LBL-9037

PROCEEDINGS

CARBONACEOUS PARTICLES IN THE ATMOSPHERE

March 20-22, 1978
LAWRENCE BERKELEY LABORATORY
UNIVERSITY OF CALIFORNIA

T. Novakov, Editor

June 1979

Sponsored By
NATIONAL SCIENCE FOUNDATION
AND
LAWRENCE BERKELEY LABORATORY
Berkeley, CA 94720

Prepared for the U.S. Department of Energy under Contract No. W-7405-ENG-48

TO: Dr. Richard A. Carrigan

of the

National Science Foundation

CONTENTS

PREFACE

The first Conference on Carbonaceous Particles in the Atmosphere was held March 20-22, 1978, at Lawrence Berkeley Laboratory (LBL), University of California at Berkeley. The 45 papers presented at this topical conference on carbonaceous particles gave a state-of-the-art review of analysis, speciation, and behavior; transport, formation, and reactions; biological effects; and sources and physical properties of carbonaceous particles in the atmosphere.

The idea for such a conference developed in a number of conversations I had with Professor R. J. Charlson of the University of Washington. From these discussions, and from the research results generated in numerous laboratories, it became apparent that carbonaceous particulate matter is an extremely important component of the overall aerosol problem, with implications to atmospheric chemistry, atmospheric physics, climate, and public health. It also became clear that in the past, carbonaceous particles have received far less attention than they deserve in view of their potential impact on air quality. Professor Charlson and I felt that the time was right to organize a conference devoted solely to carbonaceous particles and their effects on the environment. The National Science Foundation--through its program titled Chemical Threats to Man and Environment, with Dr. R. A. Carrigan as Program Manager--was receptive to the idea and provided the necessary funding for the Conference. Dr. M.O. Amdur joined us from the beginning and provided her extremely valuable input in organizing the biological and biomedical aspects of the conference.

The technical program, with invited and contributed papers, was organized by the Program Committee composed of:

T. Novakov, Lawrence Berkeley Laboratory, Chairman
R. J. Charlson, University of Washington
M. O. Amdur, Massachusetts Institute of Technology
R. A. Carrigan, National Science Foundation
D. Ballantine, U. S. Department of Energy
J. Holmes and J. Suder, California Air Resources Board
R. M. Perhac, Electric Power Research Institute
W. E. Wilson, Jr., U. S. Environmental Protection Agency

H. Rosen, Lawrence Berkeley Laboratory, served as the Conference Secretary.

The organizers intended to provide as much discussion as possible as part of the Conference program. Discussion sessions were led by a distinguished group of scientists: R. K. Stevens, U. S. Environmental Protection Agency; G. Gordon, University of Maryland; D. Hoffman, Naylor Dana Institute-American Health Foundation; and J. P. Lodge, Jr., consultant.

The consensus of the participants was that the Conference was successful and stimulating. Many individuals contributed to the success of the conference. Our thanks go to all the participants and speakers who made this Conference a scientifically important gathering. We also acknowledge the Conference Program Committee for its part in soliciting and selecting the presentations. The entire Conference ran on schedule, thanks to the session chairmen: P. T. Cunningham, L. Newman, M. O. Amdur, R. J. Charlson, and H. Rosen.

Many people at Lawrence Berkeley Laboratory gave their enthusiastic help in organizing the Conference. We would like to thank A. M. Sessler, LBL Director, E. K. Hyde, LBL Deputy Director, and R. J. Budnitz, Head of LBL's Energy and Environment Division. Organization of the Conference would have been impossible without the help of T. H. Kirksey, L. Millard, and S. Sanford from the Technical Information Division; and J. C. Baxter and J. Ortiz from the Travel Department. L. Wroth managed many of the administrative and clerical tasks before, during, and after the Conference.

Finally, members of the Atmospheric Aerosol Research group--W. H. Benner, R. Brodzinsky, S. G. Chang, M. Clemenson, R. L. Dod, L. A. Gundel, A. D. A. Hansen, S. S. Markowitz, G. E. Mason, S. Oblath, H. Rosen, A. Sawaya, R. C. Schmidt, and R. Toossi--deserve special thanks for working long hours and for performing chores well beyond their duty.

This work was performed under the auspices of the Division of Biomedical and Environmental Research of the U. S. Department of Energy under Contract W-7405-ENG-48, and also of the National Science Foundation under ENV 77-20076.

T. Novakov

Analysis, Speciation, and Behavior

SOME ANALYTICAL APPROACHES TO THE CHEMICAL CHARACTERIZATION OF CARBONACEOUS PARTICULATES

Hanns Malissa
Institute for Analytical Chemistry and Microchemistry
Technical University of Vienna
Vienna, Austria

ABSTRACT

The concept of systematic integrated dust analysis (SIDA), developed for the overall characterization of aerosol particles in terms of size distribution and chemical composition, includes the analysis of carbonaceous material. Size-segregated sampling is accomplished by a Berner ring jet impactor. Thermoanalytical methods (based on combustion of the sample in O_2) using relative conductimetric detection of evolved CO_2 and SO_2 enable temperature-dependent analyses of C and S species. About 50 µg of sample material is needed for such analyses. Flame ionization detection provides information on the volatility of carbonaceous fractions in N_2 as a function of temperature. These methods allow us to classify carbonaceous materials as 1) organic compounds volatile in N_2 and/or decomposing in O_2 at low temperatures, 2) soot, and 3) inorganic compounds (carbonates) decomposing at high temperatures. Typical analyses are given; and the role of other methods of SIDA in providing additional information is described. These methods include electron probe microanalysis, secondary electron microscopy, atomic absorption spectroscopy, infrared spectroscopy, and potentiometric analysis.

INTRODUCTION

Like many other investigators, we feel that as long as we are unable to analyze and characterize the carbonaceous fractions of atmospheric aerosol particles, we cannot adequately assess the roles of specific chemical mechanisms in atmospheric chemistry. I am very honored to be invited to report on our approach to this subject. This short report outlines only the principles and some results reflecting the cooperation between my coworkers—H. Puxbaum, R. Kellner, M. Grasserbauer—and me.

Because the analysis of carbonaceous material is part of the general scheme of airborne particle analysis, we use in principle the idea of integrated dust analysis.[1] We have advanced this idea to account for the following facts:

1. The total sample weight is small when size-segregated sampling is employed.

2. The concentration of airborne particulates in the air is small. Therefore we have to use a fairly sophisticated analytical strategy to get as much information as possible from samples weighing as little as 50 µg.

Because the quality of analytical results depends on the quality of the sampling procedure used, we have paid a great deal of attention to sampling, especially for the purposes described here. Sampling is a main part of our concept of systematic integrated dust analysis (SIDA).

SAMPLING

We feel that the following main points have to be followed to avoid or minimize unwanted reactions during ambient air sampling:

1. Sampling should be as "soft" as possible, i.e., with the least possible chemical perturbations, to minimize side reactions during sampling.

2. The sampling methods should be compatible with the analytical procedures to be employed.

3. Size fractionated sampling techniques should be used.

Consideration of these points led us to choose cascade ring impactors of the "Berner" type (University of Vienna), which employ thin annular copper foils as the depositing surface. Copper foil was chosen because it is a good supporting material for electron probe microanalysis (EPMA), and it is convenient for our thermal-analytical methods. Table 1 lists some characteristics of the impactor, while the impactor itself is shown in Figure 1.

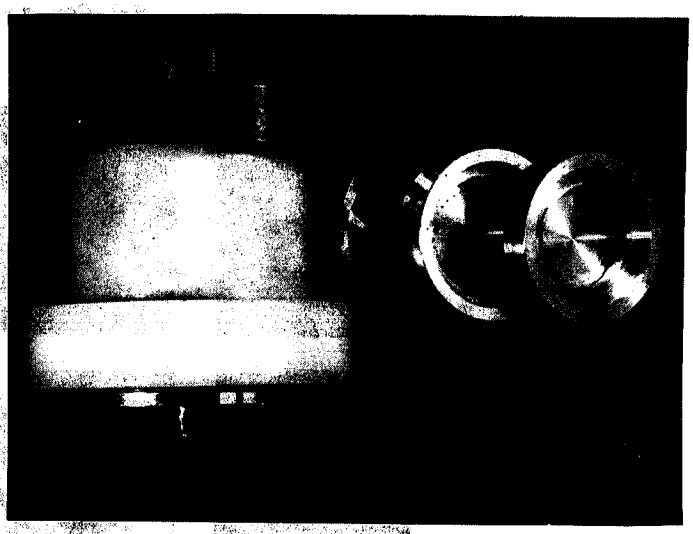

Fig. 1 Four-stage cascade impactor TU-1.

For stages 1 and 2, no treatment of the copper surface is required according to our experience, especially for soot-like materials. Stages 3 and 4

Table 1. Sampling characteristics of impactor TU-1.

Stage no.	Size range A.D. 50(μm)	No. of spots	Diameter of spot(mm)	Amount of particulate matter per spot (μg) for sampling time of 1 hour and thickness of layer (μm) Urban air	Industrial air	Rural air
1	0.14-0.40	55	0.8-1.0	3 μg 3 μm	10 μg 10 μm	0.5 μg 1 μm
2	0.4 -1.6	33	1.2-1.5	20 μg 7 μm	70 μg 20 μm	3 μg 1 μm
3	1.6 -6.4	14	2 -3	30 μg 3 μm	90 μg 10 μm	5 μg a
4	6.4-25	6	10 -12	50 μg a	150 μg a	30 μg a

Average TSP concentrations		Recommended sampling time
Urban air	300 μg/m^3	5-10 hr
Industrial air	1000 μg/m^3	1-3 hr
Rural air	50 μg/m^3	24-72 hr

Average thickness of layer calculated, specific mass = 2 g cm^{-3}.
[a]Thickness smaller than particle size, therefore incomplete coverage of substrate.

are usually coated with Apiezon grease to prevent particle bounce-off effect.

Figure 2 shows the hill-like spot deposits. The morphology of these samples. The morphology of these samples gives us an impression of the difficulties we may encounter in quantitative analysis via EPMA. Scanning electron beam microanalysis of the two small size fractions sampled by the impactor described above gives precise and satisfying results (Fig. 3). The thick line—the average result of analyses of five different spots on the foil—demonstrates that any one individual spot is representative of the size fraction collected on one stage.[2]

ANALYSIS

General Considerations

Depending on the amount of sample and on the kind of information needed, we may employ one or more of the three characterization steps, summarized in Table 2. If there is enough previous information, or if only a very small sample amount is available (< 200 μg), we will choose the short characterization and use the thermal decomposition technique in a stream of oxygen or nitrogen with relative conductimetric C and S determination, as described below.[3,4] This type of analysis provides us with a differentiation of the

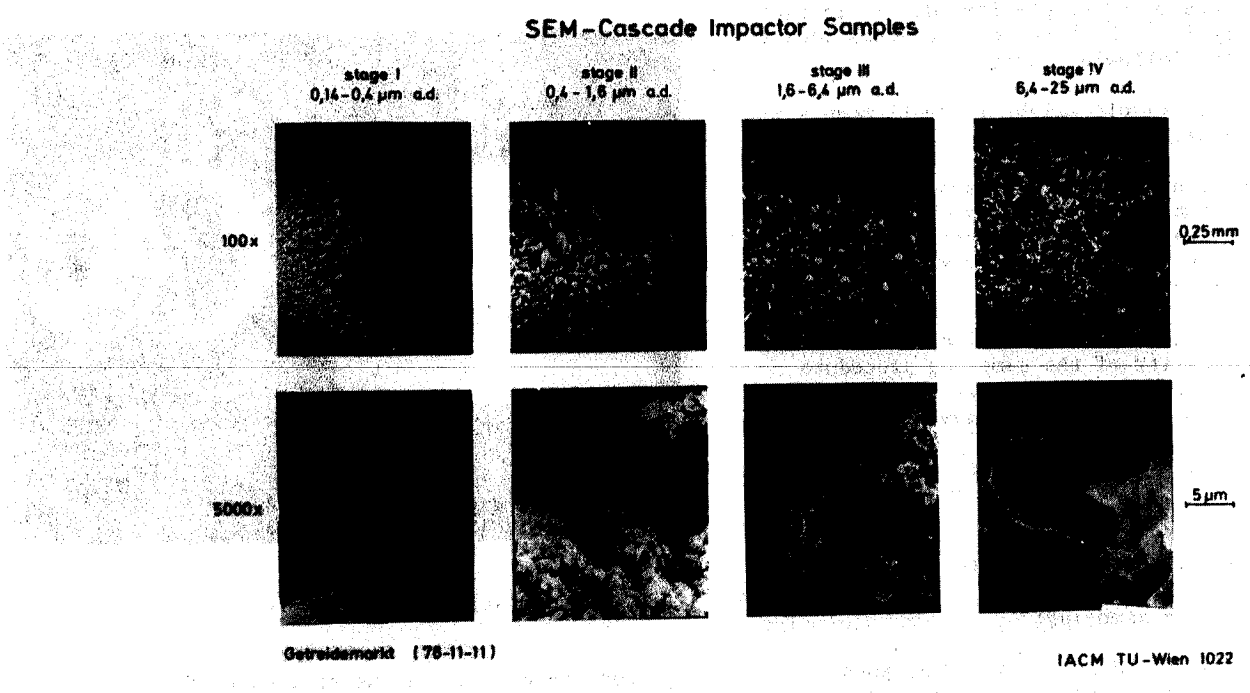

Fig. 2 Aerosol deposition by cascade impactor TU-1.

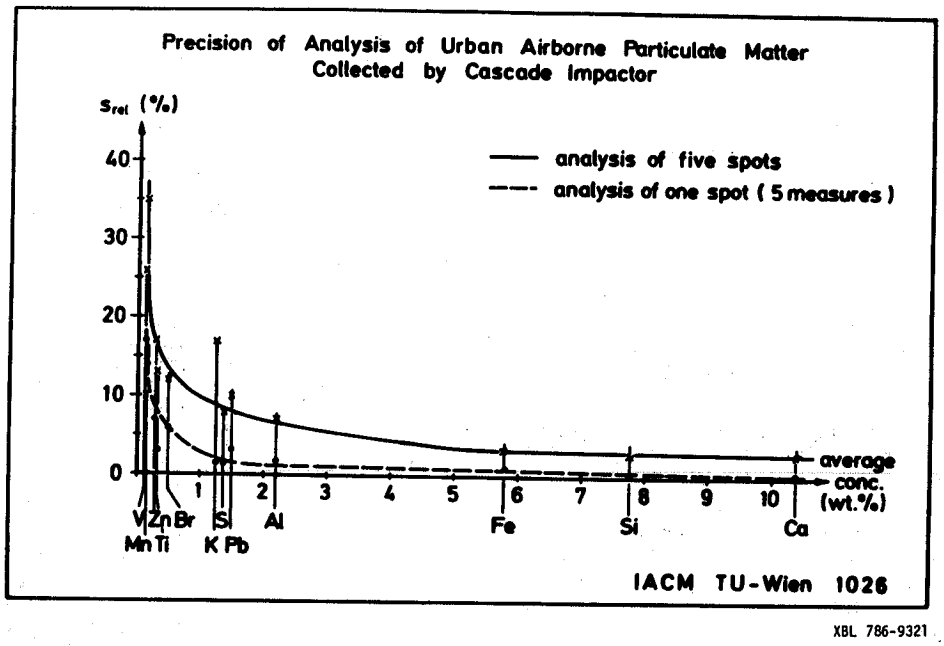

Fig. 3 Precision of the analysis of airborne particulate matter collected by cascade impactor TU-1.

Table 2. Characterization of atmospheric particulates.

Test	Short	Medium	Full
1. Total C + S	+	+	+
2. TDC + TDS	+	+	+
3. NH_4^+, NO_3^-, H^+	+	+	+
4. EPMA (EDS, WDS)	-	+	+
5. FT-IR	-	+	+
6. AAS, AES	-	-	+
7. Morphology + single particle identification	-	-	+
8. Diffraction	-	-	+
9. GC-FT/IR, GC-MS	-	-	+
10. Special tests			
Sample demand (µg)	200	500	1000

carbonaceous material into organic carbon, graphitic soot, and carbonate carbon fractions. The determination of the ammonium is also performed by relative conductometry,[5] while the nitrate is determined by an ion-sensitive electrode.[6] The time needed for this set of analyses is about 1 hour.

The full characterization is used mostly on relatively unknown samples and for transport and chemical conversion studies. Atomic absorption spectroscopy (AAS) is used for the analysis of trace elements.

Diffraction techniques (electron, X-ray, and Raman) and electron microscopic methods are now being developed in our laboratory and are of primary concern for further investigations. We have already made progress in the application of thin-layer chromatography (TLC) and the evaluation of micro-infrared (IR) techniques.

The "SIDA" Scheme

Knowing that one analytical tool alone can never give complete information in dust analysis, we introduced the concept of integrated dust analysis in 1974, at the Fourth Symposium on the Analytical Chemistry of Pollutants in Basle, Switzerland. This approach included (1) average analysis of all or individual elements, (2) identification and quantitative analysis of individual particles, (3) determination of particle mass, and (4) determination of morphology.

With the use of the impactor sampling technique, smaller sample amounts were obtained, so that a more advanced and systematic approach was necessary to obtain as much information as possible. This approach contains the following steps:

1. Sampling with cascade impactors.

2. Determination of the total amount of sample on each stage and estimation of the weight of each individual sample spot on the stage.

3. Determination of the average concentration of elements with atomic number > 11 by EPMA in the scanning mode.

4. Investigation of morphology by scanning electron microscopy (SEM), and single particle identification by SEM-energy dispersive spectroscopy (EDS).

5. Characterization of C, S, and N compounds by thermal decomposition analysis.

6. Specific compound identification by infrared techniques.

7. Trace element determination by atomic absorption.

8. Use of various other speciation methods (e.g., GC for organic compounds, diffraction techniques) if there is still sample material available.

This general outline can be varied if necessary for different research programs.

One approach of integrated analysis is shown in Figure 4. By backweighing the copper rings, the total amount of sampled matter is determined; and the weight of deposited airborne particles per spot is calculated simply by dividing by the number of spots. Because the copper foil is paper thin, the spots are cut out for further investigations. It is also possible to scrape off the deposited material carefully. (At the present time, we are investigating the use of a micro-ultrasonic device instead of scrapers.) Analysis by EPMA has been described by Grasserbauer et al.[2]; the IR-technique, by Kellner[7]; the microdetermination of halogens and ammonia, by Puxbaum et al.[5,8]; and the analysis of carbonaceous material by thermal decomposition, by Malissa et al.[3] and Gal et al.[4] For further information, the reader should consult Analysis of Airborne Particles by Physical Methods,[9]

Thermal Methods for the Characterization of Carbonaceous Material

One important step in the characterization of atmospheric aerosols is the temperature-programmed decomposition of the material, carried out either in a nitrogen atmosphere to obtain the volatile organic components or in an oxygen atmosphere to obtain the total carbon and total sulfur contents. During the temperature-programmed heating, organic and inorganic species are separated due to their different pyrolytic behavior. A schematic representation of the apparatus used is shown in Fig. 5.

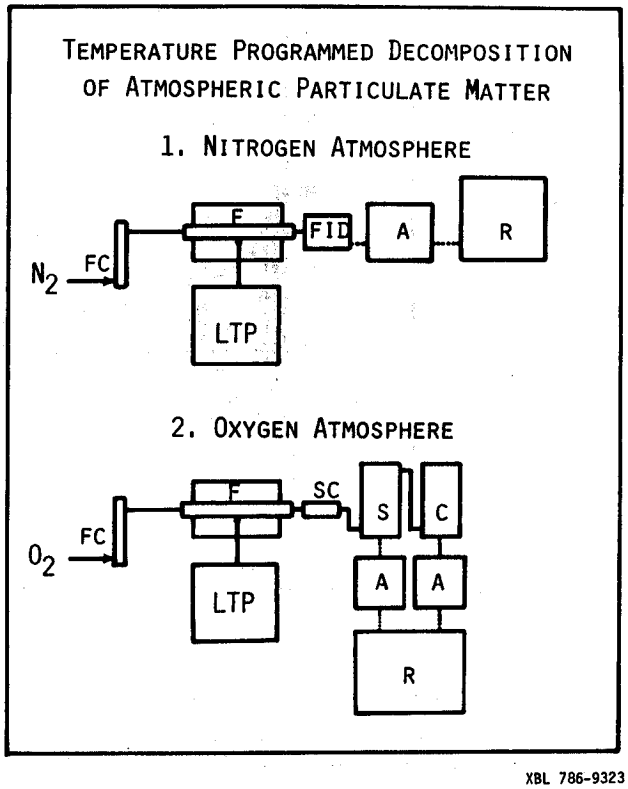

Fig. 5 Schematic presentation of the apparatus for temperature-programmed decomposition of atmospheric particulate matter.

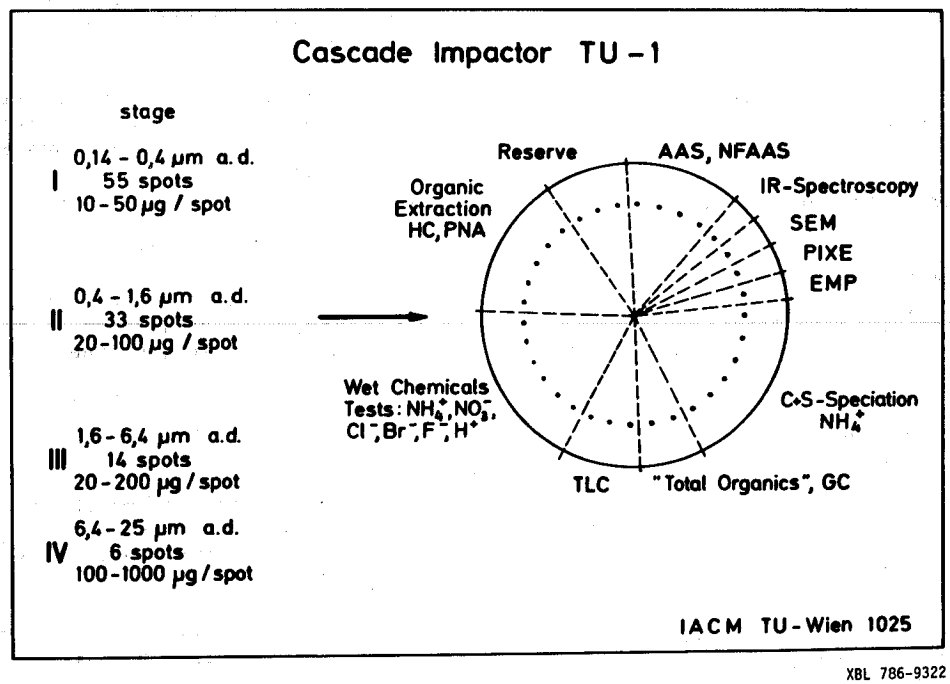

Fig. 4 Sample distribution for chemical characterization.

To determine the volatile organic components, the aerosol or dust sample is placed in a microfurnace and heated at a linear rate of 10°C/min in a nitrogen atmosphere. The evolved organic compounds are led to a flame ionization detector (FID). Peak areas of the FID response are integrated, and the result is expressed in percent volatile organic carbon (VOC). A typical result is presented in Fig. 6. Dust from a highway tunnel (Tauerntunnel), collected in the exhaust tube with a dustfall gauge, contained 4.2% VOC, evolved in two characteristic peaks with maximum evolution rates at 250°C and 400°C. To prove that the two peaks belonged to two different groups of organic compounds, the dust was extracted with methanol and the residue examined for volatile organic carbon. This sample yielded a single peak at 400°C with 2.0% VOC, showing that only the group of organic compounds volatile in the temperature range 150-350°C was extractable in methanol (Fig. 6).

The total carbon determination is carried out simultaneously with the sulfur determination. The sample is heated in an oxygen atmosphere, and the oxidation or dissociation products are absorbed in two detection units (Fig. 5). SO_2 is absorbed in a weak H_2O_2/H_2SO_4 solution; CO_2 is absorbed in a NaOH solution. The change of conductivity of the solution during the sample heating (10°C/min linear temperature rate) is shown in Fig. 7. The total carbon evolution reveals three main peaks, which we interpret as organic carbon, soot carbon, and inorganic carbon. The dust sample from the Tauerntunnel contained 8.1% organic carbon, 10.4% soot carbon, and 5.1% inorganic carbon. A comparison with the VOC trace in Fig. 6 shows that only 52% of the organic compounds was volatile. Much of the carbonaceous material must be present in

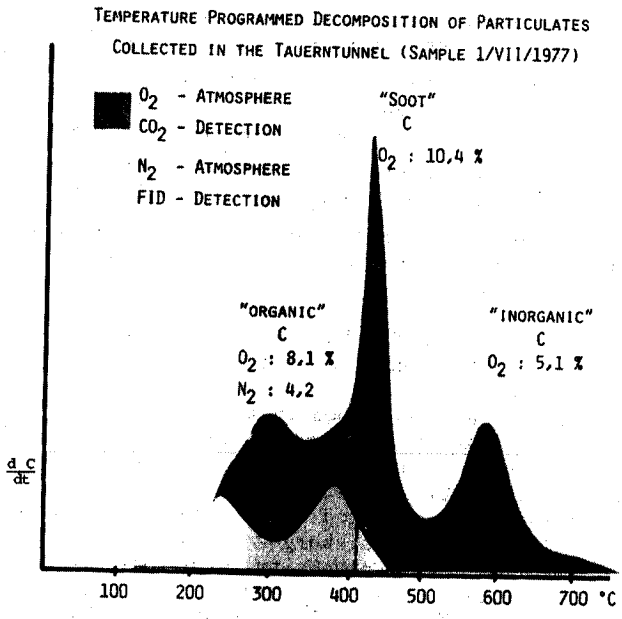

Fig. 7 Record of the carbon evolution in an oxygen atmosphere compared with the record of the volatile organic carbon determination.

polymeric (nonvolatile) states. In the highway tunnel sample, 44% of the total carbon was present in a polymeric "soot" state.

The thermal evolution of the sulfur compounds also yields three groups, due to their different pyrolytic behavior. In the low temperature range (100-380°C), SO_2 from the decomposition of ammonium

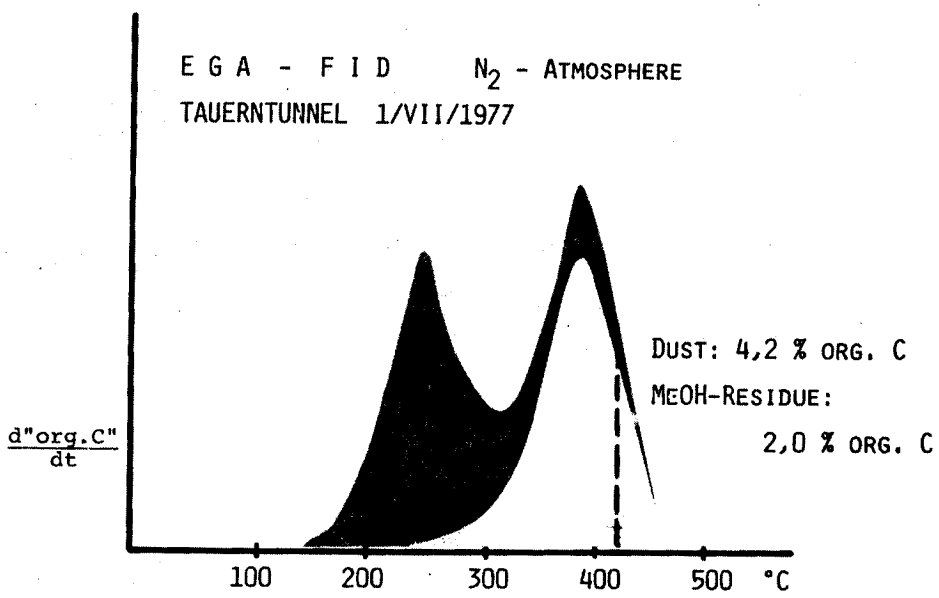

Fig. 6 Record of volatile organic carbon determination.

sulfates or sulfuric acid is liberated. Sulfur from the organic fraction should also occur in this range, but generally very low amounts of SO_2 were evolved from the organic fraction. In the medium temperature range (380-550°C), the sulfur content of the "soot" fraction is evolved as SO_2. In the high temperature range (550-1300°C), inorganic sulfates, mainly $CaSO_4$, decompose. Table 3 demonstrates the occurrence of the three groups of carbon and sulfur compounds in sediment and airborne dust samples.

The samples from Salzburg Aigen, Salzburg City, and Salzburg Hellbrunn are roadway dust. Carbon is present mainly in the carbonate state. The "soot" fraction is enriched in the city sample and low in the suburb of Hellbrunn. The sulfur content is lowest in Hellbrunn and somewhat higher in Aigen and the city of Salzburg. Sulfur is present as sulfates in the low and high temperature ranges. The samples from the Salzburg Power Station and the Vienna Technical University were collected by dustfall gauges (sampling period, 28 days), and the sample from Milan, Italy, was obtained from filters in an air conditioning unit. These coarse particle samples are similar in several respects:

1. The "soot" fraction is highly enriched.

2. A certain amount of sulfur compounds, corresponding to the "soot" fraction, is liberated.

3. The inorganic carbonate content is lower than one might expect for such samples. Since inorganic sulfates are also present, the lower carbonate could be due to possible exchange reactions between the CO_3^{2-} and SO_4^{2-} ions.

Small atmospheric particles (< 1.6 µm aerodynamic diameter [A.D.]) have a different composition (Table 4):

1. The carbon is predominantly in the "soot" state.

2. Sulfur is present mainly as ammonium sulfate.

Table 4. Characterization of the carbonaceous matter in urban aerosols, Vienna, Getreidemarkt, April 10, 1978.

Carbon fraction (wt.% C)	Size fraction (µm A.D.) 0.1-0.4	0.4-1.6	1.6-6.4	6.4-25
Total carbon	40.9	26.2	20.0	4.5
Volatile organic C	4.5	2.3	<0.2	n.d.
Total organic C	4.6	4.1	8.3	n.d.
Soot C	36.3	22.1	9.6	n.d.
Carbonate C	-	-	2.1	n.d.
Aerosol concentration (µg/m^3)	8.5	28.5	20	43

(n.d. = not determined)

3. In the size fractions < 1.6 µm A.D., the amount of inorganic carbonate is negligible.

4. Inorganic sulfates in the high temperature range are detected, but usually not to a great extent.

5. Size fractions < 1.6 µm A.D. show decreasing carbon and increasing "soot" carbon.

6. High-temperature sulfur decreases while ammonium sulfates increase.

To determine the ammonium content of dust samples, another method involving thermal evolution is applied. The sample is treated with LiOH in a nitrogen carrier gas stream at 600°C. The ammonia liberated during the reaction is quickly removed from the hot zone of the furnace and, after passing a chemical filter, is absorbed in weak sulfur acid and determined by relative conductometry. Some results are given in Table 5, indicating the enrichment of ammonium salts in the fine particle range.

CONCLUSION

In summary, Fig. 8 shows the main components of an ambient aerosol sample from Vienna as determined by systematic integrated dust analysis. Three

Table 3. Carbon and sulfur speciation in various dust samples.

Location	Sampling		Weight % total	Low temp. range 380°(%)	"Soot" fraction 380-550°	High temp. range 550°(%)
Salzburg Aigen	<50 µm, sieved	C	12.7	1	20	80
		S	0.27	40	-	60
Salzburg City	<50 µm, sieved	C	7.5	3	37	60
		S	0.40	40	-	60
Salzburg Hellbrunn	<50 µm, sieved	C	12.5	1	3	97
		S	0.05	20	-	80
Salzburg Power station	Dust jar	C	60.6	20	80	1
		S	10.9	5	55	40
Milan	ISPRA, air bag	C	41.5	15	85	1
		S	5.25	10	30	60
Vienna T.U.	Dust jar	C	8.4	1	80	20
		S	1.4	10	10	80

Table 5. Ammonium content of urban dust.

Dust	Wt.% ammonium-N
Vienna, roadway sediment	0.15
Vienna, air conditioning filter	0.83
Vienna, airborne particles	
Size fraction (µm A.D.)	
0.1-0.4	4.3
0.4-1.6	8.6
1.6-6.4	1.5
6.4-25	0.1

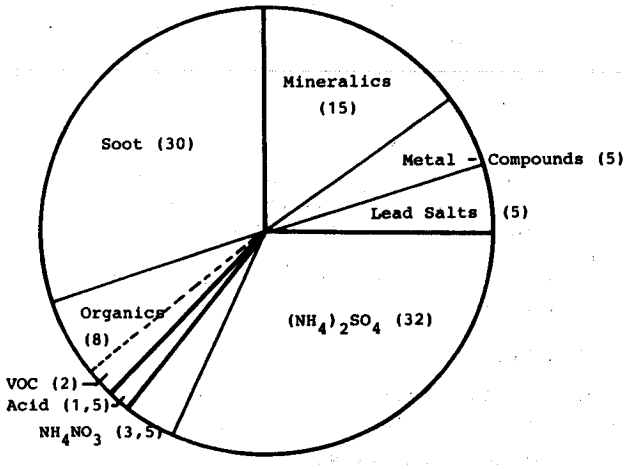

Fig. 8 Summarized result of SIDA techniques: aerosol fraction 0.4-1.6 µm A.D., Vienna, March 1977, with the relative weight percent in parentheses.

groups of components dominate the composition: mineral compounds, ammonium salts, and carbonaceous compounds. The mineral fraction can be separated into (1) mineral components from abrasion and erosion processes, (2) mineral components from various emissions, and (3) automotive lead salts. The ammonium salts are mainly sulfates and nitrates. The carbonaceous fraction contains (1) organic components, (2) soot, and (3) inorganic carbonates (negligible in this example). The "soot" fraction composes the main compound of the carbonaceous material. This fraction is not extractable in organic solvents and is stable in nitrogen up to 450°C. These are the characteristics of the highly polymeric structures present in particles from incomplete combustion processes. Our findings are consistent with the view that the major part of the carbonaceous matter in ambient aerosols is due to primary emissions.

REFERENCES AND FOOTNOTES

1. H. Malissa, "Integrated dust analysis by physical methods," Angew. Chem. Int. Ed. Engl. 15 (3), 141 (1976).
2. M. Grasserbauer, H. Puxbaum, and O. Weiss, "Analysis of the respirable fraction of airborne particles collected by cascade impactors," Fresenius Z. Anal. Chem. (in press).
3. H. Malissa, H. Puxbaum, and E. Pell, "Zur simultanen relativ-konduktometrischen Kohlenstoff- und Schwefelbestimmung in Stäuben," Z. Anal. Chem. 282, 109 (1976).
4. S. Gal, F. Paulik, E. Pell, and H. Puxbaum, "Thermoanalytical investigations on dust," Z. Anal. Chem. 282, 291 (1976).
5. H. Puxbaum, "Eine relativkonduktometrische Mikromethode zur Bestimmung von Ammonium in Stäuben," Mikrochimica Acta 1977 II, 157.
6. V. Simeonov and H. Malissa, "A model of direct potentiometric determination of nitrate," Fresenius Z. Anal. Chem. 287, 37 (1977).
7. R. Kellner, paper presented at the Scientific Session on Environmental Analysis, Szombathely, Hungary, September 1977.
8. H. Puxbuam, V. Simeonov, and J. Rendl, "Potentiometric determination of chloride and bromide in airborne dust," Microchimica Acta 1977 II, 325.
9. H. Malissa, ed., Analysis of Airborne Particles by Physical Methods (CRC Press, Miami Beach, Florida, 1978).

ANALYSIS OF VOLATILIZABLE AND ELEMENTAL CARBON IN AMBIENT AEROSOLS

Richard L. Johnson and James J. Huntzicker
Oregon Graduate Center
19600 N.W. Walker Road
Beaverton, Oregon 97005

ABSTRACT

An instrument capable of measuring both the volatilizable and elemental carbon fractions of carbonaceous aerosol on a single filter sample is described. The principle of the method is the familiar one of oxidation of the carbon to CO_2, reduction of the CO_2 to CH_4, and measurement of the CH_4 in a flame ionization detector. Organic carbon and carbonates are volatilized at 580°C in a He atmosphere and oxidized to CO_2 by MnO_2 at 850°C in the first part of the analytical cycle. Elemental carbon is measured in the second half of the cycle by oxidation in a He-O_2 atmosphere and chromatographic separation of the O_2 and CO_2. Carbonates can be separated from the organic carbon by acidification of the filter. The complete analytical cycle requires about 30 minutes. The lower limit of detection is determined primarily by the black concentration on the filter, the absolute limit being substantially less than 1 μg.

INTRODUCTION

Carbon has long been recognized as an important constituent of atmospheric aerosols. The carbonaceous aerosol consists of carbonates, a large number of organic compounds, and elemental carbon as soot. The chemical composition and mechanisms of formation of organic aerosols have been reviewed by Grosjean.[1] Recent studies have indicated that soot might also be an important component of carbonaceous aerosol and that soot can catalyze the oxidation of SO_2 to sulfate.[2,3]

Although the organic fraction can be analyzed in a number of ways, relatively few methods have been reported for the analysis of elemental carbon. Smith et al.[4] used an infrared method which required a long term grinding of the particles prior to analysis. Mueller et al.[5] reported a combustion method for total (i.e. organic plus elemental) carbon. No single, rapid, method has been reported for the analysis of both organic and elemental carbon in aerosol samples. This report concerns the development and preliminary application of such a method.

EXPERIMENTAL

The method which was developed is a variation of one used frequently for the analysis of total organic carbon.[6,7] The principle of the method is volatilization of organic carbon in a He atmosphere followed by oxidation of the carbon to CO_2, reduction of the CO_2 to CH_4, and analysis of the CH_4 in a flame ionization detector. Elemental carbon is oxidized to CO_2 in an O_2-He atmosphere followed by chromatographic separation of the O_2 and CO_2. The CO_2 is reduced to CH_4 and analyzed as above. Analyses are performed directly on the filter substrate (either glass or quartz fiber) which is used to collect the aerosol, and no pre-treatment of the sample is required. A block diagram of the instrument is shown in Figure 1 and a detailed flow diagram in Figure 2. An explanation of the speciation method, which is a two step process, follows.

The filter sample, which generally consists of four 0.25 cm^2 circles, is loaded into a quartz boat. After purging with He (O_2 content < 1 ppm) for 3 minutes, the sample is moved into the 580°C pyrolysis zone where organic carbon is volatilized. At this temperature efficient volatilization of organic carbon could be achieved without melting the glass fiber filter, and no oxidation of elemental carbon from O_2 impurities in the He was observed. The volatilized carbon is swept into the oxidation zone (MnO_2 at 850°C) by He and converted to CO_2. The He-CO_2 mixture passes through the methanator evaluation valve and valves D, A, and B (c.f. Figure 2). Column C1 between valves A and B is bypassed. After the He-CO_2 mixture leaves valve B, it is mixed with H_2 and enters the catalytic methanator (Ni on firebrick). The CO_2 is reduced to CH_4, and the CH_4 is measured in a flame ionization detector. The flame ionization detector signal is processed in an electrometer-integrator-recorder system. When the volatilizable carbon analysis is complete, a known amount of calibration gas (CH_4 or CO_2) is injected into the system through valve C and analyzed as above.

The loading, pyrolysis, and oxidation zones (i.e., the sample oven) are then isolated from the rest of the instrument and pressurized with O_2. (The sample remains in the pyrolysis zone.) After five minutes of isolation, during which time elemental carbon is oxidized to CO_2 in the O_2-He

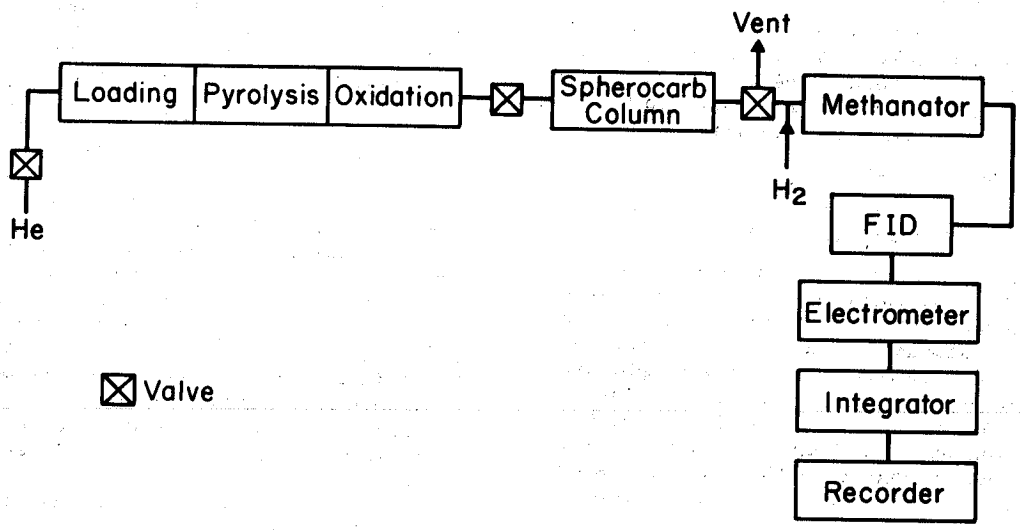

Fig. 1. Block diagram of the carbon analyzer. The loading, pyrolysis, and oxidation zones are in a single quartz tube. The pyrolysis and oxidation zones are at 580°C and 850°C respectively, and oxidation is accomplished by MnO_2. The methanator is a quartz tube containing Ni on firebrick and is at 450°C.

FID: flame ionization detector.

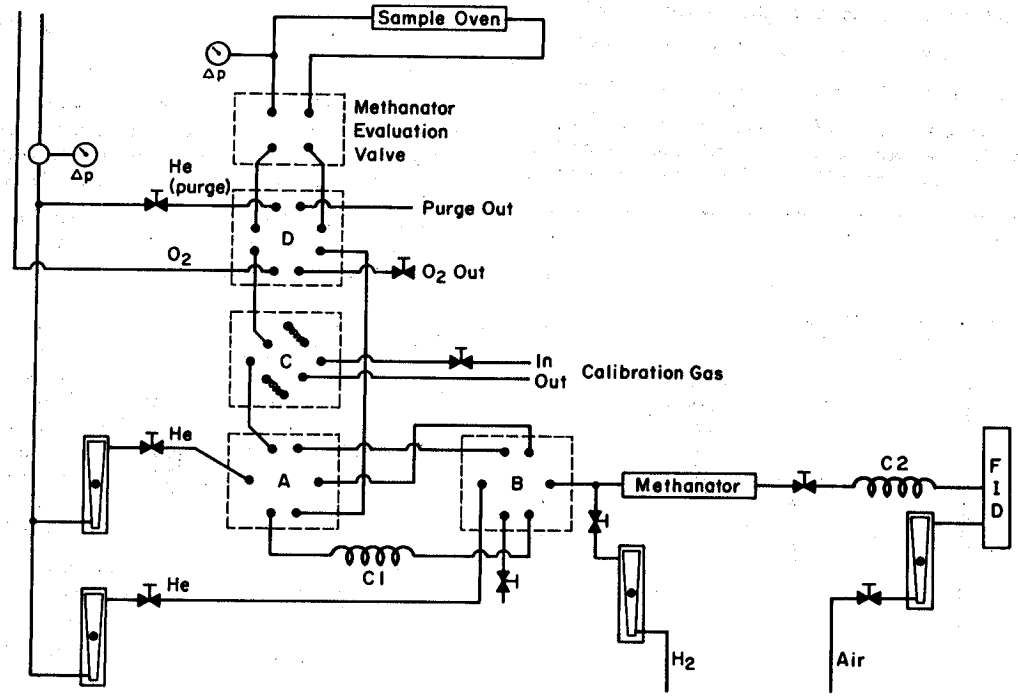

Fig. 2. Flow system for carbon analyzer. Valves A, B, C, D, and the methanator evaluation valve are multi-port, zero dead volume valves. The methanator evaluation valve is used to remove the sample oven from the flow system and permits measurement of the efficiency of methanation. C1 and C2 are Spherocarb columns. C1 is the analytical column and is 38 cm long by 0.4 cm i.d.

atmosphere, the gases in the sample oven are swept through the valves and into column C1 which separates the CO_2 from the O_2. The column contains 60/80 mesh Spherocarb (Analabs, Inc.), a spherical, non-friable, carbon molecular sieve. Oxygen is eluted first from the column and is vented to the atmosphere by valve B to prevent damage to the methanator. The CO_2 emerges from the column after four minutes, is mixed with H_2, and is directed through the methanator and into the flame ionization detector. The resultant CH_4 is measured as above. When the elemental analysis is complete, a known amount of calibration gas is added and the response measured. For both the volatilizable and elemental calibrations the flow paths of the calibration gases are the same as for the sample gases. This minimizes problems in the electronic integration which might result from different peak shapes. The length of an analytical run is 25 minutes. At the present time the analysis is partially automated, and a fully automated system is being developed.

RESULTS

Figure 3 shows the analyzer response for an aerosol sample on a Gelman A/E glass fiber filter. The peaks correspond to volatilizable carbon, volatilizable mode calibration, elemental carbon, and elemental mode calibration. The resultant carbon concentrations on the filter after blank subtraction are 20 $\mu g/cm^2$ of volatilizable carbon and 1.6 $\mu g/cm^2$ of elemental carbon. Typical blank concentrations on the filter are 4 $\mu g/cm^2$ of volatilizable carbon and 0.4 $\mu g/cm^2$ of elemental carbon. Most of the volatilizable blank corresponds to organic carbon on the filter, but most of the elemental blank probably results from an artifact in the system. Further work is underway to minimize this artifact. The atmospheric concentrations of carbon for the sample of Figure 3 are 8 $\mu g/m^3$ of volatilizable carbon and 0.6 $\mu g/m^3$ of elemental carbon (air volume sampled: 2.55 m^3/cm^2 of filter; total mass loading: 78 $\mu g/m^3$).

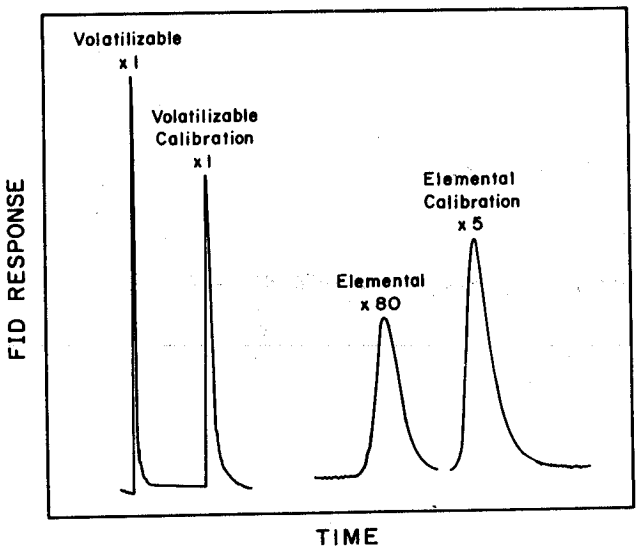

Fig. 3. Response of the carbon analyzer to carbonaceous aerosol on a glass fiber filter. In both instances the calibration peaks correspond to 54 µg of carbon. Note the difference in the ordinate scales for the four peaks.

The method has been tested for a number of model compounds by analyzing known amounts of the various substances. The results are shown in Table 1. Coronene and glutaric acid have been identified in aerosol samples, and humic acid is a soil component. All compounds were recovered at 90% or greater efficiency. Of particular importance is the lack of cross-over between the volatilizable and elemental modes; i.e., the organic compounds gave responses only in the volatilizable mode and graphite only in the elemental mode.

Table 1. Efficiency of Carbon Analyzer for Different Carbon Compounds.

Compound	% Recovered as Volatilizable	% Recovered as Elemental
Glutaric acid	105	0
Mannitol	98 ± 7	0
EDTA	95	0
Oxalic acid	91 ± 7	0
Coronene	90 ± 3	0
Humic acid	93	0
Graphite	0	94 ± 3

The response of the carbon analyzer to K_2CO_3, Na_2CO_3, and $CaCO_3$ was found to occur only in the volatilizable mode. Work is currently underway to determine the carbonate response separately by acidifying the samples and measuring the evolved CO_2. When this has been accomplished, the operational term "volatilizable" can be dropped, and the more precise terms, carbonate, organic, and elemental, can be used.

The instrument has been used to analyze a small number of ambient samples from the Portland, Oregon, metropolitan area. A total of 20 high volume samples on Gelman A/E glass fiber filters from 6 sites - both urban and rural - during four days in August 1977 were analyzed. Carbonate analysis was not performed, and so the volatilizable carbon included both organic and carbonate carbon. For these samples the average mass loading was 80 $\mu g/m^3$. The volatilizable carbon comprised an average of 9.4% of the total and elemental carbon 1.2%. The ratio of elemental to total carbon was 0.12. The heaviest concentration (2.4 $\mu g/m^3$) of elemental carbon was measured in an area in which there was considerable diesel truck activity.

ACKNOWLEDGEMENT

This work was sponsored in part by the Northwest Environmental Research Center, a consortium of Oregon and Washington industries supporting environmental research at the Oregon Graduate Center.

REFERENCES

1. D. Grosjean, chapter on "Aerosols" in "Ozone and other photochemical oxidants", National Academy of Sciences (1977).

2. T. Novakov, S.G. Chang and A.B. Harker, "Sulfates as pollution particulates: catalytic formation on carbon (soot) particles", Science 186, 259-261 (1974).

3. H. Rosen and T. Novakov, "Raman scattering and the characterization of atmospheric aerosol particles", Nature 266, 708-710 (1977).

4. D.M. Smith, J.J. Griffin and E.D. Goldberg, "Elemental carbon in marine sediments: a baseline for burning", Nature 241, 268-270 (1973).

5. P.K. Mueller, R.W. Mosley and L.B. Pierce, "Carbonate and noncarbonate carbon in atmospheric particles", in "Proceedings of the Second International Clean Air Congress" (H.M. Englund and W.T. Beery, ed., Academic Press, New York 1971) pp 532-539.

6. Y. Takahashi, R.T. Moore and R.J. Joyce, "Direct determination of organic carbon in water by reductive pyrolysis", Amer. Lab. 7, 31-38 (1972).

7. D. Grosjean, "Solvent extraction and organic carbon determination in atmospheric particulate matter: the organic extraction - organic carbon analyzer (OE-OCA) technique", Anal. Chem. 47, 797-805 (1975).

Analysis of Adsorbed Species of Commercial Polymeric Carbons

W. L. Fitch and D. H. Smith
Department of Genetics
Stanford University
Stanford, California 94305

ABSTRACT

A review of the important forms of polymeric carbon (graphitic carbon) is presented. Research directed toward the analysis of polymeric carbon and materials adsorbed on it is described. A new simple, method for measuring the adsorptivity of polymeric carbons , utilizing tritium labeled benzo[a]pyrene, has been developed. Benzene/methanol extraction and analysis by combined gas chromatography/mass spectrometry (GC/MS) indicates the presence of a series of oxidized polynuclear aromatic hydrocarbons (PAH) as adsorbates on commercial carbon black samples. The implications of this work for the study of environmental polymeric carbons are discussed.

INTRODUCTION

Polymeric carbons (also called graphitic or elemental carbons) are defined as those materials which consist structurally of fused polycyclic ring systems composed predominantly of carbon. This definition encompasses a variety of polymers ranging in homogeneity from coal and soot to graphite, but excludes diamond. Polymeric carbons can be of natural origin (coal, graphite, soots from forest fires) or man-made (carbon blacks, fossil fuel derived soots, activated carbons.) Polymeric carbons have been detected in all environments where they have been sought, including sediments [1,2], the moon [3] and atmospheric particulates. In spite of its widespread occurrence, very little is known about the environmental fate and effects of polymeric carbon.

The physical processes which produce polymeric carbons [4,5] will also produce the lower homologues, the polynuclear aromatic hydrocarbons (PAH). These materials have known health effects [6] and are routinely monitored in a variety of environmental compartments. Of the commercial polymeric carbons, the soots such as lampblack and the carbon blacks used in rubber tire manufacture have been shown to contain adsorbed PAH which are extractable with benzene. However, the finer particle size channel blacks used for pigments and the activated carbons used in water purification have not been shown to contain benzene extractable PAH in appreciable quantities. The similarities in production methods for these different carbons has led to the suspicion that the small particle size channel blacks and activated carbon will contain adsorbed PAH, but that due to a stronger adsorption these PAH are not extractable by normal means. This paper will describe our methods for measuring the adsorption of PAH by polymeric carbon samples and the analysis of adsorbed species on commercial samples of carbon.

EXPERIMENTAL

Equipment

The gas chromatographs, mass spectrometer and data analysis equipment routinely used in this laboratory have been described elsewhere [7,8]. Tritium was measured with a Packard Tri Carb Liquid Scintillation Counter. ^{3}H-Benzo[a]pyrene (158 microcuries/ug in benzene) was purchased from the Amersham Corp. Samples of polymeric carbons were obtained from commercial sources as indicated in Table 1. Elemental analyses were performed by the Stanford Department of Chemistry Microanalytical Laboratory. Authentic samples of PAH and derivatives were obtained from Aldrich Chem. Co., Eastman Organic Chem. and Analabs Inc. All solvents were Baker "Resi-analyzed" grade.

Measurement of Benzo[a]pyrene Adsorption

^{3}H-Benzo[a]pyrene solutions of specific activities 0.00123, 0.0510, 1.37 and 158 microcuries/ug in toluene were prepared from the purchased solution and unlabelled benzo[a]pyrene. These solutions are stable for several months at room temperature if protected from light. Aliquots were added to 10.0 mg of the polymeric carbon sample in a small glass vial along with toluene to a final volume of 2.0 ml. Preliminary experiments indicated that the adsorption was slow, requiring several hours to reach equilibrium. For data collection the adsorption experiments were left overnight prior to analysis. The solution was filtered through glass wool, and an aliquot of the filtrate was added to a scintillation vial containing Liquifluor scintillation fluid (New England Nuclear, 15 ml) for counting. The channel ratios method was used to correct the counts per minute for quenching. The equilibrium benzo[a]pyrene concentration in solution was then calculated from the specific activity. The concentration of adsorbed benzo[a]pyrene was calculated by subtraction using the known weights of carbon sample and benzo[a]pyrene added.

Extraction and Analysis of Carbon Samples

A polymeric carbon sample (5 g) was extracted for 20 hr in a standard soxhlet apparatus with benzene/methanol (9/1). The residue after removal of the solvent was weighed, dissolved in dichloromethane and the internal standard, 1,2,3,4-tetrachloronaphthalene (200 ug), was added. An aliquot of this solution was injected on a 6 ft. 1/8 in packed column of

Table 1. Polymeric Carbons Investigated

Name	Source	Trade Name	Particle Size (nm)
Channel 19	b	Colour Black FW200	13
Channel 18	c	Neo Spectra AG	13
Channel 15	b	Colour Black FW2	13
Channel 13	b	Special Black 5	20
Channel 12	b	Special Black 4	25
Channel 10	c	Neo Spectra Mark III	14
Channel 4	b	Colour Black S160	20
Active 9	a	Darco G60	-
Active 8	d	Norit A	-
Furnace	b	Corax L	23
Lampblack	a	Lampblack	44
Graphite	a	Powder Grade 38	<44,000

Sources:

a. Fisher Scientific Co.
b. Degussa Inc., Pigments Division
c. Cities Service Co. Columbian Division
d. Matheson Coleman and Bell.

Dexsil 300 along with a mixture of hydrocarbon standards (C_{16}, C_{20}, C_{28}, and C_{36}, about 1 ug each). The column was programmed from 120-300°C at 4°C/min. A total of 500 mass spectra were recorded with a mass range of 40-450. For the higher molecular weight PAH present in certain extracts, it was necessary to record 700 spectra to a final temperature of 325°C.

Data Analysis

The raw data from the GC/MS experiments were analyzed by the suite of computer programs, CLEANUP, TIMSEK and SEARCH, which have been described elsewhere [7,9]. The CLEANUP program produces "clean" mass spectra of components after subtracting background and resolving overlapping peaks. The TIMSEK program assigns relative retention indices (RRI) to each peak by comparison to coinjected hydrocarbon standards, and calculates relative concentrations in comparison to the added internal standard. The SEARCH program attempts to identify peaks by comparison of mass spectra and associated RRI's to a library of previously identified compounds. This library is continuously updated and now contains over 100 PAH and derivatives. Table 4 is a listing of the contents of this library.

RESULTS AND DISCUSSION

Adsorption of Benzo[a]pyrene By Polymeric Carbons

We have measured the adsorption of ^{3}H-benzo[a]pyrene from toluene by the channel black sample 13 (Table I, the numbers refer to oxygen content) over a broad range of concentrations. The resulting adsorption isotherm plotted as the

Table 2. Analytical Data on Polymeric Carbons

	Elemental analysis							
Name	C	H	N	S	O	Ash	Extract[a]	Adsorptivity[b]
Channel 18	81.3	0.5	0.0	0.1	18.0	0.1	<0.1	0.030
Channel 19	79.2	0.7	0.4	0.4	19.4	0.0	1.4	0.056
Active 8	88.0	0.6	0.1	0.0	7.6	3.7	<0.1	0.060
Channel 15	83.9	0.3	0.4	0.3	14.9	0.1	1.1	0.069
Channel 10	89.5	0.7	0.0	0.0	9.8	0.0	<0.1	0.072
Active 9	88.7	0.7	0.0	0.0	8.8	1.8	<0.1	0.083
Graphite	97.0	0.1	0.0	0.0	1.6	1.3	<0.1	0.14
Channel 13	85.6	0.6	0.3	0.4	13.2	0.0	0.85	0.15
Furnace	96.9	0.3	0.0	0.7	2.1	0.0	<0.1	0.23
Channel 12	86.0	0.7	0.4	0.4	12.4	0.0	0.48	0.36
Channel 4	94.6	0.6	0.1	0.3	4.4	0.0	1.0	3.8
Lampblack	96.7	0.6	0.0	1.5	0.9	0.3	0.37	40.0

[a] Weight percent of the benzene/methanol extract.
[b] Distribution coefficient for 10 nanograms benzo[a]pyrene between toluene (2 ml) and carbon (10 mg). Results in units of nanograms per ml toluene/nanograms per mg carbon.

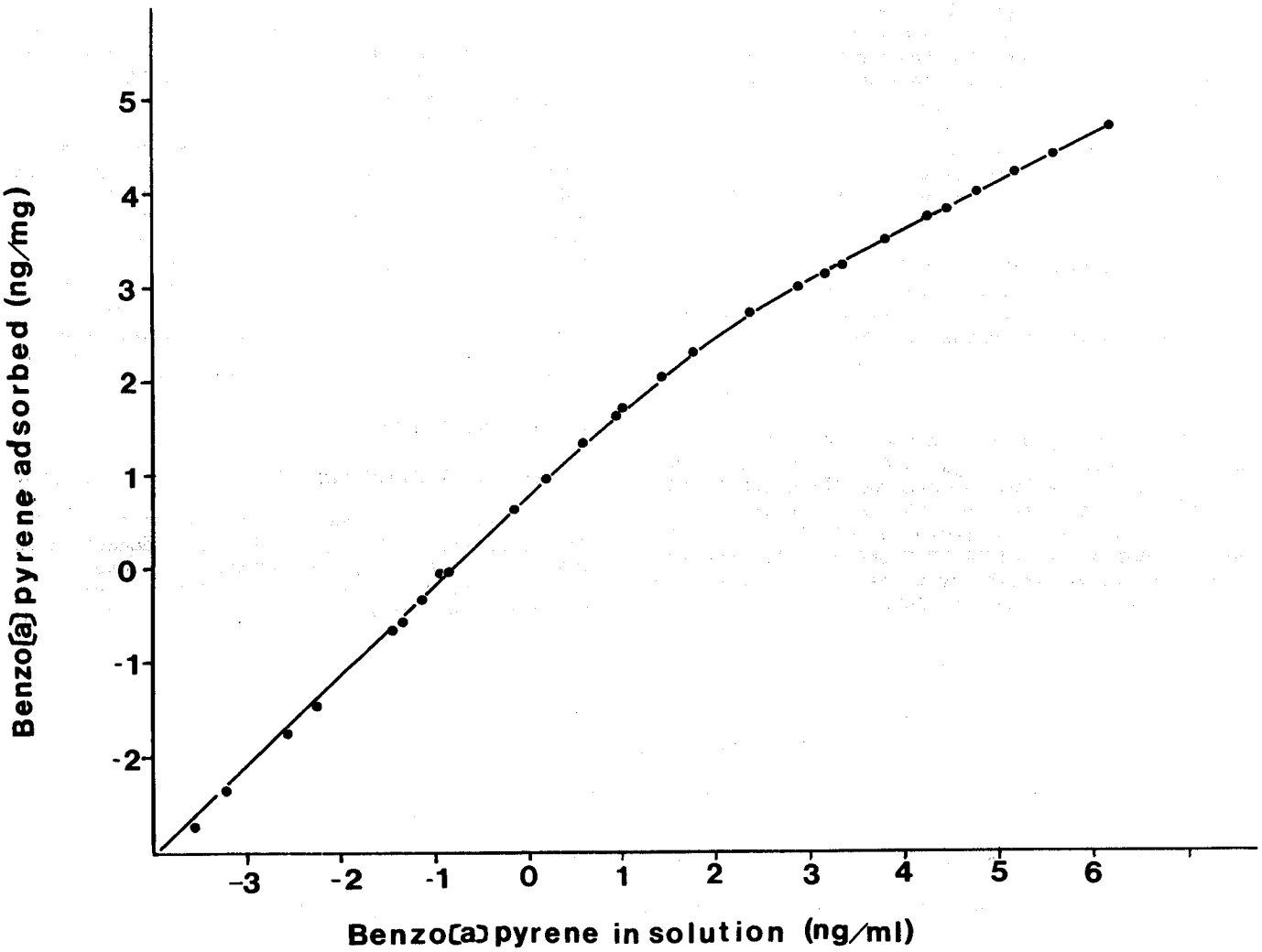

Fig. 1. Isotherm for the adsorption of benzo(a)pyrene by channel black 13 from toluene solution (plotted log/log)

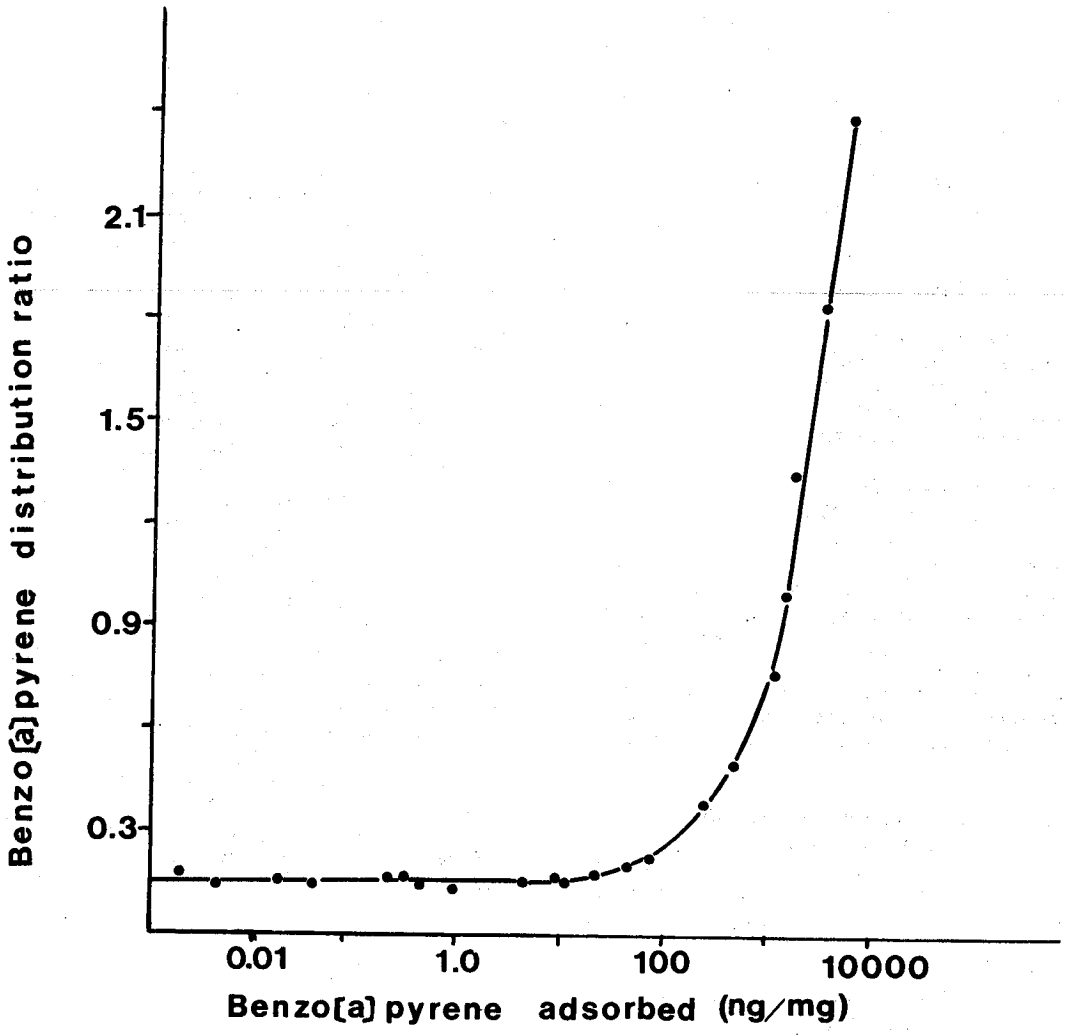

Fig. 2. Same data as Fig. 1 plotted as the ratio of the equilibrium solution concentration (in µg per µl of toluene) to the adsorbed concentration (in µg per mg of carbon) versus the adsorbed concentration.

logarithm of the adsorbed concentration versus the logarithm of the equilibrium toluene concentration, is shown in Figure 1. Another way of looking at these data is presented in Figure 2. Here the ratio of the solution concentration to that adsorbed is plotted against the logarithm of the adsorbed concentration. It can be seen that the distribution of benzo[a]pyrene is constant up to an adsorbed concentration of about 10 ppm. It was decided to compare the adsorptivities of various carbons at the 1 ppm level. These results are shown in Table 2 and are discussed below. It is felt that this simple method is a reliable way of measuring the adsorptive capacities of various polymeric carbon for PAH.

Identification of Carbon Extractables

Each of the carbons listed in Table 1 was extracted with benzene/methanol for 20 hr. The percent extractable material is listed in Table 2. The extracts were analyzed by combined gas chromatography/mass spectrometry to determine the chemical nature of the adsorbed species [10]. The total ion current traces for the extracts of the lampblack and three channel blacks are shown in Figures 3-6. The identities of individual components were determined by comparison of both mass spectra and relative retention indices to those of authentic samples, by comparison to literature spectra [11,12,13] or by analysis of fragmentation patterns [14,15]. The quantitative results (Table 3) are based on the calculation of relative concentrations by the TIMSEK program [7] using tetrachloronaphthalene as internal standard.

Table 3 lists quantitative data on the extractables from five channel blacks and a lampblack. The data are presented only for the most abundant member of each compound class for each polymeric carbon. The actual number of compounds quantitated from each carbon is too large for tabular presentation. However Table 4 is a listing of all of the compounds which we have detected in these studies, together with; 1) their retention indices on Dexsil; 2) molecular weight; and 3) the basis for the structural assignment. We have not attempted to determine which among many possible isomeric structures is present for many of the materials which occur at low concentrations.

Properties Of Specific Polymeric Carbons

a) Graphite. Graphite consists of large two dimensional sheets of fused aromatic rings [16]. The layers are held together by weak van der Waals forces which give the material its characteristic properties - lubricating ability and softness. It is found naturally in a variety of places including deep Earth deposits and meteorites. The majority of the graphite in commercial use is prepared synthetically by high temperature conversion from less pure carbon black or coke. Graphite uses range from specialized high technology items such as electrodes and nuclear fission moderators to everyday items such as pencils. Small organic molecules will not survive the high temperatures involved in graphite formation. Extraction of a commercial powdered graphite sample yielded trace quantities of naphthalene, but no other extractables. The adsorbancy of graphite for benzo[a]pyrene (Table 2) indicates that particle size (and thus surface area) is not the only factor regulating adsorption. Although the particle size of our graphite sample far exceeds that of other carbon samples, its adsorptivity for benzo[a]pyrene is intermediate to samples with much smaller particle sizes.

b) Active carbon. Activated carbons are prepared by controlled pyrolysis and subsequent oxidative activation of organic substrates, such as sugar, coconut or petroleum. Their high adsorptive properties are due to the highly porous structure formed during the oxidation process. A large increase in the production of activated carbons is anticipated over the next several years [17] due to EPA mandated use in water treatment programs. The large scale use of these materials will necessitate a greater understanding of their adsorptive/desorptive [18,19] and catalytic [20] properties. As prepared active carbons have at most trace quantities of extractable organic adsorbates [21]. We extracted two commercial active carbons and were able to detect only trace quantities of low molecular weight PAH in one of the two samples. Both of these carbons strongly adsorbed benzo[a]pyrene as expected. Active carbons tend to be irreproducible from batch to batch in their adsorbancy for water pollutants [22], and simple ways of measuring this property are of value.

c) Carbon blacks. Carbon blacks are a variety of materials, composed of microcrystalline graphite-like particles, whose properties vary greatly depending on their method of preparation [23,24]. The major forms are:

1) Lampblack - historically the classic black pigment for use in printing , now largely replaced by furnace and channel blacks. Lampblack is prepared commercially by incomplete combustion of heavy petroleum fractions. The products have particle sizes ranging from 40-200 nanometers and normally contain large amounts of adsorbed polynuclear aromatics. On extraction, a commercial lampblack sample yielded a variety of PAH and sulfer-containing PAH as shown in Figure 3. The adsorptivity of lampblack for benzo[a]pyrene (Table 2) is very low, supporting the idea that any PAH present will be readily extractable.

2) Furnace black - the largest volume black at the present time, used primarily in rubber products including tires. These blacks are prepared in large furnaces from petroleum fractions and an additional energy source such as natural gas. Their properties vary greatly depending on feedstock and process technology. Particle sizes range mainly from 20 to 50 nanometers. Furnace blacks, including those of particle size near 30 nm, have been shown to contain adsorbed PAH and sulfer and oxygen derivatives [13,25,26,27,28]. However, the small particle size furnace black which we extracted

yielded only traces of the smaller PAH, pyrene being the highest molecular weight derivative detected. A trace of dibenzofuran was also detected.

3) Channel blacks - these fine particle size blacks (10-30 nanometers) are prepared by impinging natural gas or petroleum based flames on moving metal channels. The channel blacks are the most expensive of the commercial blacks and find their use in fine pigments. To achieve maximum color properties, many channel products receive a post-oxidative treatment. The oxygen content of a channel black can range up to 20 percent.

According to the literature, channel blacks do not contain extractable PAH [25,29,30]. Indeed, it was reported that small particle size channel blacks are so strongly adsorptive for PAH that they would not be readily detected even if present[31]. Our results on the adsorption of ^{3}H-benzo[a]pyrene by channel blacks (Table 2) confirm this. The small particle size, high oxygen content channel blacks adsorb benzo[a]pyrene as strongly or more strongly than activated carbons. We have, however detected a series of PAH derivatives upon extraction of these channel black samples.

Figures 4 and 5 show the total ion current traces for the extracts of two oxidized channel black samples. Phenanthrene is seen in these extracts, but no other PAH are detectable at this level of sensitivity. However, a variety of oxidized species have been identified. These include ketones such as 9-fluorenone, quinones such as anthraquinone, nitro compounds such as 1-nitronaphthalene, anhydrides such as 1,8-naphthalenedicarboxylic anhydride and methyl esters such as dimethylphthalate. The methyl esters were not detected when benzene alone was used for extraction and are presumably formed by acid catalyzed (these channel blacks are highly acidic) esterification with the methanol solvent. Channel samples 19 and 13 yielded similar results. In general, the four oxidized channel blacks which we obtained from Degussa Inc. showed increasing extractable content with increasing oxygen content.

Interestingly, the two high oxygen content, high benzo[a]pyrene adsorption, small particle size channel blacks which were obtained from the Cities Service Corp., Columbian Division (channels 18 and 10, Table 1 and 2) had no detectable extract at all. The only noticable difference in these blacks is that they have much lower sulfer and nitrogen contents indicating differences in petroleum feedstock or post-oxidation technology or both. This discrepancy is typical of commercial products for which the quality control and marketability is based on a nonchemical criteria, such as color.

The lowest oxygen content channel (channel 4, also a Degussa product) yielded an extract (Figure 6) which contained both PAH and oxidized PAH. However it did not show either the methyl esters or the nitro-PAH. Among the channels investigated, this sample was the only one which does not receive a postoxidative treatment during its roduction. Thus, we speculate that the more highly oxidized PAH acids and nitro derivatives are formed during this high temperature air-oxidation. Channel 4 is also anomalous in its adsorption of benzo[a]pyrene compared to other samples of similar particle size.

As mentioned, the small particle size channel blacks strongly adsorb benzo[a]pyrene and presumably other PAH as well. The oxidized PAH, which appear to be readily extracted from these carbons generally have molecular weights in the 170-230 range. Whether higher molecular weight materials are present but not extractable is not known. We have detected trace quantities of oxy-PAH with molecular weights up to 270. Approaches to improving the extraction of PAH from carbon blacks are described elsewhere [8].

d) Soots. Any incomplete combustion process will produce a residue of polymeric carbon. The major environmental concerns here are soots from petrochemical energy production and uncontrolled fires. These soots are of undetermined structure and admixed with a variety of other air pollutants. It is likely that the PAH and derivatives, including ketones, quinones, which have been detected in atmospheric particulates [32,33] are associated with the polymeric carbon present. We have not investigated any environmental soots at this time.

CONCLUSIONS

Polymeric forms of carbon are widespread environmental contaminants. Very little is known about their fate in the air or on land. Furthermore, little is known about the adsorptive and catalytic properties of these materials with regards to the environmental fate of other pollutants such as PAH or sulfer dioxide. Our results on the extractable components of channel blacks indicate that the polar PAH derivatives are more prevalent and more readly solubilized than PAH for certain carbons. Whether these oxidized PAH demonstrate the same cellular toxicities as their parent molecules is unknown. The recent investigations of the mutagenic properties of nitro derivatives of benzo[a]pyrene [34] certainly indicates that more work is needed in this area. Finally, our work has particular relevance to one area of health concern. In 1976, the FDA removed carbon black from the GRAS list for food and cosmetic additives [35]. The primary rational for this delisting revolved around the question of the presence of extractable PAH. Previously, only channel blacks had been allowed for food uses as these supposedly contained no PAH. The introduction of channel blacks utilizing varied petrocarbon feedstocks led to worries about quality control. Channel black producers were unable to satisfy the FDA as to the consistent nature of their products. As our results demonstrate, materials of competitive color properties can vary tremendously in terms of extractable content. Very careful regulation will be required if carbon blacks are to be relisted as food and cosmetics additives.

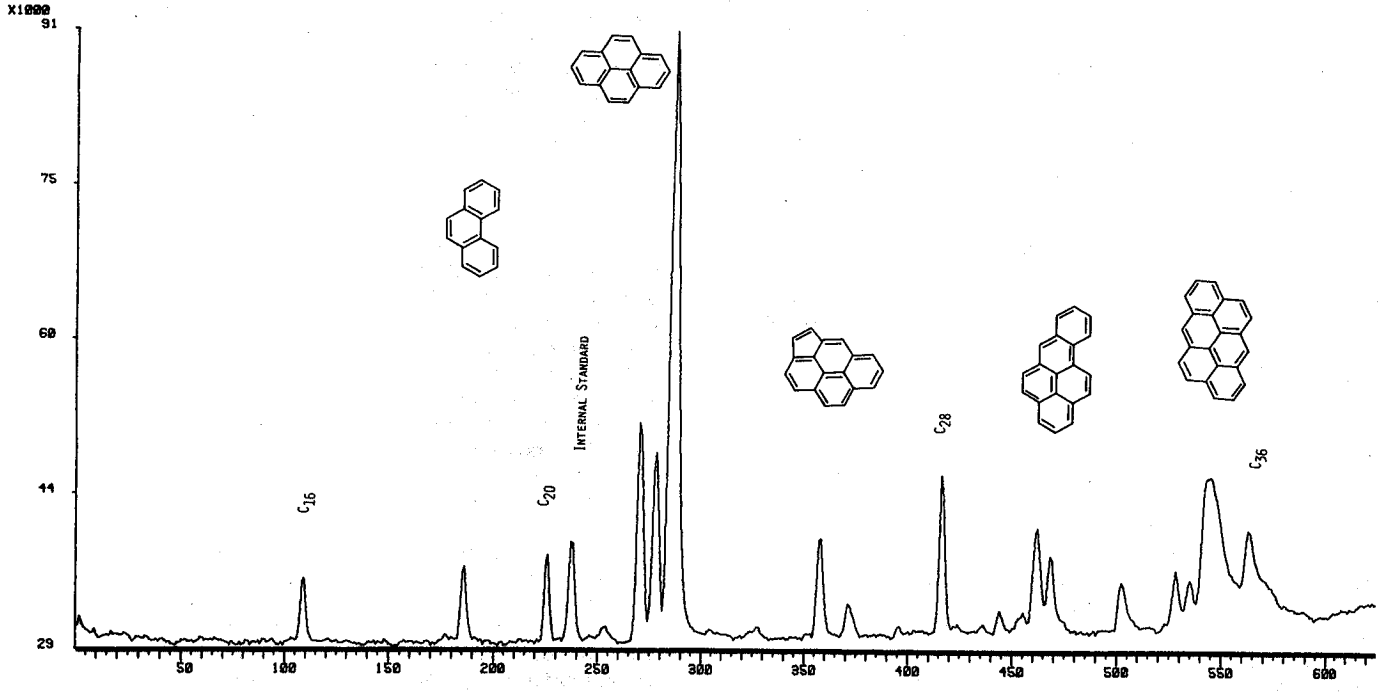

Fig. 3. Total ion current trace of the benzene/methanol extract of lampblack.

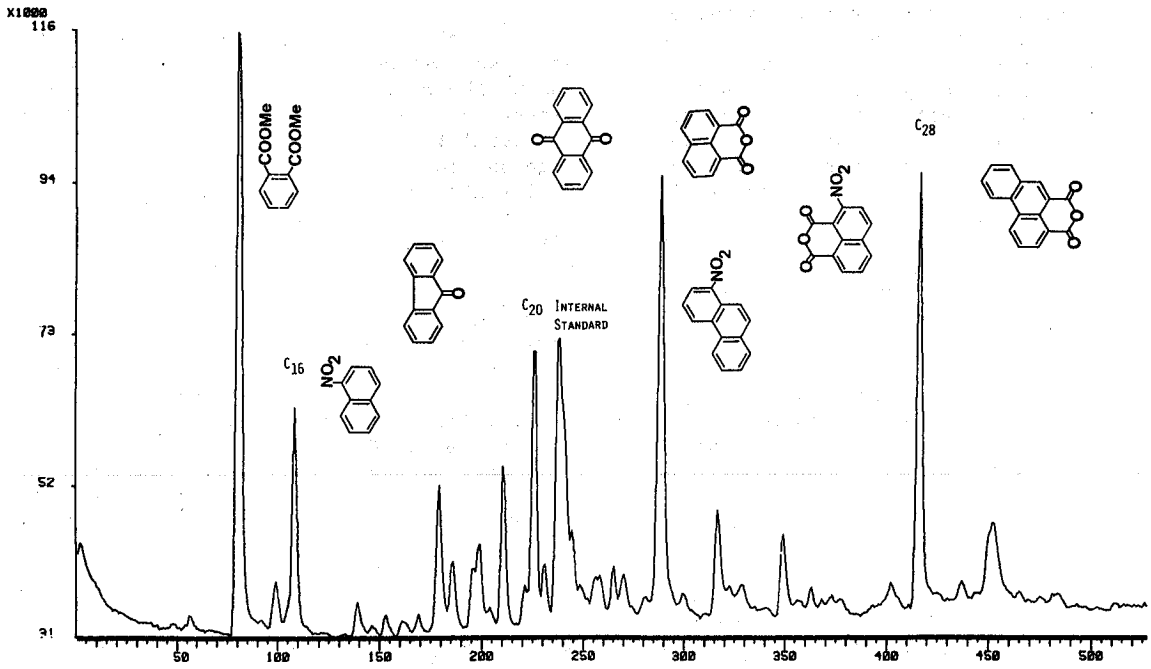

Fig. 4. Total ion current trace of the benzene/methanol extract of channel black 12.

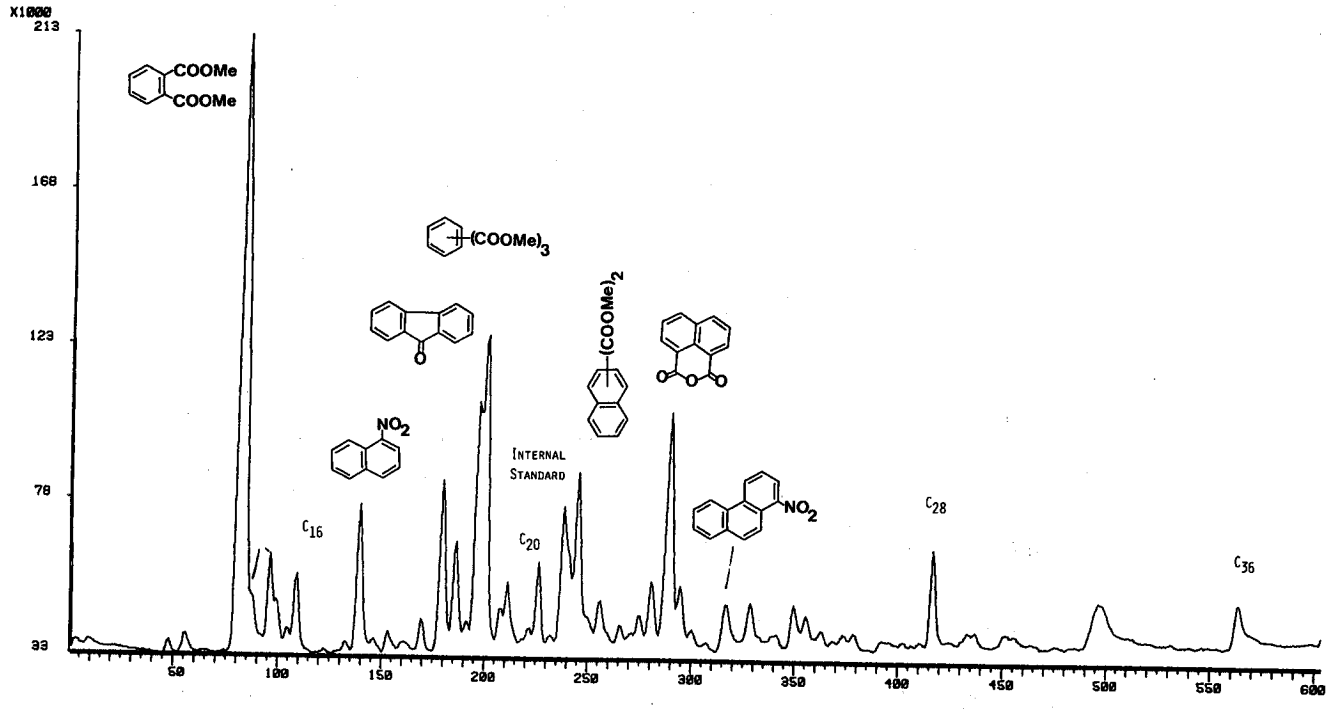

Fig. 5. Total ion current trace of the benzene/methanol extract of channel black 15.

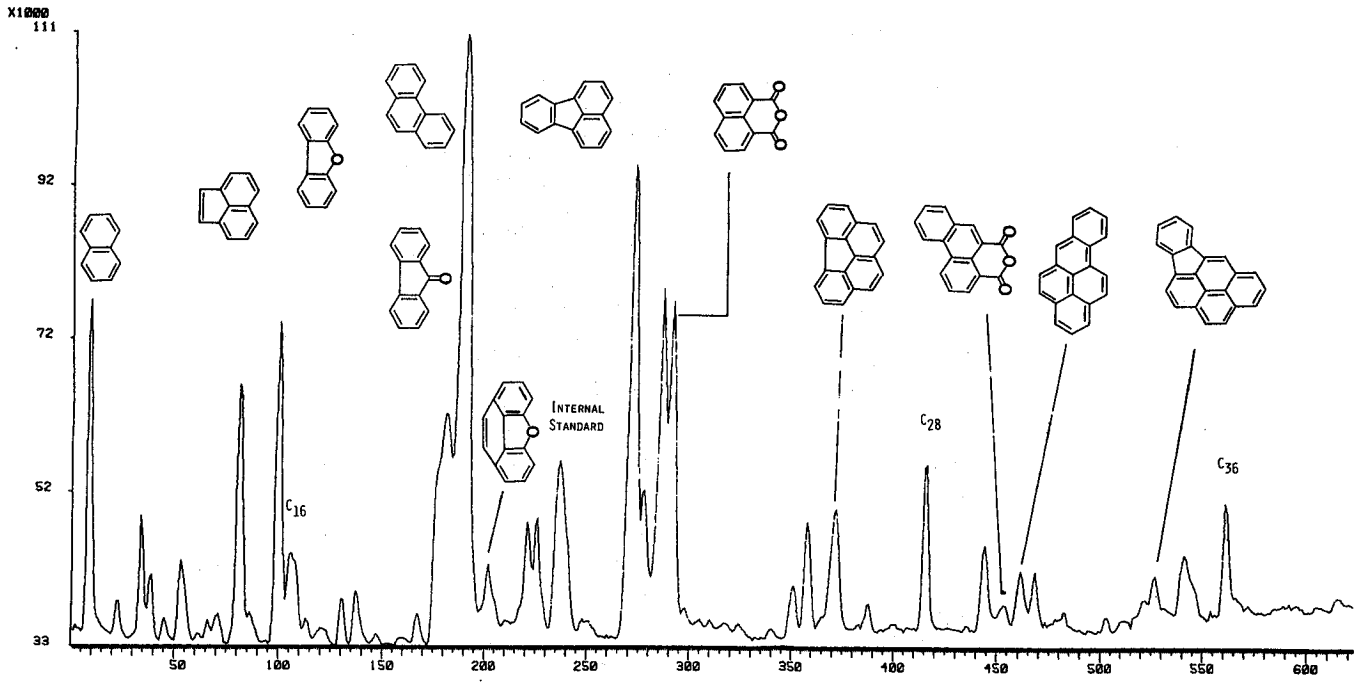

Fig. 6. Total ion current trace of the benzene/methanol extract of channel black 4.

Table 3. Quantitative Analysis of Carbon Black Samples, Concentration (ppm) of Most Abundant Member of Each Chemical Class.

Class	Lamp-black	Channel 4	Channel 12	Channel 13	Channel 15	Channel 19
PAH	Pyrene 302	Phen-anthrene 470	Phen-anthrene 12	Phen-anthrene 18	Phen-anthrene 32	Phen-anthrene 12
Heterocycles	Benzo[def] dibenzo-thiophene 70	Dibenzo-furan 190	-	-	Dibenzo-furan 11	-
NitroPAH	-	-	1-Nitro-naphtha-lene 15	A Nitro-phenan-threne 15	1-Nitro naphtha-lene 46	1-Nitro-naphtha-lene 24
OxyPAH	Benzo[def] pyrene-one 26	9-Fluoren-one 218	9-Fluoren-one 21	Anthra-quinone 23	9-Fluoren-one 53	Anthra-quinone 63
Anhydrides	-	Naphthalic 161	Naphthalic 62	Naphthalic 137	Naphthalic 79	Naphthalic 79
CarboxyPAH	-	-	Phthalic 90	Phthalic 306	Phthalic 302	Phthalic 668
Fatty acids	-	-	Palmitic 18	Palmitic 18	Palmitic 15	Palmitic 43

Table 4. Retention Indices of PAH and Derivatives.

R.I.	M.W.	Basis	Name
1208	128	a	Naphthalene
1283	129		Quinoline
1324	186		Decanoic acid methyl ester
1340	142		A Methylnaphthalene
1359	142		A Methylnaphthalene
1417	154		Biphenyl
1424	148	b	Phthalic anhydride
1439	200		Undecanoic acid methyl ester
1477	156	b	1,4-Naphthoquinone
1480	156		A C_2-Naphthalene
1481	202		Octanedioic acid dimethyl ester
1512	194		Dimethylphthalate
1516	152	a	Acenaphthalene
1529	181		Methylnitrobenzoate
1532	168		Methylbiphenyl
1542	214		Dodecanoic acid methyl ester
1555	181		Methylnitrobenzoate
1581	168	b	Dibenzofuran
1582	216		Nonanedioic acid dimethyl ester
1628	153	b	Cyclopentaquinoline
1645	228		Tridecanoic acid methyl ester
1657	166		Fluorene
1686	182	b	Xanthene isomer
1708	182		Xanthene isomer
1720	173	a	1-Nitronaphthalene
1725	170		1,8-Naphtholactone
1743	242		Myristic acid dimethyl ester
1746	193	b	3-Nitrophthalic anhydride
1765	173	a	2-Nitronaphthalene
1788	244		Undecanedioic acid
1846	184	b	Dibenzothiophene

1848	256		Pentadecanoic acid
1876	180	a	9-Fluorenone
1894	252		Benzene tricarboxylic acid trimethyl ester
1897	193	b	6-Nitrophthalic anhydride
1905	252		Benzene tricarboxylic acid trimethyl ester
1922	178	a	Phenanthrene
1928	178	a	Anthracene
1935	239		Nitrophthalic acid dimethyl ester
1946	270		Palmitic acid methyl ester
1951	192	b	Benzo(def)dibenzofuran
2020	198	b	A Naphthalenedicarboxylic anhydride
2035	192		Methylphenanthrene
2047	284		Heptadecanoic acid
2053	213	b	A Nitrodibenzofuran
2059	208	a	Anthraquinone
2071	244		Naphthalene dicarboxylic acid dimethyl ester
2078	218	b	A Dinitronaphthalene
2112	244		Naphthalene dicarboxylic acid dimethyl ester
2113	196	b	Xanthone
2140	213	b	A Nitrodibenzofuran
2143	218		A Dinitronaphthalene
2147	298		Stearic acid methyl ester
2184	225	b	A Nitrofluorenone
2193	297		Nitrobenzenetricarboxylic
2205	204	b	4-H-Cyclopenta[def]phenanthren-4-one
2207	218		A Dinitronaphthalene
2208	310		Benzene tetracarboxylic acid tetramethyl ester
2213	202	a	Fluoranthene
2232	310		Benzene tetracarboxylic acid tetramethyl ester
2239	218		A Naphthobenzofuran
2248	208		Benzo[def]dibenzothiophene
2261	198	a	Naphthalene-1,8-dicarboxylic anhydride
2263	202	a	Pyrene
2264	310		Benzene tetracarboxylic acid tetramethyl ester
2298	218		A Dinitronaphthalene
2357	243	b	A Nitronaphthalene dicarboxylic anhydride
2360	216	a	Benzo(a)fluorene
2376	232		Benzoxanthene
2386	223	b	A Nitrophenanthrene
2389	216		A Benzofluorene
2396	294		Phenanthrene dicarboxylic acid dimethyl ester
2405	208	a	9,10-Phenanthrenequinone
2430	254	a	1,1-Binaphthyl
2431	218		A Dinitronaphthalene
2433	216		A Benzofluorene
2542	243		A Nitronaphthalene dicarboxylic anhydride
2547	230		A Benzofluorenone
2562	236		A Phenanthrenediquinone
2563	226		Cyclopenta[cd]pyrene
2587	234		A Naphthobenzothiophene
2603	228	a	Benz(a)anthracene
2610	254	a	1,2'-Binaphthyl
2627	226		Benzofluoranthene
2678	242		A Naphtho[def]dibenzofuran
2698	230		A Benzofluorenone
2775	254	a	2,2'-Binaphthyl
2978	268	a	A Dinaphthofuran
2993	252		Benzo[j or k]fluoranthene
3036	243		A Phenanthrenedicarboxylic anhydride
3042	252	a	Benzo(a)pyrene
3051	258		A Naphtho[def]dibenzothiophene
3081	252	a	Perylene
3127	254		6-H-Benzo[cd]pyren-6-one
3312	256		A Pyrenequinone
3393	276		Indeno[1,2,3-cd]pyrene
3475	276		Benzo[ghi]perylene
3520	272		Pyrenedicarboxylic anhydride
3545	276	a	Anthanthrene
3950	300	a	Coronene

Basis: a - authentic sample; b - high resolution mass spectral data to support assignment.

ACKNOWLEDGMENT

This research was supported by a grant from the National Aeronautics and Space Administration, NGR-05-020-004.

References

1. K. K. Bertine and M. F. Mendeck, Environ. Sci. Technol., 12, 201 (1978).
2. D. M. Smith, J. J. Griffin and E. D. Goldberg, Anal. Chem., 47,233 (1975).
3. S. Chang, J. W. Smith, I. Kaplan, J. Lawless, K. A. Kvenvolden .and C. Ponnamperuma, "Proceedings of the Apollo 11 Lunar Science Conference", Vol. 2,p. 1857, 1970.
4. J. Lahaye and G. Prado, Amer. Chem. Soc. Symposium Series, 21, 333 (1976).
5. J. Abrahamson, Nature, 266, 323 (1977).
6. National Academy of Sciences, "Particulate Polycyclic Organic Matter", Washington D. C. ,1972.
7. D. H. Smith, M. Achenbach, W. J. Yeager, P. J. Anderson, W. L. Fitch and T. C. Rindfleisch, Anal. Chem., 49, 1623 (1977).
8. W. L. Fitch, E. T. Everhart and D. H. Smith, submitted to Anal. Chem.
9. R. G. Dromey, M. J. Stefik, T. C. Rindfleisch and A. M. Duffield, Anal. Chem., 48, 1368 (1976).
10. R. C. Lao, R. S. Thomas and J. L. Monkman, J. Chromatogr., 112, 681 (1975).
11. Eight Peak Index of Mass Spectra, Mass Spectrometry Data Centre, AWRE, Reading, RG74PR, UK, 1974.
12. S. P. Markey, W. G. Urban and S. P. Levine, Mass Spectra of Compounds of Biological Interest, U. S. Atomic Energy Comm. Rep. No. TID-26553, National Technical Information Service, U. S. Dept. of Commerce, Springfield, Va. 22161.
13. A. Gold, Anal. Chem., 47, 1469 (1975).
14. H. Budzikiewicz, C. Djerassi and D. H. Williams, Mass Spectrometry of Organic Compounds, Holden-Day, San Francisco, 1967.
15. R. H. Shapiro and J. W. Serum, Org. Mass Spectrom., 2, 533 (1969).
16. A. K. Holliday, G. Hughes and S. M. Walker, The Chemistry of Carbon, Pergamon Press, New York, 1973.
17. Chemical and Engineering News, April 3, 1978, p. 10.
18. V. A. Garten and D. E. Weiss, Rev. Pure Applied Chem., 7, 69 (1957).
19. J. W. Hassler, Purification With Activated Carbon, Chemical Publishing Co., New
20. C. Ishizaki and J. T. Cookson, J. Water Pollution Contr. Fed., 45,, 515 (1973).
21. V. J. Borneff and R. Fischer, Arch. Fur ʰygiene, 145, 334 (1961).
22. D. F. Bishop, L. S. Marshall, T. P. O'Farrell, R. B. Dean, B.O'Conner, R. A. Dobbs, S. H. Griggs and R. V. Villiers, J. Water Pollution Contr. Fed., 39, 188 (1967).
23. C. A. Mantell, Carbon and Graphite Handbook, Interscience, New York, 1968.
24. L. L. Ban and W. M. Hess, Amer. Chem. Soc. Symposium Series, 21, 358 (1976).
25. H. L. Falk and P. E. Steiner, Cancer Res., 12, 30 (1952).
26. M. L. Lee and R. A. Hites, Anal. Chem., 48, 1890 (1976).
27. A. H. Qazi and C. A. Nau, Amer. Ind. Hyg. Assoc. J., 36, 187 (1975).
28. L. Wallcave, D. L. Nagel, J. W. Smith and R. D. Waniska, Environ. Sci. Technol., 9, 143 (1975).
29. P. E. Steiner, Cancer Res., 14, 103 (1954).
30. J. Neal, N. Thornton and C. A. Nau, Arch. Environ. Health, 4, 46 (1962).
31. H. L. Falk and P. E. Steiner, Cancer Res., 12, 40 (1952).
32. R. C. Pierce and M. Katz, Environ. Sci. Technol., 9, 347 (1975).
33. R. C. Pierce and M. Katz, Environ. Sci. Technol., 10, 45 (1976).
34. J. N. Pitts, K. A. Van Cavwenberghel D. Grosjean, J. P. Schmid and D. R. Fitz, Paper presented at the Conference on Carbonaceous particles in the Atmosphere, Berkeley (March, 1978), Chapter 26, this volume.
35. Food and Drug Administration, Color Additives, Federal Register, 41, 41852 (Sept. 23, 1976).

CYANO-ARENES PRODUCED BY THE COMBUSTION OF NITROGEN CONTAINING FUELS

George R. Dubay and Ronald A. Hites*
Department of Chemical Engineering
Massachusetts Institute of Technology
Cambridge, Mass. 02139

ABSTRACT

Cyanonaphthalenes (both isomers) and cyanoacenaphthylenes (four isomers) have been identified in the soot generated by the combustion of aromatic hydrocarbon fuels doped with 6-30% pyridine. These are by far the most abundant nitrogen containing organic compounds in this combustion effluent; multi-ring, nitrogen heterocyclic compounds, such as those commonly observed in airborne particulate matter, are a minor component. These identifications have been made by gas chromatographic mass spectrometry following a preliminary separation by alumina column chromatography. The environmental significance of these findings is discussed.

INTRODUCTION

Certain organic compounds in soot cause cancer in man[1]. Determining the structures of these compounds and understanding their biological activities have been the subjects of intense research over the last 50 years[2], and it is now known that the major class of carcinogenic compounds associated with soot are the polycyclic aromatic hydrocarbons (PAH)[3]. Nitrogen containing aromatic compounds (aza-arenes) are also associated with soot[4] and some are known to be carcinogenic[5]; but, because they are much less abundant than PAH, these compounds have received proportionately less attention. In the future, however, it is likely that the environmental abundance of aza-arenes will increase as fuels higher in organic nitrogen content are burned. We have, therefore, undertaken the identification of the major aza-arenes produced by the combustion of a model fuel containing 1-6% nitrogen.

Several researchers have developed methods for the analysis of aza-arenes in atmospheric particulate samples based on thin-layer, gas, paper, high pressure liquid, and column chromatography and on electrophoresis[6,10]. All of these techniques begin with a solvent-solvent extraction utilizing strong acid to partition the basic aza-arenes away from the PAH. This procedure obviously discriminates against neutral aza-arenes which might be present. To avoid this problem, we have separated the aza-arenes from the bulk of the PAH by alumina chromatography using gradient elution.

Once the compounds are separated from the PAH, the identification of the exact molecular structures of aza-arenes is still very difficult. Almost all assignments made in the literature are, to some degree, ambiguous. Assignments have been based on gas chromatographic retention information and on fluorescence, UV, or electron impact mass spectra[6,10]. In these analyses, all the possible isomers of a particular molecular structure have not been available; and, using these techniques, there is no criterion by which the unavailable isomers can be ruled out.

To address the problem of determining the precise molecular structure of compounds produced by combustion, we have developed a method based on charge exchange-chemical ionization mass spectrometry (CE/CIMS). We have established that isomeric PAH and aza-arenes have characteristic mass spectra when 5 or 10% methane in argon is employed as the reagent gas for CE/CIMS[11,12]. The two most prominent ions in the reacting plasma are $C_2H_5^+$ and Ar^+. A molecule reacts either with a strongly acidic $C_2H_5^+$ ion to give the protonated molecular ion (M+1), or it reacts with an Ar^+ ion to give the molecular ion (M); the relative rates of these two reactions determine the intensity ratio of the two ions. A high, positive correlation was found between ionization potential and M+1/M ratio[11]. We have also established that this relationship holds for some aza-arenes and for some methylated PAH[12]. Aza-arenes which have ionization potentials differing by more than 0.1 ev can be distinguished using this method.

The great potential of this technique lies in its predictive ability. The relationship between ionization potentials and M+1/M intensity ratios can be established for all available isomers. Calculation of ionization potentials from molecular orbital theory will then allow prediction of the M+1/M ratio for unavailable isomers.

EXPERIMENTAL

Combustion Conditions

Soot was obtained in two ways: 1. A solution of 32% pyridine in o-xylene (6% fuel nitrogen) was burned in a wick-fed, alcohol-lamp burner. Soot was collected on the exterior of a pre-cleaned, water-cooled, filter flask. The soot was removed by scrubbing the flask with CH_2Cl_2-soaked glass wool. The soot, glass wool, and associated CH_2Cl_2 were put in a pre-cleaned Soxhlet thimble and extracted with 200 ml CH_2Cl_2 overnight. The extract volume was reduced to 1 ml

on a rotary evaporator operating at 30° C and 15 torr. Samples were stored in the dark at 6° C.

2. A Meker burner was modified by replacing the air inlets with oxygen feeds; the fuel inlet was attached to a stainless steel tube through which a benzene/methane mixture was passed. The fuel mixture was preheated to vaporize the benzene, and the plumbing was heated (300°C) to prevent condensation. Methane and O_2 flows were maintained by critical orifices, and the benzene flow was measured before vaporization by passing the liquid through a capillary tube in which the upstream and downstream pressures were carefully measured. The liquid flows corresponded to Reynold's numbers of 800-1000 through the capillary tube; thus, the flow was always laminar and proportional to the pressure drop throught the tube. The benzene was doped with sufficient pyridine (5.3%) to give a fuel containing 1% nitrogen. Fuel equivalence ratios of 4.0 and 4.5 were used, the CH_4/C_6H_6 ratio was 1.5, and the cold gas velocity was 31.8 cm/sec. Soot was collected by a water-cooled spray probe[13] and was trapped in glass wool packed filters. The organic compounds were extracted first with acetone and then with CH_2Cl_2.

Column Chromatography

In order to eliminate interferences caused by PAH and to obtain an enrichment of the nitrogen compounds, the soot extracts were fractionated as follows: The sample (1 ml) was added to 1 g of neutral alumina (activity grade 1, ICN Pharmaceuticals) in a 25 ml beaker, and the CH_2Cl_2 was allowed to evaporate at room temperature (15 min.). This pre-coated alumina was added to the top of a column prepared from 5 g of alumina with hexane as the solvent. Six fractions were then eluted (see Table I). These fractions were then concentrated to the necessary degree on a rotary evaporator for analysis.

Instrumentation

A Hewlett-Packard 5730A gas chromatograph equipped with dual nitrogen-phosphorous flame ionization detectors (FID) was used for GC analyses. A Hewlett-Packard 5982A mass spectrometer interfaced to a 5933A data system was utilized for gas chromatographic mass spectrometry. Charge exchange-chemical ionization mass spectrometry was performed with 5% methane in argon (supplied by Matheson Gas Products). The flow of carrier gas was 10 ml/min. and the ion source temperature was 195° ± 2° C. The ratios of the protonated molecular ion to the molecular ion were established by adding all spectra scanned within a given GC peak.

RESULTS AND DISCUSSION

The two different combustion systems gave virtually identical results; therefore, they will not be distinguished in the following discussion. As indicated in Table I, all of the aza-arenes were collected in fractions 3 and 4. The gas chromatogram of fraction 4 was extremely complex. Because this fraction contained less than a third of the aza-arenes and because the identities of most of the components in this fraction corresponded to those reported elsewhere[10], further analyses of this fraction have not been pursued.

Fraction 3 contained most of the aza-arenes, and gas chromatograms of this fraction are shown in Figure 1. The upper trace was obtained with a normal FID and the lower with a nitrogen specific FID. Comparison of these two traces show that the nitrogen-FID and the normal FID respond equally to the early eluting peaks, indicating that nitrogen is present in all of these constituents. The later eluting peaks were detected only by the normal FID, indicating that they are probably PAH.

The electron impact and CE/CI mass spectra of peaks 1 to 7 are given in Table II. The spectra of peak 1 were interpreted as those of either 1- or 2-cyanonaphthalene, and authentic samples of these two compounds were obtained (K and K Laboratories). The exact retention time (by co-injection) and the electron impact and CE/CI mass spectra of 1-cyanonaphthalene were identical with those of peak 1. The identification of peak 2 as 2-cyanonaphthalene was proven in a similar fashion.

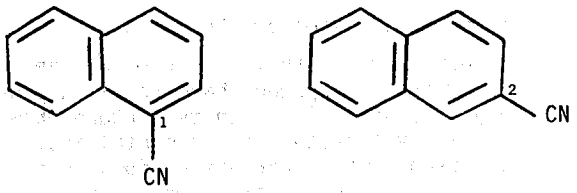

Peaks 3-6 all show molecular weights of 177 ($C_{13}H_7N$) (see Table II). Based on analogy and on the abundant presence of a parent hydrocarbon, these peaks have been tentatively identified as the four isomers of cyanoacenaphthylene.

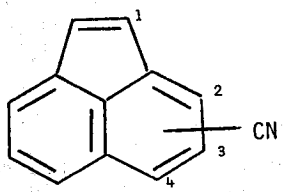

These are not known compounds and proof of their structure must await their systhesis. Peak 7 has a molecular weight of 203 ($C_{15}H_9N$) and probably represents several unresolved cyanophenanthrene isomers.

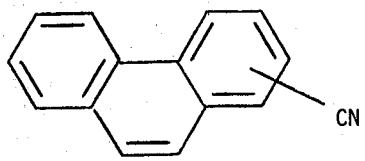

Based on the GC data, we estimate that 80% of the aza-arenes in fraction 3 are cyanonaphthalenes, cyanoacenaphthylenes, and cyanophenanthrenes; these compounds are the most abundant

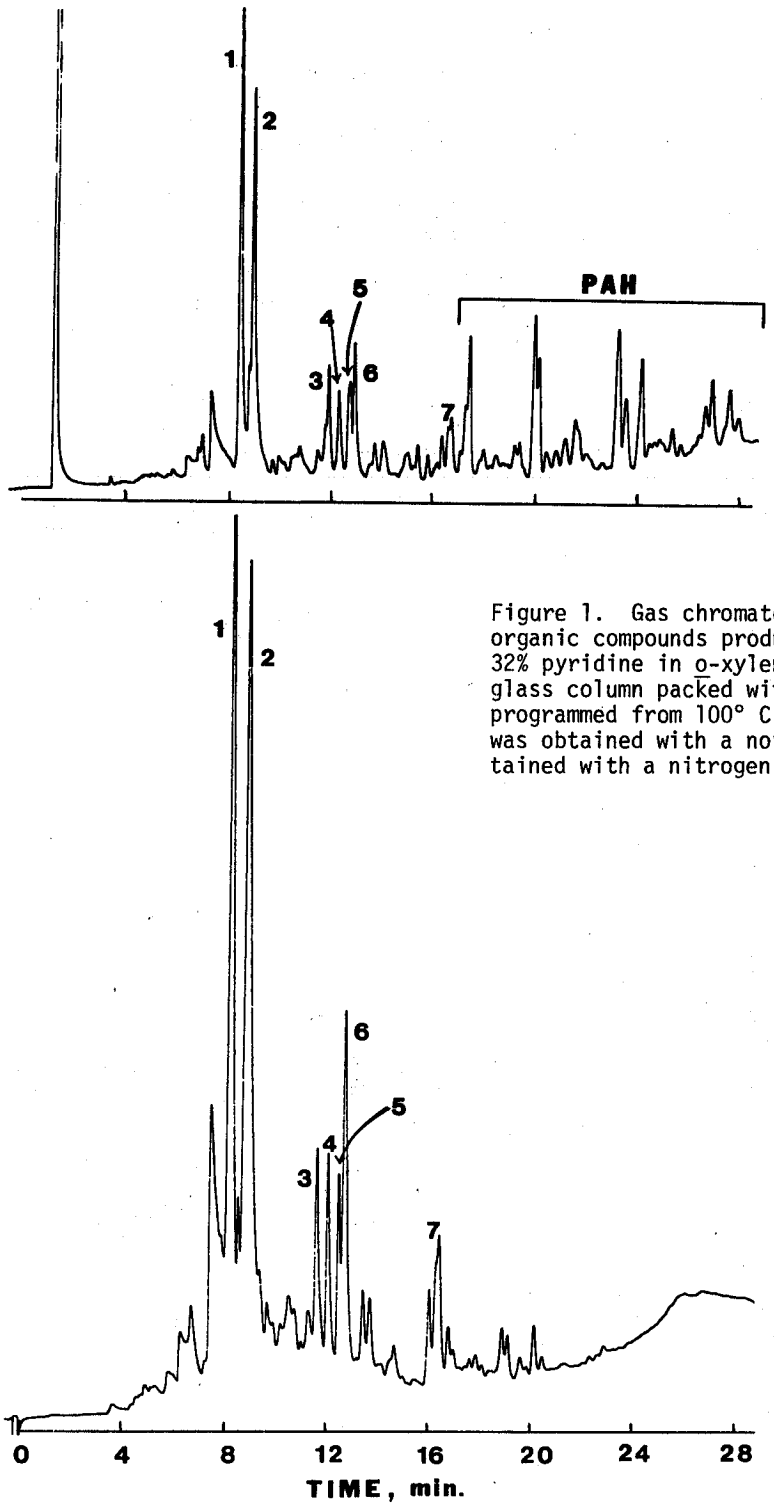

Figure 1. Gas chromatograms of fraction 3, isolated from the organic compounds produced by the combustion of a solution of 32% pyridine in o-xylene. GC conditions: 1.8 m X 6.3 mm O.D. glass column packed with 3% OV-17 on 80/100 mesh Supelcoport, programmed from 100° C to 310° C at 8° C/min. The upper trace was obtained with a normal FID and the bottom trace was obtained with a nitrogen specific FID.

class or organic nitrogen compounds in the effluent from these flames. Multi-ring, nitrogen heterocyclic compounds (such as acridine or phenanthridine) which have been commonly observed in airborne particulate matter[10] are a minor component (<7%) in these effluents.

Cyanonaphthalenes have not been found in combustion effluents before. They have, however, been found at trace levels in cigarette smoke tar[14,15], in petroleum[16], in tar from the low-temperature pyrolysis of coal[17], and in anthracene oil[18]. In all of these cases, it is presumed that cyanonaphthalenes are formed from the pyrolysis of other nitrogen compounds[19]. The biological activity of these compounds is not clear. There have been reports that cyanonaphthalenes cause irregular mitoses and chromosomal aberrations[14,20], that they have insecticidal properties[21,22], and that they are toxic to the eggs of body lice[23]. On the other hand, testing by a quantitative forward mutation assay using 8-azaguanine resistance in Salmonella typhimurium[24] indicates that these compounds have less than 1% of the activity of benzo[a]pyrene on a molar basis[25].

The environmental significance of our results is two fold. (a) The relative amount of cyano-arenes being produced by the combustion of a nitrogen containing fuel is significant (see Table I), and some of these compounds may be biologically active. Emission of large amounts of such compounds into the environment would seem to be undesirable. (b) Although several cyano-arenes are being produced in flames, it is not known if they are environmentally persistant. Nitrogen functional group analysis by ESCA have indicated the presence of the cyano functionality in certain urban air particulate samples[26], but specific cyano-arenes have not been found in the atmospheric environment. Cyano-arenes may well be present in air particulates but, because of the analytical limitations outlined above, they have not yet been detected. We suggest that the quantity (if any) of cyano-arenes in the ambient air environment should be measured using techniques designed for these compounds. Cyano-arenes may be more prevelant than the multi-ring, nitrogen heterocyclic compounds studied in the past, and their environmental chemistry and toxicity may warrent at least equal attention.

ACKNOWLEDGEMENT

The authors thank Jack B. Howard and William J. Kausch, Jr. for the design and operation of the second burner system. This work was supported by the Environmental Protection Agency (Grant R803242) and the Department of Energy (Grant EE-77-5-02-4267).

REFERENCES AND FOOTNOTES

* To whom correspondence should be addressed.

1. P. Plott, Chirugical Observations, Hawkes, Clarke, and Collins, London (1775) p.63.

2. National Academy of Sciences, Particulate Polycyclic Organic Matter, Washington, D.C. (1972).

3. D. Hoffmann, and E.L. Wynder, in Chemical Carcinogens, C.E. Searl, ed., Amer. Chem. Soc. Monograph 173, Washington, D.C. (1976) pp. 324-365.

4. E. Sawicki, S.P. McPherson, T.M. Stanley, J. Meeker, and W.C. Elbert, Int. J. Air Water Pollut. 9, 515 (1965).

5. A. Dipple, in Chemical Carcinogens, C.E. Searl, ed., Amer. Chem. Soc. Monograph 173, Washington, D.C. (1976) pp. 245-314.

6. E. Sawicki, T.W. Stanley, S. McPherson and M. Morgan, Talanta 13, 619 (1966).

7. E. Sawicki, M. Guyer, and C.R. Engel, J. Chromatog. 30, 522 (1967).

8. C.R. Engel, and E. Sawicki, J. Chromatog. 31, 109 (1967).

9. W. Cautrells, and K. van Cauwenberghe, Atmos. Environ. 10, 447 (1976).

10. M.W. Dong, D.C. Locke, and D. Hoffmann, Env. Sci. Tech. 11, 612 (1977).

11. M.L. Lee and R.A. Hites, J. Amer. Chem. Soc. 99, 2008 (1977).

12. R.A. Hites, and G.R. Dubay, in Carcinogenesis, Vol III, P.W. Jones ed., Raven Press, New York, (1978), pp. 85-87.

13. G.P. Prado, M.L. Lee, R.A. Hites, D.P. Hoult, and J.B. Howard, Sixteenth (International) Symposium on Combustion, The Combustion Institute, Pittsburg, PA (1977) pp. 649-661.

14. C. Izard and P. Moree-Testa, C.R. Acad. Sci. Ser. D 272, 2581 (1971); Chem. Abst. 75, 61573j.

15. J. Benner, C.K. Keene, and T.W. Holt, in 4th Tobacco and Health Workshop Conf. Proceedings, Univ. Kentucky, Lexington, KY (1973) pp. 408-420; Chem. Abst. 79, 89669b.

16. G.K. Hartung, and D.M. Jewell, Anal. Chem. Acta 27, 219 (1962).

17. V.J. Andre, P. Dath, J. Mahieu, and E.H. Grand'Ry, Brennstoff Chemie 48, 369 (1967); Chem. Abst. 68, 31869y.

18. E. Proksch, Oesten. Chem. Ztg. 67, 105 (1966); Chem. Abst. 64, 19251g.

19. J.M. Patterson, N.F. Naidar, and W.T. Smith, Jr., Chem. Ind. (London) 1975, 128 (1975).

20. P.R. Bhalla, R.C. Arnold and P.S. Sabharwal, J. Hered. 65, 311 (1974).

21. M.C. Swingle, E.L. Mayer, and J.B. Gahan, J. Econ. Entomol. 37, 672 (1944); Chem. Abst. 39, 764(6).

22. E.L. Mayer, C. Robertson, R.H. Nelson and C.F. Woodward, Bur. Etomol. Plant Quarantine, E-836 (1952); Chem. Abst. 46, 5251a.

23. G.W. Eddy and N.B. Carson, J. Econ. Entomol. 41 31 (1948); Chem. Abst. 42, 5156g.

24. T.R. Skopek, H.L. Liber, J.J. Krolewski, and W.G. Thilly, Proc. Nat. Acad. Sci., 75, 410 (1978).

25. D.A. Kaden and W.G. Thilly, Massachusetts Institute of Technology, (1977), provate communication.

26. S.G. Chang and T. Novakov, Atmos. Environ. 9, 495 (1975).

Table I

Fractionation of the Soot Extracts

Fraction	Solvent	Volume (ml)	%PAH*	%Aza-arene*
1	hexane	30	0	0
2	30% benzene, 70% hexane	30	64	0
3	70% benzene, 30% hexane	30	12	15
4	benzene	30	2	7
5	benzene	50	0	0
6	CH_2Cl_2	50	0	0
		TOTAL	78	22

*Percent of total material in the various fractions as measured from the normal FID or nitrogen-specific FID responses, respectively.

Table II

Mass Spectra of Peaks 1 to 7 in the

EI (top) and CE/CI (bottom) Modes

	PEAK 1		2		3		4		5		6		7	
	m/e	int	m/e	int	m/e	int	m/e	int	m/e	int	m/e	int	m/e	int
M + 1	154	13	154	13	178	15	178	16	178	18	178	19	204	22
M	153	100	153	100	177	100	177	100	177	100	177	100	203	100
M - H	152	7	152	8	176	15	176	8	176	11	176	11	202	13
M - CN	127	5	127	5	151	9	151	6	151	4	151	4	177	6
M - HCN	126	17	126	15	150	18	150	15	150	13	150	18	176	10
Others	125	4	125	3	179	5	179	7	179	4	179	4	201	13
					175	6	175	4	175	7	175	6	175	7
					149	4	149	6	149	7	149	3	151	6
M	153	38	153	40	177	41	177	45	177	38	177	42	203	46
M + H	154	100	154	100	178	100	178	100	178	100	178	100	204	100
M + 2	155	15	155	14	179	25	179	18	179	17	179	16	205	17
M + CH_3	168	9	168	9	192	6	192	8	192	13	192	16	218	11
M + C_2H_5	182	35	182	37	206	34	206	40	206	45	206	44	232	41
M + 30	183	6	183	5	207	14	207	8	207	11	207	11	233	9
Others	156	6	156	3	180	14	180	9	180	10	180	8	206	10
					208	6	208	6	208	3	208	5	234	5
M + 1/M*	2.63		2.37		2.33		2.10		2.49		2.27		2.01	

*corrected for ^{13}C.

CONTRIBUTION OF HIGH-RESOLUTION MASS SPECTROMETRY TO SPECIATION OF PARTICULATE CARBON

Dagmar Rais Cronn
Washington State University
Pullman, WA 99164

ABSTRACT

The analytical technique to be discussed was developed as a result of interest in the molecular nature of atmospheric aerosols. Particular attention has been given to the organic material present in photochemical smog in field studies in St. Louis and Los Angeles. Quantitative molecular information is obtained by computer-controlled, high-resolution, mass spectrometric thermal analysis (HRMSTA). A descriptive explanation of the technique is given. Examples which demonstrate the utility of the method as well as the unique information available from the method are presented.

INTRODUCTION

The first paper to appear on the application of computer-controlled, high-resolution, mass spectrometry (CCHRMS) to air pollution analysis, as developed at the University of Washington, appeared in 1973[1]. The analytical technique has not yet been utilized by others for analysis of air pollutants despite the unique capabilities of the method. This is presumable due to the expense of acquiring and operating a high resolution mass spectrometer. Quantitative molecular information about atmospheric aerosols is obtained using techniques designed to minimize sample handling. The sensitivity is sufficient to report results for real samples of urban smog aerosol in addition to studies of simulated atmospheres in smog chambers. The technique is especially important due to attainment of molecular identification as opposed to the ionic information available from more traditional wet chemical analyses or elemental information from such methods as X-ray fluorescence or neutron activation. Furthermore, this method provides qualitative identification of specific organic components as well as several inorganic compounds rather than such information as total organics identified as benzene soluble material. And, as mentioned, the information available from this MS technique is quantitative, providing concentrations of components in micrograms per cubic meter.

The CCHRMS method also has one distinct advantage over gas chromatography mass spectrometry (GCMS). The method does not require the solvent extraction and concentration steps necessary for GCMS analysis. The filter punches or impaction plates are inserted directly into the mass spectrometer by a probe specially designed to temperature program the sample after insertion into the instrument. Thus, the individual compounds in the aerosol sample are thermally desorbed into the source region of the mass spectrometer according to their vapor pressures. Further separation of the multicomponent mixture can then be achieved due to the high resolution capability of the instrument. Most GCMS equipment only provides so-called unit mass resolution so that mass fragments of a single nominal mass cannot be resolved from each other as in high resolution instruments.

Two additional papers have been published describing the results of the application of this analysis method to urban smog aerosols.[2,3] The first of these papers reports the initial identification in ambient urban particulate matter of a number of different highly oxidized secondary organic aerosol components. The second paper delineates the diurnal pattern of various organic aerosol components with sampling periods as short as two hours and shows that the temporal behavior of presumed primary organic constituents differs from that of the secondary organic components. Additional details about the aerosol analysis technique used at the University of Washington can be found in the dissertations which have resulted from the program [4,5,6] and the final report to the Environmental Protection Agency.[7]

EXPERIMENTAL

Since atmospheric aerosol size distributions at the earth's surface are bimodal, the sampling apparati used for sample collection for CCHRMS analysis separate the particles into two fractions. Early work showed that most of the organic aerosol pollutants exist in the so-called accumulation mode between 0.1 and 1-2 microns. In one sampling system, the coarse particles above 1-2 microns are collected by impaction before the accumulation mode is collected on a glass fiber filter. In the other sample collection device, respirable particles are collected with a high volume sampler equipped with a cyclone to remove particles above 3.5 microns.

The sample analysis scheme is shown in Fig. 1. Filters are baked at 500°C for 24 h to remove organic impurities before sampling. After the samples have been collected, 7 mm discs are punched from the filters and both filter and impaction samples are transported and stored until analysis at dry ice temperatures to minimize sample reactions or loss due to volatilization.

After a sample is inserted into the source region of the mass spectrometer using the temperature programmable probe, the aerosol constituents

SAMPLE ANALYSIS SCHEME

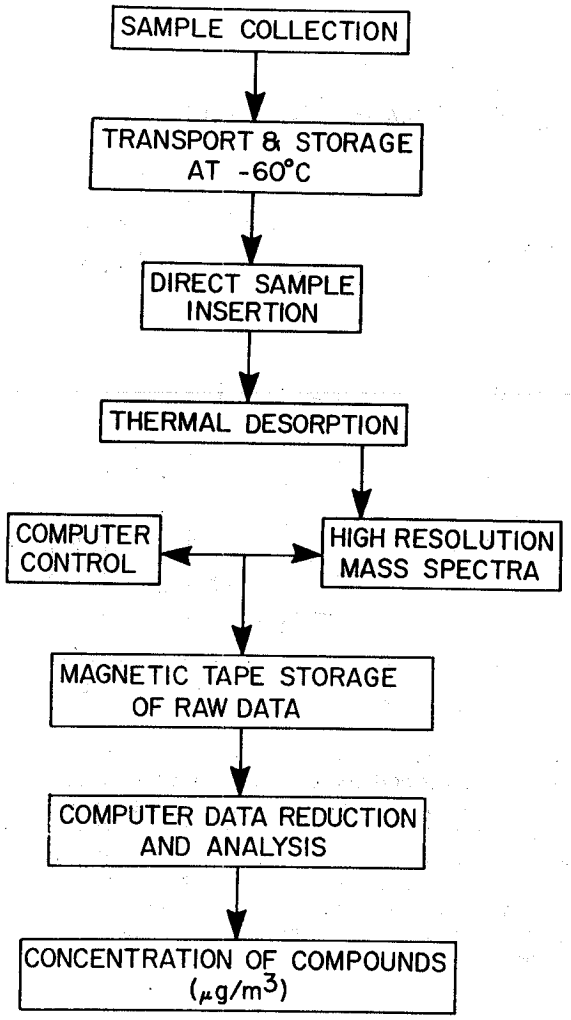

Fig. 1. Flow diagram of the sample analysis scheme used for CCHRMS analysis.

are thermally desorbed by heating from room temperature to about 380°C. The probe is maintained isothermally until data acquisition is complete.

As the aerosol is being vaporized, mass spectral scans are acquired by the computer and the raw mass spectral data is stored on magnetic tape. Subsequent computer data reduction and analysis is required before the final output in the form of concentrations of various aerosol constituents in micrograms per cubic meter is obtained. After acquisition and storage of mass spectral scans, the computer is used to calculate peak centroid times and heights. Then the mass of every fragment in every mass scan of a sample is calculated by interpolation from a few known mass fragments. The calculated masses are then compared to a mass file which contains mass and elemental composition of the fragments so far identified in air particulate matter samples. The computer than compiles for each mass in the mass file the intensity or peak height as a function of time and hence temperature. This time-height compilation for each mass is referred to as a mass thermogram. An example of a mass thermogram for the NO_2^+ peak is shown in Fig. 2. The area under the curve within the appropriate temperature limits is proportional to the amount of some compound in the sample. In this case, the mass thermogram can give the amounts of both NH_4NO_3 and $NaNO_3$ since the two compounds vaporize into the MS at different temperatures (or times).

Compound files stored on magnetic tape contain the parameters for calculation of concentrations of aerosol components. The computer calculates the area under the mass thermogram of the identifying mass fragments. Figure 3 shows the subsequent calculation for concentrations of the various components in the sample. About 80 components are routinely identified in urban aerosol samples.

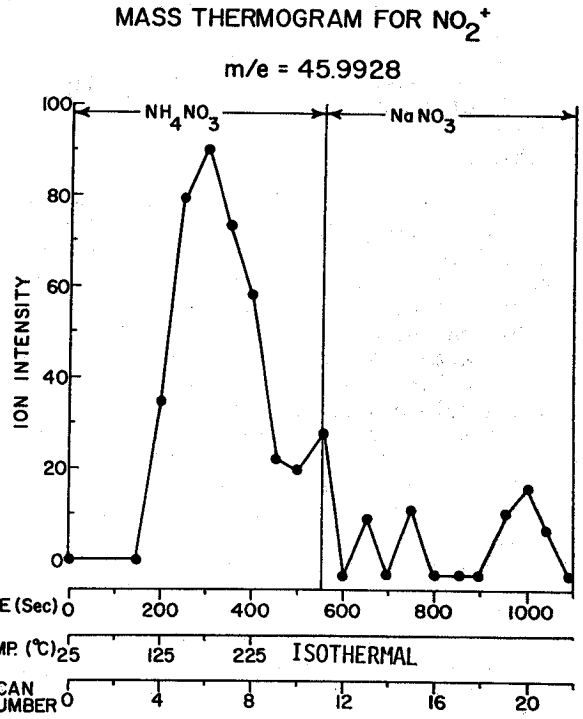

Fig. 2. An example of a mass thermogram for the mass fragment NO_2^+. The integrated area under the curve within the appropriate temperature limits is related to the concentration of the sample components NH_4NO_3 and $NaNO_3$.

$$\text{CONCENTRATION } (\mu g/m^3) = \frac{A_x}{A_s} \cdot \frac{X}{R \cdot A \cdot M}$$

A_x = AREA OF MASS THERMOGRAM FOR IDENTIFYING MASS

A_s = AREA OF MASS THERMOGRAM OF INTERNAL STANDARD

X = MICROGRAMS OF STANDARD ADDED TO SAMPLE

R = RESPONSE FACTOR

A = ALIQUOT OF SAMPLE

M = CUBIC METERS OF AIR SAMPLED

Fig. 3. The quantity of a given material present can be calculated by this formula.

DISCUSSION

Qualitative identification of compounds by mass spectral analysis is complicated by the fact that it is difficult to distinquish between various isomers which may have the same elemental composition. Therefore, attributing a particular identifying mass fragment to a particular compound is not an infallible process.

Quantitatively, the largest source of error for a compound is likely to be the response factor used for the calculation. Some response factors have been empirically determined in the lab, which lowers this source of error for those compounds for which this has been done. Other response factors have been taken from the literature or guessed at based on similarities to other compounds. Because of this, absolute accuracy may be no better than about a factor of two or three. But the relative precision of the method is much better--say 20% on a relative comparison basis between samples. Therefore, although there may be an absolute bias in the concentrations of a particular compound, the relative comparison between samples is meaningful.

The general accuracy of the method for the more abundant components is fairly good, as seen in Fig. 4 by comparing the summation of only organic material identified by mass spectrometry and the total noncarbonate carbon in each sample as analyzed on a total carbon analyzer by the California Air and Industrial Hygiene Laboratory (AIHL). The mass spectrometer data would be expected to be a little higher to account for the weight of the elements other than carbon in the organic material. An average of 23% of the total mass loading is identified as organic material for this one day in the Los Angeles area. Figure 4 also shows what portion of the total respirable mass loading ($\geq$ 3.5 μm) was identified by CCHRMS. The total mass loading of the atmosphere in $\mu g/m^3$ is shown as a function of time of day. The total mass increased from overnight low values to a maximum in the late afternoon and then decreased again during the evening. Also shown in Fig. 4 is the total mass

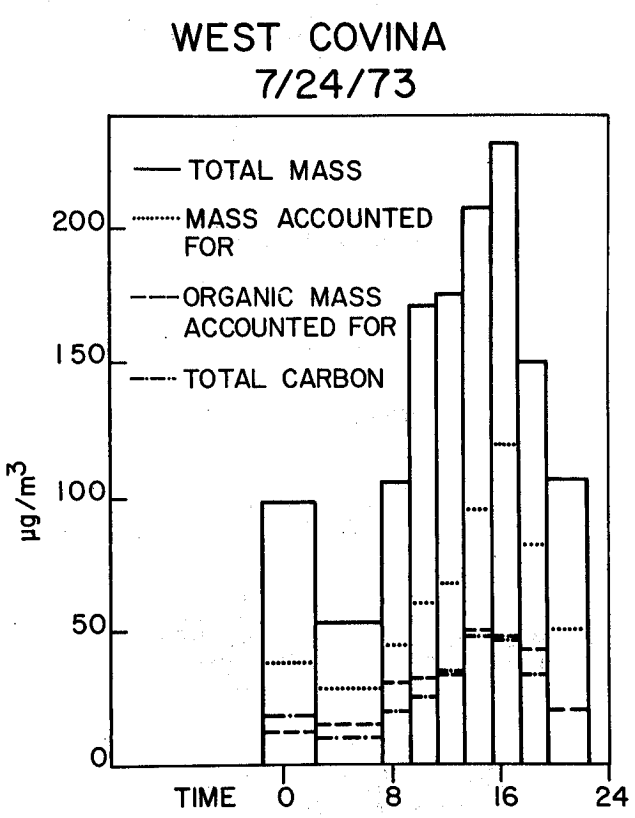

Fig. 4. Visual presentation of the diurnal variation of suspended particulate matter ≤ 3.5 microns (_), the mass of organic plus inorganic components accounted for in these samples by CCHRMS (·····), the organic mass accounted for by CCHRMS (----) which can be compared with the total carbon defined as the sum of volatile carbon determined by a Dupont Thermal Evolution Analyzer and non-volatile carbon (-·-·-).

accounted for in each sample by the mass spectrometric analysis. This figure was obtained by summing the concentration of each component identified in the sample, both organic and inorganic. An average of 45% of the total mass of each sample was accounted for by this technique. The comparison would be even more favorable if the inorganic nitrate compounds' response factors had been adjusted to agree with the total nitrate determined by wet chemical methods. The sulfate concentration of samples from the West Covina site and the Washington University site in St. Louis are shown in Fig. 5. The West Covina samples were analyzed by a classical wet chemical method by AIHL as well as by CCHRMS. The correlation coefficient for the nine samples is 0.96. The Washington University samples were analyzed by three means: (1)CCHRMS, (2) a fast cyclic scanning MS method developed by Rich Knights at the University of Washington, and (3) a flame photometric method developed by Paul Roberts at the California Institute of Technology. Again, the accuracy of the CCHRMS method is good.

Note that $SO_4^=$ dominates the submicrometer aerosol

SULFATE COMPARISONS

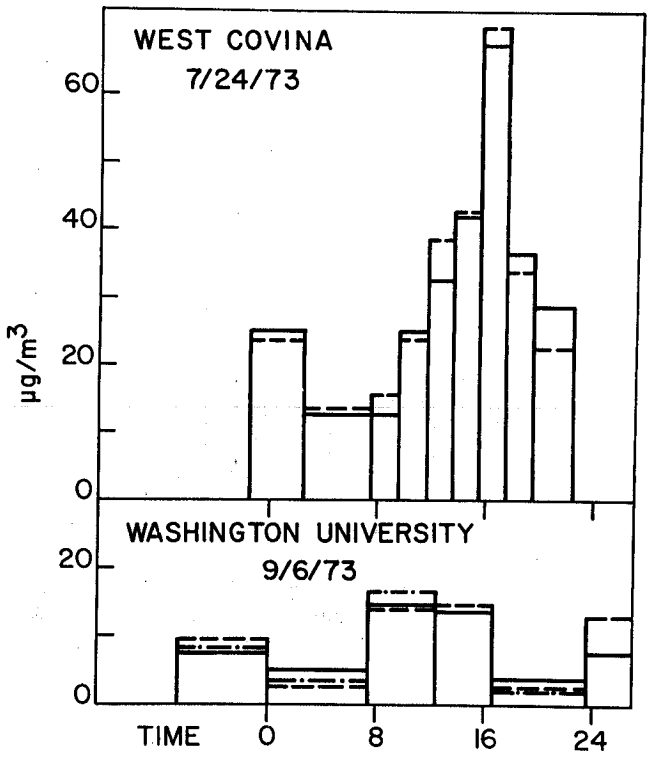

Fig. 5. Visual comparison of the temporal changes in sulfate concentration determined by four separate analysis techniques: ____ = CCHRMS; for Washington University, ---- = a computer controlled fast cyclic scan mass spectrometric thermal analysis technique developed specifically for inorganic air pollutants by R. L. Knights; for West Covina, ---- = wet chemical analysis by AIHL; -·-·- = flash varporization followed by flame photometric detection, a technique developed by P. Roberts at the California Institute of Technology.

at both sites. The largest single component in each sample is sulfate. Sulfate averaged roughly 20% of the total aerosol at West Covina on July 24, 1973.

The CCHRMS method has provided several instances of unique information about atmospheric aerosols which would not have been available by any other means. Several groups of organic compounds have been identified for the first time in airborne particulate matter. These include presumed photo-oxidation products of cycloalkenes and/or diolefins, toluene and plant emissions (especially alpha pinene). Differences in the temporal behavior of individual primary and secondary aerosol constituents have been followed and explained based on the meteorological conditions and the different sources (sources of precursors for secondary constituents).

Samples were collected in St. Louis in conjunction with intensive sampling by other research groups under an EPA grant. Other samples were collected in the Los Angeles area as part of the California Air Characterization Experiment (ACHEX) in cooperation with the Air and Industrial Hygiene Lab of the California Department of Public Health.

The site monitored in the Los Angeles area was in West Covina about 30 km east of downtown Los Angeles. Three sites were monitored in the St. Louis area: One was on a soccer field on the Washington University campus in a residential area about 12 km west of the Arch. Another was on the roof of the Holiday Inn, much closer to the congested central city and nearby industry. Tyson Hollow was a more rural location about 35 km west-southwest of the Arch. Samples providing 4-h and 2-h time resolution were obtained at St. Louis and West Covina, respectively, in 1973.

Several observations could be made about comparison between the two urban sites. First, the chemical species at both cities were much the same. Second, the amounts of materials at West Covina were generally greater than those in St. Louis. Very low concentrations of most materials were found at the rural site at Tyson. Most materials at Tyson increased when there was transport from the St. Louis direction. Third, there were greater excursions of concentration in the L.A. area. Fourth, there was a definite pronounced diurnal variation in each of the compounds appearing in sufficient amount to give reliable quantitative variations. Fifth, there were different kinds of diurnal variations shown by different compounds and sixth, the type of daily cycle of a given compound was most often the same for both cities studied.

Concentrations of materials at Holiday Inn were similar to those at Washington University despite the proximity to the downtown and industrial areas. This was attributed to better dilution at the twelfth floor height and/or differences in meteorological conditions.

The diurnal variations of inorganic secondary sulfate aerosol in the two cities have already been presented in Fig. 5. The diurnal variations in total particulate alkanes are shown in Fig. 6. The morning increases in concentrations at both cities have been attributed to primary auto emissions in the vicinity of the sampling sites. Wind trajectory analysis in the L.A. basin for July 24, 1973 indicated the mid-afternoon peak in alkanes at West Covina was likely due to advection of the emissions from the industrial complex in the vicinity of Dominquez Hills. Visual comparison of the carbon monoxide trace for the Washington University site with the behavior of total alkanes corroborates the attribution of this component of the aerosol to an automotive source. Morning and evening traffic periods account for part of the behavior. Freshman orientation week at Washington University occurred the first week in September of 1973. The heavy evening traffic generated by the dormitories near the sampling site accounted for the huge late evening primary particulate loading. High numbers of particles in the nuclei mode at the sampling site also indicated freshly generated aerosol.

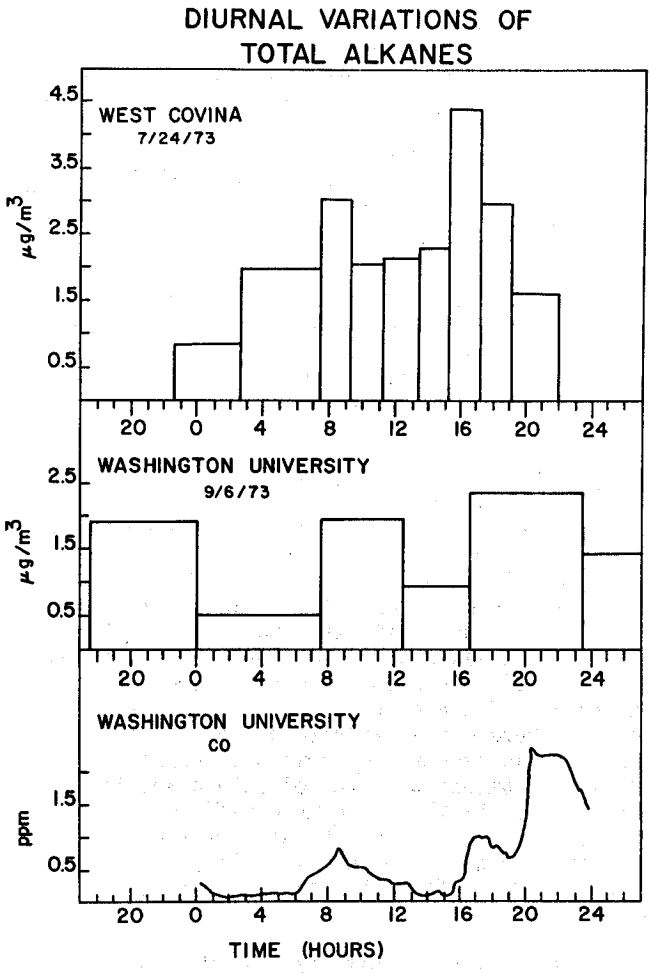

Fig. 6. The diurnal variations of total particulate alkanes for West Covina, California and St. Louis, Missouri. See text for discussion of meteorology and sources which account for the differing behavior. The correlation of carbon monoxide at the Washington University site in St. Louis with this primary component is also shown.

A clear qualitative difference from the temporal behavior of the representative primary aerosol component shown in Fig. 6 can be seen in the diurnal variation of hexanedioic acid shown in Fig. 7. The precursor for this presumed secondary air pollutant is thought to be cyclohexene. Support for classifying this compound as a secondary component of the aerosol can be seen in Fig. 8. The correlation of hexanedioic acid and ozone concentration is significant while there is no significant correlation between total particulate alkanes and ozone.

CONCLUSIONS AND RECOMMENDATIONS

High resolution mass spectrometry has already been proven a uniquely useful tool for the analysis of airborne particulate matter. The technique in its present form has not been nearly exhausted in terms of the information which could be acquired. Further analysis of a greater number of

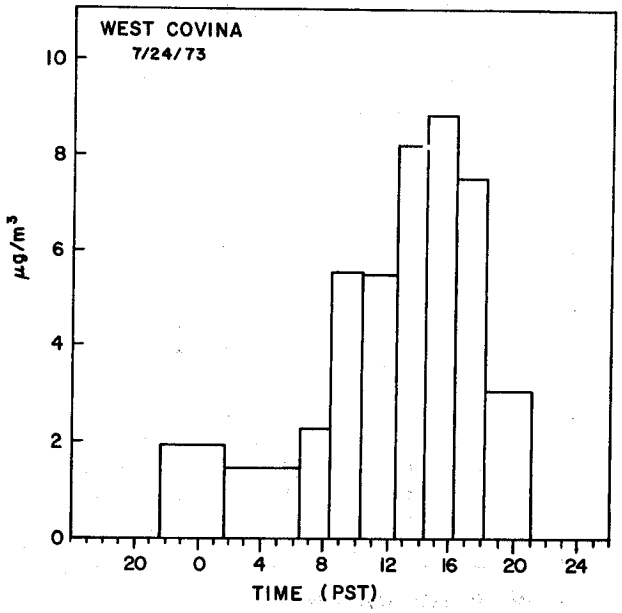

Fig. 7. Diurnal variation on July 24, 1973 at West Covina, California of hexanedioic acid, a presumed secondary component. (Atmos. Environ., 11: pg. 935, 1977).

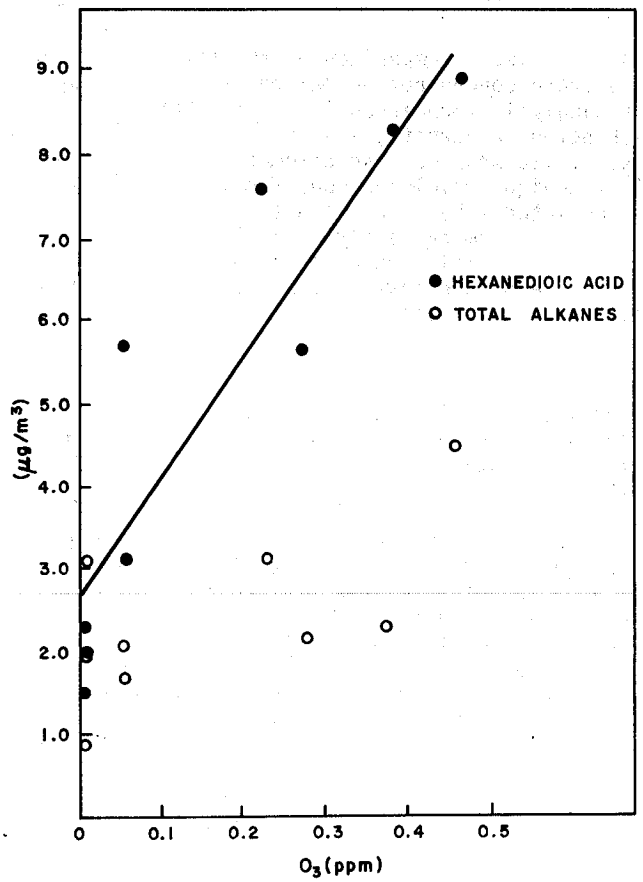

Fig. 8. The apparent correlation of hexanedioic acid and ozone concentrations on July 24, 1973 at West Covina, California. Total alkanes shown for contrast. (Atmos. Environ., 11: pg. 936, 1977).

ambient samples should be made to document the variety of organic components and their concentrations existing near specific source types. Analysis of smog chamber samples would provide information on other potential photochemically produced aerosol components. Identification of the components of auto exhaust should also be pursued utilizing this method.

Some further instrumentation developmental work would provide even further capabilities. Chemical ionization rather than the current electron impact ionization would increase the sensitivity by putting larger amounts of ion current into a fewer number of mass fragments. Since the mass fragments formed by chemical ionization are more indicative of the molecular weight of a specific component, the correct qualitative identification would be more assured and the selectivity of the technique improved. Faster cyclic scanning which is not possible with the present system would increase the precision of the quantification. Elimination of the internal mass marker standard (PFKHB), by use of a double beam instrument, or otherwise, would lessen the numbers of mass fragments in each mass scan and also lessen the chance of confusing mass marker peaks with sample peaks. Multiple ion detection would allow the sensitivity to be greatly enhanced for a few specific components of special interest.

The only disadvantage of CCHRMS for analysis of airborne pollutants is the acquisition and operating costs of a high resolution mass spectrometer system. Certainly, the information obtained to date supports the conclusion that the gain has been well worth the cost.

ACKNOWLEDGEMENTS

It was a pleasure working as a team with A. L. Crittenden, D. Schuetzle, R. J. Charlson and R. L. Knights in Seattle. William Wilson of EPA deserves credit for his support and encouragement. Daniel Grosjean and Bruce Appel spent hours in helpful discussions during the period I spent working on the project.

REFERENCES

1. D. Schuetzle, A. L. Crittenden and R. J. Charlson, "Application of Computer Controlled High Resolution Mass Spectrometry to the Analysis of Air Pollutants," J. Air Pollut. Control Assoc., 23: 704 (1973).

2. D. Schuetzle, D. R. Cronn, A. L. Crittenden and R. J. Charlson, "Molecular Composition of Secondary Aerosol and Its Possible Origin," Environ. Sci. Technol., 9: 838 (1975).

3. D. R. Cronn, R. J. Charlson, R. L. Knights, A. L. Crittenden and B. R. Appel, "A Survey of the Molecular Nature of Primary and Secondary Components of Particles in Urban Air by High Resolution Mass Spectrometry," Atmos. Environ., 11: 929 (1977).

4. D. Schuetzle, "Computer Controlled High Resolution Mass Spectrometric Analysis of Air Pollutants," Ph.D. thesis, University of Washington, Seattle, Washington (1972).

5. R. L. Knights, "Computer Controlled Fast Cyclic Scan Mass Spectrometric Thermal Analysis. I.) Platinum Surface Oxides II.) Inorganic Air Pollutants," Ph.D. thesis, University of Washington, Seattle, Washington (1973).

6. D. R. Cronn, "Analysis of Atmospheric Aerosols by High Resolution Mass Spectrometry," Ph.D. thesis, University of Washington, Seattle, Washington (1975).

7. A. L. Crittenden, "Analysis of Air Pollutants by Mass Spectrometry," report No. EPA-600/3-76-093, (1976).

ANALYSIS OF CARBONACEOUS PARTICULATES AND CHARACTERIZATION OF THEIR SOURCES BY LOW-LEVEL RADIOCARBON COUNTING AND PYROLYSIS/GAS CHROMATOGRAPHY/MASS SPECTROMETRY

L.A. Currie*, S.M. Kunen†, K.J. Voorhees‡, R.B. Murphy§, and W.F. Koch*
National Bureau of Standards
Washington, D.C. 20234

ABSTRACT

The chemical nature and fossil fuel contribution to urban, rural and indoor atmospheric carbonaceous particulate samples have been studied by a combination of pyrolysis/gas chromatography/mass spectrometry (Py/GC/MS) and low-level miniradiocarbon counting. The latter method is applied here for the first time to just milligram amounts of atmospheric particulate material (~10 mg carbon), and it has shown a striking difference between the biogenic/fossil carbon content of urban and desert samples. Application of Py/GC/MS to the insoluble carbonaceous fraction has provided information on sources and characteristics of the primary carbonaceous material.

INTRODUCTION

A major portion of atmospheric particles in urban and rural areas consists of carbonaceous material which derives from both anthropogenic and biogenic sources. These materials can enter into complex photochemical reactions leading to visibility reduction and possible health effects. A concern in contemporary atmospheric research is the development of techniques having the capacity to discern the various sources of this carbonaceous material. Two methodologies are presented which are currently being developed for source identification: low level miniradiocarbon counting and pyrolysis/gas chromatography/mass spectrometry (Py/GC/MS). For the former method 5-10 mg of carbon is necessary; for the latter about 1 mg of sample will suffice.

Through the measurement of the isotopic (^{14}C) composition, definitive conclusions can be drawn as to the relative anthropogenic versus biogenic origins of carbonaceous particulate material. A biogenic source of the compound(s) in question will result in a $^{14}C/^{12}C$ ratio which reflects the present equilibrium worldwide atmospheric value, while anthropogenic contributions—almost entirely fossil fuel derived—will be devoid of radiocarbon due to their geological age[1,2]. Py/GC/MS is used to fingerprint the insoluble carbonaceous portion (polymeric, graphitic) of particulate samples, which undergoes little chemical or physical transformation during transport from the source to the point of collection. The rationale for combining these two approaches is that they possess a very important independence and complementarity. Pattern recognition techniques applied to the Py/GC/MS data on the insoluble carbonaceous material (ICM) will yield source–correlation information, whereas radiocarbon measurements can serve for source validation because of its unique relationship to fossil versus non-fossil origin.

Samples characterized in this study include two from urban locations (Azusa [Los Angeles] and Salt Lake City), one from a remote area (desert), and one ("indoor") from within a laboratory office. Besides the radiocarbon and Py/GC/MS analyses, applied to each of three samples, one sample (Azusa) was submitted also to thermogravimetric analysis (TGA). The results of these analyses showed the desert sample to contain little carbon, most of which was natural (biogenic) in origin, while the urban samples contained three to four times as much carbon whose isotopic (radiocarbon) and molecular (ICM) composition was consistent with major input from fossil sources.

ISOTOPIC (RADIOCARBON) CHARACTERIZATION

The facility which has been developed at NBS to determine the fossil carbon content of atmospheric particles has extended the state-of-the-art of low-level radiocarbon counting in several ways. Required sample sizes are about 100 times smaller than conventionally used for radiocarbon dating; background is reduced through the use of multidimensional spectroscopy and high purity construction materials; and special measures are taken to assure background reproducibility and to eliminate spurious events (pulses) and sample contamination.

The ^{14}C measurement process consists of two steps: quantitative conversion of

the carbonaceous material to high-purity carbon dioxide (counting gas), and low-level proportional counter spectroscopy in specially-constructed small volume gas counters. (The counter used in the present study is made of high-purity quartz and has a volume of ∿15 mL.) Both phases of the measurements required special techniques. The preparation of the counting gas from air particulate samples presented special handling and purification problems, due to the relatively large sample (filter) areas involved and the large amounts of sulfur and nitrogen oxides produced during combustion. Long-term counting of the samples, on the other hand, required on-line monitoring of gas purity, system gain and background reliability. Methods for attacking these chemical and counting problems are discussed below.

Sample Preparation

Counting gas (CO_2) was prepared by means of a combustion-purification (vacuum) system, which incorporated a volumetric section for quantitative assay and transfer of the purified sample. Large air filters presented a special challenge, however, because the initial design for the combustion furnace incorporated only a 10 mm ID silica tube -- suitable for handling mg-size carbon samples which are compact. Consequently a method was sought to remove the atmospheric particulate matter from glass fiber filters in order to reduce the volume of the sample to a size compatible with the small bore combustion tube. The first approach was mechanical scraping of the deposit from the filter with a nickel spatula. This proved unsatisfactory in that it was impossible to remove the particulate matter without carrying more than half of the filter with it. The second approach involved ultrasonic agitation in distilled water to remove the particulate matter, followed by filtration of the suspended material on Nucleopore membrane filter (0.8 μm pore size), and "lifting" the resultant deposit from the membrane filter. The method was quite inefficient, leading to large and variable losses (typically ∿50 percent). The final solution to the problem was to build a (new) combustion furnace large enough to accommodate an entire glass (or quartz) fiber filter as shown in Figure 1 and described below. The advantages to this approach are minimum sample handling and preparation; the disadvantages are increased volume in the combustion train and, in the case of the glass fiber filter, the possibility of melting the filter and fusing the air particulate matter within it.

The vacuum system consists of three stages to which samples are subjected in order to recover carbon in the form of high-purity CO_2. The combustion and purification train (stage 1) includes an afterburner to decompose/oxidize organic vapors, a CuO furnace to completely oxidize CO, and an Ag furnace to remove vapors containing sulfur or halogens. Such gaseous compounds formed during combustion would otherwise remain with the gaseous CO_2 and reduce the ^{14}C counting efficiency. The trapping area (stage 2) utilizes three spiral traps: T_1 at -78 °C (dry ice-methylene chloride bath), for the removal of H_2O vapor; and T_2 and T_3 both at -196 °C (liquid nitrogen bath), for condensing CO_2. Following the combustion process, the sample is sublimed to the transfer area (stage 3), where the amount of CO_2 is determined by volumetric techniques.

The conversion of a carbonaceous sample to counting gas takes place as follows: In the first of the three stages the sample is loaded into the combustion furnace and the system is evacuated. Stopcock d is then closed, and the furnaces turned on. (Stopcock e remains open.) While the furnace temperatures are rising, trap coolants are set in position. Oxygen is admitted through stopcock a. Stopcock b. is opened slightly to maintain just less than one atmosphere in volume a-b and ∿100 mmHg pressure in the trapping area. This throttling procedure is necessary because O_2 will condense at liquid nitrogen temperature if its pressure exceeds 110 mmHg. Furnaces in the combustion area are raised to the following temperatures: Pt - afterburner (packed with platinum gauze and quartz wool), 900 °C; CuO, 800 °C; and Ag-wool, 400 °C. The combustion proceeds by raising the main combustion furnace to 900 °C over a period of about one hour. (For certain small-volume samples, like wood cellulose, a torch is more convenient for initiating combustion.)

The second stage consists of trapping water in T_1 and the CO_2 sample in T_2 and T_3. The system is continually pumped during combustion, and for at least 15 minutes after the completion of combustion, to remove any residual O_2.

The final stage consists of transfering sample CO_2 contained in traps T_2 and T_3 to the transfer area and collecting it in the sample bulb. This is accomplished by closing stopcocks b, d, and e; submersing the sample bulb in liquid nitrogen, opening stopcock f; and then removir-

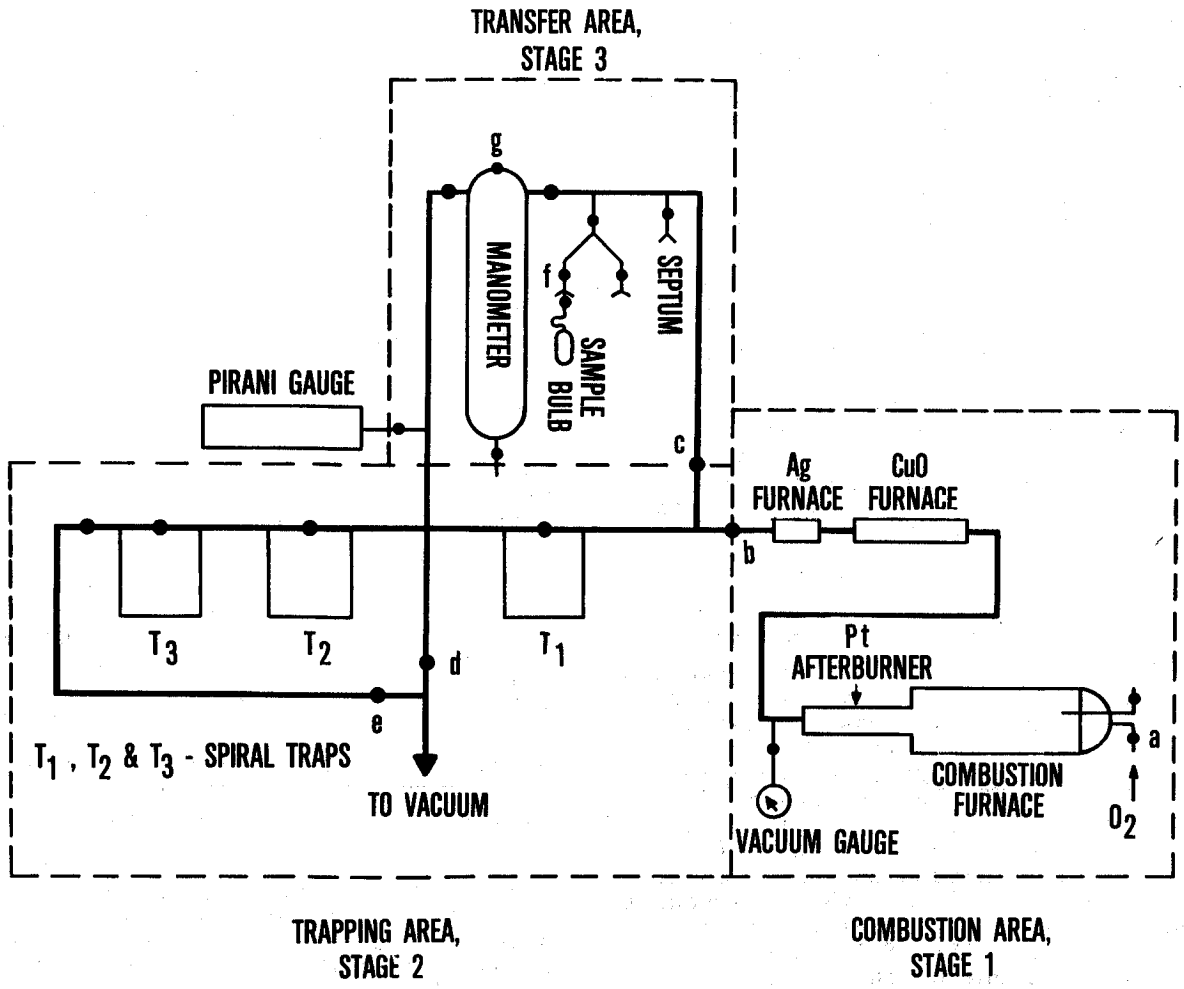

Fig. 1. Schematic diagram of the sample preparation system for the conversion of particulate carbonaceous material to purified counting gas (CO_2).

the liquid nitrogen at T_2 and T_3. CO_2 then sublimes through T_1 (still at -78 °C) and recondenses in the sample bulb. The recovery is determined by expansion of the sample CO_2 into known volume c-g and noting the pressure and temperature.

Two significant problems were encountered in the conversion of samples to counting gas: recovery and purity. Recovery was initially low and variable prior to the addition of the second liquid nitrogen trap (T_3) and to packing the first one (T_2) with glass chips. Through these steps, overall recovery—as determined by the combustion of cellulose (cotton) and oxalic acid dihydrate—was increased from about 60 to about 87 percent. Efforts to obtain quantitative recovery are still underway.

Purity requirements for CO_2 as a counting gas are extreme; even ∿ppm of electronegative species can seriously impair counting efficiency[3]. We found oxygen (because of retention in Teflon-containing valves) and nitrogen oxides (especially from air particulates) particularly troublesome. The former was eliminated by limiting the exposure of Teflon in the system; and the latter, by redistilling the sample CO_2 from (rather than through) a -78 °C bath. In this way, N_2O_4 tended to be well separated from the counting gas. Purity monitoring will be discussed in the following section.

Radiocarbon Counting

Determination of the fraction of contemporary (or fossil) carbon rests upon the accurate measurement of the $^{14}C/^{12}C$

ratio in the sample as compared to that in known contemporary, biogenic carbon. The accuracy with which we can measure this ratio depends upon (1) the Poisson (counting statistics) imprecision -- which is fixed by the counting time and the counting rates for the sample, background, and contemporary carbon; and (2) the stability of the counter efficiency (and gain) and background rate. For the current system (15 mL quartz counter, overall counting efficiency of about 80 percent) the background and (net) contemporary biogenic carbon rates (for 10 mg-carbon) are approximately 0.12 counts per minute (cpm) and 0.14 cpm, respectively. As a result, one to two days of counting time is needed to attain (Poisson) precision to adequately determine the percent of sample carbon which arises from fossil sources. A quantitative discussion and nomogram for relating counting precision, counting time, fossil carbon content, and background and contemporary rates is given in Ref. 2.

Accurate measurements of such small quantities of radiocarbon are critically dependent on stability (background, efficiency), as noted above, as well as rejection of spurious pulses and contaminants. In Table 1, an experimental assessment of background stability is shown. In this case the actual variability of a set of 15 hour observations was consistent with that expected from Poisson statistics -- equivalent to a relative standard deviation of about 8 percent. Spectroscopic discrimination, for the rejection of spurious events plus certain radioactive contaminants, is based on pulse energy (pulse height analysis) – pulse shape analysis. This permits us to distinguish between different classes of decay particles because of the dependence of the relationship between pulse height and track length (pulse shape) on the type of event. The resulting two dimensional spectra appear as in Figure 2, where pulse height is defined on the x-axis and the pulse shape parameter, on the y-axis. Pulses corresponding to short-range events (tritium, radon, ...) in the counter would be found in a narrow band at the 45-degree diagonal between

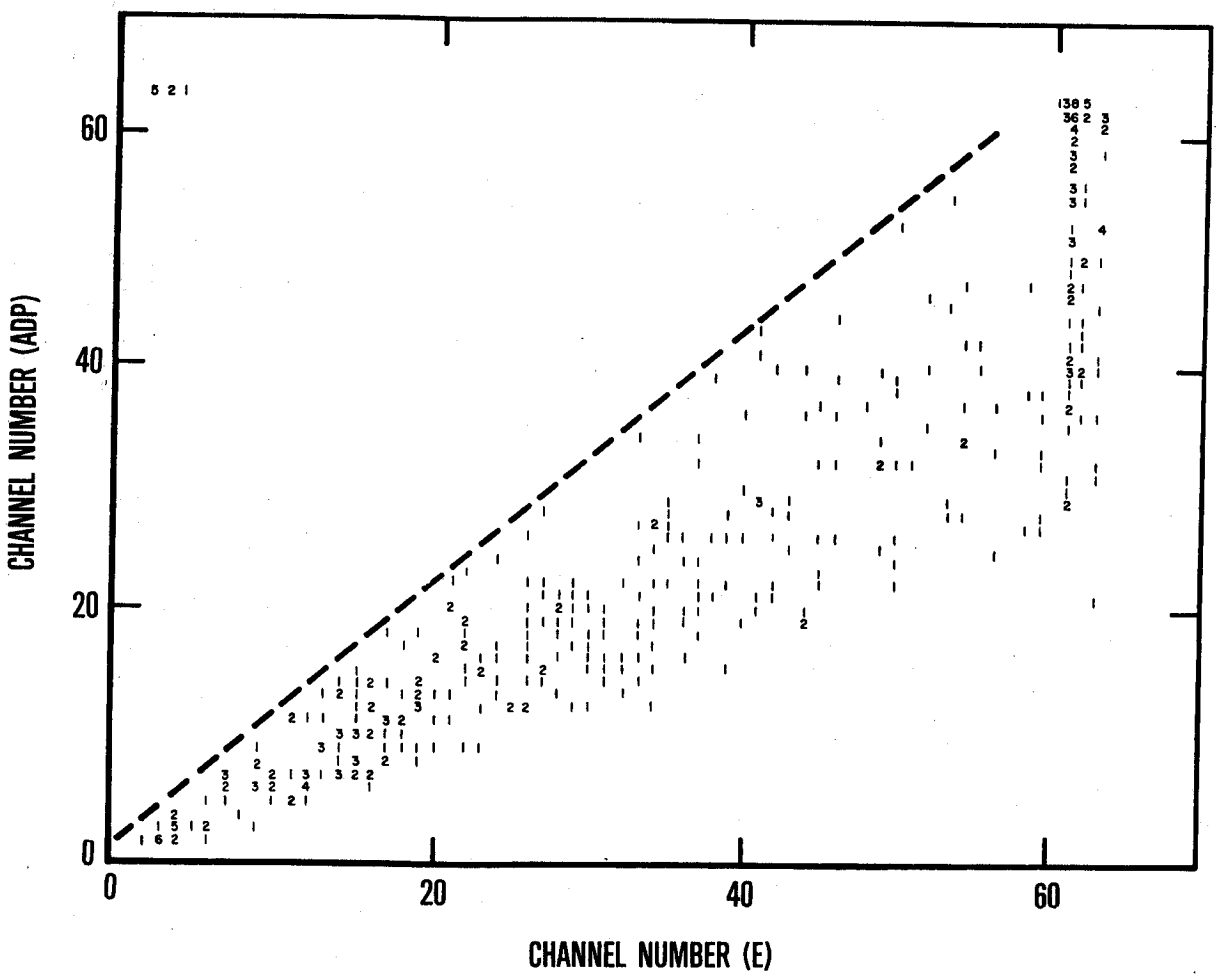

Fig. 2. Two parameter proportional-counter spectrum for the Salt Lake City sample. Abscissa represents pulse energy (E); ordinate, pulse shape (ADP). Spurious pulses appear above the 45° dashed line.

the two axes; and events above the 45-degree line may be ascribed to electrical noise. Such noise, which is a serious problem in small counters, may arise in part from electrical distortion at the ends of the counter wall. As seen in the figure the spurious pulses in this particular case are relatively few (8 out of 575) and they are well isolated (upper left-hand corner of spectrum). Such is not always the case.

Table 1. Background Reproducibility of a 15 mL Quartz Mini-Radiocarbon Counter[a].

Observation No.	Counting Time (min)	Observed Rate (cpm)
1	906	0.174
2	911	0.165
3	880	0.133
4	850	0.150
5	940	0.160
6	925	0.159

Observed mean and calculated S.D. (s):
0.154 ± 0.014 cpm
Poisson S.D. (σ): 0.013 cpm
P (χ^2) = 0.6

[a]L.A. Currie and R.B. Murphy, unpublished data. These measurements preceded improved shielding and meson cancellation experiments, which reduced the background to about 0.12 cpm.

Further information for the sample of Figure 2 (Salt Lake City sample) as well as background rates and monitoring parameters is given in Table 2. (In this and all subsequent tables, uncertainties represent Poisson standard deviations.) The upper section of the table indicates the overall background reduction by a factor of 250 through the combination of shielding, meson cancellation (anticoincidence) and pulse shape spectroscopy. The lower portion ("output data") includes the actual counting data obtained with the sample of particulate matter from Salt Lake City. Here, the residual ("AC") counting rate exceeds the background rate, indicating the presence of some biogenic carbon; and extrapolation and spurious pulse corrections are relatively minor.

Meson (coincidence) rate and channel location are critical on-line monitoring parameters. The location, which should remain between channels 10-50 for proper operation, indicates overall system gain;

Table 2. Control Parameters, Radiocarbon Counting.

Background Rates (cpm; 15 mL counter):

No shield (∿30); Fe shield (9.3); AC[a](0.12)

Output Data (Salt Lake City sample)

Counting time: 2.7 days
Barom. Pressure: 749.5/745.1 (mmHg)

Guard rate:	1021.8 ±0.5 cpm
Meson rate:	9.40±0.05 cpm
Meson location:	31.0 ±0.2 (channels)
AC rate:	0.148±0.006 cpm
Spurious pulses:	1.4 percent
Extrapolation:	+2.3 percent

Sample size: 5.3 mg (carbon)

[a]AC equals the anticoincidence rate -- i.e., the residual counting rate, due to signal and background after correction for mesons (coincidence counts) and spurious events (pulse shape analysis), and extrapolation to zero discriminator level.

and its stability is a vital index of electronic plus counting gas stability. The meson rate, on the other hand, is the control for counting efficiency. Small amounts of electronegative impurities in the counting gas lead to depression of meson (and radiocarbon) counting rates, which is doubly deleterious: (a) an already small signal is further reduced, causing poorer precision[4]; and (b) the actual efficiency, for calculating percent biogenic carbon, differs from the calibration value obtained with pure counting gas. Small efficiency losses can be tolerated and adequate corrections made, but losses in excess of about 20 percent lead to significant additional systematic and random error. Use of the meson rate as an efficiency monitor will be shown in the following section.

Fossil Carbon Content of Air Particulate Samples

$^{14}C/^{12}C$ ratios were determined for one rural (desert) and two urban air particulate samples which were collected on 20 cm x 25 cm filters as summarized in Table 3.

Table 3. Sample Collection Information, NBS Portion (∿50% of Total)

Sample Location	Date and Time	Weather Information	Burned Particulate Mass (mg)	Burn Date
Azusa, California	10/24/77 10:00 - 22:00		97	2/27/78
North Emery, Utah	3/27/77	Windy Conditions	428	3/7/78
A. Salt Lake City, Utah	5/31/77 - 6/1/77 08:29 - 08:24	After Rain	32	2/25/78
B. Salt Lake City, Utah	6/1/77 - 6/2/77 08:29 - 08:35	After Rain	22	2/25/78

NOTE: Half of NBS portion of each Salt Lake City sample was combusted and combined forming a composite sample for this location.

The collection time for the desert sample was much longer than that of the urban samples in order to obtain a sufficient amount of carbon. NBS received half of each filter; the remaining half was used by the Utah group for Py/GC/MS analysis to identify speciation of carbon. Prior to combustion for radiocarbon measurement, sample (amount) adequacy of the NBS portion was determined on a LECO infrared analyzer, which gives a measure of total carbon and total sulfur.[4]

Because of the large sulfate and nitrate contents of these samples, initial counting efficiency was not always satisfactory due to traces of electronegative species in the CO_2 counting gas. Repurification was then employed, and counting efficiency was monitored on line by means of the counting rates observed for cosmogenic mu mesons. Table 4 shows the observed meson rates as described in the preceding section for various stages of purification for the Salt Lake City sample.

Radiocarbon results for the three sampling locations given in Table 3 are shown in Table 5, together with the only other published radiocarbon urban air particulate measurements.[2,5,6] In accord with our original objective, we found that a (Poisson) uncertainty of ten percent contemporary carbon can be achieved with about one day of counting if 10 mg C is available. The general pattern obtained with the three samples, in terms of both carbon and radiocarbon content, seems reasonable. That is, the two urban

Table 4. Meson Monitoring of Sample Purity.

Purification Stage	Median Channel[a]	Meson Rate (cpm)	Relative Efficiency[b] (%)
1	39.2	1.10±0.04	12.
	16.7	1.3 ±0.1	14.
2	27.8	5.0 ±0.2	54.
	16.6	4.9 ±0.1	53.
3	45.0	9.1 ±0.1	98.

[a]Median location for meson (coincidence) spectrum -- used to set (or verify) correct overall instrumental gain. [Acceptable range: 10-50.]

[b]Relative to rate of ∿9.3 cpm when impurity quenching is negligible.

Table 5. Fossil Carbon in Atmospheric Particulate Samples.

Collection Area	Particulate Mass (grams)	Percent Carbon	Fossil Carbon as Percent of Total Carbon
Previous Investigations on Large (gram) Samples			
Detroit[a]	18.0	16	87
Los Angeles[a]	31.0	19	74
St. Louis[b]	9.8	60	73
Los Angeles[b]	38.0	48	60
St. Louis[c]	10.0	12	$\geq$80
This Investigation, "Normal" (milligram) Sample Size[d]			
Salt Lake City	0.108	14	72±13
Azusa (Los Angeles)	0.097	20	77±15
N. Emery, Utah	0.428	5.6	12±16

[a]Reference 5.

[b]Reference 6.

[c]Reference 2.

[d]Masses of carbon actually counted ranged from 5-10 mg; counting times, from 23-65 hours.

samples do imply greater abundance of carbonaceous matter and a relatively large contribution from fossil fuel. Higher precision measurements of size-sorted and chemically-fractionated material will be undertaken in the future in order to verify this trend.

The sample from Azusa merits some additional attention, because it was subjected both to radiocarbon and to chemical-structural analysis (Py/GC/MS and TGA) as described in the second part of this paper. Although the current radiocarbon measurement treated the total carbon, the breakdown into three classes of carbon species (solvent soluble [extractable], polymeric and graphitic) makes a further calculation interesting. That is, given the fact that the ratio (r) of extractable to total carbon is 14.5/20.5 (Table 6) and the assumption that the ICM (polymeric and graphitic carbon) contains fossil carbon only, we may calculate the fossil contribution (f) to the solvent-soluble fraction. Letting f_T represent the fossil contribution to the total carbon as given in Table 5 ($f_T = 0.77\pm0.15$), f is then calculated according to Eq. (1).

$$f = 1 - (1-f_T)/r \qquad (1)$$

Thus, $f = 0.67\pm0.21$, or somewhat more than half of the soluble carbonaceous material may be due to fossil sources. This value of f is, in fact, a lower limit, consistent with an all-fossil ICM.

CHEMICAL CHARACTERIZATION

Progress in understanding the physics, chemistry and photochemistry involved in the formation and growth of particulates in various atmospheric environments relies on detailed knowledge of the organic species constituting these particulates. This information has mainly resulted from research conducted on the solvent soluble organic molecules extracted from atmospheric and synthetically produced particulate material. Although the polymer-like or insoluble carbonaceous fraction has been discussed

Table 6. Species of Carbon in the Azusa Air Particulate Sample.

Carbon Species	Percent of Total Particulate Mass	Mass of Carbon
total carbon	20.5	43.0 mg
extractable carbon (polar, nonpolar solvents)	14.5	30.4 mg
insoluble carbonaceous material:		12.6 mg
polymeric carbon	4.1	
graphitic carbon	1.9	

in a few studies[7-10] it is only recently that investigations have begun on the structural determination of this material[11-13], and on its importance as both a catalyst and a direct participant in surface reactions with sulfur- and nitrogen-containing gaseous pollutants[14,15]. Because of the importance of the Insoluble Carbonaceous Material (ICM) as a tracer for particle sources and because of its possible health implications[16], the work to be described below has been primarily aimed at the determination of the amount and composition of the ICM component.

The advantage of measurements on the ICM rather than the soluble organics for source identification is two-fold. First, conventional extraction procedures for identifying particulate organic species usually utilize samples collected by Hi-Vol sampling procedures. It is known that the quantitative distribution of organic molecules is substantially altered during the high flow sampling procedure, e.g., a major portion of organic material with boiling points below 300 °C is lost by evaporation and sublimation during sampling[17,18]. Secondly, these compounds can undergo substantial changes from time of emission from a source or sorption onto existing atmospheric particles to time of analysis. This is due to reactions occurring through catalytic activity of the particulate metals and "soot" active sites, other reactive molecules present and sunlight. Barofsky and Baum[19] conducted a laboratory study showing that many polycyclic aromatic hydrocarbons adsorbed on matrix material undergo chemical modification when exposed to light -- a consideration of some importance in view of implied health concerns. For example, a polycyclic aromatic hydrocarbon sampled on particulate matter may be different than its precursor emitted from an anthropogenic source, depending on time of transport and general particulate chemistry. The insoluble carbonaceous particulate matrix, however, is likely to survive long-range transport relatively intact, and therefore yield more realistic information concerning source characteristics.

Experimental Methods

The particulate samples were initially submitted to exhaustive extraction to remove the solvent-soluble portion. Following this, the ICM was characterized by pyrolysis/gas chromatography/mass spectrometry (Py/GC/MS) and thermogravimetric analysis (TGA). Collection of the atmospheric samples (Table 3) took place on Gelman type A fiber-glass filters using Hi-Vol samplers. Blank filters as received yielded limited amounts of several organic compounds identified by GC/MS during a 600 °C pyrolysis treatment. Therefore, all filters were sonicated in redistilled spectral grade benzene and dried at 100 °C overnight before being used for particulate collection. The Salt Lake City sample was collected on a roof at the University of Utah which is located in a populated residential area about two miles east of downtown. The "indoor" sample was collected in an office at the Geospace Sciences Laboratory at the University of Arizona in Tucson. The Azusa, Los Angeles sample was sent to us by a utility company from California. The North Emery sample was collected by the mobile laboratory of the Environmental Studies Laboratory (University of Utah Research Institute) in central Utah, well-removed from any industrial or urban sources.

Solvent extraction of the three atmospheric (outdoor) samples consisted of Soxhlet extraction in hexane/chloroform (22/78, v/v) for six hours followed by benzene/methanol (60/40, v/v) extraction for twelve hours to exclude all soluble carbonaceous material from the ICM. The indoor sample was extracted with a series of solvents (chloroform:hexane, 78:22, v/v; benzene:methanol, 60:40, v/v; methanol; and distilled 90 °C water) by three times sonicating the material (total of 12 times) in each of the solvents in order to remove any soluble organic matter before analysis. The insoluble residue was then extracted with hot 10 percent HCl and washed three times with distilled water to remove carbonates. Solvents used were redistilled spectral grade quality.

Next, in order to estimate the proportions of: (1) condensed, polymer-like organic carbon including organic

compounds trapped in the insoluble particulate matrix, and (2) completely condensed graphitic or elemental nonorganic carbon, e.g., "soot" material (stable at 975 °C in helium), the insoluble material (ICM) from the Azusa sample was analyzed by Thermogravimetric Analysis followed by combustion within the Mettler TGA unit.[20] To carry out this analysis the extracted sample was first evacuated (10^{-4} mmHg) and flushed with helium three times in succession to remove any trapped volatile species not previously removed by the extraction procedures. For example, water and other partially trapped volatile species which could confound the weight loss measurements during the TGA procedure were thereby removed. Following this flushing treatment the sample was programmed from 25 °C to 975 °C in a helium atmosphere (essentially a pyrolysis treatment) while weight loss was recorded with the Mettler balance. After several minutes of isothermal operation at 975 °C, pure oxygen was added to the system and weight loss was again recorded during combustion.

To determine the nature of the carbonaceous species constituting the ICM, Py/GC/MS analysis was conducted on aliquots of the extracted samples. The Azusa and Salt Lake City ICM samples were fragmented and analyzed with a Pyroprobe pyrolysis/ gas chromatograph/mass spectrometer/data system at the University of Utah[21]. The samples were pyrolyzed with a Chemical Data System model 120 Pyroprobe directly into the injection port of a Hewlett Packard 7629A gas chromatograph using a pyrolysis time of 20 seconds. The pyrolysate was swept with helium from the injection port into a 0.5 mm ID stainless steel capillary precooled to -10 °C by liquid nitrogen. A cooling jacket, constructed of a 6mm x 50mm piece of T-shaped stainless steel tubing, was used to direct the liquid nitrogen onto a small area. A nichrome heater was incorporated into the cooling jacket to allow for fast heating and quick vaporization of the trapped samples into the capillary column. After vaporization the pyrolysate was separated on a 0.5 mm ID x 10 m SE-52 glass capillary column, using a column flow velocity of 18 mL/s and a temperature program of 40-210 °C at 2 °C per minute. A Hewlett-Packard 5930A mass spectrometer (quadrupole) and a 5933A computer system was directly coupled with the gas chromatograph.

The procedure above utilized 0.1 mg to 0.5 mg samples and the resulting signal limited component identification to major organic species. In order to identify as many trace products as possible, 20 mg of the indoor and Salt Lake City samples were pyrolyzed with a high vacuum pyrolysis/gas chromatography/mass spectrometry system developed at the University of Arizona.[22] Pyrolysis took place in vacuum (10^{-6} mmHg) in a Vycor furnace, and products trapped in a liquid nitrogen-cooled U-tube were subsequently transferred with helium to a micro injection loop (also liquid nitrogen cooled), for injection and GC/MS analysis. An OS-138 (polyphenylether) 45.7 m long, 0.5 mm diameter Support-Coated-Open-Tubular (SCOT) capillary tube was used for separation. The column was programmed from 40 °C to 190 °C at a rate of 2.5 °C per minute after being held at 40 °C for 10 minutes. At the end of the program the column was run isothermally at 190 °C. Compounds were identified with the use of a single-focusing Hitachi RMU-6E mass spectrometer coupled through a Watson-Biemann separator with a Perkin-Elmer Model 226 gas chromatograph.

Results

Species of Carbon. Prior to extraction, an aliquot of the Azusa sample was analyzed for total carbon, hydrogen, and nitrogen with a Perkin Elmer CHN analyzer. This instrument combusts the sample at 910 °C in an oxygen atmosphere and then specifically analyzes for the respective gaseous oxides. Following extraction, an aliquot of the remaining sample (ICM) was also analyzed for carbon, hydrogen and nitrogen. The results of these analyses indicated that this particular sample (before extraction) had a 20.5 percent by weight total carbon content, that 14.5 percent of the sample was extractable carbon (polar and nonpolar solvents), and 6.0 percent of the total particulate sample was ICM-carbon. That is, 29.3 percent (= 6.0/20.5) of the sample-carbon was non-extractable.

The thermogravimetric analysis (which is actually a pyrolysis in helium), followed by combustion in O_2 is represented in Figure 3. Assuming that all of the material which pyrolyzed (in He) and combusted (in O_2) is carbonaceous, then 69 percent by weight of the insoluble carbonaceous material is condensed, polymer-like organic carbon (plus trapped carbon species) while 31 percent of the ICM is completely condensed elemental or graphitic carbon. As expressed in Table 6 this means that 4.1 percent (= 0.69 x 6.0 percent) of the total sample or 20 percent (= 0.69 x 29.3 percent) of the total carbon in the sample is polymeric (or trapped) carbon, while 1.9 percent of the total sample or 9.1 percent of the total carbon in the sample is graphitic carbon. These numbers are approximations since it is possible that volatile or

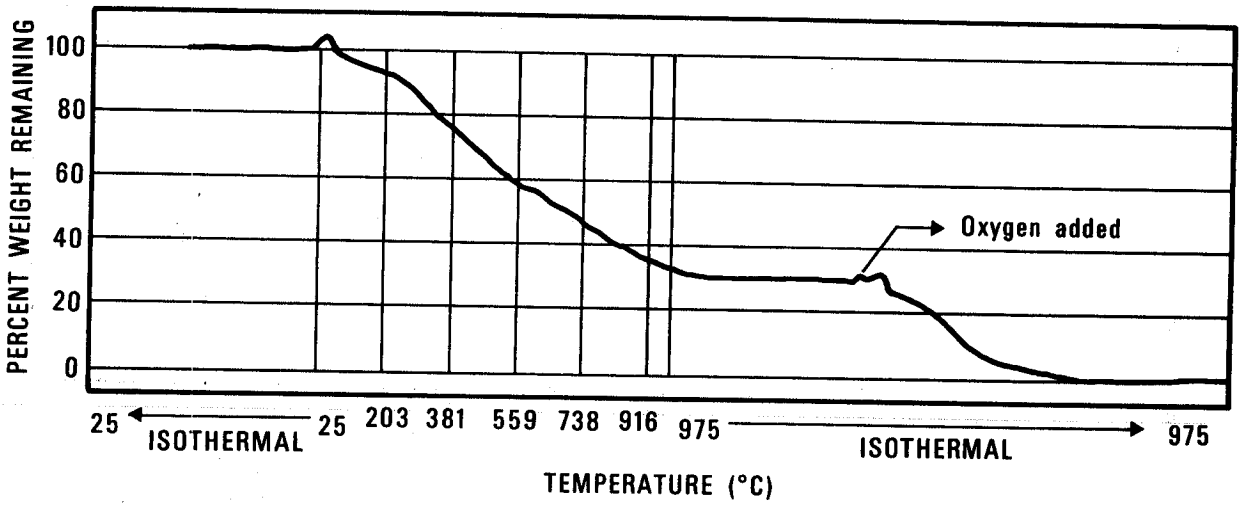

Fig. 3. Thermogravimetric analysis of the Azusa Insoluble Carbonaceous Material.

oxidizable inorganic species contributed to the weight change during the TGA procedure.

Characterization of the ICM. To qualitatively determine constituent molecules of the ICM, aliquots of the extracted samples were pyrolyzed with separation and identification of the pyrolysis products by GC/MS.

It is realized that although pyrolysis can degrade a polymer into molecular fragments indicative of the original structure, it is possible to produce new compounds (pyrosynthesized) which bear little relationship to the original polymer. Pyrolyses above 600-700 °C provide enough energy to a system to cause random carbon-carbon bond breaking. Below 600 °C low energy processes such as Diels-Alder, xanthate, ester, and Cope pyrolysis predominate. The products from the low energy reactions are usually quite indicative of the original structure. For this reason, a pyrolysis temperature of 450 °C was chosen. Thorough examination of all identified pyrolysis products is nevertheless in order, because of the possible misinterpretation of certain isolated species which can be produced at this temperature. For example, large amounts of carbohydrates pyrolyzed at 400 °C and above will form furan and other compounds which could be confused with furan and furan derivatives derived from the incomplete combustion of petroleum products.

The pyrogram shown in Figure 4 (Salt Lake City sample) is similar to the earlier results from our laboratories in which the first actual identification of discrete compounds comprising the insoluble carbonaceous component of atmospheric particulate material was made[23,24]. Most of the compounds shown represent fossil fuel constituents. The homologous series of alkanes and alkenes, up to C_{18}, can all be derived from fossil fuel sources, although it is expected that small amounts of these compounds could result from the pyrolysis of fatty acids and waxes derived from biological material collected on the filter.

Several aromatic compounds including substituted benzenes and naphthalenes as well as saturated and unsaturated five and six-membered ring compounds were also found. Some of the cyclic compounds which we observed in this and the previous studies[23,24] also occur in automobile exhaust, such as the following:

cyclopentene	cyclohexadiene
methylcyclopentene	cyclopentadiene
cyclohexane	dimethylcyclohexane
cyclohexene	

It is interesting that several of the cyclic compounds identified in the ambient particulate insoluble carbonaceous material have not been found in the extracts of ambient atmospheric particulates[25].

Due to the sample size limitation of the Pyroprobe system used for the Azusa sample, we were able to identify major compounds, but not the low concentration marker (highly source dependent) compounds that have been found in other samples. As with the Salt Lake City sample, however, the major components of the ICM are a homologous series of long chain alkanes and alkenes plus a series of alkyl substituted benzenes. Also seen were styrene

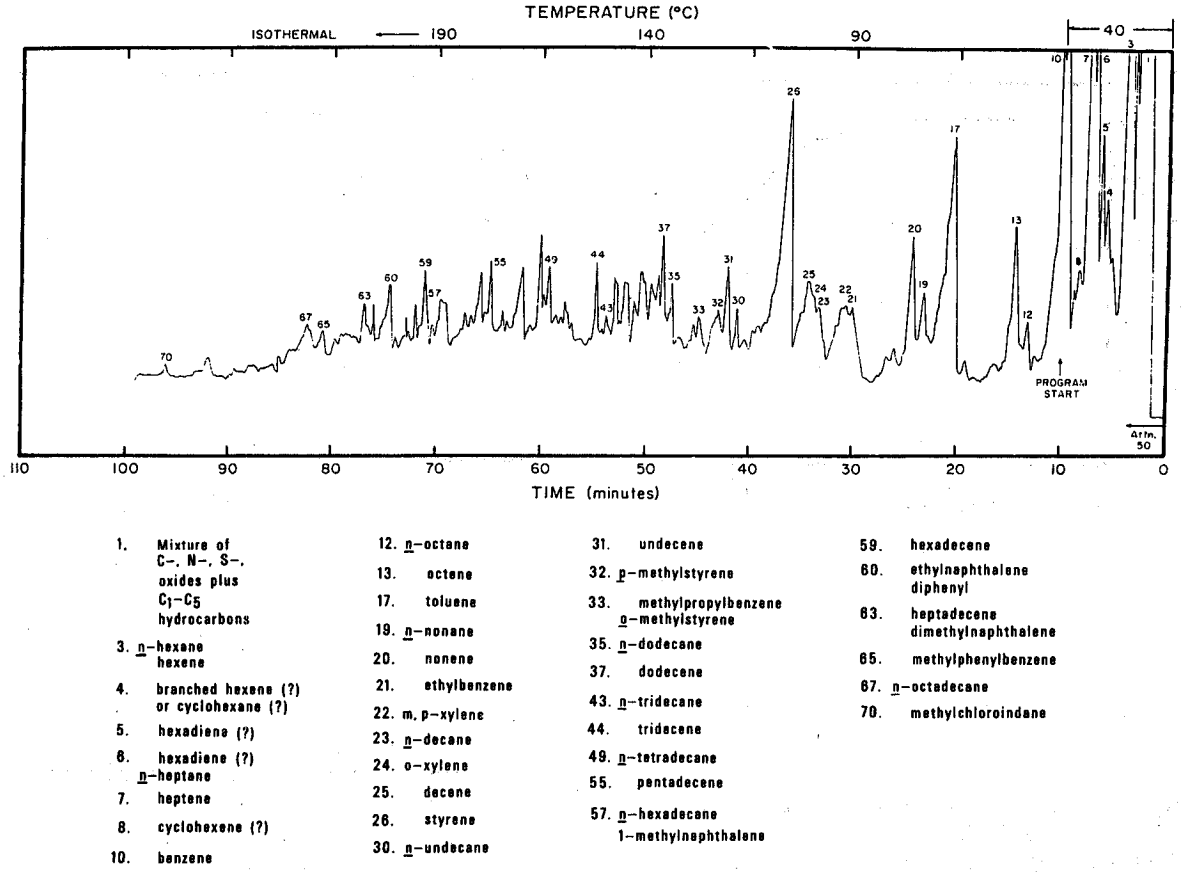

Fig. 4. 450 °C pyrolysis products of the Salt Lake City Insoluble Carbonaceous Material.

and its derivitives -- likely arising from styrenebutadiene tire rubber particles.

The indoor laboratory sample (pyrogram not shown) yielded several compounds not found in the outdoor ambient samples. A large peak was identified as methylmethacrylate, the monomer of plexiglas. A considerably smaller peak was identified as the allyl ester of methylcrotonic acid, a substance used in synthetic polymer production. Also a series of alkyl substituted pyrazoles and ethylimidazole were identified. Heteroatomic cyclic molecules such as furans and pyrazoles[23,24] could have a dual source: pyrolysis or oxidation of biogenic material (terpenes, carbohydrates, amino acids), or the combustion of fossil fuel.

CONCLUSION

This work represents the first attempt to analyze the carbon species (graphite versus polymeric carbon) in ICM together with an isotopic determination of the percent manmade versus naturally-emitted carbon in normal Hi-Vol particulate samples. With the demonstrated capacity of these new methods to discriminate between different source types and sampling regions, using as little as 10 mg of carbon for analysis, we shall be able to extend our knowledge of both the qualitative and quantitative contribution of man's activities to the atmospheric particulate burden. It is noteworthy that the desert sample, collected in advance of the construction of a large coal-fired power plant, had a relatively small carbon content practically all of which could be ascribed to natural (biogenic) sources. Future studies will be directed to the analysis of size-sorted, chemically-fractionated, and diurnal or short duration samples in order to further discern the fossil contribution and chemical nature of the primary carbonaceous material.

ACKNOWLEDGEMENT

The considerable assistance of F. D. Hileman (University of Utah) and G. A. Klouda (NBS) is gratefully acknowledged. The work was partially supported by the Office of Environmental Measurements (NBS) and the EPA Energy-Environment

Program (EPA-IAG-D6-E684). Mention of commercial products in the text does not imply endorsement by the NBS.

REFERENCES AND FOOTNOTES

*Center for Analytical Chemistry, National Bureau of Standards, Washington, D.C. 20234.

†Geospace Sciences Laboratory University of Utah Research Institute, 391 Chipeta Way, Salt Lake City, Utah 84108.

‡Flammability Research Center, University of Utah, 391 Chipeta Way, Salt Lake City, Utah 84108.

§Department of Chemistry, New York University, New York, N.Y. 10003.

1. Suess, H.E., "Radiocarbon Concentration in Modern Wood", Science, 122, 415 (1955).

2. Currie, L.A., Noakes, J., and Breiter, D., "Measurement of Small Radiocarbon Samples: Power of Alternative Methods for Tracing Atmospheric Hydrocarbons", Ninth International Radiocarbon Conference, University of California, Los Angeles and San Diego, 1976.

3. DeVries, H., and Barendsen, G.W., "Radiocarbon Dating by a Proportional Counter Filled with Carbon Dioxide", Physica 19, 987 (1953).

4. Anticipated signal, from contemporary carbon, is proportional to counting efficiency, chemical yield, and percent carbon. All of these quantities must be therefore known in advance to assess the practicability of radiocarbon measurement.

5. Clayton, G.D., Arnold, J.R., and Patty, F.A., "Determination of Sources of Particulate Atmospheric Carbon", Science, 122, 751 (1955).

6. Lodge, J.P., Jr, Bien, G.S., and Suess, H.E., "The Carbon -14 Contents of Urban Airborne Particulate Matter", International Journal of Air Pollution, 2, 309 (1960).

7. Altshuller, A.P. and J.J. Bufalini "Photochemical aspects of air pollution: a review." Environ. Sci. Technol. 5, 29 (1971).

8. Boisdron, Y. and J.R. Brock "Particle growth processes and initial particle size distribution" in Assessment of Airborne Particulates. eds. T.T. Mercer, P.E. Marrow, and W. Stober, C.C. Thomas publ., Springfield, Ill. (1972).

9. Friedlander, S.K., "Chemical element balances and identification of air pollution sources." Environ. Sci. Technol. 7, 235 (1973).

10. Appel, B.R., P. Colodny, and Wesolowski, J.J. "Analysis of carbonaceous materials in Southern California atmospheric aerosols." Environ. Sci. Technol. 10, 359 (1976).

11. Chu, R.R. and Orr, Jr., C. "Particulate products from photochemical oxidation of organic vapors in air." Paper No. 74-156 presented at the 67th Annual Meeting of the Air Pollution Control Association, Denver, Colorado, June 9-13, 1974.

12. O'Brien, R.J., Holmes, J.R., and Bockian, A.H., "Formation of photochemical aerosol from hydrocarbons: chemical reactivity and products." Environ. Sci. Technol. 9, 568 (1975).

13. Schuetzle, D., Cronn, D., Crittenden, A.L., and Charlson, R.J., "Molecular composition of secondary aerosol and its possible origin." Environ. Sci. Technol. 9, 838 (1975).

14. Novakov, T., "Chemical characterizations of atmospheric pollution particulates by photoelectron spectroscopy." 2nd Joint Conf. Sensing of Environ. Pollutants, Washington, D.C., p. 197, (1973).

15. Chang, S.G. and Novakov, T., "Formation of pollution particulate nitrogen compounds by NO-soot, and NH_3-soot gas-particle surface reactions." Atmospheric Environment. 9, 495 (1975).

16. Prado, G.P., Lee, M.L., Hites, R.A., Hoult, D.P., and Howard, J.B., "Soot and Hydrocarbon Formation in a turbulent diffusion flame," Sixteenth International Symposium on Combustion, MIT, Cambridge, Mass., Aug. 15-21, 1976.

17. Rondia, D., DeWiest, F., and Fiorentina, H.D., "Organics in atmospheric aerosols in Belgium," Paper presented at the International Conference on Environmental Sensing and Assessment, Paper No. 24-5, Las Vegas, Nevada, September 14-19, 1975, Vol. 2.

18. Fiorentina, H.D., DeWiest, F., and de Graeve, J., "Determination par Spectrometrie Infrarouge de la Matiére Organique Non Volatile Associeé aux Particules en Suspension dans l'Air-II. Facteurs Influencant L'Indice Aliphatique," Atm. Env., 9, 517 (1975).

19. Barofsky, D.F. and Baum, E.J., "Field Desorption Mass Spectral Analysis of the Photooxidation Products of Adsorbed Polycyclic Aromatic Hydrocarbons," 69th Annual APCA Meeting, Portland, 1976.

20. Fyans, R.L., "Rapid Characterization of Coal by Thermogravimetric and Scanning Calorimetric Analysis," Presented at the 28th Pittsburgh Conference, in Cleveland, Ohio, March 1977.

21. Hileman, F.D., Voorhees, K.J., Wojcik, L.H., Birky, M.M., Ryan, P.W., and Einhorn, I.N., "Pyrolysis of a flexible urethane foam," J. of Polymer Sci. 13, 571 (1975).

22. Bandurskii, E.L. and Nagy, B., "The polymer-like organic material in the Orgueil meteorite," Geochimica et Cosmochimica Acta, 40, 1397 (1976).

23. Kunen, S.M., Burke, M.F., Bandurskii, E.L., and Nagy, B., "Preliminary Investigations of the Pyrolysis Products of Insoluble Polymer-like Components of Atmospheric Particulates," Atmospheric Environment, 10, 913 (1976).

24. Kunen, S.M., Voorhees, K.J., Hill, A.C., Hileman, F.D., and Osborne, D.N., "Chemical Analysis of the Insoluble Carbonaceous Components of Atmospheric Particulates with Pyrolysis/Gas Chromatography/Mass Spectrometry Techniques", Paper No. 77-36.4, presented at the 70th Annual Meeting of the Air Pollution Control Association, Portland, Oregon, June 1976.

25. Graedel, T., Personal communication, 1975.

IDENTIFICATION OF THE GRAPHITIC CARBON COMPONENT OF SOURCE AND AMBIENT PARTICULATES BY RAMAN SPECTROSCOPY AND AN OPTICAL ATTENUATION TECHNIQUE

H. Rosen, A.D.A. Hansen, L. Gundel, and T. Novakov
Lawrence Berkeley Laboratory
University of California
Berkeley, California 94720

ABSTRACT

A series of experimental results indicates that the high optical absorptivity of aerosol particles in urban environments and particles generated from various combustion sources is due to their "graphitic" carbon component.

INTRODUCTION

Carbonaceous material represents a major fraction of the respirable particulate burden in urban areas, yet the chemical composition of this component is not well understood. Such analysis is important for evaluating the health effects, chemical activity, optical effects, and sources of these carbonaceous particles. Our paper describes the application of Raman spectroscopy and an optical attenuation technique to the identification of what appears to be a major constituent of this aerosol.

It is well known that lightly loaded particulate samples collected from both urban environments and various combustion sources have a gray or black appearance. This coloration is presumably due to a highly absorbing species in the aerosol, which could have a significant impact on the heat balance of the earth.[1-4] It is therefore important to establish the nature of these absorbing species. In this paper a series of experimental results will be presented, indicating that the high optical absorptivity of urban aerosols and various combustion source particulates is due to their "graphitic" soot content. This result is not surprising, since other major components in the aerosol, like $(NH_4)_2SO_4$, H_2SO_4, HNO_3, NH_4NO_3, and PbBrCl, are not absorbing in the visible spectral region.

"Graphitic" soot can only be produced directly from combustion; therefore this identification allows one to use the optical absorptivity as a convenient tracer for primary emissions. This "graphitic" soot tracer technique[5,6] suggests that a major fraction, possibly the dominant fraction, of the ambient carbonaceous aerosol burden is primary, i.e., due to direct particulate emissions from combustion sources. It also appears that if there are significant concentrations of secondary species, their production does not seem to depend on the photochemical activity as manifested by the ozone concentration. These results could have important consequences in terms of control strategies.

EXPERIMENTAL DETAILS

Raman Spectroscopy

A schematic of the experimental setup is shown in Fig. 1. The setup included a Coherent Radiation argon ion laser operating with 1 W of power at 514.5nm. The laser beam was focused by a 75-mm focal length cylindrical lens to a spot .06 mm × 2 mm on the sample surface via a small mirror. The backscattered radiation was collected and imaged by an f/1 lens onto the slit of a 1-m Jarrell Ashe double monochromator equipped with two 1180-grooves/mm gratings blazed at 5000 Å. The incident polarization of the laser was perpendicular to the slit of the spectrometer, and no analysis of the scattered polarization was made. The output of the spectrometer was detected by an FW130 photomultiplier cooled to -20°C and used in a photon-counting mode. The pulses, after appropriate shaping, were counted and displayed on a multichannel analyzer. The Jarrell-Ashe spectrometer was equipped with a computer-controlled grating drive made by RKB, Inc. This attachment allowed a given spectral region to be scanned many times and added to the memory of the multichannel analyzer. This multiscanning ability was used in some cases to obtain very long integration times and improved signal-to-noise.

In order to minimize heating effects, the highly absorbing samples used in these experiments were rotated at 1800 rpm by a motor. In this way one can increase the area illuminated by the laser beam by a large factor with almost no loss in signal level. The focal spot of the laser was located approximately 5 mm below the axis of rotation so that the effective illuminated area was an annulus of radius 5 mm and width 2 mm, which yielded a rather low power density of ~ 1 W/cm^2. The spectra reported in this paper were generally obtained directly from the particles collected on the filter substrate (1.2-μ Millipore or quartz fiber) without any sample preparation. The exceptions to this rule are the spectra of automobile exhaust, diesel exhaust, and activated carbon, for which there was sufficient material available to form into pellets.

Optical Attenuation

A schematic of the apparatus we developed for making optical attenuation measurements is shown in Fig. 2. This attenuation measurement apparatus compares the transmission of a 633-nm He-Ne laser beam through a loaded filter relative to that of a blank filter. The loaded filters are placed in the beam with the loaded side towards the laser; after multiple scattering through the filter substrate, the light is collected by an f/1 lens and focused on a photomultiplier tube. The data presented in

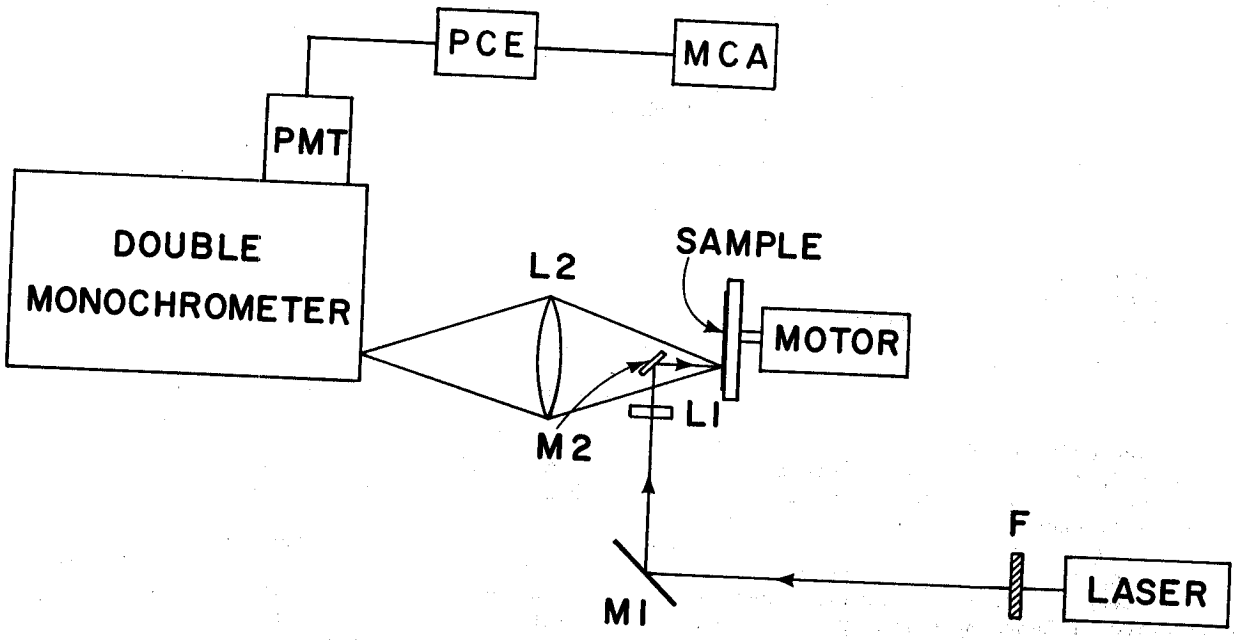

Fig. 1. Schematic diagram of experimental setup (not to scale). The elements of the apparatus are labeled in the following way: F — 30-Å interference filter, M1 — mirror, L1 — 75-mm focal length quartz cylindrical lens, M2 — small mirror, L2 — f/1 collection lens, PMT — photomultiplier tube, PCE — photon-counting electronics, and MCA — multichannel analyzer.

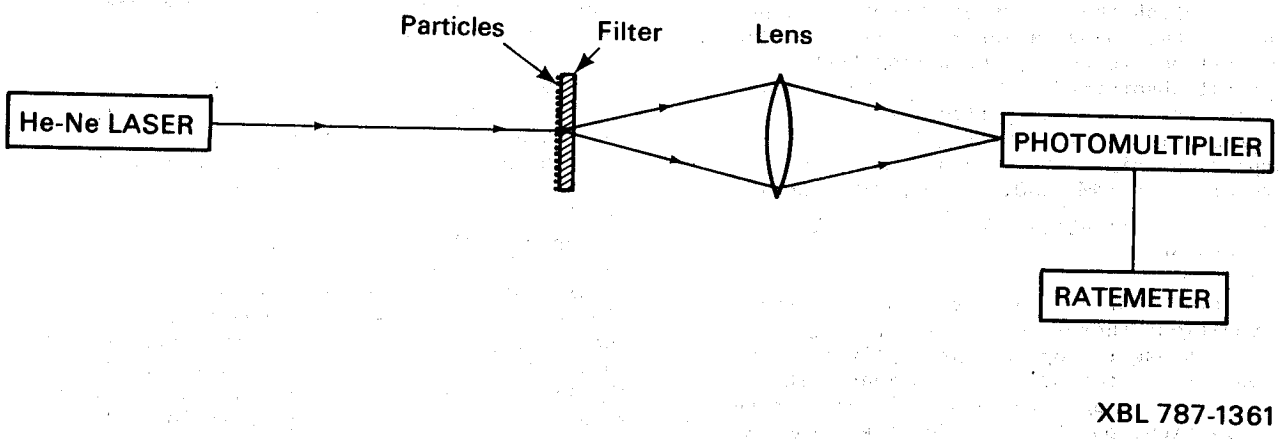

Fig. 2. Schematic of the optical attenuation apparatus.

this paper were obtained from particles collected on Millipore or quartz fiber substrates, but the optical attenuation measurement can be made with a wide variety of filter media. This technique is based on a principle similar to that of the opal glass method used by Weiss et al.[1,7] and measures the absorbing rather than the scattering properties of the aerosol. Since the real parts of the refractive indices of the filter media and the particulates are approximately equal, the addition of a few monolayers of nonabsorbing particles is expected to be a small perturbation on the transmission properties of the filter. We verified that this is indeed the case for a Millipore filter loaded with 20 $\mu g/cm^2$ on nonabsorbing 3-μm NH_4HSO_4 aerosols. Also, heat treatment and solvent extraction experiments showed that one can remove from a filter substrate most of the mass of the aerosol responsible for scattering without appreciably affecting the optical attenuation. Therefore, throughout the text, we shall attribute the optical attenuation measured in the above fashion to the absorbing component in the aerosol.

RESULTS

Raman Spectroscopy

Raman spectroscopy is a highly selective method of analysis which has only recently been applied to the characterization of air pollution particulates.[8-11] The technique can often be used to make unambiguous identifications, since different chemical species have characteristic vibrational modes and therefore characteristic Raman spectra.

The Raman spectra between 900 and 1950 cm^{-1} of ambient, automobile exhaust, and diesel exhaust particulates are compared with the spectra of activated carbon and polycrystalline graphite in Fig. 3. It is evident that the spectra of activated carbon, diesel exhaust, automobile exhaust, and the ambient sample are very similar. The positions of the two Raman modes in these spectra are coincident to within ±10 cm^{-1}, which is the estimated experimental error. The ambient sample was collected as part of the RAPS program in St. Louis, Missouri;[12] however, the same Raman modes are also evident in every urban sample studied, including samples collected in Buffalo, New York, and Berkeley, Fremont, and Anaheim, California. It should be noted that these samples were collected under a wide variety of conditions (e.g., high and low oxidant); yet for a given carbon loading, the Raman intensities are comparable. The implications of this result are fully discussed in the paper by Hansen et al.[6]

Tuinstra and Koenig[13] studied the Raman spectra of activated carbon and assigned the Raman modes near 1600 and 1350 cm^{-1} to phonons propagating within "graphitic" planes. The close correspondence of the spectra in Fig. 3 indicates the presence of physical structures similar to activated carbon in both source-enriched and ambient samples. These graphitic species are presumably formed directly in combustion, and throughout the text we shall use the term "graphitic" soot to describe them. It should be emphasized that the soot particles generated by the incomplete combustion of fossil fuels contain not only this "graphitic" soot component but also a complex mix of organic compounds.

Recently it was shown[10] that under very high laser irradiance levels (6 kW/cm^2-320 kW/cm^2), it is possible to graphitize certain organics to produce these "graphitic" Raman modes. However, the laser powers used in these experiments were typically four to five orders of magnitude larger than the rather modest average power levels used in our experiments. In order to eliminate the possibility that the laser power was making a significant perturbation in our case, we investigated the intensity of the "graphitic" mode near 1600 cm^{-1} as a function of laser power. We found that the intensity of this mode scales with the laser power down to irradiance levels as low as 10 mW/cm^2. This power level is about a factor of 10 less than the sun's radiance, and therefore we discount the above possibility as a serious source of error.

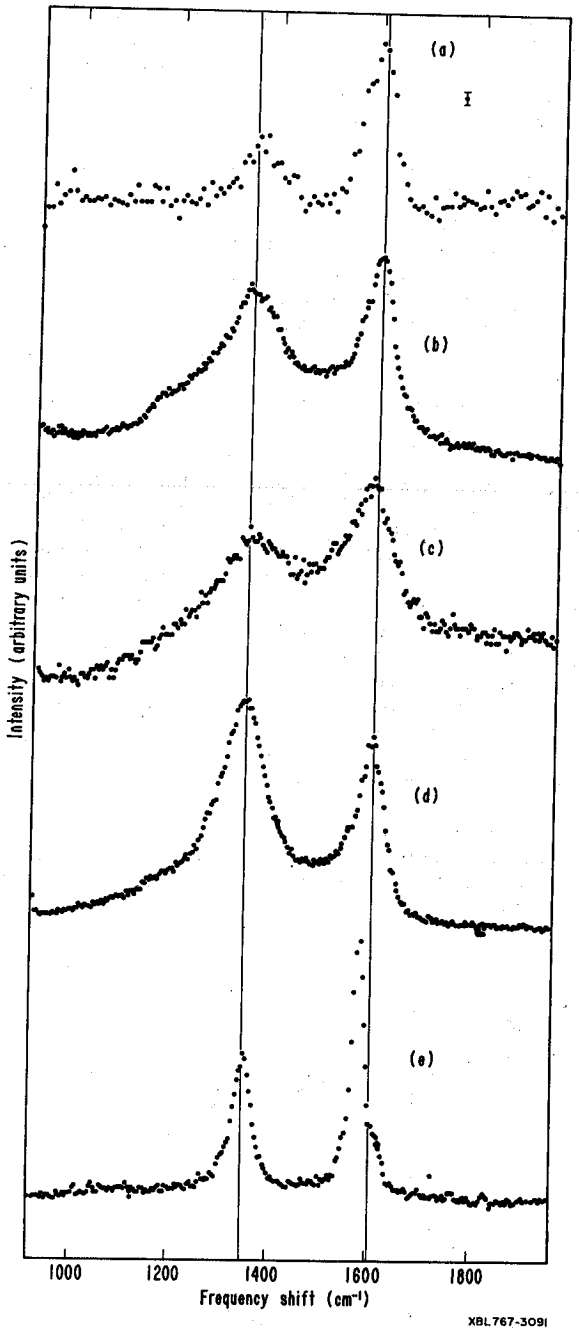

Fig. 3. Raman spectra between 920 and 1950 cm^{-1} of: a) Ambient sample collected in 1975 as part of EPA's RAPS program. The sample was collected on a dichotomous sampler and was in the small size range fraction. b) Automobile exhaust collected from a number of cold starts of a poorly tuned automobile using lead-free gas and having no catalytic converter. c) Diesel exhaust. d) Activated carbon. e) Polycrystalline graphite.

Optical Attenuation

These "graphitic" species, which have a high imaginary index of refraction,[14] are the most likely candidate for explaining the high optical absorptivity of ambient and source particulate

Table 4. Chemical analysis of the filters for the total and the fine (<0.93 μm) aerosol fraction. 1973

NOV 1973:	6	7	9	14	16	17	21
				μg/m^3			
Carbon							
Total Sample		--	--	--	--	--	
Fine Fraction		--	--	--	--	--	
MSO[a]							
Total Sample		--	--	--	--	--	
Fine Fraction		--	--	--			
Hydrogen							
Total Sample		--	--	--	--	--	
Fine Fraction		--	--	--	--	--	
Nitrogen							
Total Sample		--	--	--	--	--	
Fine Fraction		--	--	--	--	--	
Lead							
Total Sample	1.6	1.1	1.2		2.0	2.8	1.7
Fine Fraction	1.3	1.0	1.0		1.7	2.6	2.0
Sulfate							
Total Sample	8.1	4.7	18.4	4.3	4.3	7.0	10.3
Fine Fraction				3.5	3.8	5.6	8.0
Nitrate							
Total Sample	5.4	4.9	0.4	2.1	2.8	2.8	3.8
Fine Fraction				1.4	1.8	1.6	3.2
Ammonium							
Total Sample	0.5	0.2	1.4	0.2	0.2	0.3	0.4
Fine Fraction				0.1	0.1	0.2	0.3
Suspended Mass							
Total Sample	109	75	80	96	113	118	107
Fine Fraction	46	18	20	22	25	35	36

[a]Methylene chloride soluble organics

Table 5. Estimation of elemental carbon C(O) in the fine (<0.93 μm) aerosol fraction for 1971 experiment.

NOV 1971:	10	11	12	13	14
Fine Fraction Carbon, μg/m^3	10.6	11.0	7.7	5.0	7.0
BSO[a] x 0.76, μg/m^3	7.0	8.4	5.2	2.7	4.6
Estimated C(O)[a], μg/m^3	3.6	2.6	2.5	2.3	2.4
Estimated C(O)[a]/Pb[a]	1.9	1.0	1.3	2.5	1.6

[a]In the fine aerosol fraction

Table 6. Estimated elemental carbon C(O) in the fine aerosol (<0.93 μm) aerosol fraction for 1973 experiments.

NOV 1973:	6	7	9	14	16	17	21
Pb[a], μg/m^3	1.3	1.0	1.0	--	1.7	2.6	2
Estimated C(O)[a], μg/m^3	2.2	1.7	1.7		2.9	4.4	3.4

[a]In the fine aerosol fraction

exhaust is the primary contributor to the light scattering aerosol. Photochemical aerosols were not significantly present during a two-day air pollution episode in 1973, and likely do not influence visibility in the urban plume. Estimates of C(O) in the fine aerosol during episodes in 1971 were 1.0-2.5 $\mu g/m^3$, and in 1973 were 1.7-4.4 $\mu g/m^3$. However, the role that C(O) plays in coloration effects in Denver's urban plume remains to be established.

REFERENCES

1. P.A. Russell (Editor). Denver Air Pollution Study--1973. Proceedings of a Symposium. Volume I. EPA-600/9-76-007a, U.S. Environmental Protection Agency, Research Triangle Park, NC, 1976. 238 pp.

2. P.A. Russell (Editor). Denver Air Pollution Study--1973. Proceedings of a Symposium. Volume II. EPA-600/9-77-001, U.S. Environmental Protection Agency, Research Triangle Park, NC, 1977. 186 pp.

3. K. Willeke, K.T. Whitby, W.E. Clark, and V.A. Marple. "Size Distributions of Denver Aerosols--A Comparison of Two Sites." Atmos. Environ., 8: 609-633, 1974.

4. R.J. Charlson and N.C. Ahlquist. "Brown Haze: NO_2 or Aerosol?" Atmos. Environ., 3: 653-656 (1969).

5. W.C. Eaton, R.L. Penley, R.M. Burton. "Calibration of the Andersen 2000 High Volume Particle Sizing Collection Head." EPA, HERL In-house Report, 1973.

6. R.G. Draftz. "Microscopical Analysis of Ambient Aerosols from Denver, Colorado." IIT Research Institute Report No. C9928-1, 1973.

7. J.N.H. Hu. "An Improved Impactor for Aerosol Studies--Modified Andersen Sampler." Environ. Sci. Technol. 5: 251-253, 1971.

8. J.L. Durham (Editor). Denver Air Pollution Study--1973. Proceedings of a Symposium. Volume III. To be published in 1978 by U.S. EPA.

9. D.F. Miller, W.E. Schwartz, J.L. Gemma, and A. Levy. "Haze Formation: Its Nature and Origin--1975." Final Report to Coordinating Research Council, Inc. (Project CAPA 6-68) and U.S. Environmental Protection Agency. U.S. EPA Report No. EPA-650/3-75-010. 100 pp, 1975.

SECONDARY ORGANIC AEROSOLS: IDENTIFICATION AND MECHANISMS OF FORMATION

Daniel Grosjean
Statewide Air Pollution Research Center
University of California
Riverside, CA 92521

ABSTRACT

This paper addresses itself to secondary organic aerosols, with emphasis on their identification and modes of formation. Recent outdoor smog chamber studies of aerosol formation from cyclohexene, toluene, diethylhydroxylamine and amines are presented along with examples of measurements of total organic carbon and of specific secondary components (dicarboxylic acids) in ambient aerosols. Also briefly discussed are the impact of secondary organic aerosols on visibility, their possible health effects and their relative importance in urban atmospheric pollution.

INTRODUCTION

Carbonaceous particles are ubiquitous in the air environment and include elemental carbon as well as carbon combined as inorganic and organic compounds. These particles are either directly emitted into the air from combustion processes (primary carbonaceous aerosols) or formed in the atmospheres by chemical reactions involving gaseous pollutant precursors (secondary carbonaceous aerosols). While primary carbonaceous particles consist essentially of soot (elemental carbon + polycyclic aromatic hydrocarbons), secondary organic aerosols contain a variety of oxygenated species such as carboxylic acids, diacids, nitrate esters and other mono- and polyfunctional compounds.

The question of the relative importance of primary vs. secondary aerosol carbon, which has obvious implications for air pollution control strategies, is currently the object of considerable debate. Novakov and coworkers[1-3] have stressed the importance of primary soot and have carried out studies emphasizing the role of soot in the heterogeneous formation of sulfate[4] and nitrogen-containing[5] aerosols. Other investigators, including the author of this chapter, support the contention that secondary organic aerosols, largely of photochemical origin, are of major importance in polluted urban areas.[6-10]

The Conference on Carbonaceous Particles in the Atmosphere provided a timely opportunity to further discuss the experimental evidence and arguments advanced by proponents of both "sides." This paper addresses itself to recent progress in the area of secondary organic aerosols, with emphasis on their identification and on their modes of formation in ambient and simulated (smog chamber) atmospheres, and is illustrated by studies conducted at the California Institute of Technology and more recently at the Statewide Air Pollution Research Center (SAPRC), U. C. Riverside. SAPRC's work concerning the mutagenic activity of organic aerosols has also been presented at this Conference.[11] Organic aerosols have been the object of a recent review published by the National Academy of Sciences.[12]

MODES OF FORMATION OF SECONDARY ORGANIC AEROSOLS

Reactions leading to the formation of secondary organic aerosols in the atmosphere can be divided into three types, namely gas phase reactions, gas-aerosol interactions and reactions in the condensed (aerosol) phase.

Gas Phase Reactions

Since the early studies conducted by Haagen-Smit and coworkers more than twenty-five years ago,[13] considerable evidence has been accumulated concerning the formation of light-scattering organic aerosols by condensation of low volatility species formed upon irradiation of gaseous hydrocarbons (HC) in the presence of oxides of nitrogen (NO_x).[12] Thus, production of aerosols by gas phase reactions involving hydrocarbon precursors and reactive species formed in photochemical smog (ozone, hydroxyl radical, etc.) has been extensively documented in smog chamber studies conducted with paraffins, olefins, aromatics, terpenes, auto exhaust, oxygenated solvents, amines, and other organic pollutants.

However, only a few studies[14,15] have been directed to elucidating the molecular composition of the organic aerosols formed in these model systems. For example, sunlight-irradiation of 1 ppm of cyclohexene with ~0.3 ppm NO_x results in the formation of α, ω-difunctional oxygenated aerosol products bearing carboxylic, carbonyl, hydroxyl or nitrate esters groups (Table 1).

Table 1. Cyclohexene aerosol[12,15]

Product	Formula
adipic acid	$COOH-(CH_2)_4COOH$
6-nitrato hexanoic acid	$COOH-(CH_2)_4CH_2ONO_2$
6-oxo hexanoic acid	$COOH-(CH_2)_4CHO$
6-hydroxy hexanoic acid	$COOH-(CH_2)_4CH_2OH$
glutaric acid	$COOH-(CH_2)_3COOH$
5-nitrato pentanoic acid	$COOH-(CH_2)_3CH_2ONO_2$
5-oxo pentanoic acid	$COOH-(CH_2)_3-CHO$
5-hydroxy pentanoic acid	$COOH-(CH_2)_3-CH_2OH$
glutaraldehyde	$CHO-(CH_2)_3CHO$

Gas-to-aerosol rates of up to ~40 μg carbon m^{-3} min^{-1} have been measured in this system, with the final aerosol concentration accounting for up to 17%, on a carbon basis, of the initial cyclohexene concentration.[15] Similar results have been reported for another cyclic olefin, cyclopentene, and for the diolefin 1,7-octadiene. Organic aerosol products formed in these systems can be accounted for, to a large extent, in terms of olefin-O_3 and olefin-OH reactions.[15]

As shown in Fig. 1, the highly reactive olefin 2,3-dimethyl-2-butene does not form light-scattering aerosols when irradiated with NO_x under the same conditions.[15] This is because the vapor pressures of the monofunctional products formed from alkenes are several order of magnitude higher than those of the corresponding difunctional products formed from cyclic olefins.

In another outdoor smog chamber study, toluene aerosol was found to contain hydroxy nitrocresols as the major products (Table 2). A mechanism involving OH addition on toluene to form cresols and nitrotoluenes (Fig. 2), and reaction of these products with OH to form nitrocresols (Fig. 3) followed by OH reaction with nitrocresols (Fig. 4) has been proposed to account for the experimental results.[16]

Nitrogenous pollutants have also been recently investigated as precursors of organic aerosols under photochemical smog conditions. For example, we have recently shown that addition of N,N-diethylhydroxylamine (DEHA), a proposed smog inhibitor, to ambient polluted air resulted in fact in a significant <u>increase</u> (Fig. 5) in the rate of formation and levels of light-scattering aerosols.[17]

In another study, the dark (thermal) and photochemical reactions of ppm levels of secondary and tertiary amines with NO_x in humid air have been investigated.[18,19] In addition to gaseous products including nitrosamines, nitramines and amides, significant amounts of light-scattering

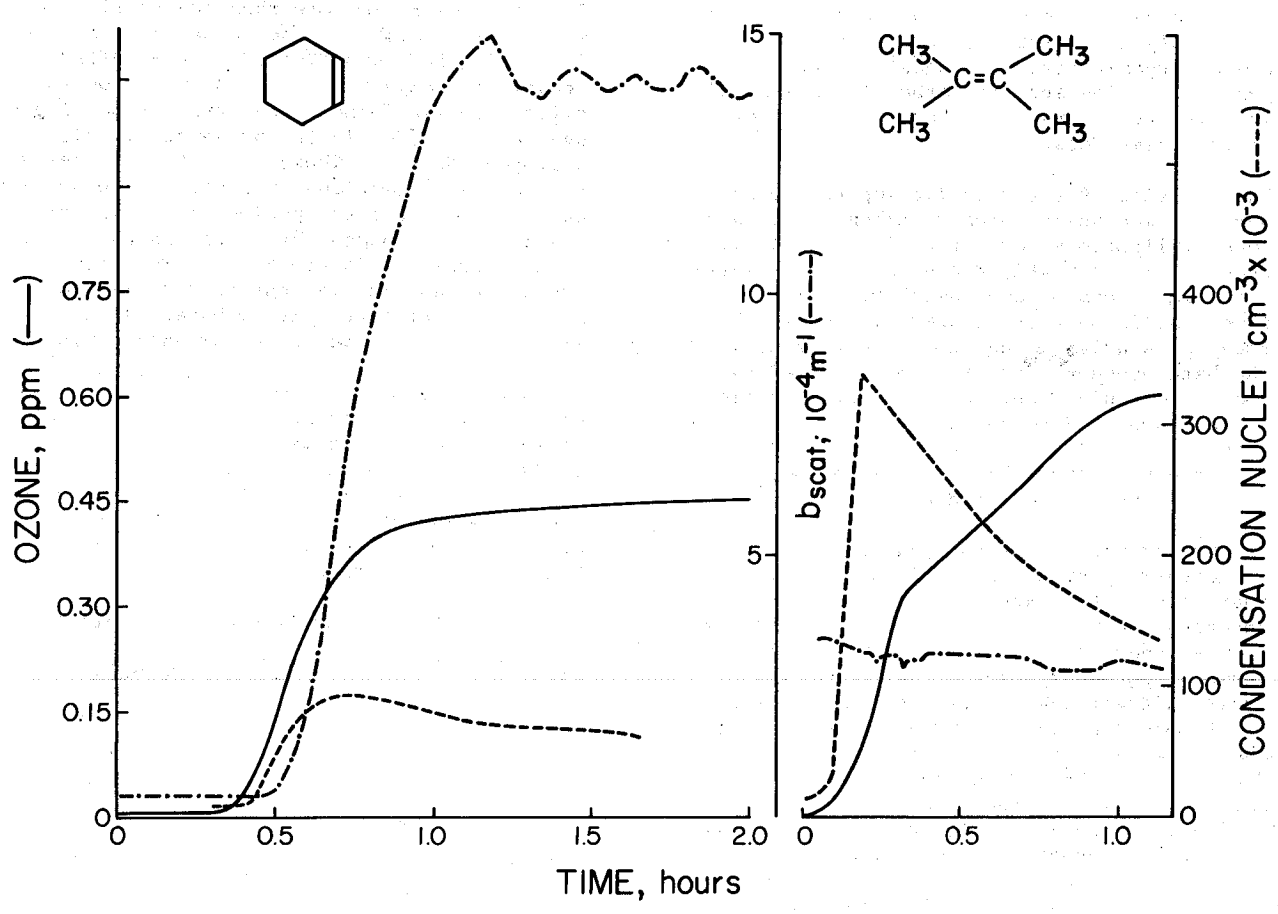

Fig. 1. Production of ozone, nuclei and light-scattering aerosols in outdoor smog chamber experiments with cyclohexene (left) and 2,3-dimethyl-2-butene (right). Initial concentrations: hydrocarbon, 1 ppm; NO, 0.33 ppm; NO_2, 0.16 ppm. From Grosjean[12].

ADDITION (SHOWN IN ORTHO): CRESOLS AND NITROTOLUENES

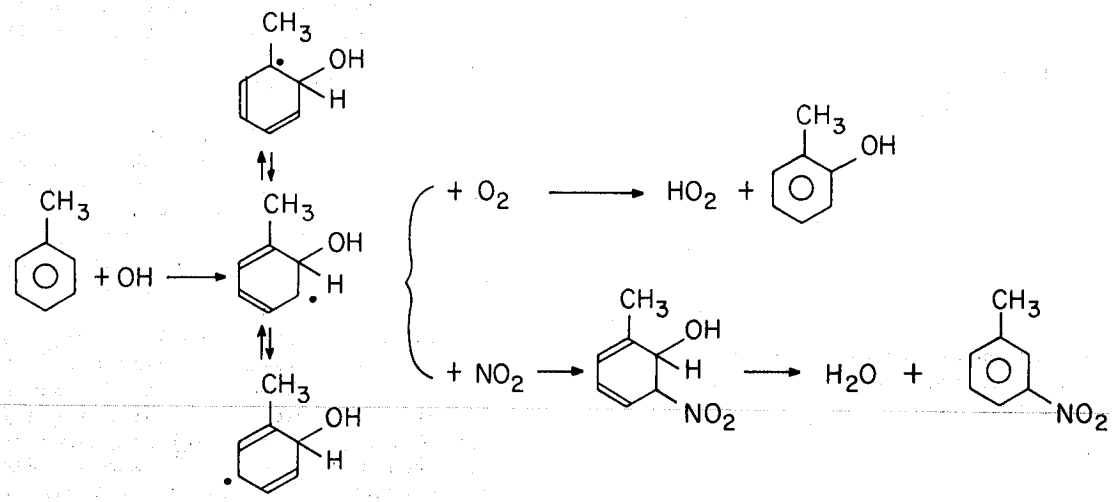

ABSTRACTION: BENZALDEHYDE

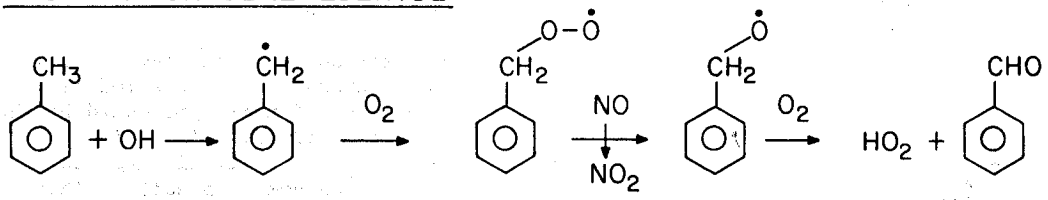

Fig. 2. Initial attack of OH on toluene: formation of cresols and nitrotoluenes. From Grosjean, Van Cauwenberghe, Fitz and Pitts.[16]

Table 2. Toluene Aerosol[a]

ACID FRACTION (MAJOR):

- Hydroxynitrocresols (4 isomers, M[b])
- Nitrocresols (4 isomers, 2M, 2m)
- Cresols (3 isomers, m)
- Benzoic acid (m)
- Hydroxybenzaldehyde (tentative, m)
- Phenol (t)

NEUTRAL FRACTION (MINOR):

- Benzaldehyde (m)
- Nitrotoluenes (ortho > para, m)
- Benzyl alcohol (t)
- MW = 110 (unidentified, 3 isomers, t)
- MW = 112 (unidentified, 2 isomers, t)

[a] From Grosjean, Van Cauwenberghe, Fitz and Pitts.[16]

[b] M = major, m = minor, t = trace.

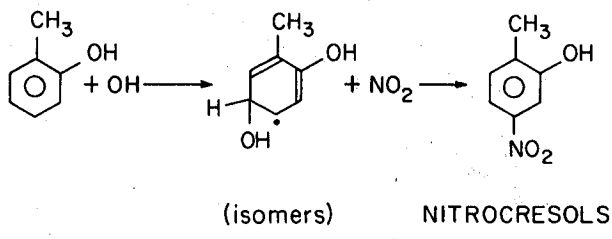

Fig. 3. Addition of OH on cresols and formation of nitrocresols. From ref. 16.

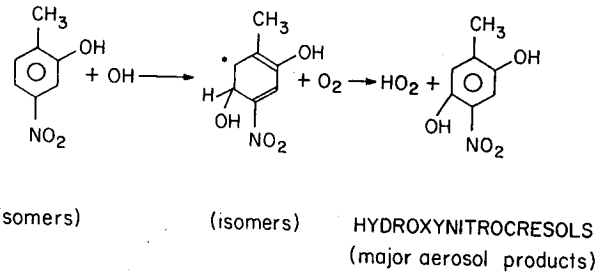

Fig. 4. Formation of hydroxy nitrocresols, the major toluene aerosol products. From ref. 16.

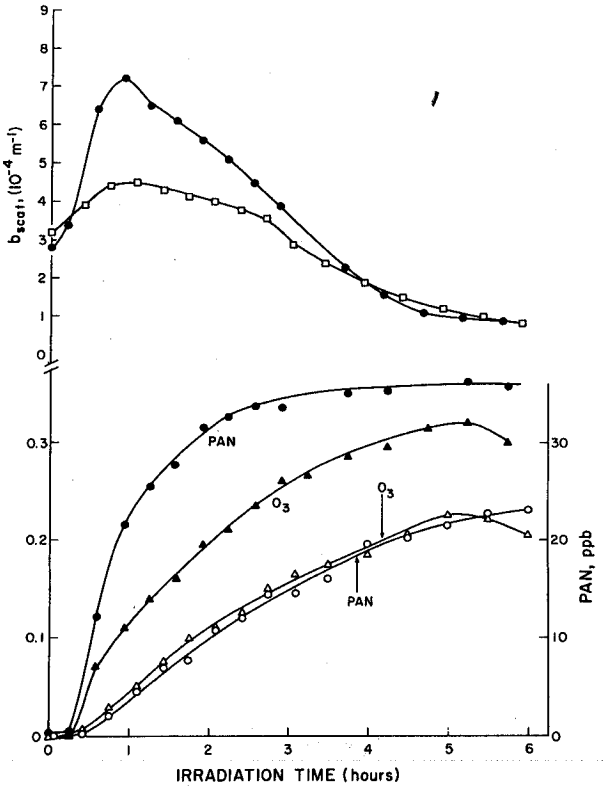

Fig. 5. Concentration-time profiles for O_3, PAN and b_{scat} during simultaneous irradiation of ambient air (open symbols) and ambient air + 0.1 ppm of DEHA (closed symbols) in a dual outdoor smog chamber, 14 October 1976, 10:00 to 16:00 PST. From Pitts, Smith, Fitz and Grosjean.[17]

aerosols were formed upon irradiation (Fig. 6). In the case of diethylamine (DEA) and triethylamine (TEA), the corresponding amine nitrate were found to be the major aerosol products. Acetamide was also found in both DEA and TEA aerosols.

Gas-Aerosol Interactions

Secondary organic aerosols may also be formed by reactions of gaseous pollutants with primary or secondary aerosol species. Reactions of this type, however, have received much less attention than those described in the previous paragraph. We have recently shown that the primary pollutant benzo(a)pyrene (BaP) deposited on a glass fiber filter reacts readily with ppm levels of ozone, peroxyacetyl nitrate (PAN) or NO_2 in air to form a variety of oxygenated products.[20] Similar reactions have been reported for BaP and other polycyclic aromatic hydrocarbons (PAH) adsorbed on other support material including alumina, soot, soil and silica gel.[21-24] Whether PAH adsorbed on the surface of airborne particles will react in a similar fashion in the atmosphere is still a matter of conjecture.

Gas-aerosol interactions involving secondary organic aerosols have received little attention. One reaction of this type would be that of ammonia with carboxylic acids (formed by reactions of olefins in photochemical smog) to form the corresponding ammonium salts. This reaction may explain in part the observed increase in light-scattering aerosols when adding ammonia to irradiated NO_x-1-octene mixtures in SAPRC's outdoor smog chamber.[25] Other possible reactions of this type may involve further oxidation, by O_3, nitric acid, etc., of aerosol oxygenates (alcohols, aldehydes) to the corresponding acids.

Reactions in the aerosol phase

Possible reactions of organic compounds with free radicals and with oxidizing species (O_3, $HONO_2$) in aqueous aerosol droplets have not been investigated experimentally. However, several studies have pointed out the possible importance of ambient aerosols as a sink for free radicals,[26,27] and an abundant literature is available concerning free radical and other oxidation reactions in the bulk aqueous phase.[28] Thus, further reactions of organics in the aerosol phase should not be overlooked. Such reactions may be responsible in part for the oxidation of 1,6 hexanedial to 6-oxo hexanoic acid and to adipic acid (Table 1) in cyclohexene aerosol.[15]

IDENTIFICATION OF SECONDARY ORGANIC AEROSOLS

Total organic carbon measurements

Measurements of the total (primary + secondary) aerosol organic carbon (AOC) concentration are generally carried out using solvent extraction[29] and/or combustion[29,30] techniques. Figure 7 shows the frequency distribution of 24-hour-averaged AOC concentrations in Riverside, CA, air, established from daily measurements made over a six-month period in 1975.[31] AOC levels

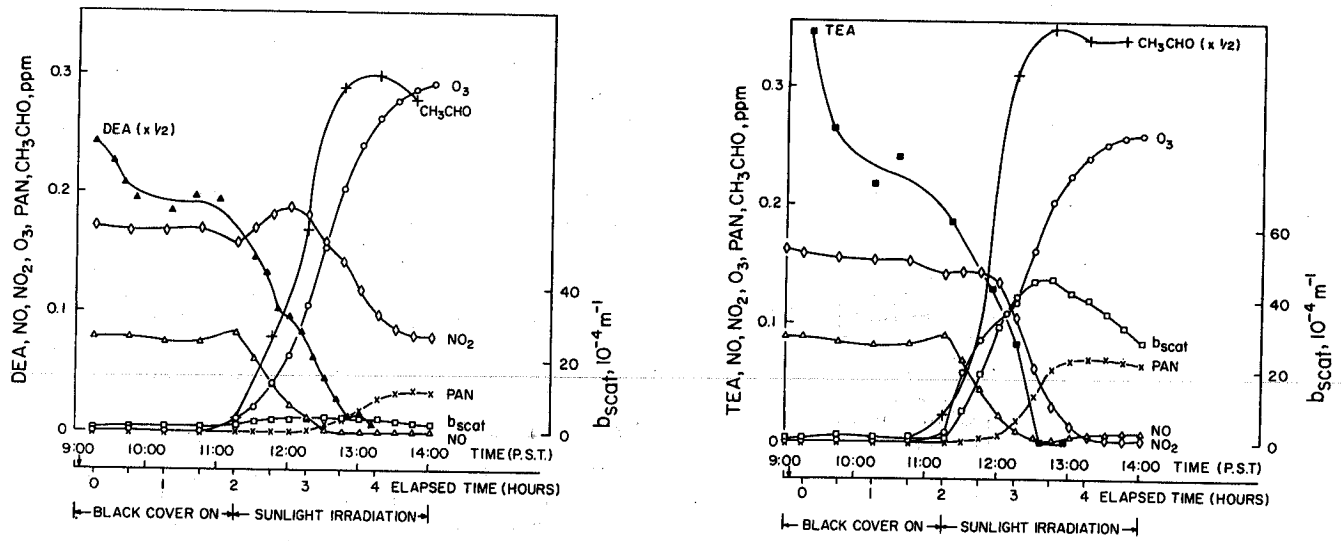

Fig. 6. Concentration-time profiles for amine, NO, NO_2, O_3, acetaldehyde and light-scattering aerosols (b_{scat}) in outdoor chamber studies conducted with diethylamine (DEA, left) and triethylamine (TEA,right). From ref. 18 and 19.

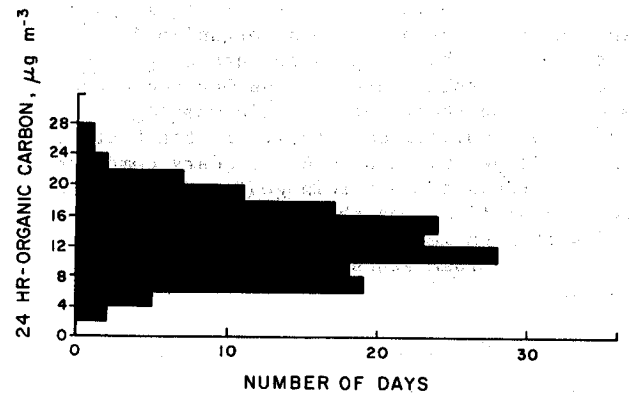

Fig. 7. Frequency distribution of 24 hr. averaged aerosol organic carbon concentrations in ambient Riverside, CA, air, from May 1 to October 31, 1975. From ref. 31.

in Southern California air have been the object of extensive measurements, including those performed as part of the Aerosol Characterization Experiment (ACHEX) study.[32,33] A breakdown into primary and secondary organics by selective extraction using solvents of increasing polarities[29] has also been recently attempted.[34]

Of increasing concern at the present time is the question of filter "artifacts," i.e., spurious retention of acidic organics gases on the basic surface of glass fiber filters and/or chemical reactions on the filter surface during sampling. Negative artifacts resulting from loss of relatively volatile aerosol organics during sampling are also of concern. Quantitative studies of organic artifact, similar to those recently conducted to investigate the formation of spurious sulfate[35] and nitrate[36] aerosol, are now in progress in several laboratories.

Molecular composition of secondary organic aerosols

In the past five years a systematic search for secondary organic aerosols has been initiated using modern analytical techniques such as mass spectrometry, combined gas chromatography-mass spectrometry and high performance liquid chromatography. The high resolution mass spectrometry-thermal analysis technique developed by Schueltze and coworkers[37,38] has proven most useful in this area.

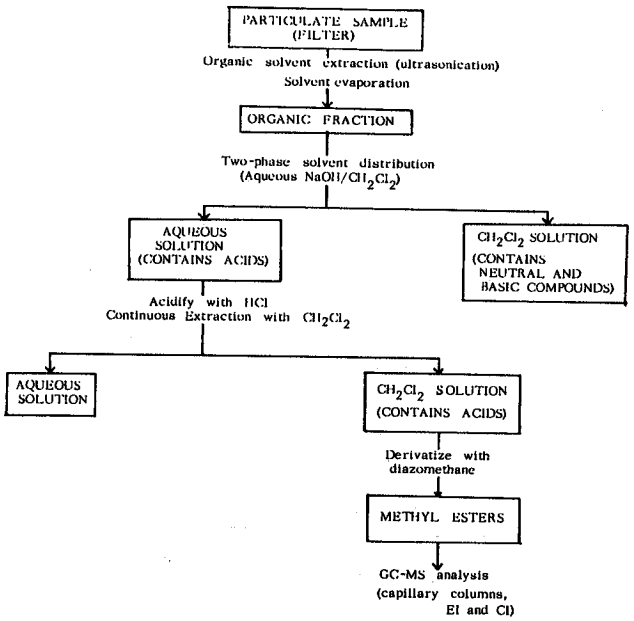

Fig. 8. Analytical protocol for GC-MS identification of carboxylic acids in ambient aerosols.

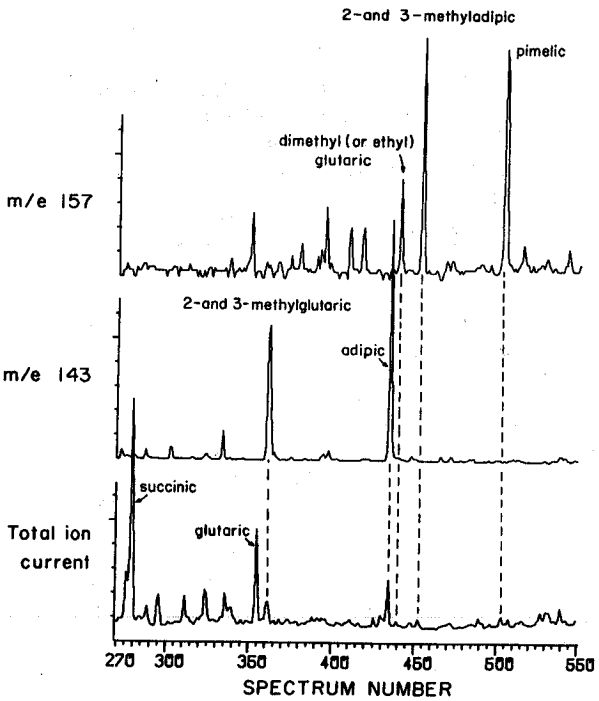

Fig. 9. Example of GC-MS analysis of dicarboxylic acid dimethyl esters using selective monitoring at m/e = 157 (esters of C_7 acids) and m/e = 143 (esters of C_6 acids). These major fragments result from the loss of a methoxy group in electron impact-MS ($M^{+\cdot}-OCH_3$) and from the loss of methanol in methane chemical ionization-MS ($MH-CH_3OH$).

Other studies include our recent analysis of the organic acid fraction of Riverside aerosols[39] using the extraction-fractionation-derivatization scheme outlined in Fig. 8. Using capillary column gas chromatography and both electron impact and chemical ionization mass spectrometry, we have identified 8 linear and 7 branched-chain dicarboxylic acids ranging from C_3 to C_{10} in ambient aerosols collected during photochemical smog episodes (Table 3 and Fig. 9).

The molecular composition of smog chamber and ambient aerosols, in which about one hundred secondary organics have been identified, has been recently reviewed.[12] It is likely that several hundred other secondary organic compounds still await identification.

SECONDARY ORGANIC AEROSOLS AND AIR QUALITY

Magnitude of the problem

The relative importance of secondary organic aerosols in the total particulate burden is extremely variable, ranging from very low in non-urban areas (and in those urban areas seldom subjected to photochemical pollution) to overwhelming in photochemically-polluted atmospheres such as the Los Angeles area.[6,9,10] Measurements of gas-to-particle distribution factors[9,40] indicate that, even during severe photochemical episodes, only a small fraction (≤3%) of the organic species emitted by pollution sources exists as aerosol organic carbon (Table 4).

Health Effects

Because of their accumulation in submicron particles, all aerosol organic compounds are potentially hazardous to human health. Moreover, organic extracts of airborne particulate matter are known to be carcinogenic in experimental animals,[41] and their mutagenic activity has been recently established.[11,20,42-45] However, although carcinogenicity has been found in oxygenated fractions of airborne organics,[46,47] most attention has focused to date on primary carcinogenic pollutants such as BaP and other PAH as well as on their heterocyclic homologs[41] (acridines, quinolines, etc.). To the best of our knowledge, not a single secondary compound has been shown to be carcinogenic or mutagenic at the present time, and the health hazards associated with high levels of secondary organic aerosols in urban atmospheres are virtually unknown.

Visibility Degradation

Studies available to date, which are limited to California aerosols,[46,47] indicate that the contribution of organic aerosols to the reduction of visibility in urban areas is small compared to that of inorganic species such as sulfates and nitrates. The reasons for this are not fully understood at the present time. The relatively "poor" light-scattering efficiency or organic aerosols may involve several factors such as refractive index, selective adsorption on amorphous material (soot) and generally hydrophobic

character retarding the growth into the size range of maximum light scattering efficiency.

RECOMMENDATIONS

It seems appropriate to conclude this brief review of the current status of research on secondary organic aerosols by stressing the need for further research in the following areas:

- chemical and physical characterization of aerosols formed in model systems (single HC precursor + NO_x in smog chamber), and application of the knowledge acquired in these studies to a better characterization of organic species in ambient aerosols.
- development of new sampling and analytical techniques, as well as optimization of the ones now available, in order to obtain information on both molecular composition and size distribution of organic aerosols.
- development of a comprehensive data base concerning the chemical nature, the physical properties and the rates of formation of organic aerosols. Such an experimental data base is now essential to improve the predictive ability of aerosol modeling techniques.
- Assessment of impact on health by combining chemical analysis and microbiological screening techniques to identify hazardous species. If such aerosol compounds (classes of compounds) are identified, selective control of their gas phase precursors could be implemented.

ACKNOWLEDGMENTS

I thank Dr. T. Novakov for his kind invitation to present this work at the Conference on Carbonaceous Particles in the Atmosphere, Berkeley, CA, March 20-22, 1978, and Dr. J. N. Pitts, Jr., for useful discussions during the preparation of this manuscript. Work performed at the California Institute of Technology was supported in part by the Environmental Protection Agency, Grant No. R802160. Work performed at SAPRC, U. C. Riverside was supported in part by the National Science Foundation, Research Applied to National Needs, Grants No. ENV73-02904-A03 and No. ENV73-02904-A04. The Contents do not necessarily reflect the views and policies of the sponsoring agencies, nor does mention of trade names or commercial products constitute endorsement or recommendation for use.

REFERENCES

1. H. Rosen, A. D. A. Hansen, R. L. Dod and T. Novakov, Paper No. 171, Proceedings of the 4th Joint Conference on Sensing of Environmental Pollutants, New Orleans, LA, Nov. 6-11, 1977, pp. 640-643.

2. H. Rosen and T. Novakov, Nature, 266, 708 (1977).

Table 3. Dicarboxylic acids identified in ambient particulate samples.[39]

linear, $HOOC-(CH_2)_n-COOH$	branched
n = 1 malonic	Me-malonic[a]
2 succinic	Me-succinic
3 glutaric	2-Me-glutaric
4 adipic	3-Me-glutaric
5 pimelic	di Me-glutaric[b]
6 suberic	2-Me-adipic
7 azelaic	3-Me-adipic
8 sebacic	

[a]Me = methyl; [b]isomer not specified.

Table 4. Organic Carbon Gas-Particle Distribution Factors (f_C) in Southern California[a]

1. Yearly average 1972[b]:

Southwestern-coastal area:	
West Los Angeles	1.0
Long Beach	1.1
Lennox	1.1
Central area:	
Los Angeles	2.2
Pasadena	2.2
Anaheim	1.9
Reseda	2.4
Inland area:	
Azusa	4.0
San Bernardino	3.1
Ontario	3.3
Chino	3.8

2. Pasadena, 7/25/73, 1 hr samples[c]:
1.6, 2.0, 3.6, 2.9, 0.9, 2.1, 3.8, 5.1, 6.1, 4.9, 2.0.

3. Riverside, 24 hr. size-resolved samples[d]:

day(1975)	f_C	f_C<0.6μ
8/15	2.05	0.73
8/22	3.09	1.29
8/26	3.05	1.38
9/2	3.53	1.50
9/12	2.71	0.77
9/13	3.07	0.56
9/14	2.64	0.69
9/15	2.47	0.82
9/21	3.40	1.57
9/28	1.82	0.54
10/1	3.43	1.19
10/2	3.31	1.38
10/17	3.08	1.61
10/18	3.49	1.09

[a]f_C = 100 x P/(P + G), where P = particulate organic carbon, μg carbon m^{-3}, and G = gas phase non-methane hydrocarbons, converted from ppm to μg carbon m^{-3}.

[b]From ref. 40.

[c]One hour samples collected from 6:30 to 17:30 PST during a severe photochemical smog episode. From ref. 9.

[d]From ref. 25, p. V-27.

3. A. D. A. Hansen, H. Rosen, R. L. Dod and T. Novakov, Paper No. 18, Conference on Carbonaceous Particles in the Atmosphere, Berkeley, CA, March 20-22, 1978.

4. T. Novakov, S. G. Chang and A. B. Harker, Science, 186, 259 (1974).

5. S. G. Chang and T. Novakov, Atmos. Environ., 9, 495 (1975).

6. G. Gartrell, Jr., and S. K. Friedlander, Atmos. Environ., 9, 279 (1975).

7. W. E. Wilson, Jr., W. E. Schwartz, and G. W. Kinzer, "Haze Formation--Its Nature and Origin," Battelle Columbus Laboratories, Columbus, Ohio, 1972.

8. R. J. O'Brien, J. H. Crabtree, J. R. Holmes, M. C. Hoggan, and A. H. Bockian, Environ. Sci. Technol., 9, 577 (1975).

9. D. Grosjean and S. K. Friedlander, J. Air Pollut. Control Assoc., 25, 1038 (1975).

10. S. L. Heisler and S. K. Friedlander, Atmos. Environ., 11, 157 (1977).

11. J. N. Pitts, Jr., K. A. Van Cauwenberghe, D. Grosjean, J. P. Schmid, D. R. Fitz, W. L. Belser, Jr., G. B. Knudson and P. M. Hynds, Paper No. 26, Conference on Carbonaceous Particles in the Atmosphere, Berkeley, CA, March 20-22, 1978.

12. D. Grosjean, "Aerosols," in Ozone and Other Photochemical Oxidants, National Academy of Sciences, Washington, D.C., 1977, Chapt. 3, pp. 45-125.

13. A. J. Haagen-Smit, Ind. Eng. Chem., 44, 1342 (1952).

14. W. Schwartz, "Chemical Characterization of Model Aerosols," U. S. Environmental Protection Agency Report No. EPA-650/3-74-011 (1974).

15. D. Grosjean, "Formation of Organic Aerosols from Cyclic Olefins and Diolefins," Chap. 19 in The Character and Origins of Smog Aerosol, G. M. Hidy et al, Edit., Adv. Environ. Sci. Technol., Wiley, New York, in press (1978).

16. D. Grosjean, K. Van Cauwenberghe, D. R. Fitz and J. N. Pitts, Jr., Photooxidation Products of Toluene-NO_x Mixtures Under Simulated Atmospheric Conditions," Paper No. ENVT. 115, Symposium on Chemical and Biological Implications of Nitrogenous Air Pollutants, 175th National American Chemical Society Meeting, Anaheim, CA, March 12-17, 1978. Div. Environ. Chem. Preprints, 18, No. 1, pp. 354-356.

17. J. N. Pitts, Jr., J. P. Smith, D. R. Fitz and D. Grosjean, Science, 197, 255 (1977).

18. D. Grosjean, K. A. Van Cauwenberghe, J. P. Schmid and J. N. Pitts, Jr., Paper No. 54, Proceedings of the Fourth Joint Conference on Sensing of Environmental Pollutants, New Orleans, LA, Nov. 6-11, 1977, pp. 196-199.

19. J. N. Pitts, Jr., D. Grosjean, K. A. Van Cauwenberghe, J. P. Schmid and D. R. Fitz, Environ. Sci. Technol., accepted for publication, March 1978.

20. J. N. Pitts, Jr., K. A. Van Cauwenberghe, D. Grosjean, J. P. Schmid, D. R. Fitz, W. L. Belser, Jr., G. B. Knudson and P. M. Hynds, Science, accepted for publication, June 1978.

21. H. L. Falk, I. Markul and P. Kotin, AMA Arch. Ind. Health, 13, 13 (1956).

22. G. Kortum and W. Braun, Justus Liebigs Ann. Chem., 632, 104 (1960).

23. A. J. Fatiadi, Environ. Sci. Technol., 1, 570 (1967).

24. B. D. Tebbens, M. Mukai and J. F. Thomas, J. Am. Ind. Hyg. Assoc., 32, 365 (1971).

25. J. N. Pitts, Jr., D. Grosjean, A. M. Winer, A. C. Lloyd and G. J. Doyle, Chemical Transformations in Photochemical Smog and their Applications to Air Pollution Control Strategies," Third Annual Progress Report to the National Science Foundation, NSF-RANN Grant ENV73-02904 A03, 1977.

26. R. E. Graedel, L. A. Farrow and T. A. Weber, Int. J. Chem. Kinetics Symp. 1, 581 (1975).

27. H. S. Judeikis and S. Siegel, Atmos. Environ., 7, 619 (1973).

28. L. M. Dorfman and G. E. Adams, "Reactivity of the Hydroxyl Radical in Aqueous Solutions," National Bureau of Standards Pub. No. NSRDS-NBS 46, U. S. Govt. Printing Office, Washington, D.C., June 1973.

29. D. Grosjean, Anal. Chem., 47, 797 (1975).

30. J. J. Huntzicker and R. L. Johnson, Paper No. 2, Conference on Carbonaceous Particles in the Atmosphere, Berkeley, CA, March 20-22, 1978.

31. J. N. Pitts, Jr., D. Grosjean, B. Shortridge, G. J. Doyle, J. P. Smith, T. M. Mischke and D. R. Fitz, Paper No. ENVT-1, Symposium "Chemistry of Air Pollutants--1976," American Chemical Society Centennial Meeting, New York, N.Y., April 4-9, 1976; Div. of Environ. Chem. Preprints, 16, No. 1, pp. 1-3 (1976).

32. G. M. Hidy, B. R. Appel, R. J. Charlson, W. E. Clark, S. K. Friedlander, D. H. Hutchinson, T. B. Smith, J. Suder, J. J. Wesolowski, K. T. Whitby and P. K. Mueller, J. Air Pollut. Control Assoc., 25, 1106 (1975).

33. B. R. Appel, P. Colodny and J. J. Wesolowski, Environ. Sci. Technol., 10, 359 (1976).

34. R. B. Appel, E. M. Hoffer, M. Haik, S. M. Wall and E. L. Kothny, "Characterization of Organic Particulate Matter," National Technical Information Service Report No. PB-279 209/1WP, July 1977.

35. R. W. Coutant, Environ. Sci. Technol., 11, 873 (1977).

36. C. W. Spicer and P. M. Schumacher, Atmos. Environ., 11, 873 (1977).

37. D. Schueltzle, A. L. Crittenden and R. J. Charlson, J. Air Pollut. Control Assoc., 23, 704 (1973).

38. D. Schueltzle, D. Cronn, A. L. Crittenden and R. J. Charlson, Environ. Sci. Technol., 9, 838 (1975).

39. D. Grosjean, K. Van Cauwenberghe, J. P. Schmid, P. E. Kelley and J. N. Pitts, Jr., Environ. Sci. Technol., 12, 313 (1978).

40. D. Grosjean, J. P. Smith, T. M. Mischke and J. N. Pitts, Jr., "Chemical and Physical Transformations in Urban-Suburban Transport of Air Pollutants" in Atmospheric Pollution, M. M. Benarie, Ed., Elsevier, Amsterdam, 1976, pp. 549-563.

41. D. Hoffman and E. L. Wynder, in Air Pollution, Vol. II, Third Ed., A. C. Stern, Ed., Academic Press, New York, 1977, pp. 361-455.

42. J. N. Pitts, Jr., D. Grosjean, T. M. Mischke, V. F. Simmon and D. Poole, Toxicol. Lett., 1, 65 (1977).

43. H. Tokiwa, H. Tokeyoshi, K. Morita, K. Takohashi, N. Soruta and Y. Ohnishi, Mutation Res., 38, 351 (1976).

44. R. Talcott and E. Wei, J. Nat. Cancer Inst., 58, 449 (1977).

45. J. M. Daisey, I. Hawryluk, T. J. Kneip and F. H. Mukai, Paper No. 28, Conference on Carbonaceous Particles in the Atmosphere, Berkeley, CA, March 20-22, 1978.

46. W. H. White and P. T. Roberts, Atmos. Environ. 11, 803 (1977).

47. D. Grosjean, G. J. Doyle, T. M. Mischke, M. P. Poe, D. R. Fitz, J. P. Smith and J. N. Pitts, Jr., Paper No. 76-20.3, 69th Air Pollut. Control Assoc. Annual Meeting, Portland, OR, June 27-July 1, 1976.

OPTICAL CHARACTERIZATION OF AMBIENT AND SOURCE PARTICULATES

A.D.A. Hansen, H. Rosen, R.L. Dod, and T. Novakov
Lawrence Berkeley Laboratory
University of California
Berkeley, California 94720

ABSTRACT

The high optical absorptivity of urban particulates is used as a tracer for the "graphitic" component of the carbonaceous aerosol. The results of the analyses of over 900 ambient samples collected over a wide range of atmospheric conditions show a strong correlation between the "graphitic" and the total carbon content of the aerosol. No systematic difference in the correlation is observed under conditions of high or low ozone, indicating that ozone-related reactions do not produce substantial quantities of secondary particulates. A comparison between these measurements and similar measurements on sources indicates that a major component of the urban carbonaceous aerosol is due to primary emissions.

INTRODUCTION

Characterization of the ambient carbonaceous aerosol in terms of its primary and secondary components is essential if meaningful control strategies are to be devised. Primary carbonaceous particulate material is defined as that emitted directly from anthropogenic sources, usually combustion. It contains extractable organic matter and nonextractable material, including "graphitic" soot. Secondary carbonaceous particulate material is material originally emitted in a gaseous state that has been transformed into a particulate state by atmospheric processes. Examples of these processes are (1) the accretion by adsorption of vapors onto the surface of primary particles, and (2) gas-to-particle conversion reactions whose occurrence in the atmosphere has been postulated under highly photochemically active conditions. If primary particulate material is dominant in the ambient aerosol, then particulate air pollution abatement strategies should include particulate emission control. If secondary particulate material dominates, emphasis should be on the control of the gaseous precursors involved in these secondary reactions. Due to the complex nature of the ambient aerosol, it has been a difficult analytical problem to clearly distinguish the contributions from these two sources of particulate carbon.

The most striking feature of filter deposits collected in urban environments is their dark coloration, which we believe is due to the strongly absorbing primary "graphitic" soot component. We assume that secondary reactions cannot produce this material. The "graphitic" component of filter-collected particulates may be conveniently measured because of its large optical absorption and used as a tracer for primary carbonaceous particles. In this paper we report on the optical characterization of a statistically large number of ambient and source samples taken under a wide range of conditions.

Our central result is that primary material appears to compose a major fraction of the ambient carbonaceous aerosol studied in two California air basins under widely varying conditions. Furthermore, we have seen no evidence for the significant production of secondary carbonaceous particulate matter in correlation with the ozone concentration, a conventional indicator of photochemical activity.

EXPERIMENTAL DETAILS

Sample Collection

Ambient aerosol samples have been collected daily since 1 June 1977 at Lawrence Berkeley Laboratory, Berkeley, California; since 15 July 1977, at the Bay Area Air Quality Management District monitoring station, Fremont, California; and since 19 August 1977, at the South Coast Air Quality Management District monitoring station, Anaheim, California. Samples were also taken from 23 March 1978 to 9 April 1978 at Argonne, Illinois. All these samples were taken in parallel on 47-mm diameter Millipore filter membranes (1.2-μm nominal pore size, type RATF) and prefired quartz fiber filters (Pallflex type 2500 QAO). The monitored flow rates varied between 1.0 and 2.6 m^3/cm^2-day (i.e., 0.24 to 0.62 CFM for the total exposed filter area of 9.6 cm^2), corresponding to face velocities of 11.6 to 30.1 cm/sec. The samples were not size segregated, but the filter holders faced vertically downward to avoid settling deposition of dust, etc. Three-day samples collected over each weekend are not included in the data presented. The samples spanned almost the entire range of weather and pollution conditions. To date, in excess of 900 filter pairs have been analyzed.

A number of representative sources have also been sampled. About 100 analyses have been made of the following particulate emissions: (1) exhaust collected in a freeway tunnel under conditions of moving traffic with few diesel trucks; (2) automobile exhaust collected in an underground parking garage under start-stop driving conditions with no diesel trucks; (3) exhaust from a small 2-stroke engine; (4) exhaust from a small 4-stroke diesel engine; and (5) stack samples from a natural-gas-fired domestic water heater.

Optical Attenuation Measurement

Both source and ambient aerosol samples have a large and uniform optical absorption throughout the visible spectral region; the dark coloration

of the exposed filters is due to the "graphitic" soot component.[1,2] The attenuation measurements are made by a laser transmission method on samples collected on Millipore filter membranes. The quantity recorded is defined as

$$ATN = -100 \ln (I/I_0) \quad (1)$$

where I_0 is the intensity of light transmitted through a blank Millipore filter, and I is that through the loaded filter.

Carbon Analysis

The carbon loading on the quartz fiber filters is determined by a total combustion/CO_2 evaluation method.[3] The filters are prefired overnight at 800°C to remove all combustible carbon before sample collection. Periodic analysis of blanks typically yields about 0.5 μg C/cm^2 compared with loadings after exposure in the range 20-100 μg C/cm^2.

OPTICAL ATTENUATION CHARACTERIZATION

Theory

As shown in Refs. 1 and 2, the dark coloration of ambient and source samples can be ascribed to the "graphitic" component of the carbonaceous particulates. We assume that a quantitative relationship between the optical attenuation and the "graphitic" carbon component can be written as

$$[GRAPH] = (1/K) \times ATN \ . \quad (2)$$

In addition to "graphitic" soot, primary particulate material also contains organic material, which is not strongly optically attenuating. The total amount of carbon is

$$[C] = [GRAPH] + [ORG] \ . \quad (3)$$

A fundamental characterization of a particulate sample is given by its attenuation per unit mass, i.e., its specific attenuation, σ, since this is a measure of the fraction of "graphitic" carbon to total carbon:

$$\sigma \equiv ATN/C = K \times [GRAPH]/[C] \ . \quad (4)$$

Measurements of the specific attenuation of numbers of source samples give insights into the relative graphitic-to-total-carbon fraction of primary emissions and the source variabilities.

The ambient aerosol contains primary carbonaceous particulates from a large number of individual sources and secondary material (as defined in the introduction). The total optical attenuation and total particulate carbon mass are then given by a summation over all components, i.e.,

$$ATN_T = \sum_i ATN_i \quad (5)$$

$$C_T = \sum_i C_i$$

and the specific attenuation of the ambient sample is

$$\sigma_T = (ATN/C)_T = \frac{\sum_i ATN_i}{\sum_i C_i} = \frac{\sum_i \sigma_i C_i}{\sum_i C_i} \ . \quad (6)$$

In other words, the specific attenuation of an ambient sample is an average of the specific attenuations of all its components, weighted according to the mass of carbon they each contribute.

Secondary material will not contain a "graphitic" component and therefore should not appreciably increase the total optical attenuation; its value of σ is very small. However, it does increase the total mass of carbon, and will therefore reduce the graphitic-to-total-carbon fraction and dilute the specific attenuation of the ambient sample. This is seen in Equ. (6) as the addition of secondary contributors, is, where σ_{is} is zero but C_{is} is non-zero. The presence of large amounts of secondary carbonaceous particulate material in the ambient aerosol will have the effect of reducing the specific attenuation of ambient samples relative to that of source samples.

Results

Results on Source Samples. We first present quantitative support for the assumption of Equ. (2) that the optical attenuation of a particulate sample collected on a filter (i.e., the degree of its dark coloration) is proportional to the total carbon loading. This occurs if the "graphitic" soot component, responsible for the coloration, constitutes a constant fraction of the total amount of particulate carbon. Figure 1 shows results from one series of samples taken from a small diesel engine under identical load and speed conditions. The correlation between optical attenuation and total carbon loading is extremely good (r = 0.99) even up to heavy loadings, giving a constant specific attenuation of σ = 5.6. In contrast, Fig. 2 shows the results for a number of freeway tunnel samples spanning a wide range of traffic conditions. Although a similar correlation obviously exists, it is clear that the specific attenuation of these samples shows a greater variability (ranging from σ = 3.75 to σ = 12.5). We postulate that this is due to a varying fraction of "graphitic" soot to total particulate carbon in the mix of exhaust, depending on the mix of vehicles and driving conditions. Similar results have been obtained for the other sources: in all cases, samples of different loadings taken under identical source conditions show good correlation, while samples of mixed composition show variability.

Results on Ambient Samples. In view of the variability of specific attenuation shown by source samples, the uniformity of results obtained from ambient samples is remarkable. Figure 3 shows optical attenuation vs. carbon loading for the samples collected at Berkeley, Fremont, Anaheim, and Argonne. All the graphs have the same scale of axes, enabling direct comparison and determination of the following very important results:

1. There is a strong correlation (r > 0.85) between optical attenuation and total suspended particulate carbon mass at every site.
2. The mean specific attenuation, i.e., the

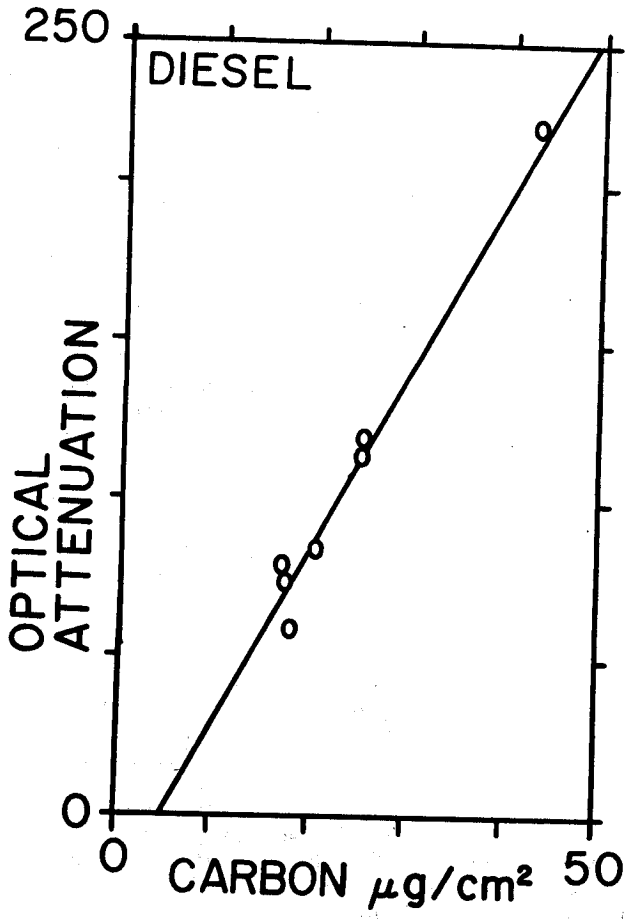

XBL 788-9881

Fig. 1. Optical attenuation versus carbon loading for samples of diesel exhaust particulates from an engine running at constant speed under constant load. Least-squares fit line shown.

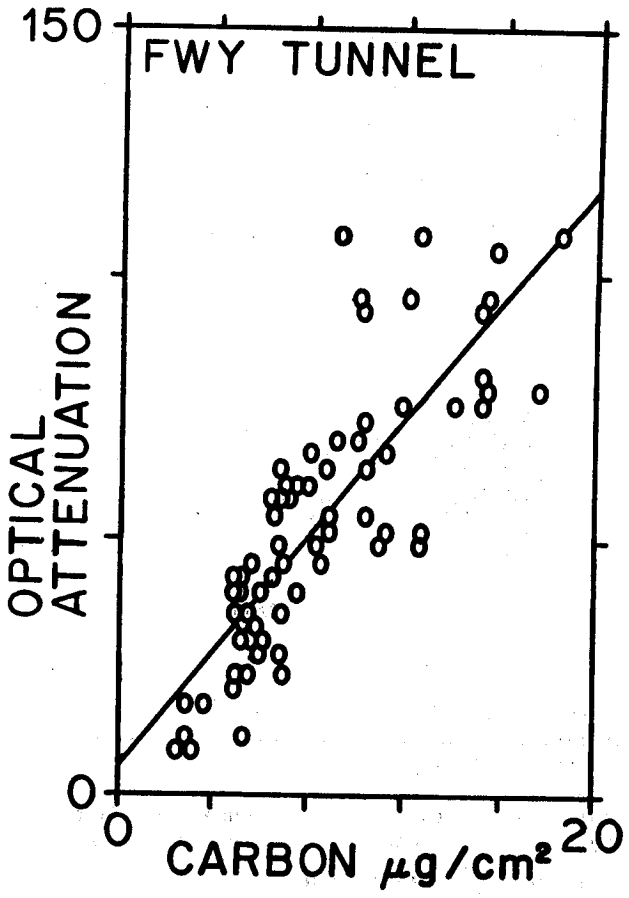

XBL 788-9882

Fig. 2. Optical attenuation versus carbon loading for samples of vehicle exhaust particulates obtained in the vent bore of a freeway tunnel. Least-squares fit line shown.

coefficient of this proportionality, is virtually identical at each site.

DISCUSSION

Source and Ambient Samples' Specific Attenuation Results

The diesel source results show that the method of optical attenuation can indeed be used as an accurate quantitative measure of total particulate carbon mass for samples from individual sources under constant operating conditions, i.e., a presumed constant fraction of "graphitic" soot to total particulate carbon. The freeway tunnel results show that the net value of σ_T for an aerosol derived from many sources can vary according to the mix of contributions (C_i) and characteristics (σ_i) of each source. The ambient air contains material from a very large number of primary and secondary sources covering the entire spectrum of "graphitic" content (i.e., of σ); if the patterns of daily input remain approximately constant, the net composition of our 24-hour samples may also remain constant. This, we believe, is the basic explanation for the results obtained from the ambient sampling program. Result (1) shows that for a particular site it is possible to estimate the amount of total suspended particulate carbon with a root mean square error of 25% by means of the simple measurement of optical attenuation. Furthermore, this is true independent of season, meteorology, or conventional air pollution indicators. This remarkable result implies that the fraction of "graphitic" soot to total particulate carbon is approximately constant under all circumstances studied.

The specific attenuation distribution of samples collected during summer pollution episodes in Anaheim is virtually identical to that of samples collected in Berkeley on extremely clear winter days or in Argonne in winter, although the loading of these samples varied widely (from 2.9 μg C/m^3 to 52.4 μg C/m^3). Because the specific attenuation σ reflects only the aerosol's fractional "graphitic" composition, this result implies that the fraction

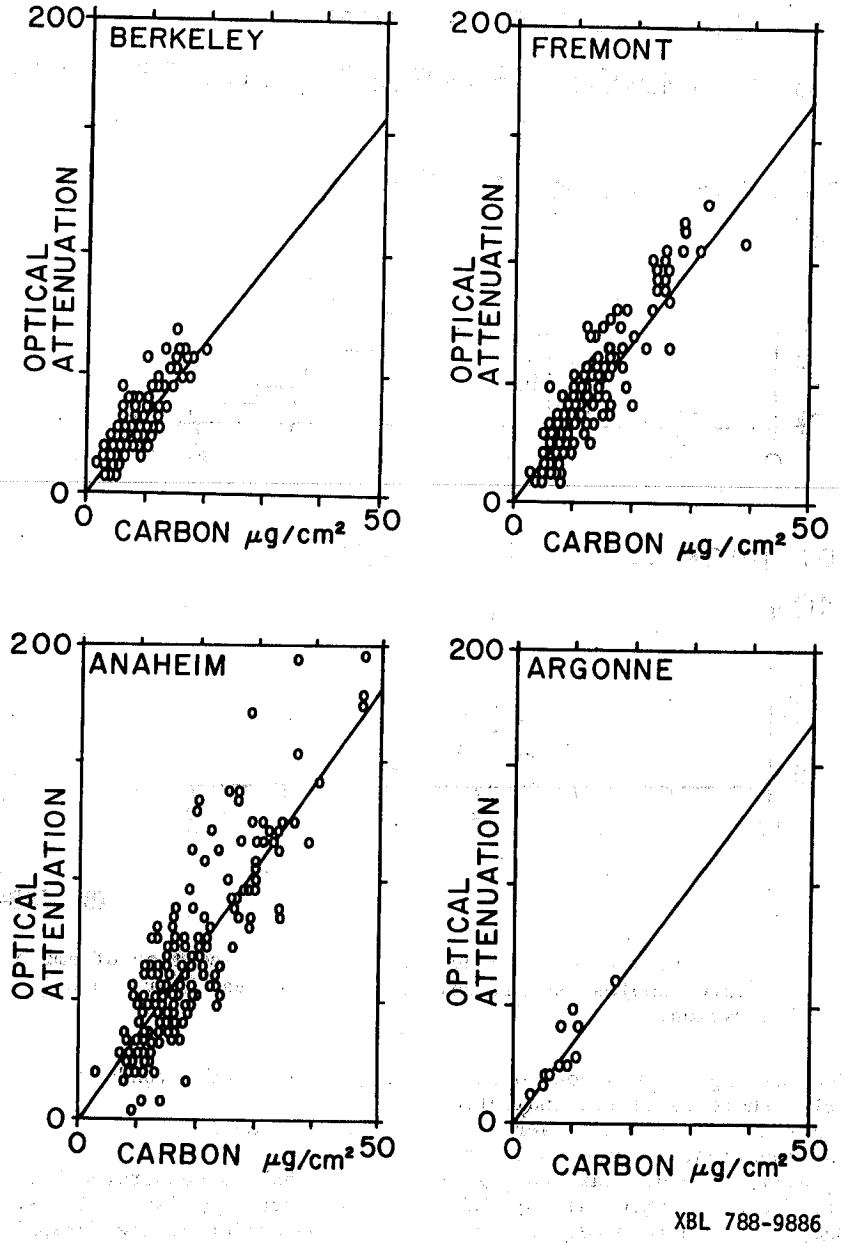

Fig. 3. Optical attenuation versus particulate carbon loading for ambient samples collected at Berkeley, Fremont, Anaheim, and Argonne. Least-squares fit line shown. Note same scale of axes of graphs.

of "graphitic" soot to total carbon in all these locations is approximately equal and constant.

The range of values of specific attenuation measured on ambient samples is overlapped by the range measured on source samples. This suggests that a major fraction of the ambient aerosol is due to primary emissions.

Secondary Particulate Carbon

The category of secondary carbon includes particulates formed from precursor gases in gas-to-particle conversion reactions in the atmosphere. Most of the proposed reactions responsible for the formation of secondary organic particles involve ozone as a reactant. If ozone-related atmospheric reactions are a substantial contributor of secondary particulate carbonaceous material in the ambient aerosol, we would expect larger contributions of this material on days characterized by higher ozone concentrations. This secondary material cannot contain a "graphitic" component and so would have a low specific attenuation, thereby diluting the total ambient aerosol's attenuation. The specific attenuation of the ambient aerosol on days characterized by high ozone levels would be expected to be lower than on days with low ozone levels.

Figure 4 shows the distribution of specific attenuation of ambient samples from all sites taken

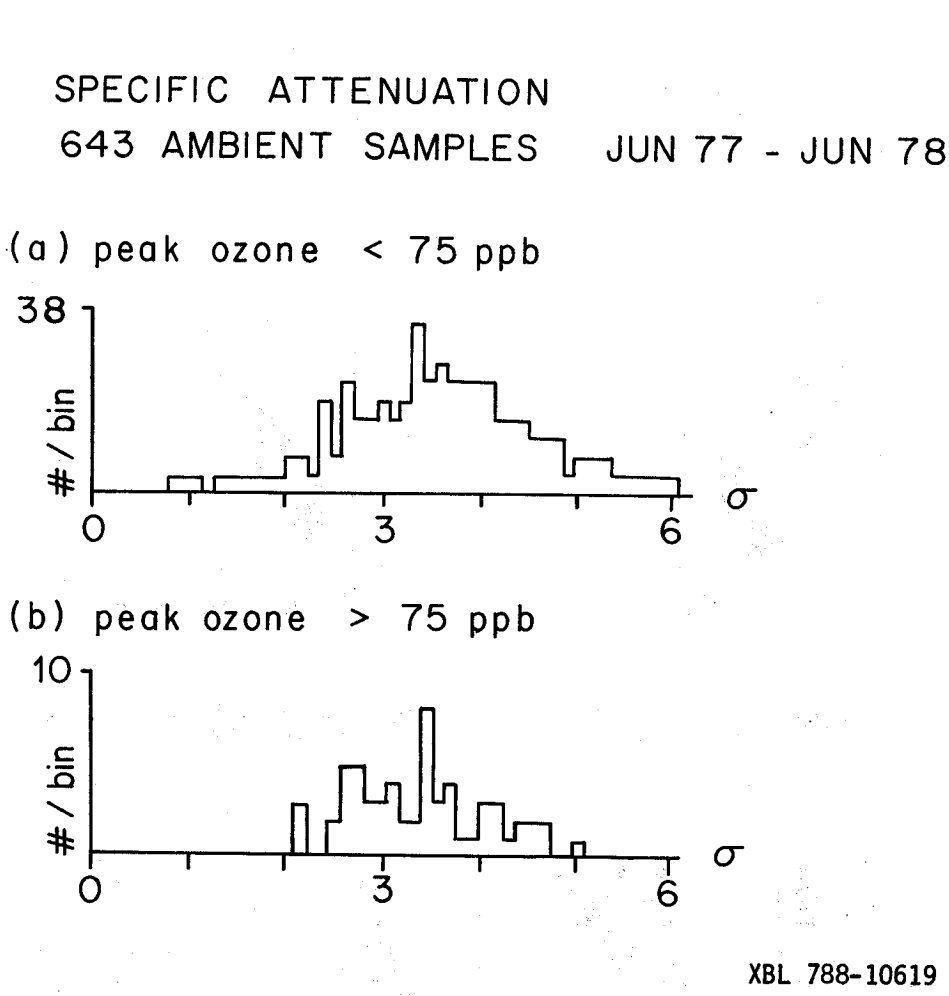

Fig. 4. Distribution of values of specific attenuation of ambient particulate samples, subdivided according to peak hour ozone concentration.

together, subdivided according to peak hour ozone concentration. Clearly, there is little indication that high-ozone days are characterized by aerosols of strongly diluted attenuation. Furthermore, the maximum correlation coefficients of peak hour ozone concentration and specific attenuation at any individual site or all samples taken together are only $r = 0.24$ and $r = 0.11$ respectively. This places a rather low limit on the maximum importance of secondary carbonaceous particulates formed in ozone-related atmospheric reactions.

Figure 5 shows the average diurnal cycles of specific attenuation for samples collected at the same time of year in Berkeley (relatively clean conditions, average particulate carbon loading 5.7 $\mu g/m^3$) and Riverside, California (severe air pollution conditions, 33.2 $\mu g/m^3$ average particulate carbon loading). These cycles, averaged over many days, are essentially identical in form and magnitude in spite of very different atmospheric chemical conditions at the two sites, including an average peak 1-hr ozone concentration of 240 ppb in Riverside vs. < 30 ppb in Berkeley. Certainly there is no evidence for the dilution of the specific attenuation of the Riverside aerosol relative to the Berkeley aerosol that would be expected if high ozone levels were associated with significant production of secondary particulate carbon.

CONCLUSIONS

We have demonstrated that the optical attenuation technique is a valid semiquantitative method for detection of the "graphitic" soot component of ambient aerosols, and that this component is an approximately constant fraction of the total suspended carbonaceous particulate loading under the atmospheric conditions so far encountered at widely differing sites. We find that this "graphitic" fraction of the ambient aerosol is comparable to that of representative source emissions. We also find a lack of evidence for the substantial production of carbonaceous particulates from gaseous precursors in atmospheres characterized by high ozone levels. Unless we can find secondary reaction mechanisms (1) that are not accompanied by ozone formation, (2) that are independent of location, season, or meteorology, and (3) whose contribution to the total ambient aerosol mass is linked to the primary particulate loading (in order to maintain a constant composition fraction), the results obtained from our ambient sampling programs so far indicate that primary particulates constitute a major fraction of the ambient carbonaceous aerosol in the two California air basins we have studied.

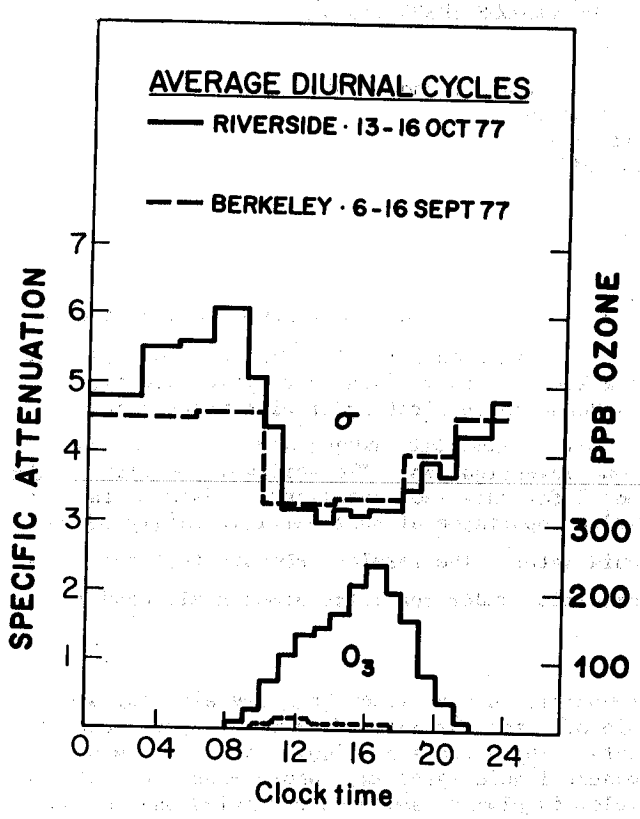

Fig. 5. Average diurnal cycles of specific attenuation and ozone concentration at Berkeley and Riverside.

ACKNOWLEDGMENTS

We would like to express our thanks to the following for their assistance and cooperation with the sampling program:

Dr. Paul Cunningham, Dr. Romesh Kumar, and Dr. Stanley Johnson, Argonne National Laboratory

The Bay Area Air Quality Management District and the South Coast Air Quality Management District

Mr. E.R. Mayo, Highway Superintendent, California State Department of Transportation, Caldecott Tunnel

Mr. K.M. Hagerty, Assistant Manager, University of California Parking Services Administration

REFERENCES

1. H. Rosen, A.D.A. Hansen, L. Gundel, and T. Novakov, "Identification of the graphitic carbon component of source and ambient particulates by Raman spectroscopy and an optical attenuation technique," Conference on Carbonaceous Particles in the Atmosphere, Proceedings, Lawrence Berkeley Laboratory, Berkeley, California (1979).
2. H. Rosen, A.D.A. Hansen, L. Gundel, and T. Novakov, "Identification of the optically absorbing component in urban aerosols," Applied Optics 17, 3859 (1978).
3. P.K. Mueller, R.W. Mosley, and L.B. Pierce, "Carbonate and non-carbonate carbon in atmospheric particulates," Second International Clean Air Congress, Proceedings (New York, Academic Press, 1971).

CATALYTIC OXIDATION OF SO_2 ON CARBON IN AQUEOUS SUSPENSIONS

S.-G. Chang, R. Brodzinsky, R. Toossi, S. S. Markowitz, and T. Novakov
Lawrence Berkeley Laboratory
University of California
Berkeley, California 94720

ABSTRACT

Combustion-produced soot particles are efficient catalysts for SO_2 oxidation, especially when surrounded by a layer of liquid water. Liquid water may dissolve the species formed on particle surfaces and thus regenerate the catalytically active sites. We have carried out a kinetic study of the catalytic oxidation of SO_2 on soot particles suspended in water. The reaction was found to be first order with respect to the concentration of carbon, 0.69^{th} order with respect to dissolved oxygen, and independent of the concentration of sulfurous acid and the pH under the conditions of our investigation. The activation energy of the reaction is 11.7 kcal/mole. A four-step mechanism is proposed for this soot-catalyzed oxidation reaction. A box-type calculation was carried out to compare the relative importance of soot-particle-catalyzed SO_2 oxidation with other SO_2 oxidation reactions involving liquid water. The results indicate that the soot-catalyzed reaction can be the dominant mechanism for SO_2 oxidation under realistic atmospheric conditions.

INTRODUCTION

During the early days of environmental awareness, primary particulate emissions were easily visible. Smoke (or soot) was the first air pollutant to be recognized and controlled. In more recent time, improvements in combustion technology and use of better-grade fuels have led to a substantial reduction of visible smoke emissions. Nevertheless, there is considerable evidence[1-4] that primary soot particles are still very important contributors to atmospheric pollution in California and elsewhere.

Soot particles, a major constituent of ambient particles, are also catalytically and surface chemically active material. For example, Novakov et al.[1,5] have shown by photoelectron spectroscopy that SO_2 oxidation to sulfate can be catalyzed by combustion-generated soot particles. They reached the following conclusions:

1. Soot-catalyzed oxidation of SO_2 is more efficient at a higher humidity.
2. The oxygen in air plays an important role in SO_2 oxidation.
3. Soot-catalyzed oxidation exhibits a saturation effect.
4. The saturation level of sulfate produced is probably related to such properties of soot particles as size, active surface area, and adsorbed surface oxygen.
5. The sulfate produced on soot particles is water soluble and contributes to the acidification of the solution.
6. SO_2 can be oxidized on other types of graphitic carbonaceous particles, such as ground graphite particles and activated carbon.

Although these authors have shown that the soot-catalyzed oxidation of SO_2 is more efficient in prehumidified air rather than dry air, the specific role of water was not made clear in their experiments. The effects of liquid water are important because liquid water may condense on the soot particles in plumes, and soot particles may encounter liquid water in their passage through fogs and clouds. Also, hygroscopic and deliquescent materials associated with soot particles may hold significant amounts of liquid water, even at a comparatively low relative humidity.[6]

We recently extended this research on the role of soot particles as catalysts for SO_2 oxidation by studying the effect of liquid water on the soot-catalyzed reaction. In this paper, we present a reaction rate law and propose a reaction mechanism for the catalytic oxidation of SO_2 on soot particles in an aqueous suspension. We also compare the soot-particle-catalyzed reaction with other reactions involving liquid water.

EXPERIMENTAL METHODS AND RESULTS

The reaction was studied in systems containing various concentrations of sulfurous acid and suspended carbonaceous particles. The carbon concentrations used in the suspensions ranged from 0.005% to 0.32% by weight, and the sulfurous acid concentration ranged from 1.5×10^{-4}M to 1.00×10^{-3} M. The concentration of sulfurous acid was monitored using iodometric titrations during the course of the reaction. In some selected runs, the concentration of sulfuric acid was followed by the turbidimetric method. Soot produced by the combustion of acetylene and natural gas, as well as that produced by a diesel engine, were collected by impinging the effluent into water, and were used in this study and found to be efficient catalysts.

Figure 1 shows the typical reaction curves of the oxidation of H_2SO_3 by dissolved oxygen in

aqueous suspensions of soot particles collected from acetylene and natural gas flames. The reaction occurs in two steps. The rate of the initial disappearance of H_2SO_3 is so fast that it could not be followed by the analytical technique used. The second process is characterized by a much slower linear reduction of H_2SO_3. The results obtained with these combustion-produced soot were essentially reproduced (Fig. 2) by suspensions of similar concentrations of activated carbon[7] (Nuchar C-190).[8] Figure 2 also shows that there is a mass balance between the sulfurous acid consumed and the sulfuric acid produced. Since it is difficult to reproducibly prepare soot suspensions, suspensions of Nuchar were used as a model system.

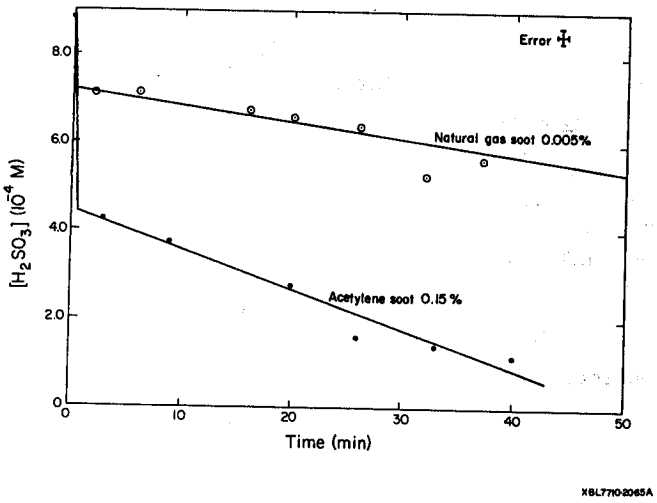

Fig. 1. H_2SO_3 concentration as a function of time for acetylene and natural gas soot suspensions.

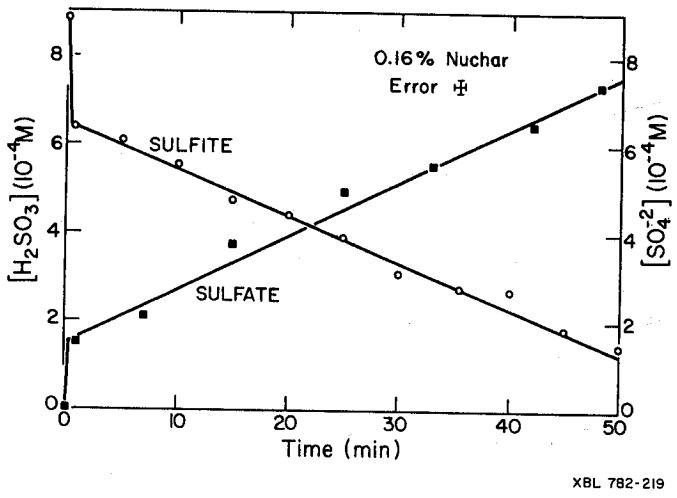

Fig. 2. H_2SO_3 and H_2SO_4 concentrations as a function of time for activated carbon suspensions.

In order to investigate the reaction rate and mechanism, a series of experiments was done with Nuchar as a model catalyst. The BET surface area of the Nuchar is 550 m^2/g. Its elemental composition (determined by combustion and X-ray fluorescence techniques) is shown in Table 1. The effects of the concentrations of carbon, sulfurous acid, and dissolved oxygen on the rate of oxidation of sulfurous acid were studied (Figs. 3, 4, and 5). The amount of sulfurous acid oxidized, at a constant temperature, by the rapid first step process is linearly proportional to the concentration of the carbon particles. A linear relationship was found between the half-life of the second process and the reciprocal of the carbon concentration and the initial sulfurous acid concentration respectively (Figs. 6 and 7). This behavior suggests a first order reaction with respect to the carbon catalyst concentration and zeroth order with respect to the sulfurous acid concentration under the conditions of this experiment (Nuchar, between 0.005% and 0.32% by weight; sulfurous acid, between 1.5×10^{-4} M and 10^{-3} M; pH, between 1.5 and 7.5). The rate of reaction with respect to the concentration of dissolved oxygen was found to be a fractional order (0.69) in Fig. 8, which was plotted by using data given in Fig. 5.

Table 1. Elemental composition of Nuchar C-190 (%)

C	74.7	K	0.091	Ni	0.001
O	23.6	Al	> 0.055	Cl	< 0.001
H	0.9	Ti	0.016	As	0.0004
N	0.1	Mn	0.013	Br	0.0004
Ca	0.221	Cr	0.002	Rb	0.0004
S	> 0.166	Cu	0.002	Zr	0.0004
Si	> 0.111	Zn	0.002	Pb	0.0004
Fe	0.117	Sr	0.002	Ga	0.0001

BET surface area = 550 m^2/g.

In order to assess the dependence of the SO_2 oxidation reaction on pH, a known volume of H_2SO_4 or NH_4OH was mixed into the sulfurous acid solution before adding Nuchar. In a separate run at a high pH, Na_2SO_3 solution was used for the experiment. The pH of the solution decreased during the course of the reaction. The change in pH varied from 0.05 to 1.0 pH unit, depending on the initial pH of the solution: the larger the initial pH, the larger the change. The results, represented in Fig. 9, demonstrate that the reaction rate essentially does not depend on the pH of the aqueous suspension under the conditions of this investigation. The pH of these experiments ranged from 1.45 to 7.5, which should cover the entire range of interest at atmospheric conditions. The latter observation is very striking, as it differs from other heterogeneous reactions involving liquid water which are dependent on the pH of the liquid water.

The reaction is accelerated by temperature, as may be seen from the results shown in Fig. 10. The activation energy is 11.7 kcal/mole between 5.5°C and 50°C (Fig. 11).

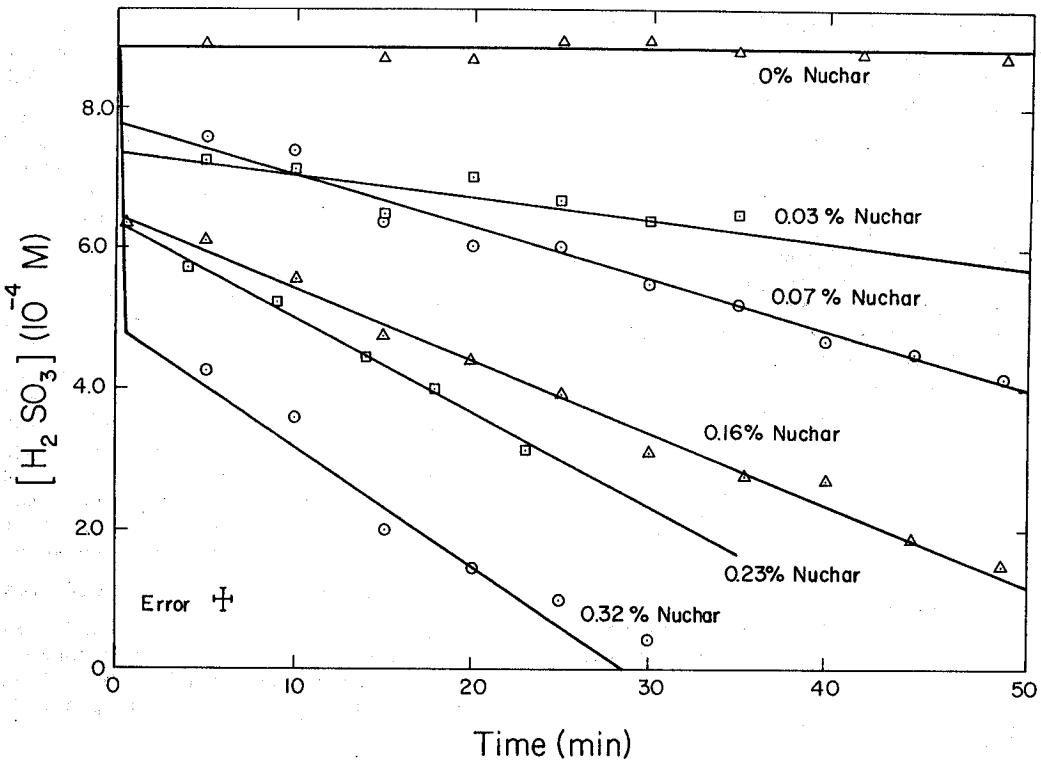

XBL7710-2070

Fig. 3. H_2SO_3 concentration as a function of time for various activated carbon concentrations. Initial H_2SO_3 concentration was 8.85×10^{-4} M.

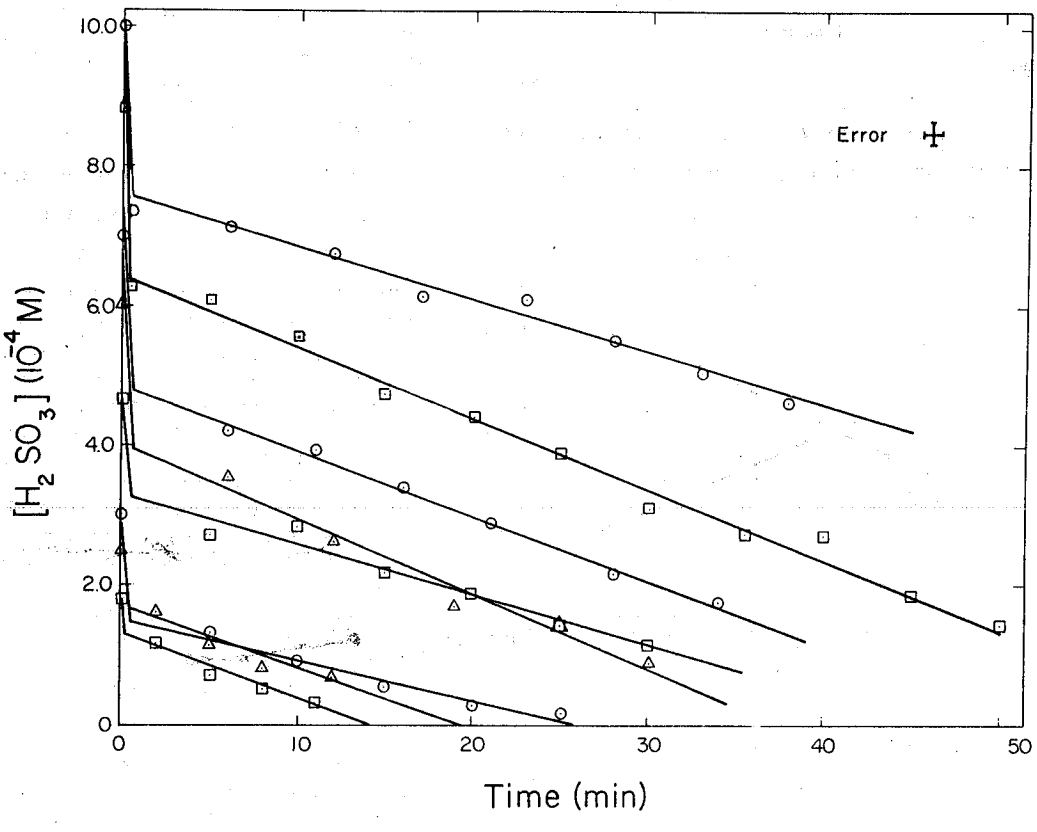

XBL7710-2068A

Fig. 4. H_2SO_3 concentration as a function of time for various initial concentrations of H_2SO_3 at a fixed activated carbon concentration of 0.16% by weight.

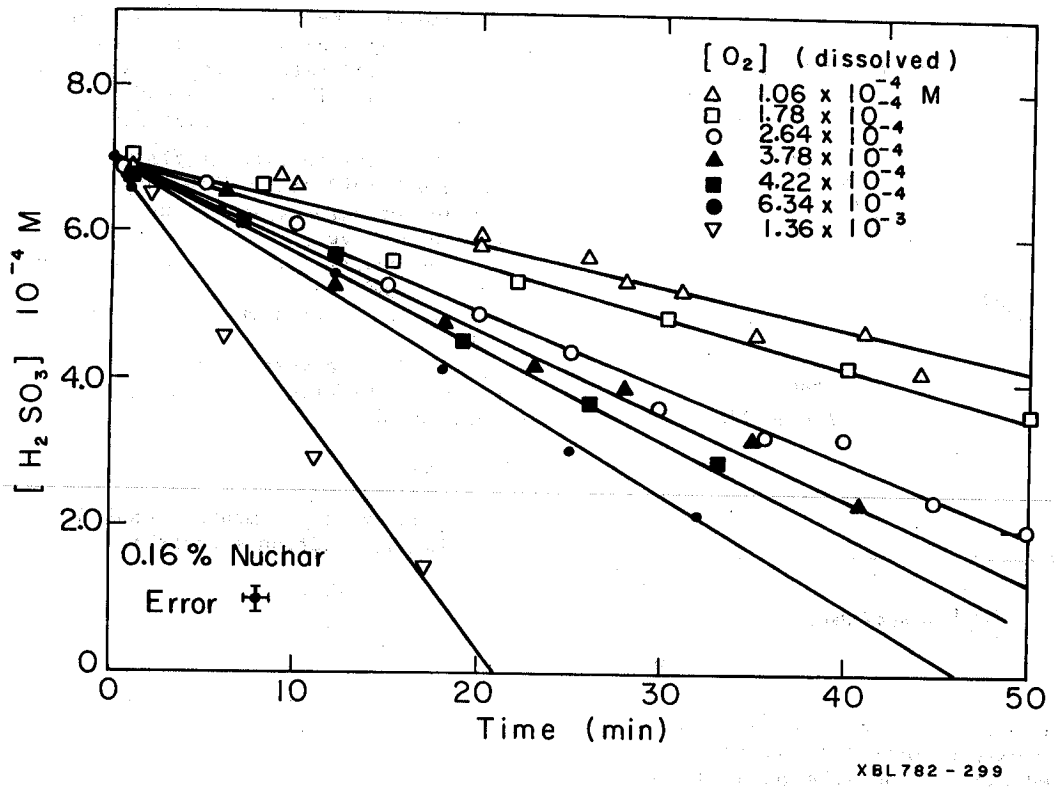

Fig. 5. H_2SO_3 concentration as a function of time for various concentrations of dissolved oxygen at a fixed activated carbon concentration of 0.16% by weight.

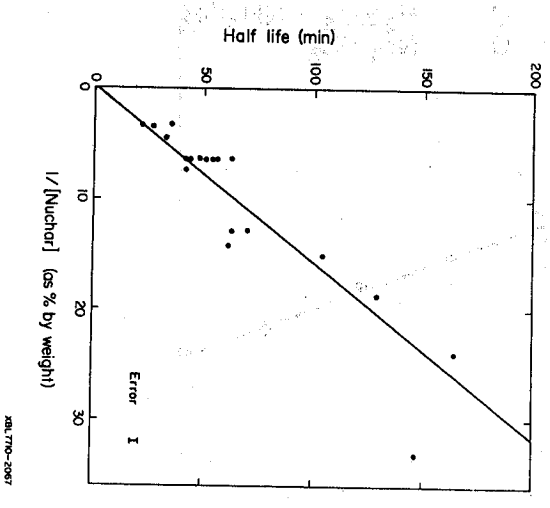

Fig. 6. Reaction half-life versus reciprocal of activated carbon concentration. The plot shows first order dependence with respect to activated carbon.

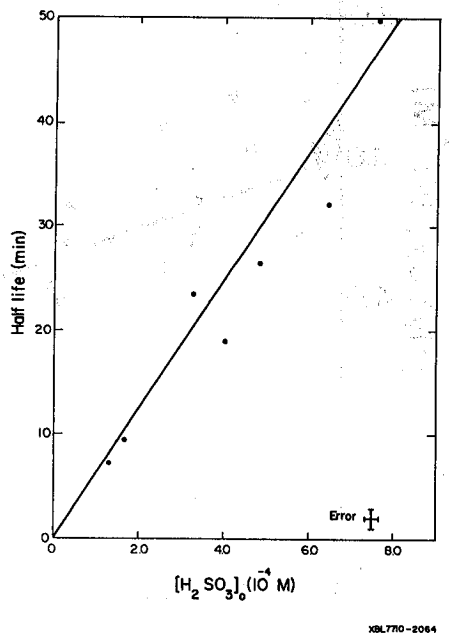

Fig. 7. Reaction half-life versus initial H_2SO_3 concentration. The plot shows zeroth order dependence with respect to H_2SO_3.

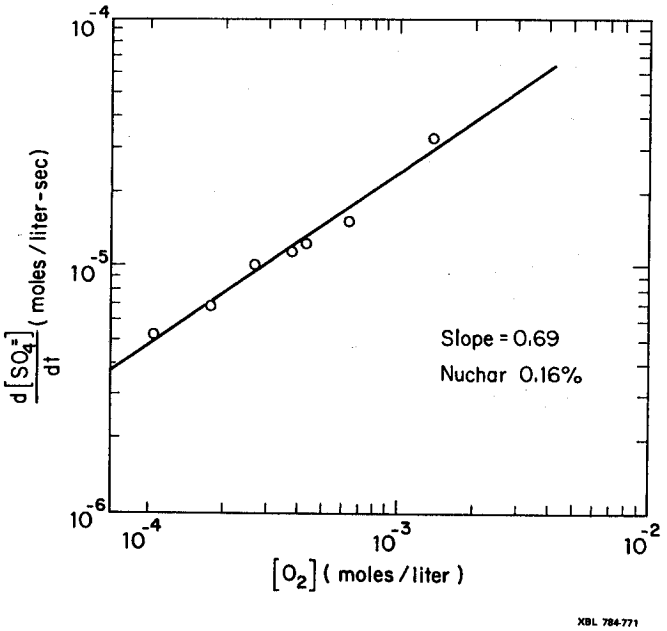

Fig. 8. The rate of formation of sulfuric acid versus dissolved oxygen concentration at a fixed activated carbon concentration of 0.16% by weight.

In summary, the reaction occurs in two steps—an initial rapid oxidation followed by a much slower one. The rate of the first process is too fast to follow. The reaction of the second process has the following characteristics:

1. The reaction rate is first order, zeroth order, and 0.69th order with respect to the concentration of carbon, sulfurous acid, and dissolved oxygen respectively.
2. The reaction rate is pH independent (between pH of 1.45 and 7.5).
3. The activation energy of the reaction is 11.7 kcal/mole.
4. There is a mass balance between the consumption of sulfurous acid and the production of sulfuric acid.

DISCUSSION

Based on the experimental results, we propose the following reaction mechanism:

$$C_x + O_2(\ell) \underset{k_{-1}}{\overset{k_1}{\rightleftharpoons}} C_x \cdot O_2(\ell) \qquad (1)$$

$$C_x \cdot O_2(\ell) + Su \underset{k_{-2}}{\overset{k_2}{\rightleftharpoons}} C_x \cdot O_2(\ell) \cdot Su \qquad (2)$$

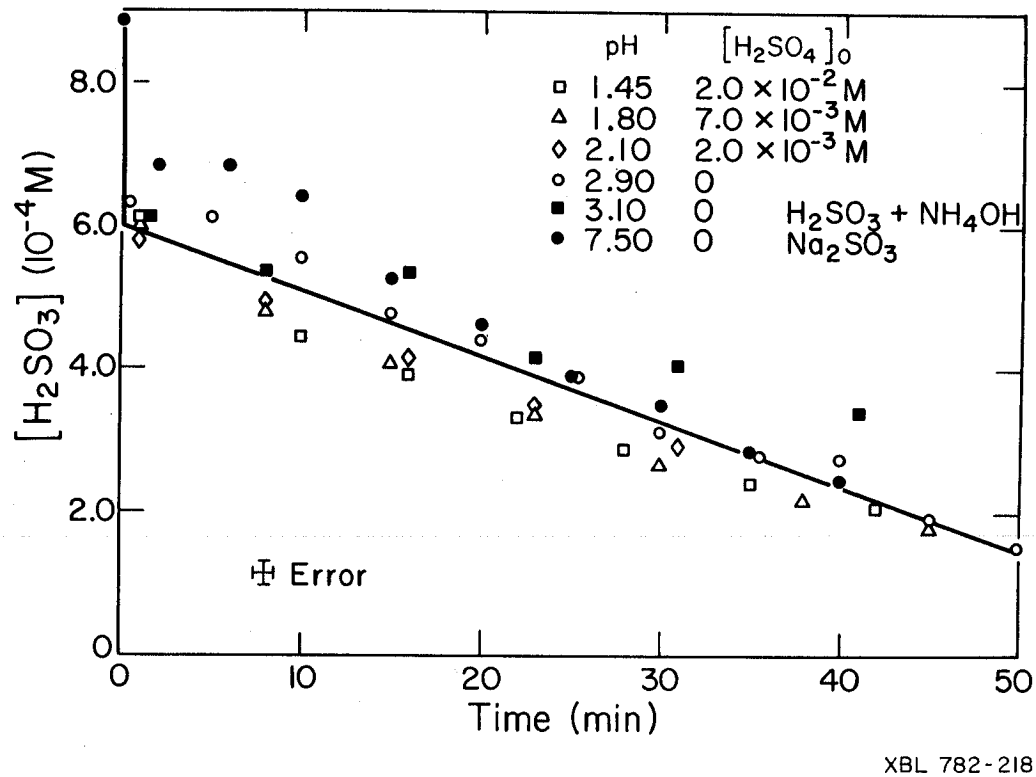

Fig. 9. H_2SO_3 concentration as a function of time at an activated carbon concentration of 0.16% by weight at various pH values. Initial H_2SO_3 concentration was 8.85×10^{-4} M.

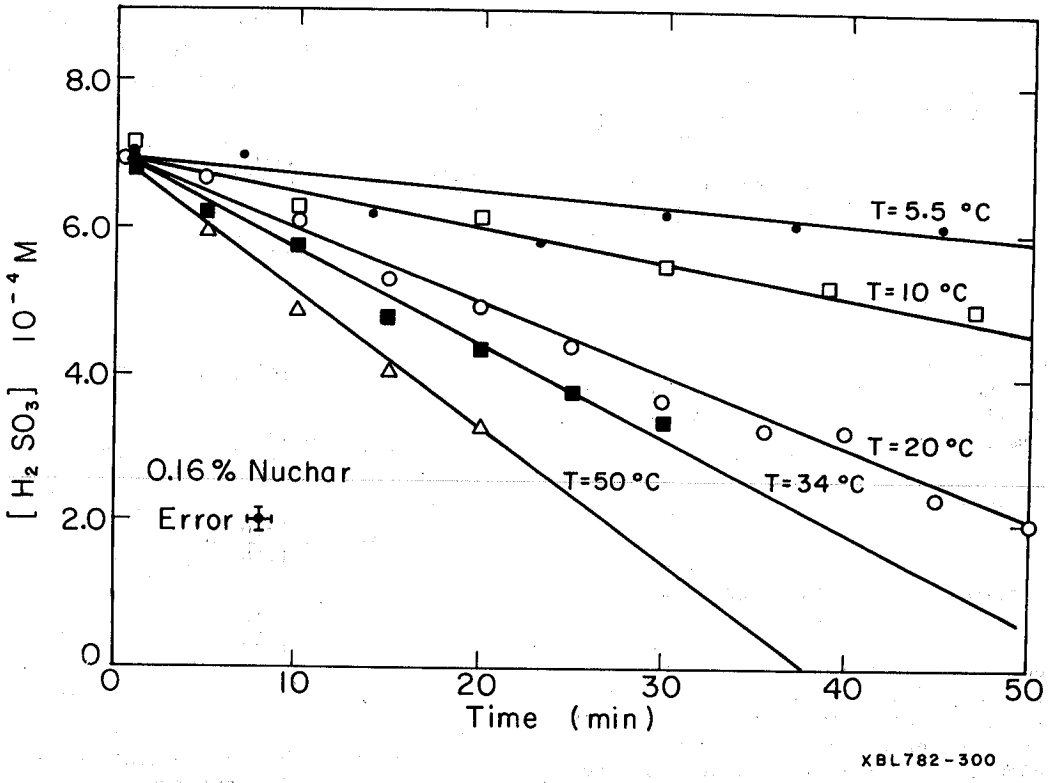

Fig. 10. H_2SO_3 concentration as a function of time at an activated carbon concentration of 0.16% by weight at various temperatures.

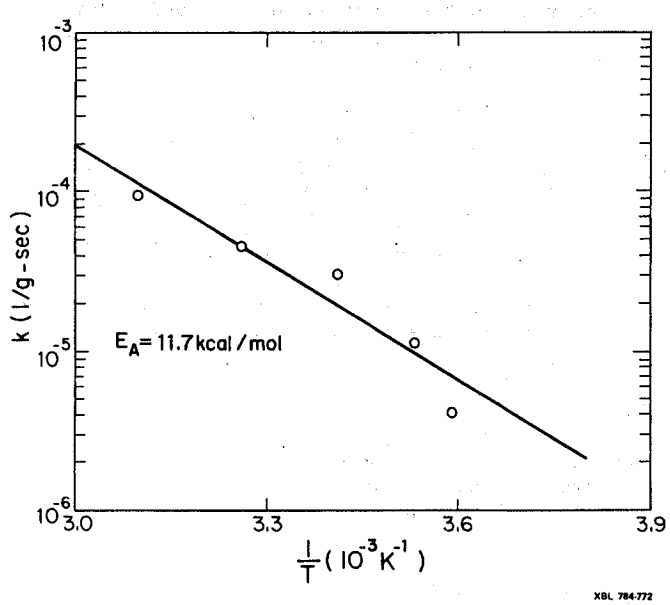

Fig. 11. A plot of the rate constant versus reciprocal of reaction temperature (the Arrhenius equation). The activation energy is calculated to be 11.7 kcal/mole.

$$C_x \cdot O_2(\ell) \cdot Su + Su \underset{k_{-3}}{\overset{k_3}{\rightleftharpoons}} C_x \cdot O_2(\ell) \cdot 2Su \qquad (3)$$

$$C_x \cdot O_2(\ell) \cdot 2Su \xrightarrow{k_4} C_x + 2\ SuO \qquad (4)$$

where C_x = soot, $O_2(\ell)$ = dissolved oxygen molecule, Su = sulfite species, and SuO = sulfate species.

Equation (1) indicates that dissolved oxygen is adsorbed on the soot particle surface to form an activated complex. This adsorbed oxygen complex then oxidizes the sulfurous acid to form sulfuric acid according to Equations (2)-(4). If one assumes that the reaction follows the condition of Langmuir adsorption equilibrium,[9] the rate of acid formation is:

$$\frac{d[SuO]}{dt} = 2k_4\ [C_x \cdot O_2(\ell) \cdot 2Su]$$

$$= 2k_4 [C_x] \left\{ \frac{K_1 [O_2(\ell)]}{1 + K_1 [O_2(\ell)] + K_W [H_2O] + K_{Su} [Su]} \right\}$$

$$\times \left\{ \frac{K_2 [Su]}{1 + K_2 [Su]} \right\} \left\{ \frac{K_3 [Su]}{1 + K_3 [Su]} \right\}$$

where K_1, K_2, and K_3 are the equilibrium constants of reactions (1), (2), and (3) respectively. K_W and K_{Su} are the equilibrium constants of the adsorption of water and sulfite species on carbon particles respectively. If $k_2[Su] \gg k_{-2}$ and

$k_3[Su] >> k_{-3}$, the rate law simplifies to

$$\frac{d[SuO]}{dt} = 2k_4[C_x]\left\{\frac{K_1[O_2(\ell)]}{1+K_1[O_2(\ell)]+K_W[H_2O]+K_{Su}[Su]}\right\} .$$

If the power rate form is used (Freundlich isotherm[9]) instead of the Langmuir form, the rate law becomes

$$\frac{d[SuO]}{dt} = k[C_x][O_2(\ell)]^n ,$$

which corresponds to the experimental results where n = 0.69. The activation energy (E_a) was determined to be 11.7 kcal/mole. The rate law as a function of temperature is

$$\frac{d[SuO]}{dt} = A[C_x][O_x(\ell)]^n \exp-(\frac{E_a}{RT})$$

where $A = 1.17\times10^5$ mole$^{0.3}$ $\ell^{0.7}$/g-sec, which is the average value determined for natural gas and acetylene soot.

We have ruled out the possibility that the oxidation of sulfurous acid is due to a reaction involving impurities such as iron in carbon particles. This was done by leaching a carbon sample with concentrated sulfuric acid for about a week before it was used for the study. This sample contained less than one-third of the original iron content; however, it still exhibited the same reaction rate as all samples without this treatment.

The possibility that the outgassing of SO_2 from the solution might contribute to the disappearance of sulfurous acid is ruled out by the fact that there is a mass balance between the amount of sulfurous acid consumed and the amount of sulfuric acid produced and that no significant consumption of sulfurous acid was observed over a 30-min interval for a solution without the addition of carbon particles.

We have examined the role of dissolved oxygen on the behavior of the reaction. It is conceivable that the initial rapid consumption of sulfurous acid could be due to the depletion in the amount of dissolved oxygen in the solution. The second, slower rate of consumption would then be limited by the rate of diffusion of the oxygen into the solution. This hypothesis was ruled out by noting that the behavior and the rate of the reaction were not affected by bubbling air into the solution or by increasing the stirring speed. The reaction rate speeds up, however, if one increases the concentration of dissolved oxygen (Fig. 5). We therefore conclude that the reaction rate is not limited by the mixing rate of gaseous oxygen molecules into the solution, but rather by the rate of formation of the activated oxygen complex.

The reaction will behave independently of the concentration of sulfite species and the pH of the solution as long as the following conditions are satisfied:

k_2[oxidizable sulfite species] >> k_{-2} and

k_3[oxidizable sulfite species] >> k_{-3} .

The pH ranges from 1.45 to 7.5 in this study. Therefore the ratio of $[SO_2\cdot H_2O]:[HSO_3^-]:[SO_3^=]$ ranges from $1:0.48:8.4\times10^{-7}$ to $9.4\times10^{-7}:0.51:1$. Then the conditions

$$k_2[1.5\times10^{-4}\times\frac{9.4\times10^{-7}}{1.51}] >> k_{-2} \text{ and}$$

$$k_3[1.5\times10^{-4}\times\frac{9.4\times10^{-7}}{1.51}] >> k_{-3} \text{ , or}$$

$$k_2[1.5\times10^{-4}\times\frac{0.48}{1.48}] >> k_{-2} \text{ and}$$

$$k_3[1.5\times10^{-4}\times\frac{0.48}{1.48}] >> k_{-3} \text{ , or}$$

$$k_2[1.5\times10^{-4}\times\frac{8.4\times10^{-7}}{1.48}] >> k_{-2} \text{ and}$$

$$k_3[1.5\times10^{-4}\times\frac{8.4\times10^{-7}}{1.48}] >> k_{-3}$$ should be satisfied respectively if $[SO_2\cdot H_2O]$, $[HSO_3^-]$, or $[SO_3^=]$ is the oxidizing species (1.5×10^{-4} mole/ℓ being the smallest sulfite concentration used). However, the possibility that the two or three sulfite species are oxidized cannot be ruled out.

We have investigated the kinetics at a much lower sulfite concentration and at a much higher pH of the solution. Preliminary results indicate that the oxidation rate is considerably slower at pH > 7.6. This behavior could indicate that a reaction mechanism, different from the proposed one, is operating. However, the proposed mechanism reproduces the results obtained under our experimental conditions. Further work is necessary to completely understand the actual reaction mechanism.

We are trying to determine whether there are any chemical species in the atmosphere which might inhibit the soot-catalyzed process, as some organic substances are known to retard SO_2 aqueous oxidation catalyzed by transition metal ions.[10] The liquid water collected by condensing the water vapor from the Berkeley atmosphere was used for the kinetic study and was found to have no effect on the oxidation rate of sulfurous acid. In a separate experiment, a gummy deposit taken from the wall of a highway tunnel was used for the study. The reaction rate of this sample is 50% faster compared with the same amount of Nuchar C-190. Therefore, no indication of inhibition from atmospheric contaminants has been observed so far.

The rate constants of several different types of carbon particles were studied and found to differ from type to type. In principle, the reaction rate should be proportional to the concentration of active sites on the carbon particles, rather than to the concentration of carbon particles. The number of active sites per unit mass of carbon particles is different from type to type and is not necessarily proportional to the surface area. Sidelewski[11] has shown, by means of the

electron paramagnetic resonance method, that free electrons on carbon particles can serve as active centers for the adsorption of oxygen molecules and for the oxidation of SO_2. The concentration of free electrons is related to the origin and thermal history of the carbon particles. The rate constant reported in this study represents the average value between the values of natural gas and of acetylene soot particles produced under rich flame conditions. Benner et al.[12] have recently found in a fog chamber study that the reaction rate of soot particles from a natural gas diffusion flame can be considerably faster than the reaction rate reported here for aqueous soot suspensions.

We have carried out a box-type calculation to compare the relative importance of soot-particle-catalyzed reactions with other reactions involving liquid water. The systems which were considered are: SO_2-$H_2O(\ell)$-air; NH_3-SO_2-$H_2O(\ell)$-air; O_3-SO_2-$H_2O(\ell)$-air; NH_3-O_3-SO_2-$H_2O(\ell)$-air; Fe^{+3}-SO_2-$H_2O(\ell)$-air; NH_3-Fe^{+3}-SO_2-$H_2O(\ell)$-air; Mn^{+2}-SO_2-$H_2O(\ell)$-air; and soot-SO_2-$H_2O(\ell)$-air. The kinetics of each of these processes, other than the soot-catalyzed reactions, have been studied by many investigators. The results of Beilke et al.,[13] Erickson et al.,[14] Freiberg,[15] and Matteson et al.[16] for oxygen, ozone, iron, and manganese systems respectively were used in this calculation. The following initial conditions were used in the calculation: liquid water, 0.05 g/m^3; SO_2, 0.01 ppm; O_3, 0.05 ppm; and CO_2, 0.000311 atm. For NH_3 a concentration of 5 ppb was used, which is higher than the highest equilibrium partial pressure of NH_3 over the United States as calculated by Lau and Charlson.[17] Concentrations of particulate Fe and Mn of 250 ng/m^3 and 20 ng/m^3 respectively were assumed. However, only 0.13% of the total iron and 0.25% of the manganese are water soluble, according to Gordon et al.[18] A soot particle concentration of 10 μg/m^3 was assumed.

The following assumptions were made in the calculations:

1. The size of liquid water drops suspended inside the box is so small that the absorption rate of gaseous species (SO_2 and NH_3) is governed by chemical reactions.
2. There is no mass transfer of any species across the box during the reaction. Therefore, the SO_2 (and NH_3) in each box is depleted with time. The mass balance of the sulfur and ammonia (i.e., $\Delta[SO_2]g = \Delta[SO_2\cdot H_2O] + \Delta[HSO_3^-] + \Delta[SO_3^=] + \Delta[HSO_4^-] + \Delta[SO_4^=]$, and $\Delta[NH_3]g = \Delta[NH_3\cdot H_2O] + \Delta[NH_4^+]$) is always maintained.
3. The growth of liquid water droplets due to the vapor pressure lowering effect of the sulfuric acid formed in the droplets is neglected.

The amount of sulfate formed as a function of time was calculated according to the following procedure:

1. Initially the droplets achieve chemical equilibrium with CO_2, SO_2, and NH_3 at the partial pressures adopted. The $[H^+]$, $[SO_2\cdot H_2O]$, $[HSO_3^-]$, $[SO_3^=]$, $[NH_3\cdot H_2O]$, and $[NH_4^+]$ are calculated when $[HSO_4^-]$ and $[SO_4^=]$ are equal to zero.
2. Assuming a time step Δt, the $[HSO_4^-]$ and $[SO_4^=]$ are calculated with the aid of the corresponding reaction rate law for each process.
3. Gaseous SO_2 and NH_3 are depleted. The remaining $[SO_2]$ and $[NH_3]$ are calculated using the mass balance equation.
4. Then the $[H^+]$, $[SO_2\cdot H_2O]$, $[HSO_3^-]$, $[SO_3^=]$, $[NH_3\cdot H_2O]$, and $[NH_4^-]$ are again calculated and the process is repeated until a 24-hr period is completed.

The result of this calculation is given in Table 2 and in Fig. 12. From this calculation, we can conclude that the soot-catalyzed oxidation of SO_2 can be the dominant mechanism under realistic atmospheric conditions.

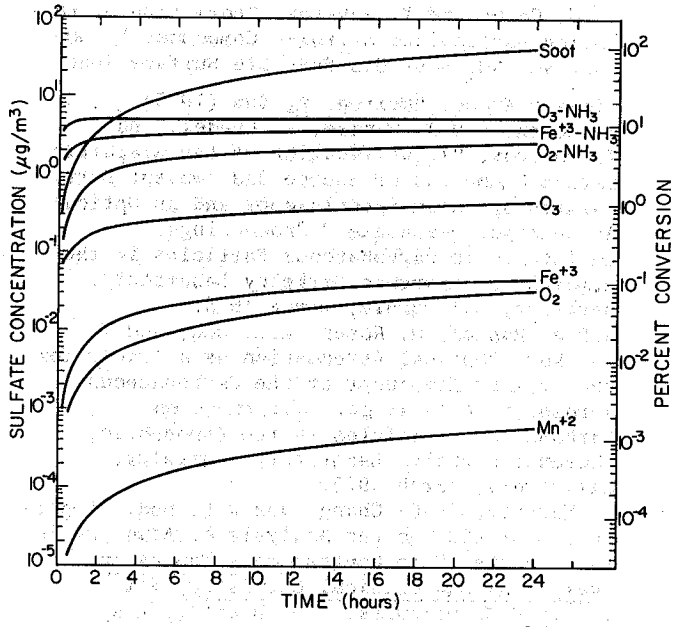

Fig. 12. Comparison of relative significance of various SO_2 conversion processes in aqueous droplets.

ACKNOWLEDGMENT

This work was supported by the Division of Biomedical and Environmental Research, Department of Energy, and by the National Science Foundation. The authors would like to thank Prof. Leo Brewer, Prof. H. S. Johnston, and especially Prof. R. J. Charlson and Dr. R. C. Carrigan for helpful discussions.

Table 2. Comparison of the relative significance of various SO_2 conversion processes in aqueous droplets.

Mechanisms	1 hr		6 hr		12 hr		24 hr	
	$SO_4^=$ μg/m^3	% conv.	$SO_4^=$ μg/m^3	% conv.	$SO_4^=$ μg/m^3	% conv.	$SO_4^=$ μg/m^3	% conv.
Mn^{+2}	2.55×10^{-5}	6.2×10^{-5}	1.6×10^{-4}	3.9×10^{-4}	3.1×10^{-4}	7.5×10^{-4}	6×10^{-4}	1.45×10^{-3}
O_2	1.8×10^{-3}	4.3×10^{-3}	9.6×10^{-3}	2.3×10^{-3}	1.8×10^{-2}	4.4×10^{-2}	3.4×10^{-2}	8.2×10^{-2}
Fe^{+3}	4.7×10^{-3}	1.1×10^{-2}	2.1×10^{-2}	5×10^{-2}	3.3×10^{-2}	8.0×10^{-2}	4.8×10^{-2}	0.12
O_3	0.13	0.33	0.27	0.66	0.35	0.85	0.47	1.13
O_2-NH_3	0.52	1.26	1.54	3.7	2.02	4.89	2.50	6.1
Fe^{+3}-NH_3	2.3	5.6	3.2	7.76	3.6	8.73	3.9	9.45
O_3-NH_3	4.51	10.94	5.14	12.5	5.28	12.8	5.28	12.8
C_x	1.8	4.4	10.8	26.4	21.6	52.4	41.25	100

Concentration: $H_2O(\ell)$: 0.05 g/m^3; SO_2: 0.01 ppm (10^{-8} atm); NH_3: 5 ppb (5×10^{-9} atm); O_3: 0.05 ppm (5×10^{-8} atm); $Mn^{+}2$: 20 ng 0.25%/m^3; Fe^{+3}: 250 ng 0.13%/m^3; C_x: 10 μg/m^3; temp.: 10°C.

REFERENCES AND FOOTNOTES

1. T. Novakov, S.-G. Chang, and A.B. Harker, "Sulfates as Pollution Particulates: Catalytic Formation on Carbon (Soot) Particles," Science 186, 259 (1974).
2. S.-G. Chang and T. Novakov, "Formation of Pollution Particulate Nitrogen Compounds by NO-Soot and NH_3-Soot Gas-Particle Surface Reactions," Atmos. Environ. 9, 495 (1975).
3. H. Rosen, A.D.A. Hansen, L. Gundel, and T. Novakov, "Identification of the Graphitic Carbon Component of Source and Ambient Particulates by Raman Spectroscopy and an Optical Attenuation Technique," Proceedings, Conference on Carbonaceous Particles in the Atmosphere, Lawrence Berkeley Laboratory, Berkeley, California, March 1978.
4. A.D.A. Hansen, H. Rosen, R.L. Dod, and T. Novakov, "Optical Attenuation as a Tracer for the Primary Component of the Carbonaceous Aerosol," Proceedings, Conference on Carbonaceous Particles in the Atmosphere, Lawrence Berkeley Laboratory, Berkeley, California, March 1978.
5. T. Novakov, S.-G. Chang, and R.L. Dod, "Application of ESCA to the Analysis of Atmospheric Particulates," in Contemporary Topics in Analytical and Clinical Chemistry, Vol. I, ed. by D.M. Hercules, G.M. Hieftje, L.R. Snyder, and M.A. Evenson (New York, Plenum, 1977), p. 249.
6. R.J. Charlson, D.S. Covert, T.V. Larson, and A.P. Waggoner, "Chemical Properties of Tropospheric Sulfur Aerosols," Atmos. Environ. 12, 39 (1978).
7. For previous works related to this subject, see M. Hartman and R.W. Coughlin, "Oxidation of SO_2 in a trickle-bed reactor packed with carbon," Chem. Eng. Sci. 27, 867 (1972), and references therein.
8. Nuchar: Trademark of West Virginia Pulp & Paper Co.
9. Alfred Clark, The Theory of Adsorption and Catalysis (New York, Academic, 1970).
10. L.C. Schroeter, Sulfur Dioxide: Application in Foods, Beverages, and Pharmaceuticals, (Oxford, Pergamon, 1966), p. 56.
11. J. Siedlewski, "The Mechanism of Catalytic Oxidation on Activated Carbon; The Influence of Free Carbon Radicals on the Adsorption of SO_2," Int. Chem. Eng. 5, 297 (1965).
12. W.H. Benner, private communication, 1978.
13. S. Beilke, D. Lamb, J. Müller, "On the Uncatalyzed Oxidation of Atmospheric SO_2 by Oxygen in Aqueous Systems," Atmos. Environ. 9, 1083 (1975).
14. R.E. Erickson, L.M. Yates, R.L. Clark, and D. McEwen, "The Reaction of Sulfur Dioxide with Ozone in Water and Its Possible Atmospheric Significance," Atmos. Environ. 11, 813 (1977).
15. J. Freiberg, "The Mechanism of Iron Catalyzed Oxidation of SO_2 in Oxygenated Solutions," Atmos. Environ. 9, 661 (1975).
16. M.J. Matteson, W. Stöber, and H. Luther, "Kinetics of the Oxidation of Sulfur Dioxide by Aerosols of Manganese Sulfate," Ind. & Chem. Fund. 8, 677 (1969).
17. N.-C. Lau and R.J. Charlson, "On the Discrepancy Between Background Atmospheric Ammonia Gas Mesurements and the Existence of Acid Sulfates as a Dominant Atmospheric Aerosol," Atmos. Environ. 11, 475, 1977.
18. G.E. Gordon, D.D. Davis, G.W. Israel, H.E. Landsberg, and T.C. O'Haver, Atmospheric Impact of Major Sources and Consumers of Energy, NSF/RA/E-75/189 (Grant NSF-ESR75-02667 to Univ. of Maryland), 1975.

OXIDATION OF SULFITE BY ACTIVATED CHARCOAL

D. J. Eatough, W. P. Green, and L. D. Hansen
Thermochemical Institute (Contribution No. 149), and Department of Chemistry
Brigham Young University, Provo, Utah 84602

ABSTRACT

One possible mechanism for the conversion of SO_2 to sulfate in atmospheric aerosols is the catalyzed conversion on soot particles. Previous work has indicated that activated charcoal is a good model for this catalytic conversion. We report here a calorimetric study of the conversion of sulfite to sulfate in aqueous suspensions of activated charcoal. The results indicate that groups are present in the charcoal which are capable of complexing with sulfite and rapidly oxidizing sulfite to sulfate, resulting in the formation of new reduced species in the charcoal. This reaction mechanism does not appear to involve simple reaction with surface adsorbed oxygen. The rate limiting step for oxidation of sulfite by the charcoal will be the oxidative regeneration of this active site.

INTRODUCTION

It has previously been well documented that activated charcoal is an effective catalyst for the conversion of SO_2 to SO_4^{2-} in the presence of water.[1] It has been postulated that this mechanism may be important in the production of sulfate in the atmosphere if significant quantities of soot are present from the combustion of fossil fuels.[2] It has also been suggested that commercially available activated charcoal can serve as a good model system for carbonaceous material in the atmosphere.[3] Recent work by Chang, et. al.[3] has shown that the removal of SO_2 from aqueous suspensions of activated charcoal is a two step process involving the very rapid removal of about 0.3 μeq of SO_2/mg of suspended soot followed by a slower removal process. Sulfate is the reported end product of these reactions. The slow reaction was observed to be first order in activated charcoal concentration and independent of initial H_2SO_3 concentration or pH from pH = 1.4 to 2.9. We report here a thermodynamic study of the interaction of HSO_3^- with activated charcoal in aqueous solution. The results are interpreted in terms of both binding of sulfite by the charcoal and charcoal catalyzed oxidation of sulfite to sulfate.

EXPERIMENTAL AND RESULTS

Two ml of a 0.5 wt % suspension of Nuchar C-190N (Bios Laboratory) in argon purged distilled water was titrated calorimetrically[4] with 0.2 ml of a 0.03 M $NaHSO_3$ solution in argon purged distilled water. The titration required five minutes. Immediately after titration, any remaining sulfite was fixed in 0.1 M HCl, 2.5 mm $FeCl_3$, and SO_3^{2-} and SO_4^{2-} determined by a calorimetric analytical procedure.[5] Blank determinations were also made by determination of SO_3^{2-} and SO_4^{2-} in water equilibrated with 0.5 wt % Nuchar by the calorimetric procedure and by ion exchange chromatography. The results of these experiments are summarized in Tables 1 and 2. The results in Tables 1 and 2 suggest that sulfite is rapidly oxidized by Nuchar under the conditions of these experiments, presumably resulting in the production of reduced functional groups in the Nuchar. To test this postulate, suspensions of 0.06 wt % Nuchar in argon purged 0.1 M HCl with and without added $NaHSO_3$ were titrated calorimetrically with a 0.1 M HCl solution of $K_2Cr_2O_7$ to determine any reduced species present.[5] In all of these experiments, aqueous HCl was added to a solid mixture of Nuchar and $NaHSO_3$. Titration of the solutions containing no added $NaHSO_3$ indicated the presence of 0.11 μeq/mg Nuchar of a species which titrated with a ΔH value of -9 kcal/eq and of about 3 μeq/mg Nuchar of species which titrated with a ΔH value of from -2 to -4 kcal/eq. Presumably these are the residual S(IV) (see Table 1) and surface associated C-OH and C=O groups present in the Nuchar. The groups which titrated with a ΔH value of -2 to -4 kcal/eq were essentially unchanged by the addition of $NaHSO_3$. The amount of species present which titrated with a ΔH value of -9 kcal/eq was increased by the addition of $NaHSO_3$. Also several new reduced species were formed as summarized in Table 3.

Table 1. Observed chemical reactions associated with the addition of HSO_3^- to an aqueous Nuchar suspension.

Region	Endpoint, μeq of total HSO_3^- added/mg Nuchar[a]	Heat of reaction in region, kcal/eq HSO_3^-
1	0.15 ± 0.02	-3.9
2	0.93 ± 0.09	-0.9
3	1.15 ± 0.07	+4.7

[a]The uncertainty is the standard deviation between two determinations.

Table 2. Analysis of fixed solutions of the products of addition of HSO_3^- to an aqueous Nuchar suspension

Total $NaHSO_3$ added, μeq/mg	Analyzed products, μeq/mg SO_3^{2-}	SO_4^{2-}
0	0.07 ± 0.01	0.17 ± 0.01 (0.25 ± 0.01)[a]
1.39	0.39	1.08
1.48	0.95	0.98

[a]Sum of SO_3^{2-} and SO_4^{2-} determined by ion exchange chromatography.

DISCUSSION

The results given in Tables 1 and 2 indicate that the rapid reaction of HSO_3^- with Nuchar involves at least three different reactions up to a ratio of HSO_3^-:Nuchar of 1.15 μeq/mg. The SO_4^{2-}

Table 3. Reduced species titrated with $K_2Cr_2O_7$ in 0.1 M HCl solutions of $NaHSO_3$ with 0.06 wt % Nuchar.

$NaHSO_3$ Added,	μeq/mg of Titrated Species ΔH(kcal/eq) =				
μeq/mg	-74±4	-39±3	-23±2	-12±1	-9±1
0	0.00	0.00	0.00	0.00	0.11
1.22	0.00	0.00	0.00	0.00	0.19
1.65	0.20	0.08	0.06	0.11	0.15
2.59	0.26	0.09	0.10	0.09	0.25

produced by this interaction is from 0.8 to 0.9 μeq/mg. These data suggest that the reaction represented by Region 1 involves the quantitative and rapid conversion of 0.15 μeq HSO_3^-/mg Nuchar to SO_4^{2-}. Regions 2 and 3 involve an equilibrium between complexed sulfite and sulfate, according to reactions (1) and (2)

$$HSO_3^- + C_O = HSO_3^- \cdot C_O \quad (1)$$

$$HSO_3^- \cdot C_O = C_R + H^+ + SO_4^{2-} \quad (2)$$

where C_R and C_O are the reduced and oxidized form of the reactive Nuchar sites. The existence of sulfite complexes with the Nuchar is also suggested by the observation that sulfite is extractable from Nuchar itself, Table 2. The ΔH value for the aqueous reaction

$$HSO_3^- + 1/2\ O_2 = H^+ + SO_4^{2-} \quad (3)$$

is -33.8 kcal/eq.[6] This is significantly higher than the ΔH values measured for the oxidation of sulfite to sulfate in the presence of Nuchar due to the formation of C_R species. The measured ΔH values given in Table 1 are the sum of the ΔH values for reaction (1) plus some fraction of reaction (2), depending on the extent of SO_4^{2-} formation. Assuming the ΔH value measured in Region 1 represents the sum of reactions (1) and (2) and the ΔH value measured in Region 3 is due only to reaction (1), these results suggest that the ΔH value for reaction (1) is endothermic and about 5 kcal/eq in magnitude and the ΔH value for reaction (2) is exothermic about -8 kcal/eq.

The data summarized above suggest that while HSO_3^- interacts with Nuchar, more stable S(IV) species may not. This was investigated by conducting experiments identical to those summarized in Tables 1 and 2 except the adduct of HSO_3^- with formaldehyde, $H\text{-}\underset{H}{\overset{OH}{C}}\text{-}SO_3Na$, was used instead of $NaHSO_3$. The results of these experiments indicate that the adduct will not bind to Nuchar and is not oxidized to sulfate by aqueous suspensions of Nuchar.

Additional information on the Nuchar sulfite binding and oxidizing sites is obtained from the $K_2Cr_2O_7$ titration data given in Table 3. The solutions prepared for these analyses equilibrated for 45 minutes before the dichromate titration so that equilibrium should have been established[3] and the majority of the added HSO_3^- converted to SO_4^{2-}. The ΔH value for the oxidation of HSO_3^- by $Cr_2O_7^{2-}$ in acidic solution is -30 kcal/eq.[5] Any sulfite complexes present should be oxidized with a ΔH value smaller than this. Thus it seems probable that the species titrated with ΔH values of -23, -12, and -9 kcal/eq probably are due to titration of $HSO_3^- \cdot C_O$ species. However the species titrated with ΔH = -74 and -39 kcal/eq must represent the C_R species formed in the Nuchar by the oxidation of HSO_3^- in Regions 1 and 2 of Table 1, respectively. The sum of the ΔH_{ox} value for oxidation of the reduced species by $Cr_2O_7^{2-}$ plus the ΔH value given in Table 1 for the redox process represented by Eq. (1) and (2) should be equal to the ΔH value for reaction (4), -39 kcal/eq. The

$$3HSO_3^- + Cr_2O_7^{2-} = 3SO_4^{2-} + 2Cr^{3+} + H_2O \quad (4)$$

value calculated for this process for Region 2, -39 kcal/eq, is in excellent agreement with the expected value, indicating the end product of the $Cr_2O_7^{2-}$ titration is the species which oxidized sulfite. In contrast, the value calculated for this process for Region 1, -78 kcal/eq, differs markedly from the predicted value of -39 kcal/eq, indicating the species resulting from oxidation by $Cr_2O_7^{2-}$ is markedly different from that involved in the sulfite oxidation.

CONCLUSIONS

The interaction of HSO_3^- with Nuchar in aqueous solution results in both oxidation and complexation of the HSO_3^- by the Nuchar. These reactions are rapid. In addition to these rapid reactions, it has also been reported[3] that there is a subsequent slow conversion of sulfite to sulfate which is dependent only on the concentration of Nuchar. This observation is consistent with results obtained in this study which suggest that the rate limiting step for continued conversion of sulfite to sulfate is the oxidative regeneration of the active site in the charcoal.

ACKNOWLEDGMENTS

This work was supported by the U.S. Department of Energy (Contract No. EY-76-S-02-2988) and the Electric Power Research Institute (Contract No. RP1154-1).

REFERENCES

1. F. C. Riesenfeld and A. L. Kohl, "Gas Purification", Gulf Publishing, Houston, 1974, pp. 329-333.
2. T. Novakov, S. G. Chang, and A. B. Harker, Science, 186, 261 (1974).
3. S. G. Chang, R. Brodzinsky, S. S. Markowitz, and T. Novakov, "Catalytic Oxidation of SO_2 on Carbon in Aqueous Suspension", Atmospheric Aerosol Research Annual Report 1976-77, LBL-6819, University of California, pp. 42-56.
4. L. D. Hansen, R. M. Izatt, D. J. Eatough, T. E. Jensen, and J. J. Christensen, "Recent Advances in Titration Calorimetry", in "Analytical Calorimetry", Vol. 3, Plenum Press, New York, 1974, p. 7.
5. L. D. Hansen, L. Whiting, D. J. Eatough, T. E. Jensen, and R. M. Izatt, Anal. Chem., 48, 634 (1976).
6. "Selected Values of Chemical Thermodynamic Properties", National Bureau of Standards, Circular 500, 1952.

CARBONACEOUS PARTICULATES IN THE ATMOSPHERE: ILLUMINATION BY ELECTRON MICROSCOPY

Philip A. Russell
Denver Research Institute
University of Denver
Denver, Colorado 80208

ABSTRACT

Particulates in the "submicrometer" size range, collected from four western states, were examined by analytical electron microscopy; carbonaceous particulates usually were the predominant species observed. Whenever non-mineral sulfur was present in the samples examined, it was always observed to be associated with these carbon particles. In most cases, varying levels of associated sulfur did not affect particle size or morphology. Using electron diffraction and particulate thermal characteristics, it was unequivocally demonstrated that particulates of ammonium sulfate, ammonium hydrogen sulfate, sulfamic acid and sulfuric acid were not present among any of the samples examined.

INTRODUCTION

Carbonaceous particulates in the atmosphere have received limited attention in their importance as an influential component of pollution air masses even though these "soot" particulates can occur in rather large relative concentrations and have demonstrated capabilities to catalytically oxidize SO_2 to sulfate species.[1] Presently, the most widely suggested particulate types considered to be of importance in the production of highly visible pollution air masses are secondary particulates produced by gas-to-particle conversion of SO_2 to ammonium sulfate $[(NH_4)_2SO_4]$, ammonium hydrogen sulfate $[NH_4HSO_4]$, and/or sulfuric acid $[H_2SO_4]$.[2,3,4,5,6,7] However, little is understood about the chemical and physical properties of the individual sulfur-rich particulates and analytical high-resolution electron microscopy has yet to be utilized to its full potential in examining their microstructure and chemistry.[8]

A study of Denver, Colorado's urban air pollution plume utilized electron microscopy as part of an integrated program to better define critical factors associated with observed light scattering phenomena. It was observed that the most prevalent and universal particulates in the size range from $\sim$ 0.1 - 3.0 μm were, typically, agglomerates of very small (< 0.05 μm) particulates (Figs. 1,2). These particulates were identified by morphology and lack of elements, atomic number $\gtrsim$ 11, as carbon black, *i.e.* "soot." An interesting phenomenon related to the nature of these particulates was that sulfur, if observed in the overall sample, was always associated with them although no obvious changes in microstructural morphology were observed.[9] It was also demonstrated, using selected area electron diffraction, that no crystalline material was present in association with these particulates. The source of sulfur was determined to be independent of the automobile;[10] while the particulates themselves were identified as carbon black most likely produced by internal combustion engines.[11] This paper reports the results of analyses of carbonaceous particulates collected in Colorado, California, Nevada and Utah which were examined using analytical electron microscopy.

METHODS AND MATERIALS

Atmospheric samples examined include: (1) Lo Vol and impactor stages using Millipore and Nuclepore substrates, collected in and around Denver, Colorado, during the 1973 winter field study, (2) paraffin-coated mylar stage-3 substrates collected using a Multiday impactor operated in the Los Angeles basin November 12th and 13th, 1973, (3) Lo Vol Nuclepore substrates collected in the vicinity of Provo, Utah, November, 1976 and (4) Lo Vol Nuclepore substrates collected in the vicinity of Las Vegas, Nevada, November-December 1977.

Particulates were examined *in situ* on collection substrate samples by sequentially excising a portion of the collection substrate, attaching it to an SEM stub, and vacuum evaporating a conductive coating of $\sim$ 20.0 nm of carbon. Particulates on the substrates were examined for morphology, size and elemental composition using a scanning electron microscope (SEM) equipped with an energy dispersive X-ray spectrometer. Because X-rays could only be detected from elements with atomic numbers higher than sodium (Z = 11), the presence of carbon was assumed to be indicated by the lack of any X-ray spectra from particles or an excessive background spectrum when elements were present in larger particulates (diameter $\gtrsim$ 0.5 μm).

Selected samples from the four locations were examined by transmission electron microscopy (TEM) to provide ultra structural information beyond the normal resolution of the SEM, including interior microstructure. Using selected area electron diffraction (SAED) it was also possible to determine if particulates < 0.1 μm and larger in size were crystalline, and, providing the particulates were crystalline, unequivocally determine their species.[12,13,14] Particulates were transferred to carbon coated TEM grids from the various thin film substrates using appropriate solvents and wicking

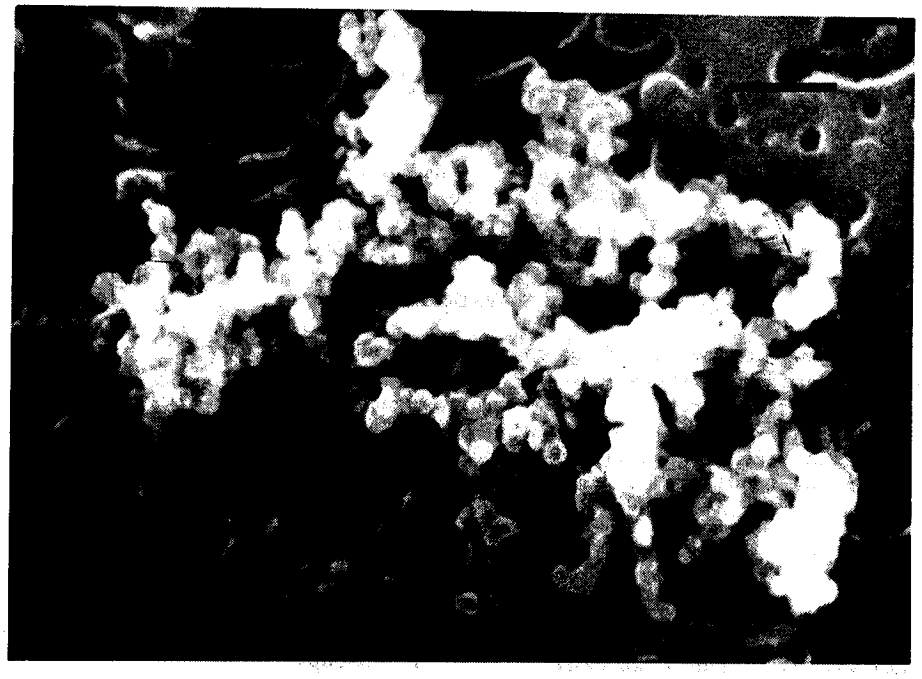

Figure 1. Typical carbonaceous particulate associated with the submicron size fraction of urban plumes of Denver and Las Vegas. Scanning electron micrograph; the bar represents 1.0 micrometer.

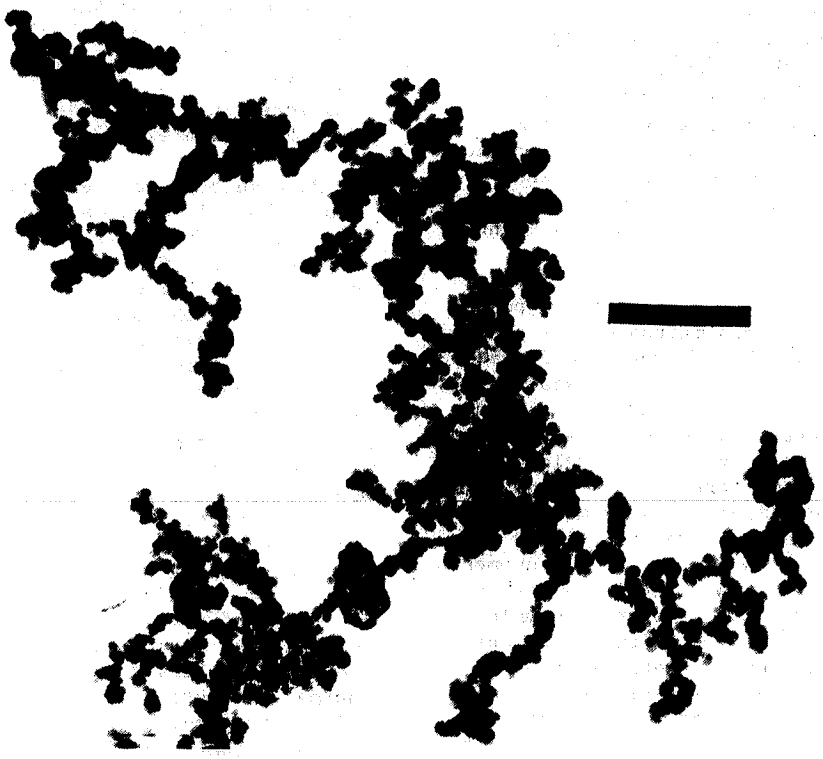

Figure 2. Typical carbonaceous particulate associated with the submicron size fraction of urban plumes of Denver and Las Vegas. Transmission electron micrograph; the bar represents 1.0 micrometer.

dissolution as described in detail elsewhere.[15,16] In one case, it was necessary to transfer particulates directly from the substrate to the carbon coated grid by using carefully directed pressure. All transferred samples were coated with ∿ 10.0 nm of carbon by vacuum evaporation prior to observation. Samples of particulate auto emission, carbon black (soot), sulfuric acid, ammonium sulfate, ammonium hydrogen sulfate and sulfamic acid deposited on thin film membrane substrates were also examined using the SEM and TEM techniques described above.

RESULTS

Denver, Colorado

The carbonaceous particulates observed in association with Denver's urban plume were consistently the same in agglomerate morphology, and individual particle size and ultra morphology. The particulates were typically chain agglomerates composed of particulates < 0.1 μm in diameter which were identical in morphology and configuration to carbon black and automotive carbonaceous emissions.[17,18,19,20,21,22] Sulfur, when present, was always associated with these carbon particles and was accompanied by no obvious changes in particulate morphology when examined by SEM or TEM. These particulates, regardless of the associative concentration of sulfur, were always observed to be noncrystalline and non heat labile. Figures 1, 2, 3 and 4 illustrate typical carbonaceous particulate material associated with Denver's plume. The reason for the subtle laminar ring structure sometimes observed in association with individual carbon particles (Fig. 3) is unknown. A similar phenomenon occurs when uncoated carbon black particulates are examined by TEM; selective, thermal decomposition of normally present hydrocarbons in the vacuum system produces a laminar pattern reflecting particle size growth. Confirmation that doubly coated specimens of carbon black do not manifest this phenomenon was made by sequentially observing the same particle over a 30 minute time period; observed laminar structures did not change.

Los Angeles, California

The particulates collected in Los Angeles air basin during a typical episode were very rich in sulfur and were expected to be representative of secondary formation. These particulates were observed to be agglomerates (0.5-3.0 μm) of inhomogeneous smaller particulates (∿ 0.1 μm) composed of a hard, granular, probably carbonaceous, core surrounded by a less electron dense layer of material, Figs. 5,6. No electron diffraction was produced by any of these particles, nor was the material observed to be heat labile.

Las Vegas, Nevada

Carbonaceous particulates similar to those found in Denver (Figs. 1,2,3,4) were prevalent in the samples examined. However, in one sample area, organic particulates that were of obvious secondary origin were observed (Figs. 7,8). These particulates were soluble in dissolution solvents and required direct transfer techniques to permit observation. Their exact composition is unknown, and they are not representative of the major carbonaceous particulate species observed in the Las Vegas area.

Provo, Utah

Carbonaceous particulates are prevalent throughout the area and are of two types--chain agglomerates similar to Figs. 1 and 2, which are usually in a minority of the < 1.0 μm particles, and singular carbon particulates ranging from ∿ 0.2 - 0.6 μm in diameter. The singular carbon particulates are often, but not consistently, rich in sulfur, thermally stable in the TEM beam and do not produce electron diffraction. Only a limited number of these particulates have been examined to date by TEM-SAED, so some caution is warranted in assuming that these are representative particles. It should be noted, however, that an active steel mill is located within the vicinity and has been observed to produce carbon particulates during its coking process similar in size and morphology to those found in the environmental samples. Figure 9 is an environmental example of these particulates.

Control Samples

Relatively stable diffraction patterns are produced by particles of ammonium sulfate (Fig. 10) and sulfamic acid when using the transfer techniques described previously. Ammonium bisulfate produces patterns which rapidly fade as the individual particulates sublime. Observations of deposited sulfuric acid aerosols made using an SEM demonstrate that it is fairly heat stable, only being affected when a direct beam is focused for small area X-ray analysis. Thus the particulates of the sulfur species of interest, as mentioned in the introduction, can often be unequivocally identified as being absent or present by using analytical electron microscopy techniques.

DISCUSSION

Although the samples examined probably do not constitute a representative sample size, some important airborne particulate information is brought to light:

1. submicrometer sized individual carbon particulates and agglomerates are consistently observed to be a major component of the submicrometer sized particulate population in air pollution air masses.

2. sulfur, except mineral sulfate, is consistently associated with carbon particulates when present in the observed samples.

3. the sulfur associated with carbon particulates has been unequivocally demonstrated not to be ammonium sulfate, ammonium hydrogen sulfate, sulfamic acid or sulfuric acid, in samples collected from four different sampling areas, by comparing heat

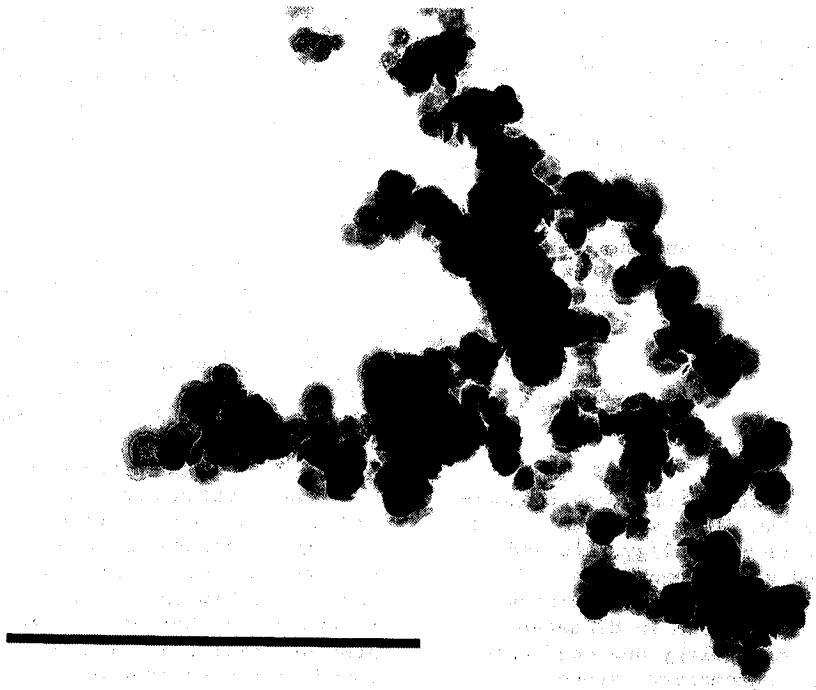

Figure 3. Typical carbonaceous particulate associated with the submicron size fraction of urban plumes of Denver and Las Vegas. Transmission electron micrograph; the bar represents 1.0 micrometer. Note the laminar ring pattern associated with the individual carbon particles.

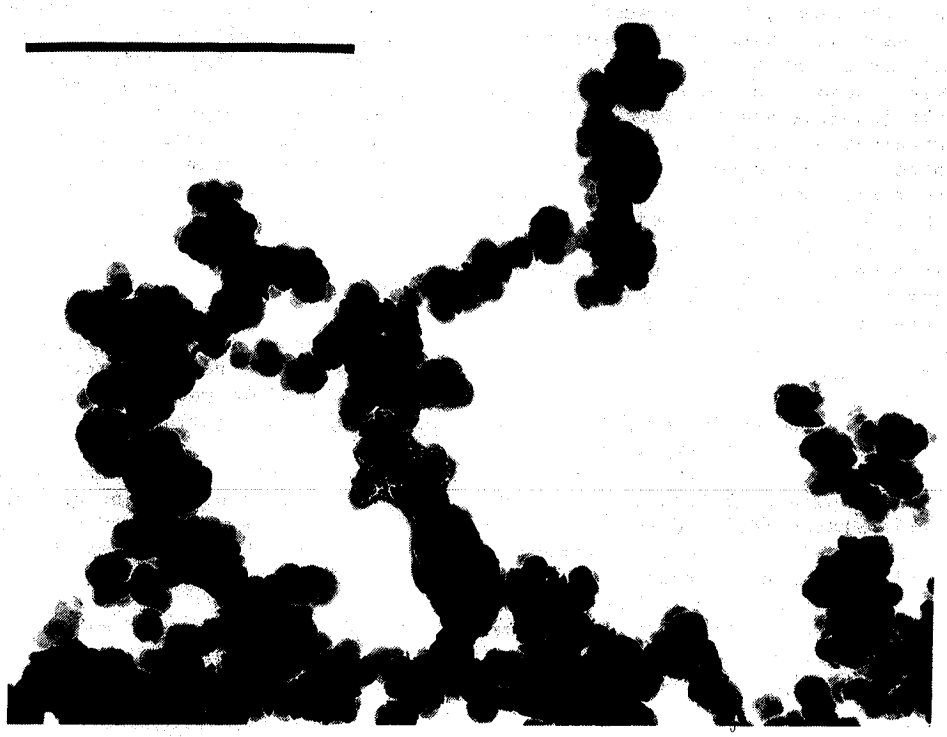

Figure 4. Typical carbonaceous particulate associated with the submicron size fraction of urban plumes of Denver and Las Vegas. Transmission electron micrograph; the bar represents 1.0 micrometer.

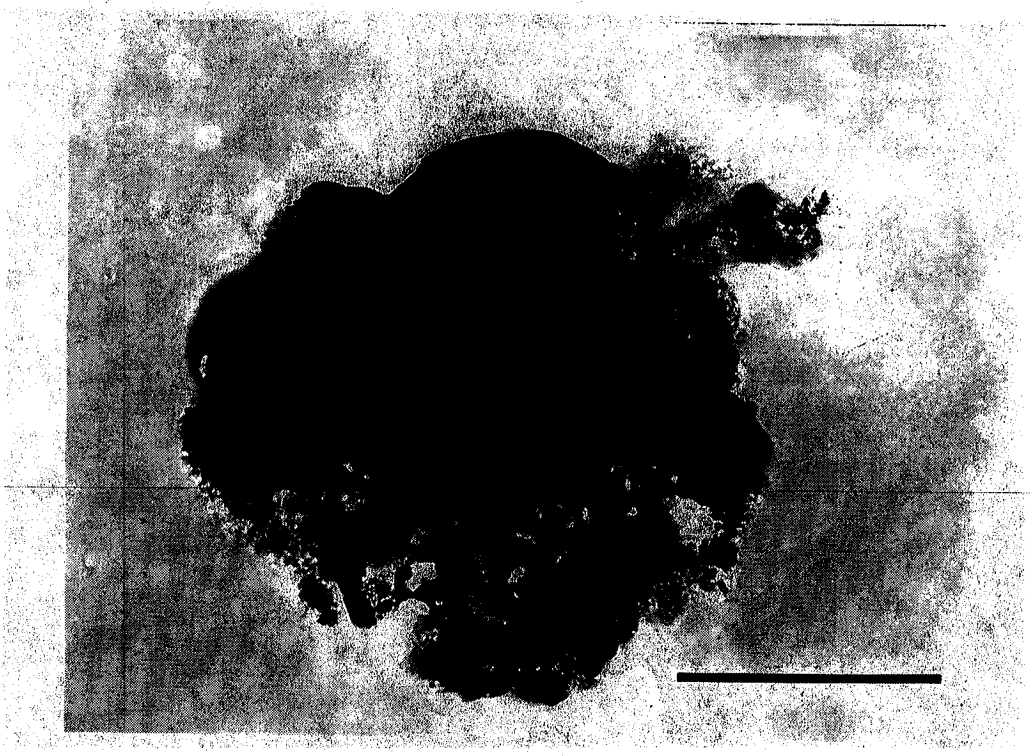

Figure 5. Carbonaceous sulfur-rich particulate associated with the Los Angeles urban plume Nov. 12-13, 1973; note the inhomogeneous agglomerate composition.

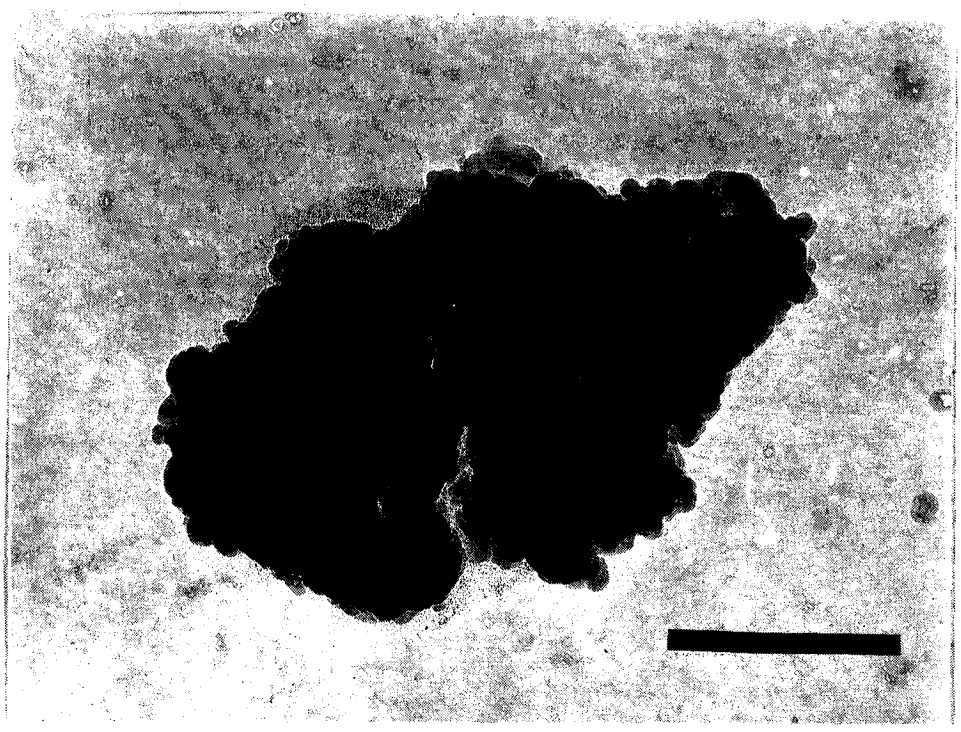

Figure 6. Carbonaceous sulfur-rich particulate associated with the Los Angeles urban plume Nov. 12-13, 1973.

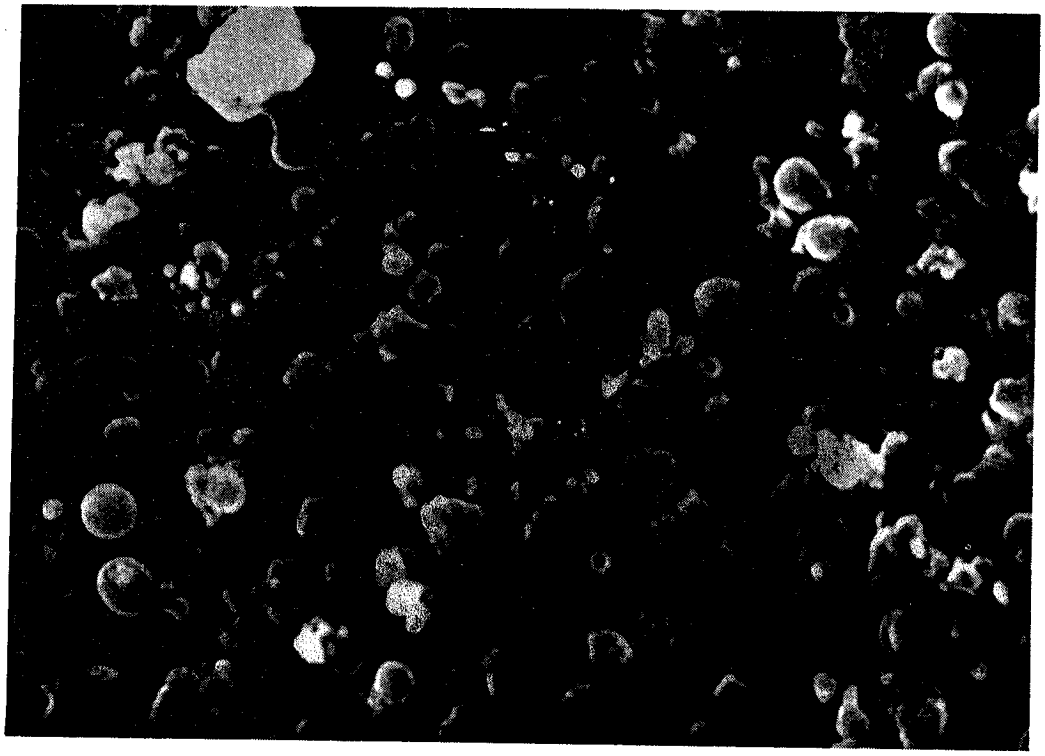

Figure 7. Scanning electron micrograph of a typical secondary particulate collected in the vicinity of Las Vegas, Nevada.

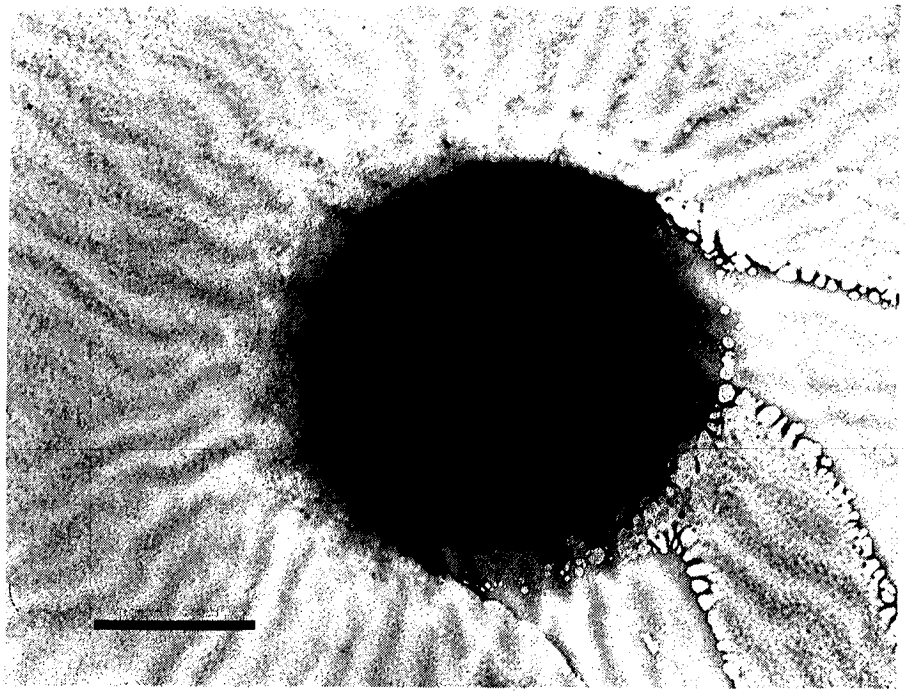

Figure 8. Transmission electron micrograph of a typical secondary particulate collected in the vicinity of Las Vegas, Nevada.

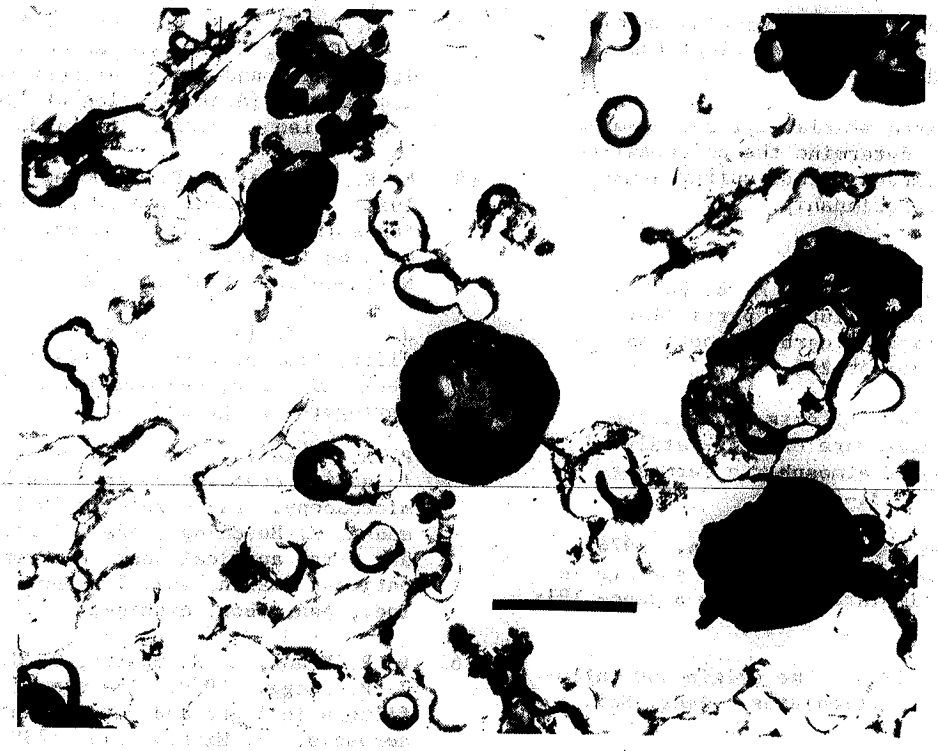

Figure 9. Typical environmental carbonaceous particulate collected in the vicinity of Provo, Utah.

Figure 10. Diffraction pattern of an artificially generated submicron size ammonium sulfate particulate.

lability and electron diffraction characteristics of atmospheric particulates and known compounds.

More samples and refined microanalytical examinations are required to determine the universality and nature of the observed carbon-sulfur atmospheric particulate relationship.

REFERENCES

1. T. Novakov, S. G. Chang and A. B. Harker. 1974. Sulfates as pollution particulates: catalytic formation of carbon (soot) particles. Science 186:259-261.

2. J. Freiburg. 1974. Effects of relative humidity and temperature on iron-catalyzed oxidation of SO_2 in atmospheric aerosols. Env. Sci. Tech. 8:731-739.

3. P. T. Cunningham and S. A. Johnson. 1976. Spectroscopic observation of acid sulfate in atmospheric particulate samples. Science 191: 77-79.

4. P. F. Fennelly. 1976. The origin and influence of airborne particulates. Amer. Sci. 64:46-56.

5. R. F. Maddalone, R. L. Thomas and P. W. West. 1976. Measurement of sulfuric acid aerosol and total sulfate content of ambient air. Env. Sci. Tech. 10:162-168.

6. P. Middleton and C. S. Kiang. 1977. A kinetic aerosol model for the growth of secondary sulfuric acid particles. [Submitted J. of Atmos. Sci.].

7. R. E. Weiss, A. P. Waggoner, R. J. Charlson and N. C. Ahlquist. 1977. Sulfate aerosol: its geographical extent in midwestern and southern United States. Science 195:979-980.

8. R. L. Tanner and L. Newman. 1976. The analysis of airborne sulfate: a critical review. J. Air Poll. Cont. Assoc. 26:737-747.

9. P. A. Russell and C. O. Ruud. 1976. An analysis of particulates from the Denver urban plume using scanning electron microscopy and energy dispersive x-ray spectrometry. Pages 165-233 *in* P. A. Russell, ed. Denver air pollution study-1973: proceedings of symposium, Vol. I. EPA publication EPA-600/9-76-007a. NTIS, Springfield, Virginia.

10. T. G. Dzubay, M. Garneau, O. Durham, R. Patterson, T. Ellestad, J. Durham. 1976. X-ray fluorescence analysis of Denver aerosol. Pages 141-164 *in* P. A. Russell, ed. Denver air pollution study-1973: proceedings of symposium, Vol. I. EPA publication EPA-600/9-76-007a. NTIS, Springfield, Virginia.

11. P. A. Russell. 1978. Further studies of particulates associated with Denver's urban plume. [To be published by EPA].

12. C. O. Ruud, C. S. Barrett, P. A. Russell and R. L. Clark. 1976. Selected area electron diffraction and energy dispersive x-ray analysis for the identification of asbestos fibers, a comparison. Micron 7:115-132.

13. B. E. P. Beeston, R. W. Horne and R. Markham. 1972. An introduction to electron diffraction. Pages 195-323 *in* A. M. Glauert ed. Practical methods in electron microscopy, vol. I. North-Holland Publishing Co., London, G. B.

14. J. A. Gard, 1976. Interpretation of electron diffraction patterns. Pages 52-67 *in* H. R. Wenk, ed. Electron microscopy in mineralogy. Springer-Verlag, N.Y.

15. P. A. Russell. 1978. Analyses of atmospheric sulfur containing particles by electron microscopy. Pages 205-210 *in* P. A. Russell and A. E. Hutchings, eds. Electron microscopy and x-ray applications: environment and occupational health, vol. I. Ann Arbor Science, Inc., Ann Arbor, Michigan.

16. E. R. Frank, K. R. Spurry, D. C. Sheesley and J. P. Lodge. 1970. The use of Nuclepore filters in light and electron microscopy of aerosols. J. Microscopie 9:735-740.

17. J. Donnet and A. Voet. 1976. Carbon black: physics, chemistry and elastomer reinforcement. Marcel Dekker, Inc., N.Y.

18. C. E. Hall. 1948. Dark-field electron microscopy, II. Studies of colloidal carbon. J. Appl. Phys. 19:271-277.

19. A. Howie, O. L. Krivanek and M. L. Rudee. 1973. Interpretation of electron micrographs and diffraction patterns of amorphous materials. Phil. Mag. 27:235-255.

20. D. B. Kittelson and D. F. Dolan. 1978. Dynamics of sampling and measurement of diesel engine exhaust aerosols. (Presented at the conference of carbonaceous particles in the atmospheres, Lawrence Berkeley Laboratory, 1978).

21. M. L. Rudee. 1976. Amorphous material. Pages 476-487 *in* H. R. Wenk, ed. Electron microscopy in mineralogy. Springer-Verlag, N.Y.

22. M. L. Rudee. 1967. A study of the domain structure of carbon black by both high-resolution dark-field electron microscopy and x-ray diffraction. Carbon 5:155-157.

PRELIMINARY OBSERVATIONS OF SO_2 - SOOT INTERACTION BY CONTROLLED ATMOSPHERE TRANSMISSION ELECTRON MICROSCOPY

Thomas T. Chung & John Dash
Department of Physics
and
Robert J. O'Brien
Department of Chemistry
Portland State University
P.O. Box 751
Portland, Oregon 97207

ABSTRACT

Using a special chamber, it was possible to observe directly in the transmission electron microscope the interaction of soot with a mixture of SO_2, O_2 and H_2O gases. Growth occurred on the soot, and subsequent passage of NH_3 over the soot produced additional growth. No crystalline products were observed in the in situ experiments, but a similar experiment outside the microscope did produce a small amount of crystalline product.

INTRODUCTION

The electron microscope is a very useful instrument for identifying submicron particles collected from the atmosphere[1]. The chief disadvantage in its use, the necessity of high vacuum, is eliminated by the technique of controlled atmosphere electron microscopy (CAEM)[2]. We have been developing this technique for in situ study of gas/particle interactions in a transmission electron microscope (TEM). The technique we use consists of inserting a small chamber with thin film windows into the specimen chamber of the electron imaging system. Gases are admitted into the chamber from an external source and are allowed to interact with aerosol particles which were previously collected on the lower window of the chamber. We can follow the interaction of the gases with the particles in real time.

We have used this system to observe the interaction of soot particles with sulfur dioxide gas. Soot particles have been implicated by Novakov et al[3] as important intermediates in the oxidation of atmospheric SO_2 to sulfates. A major question of concern is the extent to which soot interacts with SO_2, i.e., whether covering of the catalytic sites limits the extent of reaction. Our initial experiments were designed to observe any structural changes which occur in soot particles exposed to SO_2.

EXPERIMENTAL DETAILS

The gas-aerosol reactions are performed in an environmental chamber situated inside the tilting specimen stage of a Hitachi HU125C TEM. The chamber is formed by mounting two thin film windows separated by a metal spacer as shown in Figure 1. The main body of the chamber, made of phosphor bronze, contains two ports for gas inlet and outlet and one hole for the electron beam passage. Seals are made with the two O-rings and by mechanical pressure applied against the windows and the spacer by the chamber body. The windows, purchased from E.F. Fullam, Inc., are composite films of Formvar and evaporated SiO deposited on 400 mesh, 2.3 mm diameter copper grids[4]. The lower window is used as a specimen support for the aerosol samples. Temperature of the gaseous environment surrounding the specimen is measured by a Cu-Constantan thermocouple, which passes through a gas port into the chamber. The hot junction is located between the two windows so that it is possible to monitor the temperature of the gas in the chamber.

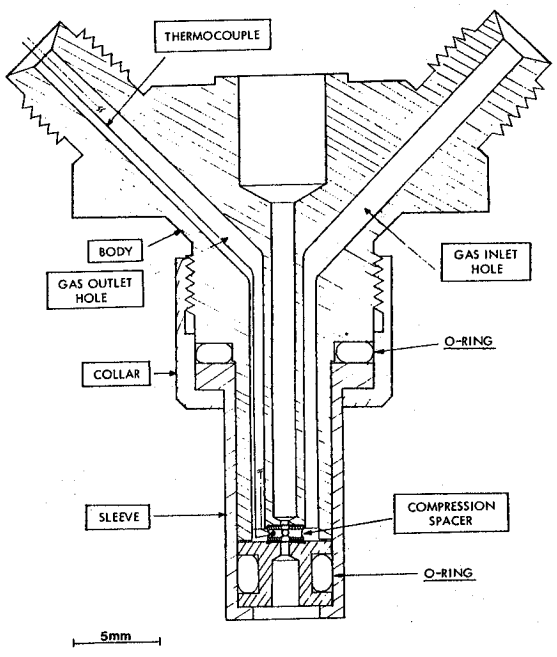

Fig. 1. Longitudinal section through the chamber used in TEM for in situ gas-particle studies. The thin film windows are above and below the compression spacer.

Gas pressure is measured with a Pace variable reluctance differential pressure gauge, which is situated on a gas handling system outside of the microscope. Two teflon tubes carry reactant gases to and from the chamber, with a needle value installed on the outlet tube for controlling gas flow out of the chamber. Thus, the pressure inside the chamber should be nearly the same as that given by the pressure gauge.

Observation in the microscope can be made on the phosphor screen or on a TV display connected to an image intensifier under the screen. Reactions may be observed in real time and recorded on videotape or in a "before and after" mode with the beam off during the reaction. Images and diffraction patterns are recorded both on videotape and on film. The soot aerosol was generated from natural gas in an oxygen-deficient Bunsen burner flame. The aerosol was collected on the inner surface of a glass cylinder held above the flame, and then scraped off onto a thin film window.

RESULTS

Experiments were conducted to determine the morphological changes which occur on soot particles exposed first to SO_2 in moist O_2 and subsequently to NH_3.

Figure 2a shows several soot particles before SO_2 was admitted. Considerable fine structure is apparent at the edges and in the holes within the particles, which are clearly agglomerations of many smaller particles. No diffraction pattern was produced by the particles indicating they are amorphous. Figure 2b shows the same particle after being exposed to SO_2 (0.5 torr), H_2O (4 torr), and O_2 (13 torr) for ten minutes with the electron beam on. All particles have increased in size by a few hundred Å, and lack of a diffraction pattern indicates the absence of crystallinity.

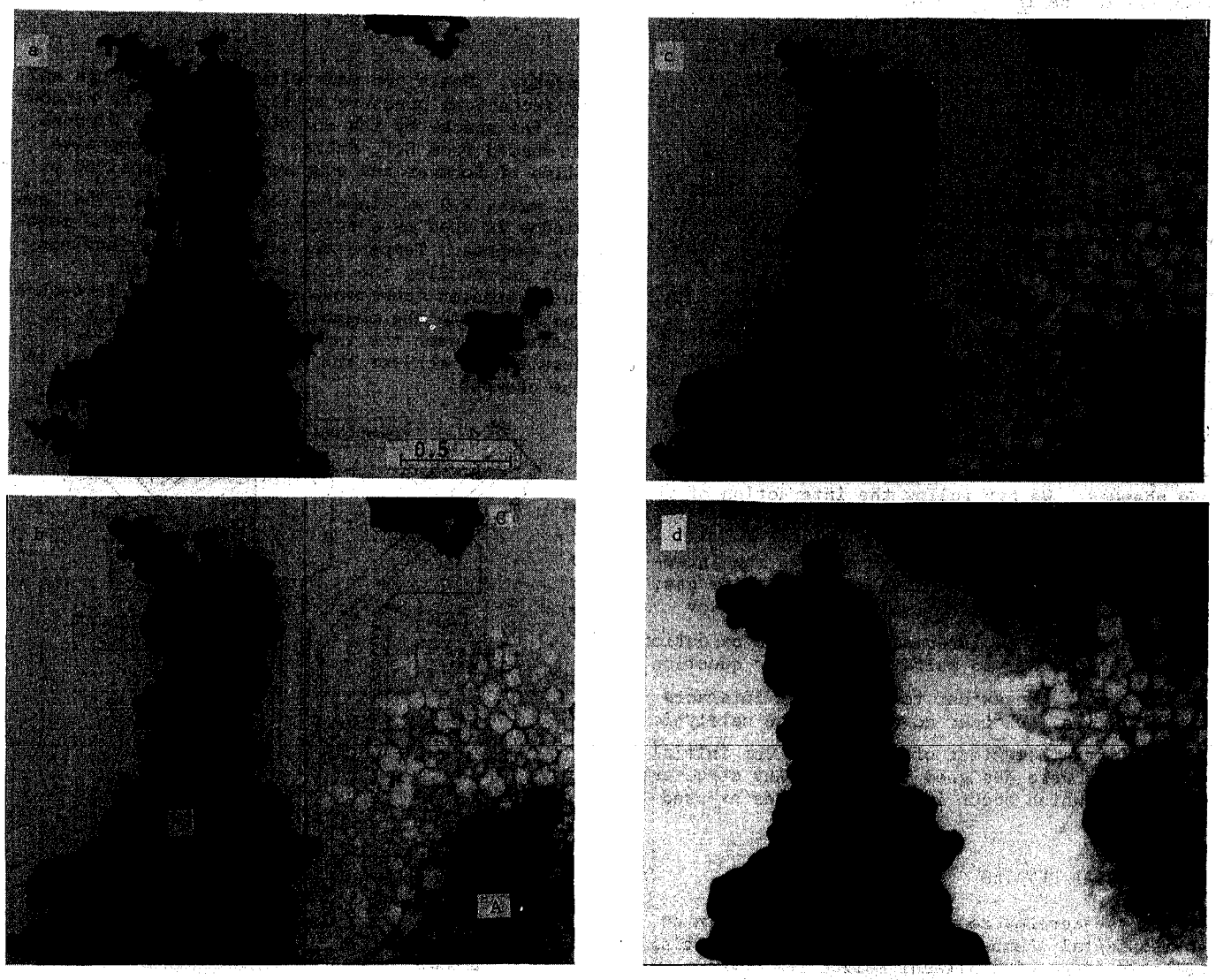

Fig. 2. TEM photographs of soot particles (75 KV): (a) In vacuum before reaction; (b) after passage through the chamber for ten minutes of a mixture of SO_2 (0.5 torr), H_2O (4 torr), and O_2 (13 torr); (c) after additional reaction with NH_3 (1.5 torr) for 5 minutes; (d) after additional reaction with H_2O (19 torr) for about one hour and subsequent drying.

Subsequent passage of NH_3 (1.5 torr) for five minutes caused further growth of the particles as shown in Figure 2c. This additional material does not produce electron diffraction either, in spite of the crystalline nature of $(NH_4)_2SO_4$ which would be a possible reaction product. The particle coating did not change, either in size or in diffraction characteristics, when pumped on with a mechanical pump. Water vapor (19 torr) was then passed through the chamber for about one hour, and the soot became less transparent near the edges, Figure 2d. Again, electron diffraction gave no evidence of crystalline material.

The particles in region A of Figure 2b were observed continuously under the electron beam during passage of the gases through the chamber. The substrate in this region became mottled, apparently because of interaction of the gases with the substrate under the influence of the electron beam. There is no mottling on the substrate to the left of the conglomeration of soot (B) or near particle C. These regions were exposed to the electron beam only before and after passage of the gases. The soot particles which were not under continuous exposure to the beam appear to have changed to approximately the same extent as those which were under continuous exposure. It therefore seems that the electron beam did not affect the soot-gas interaction but that it did cause interaction between the substrate and the gas.

An experiment under similar conditions was performed outside of the microscope with soot particles collected from partially-burned natural gas on a glass slide. This slide with soot particles was put into a glass flask connected to the gas system. After removing the air with a mechanical pump, a mixture of SO_2, O_2, and H_2O of the same partial pressure as before was passed through the flask for 10 minutes. No change was observable with the naked eye at this stage, but evacuation of the flask followed by introducing NH_3 (12 torr) caused a layer of white material to deposit on the soot particles on the slide and also on the walls of the flask. When exposed to air, it was found that the white material partially disappeared. Using an x-ray diffractometer, it was found that no sharp scattering peaks were produced by the residual deposit on the slide. A small number of white specks were still observable on the soot surface with a light microscope. Some of these were removed and examined in vacuum with the electron microscope. These specks were found to be thin, crystalline platelets, Figure 3. The diffraction pattern, Figure 4 was obtained from the platelet in Figure 3, and the same pattern was obtained from other, similar platelets. Further work is necessary to determine the crystal structure and composition of these platelets. These platelets were not observed in the <u>in situ</u> electron microscope experiments.

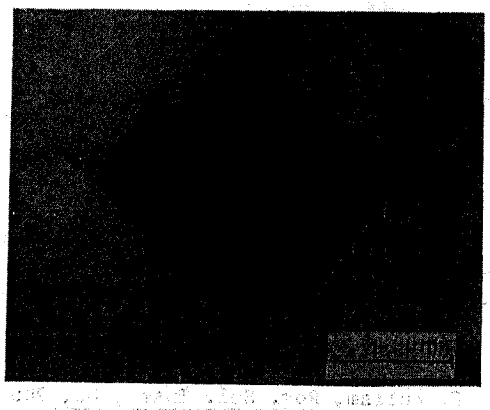

Fig. 3. Crystalline platelet which formed outside the TEM on soot particles which were subjected to same treatment as those in Figure 2. See text for explanation.

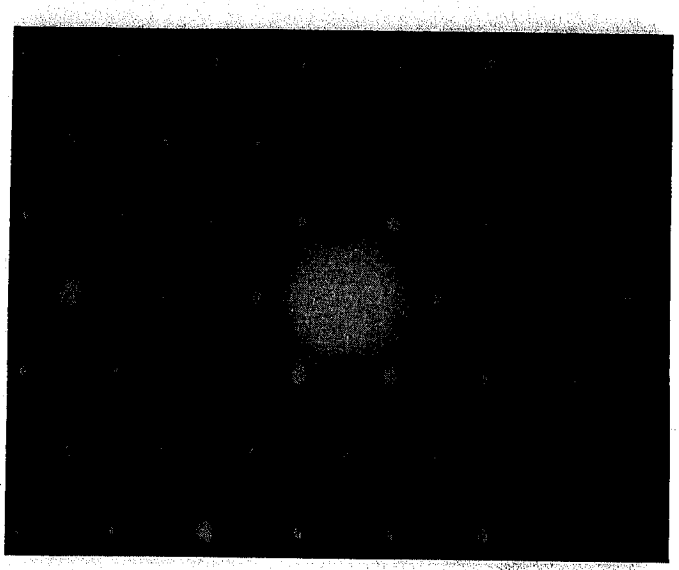

Fig. 4. Electron diffraction pattern from the platelet in Figure 3. The plane spacing for the innermost spots is 4.39 Å. The structure has not yet been determined.

DISCUSSION OF RESULTS

These results demonstrate that <u>in situ</u> electron microscopy can be used to study fine-scale, heterogeneous reactions. Identification of crystalline reaction products is possible by electron diffraction, as we have shown in other experiments (5). No crystalline products were detected in the above <u>in situ</u> experiments, but the larger-scale experiment indicated that crystalline material does form to a small extent.

Although these results are preliminary in nature, they do appear to support the previous report[3] that soot in the atmosphere may be a significant catalyst for the oxidation of SO_2.

ACKNOWLEDGEMENT

This research was supported by NSF Grant No. SER 76-18132.

REFERENCES

1. R.D. Cadle, "The Measurement of Airborne Particles," (John Wiley & Sons, N.Y., 1975).

2. R.T.K. Baker, CRC Critical Review in Solid State Science, 6, 375 (1976).

   D.F. Parsons, Science, 186, 407 (1974).

3. T. Novakov, et al., Science, 186, 259 (1974).

4. E.F. Fullam, Rev. Sci. Inst., 43, 245 (1972).

5. J. Dash, T.T. Chung, & R.J. O'Brien, To be published.

ON THE IMPORTANCE OF CARBONACEOUS PARTICLES TO THE HETEROGENEOUS FORMATION OF SULFATE IN PLUMES

J. Freiberg
Department of Environmental Science
Cook College, Rutgers University
New Brunswick, New Jersey 08903

ABSTRACT

Yield expressions are developed for heterogeneous oxidations occurring in expanding plumes with and without the participation of carbonaceous particles. The expressions are functionally different from each other but they indicate that all the oxidations proceed not to completion but to fractional asymptotic limits. Most of the oxidation occurs near the SO_2 source, rather than uniformly throughout the expanding plume.

The yield expressions are scaled to a chemistry-dispersion ratio for purposes of comparing their respective sensitivities to dispersion. At equal ratios and equal downwind distances, the yield of oxidation in the presence of carbonaceous particles is higher than that of oxidation in the absence of particles. The differences in yield are greatest if the ratio is small and least if the ratio is large.

INTRODUCTION

A significant aspect of carbonaceous particles is their relationship to sulfate, an air pollutant which is highly detrimental to human health[1,2]. Various laboratory studies have shown that carbonaceous particles catalyze the oxidation of SO_2 to sulfate with the conversion occurring either on the surface of the particles [3,4,5] or in a liquid film residing on the surface of the particles[6,7]. Moreover, field investigations [8,9] have suggested that sulfate formation in power plant plumes is catalyzed by carbonaceous particles containing heavy metals (e.g. iron and manganese) and a recent long-range transport investigation [6] of urban palls with high concentrations of sulfate and manganese-containing soot revealed that there was "a direct proportionality between the concentration of particle-borne sulphur and the content of dark components (soot) in the particle."

Carbonaceous particles in the atmosphere (fly ash) not only catalyze the conversion of SO_2 to sulfate but also transport the sulfate significant distances. Only 5% of the sulfate-bearing particles are removed within 20 km. from their source [10] and soot carrying sulfate may travel more than 1000 km. from the source [11]. Thus the fly ash extends the adverse impact of sulfate on air quality to areas far from the formation point.

In addition to catalyzing the conversion and transporting the sulfate, carbonaceous particles might even enhance the toxicity of the sulfates. It has long been recognized [1,12,13] that more of a gas may reach the lungs upon inhalation if the gas has been adsorbed onto aerosol particles.

Like SO_2 (the precursor of sulfate), carbonaceous particles are generated mainly by the combustion of fossil fuels. Hence increases in the use of fossil fuels can be expected to increase the amount of sulfate being formed and transported. But, as has been argued persuasively [14], prediction of the extent to which combustion increases will impact air quality (and hence human health) is hampered by the fact that the present knowledge of SO_2 conversion in plumes is very limited.

The problem of how to estimate the rates of sulfate formation in plumes is, accordingly, of major importance.

OXIDATION OF SO_2 IN PLUMES

The relative importance of the various chemical paths for sulfate formation in plumes is customarily ascertained by comparing their respective rates, which are calculated by substituting what are believed to be representative values of atmospheric concentrations into rate expressions whose rate constants are assumed to be known. This approach produces results which vary greatly with atmospheric and local conditons (such as relative humidity and temperature) and concentrations of pollutants such as HC, NO_x and metal catalysts. Moreover, it ignores a factor which has a most important influence on the rate of reaction, namely dispersion.

The assumption on which this conventional approach is based - i.e., that oxidation proceeds independently of atmospheric dispersion - is rationalized by reference to laboratory studies which found that SO_2 oxidations were first order processes.

$$[SO_4^{=}]_t = [SO_2]_o \exp(-kt) \qquad (1)$$

But in an expanding plume, unlike in a laboratory vessel of fixed volume, SO_2 is transported with the mean wind and is subjected to the forces of irregular wind eddies. This causes the SO_2 to mix with the ambient air, becoming continuously more diluted at the same time as it is oxidized to sulfate on the surface of particles or in liquid films on the surface of particles. Since the sulfate formation process requires not only that the SO_2 react chemically on a particle or in a droplet, but also that the SO_2 reach the particle or droplet to begin with, the nature of the particular dispersion of the SO_2, particles and droplets will significantly affect the rate of sulfate formation.

The object of this paper is to present a simple diagnostic model which will illustrate the effect of dispersion on heterogeneous SO_2 oxidations occurring with and without the particiof carbonaceous particles. Yield expressions which take dispersion into account will be derived. They will then be scaled to a chemistry-dispersion ratio for purposes of comparing their respective sensitivities to dispersion.

Heterogeneous Mechanisms

It is known that SO_2 in an expanding plume can be heterogeneously oxidized to sulfate in three ways:

(1) on the surface of particles;
(2) in a liquid film on the surface of particles through the participation of heavy metal catalysts dissolved in the film;
(3) in aqueous aerosols without catalysis.

Sulfate formation on the surface of particles. For example:

$$\frac{d[SO_4^=]}{dt} = k_s\,[SO_2]\,[A]\,(1-\theta) \qquad (2s)$$

where A is the total capacity (in mmgl/mg) of a given amount of particles to form sulfate and θ is the fraction of surface sites occupied by sulfate molecules at time t (This is like the rate of Chun and Quon[15]. When in-plume sulfate formation occurs by this route, SO_2 diffuses to carbonaceous particles and reacts with chemisorbed O_2).

Sulfate formation in a liquid film around a particle, catalyzed by heavy-metal solutes, buffered by ammonia. For example:

$$\frac{d\,[SO_4^=]}{dt} = \frac{k_c\,[H_2SO_3]\,[Fe^{+3}]}{[H^+]_{buff}} \qquad (2c)$$

(This is like the rate of Karraker[16], Brimblecombe[17], and Freiberg[18]. Here the SO_2 in the gas phase diffuses to the droplets and dissolves, and heavy-metal ions (e.g. Fe^{+3}) present in the carbonaceous ash within each droplet also dissolve. The ions catalyze the oxidation of SO_2 to H_2SO_4).

In aqueous aerosols, with no catalysts present, buffered by ammonia. For example:

$$\frac{d\,[SO_4^=]}{dt} = \frac{k_u\,[H_2SO_3]}{[H^+]^2_{buff}} \qquad (2u)$$

(This is like the rate of Scott and Hobbs[19] and Beilke, et al.[20] Here the SO_2 diffuses to the droplets and dissolves and is oxidized to H_2SO_4 without the participation of catalysts).

When any of the three processes described above occurs in an expanding atmosphere, the dispersion dilutes both the SO_2 and the aerosol. As the distances between the SO_2 molecules and the particles or droplets increases, the probability of reaction decreases accordingly. Thus there is a relationship between the rate of dispersion and the rate of H_2SO_4 formation.

The in-plume oxidation of SO_2 is analogous[21] to a chemical reaction occurring in an expanding volume reactor, a mechanism which was first explained by Benton[22].

Table 1. Yield and characteristic time expressions for heterogeneous oxidations in dispersing plumes ($V=bt^2$).

CHEMISTRY COUPLED TO DISPERSION / CHEMISTRY	FRACTIONAL YIELDS		CHARACTERISTIC TIMES		
	$(SO_4^=)_t/(SO_2)_o$	$(SO_4^=)_\infty/(SO_2)_o$	HALF LIFE OF REACTION τ	LIMIT OF τ FOR $R\to\infty$ / $R\to 0$	DEFINITIONS
HETEROGENEOUS SOLUTION CATALYZED Eq. (2c)	$1-E_{tc}E_{oc}$ (4c)	$1-E_{oc}<1$ (5c)	$\left[\frac{1}{t_o}+\frac{b}{K_c}\ln\left(\frac{1+E_{oc}}{2}\right)\right]^{-1}$ (6c)	t_o / $2t_o$	$E_{tc}\equiv\exp\frac{K_c}{bt}$; $E_{oc}\equiv\exp-\frac{K_c}{bt_o}$; $R_c\equiv K_c/bt_o$
HETEROGENEOUS SOLUTION UNCATALYZED Eq. (2u)	$\frac{1-E_{tu}E_{ou}}{1+\frac{(SO_2)_o}{(SO_4^=)_o}E_{tu}E_{ou}}$ (4u)	$\frac{1-E_{ou}}{1+\frac{(SO_2)_o}{(SO_4^=)_o}E_{ou}}<1$ (5u)	$\left[\frac{1}{t_o}+\frac{b}{K_u}\ln\left(\frac{(SO_4^=)+[2(SO_2)_o+(SO_4^=)]E_{ou}}{2(SO_4^=)+(SO_2)_o\,[1+E_{ou}]}\right)\right]^{-1}$ (6u)	t_o / $2t_o$	$E_{tu}\equiv\exp\frac{K_u}{bt}$; $E_{ou}\equiv\exp-\frac{K_u}{bt_o}$; $R_u\equiv K_u/bt_o$
	θ_τ	θ_∞			
HETEROGENEOUS SURFACE CATALYZED Eq. (2s)	$\frac{1-E_{ts}E_{os}}{1-\frac{A}{(SO_2)_o}E_{ts}E_{os}}$ (4s)	$\frac{1-E_{os}}{1-\frac{A}{(SO_2)_o}E_{os}}$ (5s)	$\frac{1}{t_o}+\frac{b}{K_s}\ln\frac{(SO_2)_o-[2(A)+(SO_2)_o]E_{os}}{(SO_2)_o-A\,[1+E_{os}]}$ (6s)	t_o / $2t_o$	$E'_{ts}\equiv\exp\frac{K_s}{bt}$; $E_{os}\equiv\exp\frac{K_s}{bt_o}$; $R_s\equiv\frac{K_s}{bt_o}$

Setting the expanding volume V at $V=bt^2$ and applying Benton's method to Eq.(2s), we obtain:

$$\frac{(A)}{V}\frac{d\theta}{dt} = K_s\ (SO_2)\ (A)\ (1-\theta)/V^2 \qquad (3)$$

where $K_s=k_s\ ((SO_2)_o-(A))$.

(Note: throughout this discussion, (x) ≡ amount of x in moles and [x] ≡ concentration of x in moles per liter for any substance x. Thus [x] = (x)/V. $(x)_t$ and $[x]_t$ are (x) and [x] at time t. $(x)_o$ and $[x]_o$ are (x) and [x] at time t_o). In setting $V=bt^2$ we have postulated a particular case of $V=bt^n$, a general form in which dispersion patterns can be described.[23]

Separating variables and integrating analytically, we obtain the following fractional yields:

$$\theta_t = \frac{(SO_2)_o\ (1-E_{ts}\ E_{os})}{(SO_2)_o-(A)E_{ts}\ E_{os}} \qquad (4s)$$

$$\text{and } \theta_\infty = \lim_{t\to\infty}\theta_t = \frac{(SO_2)_o\ (1-E_{os})}{(SO_2)_o-(A)E_{os}} \qquad (5s)$$

where: b is a constant whose value depends on meteorological conditions; t_o is the time at which V = initial volume V_o; $E_{ts} \equiv \exp(K_s/bt)$; and $E_{os} \equiv \exp(-K_s/bt_o)$.

Since $\theta_\infty<1$, it is appropriate to calculate the half life of the reaction (τ_s) rather than the half lives of the reactants. We obtain:

$$\frac{1}{\tau_s} = \frac{1}{t_o} + \frac{b}{K_s}\ln\frac{(SO_2)_o-2(A)+(SO_2)_o\ E_{os}}{(SO_2)_o-(A)} \qquad (6s)$$

After applying Henry's Law ($\beta_s \equiv [H_2SO_3]/[SO_2]$) and Raoult's Law ($\lambda \equiv (1-p/p_o)/[SO_4^=]$, where p/p_o is the relative humidity), as utilized, e.g. by Freiberg[24] we can couple rate expressions (2c) and (2u) to the plume dispersion model in the same manner as the rate expression (2s). We obtain the fractional yields and characteristic times shown in Table 1 (where $K_c=k_c\beta_s\ (Fe^{+3})/[H^+]_{buff}$ and $K_u=k_u\beta_s\ p/p_o\lambda\ [H^+]^2_{buff}$).

RESULTS AND DISCUSSION

In a laboratory vessel of fixed volume, the heterogeneous oxidations (Eqs. (2s), (2c) (2u)) are functionally identical to each other and to the first order reaction (Eq. (1)), and all proceed to completion. But upon coupling the oxidations to the atmospheric dispersion we obtain the yield equations (4s), (4c), and (4u), each of which is functionally different from every other, as are the reaction half life expressions (6s), (6c), and (6u).

None of the dispersion-coupled heterogeneous oxidations proceeds to completion. Each proceeds to a fractional asymptotic limit whose magnitude depends on the ratio of the chemical parameters (K_s, K_c, K_u, $(SO_2)_o$) to the dispersion parameters (b, t_o). It is easily shown that an increase in the ratios will cause an increase in the limit (so that if: $\frac{K_s}{bt_o}\to\infty, \frac{K_c}{bt_o}\to\infty, \frac{K_u}{bt_o}\to\infty$ then $\frac{(SO_4^=)_\infty}{(SO_2)_o}\to 1$ for Eqs. (5s), (5c), and (5u), respectively and vice-versa (when the ratios approach 0, $\frac{(SO_4^=)_\infty}{(SO_2)_o}\to 0$) (see Fig.1).

Moreover, the functional expression are such that at equal ratios and equal downwind distances, the yield of heterogeneous oxidation in the presence of particles (Eqs. (2s), (2c)) will be higher than that of heterogeneous oxidation in the absence of particles (Eq. (2u)). Also, the sensitivities of the reactions to the dispersion are such that the differences between the yields will be greatest if the ratio of the chemical parameters to the dispersion parameters is small and least if the ratio is large (see Table 2 and Fig. 1).

Table 2. The fractional yields of heterogeneous oxidations for various chemistry-dispersion ratios.

YIELD OF HETEROGENEOUS CATALYZED OXIDATION (in %)

Ratio° \ d/do**	1.25	1.50	2.00	4.00	5.00	10.00
0.1	1.99	3.25	4.88	7.22	7.68	8.61
0.5	9.52	15.35	22.12	31.95	32.96	36.24
1.0	18.13	28.33	39.35	52.76	55.06	59.34
2.0	32.93	48.66	63.21	77.68	79.81	83.47
10.0	86.47	96.43	99.33	99.93	99.97	99.99

YIELD OF HETEROGENEOUS SURFACE OXIDATION (in %)

0.1	2.20	3.6	5.39	8.03	8.47	9.48
0.5	10.47	16.76	23.99	34.28	35.34	38.71
1.0	19.74	30.52	41.89	55.38	57.66	61.86
2.0	35.30	51.29	65.63	79.46	81.45	84.87
10.0	87.66	96.78	99.40	99.95	99.97	99.99

YIELD OF HETEROGENEOUS UNCATALYZED OXIDATION (in %)

0.1	.18	.30	.46	.70	.75	.85
0.5	.94	1.62	2.51	4.09	4.28	4.91
1.0	1.97	3.46	5.56	9.21	10.02	11.71
2.0	4.27	7.93	13.51	24.04	26.43	31.47
10.00	36.75	71.06	93.09	99.34	99.67	99.89

* d=Distance between the source and the downwind edge of the plume.
** do=Distance between the source and the downwind edge of the plume at the time when oxidation began. (i.e. at d/do=1, the yield is zero.
° Ratio=Ratio of the product of the chemical parameters to the product of the dispersion parameters.

These results illustrate that the three oxidation paths are all to differing degrees sensitive to dispersion. The effect of dispersion is usually neglected in studies which compare the importance of various rate mechanisms. Since the ratios are not usually equal at equal downwind distances in the same dispersing atmosphere, one cannot conclude that as a general rule catalyzed oxidation proceeds faster on a particle's surface than in an aqueous film, or that both are generally faster than uncatalyzed oxidation. But by the same token, conclusions as to the relative importance of the various atmospheric oxidation paths cannot legitimately be drawn from laboratory derived rate expressions without making due allowance for the effects of dispersion.

Since the oxidations proceed not to completion but only towards a fractional asymptotic limit, it is appropriate to focus not on the half lives of the reactants but on the half lives (τ) of the reactions. Each half life expression is functionally different from every other. But, they are all functions of the ratio of chemical parameters to dispersion parameters. Also, they are all bounded above and below by the same limits (t_o, $2t_o$). Thus half the final sulfate yield of SO_2 oxidation will be obtained close to the source and in an amount of time whose limits are constant for any given dispersion pattern and do not depend on the magnitude of the rate constants and the dispersion parameters. This conclusion is in agreement with previous results [21,25].

The present analysis does not take into account dispersion coupled oxidations which are limited by diffusion of ambient gases such as O_3 and NH_3 [26]. These will have different sensitivities to disperson.

SUMMARY

This paper presents a diagnostic model for the heterogeneous oxidation of SO_2 with and without the participation of carbonaceous particles. It shows that while the rates of the various oxidation paths may be functionally identical when the oxidations take place in laboratory vessels of fixed volume, they will be functionally different from each other when the oxidations take place in expanding plumes.

The yields are functions of the ratios of chemical parameter to the dispersion parameters and are such that the oxidation does not proceed to completion but to a fractional asymptotic limit.

The half lives of reaction are also functions of the ratios. They show that the oxidation will occur close to the source and in an interval of time whose limits are constant for any given dispersion pattern and independent of the chemical parameters involved.

The same conceptual results can be obtained for an air shed expanding in three dimensions, for which $V = bt^3$ (there $t_o \leq \tau \leq \sqrt{2}\, t_o$) and, indeed, for any expanding atmosphere whose rate of expansion is higher than first order, i.e., for all dispersions $V = bt^n$ for which $n > 1$. (When $n \leq 1$, the reactions proceed to completion, but their yields and characteristic times depend on b and t_o).

The sensitivities of the heterogeneous reactions to dispersion are such that at equal ratios and equal downwind distances, the yield of oxidation in the presence of carbonaceous particles is higher than that of oxidation in the absence of particles. The differences in yield are greatest if the ratio is small and least if the ratio is large.

These results emphasize the importance of considering the sensitivity of rate expressions to dispersion when evaluating the relative importance of various rate mechanisms in dispersing atmospheres.

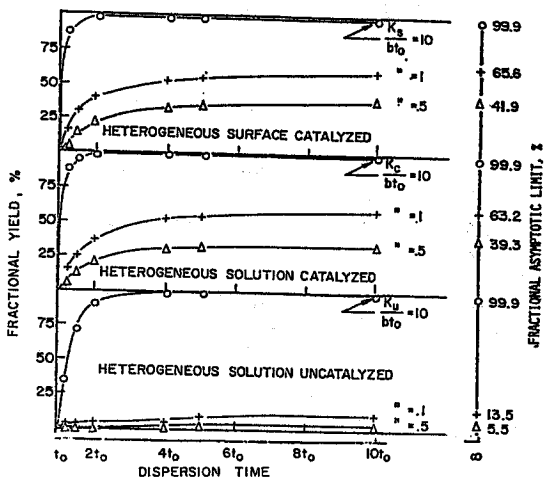

Fig. 1. Sensitivity of the sulfate yield to changes in dispersion time, for various ratios of "chemistry" to "dispersion".

ACKNOWLEDGMENTS

The author wishes to thank Cook College of Rutgers University for underwriting this work and Ms. Joan Kearney for typing this manuscript.

REFERENCES

1 M.O. Amdur, "Inhaled Particles and Vapours", C.N. Dowig, Ed., p.281-294, Pergamon Press, New York, (1961).

2 S.K. Friedlander, "Small Particles in Air Pose a Big Problem", Envir. Sci. Tech. 7, 1115 - 1118, (1973).

3 T. Novakov, S. G. Chang, A. B. Harker, "Sulfates as Pollution Particulates; Catalytic Formation on Carbon (Soot) Particles", Science 186, 259-261, (1974).

4 B. Barbaray, J. P. Contour, G. Mouvier, "Sulfur Dioxide Oxidation Over Atmospheric Aerosol", Atmospheric Environment 11, 355-356 (1977).

5 H.S. Judeikis, S. Siegel, "Particle-Catalyzed Oxidation of Atmospheric Pollutants". Atmospheric Environment 7, 619-631 (1973).

6 C. Brosset, "Water-Solube Sulphur Compound in Aerosols", Paper #2, ISSA, Dubrovnik, Yugoslavia, (September, 1977).

7 S. G. Chang, R. Brodzinsky, S.S. Markowitz, T. Novakov, "Catalytic Oxidation of SO_2 on Carbon in Aqueous Suspension", Paper #18, Conference on Carbonaceous Particles in the Atmosphere, Berkeley, California, (March 1978).

8 P. M. Foster, "The Oxidation of Sulfur Dioxide in Power Station Plumes", Atmospheric Environment 3, 157-175, (1969).

9 L. Newman, J. Forrest and B. Manowitz, "The Application of an Isotopic Ratio Technique to a Study of the Atmospheric Oxidation of SO_2 in the Oil Fired Power Plant", Atmospheric Environment 11, 345 - 353, (1977).

10 N.R. Glass, "Environmental Effects of Increased Coal Utilization" Office of Health and Ecological Development, Washington, D.C. 20470 (1977)

11 H. Rodhe, C. Persson, O. Akesson, "An Investigation into Regional Transport of Soot and Sulphate Aerosols", Atmospheric Environment 6, 675-693, (1972).

12 L. Dautrebande, "Bases Experimenteles de le Protection Contre les Gaz de Combat", J. Duculet, Gembloux, Belgium (1939).

13 A. Goetz, "An Interpretation of the Synergistic Effect Based upon Specific Surface Action of Airborne Aerosols", Final Report U.S.P.H.S. Contract SAph 69557 (Part B) (1958).

14 J. M. Hales, Tall Stacks and the Atmospheric Environment. Batelle-NW Labs Report to U.S.E.P.A. (EPA-450/3-76-007), Research Triangle Park, N. C., (January 1976).

15 K. C. Chun, J.K. Quon, "Capacity of Fe_2O_3 Particles to Oxidize SO_2 in Air", Environ. Sci. Tech. 7, 532-538 (1973).

16 D. G. Karraker, "The Kinetics between Sulfurous Acid and Ferric Ion". J. Phys. Chem. 67, 871-874, (1963).

17 T. Brimblecombe, D. J. Spedding, "The Catalytic Oxidation of Micromolar Aqueous SO_2", Atmospheric Environment 8, 937-944 , (1974).

18 J. Freiberg, "The Mechanism of Iron Catalyzed Oxidation of SO_2 in Oxygenated Solutions". Atmospheric Environment 9, 661-673 (1975).

19 W.D. Scott, P. V. Hobbs, "The Formation of Sulphate in Water Droplets", J. Atm. Sci. 24, 54-57 (1967)

20 S. Beilke, D. Lamb, J. Muller, "On the Uncatalyzed Oxidation of Atmospheric SO_2 by O_2 in Aqueous Solutions", Atmospheric Environment 9, 1083-1090, (1975).

21 J. Freiberg, "The Iron Catalyzed Oxidation of SO_2 to Acid Sulphate Mist in Dispersing Plumes". Atmospheric Environment 10, 121-130, (1976).

22 A.J. Benton, "The Kinetics of Gas Reaction at Constant Pressure", J. Am. Chem. Soc. 53, 2984-2997 (1931).

23 H. D. Slade "Meteorology and Atomic Energy", U. S. Atomic Energy Commission, (1968).

24 J. Freiberg, "Effects of Relative Humidity and Temperature on Iron-Catalyzed Oxidation of SO_2 in Atmospheric Aerosols, Environ. Sci. Techn. 8, 731-734, (1974).

25 J. Freiberg, "The Conversion Limit and Characteristic Time of SO_2 Oxidation in Plumes", Atmospheric Environment 12, 339-347, (1978).

26 W. E. Wilson, R. J. Charlson, R. B.Husar, K.T. Whitby and D. Blumenthal, "Sulfates in the Atmosphere", E.P.A.-60017-77-021 (1977).

Capture of Atmospheric Gases by Water Vapor Condensation on Carbonaceous Particles

Michael J. Matteson
Georgia Institute of Technology
Atlanta, Ga. 3C332

ABSTRACT

The oxidation of SO_2 and interaction of NO_2 with suspended carbonaceous particles (SCP) have been demonstrated by several research laboratories. Reaction rates in the aqueous phase are usually a function of the concentration of dissolved gaseous reactant. The work reported here deals with a mass transfer mechanism which enhances the concentration of dissolved gases absorbed by SCP via water vapor condensation. In the first phase of these investigations, we have suspended large (D = 2 - 3 mm) cold (5 - 7°C) water droplets in warm (25 - 30°C) Nitrogen containing various concentrations of water vapor and a representative atmospheric gas (SO_2, O_2 or NO_2). The gas was absorbed by the water droplet during the water vapor condensation process and the droplet collected after various periods of exposure. The droplet temperature was monitored with a Y/SI Hypodermic probe and the amount of condensed water calculated from this time - temperature profile. The amount of dissolved gas was measured upon collecting the droplets and time - concentration profiles were compared for the various condensation rates. All three gases were absorbed at concentrations several levels greater than when no water vapor condensation was taking place. These results are correlated with the concentrations of the gas and the water vapor in N_2. The results support the fact that non-steady state mass transfer via water vapor condensation is a strong mechanism for concentrating atmospheric gases on SCP. This type of mechanism occurs frequently in smoke plume formation at stack exits, and in cloud formation in the atmosphere. A comparison of time scales for the competing processes which utilize the dissolved gases will determine which chemical reactions are affected.

INTRODUCTION

The absorption of gases by clouds, fogs and water droplets is a key step in the removal process for many trace gases in the atmosphere. The high acid content of rainfall in many indistrial regions is attributed to the absorption of sulfur and nitrogen oxides. Upon the release of fossil fuel stack gases, containing water vapor, which are rapidly cooled from 250°F to ambient temperatures, much of the associated oxides of sulfur and nitrogen is dissolved as the water is condensed upon suspended carbonaceous particles (SCP) and the smoke plume is formed.

The object of the work reported here is to determine the rates of absorption of SO_2, NO_2 and oxygen at stack gas concentration by water droplets undergoing growth due to water vapor condensation.

PART I: SO_2 ABSORPTION

This investigation was made in an effort to determine how water vapor condensation affects the uptake of SO_2 by droplets and how this absorption compares with situations where no water vapor is condensing. We decided to use a falling drop technique here since SO_2 is very quickly absorbed (Figure 1). By letting the drop fall various distances, and knowing the drop size, we were able to vary exposure time. The SO_2 and water vapor concentration in the gas through which the drop fell were controlled, so that we were able to measure the amount of SO_2 absorbed as a function of time, water vapor condensation and SO_2 concentration. By holding the drop temperature to around 7°C and the humid gas at about 25°C, we could adjust the water vapor concentration in the gas such that supersaturation ratios (SSR) of 1.0, 1.5, 2.0 and 2.5 were obtained. The SSR is the ratio of water vapor pressure in the gas to that in equilibrium with the drop.

The droplets were collected in a container continuously flushed with nitrogen to prevent further contact with the SO_2 gas. Five ml of the solution collected were then mixed with one ml of three percent hydrogen peroxide solution, and the pH of the resultant mixture was measured.

The first experiments at a supersaturation ratio (SSR) of 1.0 were undertaken to provide a basis with which to compare SO_2 absorption during water vapor condensation (SSR = 1.5, 2.0, 2.5). The results of these tests are shown in Figures 2 and 3, where the relative average concentration C/C_s is plotted as a function of time. C_s is the equilibrium solubility measured for that particular gas phase concentration. All test results expressed in Figures 2 and 3 were normalized to this value. These tests agree quite well with the mass transfer model proposed by Groothuis and Kramers.[1]

In testing at higher water vapor concentrations, however, we noticed that the absorption of SO_2 exceeded the SSR = 1 case by a significant amount (Figures 2, 3: SSR = 1.5, 2.0, 2.5). The dashed line at $C/C_s = 1.0$ represents the equilibrium solubility of SO_2 in water measured for that gas phase concentration.

PART II: NO_2 ABSORPTION

Investigations into water absorption at low concentrations (ppm range) of nitrogen dioxide are relatively few. From Borok's[2] data, the Henry's Law constant for NO_2 in water is $H = 100\ atm.^{-1}$

Palmes, et al.[3] and Crecelius and Forwerg[4] found that the NO_2 is present primarily as NO_2^- with only trace amounts of NO_3 when absorbed by water in the ppm range. A possible reaction sequence for the low concentration range may be:

$$3\ NO_2 + H_2O \rightleftharpoons 2HNO_3 + NO \quad (1)$$

$$HNO_3 + 2\ NO + H_2O \rightleftharpoons 3\ HNO_2 \quad (2)$$

$$HNO_2 \rightleftharpoons H^+ + NO_2^- \quad (3)$$

with the ionization proceeding to 100 percent completion as the NO_2 concentration is decreased.

Dekker[4] concluded that the main resistance to mass transfer shifts from the gas phase to the liquid phase as the concentration is lowered. With this background it was decided to test NO_2 in the 100-300 ppm range for enhanced mass transfer via water vapor condensation.

Because of the very low concentrations of NO_2 in water, and since the sample volume is so small, measuring the amount of gas absorbed in water droplets as a function of time demanded a contact chamber where the droplets could be exposed to the desired test atmospheres for long enough exposure times to ensure that near-saturation conditons could be achieved. It was because of this requirement that we decided to use a suspended drop in a moving gas stream (Figure 4). This technique offered the advantage of being able to avoid the masking effects of mass transfer during droplet formation. By synchronizing the droplet injection with a solenoid gas injection switch, it was possible to assure that the droplet was fully formed and internally at rest before exposure to the NO_2 stream. Supersaturation ratios (SSR) of 1.0 (no condensation), 1.5, 2.0, and 2.5 were applied at the onset of exposure.

Because of the necessarily long (up to 1 min.) exposure time, it was not possible to maintain the droplet at a constant temperature, as was desired. Heating of the droplet occurred because of the condensation of water vapor from the gas, the convective transfer of heat from the warmer air mass (25°C) and radiation from warmer surfaces. Droplet temperature was measured with a YSI Model 524 thermistor by suspending the droplet from both the injection capillary and the thermistor needle. These tests showed that the droplet temperature rises quite rapidly during the first 20 seconds and then slows to an equilibrium value somewhat lower than the ambient gas temperature. The water vapor condenses until the droplet vapor pressure is the same as that of the ambient gas, and then evaporation begins. Figure 5 shows the case of ambient water vapor pressure at 2.5 times that in equilibrium with a 5°C droplet. The total amount of water vapor condensed varied with SSR, and there was only evaporation taking place at an SSR = 1.0.

The results presented in Figures 6 and 7 show the NO_2 absorbed by water as a function of time for various SSR and gas phase NO_2 concentrations. The results are normalized to the saturation concentration at the temperature of the droplet when sampled. For the tests at both 100 and 300 ppm NO_2 in the gas phase, the droplets were practically saturated with NO_2 within 5 seconds of exposure. The dashed lines are based on an assumed first order reaction during non-steady state diffusion into a semiinfinite medium (penetration theory).[6]

There is a definite effect on supersaturation as the SSR is increased above 1.0. This continues for about 15 seconds and then droplet concentration returns to the saturation level. Tests at 60 seconds showed that the droplets remain at the saturation concentration. An explanation for the rapid decline in NO_2 supersaturation is indicated in Figure 5 which shows that condensation ceases after 15 - 20 seconds and evaporation begins. Therefore, the supersaturation of NO_2 is strongly connected to the condensation of water vapor. For the case of SSR = 1.0, no condensation and only evaporation occurred. As expected there is no evidence of supersaturation of NO_2. Greater supersaturation was possible at the lower than at higher NO_2 level, as was experienced in the investigations of SO_2.

PART III: O_2 ABSORPTION

Oxygen was tested to determine if a non-hydrolyzing, non-reacting gas would respond to the same enhancement effects of absorption during water vapor condensation as did SO_2 and NO_2. Furthermore, many oxidation processes in fogs depend on the concentration of dissolved O_2.

Since oxygen is so sparingly soluble in water we used the same contact cell (Figure 4) as used with the NO_2 tests. To measure the amount of O_2 absorbed, we adapted a Natelson Microgasmeter, normally used for blood oxygen analysis. Concentrations of O_2 in N_2 tested were 21%, 40%, 60%, and 80%; and SSR were, again 1.0, 1.5, 2.0 and 2.5.

Results are shown in Figures 8 and 9 for 21% and 80% oxygen respectively. The results are normalized to the oxygen saturation value at that temperature. Also a curve has been inserted showing the concentration one would expect if absorption were controlled by diffusion in the liquid phase:

$$\frac{\partial c}{\partial t} = D_{O_2\text{-}H_2O}\ \nabla^2 C_{O_2} \quad (4)$$

As with the tests on SO_2 and NO_2, we noticed that oxygen absorption is definitely enhanced by water vapor condensation.

DISCUSSION

The rate of gas absorption during water vapor condensation or evaporation is a function of both the rate of diffusion in the liquid phase, and the rate at which the water is transported. In order to isolate the effect of the water vapor transport on the rate of absorption, the increase in the amount of gas absorbed and the corresponding increase in the amount of water condensed for different SSR was determined for fixed value of time.

Tests on all three gases indicate that the effect of water vapor transport on absorption follows the relation

$$\frac{d\bar{C}_A}{dt} = k(Y_A)^n \frac{d(H_2O)}{dt} \quad (5)$$

such that

$$\bar{C}_A = k(Y_A)^n (H_2O) \quad (6)$$

where Y_A = absorbed gas concentration in gas phase, mole fraction

(H_2O) = moles water condensed

Gas	k	n
SO_2	3.06×10^2	1.3
NO_2	3.68×10^{-4}	0.105
O_2	5.66×10^{-4}	0.20

A possible explanation for this absorption enhancement may be that under conditions of water condensation, there is a net movement of water vapor toward the water surface, tending to drag extra gas molecules along, whereas in steady-state conditions there exists an equimolar exchange of water molecules both to and from the surface. The gas is absorbed in both cases but in the non-steady state the amount of gas entering the surface is enhanced somewhat by the condensing H_2O molecules. The resistance to absorption is primarily in the liquid phase which is governed by the dissolved gas concentration at the air-water interface. Therefore, if more gas molecules can be "packed" into the surface, this would tend to enhance the overall absorption process.

Another possible explanation for the enhancement effect is the generation of surface instabilities. The transfer of water vapor to the liquid phase may occur in localized amounts over the surface, causing adsorbed gas to be more concentrated at some points in the surface than in neighboring regions. Consequently, at the points of higher concentration the transfer of absorbed gas to within the water bulk moved at a faster pace, dragging surface solution with it. The net result are many surface driven instabilities and an overall surface turbulence, which tends to reduce the liquid phase resistance to gas absorption.

We noted that the enhancement phenomenon is diminished at higher gas phase concentrations. There may be a limit to the number of extra molecules that the condensing water is dragging along.

It is generally assumed, in the steady-state case, that the surface of the droplet is saturated with oxygen and that the saturation concentration is determined by the gas phase concentration at the gas-liquid interface. Under evaporation conditions, this interfacial concentration may be less than that of the bulk gas phase concentration because of the migration of water molecules in opposite direction. For example, the rate of evaporation at SSR = 1.0 at 100 seconds is about 100 times faster than the rate of O_2 absorption over the range of oxygen concentrations tested. Therefore, the liquid phase saturation concentration would tend to be less than one would expect from steady-state conditions. However, acting to oppose this is the escape of water molecules from the surface solution, which would tend to concentrate the oxygen in the liquid at the interface. The net effect as shown in Figure 8 for SSR = 1.0, 1.5 is to produce an equilibrium concentration somewhat lower than the steady-state case for $t \to \infty$.

CONCLUSIONS

Droplets growing by water vapor condensation are able to concentrate gases at levels that far exceed saturation. The implication of these results when extended to growing fogs and clouds is that oxidation processes involving conversion of dissolved SO_2 or NO_2 to sulfates and nitrates may proceed much more rapidly than expected when reactant calculations are based on steady-state concentrations.

ACKNOWLEDGEMENT

This work was supported by Contract No. EE-77-S-05-5592 from the Department of Energy.

REFERENCES

1. Groothuis, H., and H. Kramers, Chem. Eng. Sci., 4, 17 (1955).

2. Borok, M. T., Zh. Prik. Khim., 33, 1761 (1960).

3. Palmes, E.D., A. F. Gunnison, J. Dimattio, and C. Tomczyk, Am. Ind. Hyg. Assoc. J., 37, 570 (1976).

4. Dekker, W. A., E. Snoek, and H. Kramers, Chem. Eng. Sci., 11, 61 (1959).

5. Sherwood, T. K., R. L. Pigford, and C. R. Wilke, "Mass Transfer," McGraw-Hill, Inc., New York, 1975.

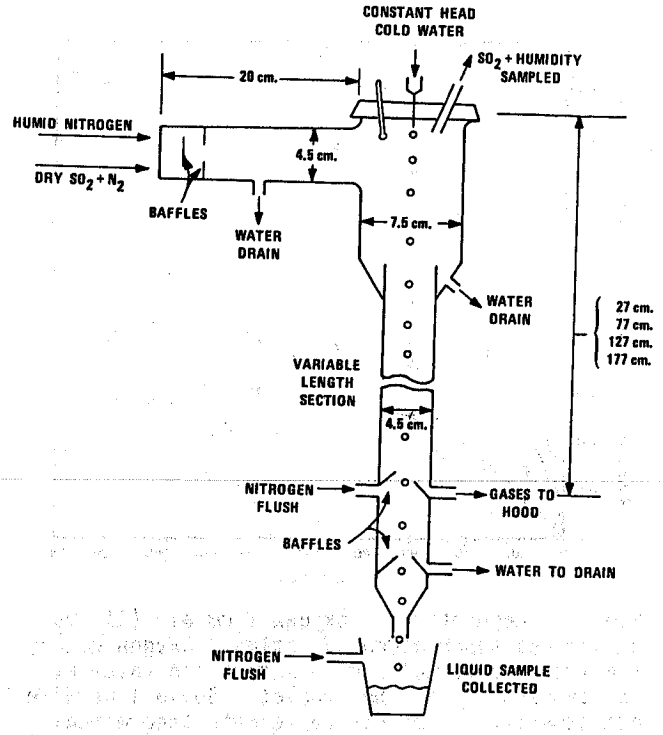

Fig. 1. Absorption Chamber

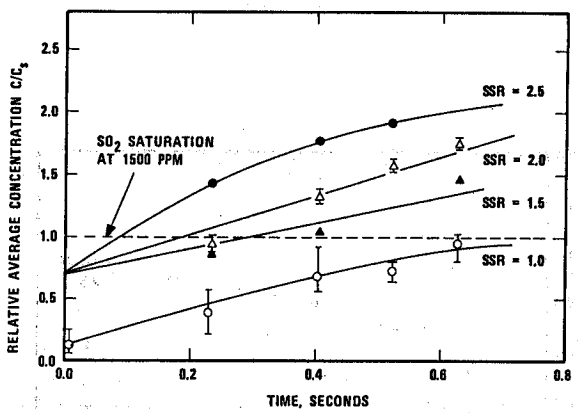

Fig. 2. Rate of absorption of SO_2 by water droplets undergoing condensation in the presence of N_2 and 1500 ppm SO_2.

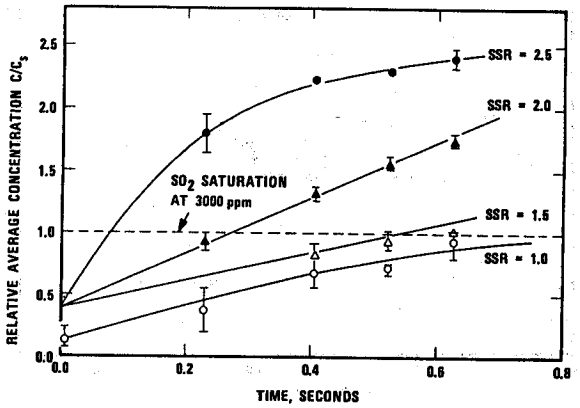

Fig. 3. Rate of absorption of SO_2 by water droplets undergoing condensation in the presence of N_2 and 3000 ppm SO_2.

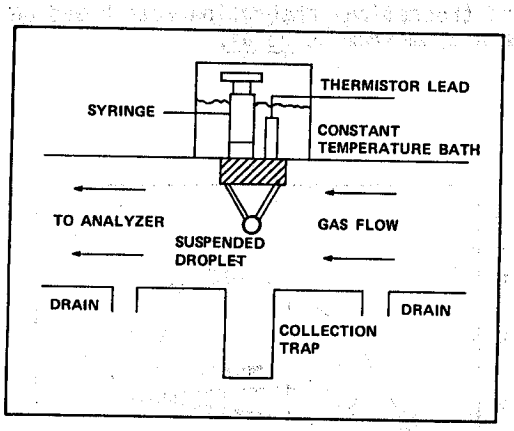

Fig. 4. Contact Cell

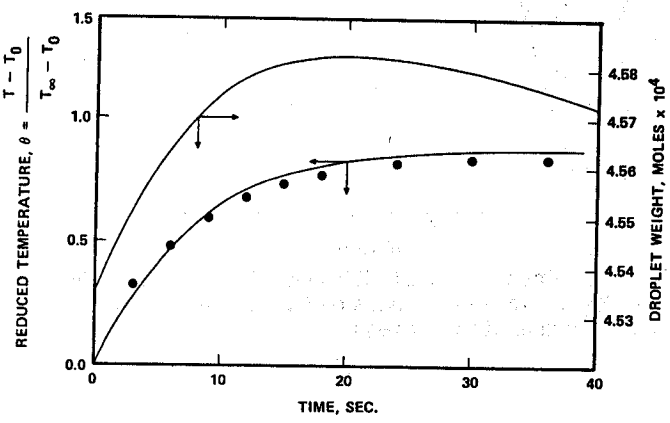

Fig. 5. Droplet temperature and mass variation time. Solid lines represent Runge-Kutta approximations[1] based on energy-material balance for droplet with initial temperature of T_0=5°C exposed to flowing air at T_∞ = 25°C and water vapor pressure = 2.5 times that for water at 5°C. Points are experimentally obtained values.

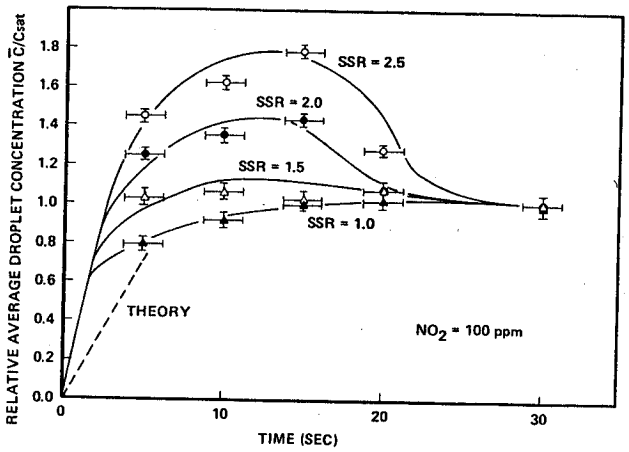

Fig. 6. Absorption of 100 ppm nitrogen dioxide from N_2 at various supersaturation ratios (water vapor condensation rates). Nitrogen dioxide concentrations are normalized to saturation value at the temperature of the droplet. Dashed line represents theoretical absorption rate based on N_2O_4 data from Kramers et al.

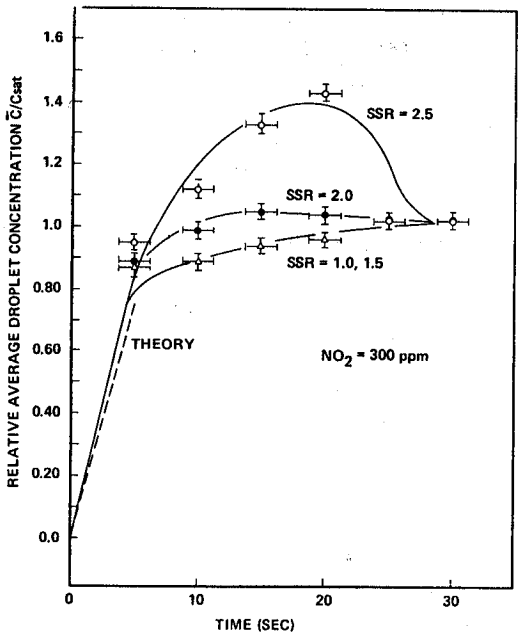

Fig. 7. Absorption of 300 ppm nitrogen dioxide from N_2 at various supersaturation ratios (water vapor condensation rates).

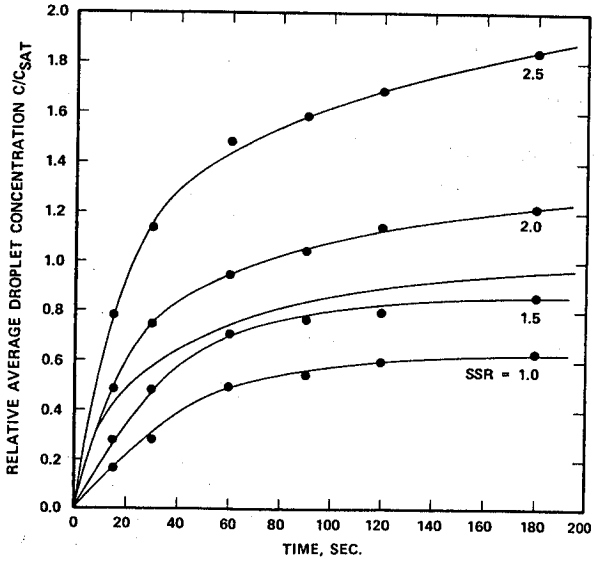

Fig. 8. Absorption of oxygen from air (21% O_2) at various supersaturated ratios. Oxygen concentrations are normalized to saturation value at the temperature of the droplet. Solid line without experimental points represents theoretical variation of average concentration vs time based on equation 2.

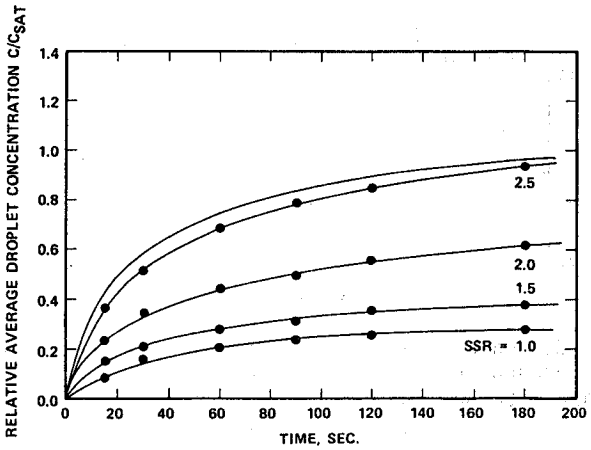

Fig. 9. Absorption of oxygen from mixture 80% O_2, 20% N_2, at various supersaturation ratios.

CATALYTIC REACTIVITY OF AIRBORNE PARTICULATE MATERIAL

Francis Menotti and John B. Hudson
Materials Engineering Department
Rensselaer Polytechnic Institute
Troy, New York

Roger J. Cheng and Volker A. Mohnen
Atmospheric Sciences Research Center
State University of New York at Albany
Albany, New York

ABSTRACT

The surface of airborne particulates may offer a convenient channel for the turnover of gaseous pollutant species by catalytic reactions. We are employing a combination of modern surface research techniques to investigate the rate of reactions of potential interest in air pollution on the surface of both real and simulated particulate materials. Initial studies of particulate materials from both oil and coal-fired power plant boilers by Auger Electron Spectroscopy (AES) showed significant amounts of metal oxides, especially vanadium and iron. Qualitative studies of sulfur uptake on laboratory-prepared iron and vanadium oxide samples indicated significant uptake of sulfur on exposure to SO_2 gas at 100°C. Quantitative studies of SO_2 adsorption and reaction on two different vanadium oxide surfaces, by a combination of AES and molecular beam mass spectrometric techniques, demonstrate that SO_2 is adsorbed non-dissociatively and reversibly on both VO and V_2O_5 surfaces. In the case of VO, the resulting adsorbed species reacts with gaseous O_2 in a process that is first order in oxygen pressure. Studies of the reactivity of adsorbed SO_2 on V_2O_5 are continuing, and will be extended to studies on actual airborne particulate surfaces.

INTRODUCTION

A cooperative effort between research groups at the Atmospheric Sciences Research Center of the State University of New York and the Surface Studies Laboratory at Rensselaer Polytechnic Institute is currently under way. The ultimate aim of this effort is to assess the role that heterogeneous catalysis of atmospheric chemical reactions at the surface of airborne particulate material plays in the overall turnover rate of pollutant gases in the atmosphere.

The approach to the problem is twofold. On the one hand, atmospheric sampling techniques are being used to collect airborne particulate materials, such as those found in fossil fuel-fired power plant boilers. These particles are characterized in terms of morphology, size distribution and chemical composition, both bulk and surface. Samples of these particles are then prepared for chemical kinetic studies in the molecular beam surface research system, to be described below. In a concurrent study, samples are being prepared to simulate those aspects of the surface composition of the airborne particulates that are felt to be of possible significance catalytically. These samples, after characterization, are being exposed to reactant gas mixtures in the molecular beam system. A combination of mass spectrometric detection of desorbed product fluxes and Auger electron spectrometric detection of non-volatile surface products is being used to characterize the rate and extent of the surface reaction. It is hoped that this combination of techniques will lead to unequivocal conclusions as to the rate-limiting steps in the chemical reactions studied.

In the work to date, we have been investigating the overall reaction

$$SO_2 + O_2 \rightarrow SO_3 + \text{Sulfates}$$

at the surfaces of both real stack particulate samples and laboratory-prepared samples, prepared so as to simulate the surface composition of the real particulates. The aim of the present work is to assess the role that catalytic reaction on particulate surfaces plays in the turnover of SO_2 in power plant plumes. The techniques used are applicable to a wide range of reactions on a wide range of surfaces, and will eventually be applied to other systems of interest to atmospheric chemistry.

Sample Preparation and Characterization

Actual airborne particulate materials were obtained by stack sampling techniques from both oil-fired and coal-fired power plant boilers. Extensive characterization measurements on these particles are reported elsewhere (1, 2, 3). Suffice it to say for the present that these particles, which covered the size range from 0.1-10μ, had surface compositions showing large amounts of both carbon and metal oxides. In the case of the oil-fired boiler, the particulates contained large amounts of vanadium, apparently

as V_2O_5. The particulates from the coal-fired boiler showed lesser amounts of iron, sodium and calcium oxides. Auger electron spectra of samples of the two types of particulate are shown in Fig. 1 (oil) and Fig. 2 (coal).

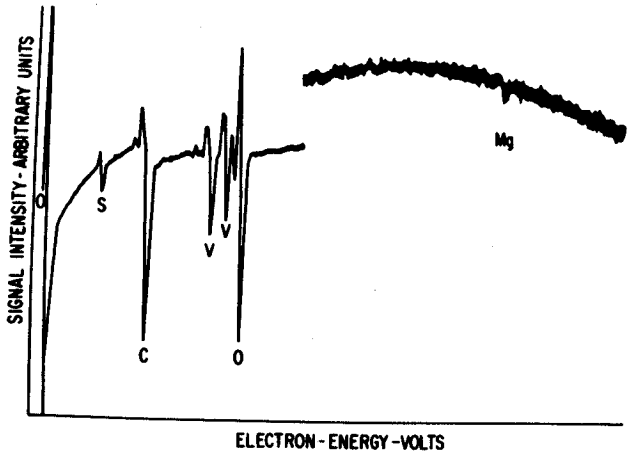

Fig. 1. Auger spectrum of flyash from oil-fired power plant boiler

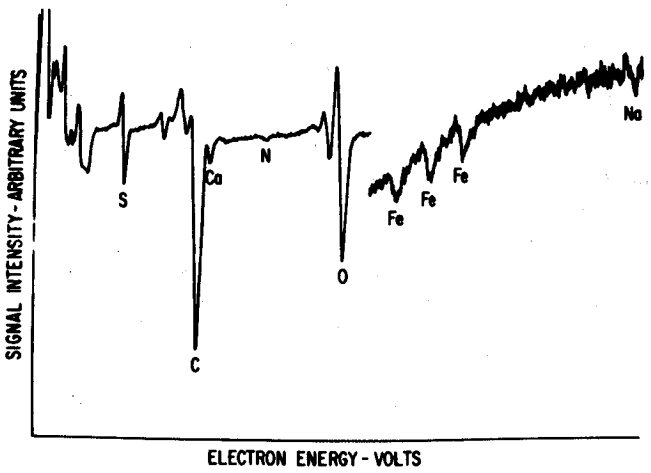

Fig. 2. Auger spectrum of flyash from coal-fired power plant boiler

Bulk samples were prepared to simulate the composition of these particulate samples by vapor deposition of metal oxides on pure graphite substrates. This technique has been used to make samples of V_2O_3, V_2O_5, FeO and Fe_2O_3, for use in reaction kinetic studies. These samples have been characterized by Auger electron spectroscopy, and show the peaks of the appropriate metal, along with carbon and oxygen. Metal-to-oxygen ratios vary due to changes in deposition conditions, but ratios close to stoichiometric have been obtained in the cases of V_2O_3 and FeO, shown in Fig. 3 (V_2O_3) and Fig. 4 (FeO). To date these samples have been used for the "static exposure" experiments described later.

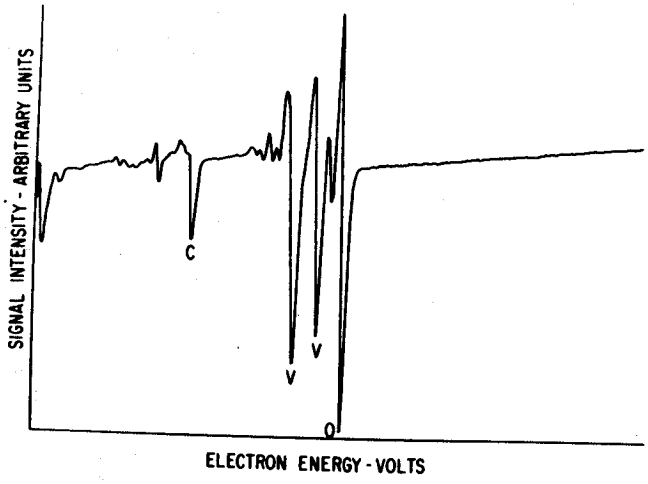

Fig. 3. Auger spectrum of sample formed by vapor deposition of V_2O_3 on graphite

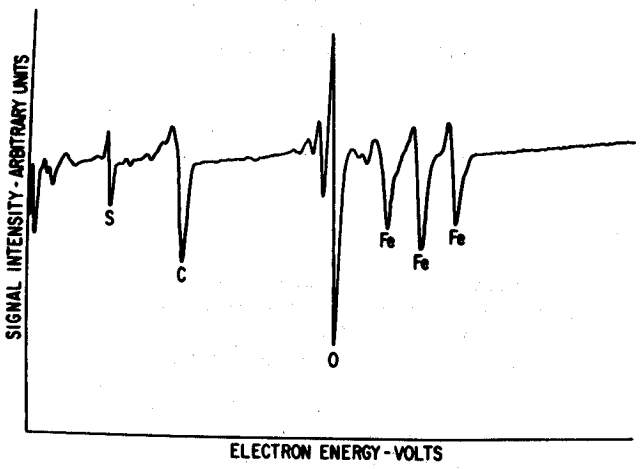

Fig. 4. Auger spectrum of sample formed by vapor deposition of FeO on graphite

A few samples, used in initial kinetic studies in the molecular beam system, were made either by oxidizing a vanadium metal ribbon or by melting

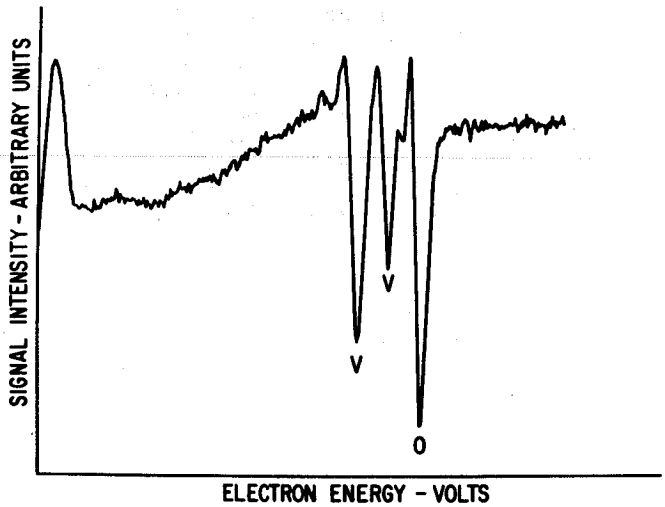

Fig. 5. Auger spectrum of sample formed by melting V_2O_5 onto a tantalum ribbon

V_2O_5 powder into a tantalum ribbon. These samples permit easy temperature control by Joule heating. An Auger spectum of the sample prepared by melting V_2O_5 is shown in Fig. 5.

Molecular Beam System

The surface kinetic measurements are being carried out in the Molecular Beam Surface Research System shown in a schematic top view in Fig. 6. The main chamber of this system, a cylinder 32 cm in diameter, 50 cm high, is pumped by a cryogenic pump to working pressures in the 10^{-8}Pa range. The sample under study is mounted on a universal positioner, from the top, on the axis of the system. Non-metallic samples are mounted on a molybdenum block and can be heated either by radiation from an enclosed filament, or by electron bombardment from this filament, metallic samples can be mounted as thin ribbons and heated by Joule heating. The available temperature range is from ambient to 1000K.

The chamber is equipped with a cylindrical mirror electron energy analyser, with a co-axial electron gun, for Auger electron spectrometric measurements, and an ion gun for surface cleaning by Argon ion bombardment and anneal. There is a stagnation chamber, connected to the main chamber through a small orifice, in the line of the molecular beam, for making absolute beam intensity measurements.

The molecular beam is formed and modulated in a second, separately-pumped chamber. Beam gas, at a pressure in the 10^3Pa range, flows through a multicapillary array into this chamber to form the molecular beam. The resulting beam is modulated by a toothed wheel mounted to an electric motor inside the chamber. This wheel also intercepts the light beam from an LED-photocell combination, to provide the reference signal necessary for signal detection using a lock-in analyser. The modulated beam passes through a collimating orifice into the main chamber, where it can be controlled in an on-off mode by a magnetically operated shutter. The maximum beam intensity provided by this system is $\sim 10^{14}$ molec/cm^2 sec at the substrate, equivalent to a static pressure of $\sim 10^{-4}$Pa. The available range of beam modulation frequencies is from 15 to 200 Hz.

The beam molecules scattered by the surface, and any volatile product species formed at the surface, are detected by a monopole mass spectrometer, mounted vertically in a third separately-pumped chamber, with the mass spectrometer ion source mounted $\sim$5 cm from the sample surface. This detector has a mass range from one to 300, and can detect a product flux from the surface as low as 10^{10}molec/cm^{2}sec. The mass spectrometer output can be detected in either an ac or a dc mode. In the ac case, the spectrometer output is fed to a two-phase lock-in analyser, which permits direct measurement of both the phase and

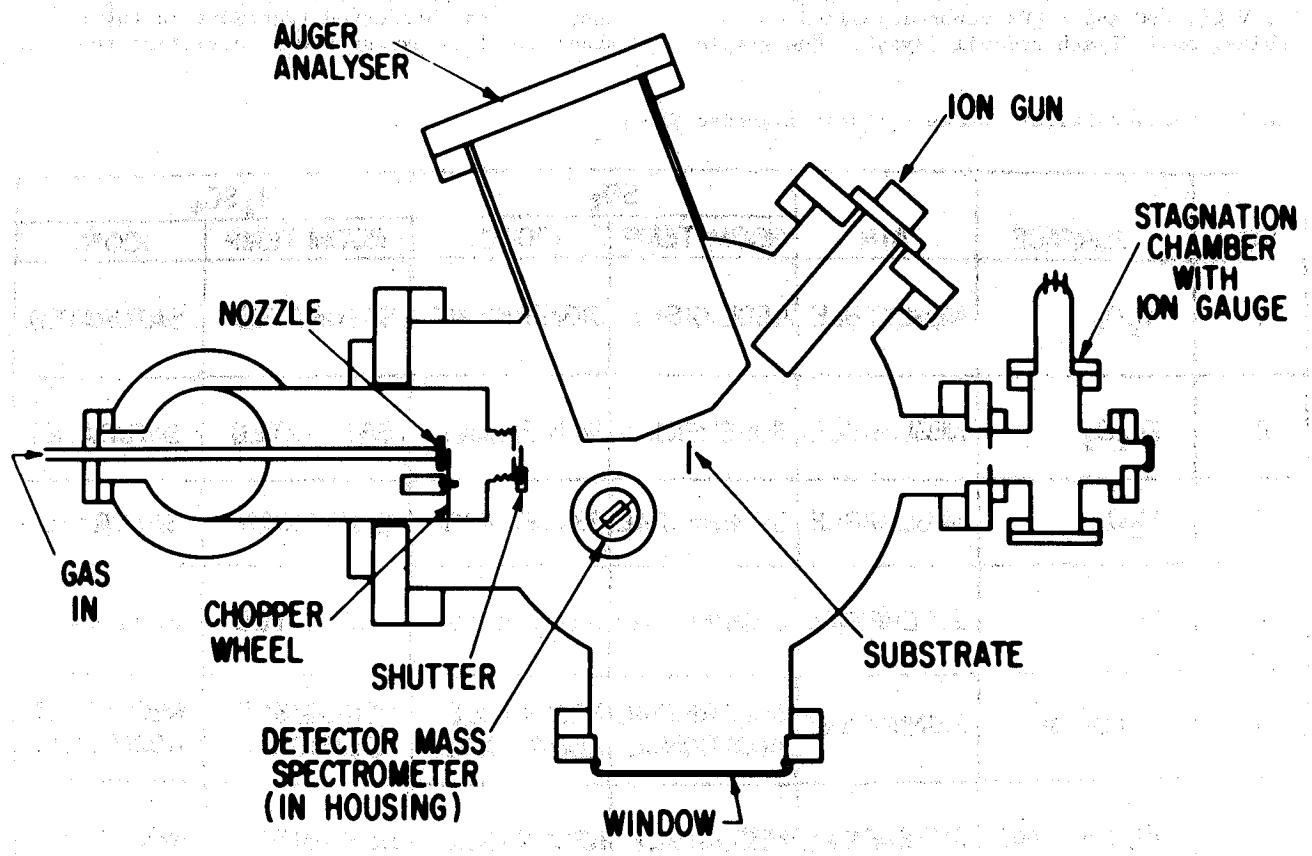

Fig. 6. Schematic top view of the molecular beam surface research system.

amplitude of the a.c. component of the mass spectrometer signal arising from either scattered beam material or reaction product species. As will be seen later, this permits measurement of surface reaction rate constants, and surface lifetimes of adsorbed species. In the dc case a signal directly proportional to the molecular flux from the surface under study is detected. This mode of operation is used in temperature programmed desorption studies, in which the surface is exposed to a gas mixture at low temperature, then heated to cause desorption of surface reaction products.

Results

To date, two different types of reaction kinetic experiments have been run. A set of exploratory measurements has been carried out in which both real particulates and simulated samples were exposed to static pressures of SO_2 or H_2SO_4, and then examined by Auger electron spectroscopy for sulfur pickup. A second set of measurements of O_2 and SO_2 interaction with the samples formed by oxidizing a vanadium ribbon or melting V_2O_5 powder onto a tantalum ribbon has been made in the molecular beam system.

The "Static exposure" experiments were intended to screen the samples tested to determine the most likely candidates for more extensive study in the molecular beam system. In these studies, five identical samples were prepared of each material studied. The materials included pure graphite, V_2O_5, V_2O_3, FeO and Fe_2O_3 vapor-deposited on graphite, coal flyash and oil flyash. One sample of each material was retained as a blank, one exposed to SO_2 at atmospheric pressure and room temperature, one to SO_2 at atmospheric pressure and 100°C, one to H_2SO_4 in atmospheric air at room temperature, and one to H_2SO_4 in atmospheric air at 100°C.

After exposure, all samples were examined by Auger electron spectroscopy to determine the extent of sulfur uptake, if any. Auger spectra were taken of the sample as received from the sulfur treatment, and at intervals as the surface was sputtered away by argon ion bombardment. The results of these measurements are summarized in Table 1. The samples that had not been sulfur-exposed showed negligible surface sulfur in all cases except the flyash samples, which showed fractional monolayer sulfur coverage. Exposure to SO_2 at room temperature resulted in only superficial sulfur uptake in all cases. That is, sulfur coverage is small compared to a monolayer. Exposure to SO_2 at 100°C caused significant sulfur uptake (i.e., sulfur was detected to a depth of several monolayers) in all of the metal oxide samples, but not in the flyash samples. Exposure to H_2SO_4 at either room temperature or 100°C resulted in saturation of the metal oxide layers, with large amounts of sulfur being detected in the Auger spectra throughout the layer, until the carbon substrate was reached. Flyash samples exposed to H_2SO_4 showed only superficial additional sulfur uptake.

Two generalizations emerge from this study. Firstly, it appears that exposure to SO_2 at 100°C should be the preferred treatment in future studies. This exposure was sufficient to cause

Table 1. Surface Sulfur Uptake - Static Exposure Study

NO.	SURFACE	AIR	SO_2		H_2SO_4	
			ROOM TEMP	100°C	ROOM TEMP	100°C
1	V_2O_5	NEGLIGIBLE	NEGLIGIBLE	SIGNIFICANT	SATURATED	SATURATED
2	Fe_2O_3	NEGLIGIBLE	SUPERFICIAL	SIGNIFICANT	SATURATED	SATURATED
3	V_2O_3	NEGLIGIBLE	SUPERFICIAL	SIGNIFICANT	SIGNIFICANT	SATURATED
4	FeO	SUPERFICIAL	SIGNIFICANT	SIGNIFICANT	SATURATED	SATURATED
5	Flyash - oil	SIGNIFICANT	SUPERFICIAL ADDITIONAL	NEGLIGIBLE ADDITIONAL	NEGLIGIBLE ADDITIONAL	NEGLIGIBLE ADDITIONAL
6	Flyash - coal	SUPERFICIAL	NEGLIGIBLE	NEGLIGIBLE	NEGLIGIBLE	NEGLIGIBLE

significant surface reaction, but not to completely saturate the bulk of the sample. The H_2SO_4 exposure appears to be "over kill." Secondly, the uptake on the metal oxide samples was definitely greater than on the flyash samples. It thus appears that either the active agent in the uptake process is the metal oxide constituent, rather than the carbonaceous matrix, or that the flyash samples were already saturated with sulfur prior to the laboratory exposure. Further studies will be required to answer this question.

The molecular beam experiments are at present in a developmental phase. Experiments performed to date have been aimed at characterizing the interaction of SO_2 and O_2 beams with surfaces of composition VO_x with $1 < X < 2.5$.

The initial measurements were made on a surface formed by exposing a cleaned vanadium metal ribbon to gaseous O_2 at a pressure of 10^{-2}Pa in the molecular beam system. Auger electron spectrometric measurements indicated that this surface had the approximate composition VO. This determination was made using the relation between Auger peak height ratio and vanadium oxidation state determined by Szalkowski and Somorjai (4).

The rate of SO_2 uptake from the molecular beam on this surface was measured by Auger electron spectroscopy, with measurements of the sulfur and vanadium Auger signals being recorded as a function of the total exposure of the surface to SO_2. In these measurements, the electron beam of the Auger analyser was turned on only when spectra were being recorded and at the lowest practical electron current level, in order to minimize electron bombardment induced uptake effects, which were observed in initial stages of the study.

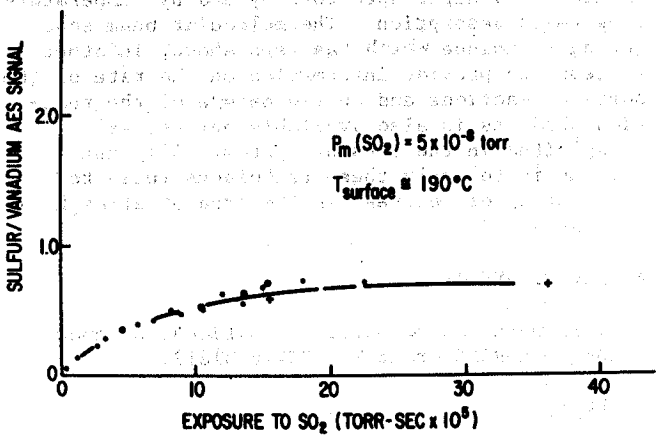

Fig. 7. SO_2 adsorption kinetics on oxidized vanadium. Sulfur Auger peak height relative to vanadium vs integrated exposure to SO_2

The resulting uptake behavior is shown in Fig. 7, where the ratio of the sulfur to vanadium Auger peaks is plotted against the integrated SO_2 flux to the surface. The rate of the process follows Langmuir type kinetics, with the rate of uptake being given by

$$\frac{dC}{dt} = I\, S_o\, (1 - \frac{C}{C_s}),$$

in which C is the surface sulfur concentration (molec/cm^2), I the SO_2 flux to the surface (molec/cm^{2}sec), S_o the adsorption probability on the uncovered surface, and C_s the saturation sulfur coverage. The solid line in Fig. 7 represents a plot of this expression with $S_o = 6 \times 10^{-3}$ and $C_s = 1.7 \times 10^{14}$ molec/cm^2. This amounts to essentially complete monolayer coverage of SO_2.

The SO_2 adlayer formed as described above was next exposed to an O_2 molecular beam, and the course of the reaction observed by Auger electron spectroscopy. It was found that the O_2 beam removed the adsorbed SO_2 layer, as shown in Fig. 8,

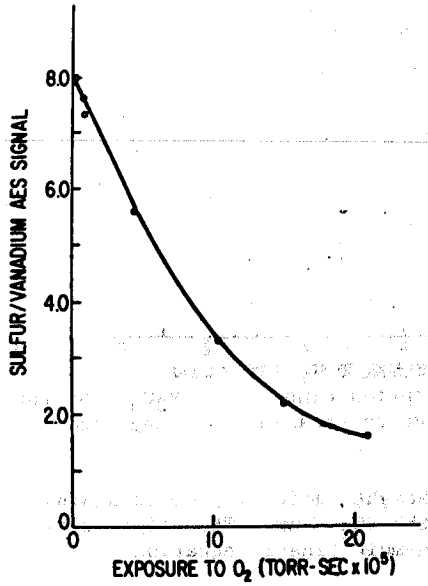

Fig. 8. Removal of adsorbed SO_2 from oxidized vanadium by gaseous O_2. Sulfur Auger peak height relative to vanadium vs integrated exposure to O_2

where the ratio of the sulfur to vanadium Auger peaks is plotted against oxygen exposure. This process was found to follow first-order kinetics with respect to oxygen exposure, with the surface sulfur concentration following the relation

$$C = C_s \exp\left(\frac{-I\, S_o\, t}{C_s}\right)$$

in which, for this case, I is the oxygen molecular impingement rate (1.9×10^{13}molec/cm^{2}sec) and S_o is the single collision reaction probability, which was found to be 4×10^{-3}. Note, however, that these measurements tell us only that sulfur is leaving the surface, and cannot tell us whether the removal process involves reaction to form SO_3, or a simple replacement adsorption process, with oxygen replacing SO_2 on the surface.

In view of the relatively low values of SO_2 sticking coefficient and O_2 reaction probability found in these studies, it was decided to switch to a surface having an oxygen to vanadium ratio closer to that observed in the flue gas particulate samples. In order to do this, a sample was prepared by melting powdered V_2O_5 onto a thin tantalum ribbon. The sample thus prepared was mounted in the molecular beam system, cleaned by argon ion bombardment and anneal, and characterized

by Auger electron spectroscopy. The observed spectrum was previously shown in Fig. 5, and shows a vanadium to oxygen Auger peak height ratio similar to that observed for powdered V_2O_5.

This sample was exposed to the SO_2 molecular beam, with Auger electron spectrometric measurements again being made as a function of SO_2 exposure. Preliminary results of these measurements are shown in Fig. 9, where again the sulfur

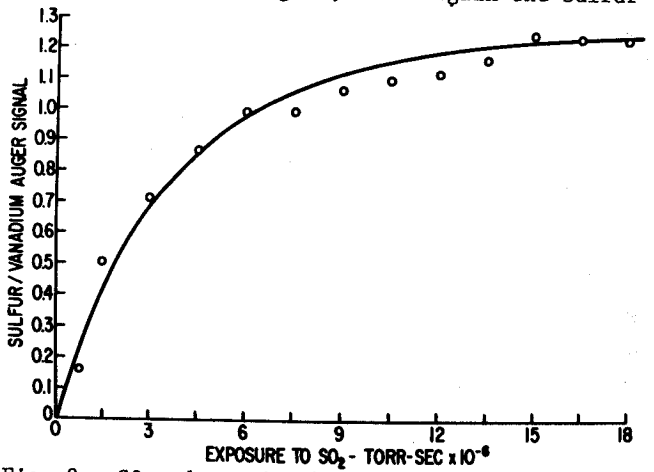

Fig. 9. SO_2 adsorption kinetics on V_2O_5. Sulfur Auger peak relative to vanadium vs integrated exposure to SO_2

to vanadium peak height ratio is plotted against exposure time to the SO_2 beam. The solid curve represents the Langmuir kinetic equation

$$C = C_s \left(1 - \exp \left(\frac{-I S_o t}{n_o} \right) \right)$$

also observed in the case of SO_2 adsorption on the oxidised vanadium surface. In this case, the saturation coverage, C_s, appears to be the same as the previous case, but the sticking coefficient, S_o, is much higher, namely 4.7×10^{-2}.

In this case, we have also been able to show, by temperature programmed desorption measurements, that the SO_2 is relatively weakly bound to the V_2O_5 surface, and probably does not dissociate on adsorption. In these measurements, the V_2O_5 surface was exposed to the SO_2 beam for a fixed time at room temperature. The sample was then heated, and the mass 64 peak (SO_2^+) monitored with the detector mass spectrometer. Results of one such measurement are shown in Fig. 10. The single peak in the desorption spectrum indicates that the majority of the adsorbed SO_2 is held in a single binding state. The temperature at which this peak occurs is consistent with a heat of adsorption of roughly 20 K-cal/mol. The long tail-off at higher temperature is generally indicative of either a range of surface sites of higher binding energy, or of migration of adsorbed SO_2 into either the bulk of the V_2O_5 sample or into pores in the sample surface. Further measurements will be required in order to resolve this question.

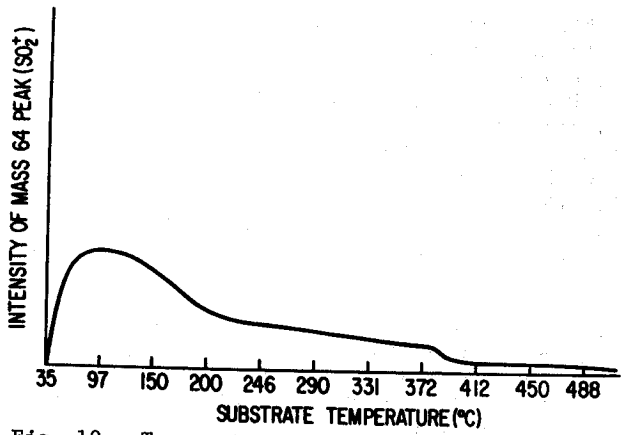

Fig. 10. Temperature programmed desorption of SO_2 from V_2O_5. Mass spectrometer signal at mass 64 (SO_2^+) vs surface temperature

Summary

The results obtained to date, while not giving a complete picture of the surface oxidation reaction under study, serve to indicate the kind of information that the techniques used can provide. It is apparent that preliminary screening by Auger spectroscopy of samples given static exposures to sulfur-containing gases can delineate the conditions under which surface uptake of sulfur takes place, and thus provide guidelines for more sophisticated kinetic studies. It is also apparent that this technique can be applied to a wide range of sample types, including powders, vapor deposited materials and bulk metal and oxide surfaces. Surface reaction kinetics of such processes as adsorption-desorption and reactive removal of previously adsorbed species may also be monitored by Auger spectroscopy and by temperature programmed desorption. The molecular beam scattering technique which has been shown, in other systems, to provide information on the rate of the surface reactions and on the nature of the reaction products is also available but as yet unexploited in the present system. All that remains is to apply these techniques fully to the systems of interest in the area of atmospheric chemistry.

ACKNOWLEDGEMENTS

This work was supported by National Science Foundation-RANN Grant No. ENV76-81817.

REFERENCES

1. R.J. Cheng, V.A. Mohnen, T. Shen, M. Current and J.B. Hudson, J.Air Pollution Cont.Assoc. 26, 727 (1976)

2. T. Shen, R.J. Cheng, V.A. Mohnen, M. Current and J.B. Hudson, Proceedings of the 4th International Clean Air Congress, p.386 (1977)

3. V.A. Mohnen, J.H. Hawley, R.J. Cheng, T.T. Shen, J.B. Hudson and M.I. Current, ASRC-SUNYA Pub.1380, Atmospheric Sciences Research Center, SUNYA, Albany, NY, Feb. 1976.

4. F.J. Szalkowski and G.A. Somorjai, J.Chem. Phys. 56, 6097 (1972)

Discussion, Glen E. Gordon (University of Maryland)

Are Carbon Soot Particles Important in the Conversion of SO_2 to Sulfates?

A major focal point of this Conference is the question: "Do carbon soot particles play a major role in the conversion of SO_2 to sulfates and sulfuric acid?" Many mechanisms have been proposed, especially gas-phase oxidation and heterogenous reactions such as the "dirty-water" mechanism in which the oxidation of SO_2 in water droplets by dissolved oxygen is catalyzed by Fe, Mn, or V ions. Although most gas-phase reactions studied are too slow to be important, it appears that reactions of radicals such as OH, HO_2, and their organic homologs are fast enough to account for much of the 1 to 2%/hr conversion typically observed over long distances during sunny, warm days. However, those photochemically produced species are surely not the major reactants with SO_2 during fall and winter, especially during pollution episodes, which are accompanied by low temperatures, haze or fog, and little sunshine. Under those conditions it is likely that heterogeneous reactions account for most of the conversion.

The dirty water mechanism was postulated years ago, but we still don't have quantitative estimates of its importance. Various groups have measured rates of Fe-catalyzed oxidation of SO_2 in solution; however, they have not determined the humidities at which particles bearing Fe, Mn, and V take on water nor have they measured the solubility of those metals in the water layers. Until these key intermediate steps are investigated, no model for the rate of SO_2 conversion by this mechanism in plumes or ambient air has any validity. Thus, while this reaction may be important, its quantitative significance is now indeterminant.

In 1973, Novakov et al. at Berkeley demonstrated in the laboratory that SO_2 oxidation is catalyzed by carbon soot particles. However, it's been only during the past year that the atmospheric chemistry community has begun to take serious note of this mechanism, as little field data relevant to it existed. But now the Berkeley group has developed various lines of evidence that point towards the possible importance of the soot mechanism: (1) Raman lines of soot are found in most ambient samples; (2) soot particles on filters cause most of the attenuation of transmitted light; (3) the light attenuation correlates strongly with total carbon mass; (4) data from several areas under different conditions (photochemical and otherwise) fall about a single line (attenuation vs. total carbon) which has the same slope as a plot for primary particles from several sources, suggesting that typically half of the particulate carbon is primary soot; (5) soot in water catalyzes sulfite oxidation and is not inhibited by low pH; and (6) SO_4/SO_2 ratios in Berkeley during winter are comparable with those of Los Angeles in summer.

Although the case for the carbon soot mechanism is now much stronger, a number of points should be subjected to further discussion and additional experiments:

1. At this conference there has been much debate about the fraction of particulate carbon that is primary and/or soot. One problem is that there are many different definitions of types of carbon dependent on the type of experiment done, e.g., extractable, primary, organic, volatilizable, water-soluble non-carbonate carbon, etc. A major step towards resolving this controversy could be taken if the investigators involved would all analyze samples of the same material (e.g., the soon available NBS Standard Reference atmospheric particulate material) in order to establish firm relationships between these variously defined fractions.

2. Both correlations and lacks thereof between sulfate and carbon on ambient particles have been been reported, but there is not necessarily a conflict here: such correlations are neither necessary nor sufficient to prove the importance of the soot mechanism. Since other mechanisms surely play an important role, especially gas-phase during summer, sulfate levels might often be uncorrelated with carbon, even if the latter is the most important under different conditions. Conversely, so many atmospheric variables correlate with meteorological parameters (especially wind speed and mixing height) that most have positive correlations with most others. Thus, the observation of a correlation on bulk samples does not prove the case. I would be much more impressed by a particle-by-particle correlation, i.e., at certain times, virtually every individual sulfate particle having a large soot component. (Or is there some natural atmospheric process by which sulfate once formed on soot can subsequently leave the particle?)

3. There appears to be a controversy about the yield of sulfate on soot as a function of humidity. Appel's experiment (covered informally during the discussion period) with SO_2 and soot generated from acetylene yielded little sulfate at humidities below 90%. The Berkeley group finds enhanced yields with increasing humidity, but an appreciable yield even at low humidity. Coupled with this question is the fact that, just as in the case of the dirty water mechanisms, the humidity at which soot particles take on water has not been established.

4. Is there enough soot released from various sources to account quantitatively for a substantial fraction of sulfate observed on an area or regional basis? What is the capacity (i.e., the maximum S/C ratio) of soot to produce sulfate? Experiments at Berkeley suggest that this ratio can go as high as 0.6. This high ratio surprises me, as I visualize the sulfate as forming a monolayer on the ~100Å soot spheres within the agglomerates. Is it possible that the 0.6 ratio reflects only the surface concentrations?

5. Several other inconsistencies have arisen at this Conference, e.g., Whitby's indication that sulfate and carbon are on different sizes of Aitken nuclei, Mohnen's finding of only superficial attachment of SO_2 to carbonaceous particles at low

temperatures, and O'Brien's failure to observe the growth of sulfate on soot particles in the TEM chamber.

In summary, great progress has been made in studies of heterogeneous conversion of SO_2, especially the soot mechanism. Although many uncertainties and inconsistencies remain, we at least have enough information to design definitive experiments to answer some of the outstanding questions.

Discussion by J. Freiberg (Rutgers University)

Chang et al. (1978) and Eatough et al. (1978) found that S(IV) species (i.e., $H_2O{\cdot}SO_2$, HSO_3^-, $SO_3^=$) are oxidized to sulfate in aqueous suspensions containing carbonaceous particles. Chang et al. (1978), who performed their experiments in bulk solutions, found the rate of oxidation to be independent of pH. This led commentators to suggest that this oxidation path might account for the "formation of acid in the presence of acid" in the atmosphere. But consideration of the solubility of gaseous SO in atmospheric droplets, the thermodynamics of equilibrium among S(IV) species in droplet solution and the kinetics given by Chang et al. (1978) suggests that, in droplets, sulfate formation in the presence of carbonaceous catalysts is pH dependent.

When a droplet is exposed to ambient SO_2, SO_2 dissolves into the droplet as $H_2O{\cdot}SO_2$, which dissociates into HSO_3^- and $SO_3^=$. With an increase in pH, the concentration of $H_2O{\cdot}SO_2$ in solution will remain constant (assuming constant temperature and SO_2 partial pressure — Henry's Law), and the concentration of HSO_3^- and $SO_3^=$ will increase. Thus the overall solubility of S(IV), where S(IV) $\equiv H_2O{\cdot}SO_2 + HSO_3^- + SO_3^=$) varies directly with pH; and, to the extent that SO_2 oxidation in carbonaceous suspension relies on HSO_3^- (as Eatough et al. [1978] have found that it does) or on $SO_3^=$, the oxidation rate can be expected to increase with pH.

The pH independence found by Chang et al. (1978) can be explained by the fact that their experiment involved a bulk sulfurous acid solution rather than a water droplet. Being "stocked" with S(IV), the solution did not depend on the atmosphere as its source of SO_2. The initial S(IV) "load" (which the authors varied over only a narrow range: 6.56×10^{-6} to 8.85×10^{-4}M) was such as would occur in nature only at high $[SO_2]_g$ (i.e., high concentrations of atmospheric SO_2). Moreover, it was observed that the reaction occurred quickly and that sulfur mass balance in the reaction was preserved (i.e., no SO_2 diffused into the atmosphere during the reaction). Thus, by virtue of the way the experiment was structured, the gas-to-liquid phase solubility of S(IV) was a factor of negligible relevance. In this way the influence of pH on the oxidation would not show up.

That the oxidation may be pH-dependent in atmospheric droplets is also supported by the fact that the Chang mechanism yields a rate expression which is independent of pH only for $K_2[SO_2{\cdot}H_2O] \gg K_{-2}$ and $K_3[SO_2{\cdot}H_2O] \geq K_{-3}$. Clearly, if [S(IV)] is small enough, the inequalities will not hold and the pH independent rate expression will be inapplicable.

Chang et al. (1978) and Eatough et al. (1978) have presented important preliminary information on the role of carbonaceous particles in atmospheric SO_2 oxidation. But it is premature to conclude on the basis of the present data that the rate of the oxidation is independent of pH. Experiments more closely simulating atmospheric conditions (e.g., using atmospheric size droplets) are warranted.

References

1. S.-G. Chang, R. Brodzinsky, R. Toossi, S.S. Markowitz, and T. Novakov, "Catalytic Oxidation of SO_2 on Carbon in Aqueous Suspensions," Proceedings, Conference on Carbonaceous Particles in the Atmosphere, Berkeley, California (1978).
2. D.J. Eatough, W.P. Green, and L.D. Hausen, "Oxidation of Sulfate by Activated Charcoal," Proceedings, Conference on Carbonaceous Particles in the Atmosphere, Berkeley, California (1978).

Discussion by B. R. Appel (Air and Industrial Hygiene Laboratory, California Dept. of Health)

I wanted to share with you what I think this conference has demonstrated with respect to the mechanism of conversion of SO_2 to sulfate, mediated by carbon. I will be referring to "wet" and dry mechanisms where the former refers to the oxidation of dissolved SO_2 by a slurry of carbon in water. I am persuaded by the papers presented that the wet mechanism is effective in accelerating the oxidation of sulfite to sulfate. One of the remaining challenges will be to demonstrate the relevance of the wet mechanism to ambient air.

With respect to the "dry" mechanism, which I'll define as operative at up to 90% R.H., I would make the following comments. First of all, Techa Novakov noted that the amount of SO_2 converted to particulate sulfur was "a couple of percent." Secondly, in the work I described to you previously, we demonstrated that the amount of sulfate formed by the dry mechanism represented 5 to 15% of the weight of carbon. We found, furthermore, that this carbon was subsequently inactive for the oxidation of SO_2 at R.H. values up to 90%. I left open the possibility that the initial 5 to 15% sulfate (as a percent of carbon) might have been formed as a result of a catalytic process on the surface of carbon. However, we heard from Ken Whitby this morning that there are two distinct size modes in the nuclei region for

particulate sulfur and flame-derived carbon, 0.03 μm for sulfur and 0.06 μm for carbon. This suggested to him that there was no mechanistic link between them. Opposing this is the work of Bob O'Brian which suggests substantial growth, presumably by sulfuric acid formation on the surface of carbon particles as viewed by EM. That work, however, was performed at 1 torr or about 1000 ppm of SO_2. One has to question the relevance of that experiment to ambient air.

The experiments I've described for the dry system are far from perfect, however. We've heard from Dave Kittleson what may be one of the major limitations of these experiments. As an example, about 40% of the particulate carbon derived from the acetylene flame in the experiment I described earlier was lost by heating to 200°C. This volatile portion was certainly not graphitic soot but may have been a liquid hydrocarbon clogging the pores of any soot formed. The particulate matter was black so we presume some soot was present. We heard from William Pierson that solvent extraction of such material can increase its surface area and, presumably, its catalytic activity. Possibly the failure in our experiments to observe oxidation reflects the degree of clogging. Another weakness in experimental studies of the dry mechanism is the lack of hygroscopicity of carbon, alone. Perhaps in mixtures with hygroscopic salts one might see catalytic activity.

Considering these limitations I would recommend three experiments relevant to the dry mechanism. First, collect carbon from propane flames on filters, wash with cyclohexane or benzene to remove the layer of organics and then expose the carbon to moist air with SO_2. Secondly, mix aerosols of carbon and ammonium nitrate, a hygroscopic salt, and while still airborne, allow them to coagulate, add SO_2 in moist air, collect on a filter and analyze for carbon and sulfate. This could also be done by initial collection on filters, washing with organic solvent to increase surface area and then expose to SO_2 in moist air. The third experiment is an evaluation of the transition region between 90 and 100% relative humidity.

Discussion by P. T. Cunningham (Argonne National Laboratory)

I am a little disturbed by the observation of hydrocarbon material in association with acidic aerosols. Over several years of analyzing materials with infrared spectroscopic methods, we have observed a strong negative correlation between the occurrence of hydrocarbons, as evidenced by the appearance of the carbon hydrogen stretching bands, and the occurrence of acidity in aerosol samples. This is not to say that carbonaceous materials may not be associated with acidic aerosols, but it does seem to suggest that these carbonaceous materials are not properly characterized as hydrocarbons.

Discussion by B. R. Appel (Air and Industrial Hygiene Laboratory, California Dept. of Health)

I want to describe the results of three experiments conducted jointly by AIHL and LBL personnel to evaluate the effects of combustion derived carbon ("soot") in converting SO_2 to sulfate at relative humdities up to 90%.* The sulfate observed represented not only sulfate and/or sulfite associated with carbon-SO_2 interactions (both suspended carbon and carbon on filters) but also sulfate from SO_2-filter media interactions, and SO_3 and sulfate formed in the flame from sulfur compounds in the acetylene used as the fuel. The experiments were as follows:

1. SO_2 was injected downstream of an acetylene flame in a region with temperature about 300°C. Filter collection of the aerosol was made using 47 mm Gelman A (pH = 7.6) glass fiber filters at 1.32 cfm. Two filters sampled for 10 hours continuously while, on the remaining two holders, filters were changed after five hours.

2. As in 1, but no SO_2 injected. This experiment was made to evaluate the significance of sulfate formed from sulfur compounds in the acetylene fuel. In addition, the volatility behavior of the soot collected on the filters was evaluated to obtain the proportion of relatively volatile, organic carbon.

3. No SO_2 injected. Two sets of four filter samples were collected sampling for five hours with each set. The filters were subsequently exposed to SO_2 under varying humidity conditions using an AIHL exposure system.

The results of Experiment 1 are summarized in Table 1 and indicate a sampling precision of 11% (C.V.) or better for carbon. The sulfate levels, with one exception, were significantly greater than those expected from SO_2-clean filter interactions alone (ca. 50 μg). It was previously established that clean Gelman A exposed to 0.1-0.5 ppm SO_2 is saturated with SO_2 in 10 minutes at the flow rate used here (1.32 cfm). If most of the observed sulfate resulted from SO_2-filter interactions then the ratio sulfate/carbon should decrease with increasing sampling time. The observed ratio was not significantly different for samples collected for five and ten hours. Accordingly much of the sulfate and/or sulfite appears to relate either to fuel sulfur oxidized in the flame or to carbon-SO_2 interaction.

The sulfate levels in Experiment 1 represented 5-15% of the weight of carbon collected and 0.1-1.0% of the SO_2 passing through the filter. If carbon collected on a filter was able to convert SO_2 to sulfate (or fix SO_2 as sulfite) without being saturated then the sulfate observed on 10-hour filter samples would exceed the sum of the

sulfate observed on the two successive five-hour samples. The observed mean sum, for two trials, 85 μg compares to the mean 10-hour value 95 μg. Thus, if carbon was functioning as a catalyst, it was relatively ineffective.

The SO_2 concentration measured near the filters varied from 0.18 to 0.34 ppm as five-hour average values. At the conclusion of the experiment the flame was turned off and the instantaneous SO_2 concentrations was observed to decrease from 0.41 to 0.13 ppm. This implied that the difference, 0.28 ppm SO_2, resulted from oxidation of the sulfur compounds present in the acetylene. The ratio of fuel-related/added SO_2 was, at that moment, 2.2. This ratio at other times during the experiment is unknown.

The LBL staff tried various techniques to obtain sulfur-free acetylene but was unsuccessful. Accordingly, the second experiment was run to serve as a "blank" for Experiment 1; no SO_2 was added to the system. The results are shown in Table 2 and indicate a reduced level of sulfate collected, in μg, but a similar level of sulfate, expressed as a percent of carbon, to that in the first experiment. Thus, it appears that most, if not all, of the observed sulfate in Experiment 1 was due to fuel sulfur which had been oxidized to $SO_3^=$, and/or sulfate by the flame and that SO_2 added downstream of flame remained almost completely unconverted even though the temperature was initially high. In two cases, the sulfate observed was less than that expected from SO_2-filter interactions. The cause of this behavior is unclear.

As part of Experiment 2 the volatility behavior of the collected soot was studied in air at atmospheric pressure. The results indicated 40-45% loss of carbon on heating the collected soot to 200°C. The carbon remaining non-volatile at $\leq$ 200°C, can be used as an upper limit estimate of the graphitic carbon present in the soot.

In the third experiment the carbon-loaded filters were subsequently exposed to 0.1 ppm SO_2 at two relative humidities, 50 and 90%. Because of the fuel sulfur, filters contained an initial sulfate level prior to deliberate SO_2 exposure. The results are shown in Table 3. Interpretation of these results is complicated by several factors. Carbon was collected on the filters in two batches of four each. Within each batch the carbon level collected varied from filter to filter (mean C.V. = 25%). Since the filters were collecting fuel-related sulfate as well, the μg sulfate would be expected to show similar variation.

In Experiments 1 and 2 the sulfate observed ranged from 5 to 15% of the carbon formed. The sulfate observed in Experiment 3 remains in all cases, within this range following SO_2 exposures. In the series run at 50% R.H. the sulfate, as a percent of carbon, appears to decrease with increasing exposure to SO_2 while at 90% R.H., an increase was noted. However, the expected variability in the control samples (7-15%) with zero SO_2 exposure, prevents conclusions of significant sulfate formation at 90% R.H.

We conclude that conversion of SO_2 to sulfate on soot at relative humidities 30 to 90% does not appear to be a significant phenomenon either on suspended soot particles or on soot pre-collected on filters under the conditions studied.

FOOTNOTES

*The wet chemical method used for sulfate did not distinguish sulfate and sulfite.

Table 1

Results of Experiment 1[a]

Filter I.D.	Sampling Time (hrs)	Average SO_2 (ppm)	Carbon Collected (µg)	Sulfate Collected (µg)	Sulfate as % of Carbon	% SO_2 Converted to Sulfate
41A	1st 5	0.18	457.7			
				70.3[b]	9	0.32
45A	2nd 5	0.34	307.1			
42A	1st 5	0.18	534.1	82.0	15	1.03
46A	2nd 5	0.34	321.2	17.2	5	0.12
43A	10	0.26	828.3	107.5	13	0.49
44A	10	0.26	750.7	83.0	11	0.37

[a]Exposure conditions: Average Relative Humidity at filters = 32%
Temperature at filters = 24.6 ± .9°C
Temperature at SO_2 injection point = 297 ± 6°C

[b]Filters 41A and 45A combined and extracted together. The amount shown is the total sulfate for the two 5-hour filters.

Table 2

Results for Experiment 2[a]

Filter I.D.	Sampling Time (hrs)	Average SO_2 (ppm)	Carbon Collected (µg)	Sulfate Collected (µg)	Sulfate as % of Carbon	% SO_2 Converted to Sulfate
47A	1st 5	.16	412.4	56.8	14	0.81
51A	2nd 5	.14	383.8	28.8	8	0.47
48A	1st 5	.16	427.6	64.8	15	0.91
52A	2nd 5	.14	369.5	26.7	7	0.44
49A	10	.15	693.6	89.4	13	0.69
50A	10	.15	705.4	65.4	9	0.51

[a]Exposure conditions: Average Relative Humidity at filters = 41%
Temperature at filters = 28 ± 2°C

Table 3

Results of Experiment 3

0.1 ppm SO_2 50% R.H.

Filter I.D.	Sampling Time (Hours)[a]	Carbon (µg)[b]	Sulfate Collected (µg)	Sulfate as % of Carbon
B 0053A	0	391.7	52.5	13
B 0054A	6	442.9	50.3	11
B 0055A	6	449.2	47.9	11
B 0056A	24	633.7	51.4	8

0.1 ppm SO_2 90% R.H.

B 0057A	0	299.4	21.4	7
B 0058A	6	353.6	23.8	7
B 0059A	24	527.2	44.3	8
B 0060A	24	517.5	55.6	11

[a] Exposure time to 0.1 ppm SO_2 not including the time for pre-loading the filters.

[b] Conditions during the initial exposure for loading filters with carbon:

SO_2 concentration (from fuel) = .19 ± .01 ppm

Relative Humidity at filters = 71 ± 3%

Temperature at filters = 29 ± 2°C

Chemical Structure and Biological Effects

CHEMICAL AND BIOLOGICAL ASPECTS OF ORGANIC PARTICULATES IN REAL AND SIMULATED ATMOSPHERES

James N. Pitts, Jr., Karel A. Van Cauwenberghe, Daniel Grosjean,
Joachim P. Schmid and Dennis R. Fitz
Department of Chemistry and Statewide Air Pollution Research Center
University of California
Riverside, CA 92521

and

William L. Belser, Jr., Gregory B. Knudson, and Paul M. Hynds
Department of Biology and Statewide Air Pollution Research Center
University of California
Riverside, CA 92521

ABSTRACT

The discovery of direct mutagenic activity, as determined by the Ames Salmonella typhimurium reversion assay, in the organic fractions of ambient aerosols collected throughout Southern California, led us to investigate the reactions of benzo(a)pyrene (BaP) deposited on glass fiber filters with ambient photochemical smog, as well as with O_3, NO_2, and peroxyacetyl nitrate (PAN) in simulated atmospheres. A variety of products are readily formed, including phenols, diphenols, dihydrodiols, quinones, etc. Directly mutagenic nitroderivatives are formed upon exposure of BaP (a carcinogen) and of perylene (a non-carcinogen) to 1 ppm of NO_2 in air containing traces of nitric acid (~10 ppb). If such reactions occur in urban atmospheres they may account in part for the "excess" carcinogenicity (over BaP and certain other polycyclics)observed in organic particulates collected from smog and exhausts of gasoline and diesel engines. However, historically, such gas-solid interface processes may also have occurred on the filters used in particulate sampling. Thus the possibility of "filter artifacts" must be recognized.

It has been known for over two decades that extracts of the organic fraction of condensates from auto exhaust and from particulates collected in ambient urban air in the U. S. are carcinogenic when administered subcutaneously to mice [1,2]. Subsequently, this effect was seen in experimental animals administered extracts from ambient particulates collected in 1954 from Los Angeles photochemical smog[3] and in seven U. S. cities[4]. Similar results have been found with ambient samples collected in major urban centers throughout the world.

The carcinogenicity of the neutral fraction of organic particulates has been mainly attributed to the presence of PAH such as BaP and benz(a)-anthracene. However, a large number of other PAH have also been identified recently in ambient particulates[5,6], auto exhaust[7], diesel engine exhaust[8] and in soil near mountain highways[9].

In addition to PAH, other chemical carcinogens have been identified in ambient particulates, especially aza-arenes such as benzocarbazoles in the neutral fraction and benzacridines and dibenzacridines in the basic fraction[10,11,12,13,14].

However, it is noteable that the observed carcinogenicity in animals or transformation in cell cultures is significantly greater than can be accounted for by the amounts of carcinogenic polycyclics present in the samples administered [3,4,15-19]. Thus, Gordon and coworkers reported that in airborne particles collected in the Los Angeles area, the benzene extract had 100 to 1000 times the cell transformation activity attributable to its BaP content. Furthermore, the methanol extract, while containing only about 1/30 of the BaP in the total sample, had activity comparable to the benzene extract[20].

With respect to auto exhaust, Mohr and coworkers studied the effects of the condensate on the Syrian golden hamster lung. They concluded not only that the condensate displayed a carcinogenic effect (100% rate of multiple pulmonary tumors) but also "Considering the relatively low total dose of BaP contained in the condensate, this pronounced neoplastic response cannot be explained alone by the effects of this well known carcinogenic hydrocarbon".[18]

Elucidation of the compound(s) responsible for this "excess carcinogenicity" is complicated by the fact that, during transport in the atmosphere, in the presence of light, oxygen, water and a spectrum of co-pollutants, such as NO_2, O_3, etc., primary organic pollutants, including PAH, may undergo a variety of chemical and physical transformations. Thus, ambient organic particulates are very complex mixtures and their detailed analysis by conventional chemical (e.g., gc-ms) techniques alone is difficult indeed. However, it is axiomatic that reliable evaluation of the impact on man of environmental contaminants requires accurate delineation of the dose-response curves. Thus, despite the complexity of the system, it is essential that we acquire detailed knowledge of the physical and chemical

We first performed experiments in which BaP, deposited on washed and fired glass fiber filters of the type used in ambient sampling, was exposed in the dark to particle-free, pure air containing (a) O_3 [11 parts per million (ppm), exposure time 24 hours at a flow rate of 3 cubic feet per minute (cfm)], (b) NO_2 (1.3 ppm, 24 hr, 1 cfm), and (c) PAN (1.1 ppm, 16 hr, 3 cfm). All these exposures resulted in the formation of directly active mutagenic products. Control runs with BaP exposed to pure air (24 hr at 3 cfm) and with blank filters exposed to NO_2, O_3 or PAN were also included. These did not yield any direct mutagens.

After extraction, of the filters, the products and unreacted BaP were separated by thin layer chromatography (TLC). The major TLC bands were then analyzed by mass spectrometry and were tested for mutagenic activity with Salmonella typhimurium strains TA1535, TA1537, TA1538, TA98 and TA100, with and without addition of a mammalian metabolic activation system [0.5 ml of rat liver S-9 mix.] For comparison purposes, a sample of 9 mg of BaP incubated for 30 minutes at 37°C with liver S-9 mix was analyzed and tested in the same way.

As shown from the TLC bands in Figure 1, BaP reacted with O_3 and PAN to form a variety of oxygenated products and with NO_2 to form nitro derivatives. As expected, the TLC bands containing the unreacted BaP (R_f = 0.77) were not directly active and required metabolic activation. The bands containing the BaP-quinones (R_f = 0.54) were complex and contained, in addition to the inactive quinones, a directly active compound as yet unidentified.

Treatment of BaP with liver S-9 mix resulted in the appearance of a complex TLC band as seen with ambient smog but not with the single gases (Figure 1). This contained directly active mutagens. Its R_f (0.35) and the molecular weight of its components (MW = 268) are consistent with those of isomers of hydroxybenzo(a)-pyrene.

Exposure of BaP to 1 ppm of NO_2 containing traces of nitric acid (~10 ppb) resulted in the appearance of only one major TLC band. This contained a directly active mutagen whose R_f (0.74) and MW (297) were consistent with the nitrobenzo(a)pyrene (nitro-BaP) structure.

By changing the TLC solvent system described in Figure 1 to toluene alone, the band containing nitro-BaP was further resolved into two bands, one yellow and one orange, the latter having a lower R_f value. From the mass spectra and ultraviolet-visible spectra shown in Figure 2, and by comparison with those of authentic samples synthesized according to Dewar[65], we assign the structure 6-nitro-BaP to the component

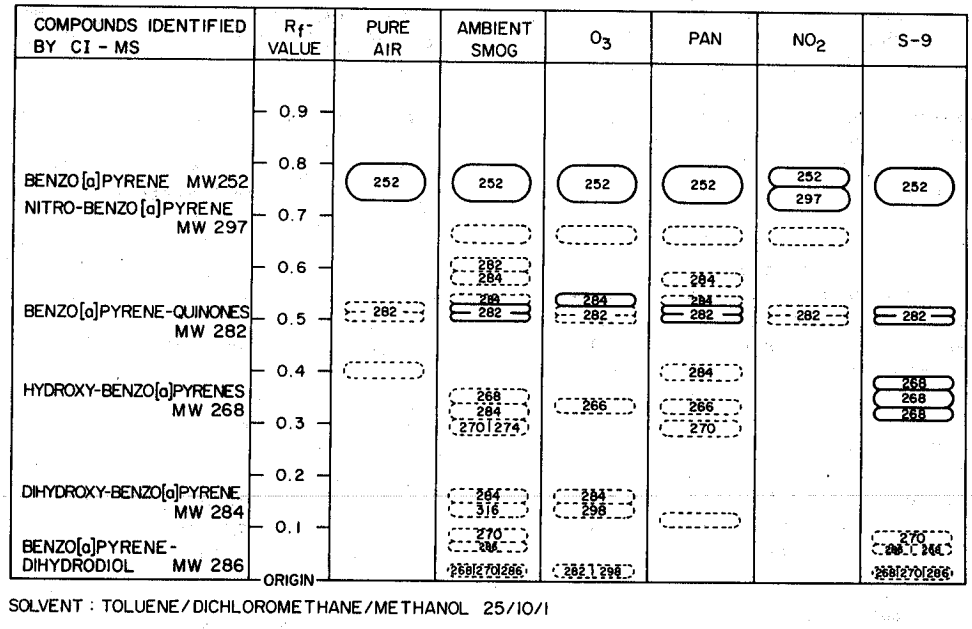

Figure 1. Thin layer chromatograms of products formed upon exposure of BaP (6-10 mg, deposited on two 8 x 10 in. Gelman AE glass fiber filters) to pure air, ambient smog, O_3, PAN and NO_2 and upon treatment of BaP with liver S-9. Each TLC band (separation on Merck silica gel plates No. 5763) was recovered in methanol and analyzed by methane chemical ionization mass spectrometry (CI-MS, direct introduction probe). Each band (solid line = major, dashed line = minor) shows the molecular weight(s) of the product(s) found in it. Also shown are the products identified by CI-MS in each band (first column from left) and the TLC R_f values (second column). See text for exposure levels, experimental conditions and results of mutagenic assay.

nature of the constituents of particulate matter, both PAH and others. Furthermore, we must do so insofar as possible, at, or near, the site of their impact upon the biological target.

Because of the chemical complexity of ambient particulates and auto exhaust, and because animal tests for suspected carcinogens are time consuming and expensive, experiments directed to establishing the identity of the compounds responsible for the "excess" carcinogenicity have been in general relatively limited. Recently however, a rapid and relatively inexpensive microbiological assay for mutagenic activity has been developed by Ames and co-workers[21-23]. It is a reverse mutation system employing histidine-requiring mutants of the bacterium Salmonella typhimurium. In tests of some 300 compounds, about 85 to 90% of the known carcinogens were also found to be mutagens, while the number of false positives and negatives ranged from 10 to 15%[24]. This observation has been confirmed by other investigators[25] and the Ames test is now generally recognized as a useful, though by no means exclusive, screening test for chemical mutagens in complex environmental samples[26-32].

We have been using the Ames test to screen for mutagenic activity in particulate samples collected from real and simulated atmospheres, and as a means of obtaining microbiological clues to the chemical nature of the compounds responsible for the "excess" carcinogenicity.

In 1975 the mutagenicity of organic fractions from particulates collected at several sites in the Los Angeles Basin was demonstrated using the Ames assay system[33]. This phenomenon has now been reported in studies in Ohmura and Fukuoka, Japan[34], Kobe, Japan[35], Buffalo, New York and Berkeley, California[36], New York City, New York[37], and Chicago, Illinois[38].

Recently, we collected 23 samples of airborne particulates at 11 urban sites in California's South Coast Air Basin[39,40]. Results of the Ames tests can be summarized as follows:

- All 23 samples exhibited frameshift-type mutagenic activity without requiring metabolic activation with strains TA1537, TA1538 and TA98.
- All solvent and filter blanks were inactive.
- Typically, assay of 0.1 to 2 mg of airborne organic particulates resulted in a five to 20-fold increase in the number of histidine revertants per plate above the background of spontaneous revertants in strains TA1537, TA1538 and TA98, and in up to a two-fold increase in strain TA100.
- No activity was observed in any of the assays with strain TA1535, which is reverted by base-pair substitution mutations.
- Microsomal activation by S-9 solution did not increase the activity of the majority (20 out of 23) of the samples tested.
- Assay of extracts of a size-resolved sample collected in downtown Los Angeles revealed that all mutagenic activity was associated with organic species present in particles of diameter 1.1 micron or less. This is consistent with the well-documented distribution of organic particulate pollutants such as BaP with respect to particle size[41-44].

As noted earlier, the carcinogenic activity of organic fractions extracted from ambient particulates taken from the Los Angeles atmosphere is well known, so that our finding frameshift-type mutagenic activity in all urban samples is not surprising. What is interesting chemically is that metabolic activation was not required for any sample. In fact, addition of S-9 had an enhancing effect in only three out of 23 samples. Thus, these urban particulates must contain mutagens other than the carcinogenic PAH, such as BaP, which require such activation. This is consistent with the numerous observations of "excess" carcinogenicity in animal or in cell transformation activity discussed above, and the low average concentrations of BaP in the Los Angeles Basin[3].

We recently proposed that the presence of these direct mutagens in ambient particulates may be due in part to the reactions of BaP and other PAH with such species as nitrogen dioxide, ozone, peroxyacetyl nitrate (PAN), singlet molecular oxygen ($O_2{}^1\Delta$), and free radicals present in photochemical smog such as OH and HO_2[45,46]. If some of the products formed in these reactions are analogous to the metabolites of BaP and other PAH in mammalian cells[47,48,49], reactions of PAH in exhaust effluents and in the atmosphere could account for the presence of directly active mutagens in urban particulates.

Relevant to the postulated importance of oxidative processes during atmospheric transport of PAH are several reports of the carcinogenic activity of polar fractions of organic particulates[4,20, 50-52], products of ozonized gasolines[53] and products of oxidation of aliphatic hydrocarbons[54] and of the toxicity of the photooxidation products of a commercial fuel oil[55].

There are also several reports that BaP and other PAH readily undergo photochemical transformations when adsorbed on a variety of support materials such as filters. silica gel and carbon (soot) particles[3,7,56-59].

Finally, there is evidence that polycyclic quinones are present in ambient particulates and that they may be formed atmospheric photooxidation of PAH[60-63].

In order to test our hypothesis that oxidative reactions of PAH in the atmosphere may lead to the formation of directly active mutagens, we conducted one set of experiments in which the carcinogen, BaP, and perylene, reportedly a non-carcinogen[14,64], were each exposed to pollutant gases under simulated atmospheric conditions and one set in which BaP was exposed to the gases in ambient photochemical smog.

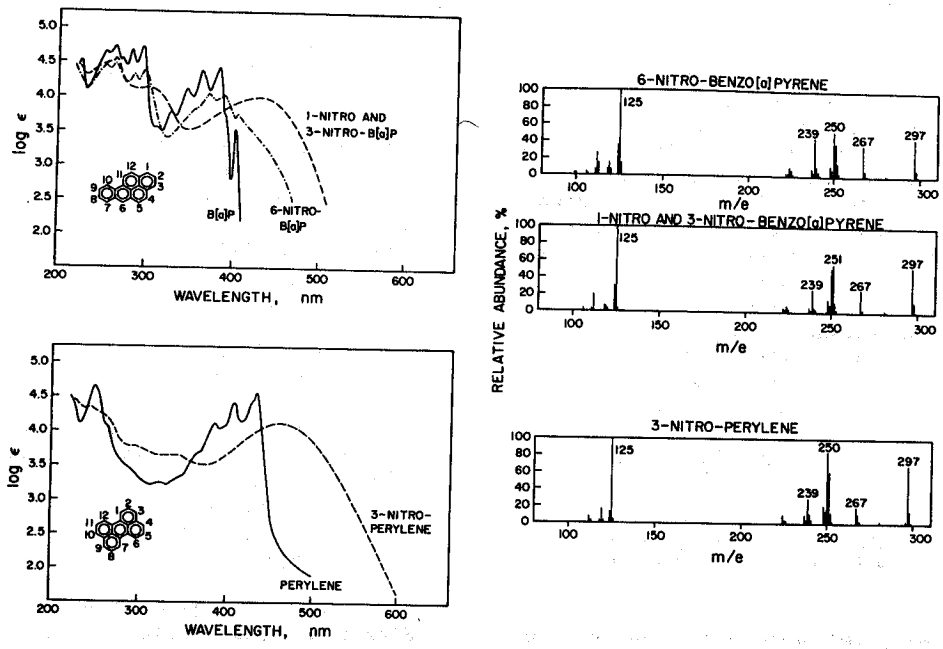

Figure 2. Ultraviolet-visible (uv/vis) spectra in methanol (left) and electron impact mass spectra (right) of 6-nitro-BaP, 1-nitro- and 3-nitro-BaP, and 3-nitro-perylene formed upon exposure of BaP or perylene to NO_2. Also shown are the formulas and uv/vis spectra of the parent PAH (left).

present in the yellow TLC band while the orange TLC band consists of a mixture of the 1-nitro and 3-nitro isomers.

As shown in Figure 3, both 6-nitro-BaP and the mixture of the 1-nitro- and 3-nitro-BaP isomers are direct mutagens in the Ames test. They are directly active with strains TA1537, TA1538, TA98 and TA100 which are reverted by frameshift mutagens. Addition of liver S-9 significantly enhanced their activity in strains TA1537, TA1538 and TA98, and reduced the activity of the 1-nitro- and 3-nitro-BaP mixture with strain TA100.

Dose-response curves for the authentic samples, also shown in Figure 3, are in good agreement with those of the nitro-BaP isomers formed upon exposure of BaP to NO_2. No activity was found with strain TA1535 which is reverted by base-pair substitution mutations.

Since exposure of BaP, a known carcinogen and activatable mutagen, to ppm levels of NO_2 results in the formation of mutagenic nitro-derivatives, it seemed interesting to see if, under the same conditions, similar products could also be formed from a non-carcinogenic PAH. To address this point, NO_2 exposure studies were repeated with perylene, an isomer of BaP present in ambient air and emitted in many combustion processes[14,64], including vehicle exhaust. Unlike BaP, we found perylene to be non-mutagenic with or without S-9 in the Ames reversion assay (Figure 3d).

Perylene deposited on glass fiber filters was exposed to 1 ppm of NO_2 for 24 hours at a flow rate of 1 cfm. The major resulting TLC band (brick-red color on silica gel) consisted of 3-nitroperylene, identified on the basis of its mass spectrum and by comparison of its UV spectrum with literature data[66,67]. Both spectra are shown in Figure 2. When tested with strains TA98 and TA1538, 3-nitroperylene was found to be a directly active mutagen whose activity was significantly enhanced by the addition of liver S-9 (Figure 3).

The above studies conducted in simulated atmospheres clearly demonstrate that directly active mutagens, including nitro-derivatives, can form upon exposure of PAH to gaseous pollutants. Additional evidence for the possible occurrence of such transformations in real atmospheres was obtained by drawing ambient photochemical smog through two glass fiber filters mounted in series for 72 hours at a flow rate of 40 cfm using BaP as our "model" PAH. The upstream filter collected ambient particulates, thus allowing BaP deposited on the downstream filter to be exposed only to gaseous pollutants.

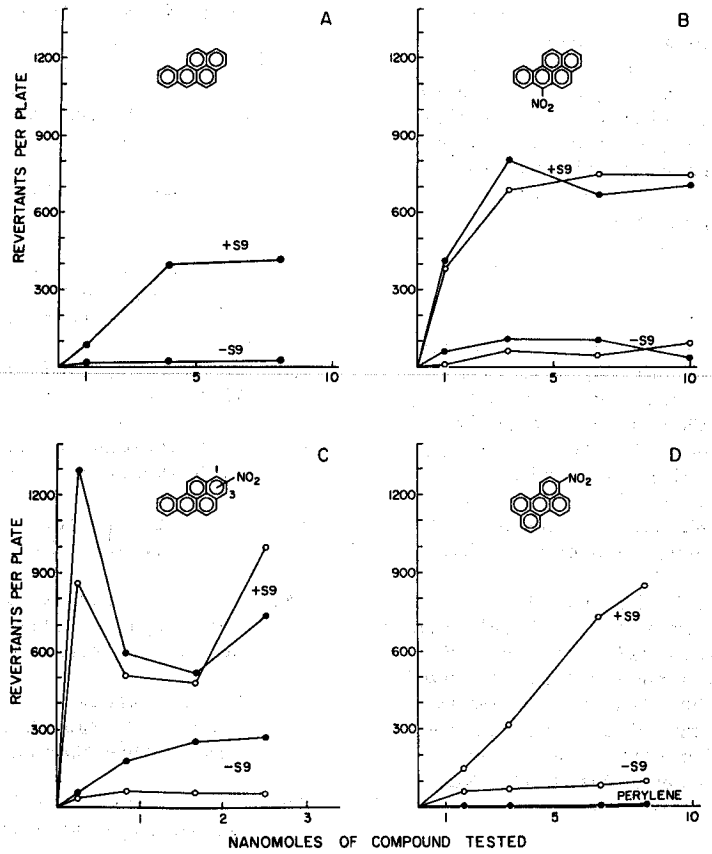

Figure 3. Mutagenic activity of BaP (A), 6-nitro-BaP (B), 1-nitro- and 3-nitro-BaP (C) and 3-nitroperylene (D) in the Ames assay system. Dose-response curves are shown only for the most sensitive strain, TA100 (A,B), TA98 (C) and TA1538 (D) with (+S9) and without (-S9) metabolic activation. Each point represents the mean of at least triplicate plates. Subtracted spontaneous revertant backgrounds were: TA100:118-130 (-S9), 130-152 (+S9); TA98:24 (-S9), 44 (+S9); TA1538:12 (-S9), 41 (+S9). Also shown (full circles) are the corresponding curves for perylene (D) and for the nitro-BaP isomers (B,C) synthesized according to Dewar [65].

The results are shown in Figure 1 along with those of the BaP-exposure studies conducted in simulated atmospheres. Many of the resulting products were analogous to those formed in the laboratory exposures of BaP to the individual gaseous pollutants or in solution to the liver S-9 mix. On the basis of their molecular weights, determined by C.I.-mass spectrometry, and their R_f values, these oxidation products appear to include hydroxy-, dihydroxy- and dihydrodiol-derivatives. These are known metabolites of BaP in mammalian cells[47].

Since NO_2, BaP, perylene (and a host of other PAH) are present in auto exhaust, as well as emissions from, for example, coal burning fossil fuel power plants, it seems possible that the compounds 6-nitro-, 1-nitro-, and 3-nitro-BaP and 3-nitroperylene we isolated in these experiments using simulated atmospheres may also be formed in real atmospheric systems. Indeed, such nitro-PAH and/or their photodegradation product systems may be responsible for at least part of the direct mutagenicity we observed in the urban aerosol samples, and the "excess carcinogenicity" in animals cited above for auto exhaust and ambient particulates.

Finally, we would like to reemphasize that our studies were conducted with PAH deposited on the surface of glass fiber filters. Whether PAH adsorbed on the surface of airborne particles (soot, fly ash, etc.) will react in a similar fashion in the atmosphere is a matter of conjecture and will be investigated. This is a complex problem because atmospheric reactions of PAH may

be influenced by many factors typical of surface chemistry as well as by pollutant levels, particle size, sunlight intensity, atmospheric mixing and transport time. Similarly, little is known about the extent of possible reactions of PAH on glass fiber filters widely employed for decades to collect ambient particulates; our results suggest that they may indeed be significant. Therefore, the determination of possible filter "artifacts" is of major importance since historically most evaluations of the carcinogenic and mutagenic activity of organic particulates have been based upon filter samples.

ACKNOWLEDGMENT

This lecture is primarily based on the following recent research papers currently in press: "Atmospheric Reactions of Polycyclic Aromatic Hydrocarbons: Facile Formation of Mutagenic Nitro-Derivatives," Science, in press (1978), and "Photochemical and Biological Implications of the Atmospheric Reactions of Amines and Benzo(a)pyrene," Philosophical Transactions of the Royal Society of London, in press (1978).

We want to thank Mr. T. M. Mischke of the Department of Chemistry, University of California, Riverside, who was involved with the chemical aspects of collection and analysis of the urban particulates, and Dr. Vincent F. Simmon and Mr. Dennis Poole, Stanford Research Institute, who kindly carried out the Ames tests during our initial screening program of urban aerosols collected in the Los Angeles Basin.

We also want to express our appreciation to the University of California and to the Federal agency who generously funded this research-the National Science Foundation-Research Applied to National Needs (Grant No. ENV73-02904-A04, Dr. R. Carrigan, Project Officer).

The contents do not necessarily reflect the views and/or policies of the NSF-RANN nor does mention of trade names or commercial products constitute endorsement or recommendation for use.

REFERENCES

1. J. Leiter, M. B. Shimkin, M. J. Shear, 1942 J. Natl. Cancer Inst. 3 155-165.

2. J. Leiter and M. J. Shear, 1943 J. Natl. Cancer Inst. 3, 455-477.

3. P. Kotin, H. L. Falk, P. Mader and M. Thomas, 1954 Arch. Indust. Hyg. 9, 153-163.

4. W. C. Hueper, P. Kotin, E. C. Tabor, W. W. Payne, H. L. Falk, and E. Sawicki, 1962 Arch. Pathol. 74, 89-116.

5. R. J. Gordon and R. J. Bryan, 1973 Environ. Sci. Technol. 7, 1050-1053.

6. R. C. Lao, R. S. Thomas, H. Oja, and L. Dubois, 1973 Anal. Chem. 45, 908-915.

7. K. W. Boyer and H. A. Laitinen, 1975 Environ. Sci. Technol. 9, 457-469.

8. R. S. Spindt, 1974 First annual report on polynuclear aromatic content of heavy duty diesel exhaust gases, Gulf Research and Development Co.

9. M. Blumer, W. Blumer, and T. Reich, 1977 Environ. Sci. Technol. 11, 1082-1084.

10. E. Sawicki, S. P. McPherson, T. W. Stanley, J. Meeker, and W. C. Elbert, 1965 Int. J. Air Water Pollut. 9, 515-524.

11. E. Sawicki, 1967 Arch. Environ. Health 14, 46-53.

12. W. Cautreels and K. A. Van Cauwenberghe, 1976 Atmos. Environ. 10, 447-457.

13. M. Dong, D. Locke, and D. Hoffmann, 1977 Environ. Sci. Technol. 11, 612-618.

14. National Academy of Sciences, 1972 Particulate organic matter. Washington, D.C.: National Academy of Sciences.

15. S. S. Epstein, S. Joshi, J. Andrea, N. Mantel, E. Sawicki, T. Stanley, and E. C. Tabor, 1966 Nature 212, 1305-1307.

16. R. H. Rigdon and J. Neal, 1971 Texas reports on biology and medicine 29, 110-123.

17. A. E. Freeman, P. J. Price, R. J. Bryan, R. J. Gordon, R. V. Gilden G. J. Kelloff, and R. J. Huebner, 1971 Proc. Nat. Acad. Sci. USA 68, 445-449.

18. U. Mohr, H. Reznik-Schuller, G. Reznik, G. Grimmer and J. Misfeld, 1976 Zbl. Bakt. Hyg., I Abt. Orig. B 163, 425-432.

19. G. Grimmer, 1977 International Agency for Research on Cancer (IARC) Scientific Pub. No. 16, 29-39 Lyon, France.

20. R. J. Gordon, R. J. Bryan, J. S. Rhim, C. Demoise, R. G. Wolford, A. E. Freeman, and R. J. Huebner, 1973 Int. J. Cancer 12, 223-227.

21. B. N. Ames, W. E. Durston, E. Yamasaki, and F. D. Lee, 1973 Proc. Nat. Acad. Sci., 70, 2281-2285.

22. B. N. Ames, J. McCann, and E. Yamasaki, 1975 Mutation Res. 31, 347-364.

23. B. N. Ames and J. McCann, 1976 Carcinogens are mutagens: a simple test system, in Screening Tests in Chemical Carcinogens, Lyon: IARC Scientific Publication No. 12.

24. J. McCann, E. Choi, E. Yamasaki, and B. N. Ames, 1975 Proc. Nat. Acad. Sci. 72 5135-5139.

25. T. Sugimura, T. Yahagi, M. Nagao, M. Takenchi, T. Kawachi, K. Hara, L. Gamasaki, T. Matsushima, Y. Hashimoto, and M. Okada, 1976 Validity of mutagenicity tests using microbes as a rapid screening method for environmental chemicals, in R. Montesano, H. Hartsch and L. Tomatis (eds.) Screening tests in chemical carcinogens. Lyon: IARC Scientific Publication No. 12.

26. H. Bartsch 1976 Mutation Res. 38, 177-190.

27. N. P. Bochkov, R. J. Sram, N. P. Kuleshov, and V. S. Zhurkov, 1976 Mutation Res. 38, 191-202.

28. B. Commoner, 1976 "Reliability of bacterial mutagenesis techniques to distinguish carcinogenic and non-carcinogenic chemicals" EPA Report EPA600/1-76-022, Washington, DC.

29. B. J. Dean, 1976 Mutation Res. 41, 83-88.

30. F. J. de Serres, 1976a Mutation Res. 38, 355-357.

31. F. J. de Serres, 1976b Mutation Res. 41, 43-50.

32. F. H. Sobels, 1977 Mutation Res. 46, 245-260.

33. J. N. Pitts, Jr., 1975 Chemical transformations in photochemical smog and their applications to air pollution control strategies. Second Annual Report, National Science Foundation-Research Applied to National Needs Grant No. AEN73-02904-A02, p. V-8.

34. H. Tokiwa, H. Tokeyoshi, K. Morita, K. Takahashi, N. Soruta, and Y. Ohnishi, 1976 Mutation Res. 38, 351-359.

35. K. Teranishi, K. Hamada, and H. Watanabe, 1978 Mutation Res. 56, 273-280.

36. R. Talcott and E. Wei, 1977 J. Natl. Cancer Inst. 58, 449-451.

37. J. M. Daisey, I. Hawryluk, T. J. Kneip, F. H. Mukai, 1978 "Mutagenic activity in organic fractions of airborne particulate matter," presented at the Conference on Carbonaceous Particles in the Atmosphere, March 20-22, Berkeley, California.

38. B. Commoner, P. Madyastha, A. Bronsdon and J. Vithayathil, 1978 J. Toxicol. Environ. Health, 4, 59-77.

39. J. N. Pitts, Jr., D. Grosjean, T. M. Mischke, V. F. Simmon and D. Poole, 1977b Presented at Symposium on mutagenic activity of airborne particulate organic pollutants, American Chemical Society, August 1977, and to be published S. D. Lee (ed.) 1978 Biological effects of environmental pollutants, in press. Ann Arbor, Michigan: Ann Arbor Science Pub., Inc.

40. J. N. Pitts, Jr., J. P. Smith, D. R. Fitz, and D. Grosjean, 1977c Sceince 197, 225-257.

41. M. Kertesz-Saringer, E. Meszaros, and T. Varkonyi, 1971 Atmos. Environ. 5, 429-431.

42. D. F. Natusch and J. R. Wallace, 1974 Science 186, 695-699.

43. R. C. Pierce and M. Katz, 1975 Environ. Sci. Technol. 9, 347-353.

44. S. K. Friedlander and A. Miguel, 1978 Atmos. Environ., in press.

45. J. N. Pitts, Jr., D. Grosjean, T. M. Mischke, V. F. Simmon, and D. Poole, 1977a Toxicol. Lett. 1, 65-70.

46. J. N. Pitts, Jr., K. A. Van Cauwenberghe, D. Grosjean, J. P. Schmid, D. Fitz, W. L. Belser, Jr., G. B. Knudson, and P. M. Hynds, 1978c Science 1978 in press.

47. D. M. Jerina, R. E. Lehr, H. Yagi, O. Hernandez, P. M. Dansette, P. G. Wislocki, A. W. Wood, R. L. Chang, W. Levin, and A. H. Conney, 1976a in, F. J. de Serres, J. R. Fouts, J. R. Bend, and R. M. Philpot (eds.) In vitro metabolic activation in mutagenesis testing, Amsterdam: Elsevier.

48. D. M. Jerina, H. Yagi, O. Hernandez, P. M. Dansette, A. W. Wood, W. Levin, R. L. Chang, P. G. Wislocki, and A. H. Conney, 1976b Synthesis and biologic activity of potential benzo(a)pyrene metabolites in Freudenthal and Jones (eds.) Polynuclear aromatic hydrocarbons: chemistry, metabolism and carcinogenesis, New York, N.Y.: Raven Press.

49. O. G. Fahmy and M. J. Fahmy 1976 Cancer Res. 36, 4504-4512.

50. S. S. Epstein, N. Mantel and T. W. Stanley, 1968 Environ. Sci. Technol. 2, 132-138.

51. E. L. Wynder and D. Hoffmann, 1965 J. Air Pollut. Control Assoc. 15, 155-158.

52. J. Asashina, J. Andrea, A. Carmel, E. Arnold, Y. Bishop, S. Joshi, D. Coffin, and S. S. Epstein, 1972 Cancer Res. 32, 2263-2268.

53. P. Kotin, H. L. Falk and C. J. McCammon, 1958 Cancer 11, 473-481.

55. R. A. Larson, L. L. Hunt and D. W. Blankenship, 1977 Environ. Sci. Technol. 11, 492-496.

56. H. L. Falk, I. Markul, and P. Kotin, 1956 AMA Arch. Ind. Health 13, 13-17.

57. B. D. Tebbens, J. F. Thomas, and M. Mukai, 1966 J. Amer. Ind. Hyg. Assoc. 27, 415-422.

58. B. D. Tebbens, M. Mukai, and J. F. Thomas, 1971 J. Amer. Ind. Hyg. Assoc. 32, 365-372.

59. D. F. Barofsky and E. J. Baum, 1976 J. Amer. Chem. Soc. 98, 8286-8287.

60. Y. Masuda and M. Kuratsune, 1966 Air Water Pollut. 10, 805-811.

61. A. J. Fatiadi, 1967 Environ. Sci. Technol. 1, 10-12.

62. J. Jaeger, 1971 Fresenius' Z. Anal. Chem. 225, 281-284.

63. R. C. Pierce and M. Katz, 1976 Environ. Sci. Technol. 10, 45-51.

64. D. Hoffmann and E. L. Wynder, 1977 Organic particulate pollutants - chemical analysis and bioassays for carcinogenicity. A. C. Stern (ed.) Air Pollution, Third Ed., vol. II (361-455), New York: Academic Press.

65. M. J. S. Dewar, T. Mole, D. S. Urch, and E. W. T. Warford, 1956a J. Chem. Soc. 3572-3575.

66. M. J. S. Dewar and T. Mole, 1956, J. Chem. Soc., 1441.

67. H. Hopff and H. R. Schweizer, 1957, Helv. Chim. Acta, 42, 2315.

samples. To test this hypothesis, we developed an optical attenuation technique to quantitatively measure various properties of the absorbing species. A schematic of the apparatus used for these measurements is shown in Fig. 2.

Using this apparatus we studied the temperature stability and solubility of the absorbing species in ambient and source particulate samples. The temperature stability was determined by measuring the attenuation by particulates collected on quartz fiber filters before and after heat treatment at various temperatures. The heat treatment procedure consisted in heating the sample at the prescribed temperature for 30 min in air. The results of these measurements are plotted in Fig. 4, which shows clearly that in all cases the absorbing species are stable in air until approximately 400°C, and then undergo what is presumably a rapid oxidation process to essentially disappear by 550°C. Note that this threshold is similar to that of polycrystalline graphite.[15] The oxidation threshold appears to be slightly higher for the laboratory soot samples than for the other samples, which may be due to differences in particle sizes or morphology. The stability of the absorbing species at elevated temperatures suggests that they are graphitic in structure, as most other organic species expected to be present in ambient and tunnel samples should oxidize or vaporize at significantly lower temperatures.

We measured the optical attenuation of source and ambient samples before and after removal of adsorbed organic compounds by solvent extraction. Sequential 6-hr soxhlet extractions with benzene and a chloroform methanol mixture (2:1 v:v), following the technique of Appel et al.,[16] should remove all soluble organic material and some inorganic ions. Ambient Berkeley samples, Caldecott Tunnel vehicle exhaust, and natural gas soot were collected on prefired quartz filters by hi-vol sampling, with optical attenuation and carbon loading measurements performed before and after extraction. In Fig. 5 we show that the optical attenuation decreases only slightly, even though a substantial fraction of the carbon is removed by solvent extraction (around 70% for ambient Berkeley filters). This result indicates that soluble adsorbed organic compounds do not contribute appreciably to the attenuation properties of the ambient and source particulates. This confirms the results of Weiss and his coworkers,[7] who found that an acid wash of ambient-particulate-loaded filters does not change their optical properties.

We also measured the wavelength dependence of the absorptivity of ambient and source particulate samples using a spectrophotometer. As shown in Fig. 6, the optical attenuation, to within 20% over the visible spectral region (4500 Å-7000 Å), has a $1/\lambda$ wavelength dependence characteristic of a constant imaginary index of refraction. This result is consistent with the hypothesis that the absorption is due primarily to "graphitic" soot since the imaginary index of refraction of both acetylene and propane soot is essentially constant throughout the visible region.[14] In fact it is difficult to find many organic species which meet this criterion: of the 13,000 organics in the 54th ed. of the CRC Handbook, only 5 are listed as gray or black in appearance.

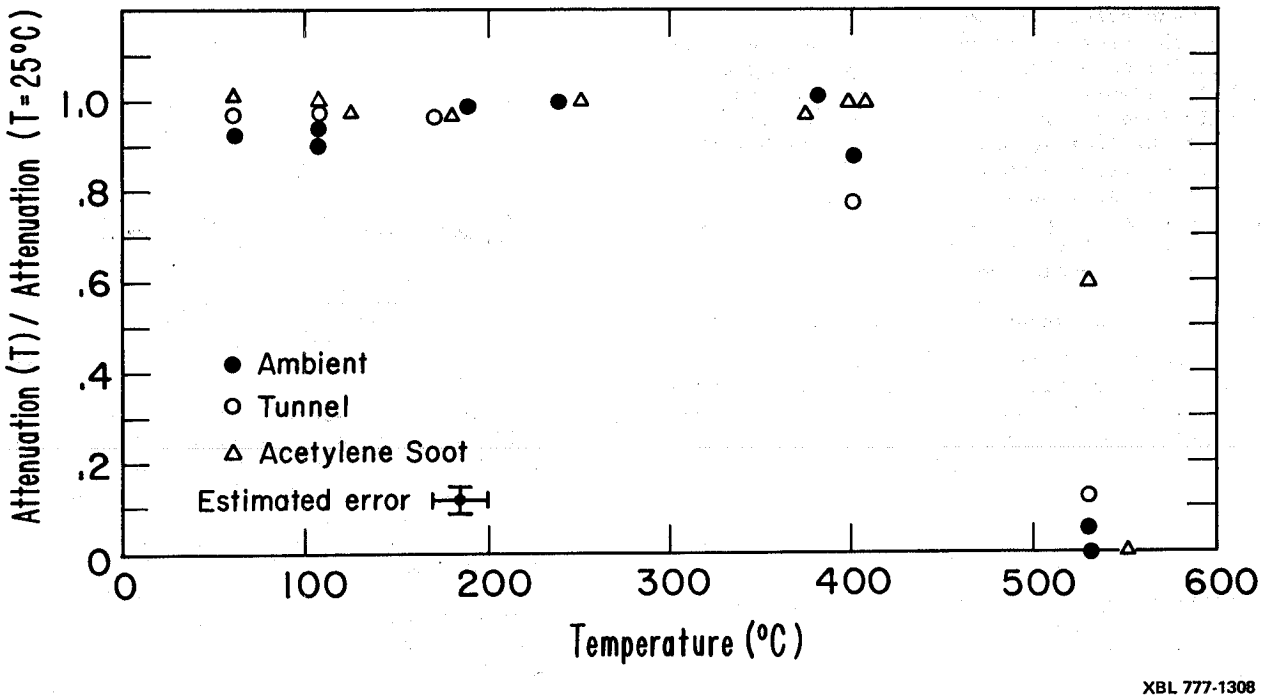

Fig. 4. Plot of the ratio of the attenuation of various samples after heat treatment at temperature T to the attenuation at T = 25°C as a function of the heat treatment temperature. The heat treatment procedure consisted in heating the sample in air for 1/2 hr at the prescribed temperature.

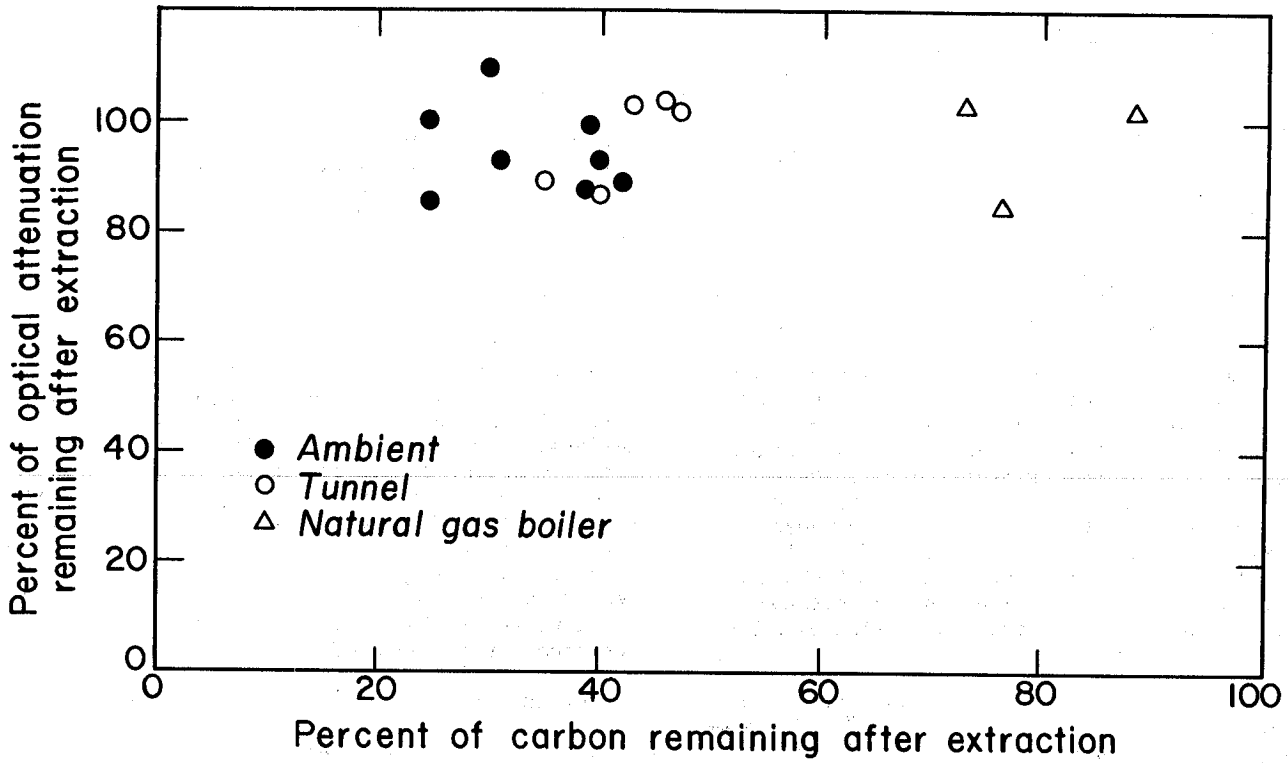

XBL 783-344

Fig. 5. Plot of the percent of the optical attenuation remaining after soxhlet extraction as a function of the carbon remaining after extraction for various ambient and source particulate samples.

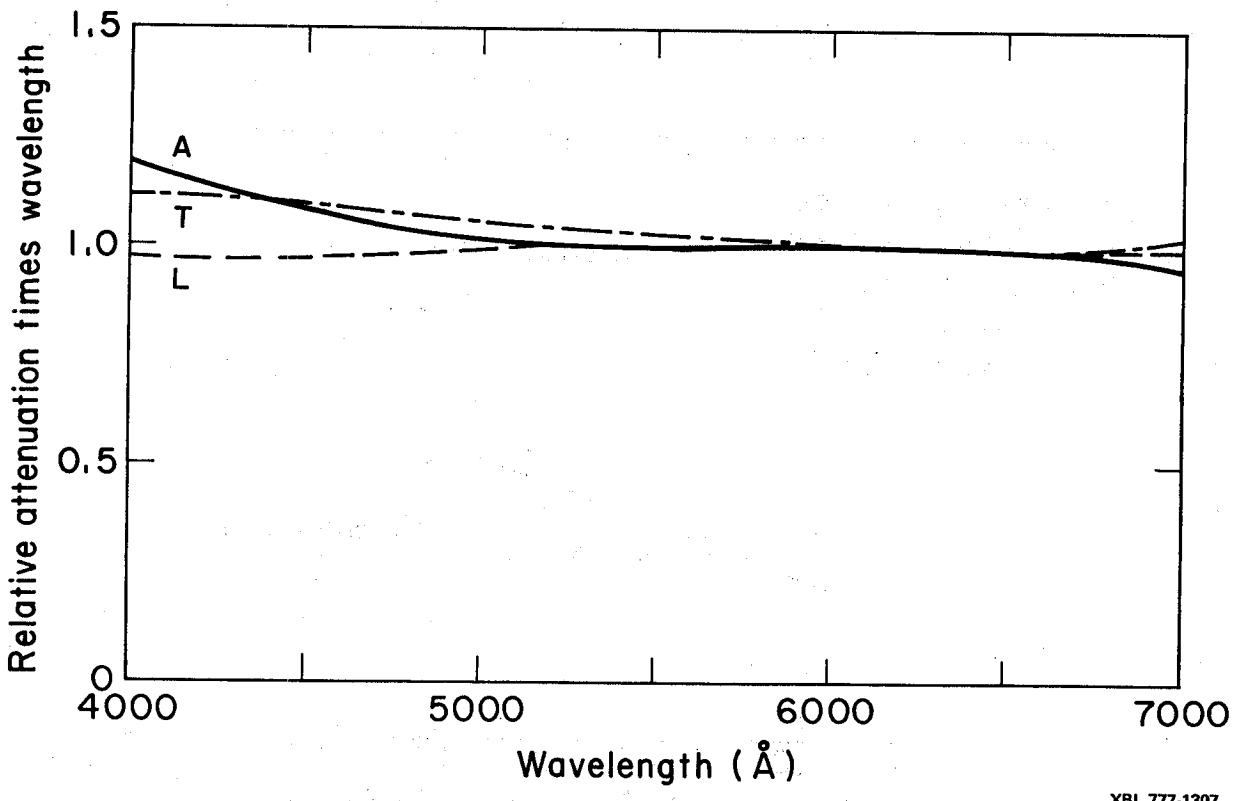

XBL 777-1307

Fig. 6. Plot of the product of attenuation and wavelength vs. wavelength for A — ambient samples, T — tunnel samples, and L — laboratory-generated soot samples. Such a plot would be flat for a wavelength independent imaginary index of refraction.

Comparison Between Raman Spectroscopy and Optical Attenuation

All these results strongly suggest that the coloration of ambient and source particulate samples is due to their "graphitic" soot content. However, we wanted to have a more direct substantiation of this result. Substantiation was provided by comparing the integrated intensity of the 1600 cm^{-1} Raman mode with the optical attenuation of the same filter sample. These measurements were done on acetylene soot samples (which were essentially pure carbon with only trace amounts of metallic impurities), highway tunnel samples, and ambient samples collected in Berkeley and Fremont in the San Francisco Air Basin and in Anaheim in the Los Angeles Air Basin. The results are shown in Figure 7. Within experimental error, these data show that there is a direct correspondence between the optical absorptivity and the Raman intensity or "graphitic" soot content for all samples studied, despite widely different chemical compositions (e.g., for a given optical attenuation, the Pb and Fe concentrations varied by more than a factor of 100.

This result can be put in a mathematical form if we neglect particle size effects[17,18] and assume an optically thin homogeneous media. With these assumptions, it is easy to show that the data in Fig. 7 imply that the ratio $\sigma_R M_R/\sigma_A M_A$ is a constant where M_R is the concentration of "graphitic" soot as defined by Raman spectroscopy, M_A is the concentration of the absorbing species, σ_R is the Raman cross section for "graphitic" soot, and σ_A is the absorption cross section for the absorbing species. For fixed optical constants, this implies that the ratio of the "graphitic" soot content to the content of the absorbing species is constant for a wide variety of ambient and source particulate samples. The most obvious and most reasonable explanation for this observation is that the absorptivity is due to "graphitic" soot.

CONCLUSION

In summary, we have shown that the species responsible for the coloration of particulate samples has high temperature stability in air, is insoluble in a variety of solvents, and absorbs uniformly throughout the visible region. We have also demonstrated that the amount of the absorbing species is directly proportional to the "graphitic" soot content as defined by Raman spectroscopy. All these results taken together indicate that the high optical absorptivity of ambient samples collected in urban environments and of various source particulate samples is due to the "graphitic" component of the aerosol.

ACKNOWLEDGMENT

This work was supported by the Division of Biomedical and Environmental Research, Department of Energy, and by the National Science Foundation. The authors would like to thank R.D. Giauque and B.W. Loo for providing elemental analyses of the samples. We would also like to thank the Bay Area Air Pollution Control District and the South Coast Air Quality Maintenance District for cooperating in our sampling program. Helpful discussions with R.J. Charlson are also gratefully acknowledged.

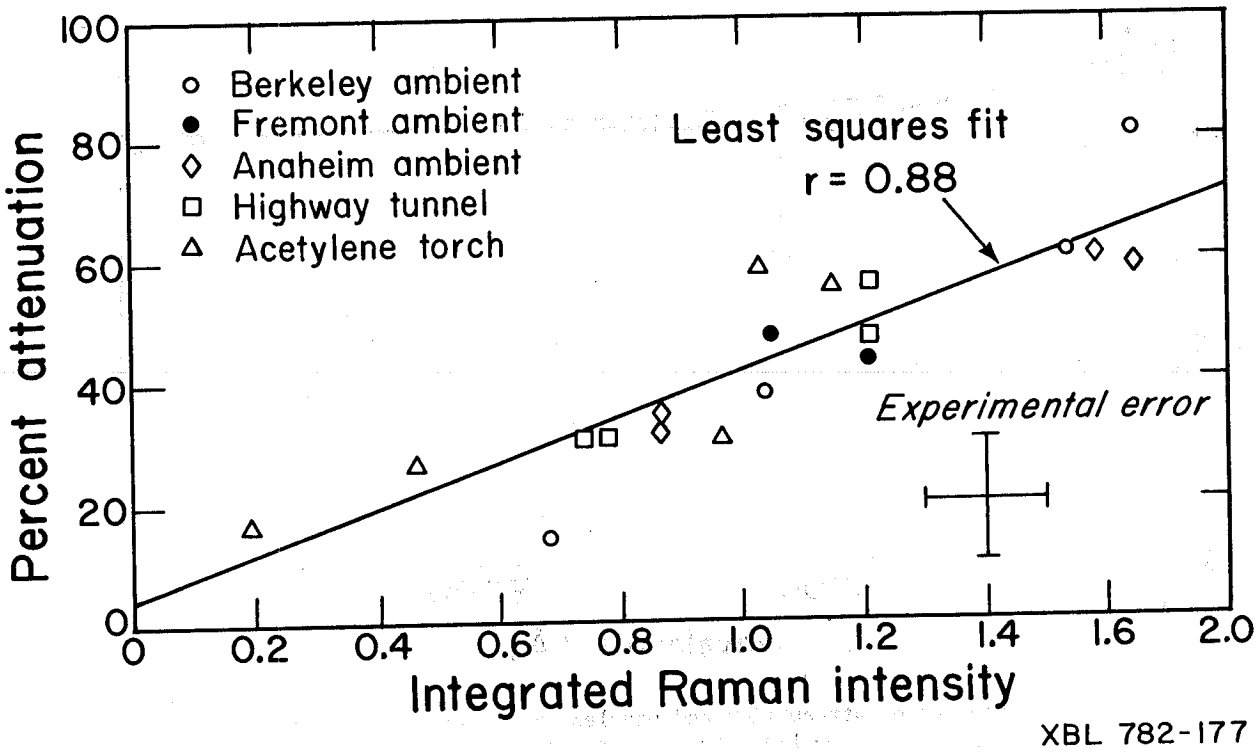

Fig. 7. Plot of integrated Raman intensity of the 1600 cm^{-1} mode versus percent optical attenuation at 6328 Å for ambient, acetylene soot, and tunnel samples.

REFERENCES AND FOOTNOTES

1. R. Weiss et al., "Application of Directly Measured Aerosol Radiative Properties to Climate Models," Proceedings, Symposium on Radiation in the Atmosphere, Garmisch-Partenkirchen, FRG, p. 469 (1976).
2. R.A. Reck, "Thermal and Radiative Effects of Atmospheric Aerosols in the Northern Hemisphere Calculated Using a Radiative-Convective Model," Atmos. Environ. 10, 611 (1976).
3. P. Chylek and J.A. Coakley, Jr., "Aerosols and Climate," Science 183, 75 (1974).
4. S.I. Rasool and S.H. Schneider, "Atmospheric Carbon Dioxide and Aerosols: Effects of Large Increases on Climate," Science 173, 138 (1971).
5. H. Rosen, A.D.A. Hansen, R.L. Dod, and T. Novakov, "Application of the Optical Absorption Technique to the Characterization of the Carbonaceous Component of Ambient and Source Particulate Samples," Proceedings, Fourth Joint Conference on Sensing of Environmental Pollutants, New Orleans, Paper 171 (1977).
6. A.D.A. Hansen, H. Rosen, R.L. Dod, and T. Novakov, "Optical Attenuation as a Tracer for the Primary Component of the Carbonaceous Aerosol," Proceedings, Conference on Carbonaceous Particles in the Atmosphere, Berkeley, California (1978).
7. R.E. Weiss, A.P. Waggoner, R.J. Charlson, D.L. Thorsell, J.S. Hall, and L.A. Riley, "Studies of the Optical, Physical and Chemical Properties of Light Absorbing Aerosols," paper presented at the Conference on Carbonaceous Particles in the Atmosphere, Berkeley, California (1978).
8. H. Rosen and T. Novakov, "Raman Scattering and the Characterization of Atmospheric Aerosol Particles," Nature 266, 708 (1977).
9. H. Rosen and T. Novakov, "Identification of Primary Particulate Carbon and Sulfate Species by Raman Spectroscopy," Atmos. Environ. 12, 923 (1978).
10. J.J. Blaha, G.J. Rosasco, and E.S. Etz, "Raman Microprobe Characterization of Residual Carbonaceous Material Associated with Urban Airborne Particulates," Appl. Spectros. 32, 292 (1978).
11. R.G. Stafford, R.K. Chang, and P.J. Kendlmann, "Laser-Raman Monitoring of Ambient Sulfate Aerosols," presented at the National Bureau of Standards 8th Materials Research Symposium on Methods and Standards for Environmental Measurement, Gaithersburg, Maryland (1976).
12. B.W. Loo, J.M. Jaklevic, and F.S. Goulding, "Dichotomous Samplers for Large-Scale Monitoring of Airborne Particulate Matter," in Fine Particles: Aerosol Generation, Measurement, Sampling and Analyses (Academic, New York, 1976), ed. B.Y.H. Liu, p. 311.
13. F. Tuinstra and J.L. Koenig, "Raman Spectrum of Graphite," J. Chem. Phys. 53, 1126 (1970).
14. W.H. Dalzell and A.F. Sarofim, "Optical Constants of Soot and Their Application to Heat-Flux Calculations," J. Heat Transfer 91, 101 (1969).
15. See, for example, Union Poco Comparison Chart, Publication PGI-S-2021, Poco Graphite Inc., 1601 South State Street, Decatur, TX 76234.
16. B.R. Appel, E.M. Hoffer, M. Haik, S.M. Wall, E.L. Kothny, R.L. Knights, and J.J. Wesolowski, Final Report to California Air Resources Board, Contract No. ARB 5-682, Characterization of Organic Particulate Matter (1977).
17. H. Chew, P.J. McNulty, and M. Kerker, "Model for Raman and Fluorescent Scattering by Molecules Embedded in Small Particles," Phys. Rev. A 13, 396 (1976).
18. H. Chew, M. Kerker, and P.J. McNulty, "Raman and Fluorescent Scattering by Molecules Embedded in Concentric Spheres," J. Opt. Soc. Am. 66, 440 (1976).

MASS MONITORING OF CARBONACEOUS AEROSOLS WITH A SPECTROPHONE

T. J. Truex and J. E. Anderson
Ford Motor Company, Scientific Laboratory
Dearborn, Michigan 48121

ABSTRACT

The feasibility of using light absorption as an *in situ* mass monitor for carbonaceous aerosols has been studied. The absorption measurements were made using a helium-cadmium laser with a measured output of 3 mw at 4166Å chopped at 4000 Hz to power an acoustically resonant spectrophone. Coupling of the spectrophone with a laboratory flow tube system for generating carbonaceous aerosols has produced the following results: (1) spectrophone output is proportional to carbonaceous aerosol mass concentration as independently determined by filter collection and weighing; (2) the absorption coefficient of the carbonaceous aerosols is 17 m^2/gm at 4166Å in rough agreement with previously measured values for bulk carbon and graphite samples of 1.4-15.0 m^2/gm. The spectrophone provides a means of continuous monitoring of carbonaceous aerosols and is far less time-consuming than filter collection techniques. Potential applications include real time monitoring of vehicle exhaust, laboratory combustion research studies and field measurements.

One of the unique features of carbonaceous aerosols - particularly primary emissions - is that they contain a large "graphitic" soot component which strongly absorbs light throughout the visible spectral region. Absorption of sunlight by carbonaceous aerosols can be a major influence on climate and on the radiation balance determining the temperature of the earth.[1-3] The absorption of visible light by carbonaceous particles also suggests a selective monitoring technique for carbonaceous aerosols since most inorganic aerosols are virtually transparent in the visible spectral region. We report results of a feasibility study of light absorption measurements with a spectrophone as an *in situ* mass monitor for carbonaceous aerosols.

The use of an acoustically resonant spectrophone for *in situ* measurements of visible light absorption in the atmosphere has been reported.[4] Inorganic aerosols, e.g., NaCl, are virtually transparent in the visible and are not detected.[4] NO_2 is the only common gas that absorbs strongly in the visible. It should not present a sizeable interference at atmospheric concentrations. Spectrophone measurements, with and without input gas filtering, can be used to evaluate NO_2 interferences.[4]

The spectrophone used in these experiments has been described in detail previously.[4] In this work, we substituted a helium-cadmium laser with a measured output of 3 mw at 4166Å in place of the 500 mw argon laser used previously. This substitution was made because of equipment availability, but it demonstrates that useful results can be obtained with very modest light intensities. The laser beam is chopped at 4000 Hz to power an acoustically resonant spectrophone. The spectrophone operates on the principle of detecting sound waves generated by localized time-dependent heating of the air. In the case of absorption of light by aerosols, sound generation in the spectrophone is limited by the rate at which the heat is transferred to the gas from the particles. The modulated heating of particles at 4000 Hz is efficient in generating sound for particles up to about 3μm in diameter. Therefore, the 4000 Hz spectrophone will only measure the light absorption of particles less than about 3μm in diameter.

A cylindrical brass resonant acoustic cavity, 5 cm in diameter and 12 cm long, was used in the spectrophone.[5-7] The cavity was used in its lowest order circumferential mode which had a Q near 200. The laser beam was passed through 8-mm-diameter holes in the end walls. A 2.54-cm B & K microphone with a sensitivity of 42 mV/Pa was mounted flush with the cavity wall on the opposite side. Acoustic isolation was achieved by placing the spectrophone within a heavy metal cylinder and constructing several sound barriers using Conoflex, a commercial multilayer acoustic shielding material. Normal room noise did not interfere with the measurements. A variable-speed mechanical chopper, acoustically isolated in a separate enclosure, was used to modulate the laser beam. Synchronous detection was used to measure the acoustic signal. The aerosol was introduced to the cell by a line connected to a sample inlet hole in the end of the spectrophone. The aerosol flowed out of the spectrophone through the ports used by the laser beam.

Carbonaceous aerosols were produced by burning propane in oxygen. A flow tube system, patterned after that of Novakov et al.[8], was used. The propane/oxygen combustion products were diluted with nitrogen and either passed through a 0.2-μm Fluoropore filter or alternatively diverted through a sample line directly into the spectrophone. Aerosol concentrations were varied by changing the propane and oxygen flow rates. As shown in Figure 1, spectrophone output is proportional to carbonaceous particle loading as determined by filter collection and weighing. It should be noted that the particulate loadings used in this study are roughly a factor of 100 larger than those found in ambient air. Previous work[4] on this spectrophone indicates that with minor engineering changes and a more powerful laser, detection of ambient levels of particulate should not be a problem. It is noteworthy that several hours were often required to collect weighable filter samples, whereas the time scale of the spectrophone measurement was limited by the aerosol sampling time (< 1 min).

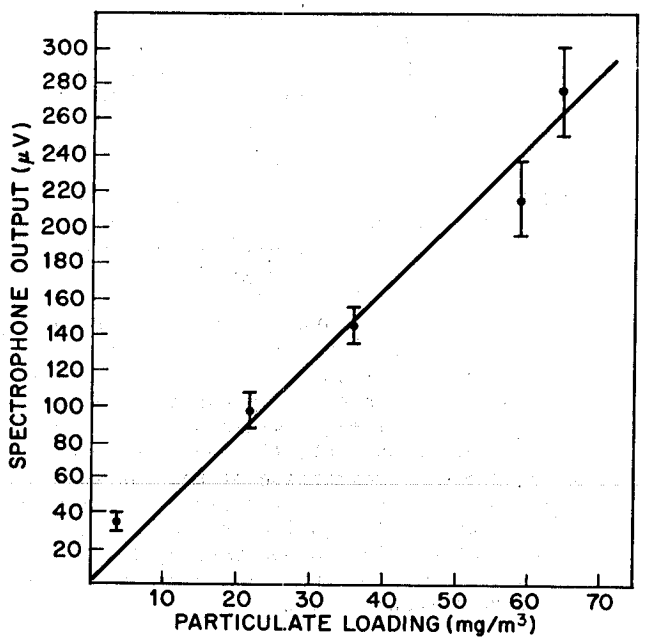

Fig. 1. Spectrophone output as a function of carbonaceous aerosol concentration. The particle concentration was determined by passing a known volume of aerosol through a 0.2-μm Fluoropore filter, where all aerosol particles were collected and subsequently weighed.

We calibrated the spectrophone output against absorption of a gaseous sample of 26 ppm NO_2 in nitrogen. Hall and Blacet[9] measured an absorption of 0.72 m^2/gm for NO_2 at 4166Å. Using these parameters, and the spectrophone output as a function of particulate loading for carbonaceous aerosols, an absorption coefficient of 17 m^2/gm was found for the carbonaceous aerosol. For purposes of comparison, Gilbert[10] and Ergun, McCartney and Walline[11] report absorption coefficients of 1.4 - 15.0 m^2/gm for various bulk coal and graphite samples at 4166Å. Medalia and Richards[12] calculate an absorption coefficient for sperical carbon black particles much smaller than the wavelength of light of 10 - 12 m^2/gm. From data presented by Vuk, et al.[13], an upper limit for the absorption coefficient of diesel particulate of $\sim$ 9 m^2/gm can be inferred. The measured spectrophone absorption coefficients are somewhat larger than these values.

It should be emphasized that the spectrophone measures the light absorption by carbonaceous particulates. Carbonaceous aerosols from different sources may differ in chemical composition, particularly in their "graphitic" to "organic" carbon ratios, and have different absorption coefficients. This point merits further study for the absorption coefficient directly influences the relationship between spectrophone output and mass loadings. At present there is no definitive

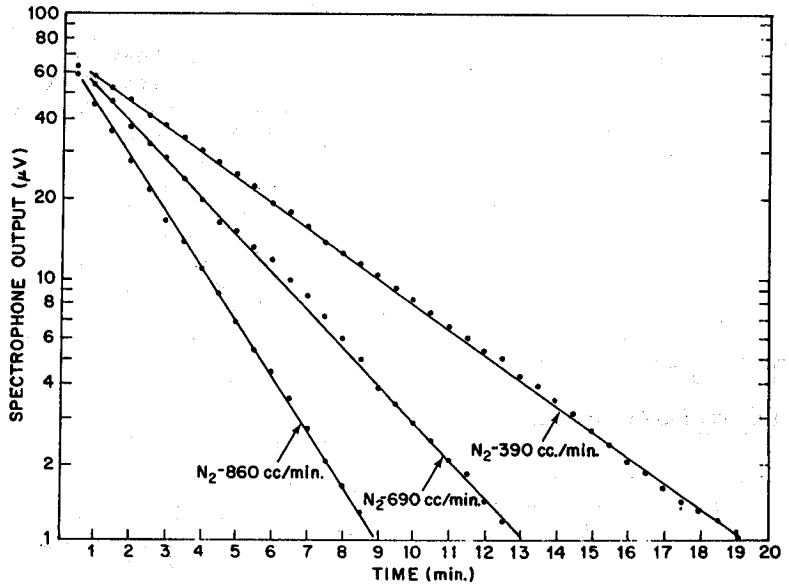

Fig. 2. Spectrophone output plotted logarithmically against time for three different aerosol dilution experiments. The initial carbonaceous particle concentrations were $\sim$ 50 mg/m^3. The nitrogen flow rates during the dilution experiments are shown on the graph.

evidence for how constant, or how variable, the absorption coefficients for carbonaceous aerosols are. Rosen, et al.[14] have presented results indicating relatively constant absorption coefficients in the visible for filter samples from a number of ambient and laboratory sources.

In a second experiment, we filled a stirred residence chamber (2-ℓ flask) with a carbonaceous aerosol. The aerosol contained in the residence chamber was then flushed into the spectrophone with pure nitrogen. Under these conditions, the aerosol concentration decays as $C(t) = C(o) \exp(-kt)$. Figure 2 shows spectrophone output plotted logarithmically against time for three different nitrogen flushing rates. The obvious first-order decay demonstrates the linearity of the system, and the expected increase in signal decay rate with increased nitrogen flow rate.

In a third set of experiments, the spectrophone was used to monitor aerosol concentrations as a function of the oxygen/propane ratio. These results, shown in Figure 3, are consistent with concurrent filter data. Spectrophone results were obtained in a few minutes, while the companion filter results required several hours per data point.

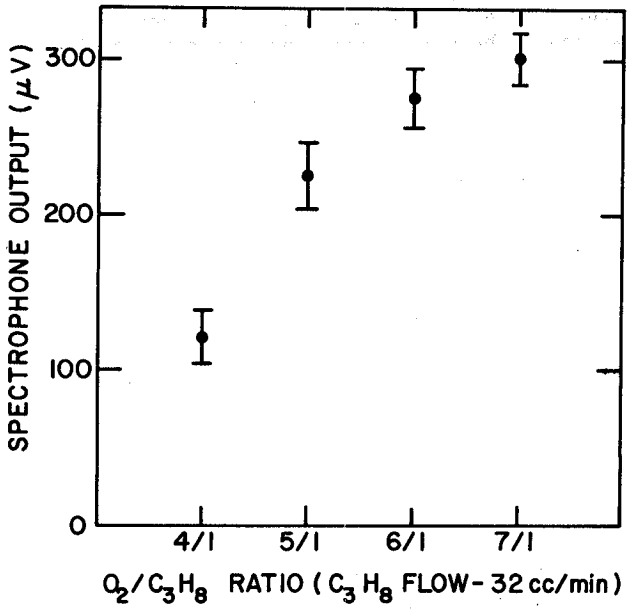

Fig. 3. Spectrophone output as a function of oxygen/propane ratio. The propane flow rate was 32 cc/min. The nitrogen flow rate in the flow tube was 9000 cc/min.

These experiments demonstrate the potential of the spectrophone in studies of carbonaceous aerosols. It provides a means of continuous monitoring and is far less time consuming than filter collection techniques. In situ monitoring of carbonaceous aerosols has potential application in (1) real time sampling of vehicle exhaust; (2) combustion research directed at understanding the formation of carbonaceous aerosols; (3) field measurements directed at the concentration of carbonaceous particles in the atmosphere, and the influence of their light absorption on the radiation balance determining the surface temperature of the earth. It should also be reaffirmed here that measurements of light absorption in the atmosphere by the spectrophone is of considerable importance in its own right. This is particularly true in assessing the visual impact of diesel particulates with increased use of this engine type and in determining the contribution of absorption to total extinction in certain urban areas.

Areas which require further experimentation include: (1) the effects of size distribution on absorption by carbonaceous aerosols (in the first approximation, the absorption by particles less than about 0.1μm in diameter would be independent of their size distribution); (2) the effects of changes in chemical composition of the carbonaceous aerosols - particularly those from different sources which may have significantly different "graphitic" to "organic" carbon ratios; (3) studies to determine if the laser beam induces changes in the atmosphere-aerosol system.[15]

ACKNOWLEDGEMENTS

We are grateful to R. W. Terhune and W. R. Pierson for illuminating discussions in the course of this work.

REFERENCES

1. J. R. Hodkinson in Aerosol Science, C. N. Davies, Ed. (Academic Press, New York, 1966) pg. 287.
2. R. A. Bryson and G. J. Dittberner, J. Atmos. Sci., 33, 2094 (1975).
3. B. M. Herman, S. R. Browning, and R. Rabinoff, J. Appl. Meteorol., 15, 1057 (1976).
4. R. W. Terhune and J. E. Anderson, Optics Letters, 1, 70 (1977).
5. C. F. Dewey, Jr., R. D. Kamm, and C. E. Hackett, Applied Phys. Lett., 23, 633 (1973).
6. P. L. Goldan and K. Goto, J. Appl. Phys., 45, 4350 (1974).
7. E. Max and L. G. Rosengren, Opt. Commun., 11, 422 (1974).
8. T. Novakov, S. G. Chang and A. B. Harker, Science, 186, 239 (1974).
9. T. C. Hall, Jr. and F. E. Blacet, J. Chem. Phys., 20, 1745 (1952).
10. L. A. Gilbert, Fuel, 41, 351 (1962).
11. S. Ergun, J. T. McCartney and R. E. Willine, Fuel, 40, 109 (1961).
12. A. I. Medalia and L. W. Richards, J. Colloid Interface Sci., 40, 233 (1972).
13. C. T. Vuk, M. A. Jones, and J. H. Johnson, SAE Paper 760131 (1976).
14. H. Rosen, A. D. A. Hansen, R. L. Dod and T. Novakov, Report LBL-6819, Lawrence Berkeley Laboratory, U. of Calif., Berkeley, CA, 8-17 (1977)
15. M. B. Baker, Atmos. Environ., 10, 241 (1976).

DETECTION AND IDENTIFICATION OF AIRBORNE CARBONACEOUS MATTER WITH A RAMAN MICROPROBE

E. S. Etz, J. J. Blaha, and G. J. Rosasco
National Measurement Laboratory
National Bureau of Standards
Washington, D. C. 20234

ABSTRACT

The laser-Raman microprobe developed at the NBS is employed in the spectroscopic characterization of carbonaceous matter associated with air pollution particulate samples. Two types of investigations are described. In the first, the new instrument is applied to the molecular analysis of single microparticles in urban air particulate samples. Of particular interest is the study of the origin and spectral behavior of two bands centered at ∿1350 and ∿1600 cm^{-1} frequently observed in the spectra of carbonaceous particles. The effects of laser irradiance conditions used in the measurement on the appearance of these bands is examined. The results of modeling experiments demonstrate that these two bands can be attributed to elemental carbon with structures similar to polycrystalline graphite. In air particulates, the source of this carbon can be either graphitic soot or residual organic matter which converts to polycrystalline graphite on exposure to high-intensity laser radiation. The second study evaluates the analytical potential of micro-Raman spectroscopy (MRS) in the trace characterization of solid organic pollutants. In these experiments, the microprobe is used to obtain vibrational Raman spectra of microsamples of polynuclear aromatic hydrocarbons (PAHs). Potential interferences arising from sample heating and sample fluorescence are examined. The PAHs are measured as single microparticles, generally of size 2-10 μm, and include representative compounds of the 3-ring (e.g., phenanthrene) and 4-ring (e.g., chrysene, pyrene, fluoranthene) systems. The Raman spectra of these organic solids are highly characteristic of crystal lattice (external) and molecular (internal) vibrations. They can therefore form a basis for the positive identification of the compounds in this class. A detection limit (with the Raman microprobe in its present state of development) of 10-100 pg is indicated for many of these environmentally significant hydrocarbons. These results demonstrate a considerable analytical potential of the MRS technique for application as a sensitive and specific method for the detection and identification of trace level PAHs separated by chromatographic procedures.

INTRODUCTION

A major portion of atmospheric particles consists of carbonaceous material which derives from both natural and anthropogenic sources. The carbonaceous material present in atmospheric particulate matter is a combination of elemental carbon (e.g., soot), inorganic (e.g., carbonates) and organic (e.g., hydrocarbon and polymeric) carbon compounds.[1] Of importance in contemporary atmospheric research is the development of analytical techniques that - quite generally - can furnish information on the molecular nature of atmospheric aerosols and in particular are capable of discerning the various forms of environmental particulate carbon. The Raman microprobe technique described here is one which allows the speciation of carbonaceous compounds when present as major constituents of single microparticles or when analyzed as trace level components (chromatographically) isolated from bulk sample collections.

The instrument employed in these studies is the Raman microprobe developed at the National Bureau of Standards.[2] It is a conventional laser-Raman spectrometer especially designed for microanalytical applications and permits the acquisition of analytical-quality Raman spectra from discrete microparticles of size 1 μm and larger or other forms of microsamples approaching 1 pg in mass.

We describe in this paper the application of the Raman microprobe to two types of study. In one we have used the instrument for the molecular characterization of single microparticles in urban air particulate samples[3,4] and are emphasizing in this discussion the characterization of the residual carbonaceous material frequently found associated with ambient air particulates.[5] Of particular interest in this study is the identification of the origin of two broad bands at ∿1350 and ∿1600 cm^{-1} which are generally observed in the spectra of carbon-bearing particles in addition to the spectral features which can be assigned to the principal component(s) of the particle. These two bands are the most well known bands in the Raman spectrum of carbons and can be used to characterize carbon structures of all

types.[6] We have studied the spectral behavior of these bands as a function of the laser irradiance (power/unit area) employed in the microprobe measurement. This was to examine their sensitivity to changes in the structural order of the carbon as a result of heating brought on by absorption of the laser radiation. By way of modeling experiments we show that these features can be ascribed to the presence of elemental carbon in a form analogous to polycrystalline graphite.[5-10] Our results are in agreement with recent Raman studies performed on bulk sample collections of airborne particulates which find carbon as a major constituent present in the form of graphitic soot.[11,12] We further show that these bands can result from the laser-induced decomposition of hydrocarbon matter adsorbed on the surfaces of particles.

The second study reported here presents the results of feasibility experiments performed to evaluate the analytical potential of micro-Raman spectroscopy (MRS) in the trace characterization of solid organic pollutants. In these preliminary investigations, the Raman microprobe has been used to obtain the Raman spectra of microsamples of selected polynuclear aromatic hydrocarbons (PAHs). A major aim of this ongoing research is an assessment of the viability of the MRS technique for use as a sensitive and specific detection method for the identification of PAH components in fractions separated by liquid chromatography procedures. The development of liquid chromatograph-Raman spectrometer interface systems has been suggested as a further advance over contemporary analytical chromatography systems.[13]

The polynuclear aromatic hydrocarbons represent a significant component of the carbonaceous material in atmospheric aerosols. Organic fractions of airborne particulate matter have been found to contain over 100 different PAH compounds.[14] The major sources of these compounds are from fossil fuel combustion and other high-temperature processings of organic materials. The predominant fraction (approximately 70-90 percent) of the total PAH content of airborne particulates is known to be associated with particles in the respirable size range of less than 5 μm.[15] In this size fraction of the aerosol, the PAH compounds are generally thought of as being adsorbed onto inorganic-core microparticles. We have not, to this point, detected and identified these compounds - presumed to be present as surface layers (or films) - in any of our measurements on single microparticles collected from the ambient air. Our Raman microprobe measurements have, however, furnished indirect evidence for the existence of thin films of organic matter on the surfaces of inorganic microparticles, - observations which are alluded to in the discussion of the origin of the "graphitic carbon" bands observed in the spectra.

We have investigated the PAH compounds by the method described here because increasingly sophisticated measurement techniques are required for the assessment of environmental pollution by trace level organics. In the trace analysis of major PAHs - many of which are either known or suspected potent carcinogens - a fair number of techniques are employed for the analysis of these compounds in complex environmental samples.[16] Of the contemporary techniques for the analysis of trace levels of PAHs, high-performance liquid chromatography (HPLC) with combined UV absorption/fluorescence emission detection is probably the most widely used and successful method.[16-18] While fluorescence detection of HPLC-separated fractions of PAHs routinely achieves high sensitivity and good selectivity, there remains a continuing demand for both increased sensitivity and increased selectivity in the determination and measurement of polycyclic organic matter.

In earlier published work[2-5] the capability of performing (qualitative) Raman spectroscopic analysis of discrete microsamples has been demonstrated. In these studies, a principal area of application of the Raman microprobe has been the chemical identification of airborne particles. It was shown that this new technique of microprobe analysis can obtain information on the molecular composition of microsamples which heretofore have yielded only to elemental analysis. The spectra obtained with the Raman microprobe are - for analytical purposes - in one to one correspondence with those reported for macroscopic samples of the same materials. In most cases, the spectra obtained from individual microparticles are relatively simple and easily interpreted.

THE MICRO-RAMAN TECHNIQUE

Detection and measurement in the Raman microprobe are based on the observation of the normal or spontaneous Raman effect. This effect provides the basis for Raman spectroscopy and has been reviewed in the context of modern chemical analysis.[19,20] In the Raman measurement, a beam of monochromatic, visible laser light is focused on the sample. The radiation scattered by the sample contains weak lines, at frequencies both lower and higher than the exciting radiation. The frequency differences, called Raman shifts,

are characteristic of the sample and are independent of the exciting frequency. The spectra obtained with the Raman microprobe are so-called Stokes-Raman spectra. They arise from molecules which scatter photons of lower frequency (Stokes lines) than that of the exciting line. The Raman pattern they represent provides a molecular fingerprint for identification and characterization. The spectrum is usually excited in a region where the sample does not absorb. Appreciable absorption of the exciting radiation generally leads to sample heating, frequently attended by sample modification or destruction. In microprobe measurements, such problems can be particularly severe because of the high irradiances (power/unit area) that must be employed to excite analytically useful spectra. A major potential limitation in all Raman work is sample fluorescence which may totally swamp the Raman effect. With a choice of laser frequencies, problems of radiation absorption and sample fluorescence can often be minimized, if not virtually eliminated. Thus, it is often possible to select such an excitation frequency that color of a sample is not a limiting factor.

Identification and characterization of molecular species present as major components of microsamples are made by qualitative comparison with reference spectra. If these are not available in the literature from measurements on bulk samples, the information is obtained from microprobe measurements of well-characterized materials.

EXPERIMENTAL PROCEDURES

The Raman Microprobe

Details on the design and construction of the NBS laser-Raman microprobe have been presented in earlier published work.[2-4] The instrument is a monochannel spectrometer, schematically depicted in Fig. 1. For excitation of the Raman spectrum, the light from an argon/krypton ion laser is focused to a small (typically 2-20 μm) spot on the sample. Nonlasing plasma lines are removed through the use of a predispersing prism. The light scattered by the sample is collected by an ellipsoidal mirror in a 180° backscattering geometry and transferred into a double monochromator equipped with concave holographic gratings. The signal is detected by a thermoelectrically cooled photomultiplier tube and processed by photon counting electronics. The sample is supported by a substrate (typically sapphire or lithium fluoride) mounted on a remotely-controlled sample stage. A built-in microscope allows viewing of the sample in transmitted light at magnifications up to 400 X. Irradiance levels

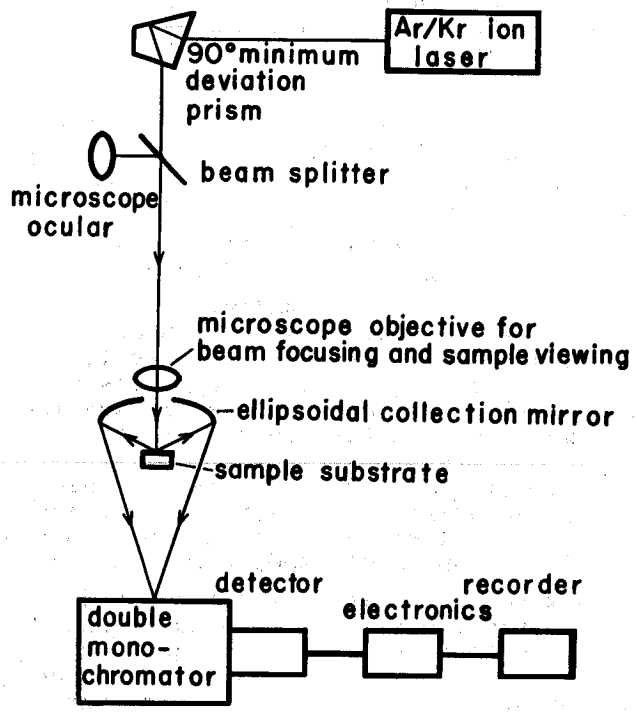

Fig. 1. Schematic of the NBS-developed Laser-Raman Microprobe. Typical measurement parameters employed: Excitation, 514.5 nm (green), 568.2 nm (yellow) and 647.1 nm (red); laser power, 5-60 mW (at sample); beam spot, 2-20 μm diameter, time constant, 0.2-4.0 sec; scan rate, 200-10 cm^{-1}/min; spectral slit width, 3 cm^{-1}.

employed in routine probe measurements range from several megawatts/cm^2 to several kilowatts/cm^2. Measurement times for solid microsamples of mass 10-100 pg may vary from 20 minutes for (fast) survey spectra to scans requiring 3-5 hours for radiation-sensitive materials.

Samples and Their Measurement

For measurement in the Raman microprobe, the microsamples are usually supported by either a sapphire (α-Al_2O_3) or a lithium fluoride (LiF) substrate. Various methods of sample preparation used with this technique have been described.[2-4] Airborne particles are collected by conventional aerosol sampling techniques, in this work consisting primarily of bulk sample collections on various types of filters and size-classified particle collections obtained through the use of multi-stage cascade impaction samplers.

The Raman microprobe spectra obtained in the study of carbonaceous matter on microparticles were all obtained using

514.5 nm (green line) excitation. Of concern in all microprobe measurements of non-transparent (i.e., colored) materials are the possible deleterious effects of the high irradiance levels which can be utilized in the measurement. In order to assess such effects in the present study, the probe measurements were performed employing low irradiance conditions (typically ∿5 kW/cm^2) at first and then repeated using higher irradiance conditions (typically ∿0.5 MW/cm^2). The spectra are compared and any changes that might have occurred in the physical, morphological or optical properties of the particle are noted by re-examination of the sample in the light microscope.

The modeling experiments designed to study the origin of carbon bands in the spectra involved the preparation of microparticle samples of $CaSO_4$ prepared from a commercial sample of soluble anhydrite. In one experiment, a sample was flash coated with a thin film (∿20 nm thick) of elemental carbon in a vacuum deposition apparatus. For the second experiment, two separate samples of soluble anhydrite microparticles were prepared to bear a surface film of n-hexadecane in one case and a film of shale oil (a hydrocarbon mixture rich in optically absorbing polynuclear aromatic hydrocarbons) in the second case. The details of these sample preparations have been described.[5]

For the study of microparticle samples of polynuclear aromatic hydrocarbons, representative compounds of the 3-ring (e.g., anthracene, phenanthrene), 4-ring (e.g., chrysene, pyrene, fluoranthene) and 5-ring (e.g., benzo[a]pyrene) systems were chosen. The samples investigated were prepared from commercially available PAH standards obtained from several sources and used without further purification. The spectrum of each compound was examined employing green line (514.5 nm), yellow line (568.2 nm) and red line (647.1 nm) excitation. This was to specifically examine effects of sample heating and sample fluorescence. In all cases it has been possible to record analytically useful (with a signal-to-background ratio for the major Raman peaks generally better than 10:1) spectra from discrete PAH microcrystals generally of size 2-10 μm, corresponding to sample masses estimated at well under 1 ng.

RESULTS AND DISCUSSION

Characterization of Carbonaceous Particles

In earlier studies of microparticles from urban air particulate samples, we demonstrated detection and identification of a wide range of inorganic materials, and mineral species in particular.[2-4] The results included evidence for chemical transformation of particles in cases where high-volume, bulk sample collections were made over extended sampling times.[4] An example of the spectroscopic evidence for such a finding is presented in Fig. 2. The particle investigated here was one isolated from a bulk sample of St. Louis urban dust, which had been collected on a glass fiber filter employing a high-volume air sampler. The particle is identified as one of complex composition with the major constituent being calcite ($CaCO_3$) and the minor constituent being insoluble anhydrite ($CaSO_4$). All five Raman active modes of $CaCO_3$ (1432, 1088,

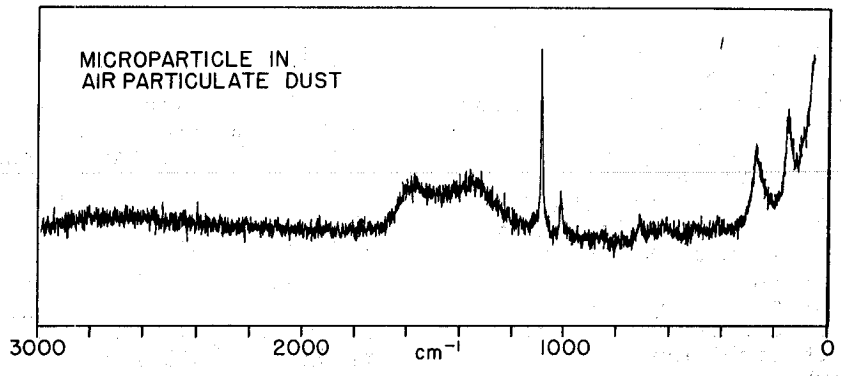

Fig. 2. Raman Spectrum of a Particle of Calcite ($CaCO_3$) in Urban Air Particulate Dust. Measurement parameters: particle size, 5 x 5 μm; substrate, LiF; laser, λ_0 = 514.5 nm; power, 48 mW (at sample); beam spot, ∿12 μm diameter; spectral slit width, 3 cm^{-1}; time constant, 0.5 sec; scan rate, 100 cm^{-1}/min; intensity, 1000 counts full scale.

714, 283, and 156 cm^{-1}) are present. The 1432 cm^{-1} band is partially obscured by the broad spectral feature in the 1200 to 1700 cm^{-1} region. The presence of $CaSO_4$ as a detected, second constituent is indicated primarily by the band at 1018 cm^{-1}. The presence of $CaSO_4$ in the particle has been interpreted to indicate the partial transformation of $CaCO_3$ by acid aerosol.[4] After accounting for both constituents, calcite and anhydrite, there remains to be assigned the rather broad, double-maximum feature centered at ∿1350 and ∿1600 cm^{-1}. Bands similar to these have been observed in the spectra of many different types of environmental particles (e.g., sulfates, oxides, nitrates, and silicates). These features have been ascribed to polycrystalline graphite[6-10] and are in agreement with recent Raman studies of bulk samples of pollution particulates which find evidence for carbon present as graphitic soot.[11,12]

We proceeded to verify that the observed spectral features were indeed attributable to a form of elemental carbon and also designed experiments to explore the possibility that these carbon bands could result from the decomposition - in the measurement process - of particle-adsorbed hydrocarbons.

Thus, two separate studies were performed. The first consisting of spectroscopic measurements on elemental carbon vacuum deposited on a particle sample of soluble anhydrite. The second type of modeling experiment involving parallel samples of the same material treated to result in microparticles coated with two types of hydrocarbon liquids. Soluble anhydrite was chosen as the host since it has a high surface area and at elevated temperatures will convert to the insoluble form, allowing some estimate of heating effects. It is known that temperature-induced conversion of soluble anhydrite to insoluble anhydrite occurs gradually, with the conversion being quite rapid above 400 °C and very slow below 200 °C. The two forms are distinguishable by their Raman spectra.[5]

In the first modeling experiment, a particle sample of soluble anhydrite was coated with an approximately 20 nm thick layer of vitreous carbon, deposited by flash evaporation in a vacuum chamber. Particles in this sample and in a parallel sample not overcoated with carbon were measured in the microprobe. Figure 3 shows the results of these measurements. The top spectrum is that of a particle not bearing a carbon film. Bands arising from

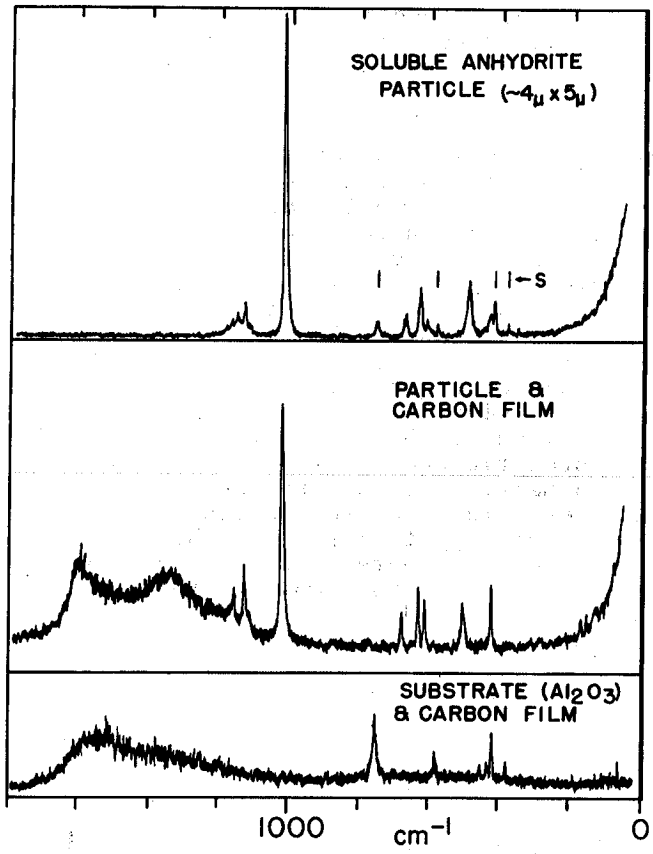

Fig. 3. Raman Spectra of Soluble Anhydrite ($CaSO_4$) Coated with a Vitreous Carbon Film. Top: not-coated particle, 4 x 5 μm; substrate, Al_2O_3; laser, λ_0 = 514.5 nm; power, ∿90 mW (at sample); beam spot, ∿6 μm diameter; spectral slit width, 3 cm^{-1}; time constant, 0.3 sec; scan rate, 200 cm^{-1}/min; intensity, 1000 counts full scale. Middle: vitreous carbon coated particle, 4 x 5 μm; same conditions as for top spectrum. Bottom: carbon film on substrate; same conditions as for top.

the (weak) interference by the sapphire substrate are indicated above the recording trace. The middle spectrum was observed from a particle of the carbon coated sample measured under high irradiance conditions. This spectrum is now that characteristic of $CaSO_4$ in the insoluble anhydrite form. In addition, the spectral features at ∿1350 and ∿1600 cm^{-1} are apparent. Heating of the particle to temperatures above 300 °C has taken place as indicated by the change from the soluble to the insoluble anhydrite form. The two distinct carbon bands have developed as a consequence of sample heating. This can be seen by comparing the carbon bands in the middle spectrum to the single, broad band characteristic of vitreous carbon, as obtained

from the measurement of the carbon film on the sapphire substrate (bottom spectrum).

We conclude that heating of the coated $CaSO_4$ sample has taken place and that the heating induced by the optical absorption of the vitreous carbon film has resulted in the formation of microcrystalline graphite. The film on the substrate is not expected to experience a large temperature rise inasmuch as the substrate with which it is in contact is an effective heat sink.

The second modeling experiment was concerned with the possibility that these carbon bands might arise from the thermal or photolytic decomposition of hydrocarbon matter sorbed onto particle surfaces. In order to examine this possibility, particles of soluble anhydrite were coated with n-hexadecane and shale oil in two separate tests. The results obtained from measurements of these samples are shown in Fig. 4. Figures 4A and 4C, respectively, show the reference spectra of soluble and insoluble anhydrite. Figure 4D is the spectrum of soluble anhydrite coated with a film of shale oil. The spectrum has changed to that of insoluble anhydrite even under the lowest irradiance conditions. The two carbon features have also been produced. Figure 4B is the spectrum of soluble anhydrite coated with n-hexadecane. In contrast to the corresponding sample coated with shale oil, this sample did not convert to the insoluble form even though the two carbon bands have been produced. These bands are exceptionally well resolved here. The complete spectral separation of the carbon bands has been reported for samples where the size of microcrystallites is greater than 5 nm.[7] The broader overlapped features are observed from samples with structures

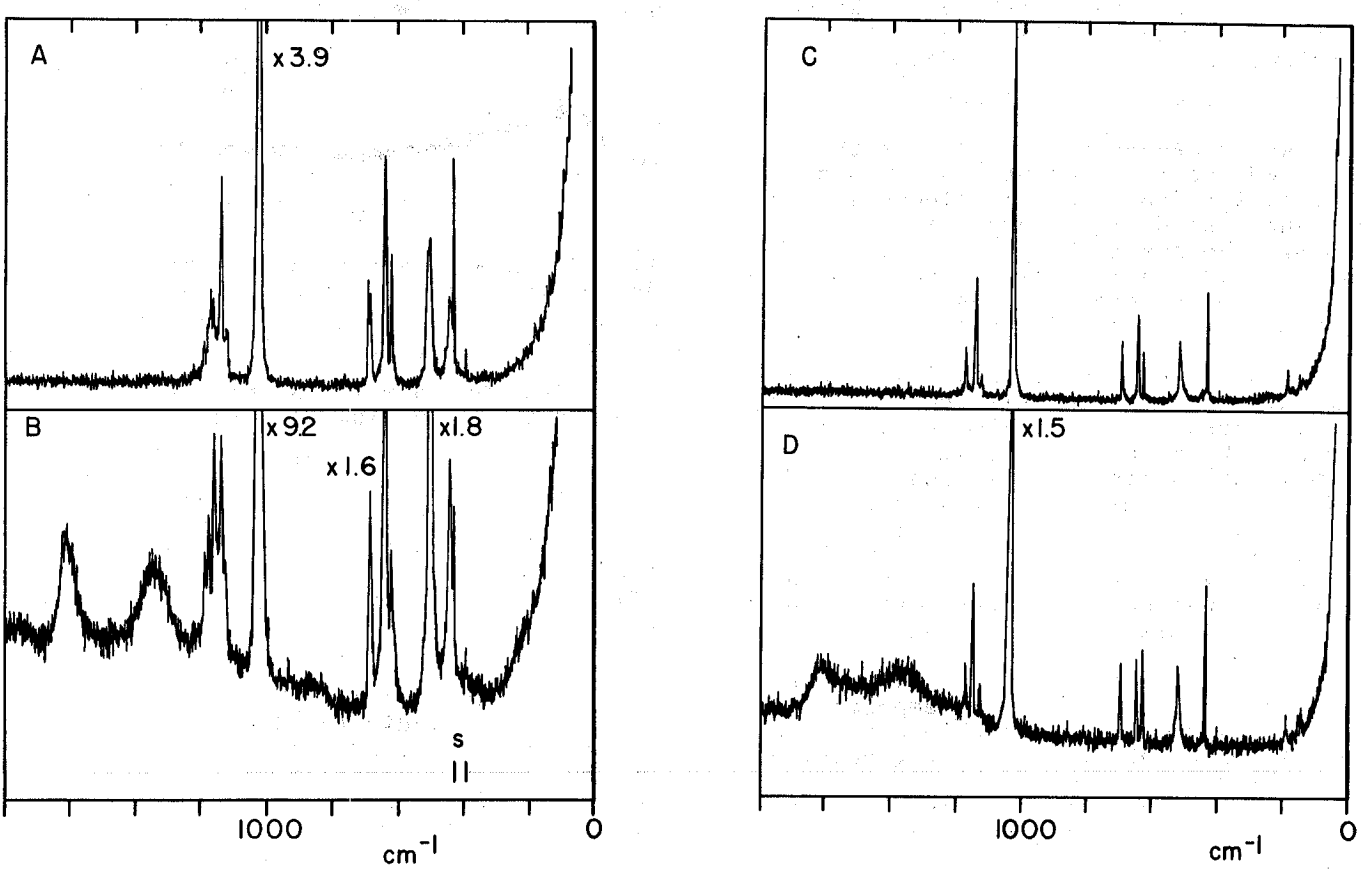

Fig. 4. Raman Spectra of $CaSO_4$ Particles Coated with Hydrocarbon Liquids. A. Soluble anhydrite particle (not coated), 6 x 16 μm; substrate, Al_2O_3; laser, λ_0 = 514.5 nm; power, 90 mW (at sample); beam spot, ∿6 μm diameter; spectral slit width, 3 cm^{-1}; time constant, 0.5 sec; scan rate, 100 cm^{-1}/min; intensity, 1000 counts full scale. B. Soluble anhydrite particle coated with n-hexadecane, 8 x 12 μm; same conditions as for A, except: time constant, 1.0 sec; scan rate, 50 cm^{-1}/min. C. Insoluble anhydrite particle (not coated), 3 x 5 μm; same conditions as for A, except: time constant, 0.3 sec; scan rate, 50 cm^{-1}/min. D. Soluble anhydrite particle coated with shale oil, 3 x 7 μm; same conditions as for B.

made up of smaller microcrystallites. Continued exposure of this sample to laser irradiation brought on a partial conversion to insoluble anhydrite over an 8-hour period. This conversion probably arises from the heating of the particle as a result of the formation of the optically absorbing carbon film.

We have demonstrated in these studies that the two broad features at ∿1350 and ∿1600 cm^{-1} - so frequently observed in the spectra of airborne particles - are indeed attributable to elemental carbon present in a form analogous to polycrystalline graphite. This carbon can be traced either to graphitic soot or to residual organic matter which can be converted to graphitic soot on exposure to high intensity laser radiation. The examples discussed here also illustrate that certain chemical and/or structural transformations - as reflected in the resulting spectroscopic changes - can be induced in microparticles as they are subjected to the conditions of the microprobe measurement. This, in many cases, calls for a circumspect analysis procedure both in the acquisition and interpretation of Raman microprobe spectra.

Spectra of Microparticles of PAHs

In this section are reported partial, representative results from the feasibility study on the potential of micro-Raman spectroscopy in the trace characterization of polynuclear aromatic hydrocarbons.[21]

Figures 5-8 show the Raman spectra of microparticles of four PAHs representative of the four- and three-membered ring systems. The spectra of these organic solids are highly characteristic of crystal lattice (external) and molecular (internal) vibrations.[22] They can therefore form a basis for the positive identification of the compounds in this class. In these measurements of microsamples of selected PAHs, a detection limit - with the Raman microprobe in its present state of instrumental configuration - of 10-100 pg is indicated for many of these environmentally significant hydrocarbons. The spectra presented in Figs. 5-7 are those of three structurally very similar PAHs in the four-ring system. These are chrysene, and the isomeric pair pyrene and fluoranthene. Their molecular structures are shown in each figure. The microparticle spectrum of chrysene is that given in Fig. 5. This example is exceptional in that a useful spectrum could be obtained of this PAH using green line excitation. In the case of all other compounds studied, 514.5 nm excitation furnished spectra that were characterized by moderate to high background luminescence levels thought to arise from broad-band fluorescence of the sample. The fluorescence emission in these cases can be so pronounced as to completely swamp the Raman signal. Sample heating was not observed in these low-irradiance measurements of chrysene microparticles and is not indicated in the spectrum. Excitation with 568.2 nm (yellow line) radiation results in chrysene spectra that have appreciably lower background levels, indicating diminished fluorescence emission at this longer wavelength. This has been a general observation made for all the PAHs investigated to this point. In the spectrum of Fig. 5, spectral interferences from the weak Raman scattering

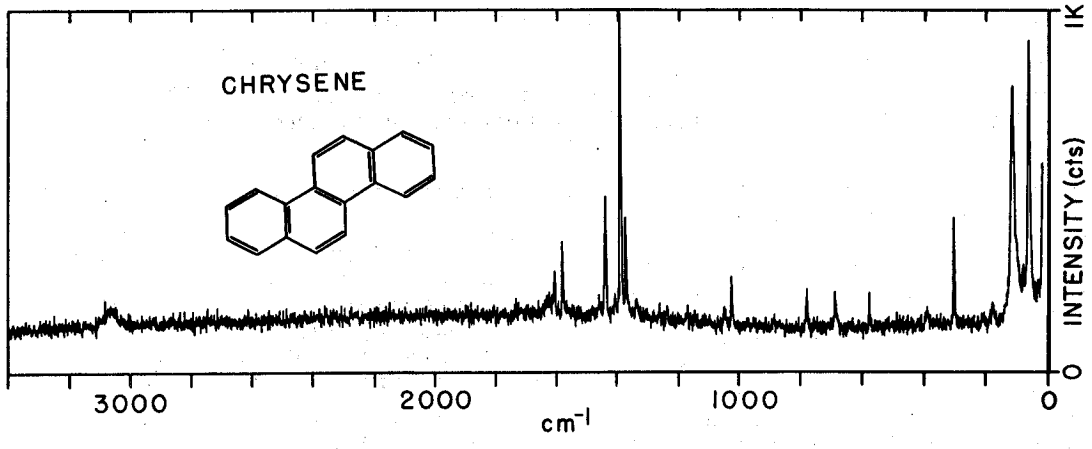

Fig. 5. Raman Spectrum of a Microparticle of Chrysene ($C_{18}H_{12}$). Measurement parameters: particle size, 7 x 9 μm; substrate, Al_2O_3; laser, λ_0 = 514.5 nm; power, 5 mW (at sample); beam spot, ∿18 μm diameter; spectral slit width, 3 cm^{-1}; time constant, 0.25 sec; scan rate, 200 cm^{-1}/min; intensity, 1000 counts full scale.

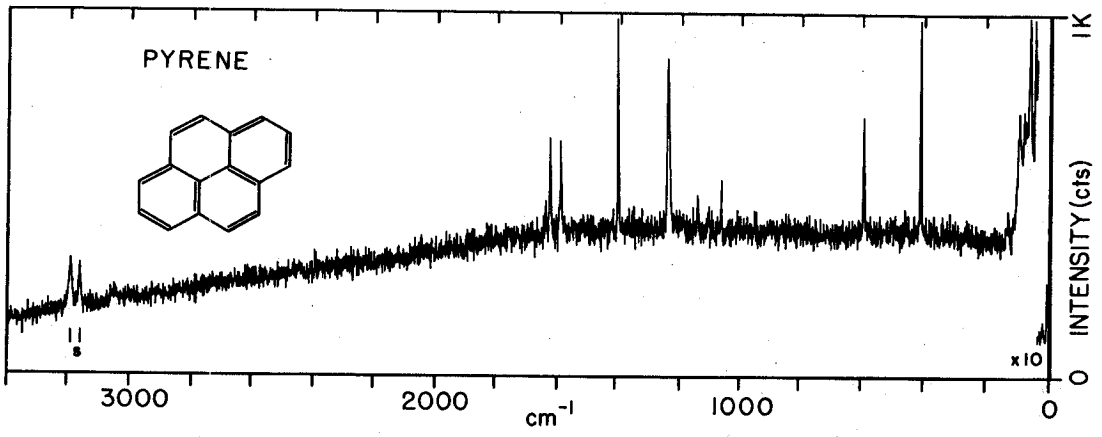

Fig. 6. Raman Spectrum of a Microparticle of Pyrene ($C_{16}H_{10}$). Measurement parameters: particle size, 30 μm; substrate, Al_2O_3; laser, λ_0 = 568.2 nm; power, 4 mW (at sample); beam spot, ∿18 μm diameter; spectral slit width, 3 cm^{-1}; time constant, 0.2 sec; scan rate, 200 cm^{-1}/min; intensity, 1000 counts full scale. Bands marked S arise from the fluorescence of the substrate.

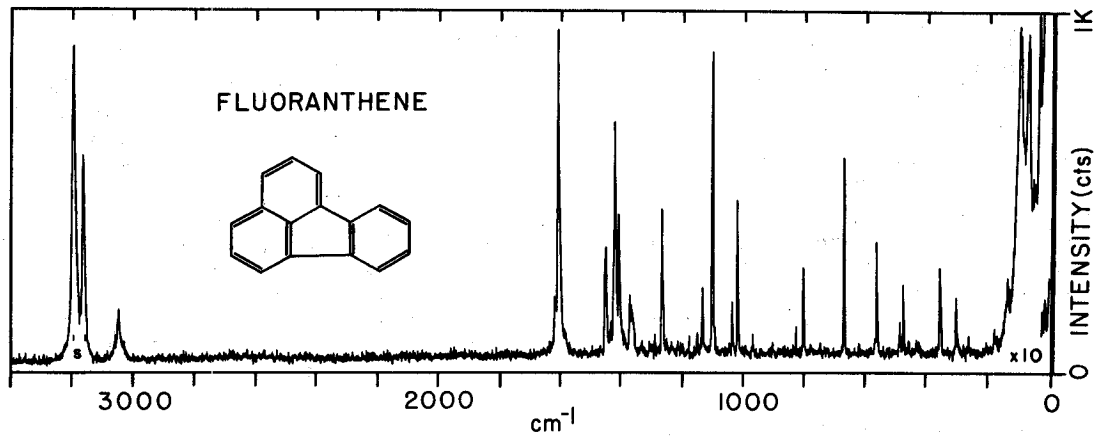

Fig. 7. Raman Spectrum of a Microparticle of Fluoranthene ($C_{16}H_{10}$). Measurement parameters: particle size, 7 x 9 μm; substrate, Al_2O_3; laser, λ_0 = 568.2 nm; power, 5 mW (at sample); beam spot, ∿18 μm diameter; spectral slit width, 3 cm^{-1}; time constant, 0.2 sec; scan rate, 200 cm^{-1}/min; intensity, 1000 counts full scale. Bands marked S arise from the fluorescence of the substrate.

of the sapphire substrate are not observed above the background luminescence level.

The spectrum of a microcrystal of pyrene, shown in Fig. 6, was excited with the 568.2 nm laser line. Attempts to obtain spectra from microsamples of this compound employing 514.5 nm excitation were unsuccessful due to the overwhelming fluorescence emission from the sample. The spectrum obtained here at rather low irradiance has a tolerable fluorescence background upon which the major Raman bands appear with good intensity. The Raman spectrum and vibrational assignments of pyrene have been reported in the literature, based on a study of single crystal samples.[23] The microprobe spectra obtained in this study are consistent with the results of these bulk Raman measurements. The doublet at the high frequency end (i.e., at higher wavenumber shifts) is not attributed to the spectrum of pyrene but arises from the ruby (Cr_2O_3, present as a trace impurity) fluorescence in sapphire. This fluorescence doublet (R lines) appears at wavenumber shifts 3167 cm^{-1} (R2 line, 692.9 nm) and 3196 cm^{-1} (R1 line, 694.3 nm) with 568.2 nm spectral excitation.

Subnanogram microsamples of fluoranthene have been examined in the microprobe, and the spectrum of a microparticle excited with 568.2 nm radiation is shown in Fig. 7. Whereas 514.5 nm excitation stimulated enormous fluorescence emission from this PAH, good spectra could be obtained with both yellow line and red line excitation. The compound is characterized by a larger number of bands of good intensity than has been observed for the two other four-ring compounds. The sapphire fluorescence doublet is pronounced in this measurement and is seen in the 3100-3250 cm^{-1} region. A qualitative comparison of the spectra (Figs. 5-7) of the three structurally similar PAHs shows that these are sufficiently different to allow unequivocal identification of these closely related molecular solids. Microprobe measurements on selected isomeric compounds of the five-ring system (e.g., benzo[a]pyrene, perylene) indicate a similarly high specificity of the Raman spectrum.

Three-membered ring compounds have been investigated along with several of their mono-methyl derivatives (e.g., 1-methyl and 2-methyl phenanthrene). Here the interest is to characterize spectral differences among the (unsubstituted) parent compound and its various methyl derivatives. The results indicate that within a given series of mono- (or di-) substituted PAHs, the various derivatives can be distinguished on the basis of the characteristic Raman shifts of the predominant, strong bands. An example from this series of measurements is the spectrum of a microparticle of phenanthrene presented in Fig. 8. The particle is supported by a lithium fluoride substrate which does not give rise to any spectral interferences. Red line excitation has been used. The standard sapphire substrate is much less suitable for measurements employing 647.1 nm excitation since the R-lines of the trace Cr^{3+} fluorescence appear at shifts 1021 and 1050 cm^{-1} and thereby represent a serious interference in a diagnostic region of the spectrum. With 647.1 nm excitation, Raman spectra can be recorded with the microprobe from near the exciting line to about 2700 cm^{-1} (wavenumber shift). This corresponds to the upper frequency limit (which is 12,750 cm^{-1} absolute or 784 nm in wavelength) of the spectral range of the monochromator with the gratings presently in the instrument. Thus, the CH stretching vibrations for these compounds - whose frequencies fall in the range 3000-3100 cm^{-1} - are not accessible with the present instrument when red line excitation is employed.

The phenanthrene spectrum in Fig. 8 is consistent with the results of bulk-Raman measurements performed on single crystal samples of phenanthrene.[24] The more predominant internal vibrational modes give rise to bands with Raman shifts at 410, 713, and 1443 cm^{-1}. By comparison, the most intense bands in the spectrum of the structural isomer anthracene appear at 396, 748, and 1403 cm^{-1}.[22]

We have shown with these examples that the micro-Raman spectroscopy technique can furnish analytically useful

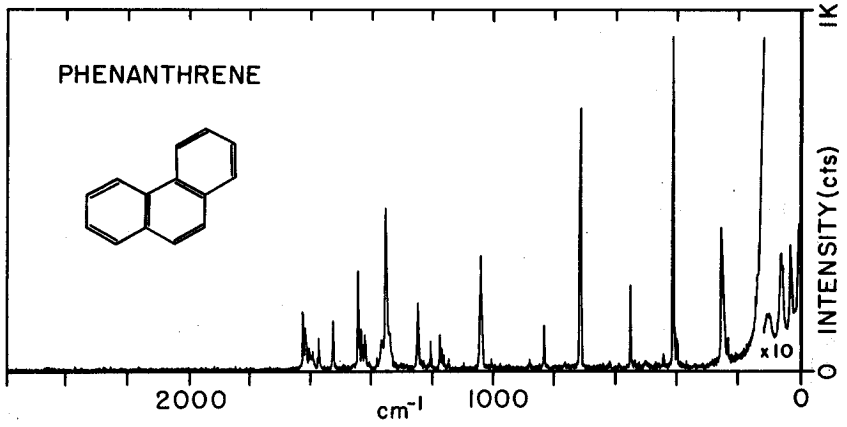

Fig. 8. Raman Spectrum of a Microparticle of Phenanthrene ($C_{14}H_{10}$). Measurement parameters: particle size, 7 x 7 μm; substrate, LiF; laser, λ_0 = 647.1 nm; power, 20 mW (at sample); beam spot, ∿16 μm diameter; spectral slit width, 3 cm^{-1}; time constant, 1.0 sec; scan rate, 50 cm^{-1}/min; intensity, 1000 counts full scale.

vibrational spectra from microsamples of PAHs of interest in environmental pollution studies. The results indicate that this new technique of (qualitative) microanalysis may potentially be applied as a post-column detection method in the identification of trace organics isolated by column chromatography. The technique appears to be especially suited as a sensitive and highly specific method of detection for liquid chromatography separations of many classes of organic compounds.

These initial studies on the characterization by micro-Raman spectroscopy of PAHs are continued. The scarcity in the literature of Raman data on PAHs makes necessary the acquisition of a library of reference spectra. Work has been initiated on the characterization of multicomponent synthetic mixtures separated by high-performance liquid chromatography. Procedures are being developed that will allow the analysis of the chromatographic effluent in a static mode whereby a portion of the effluent is trapped and the solid analyte is isolated on the Raman substrate for spectroscopic measurement.

REFERENCES

1. B. R. Appel, P. Colodny, and J. J. Wesolowski, "Analysis of Carbonaceous Materials in Southern California Atmospheric Aerosols," Environ. Sci. Technol. 10, 359 (1976).

2. G. J. Rosasco and E. S. Etz, "The Raman Microprobe: A New Analytical Tool," Research & Development 28, p. 20 (June 1977).

3. E. S. Etz, G. J. Rosasco, and W. C. Cunningham, "The Chemical Identification of Airborne Particles by Laser Raman Spectroscopy," in Environmental Analysis (G. W. Ewing, Ed.), Academic Press, Inc., New York (1977), pp. 295-340.

4. E. S. Etz, G. J. Rosasco, and J. J. Blaha, "Observation of the Raman Effect from Small, Single Particles: Its Use in the Chemical Identification of Airborne Particulates," in Environmental Pollutants: Detection and Measurement (T. Y. Toribara, J. R. Coleman, B. E. Dahneke, and I. Feldman, Eds.), Plenum Publishing Corporation, New York (1978), pp. 413-456.

5. J. J. Blaha, G. J. Rosasco, and E. S. Etz, "Raman Microprobe Characterization of Residual Carbonaceous Material Associated with Urban Airborne Particulates," Appl. Spectrosc. 32, 292 (1978).

6. R. Vidano and D. B. Fischbach, "New Lines in the Raman Spectra of Carbons and Graphite," J. Am. Ceramic Soc. 61, 13 (1978).

7. F. Tuinstra and J. L. Koenig, "Raman Spectrum of Graphite," J. Chem. Phys. 53, 1126 (1970).

8. S. A. Solin and R. J. Kobliska, "Raman Scattering from Carbon Microcrystallites and Amorphous Carbon," in Amorphous and Liquid Semiconductors, Vol. 2 (J. Stuke and W. Brenig, Eds.), Taylor & Francis Ltd., London (1974), pp. 1251-1258.

9. R. A. Friedel and G. L. Carlson, "Difficult Carbonaceous Materials and their Infrared and Raman Spectra. Reassignments for Coal Spectra," Fuel 51, 194 (1972).

10. M. Nakamizo, R. Kammereck, and P. L. Walker, Jr., "Laser Raman Studies on Carbons," Carbon 12, 259 (1974).

11. H. Rosen and T. Novakov, "Raman Scattering and the Characterization of Atmospheric Aerosol Particles," Nature 266, 708 (1977).

12. H. Rosen and T. Novakov, "Identification of Primary Particulate Carbon and Sulfate Species by Raman Spectroscopy," Atmos. Environ. 12, 923 (1978).

13. R. P. W. Scott, "Highlights from Contemporary Analytical Liquid Chromatography," Analyst 103, 37 (1978).

14. R. C. Lao, R. S. Thomas, H. Oja, and L. Dubois, "Application of a Gas Chromatograph-Mass Spectrometer-Data Processor Combination to the Analysis of the Polycyclic Aromatic Hydrocarbon Content of Airborne Pollutants," Anal. Chem. 45, 908 (1973).

15. R. C. Pierce and M. Katz, "Determination of Atmospheric Isomeric Polycyclic Arenes by Thin-Layer Chromatography and Fluorescence Spectrophotometry," Anal. Chem. 47, 1743 (1975).

16. H. S. Hertz, W. E. May, S. A. Wise, and S. E. Chesler, "Trace Organic Analysis," Anal. Chem. 50, 428A (1978).

17. B. S. Das and G. H. Thomas, "Fluorescence Detection in High Performance Liquid Chromatographic Determination of Polycyclic Aromatic Hydrocarbons," Anal. Chem. 50, 967 (1978).

18. M. Katz, T. Sakuma, and A. Ho, "Chromatographic and Spectral Analysis of Polynuclear Aromatic Hydrocarbons-Quantitative Distribution in Air of Ontario Cities," Environ. Sci. Technol. 12, 909 (1978).

19. D. E. Irish and H. Chen, "The Application of Raman Spectroscopy to Chemical Analysis," Appl. Spectrosc. 25, 1 (1971).

20. A. C. Eckbreth, P. A. Bonczyk, and J. F. Verdieck, "Laser Raman and Fluorescence Techniques for Practical Combustion Diagnostics," Appl. Spectrosc. Revs. 13, 15-164 (1978).

21. E. S. Etz, S. A. Wise, and K. F. J. Heinrich, paper presented at the 9th Materials Research Symposium, Trace Organic Analysis: A New Frontier in Analytical Chemistry, National Bureau of Standards, Gaithersburg, Md., April 10-13, 1978. To appear in the proceedings of the symposium.

22. F. R. Dollish, W. G. Fateley, and F. F. Bentley, Characteristic Raman Frequencies of Organic Compounds, John Wiley & Sons, New York (1974).

23. A. Bree, R. A. Kydd, T. N. Misra, and V. V. B. Vilkos, "The Fundamental Frequencies of Pyrene and Pyrene-d_{10}," Spectrochim. Acta 27A, 2315 (1971).

24. A. Bree, F. G. Solven, and V. V. B. Vilkos, "A Vibrational Analysis for Phenanthrene," J. Mol. Spectrosc. 44, 298 (1972).

THE DETERMINATION, SPECIATION, AND BEHAVIOR OF PARTICULATE CARBON*

Edward S. Macias, Richard Delumyea, Lih-Ching Chu, Howard R. Appleman,
C. David Radcliffe and Laurel Staley
Department of Chemistry
Washington University
St. Louis, MO 63130

ABSTRACT

Two compatible methods for carbon analysis of atmospheric fine particles are presented. The amount of soot (as elemental carbon) is determined from the reflectance of an aerosol filter sample. The sample is then analysed by the gamma ray analysis of light elements (GRALE) technique to determine the total carbon. Organic carbon is determined from the difference between total carbon and soot. Results are presented for the soot, organic and total carbon content of aerosol samples collected in St. Louis during the summer of 1977 and the winter of 1977/78.

INTRODUCTION

Airborne particulate matter has a complicated chemical composition which is strongly size dependent and comes from a wide variety of sources, both natural and anthropogenic. It is anticipated that in the next decade the increased reliance on coal for energy production will lead to further reduction of air quality. Of most concern are the fine or respirable particles (diam <3.5 μm) which are associated with visibility degradation, adverse health effects and climatic changes. Recent work indicates that it is necessary to further investigate the chemical composition of atmospheric aerosols (particles) in order to make rational decisions regarding future strategies.

Ultimately it is necessary to have a complete mass balance of the chemical constituents of the aerosol as a function of size. The fine particle chemical mass balance determined in a 21 day period in Charleston, West Virginia, reported previously,[1,2] is shown in Fig. 1. The major constituents in the urban fine particles are ammonium sulfate (42%), lead oxide (1%), trace elements (4%) and carbonaceous compounds (18% expressed as methylene groups, $-CH_2-$). In the same

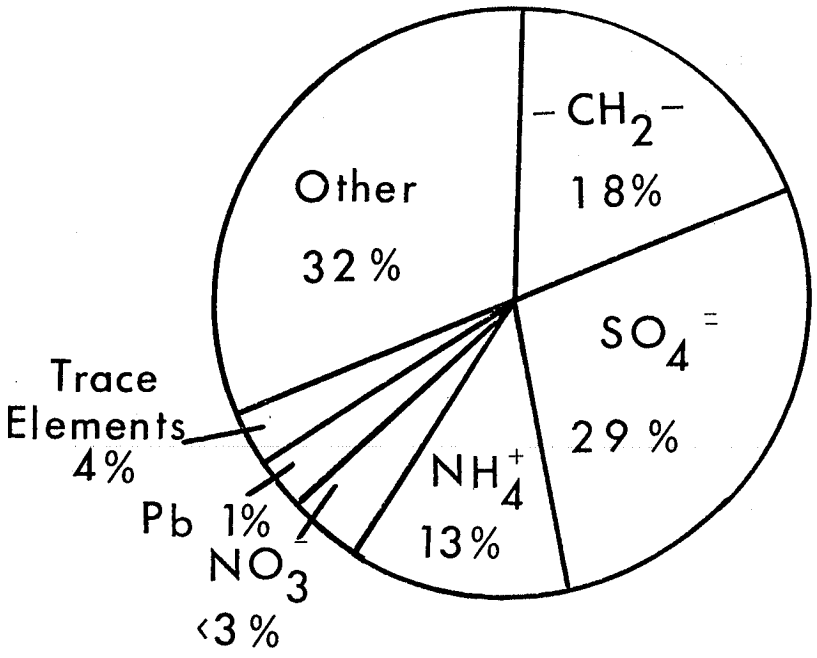

Fig. 1. Chemical mass balance of atmospheric fine particles determined in Charleston, West Virginia in summer 1976.[1,2]

study, carbon was found to constitute 12% of the coarse particle (diam >3.5 μm) mass. While there has been much emphasis placed on the first three species, much is left to be studied about the carbonaceous constituents. Particulate carbon in the atmosphere exists predominantly in three forms: soot, a substance which is largely elemental carbon with organics and other compounds adsorbed on the surface; organic compounds; and carbonates. In the Charleston study[1,2] it was found that an average 62% of the particulate carbon was in the fine particle size range but this value had large fluctuations (Fig. 2). The

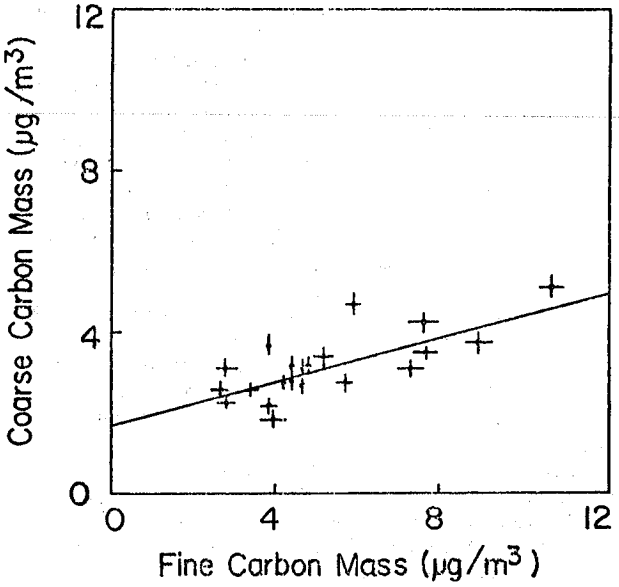

Fig. 2. Comparison of carbon mass in coarse and fine particles in Charleston, West Virginia.[1,2]

chemical composition of the carbon in the fine particles has been fairly well characterized. The fine particle carbon composition is 20-50% soot (elemental carbon), less than 5% carbonate[3] and the rest organic compounds. The detailed chemical composition of the coarse particle carbon is not well known.

Diesel emissions and the combustion of distillate oil and natural gas are thought to be the major sources of soot carbon.[4] Sources of primary organic aerosols include combustion of fossil fuel and automotive emissions. Secondary particulate organic species are formed from gaseous organic compounds through gas-to-particle conversion processes or adsorption onto soot and other particles. Fine particle lead has often been used as a tracer for automotive emissions.[5] It may be possible to estimate the extent of automotive sources of particulate carbon by correlating fine particle carbon and lead concentration. The relationship between carbon and lead from the Charleston study[1,2] is shown in Fig. 3. The two elements correlate very well (r = >0.9) for 16 of the 21 days when the carbon concentration was <6 μg/m³. However on the 5 days when the carbon concentration exceeded 6 μg/m³ there appeared to be an excess of carbon relative to lead compared to the other 16 days. This indicates that

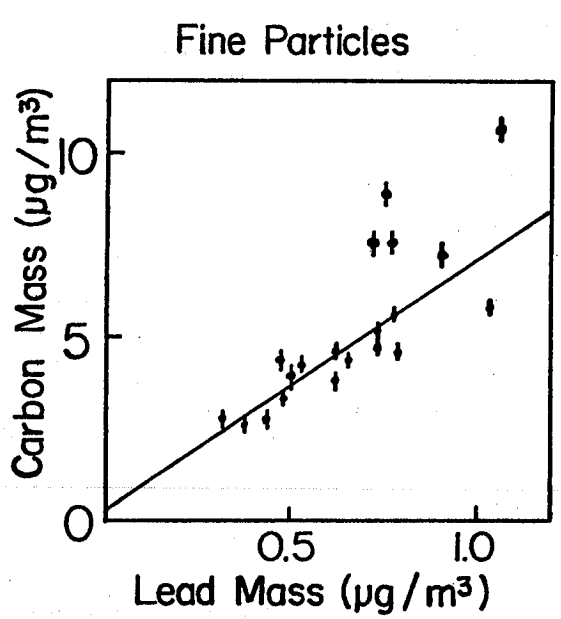

Fig. 3. Comparison of carbon and lead concentration of fine particles in Charleston, West Virginia.[1,2] The solid line is the least squares fit to the data.

during periods of high aerosol concentration non-automotive particulate carbon sources are significant.

Early methods of analysis of aerosol particulate matter relied on the differences in the chemical properties of organic and inorganic carbon. McCarthy and Moore[6] treated aerosol samples with 70% HNO_3 to oxidize organic compounds and determined the elemental carbon gravimetrically from the weight loss on heating to 140° and 700° C. Kukreja and Bove[7] treated samples collected on glass fiber filters with HF, NH_4OH, HNO_3 and HCl prior to gravimetric analysis for free carbon as above. Mueller *et al.*[3] determined total carbon content by quantitative conversion of the particulate carbon to CO_2 *via* acidification and combustion. They then determined the amount of CO_2 with a gas chromatograph equipped with a thermal conductivity detector. Appel *et al.*[8] used this method to determine the organic carbon content of various solvent extracts of atmospheric samples. Huntzicker and Johnson[9] have modifed this method by reduction of the CO_2 to CH_4 and analysis of CH_4 in a flame ionization detector. A variety of methods have been used for organic analysis of aerosols,[10] particularly mass spectrometry coupled with gas chromatography. All of the preceeding techniques are destructive. Non-destructive methods such as electron spectroscopy for chemical analysis (ESCA),[11] gamma-ray analysis for the light elements (GRALE)[12] and proton elastic scattering (PESA)[13] have been used to analyse total carbon content of ambient aerosols.

A few methods exist for the analysis of soot carbon which are non-destructive. Infrared[14] and Raman[15] spectroscopy have been employed to determine various forms of elemental carbon in aerosols based on their characteristic adsorption spectra. Two groups[16] have employed a simple

photometric technique based on the decrease in transmittance of light caused by increasing mass of particulate matter on a filter for the analysis of soot carbon.

In this paper we present two compatible methods of carbon analysis of atmospheric fine particles. The amount of soot (as elemental carbon) is determined from the reflectance of a sample measured relative to a filter blank. The sample is then analysed by the gamma ray analysis of light elements (GRALE) technique[12] to determine the total carbon. Organic carbon is determined from the difference between total carbon and soot. Results are presented for the soot, organic and total carbon content of aerosol samples collected in St. Louis during the summer of 1977 and the winter of 1977/78.

EXPERIMENTAL PROCEDURES

Aerosol Collection

A TWOMASS automated sequential tape sampler[17] was used to collect laboratory and ambient aerosols. The flow system of this sampler separated particles into two size fractions. Coarse particles were impacted on a glass fiber filter; the remaining particles were collected on an identical high-efficiency glass fiber filter. The single-stage impactor head had a 4.5-mm diam inlet aperture with a 4.5-mm jet-to-plate distance. The impactor was designed to have 50% efficiency for particles of 3.5 μm diam. Samples and standards were collected on Pallflex E70 glass fiber filter with a detachable cellulose backing. This medium was chosen because of its low mass density, efficient impaction properties, uniform thickness and low carbon, nitrogen and sulfur blank. Both the impaction and filtration heads of the TWOMASS had independent source-detector systems for beta attenuation mass measurements. The beta source was 1 mCi of ^{14}C. The cross sectional areas of the collection spots in the filtration and impaction stages were 32 and 16 mm^2, respectively.

The beta detector (ORTEC) was a silicon surface-barrier detector with a 50-mm^2 surface area, a 40-μg aluminum window, and a noise width less than 11 keV. The amplified output of each detector was acquired with two high-speed counters and further processed by a Tektronix programmable calculator with an x-y point plotter, printer, and magnetic tape cassette.

For the collection of ambient samples, the tape was automatically advanced at 3-hr intervals except during periods of high aerosol concentration ($\geq$ 40 $\mu g/m^3$) when the collection time was reduced to 2 hr. A nominal flow rate of 18 ℓ/min was used. The exact flow was determined from the output of a calibrated recording pressure transducer which monitored the pressure below the lower stage of the TWOMASS. This pressure changes linearly with flow rate, and calibration points were made at random intervals to check on linearity. During a 24 day period in St. Louis, two TWOMASS samplers were run side-by-side. The difference in fine concentrations between the two samplers was approximately 7% indicating the reliability of the collection, flow monitoring, data acquisition and analysis systems.

Total Carbon Analysis by the GRALE Technique

The total carbon content of the atmospheric fine particle samples was determined using the gamma ray analysis of light elements (GRALE) technique.[12] This non-destructive technique is based on the measurement of gamma-ray emission induced by proton bombardment of aerosol samples. The gamma-ray energy is, in general, unique to a particular nuclide and thus can be used as a signature for the chemical element. Elemental concentrations are obtained in units of $\mu g/cm^2$ and are not affected by the chemical form of the elements.

Following collection, the filter samples were mounted in 5 x 5 cm slide mounts after removal of the cellulose backing. The samples were then analyzed for carbon, nitrogen and sulfur in the external beam facility of the Washington University 135-cm sector focused cyclotron by irradiation with a collimated 7-MeV proton beam. The irradiation chamber, shown in Fig. 4, was built around a modified commercial 35-mm slide projector with a remote slide changing mechanism to automate the sample changing. The samples in the chamber were maintained in 1 atm of helium. The identity of the sample being irradiated was monitored with a closed circuit television camera. A 0.003-mm thick Havar foil served as a vacuum seal between the irradiation chamber and the cyclotron beam tube. Samples were typically irradiated with an 80-namp beam for 800-1000 sec. The beam current was determined with a digital current integrator which measured the total charge collected on the Faraday cup.

In general, inelastic proton scattering excites a nucleus to its lowest lying excited states which deexcite by the emission of gamma rays. The resulting in-beam gamma-ray spectrum includes at least one gamma ray from each element of interest.

Gamma rays produced in the proton bombardment were detected with a 60-cm^3 lithium drifted germanium Ge(Li) detector (11.7% efficient relative to a 3" x 3" NaI(Tl) detector of 1332 keV gamma rays), with energy resolution of 2.5 keV full width at half maximum for 1332 keV gamma rays. The output of the Ge(Li) detector was sent to a high-resolution preamp and amplifier which were able to process high count rates (<20,000 count/sec) without appreciable degradation of energy resolution. The amplified signals were sent to a 13-bit 200-MHz analog-to-digital converter (Tracor Northern). Digital information was stored and processed in a PDP-11 mini-computer with a 28000 word memory (Digital Equipment). The spectra were analysed immediately after each irradiation with the on-line computer. The intensity of each peak was determined from the integrated peak area after subtraction of background. The peak intensity was corrected for system dead time losses (typically 20%) determined from the area of a pulser peak in the spectrum produced from a 60 Hz tail-pulse generator. These data were normalized to the proton beam intensity determined from the integrated current measured in the Faraday cup. The

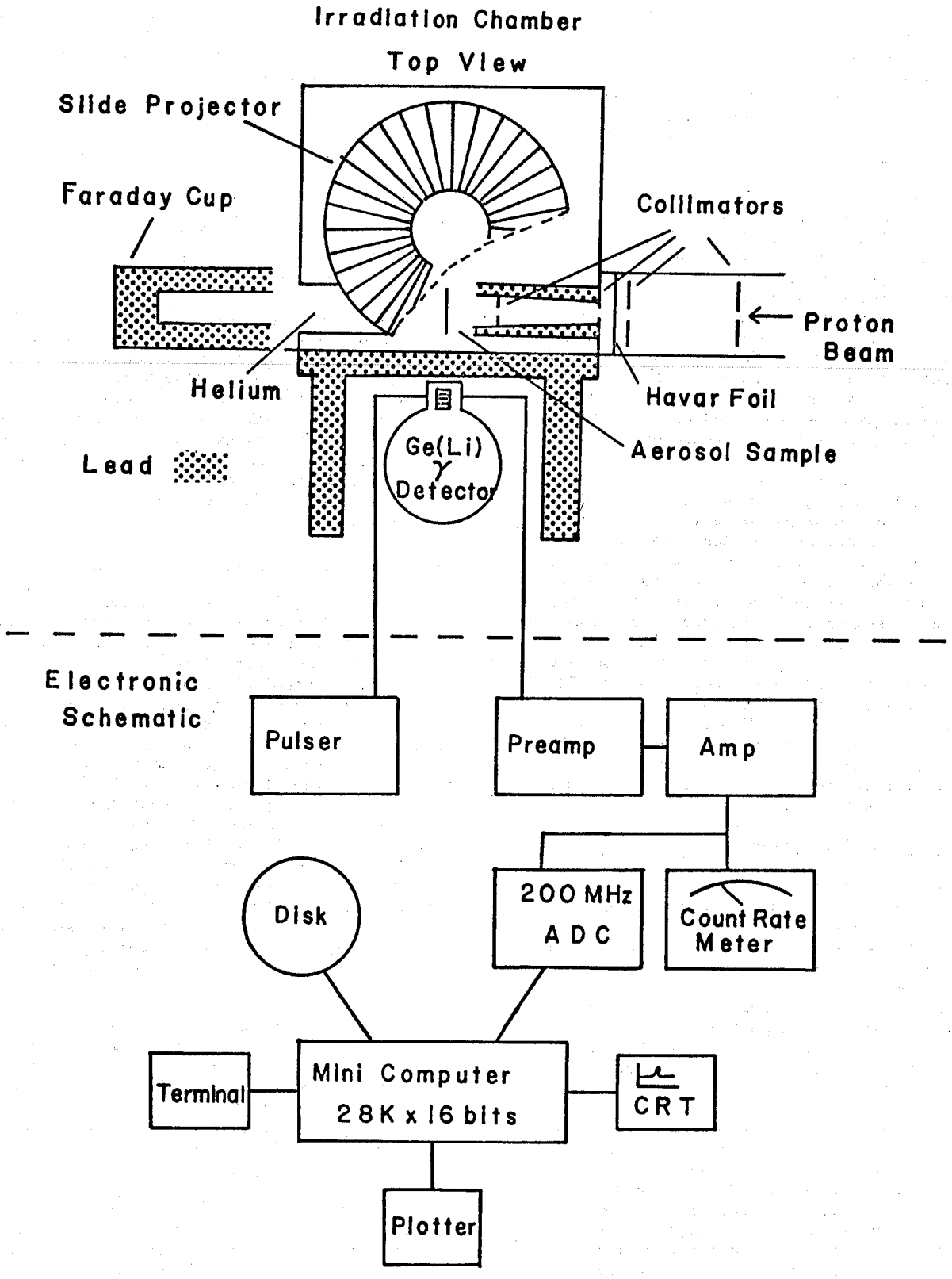

Fig. 4. Schematic diagram of the GRALE irradiation chamber and electronics.

normalized peak intensities of the filter blanks were subtracted from the aerosol results. The conversion of peak intensity into mass was carried out using standard methionine aerosols as described below. Filter blanks, atmospheric, laboratory and methionine standard aerosol samples were run under nearly identical conditions which yielded nearly equal detector count rates. All samples were analysed in the same way.

The identification of a given element in a sample was determined on the basis of peak energy determined for the large peaks by the use of external standards before and after each run. The large known peaks were then used as internal standards for energy determination of the smaller peaks. The amount of a given element in a sample was determined from the ratio of the peak area in the sample to the area of the corresponding peaks in a standard fine particle sample of methionine aerosol ($C_6H_{11}O_2SN$) on the same type of filter. The mass of methionine deposited on the filter was determined using a beta attenuation mass monitor.

The GRALE technique has been extensivly compared to other techniques in a previous study.[12] In that work the total carbon analysis of the same or duplicate filters was carried with the GRALE method, the Dohrmann DC-50 carbon analyser, (Envirotech) and the Perkin-Elmer Model 240 Elemental Analyser (Perkin-Elmer). The latter two methods are based on the high temperature combustion of carbon compounds with subsequent detection of CH_4 and CO_2, respectively. This method of intercomparison indicated that to within 5% there are no systematic discrepancies in any of the methods investigated. The advantages of the GRALE technique over combustion methods are that it is fast, non-destructive, totally instrumental, unaffected by the chemical form of the aerosol and easily automated.

Soot Analysis by Reflectance

The non-destructive quantitative analysis of soot, calibrated as elemental carbon, was determined from the reflectance of the aerosol deposit. This technique assumes that soot is the predominant species which is dark in color in the fine particle aerosol and therefore the darkness of the deposit is due primarily to soot. This technique is simple, inexpensive and sensitive. Because the light is not transmitted through the filter the method can be used with thick and inhomogeneous filters.

Two reflectance photometers, one built into a sampler for soot analysis during sample collection and the other for use off-line in the laboratory, were designed and constructed in our laboratory to conform to sampling requirements of the TWOMASS sampler and to be compatible with GRALE analysis. The on-line monitoring reflectometer was constructed from a TWOMASS sampler modified by the addition of a small tungsten filament lamp and a solid state photodetector mounted at 45° to the lower filter stage and at right angles to each other. The light source and detector were collimated to focus on the 0.3 cm^2 sample deposit. A stabilized power supply provided 5 v bias for the detector and 12 v power for the lamp. The amplified output signal from the photodetector was monitored on a strip chart recorder. Under conditions where the atmospheric soot content remained constant, the output decreased exponentially with time.

The off-line laboratory reflectometer, constructed for use with TWOMASS samples, is shown in a schematic diagram (Fig. 5). This light tight system consists of two blackened aluminum tubes (5.5 cm diam) each mounted at 45° to an aluminum sample chamber which holds standard 5 x 5 cm slide mounts. A 12-v tungsten filament lamp powered by a stabilized 12-v supply was used as a light source. Plano-convex lenses (2.3-cm diam, 4.5-cm focal length) were used to focus the incident light onto the sample (0.3 cm^2) and reflected light onto a solid-state detector. The intensity of the reflected light was measured with a N/P silicon solar cell (Centerlab Semiconductor). The solar cell output was monitored with a digital voltmeter. Blank filter paper taken from the same roll as the samples, was used to determine the initial (or blank) intensity. Blank values were obtained after the intensity of each sample was determined in order to detect any drifts in the electronics.

Calibration of the Reflectance Systems

Aerosol particles of elemental carbon (as soot) were prepared from the combustion of butane, polystyrene and paraffin. The generated aerosols were aspirated into a 5 liter container, mixed with filtered air and drawn through a TWOMASS sampler equipped as described above. A typical calibration curve for carbon generated from a butane flame is shown in Fig. 6. This curve was prepared by plotting the ratio of reflectance of the blank filter (I_o) and the reflectance after addition of soot (I) on a log scale versus carbon mass determined by beta attenuation. At low carbon masses, the decrease in log (I/I_o) is linear up to the point where the filter surface becomes saturated (covered) with carbon. Beyond that region, the reflectance does not significantly decrease with increasing carbon mass. By choosing the proper sampling conditions, saturation of ambient samples can be avoided.

A calibration was also carried out with ambient samples in the following manner. Atmospheric fine particle samples were collected with the TWOMASS sampler. The reflectance of these samples was determined with the laboratory reflectance photometer. The samples were then heated to 400° C for 5 minutes in a helium atmosphere. At this temperature organic compounds were volatilized leaving mainly elemental carbon (and carbonates). The samples were then analysed for total carbon by GRALE analysis to determine the remaining non-volatile carbon. Only fine particle samples were used in this calibration procedure. The amount of carbonate in these samples is expected to be very small, therefore the non-volatile carbon is predominantly soot carbon. With this procedure the reflectance of atmospheric samples before heating was calibrated in terms of elemental carbon by after-heating GRALE carbon analysis. The reflectance

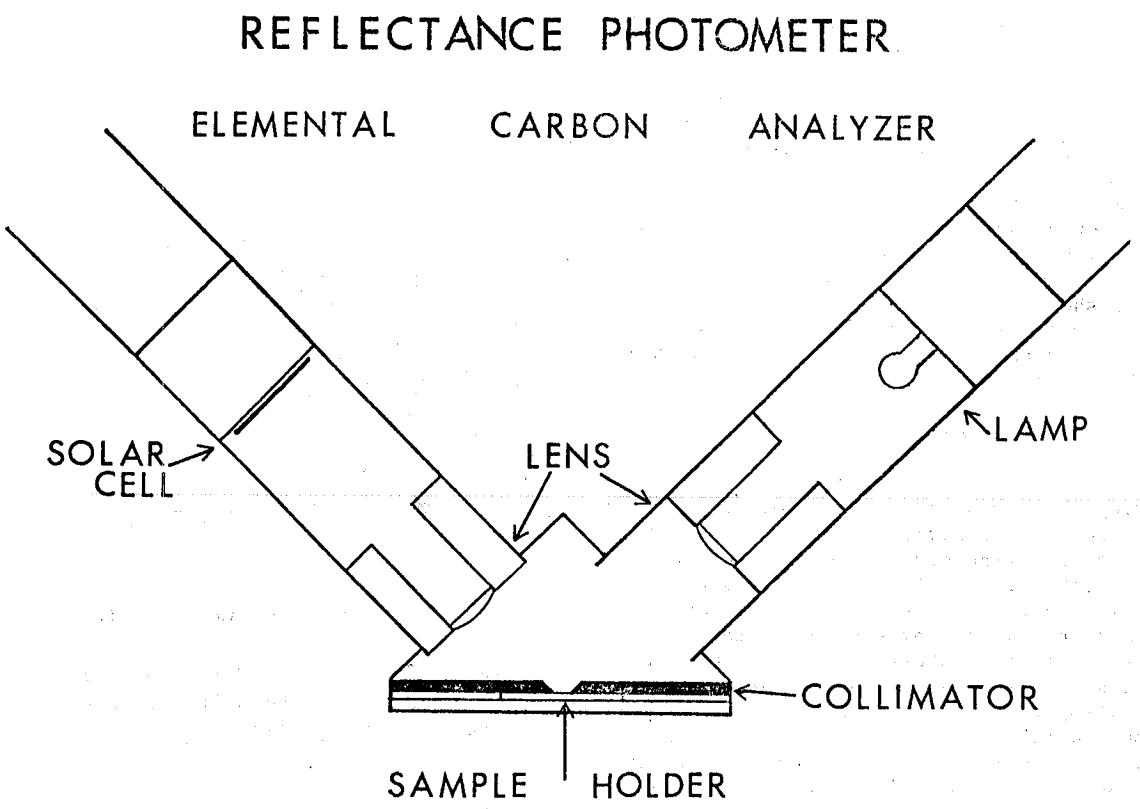

Fig. 5. Schematic diagram of the laboratory reflectance photometer.

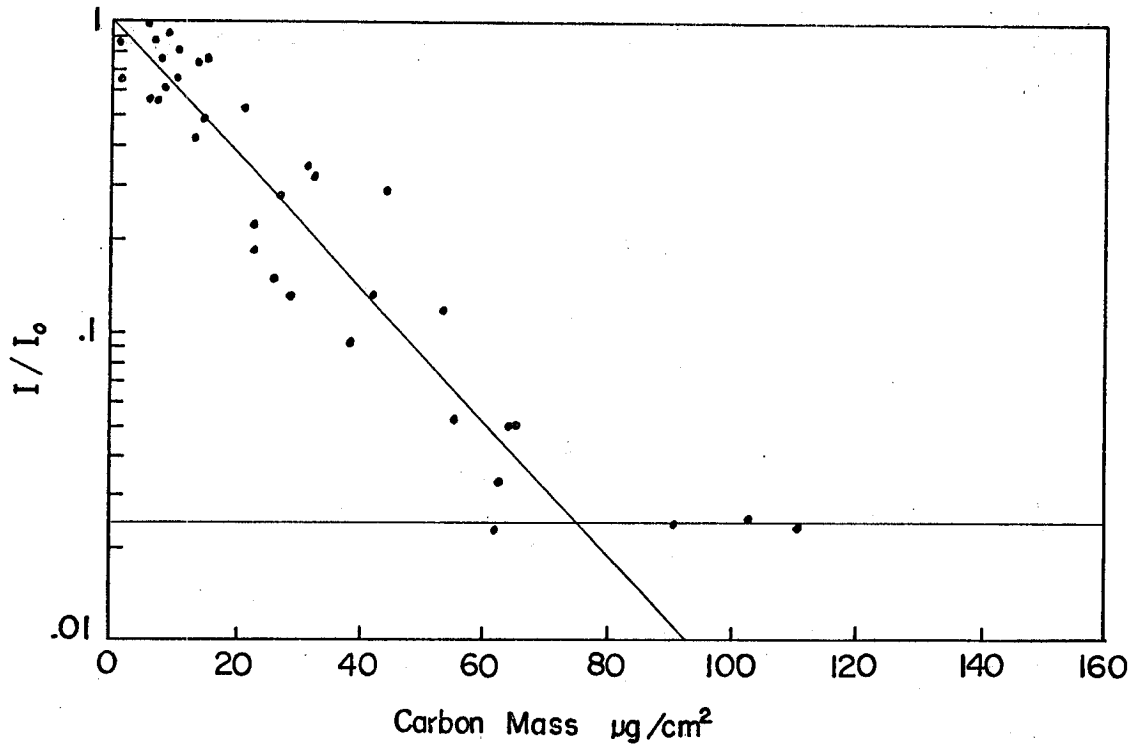

Fig. 6. Calibration of the laboratory reflectance photometer for carbon generated from a butane flame.

calibration of atmospheric samples and laboratory generated soot samples agreed to within 10%.

The on-line monitoring reflectometer was calibrated against the laboratory reflectometer in the following way. Ambient samples were collected and the reflectance was determined with the on-line reflectometer. The samples were then mounted and their reflectance determined with the laboratory reflectance photometer. A high correlation ($r = 0.96$) was obtained for results from the two systems as shown in Fig. 7. This indicates that the on-line monitoring reflectometer can be indirectly calibrated in terms of elemental carbon mass with the laboratory reflectance photometer.

TOTAL AND ELEMENTAL CARBON CONTENT OF AMBIENT SAMPLES

During the period of July 15-20, 1977, an air pollution episode occurred in the St. Louis area, during which the fine particle concentration reached a peak value of 116 $\mu g/m^3$. Fine particle aerosol samples were monitored for total mass during collection followed by the determination of soot carbon with the laboratory reflectometer. The samples were then subjected to GRALE for total carbon, nitrogen and sulfur analysis. The organic carbon fraction of the fine particles was obtained from the difference between total carbon (TC) and soot, as elemental carbon (EC). Figure 8

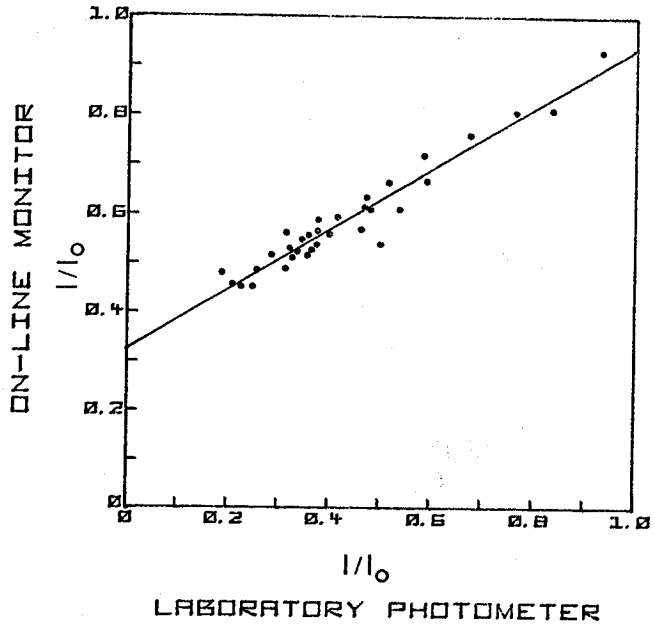

Fig. 7. Indirect calibration of the on-line reflectance photometer with the laboratory off-line reflectance photometer.

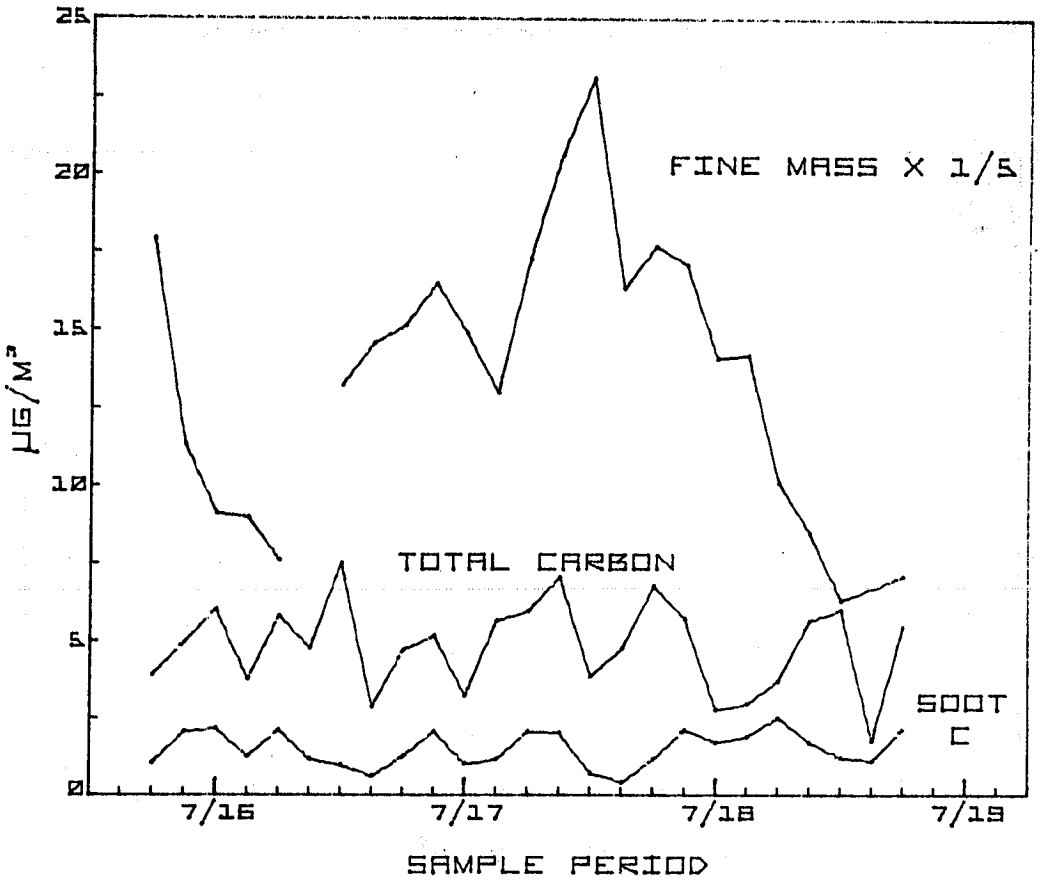

Fig. 8. Temporal variations of fine particle total carbon, soot carbon and mass in St. Louis, summer, 1977.

shows the temporal variations of fine particle total carbon, soot carbon and mass. During the peak of the event, the total carbon fraction decreased to approximately 6% of the fine particle mass, compared to 13% before and after the episode. Thus the increased mass was not accompanied by a corresponding rise in carbon content. The correlation coefficient (r) for fine particle carbon and mass was 0.44 for 22 samples. Of the total carbon, 35 ± 16% was found to be elemental carbon (soot). Correlation between the elemental carbon mass and total carbon mass was low (r = 0.33) as shown in Fig. 9a. On the other hand, the organic fraction (TC-EC) correlated well (r = 0.92) with total carbon, as expected (Fig. 9b).

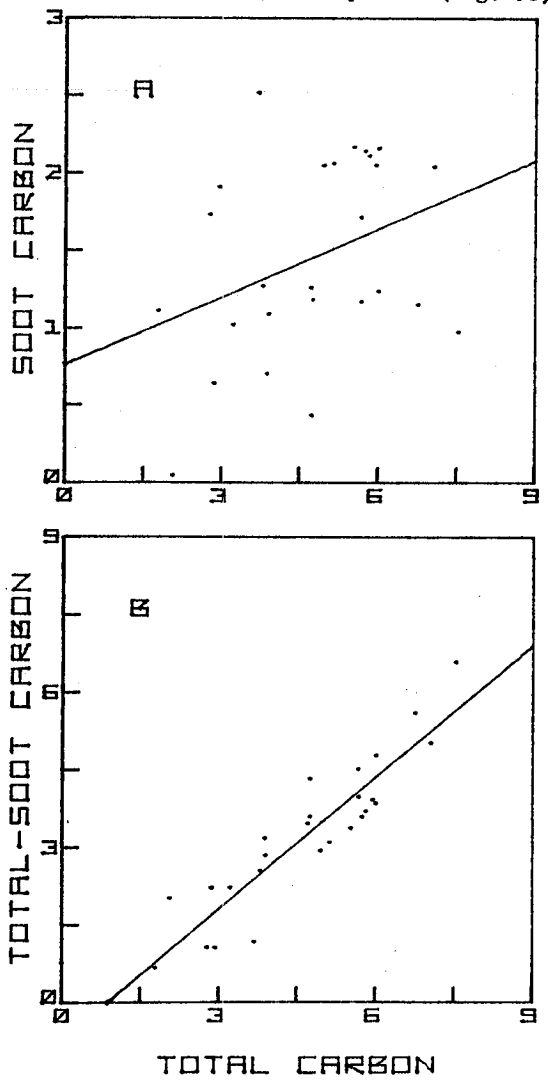

Fig. 9. a) Correlation between soot carbon and total carbon. b) Correlation between organic carbon and total carbon.

As shown in Fig. 8, the soot carbon concentration is relatively constant and independent of the fine particle concentration. One interpretation of these data is that the source of elemental carbon is relatively constant and independent of a major source of fine particle mass during the event.

Correlation coefficients were determined for sulfur and the various carbon fractions. The r for the correlations between sulfur and organic carbon (total carbon minus soot carbon), total carbon, and soot carbon were 0.06, 0.16, and 0.55, respectively. The correlation between soot and sulfur has been reported previously[11] and may be an indication of the catalytic activity of soot in the conversion of SO_2 to sulfate. However, the moderate correlation of soot with sulfur in this study is inconclusive evidence for this hypothesis.

During a 24 day winter period beginning January 26, 1978, a total of 305 samples were collected on each of two β-attenuation mass monitors. While analysis of the data set is incomplete, fine particle concentration and the EC concentration of the samples has been determined. The winter fine particle concentration was considerably lower than during the summer. Even during peak periods the winter fine particle concentration only rose to 78 $\mu g/m^3$. During the entire period, the soot carbon concentration remained relatively constant. The 24-hr average for the percentage of soot carbon in fine particles was found to be 13 ± 1%. This agrees with the summer value before and after the high concentration episode.

REFERENCES AND FOOTNOTES

*This work has been supported in part by the USEPA, Atmospheric Instrumentation Branch under grant R803115.

1. E.S. Macias and C.W. Lewis, paper No. 25 presented at the 173rd National American Chemical Society Meeting, Environmental Chemistry Division, New Orleans, La, March 21, 1977.

2. C.W. Lewis and E.S. Macias, Atmospheric Environ. (in preparation).

3. P.K. Mueller, R.W. Mosley and L.B. Pierce, J. Colloid Interface Sci. 39, 235 (1972).

4. J.I. Noland, Proceedings of the Conference on Carbonaceous Particles in the Atmosphere, Berkeley, Calif. (1978).

5. W.R. Pierson and W.W. Brachaczek, SAE Report 760039 (1976).

6. R. McCarthy and C.E. Moore, Anal. Chem. 24, 411 (1952).

7. V.P. Kukreja and J.L. Bove, Environ. Sci. Technol. 10, 187 (1976).

8. B.R. Appel, P. Colodny, and J.J. Wesolowski, Environ. Sci. Technol. 10, 359 (1976).

9. J.J. Huntzicker and R.L. Johnson, Proceedings of the Conference on Carbonaceous Particles in the Atmosphere, Berkeley, Calif. (1978).

10. E.S. Macias, K.S. Kumar, and M.K. Hoffman, Proceedings of the 9th Materials Research Symposium on Trace Organic Analysis, Gaithersburg, MD (1978).

11. T. Novakov, S.G. Chang and A.B. Harker, Science 186, 259 (1974).

12. E.S. Macias, C.D. Radcliffe, C.W. Lewis, and C.R. Sawicki, Anal. Chem. (in press).

13. J.W. Nelson in X-Ray Fluorescence Analysis of Environmental Samples, T.G. Dzubay, Ed., Ann Arbor Science, Ann Arbor, Mich. (1977) p. 19-34. Also: B.L. Cohen and R.A. Moyer, Anal. Chem. 43, 123 (1971).

14. R.A. Friedel and L.J.E. Hofer, J. Phys. Chem. 74, 2921 (1970).

15. H. Rosen and T. Novakov, Nature 266, 708 (1977).

16. C.I. Lin, M. Baker, and R.J. Charlson, Appl. Opt. 12, 1356 (1973). Also: H. Rosen, A.D.A. Hansen, R.L. Dod and T. Novakov, LBL-6819, p. 8 (1977).

17. E.S. Macias and R.B. Husar, Environ. Sci. Technol. 10, 904 (1976).

ORGANIC MATTER IN NEW YORK CITY TSP: COMPARISONS OF SEASONAL VARIATIONS AND RELATIONSHIPS TO SOURCE TRACERS

Theo. J. Kneip, M.A. Leyko, M.T. Kleinman*
M. Lippmann and J.M. Daisey
New York University Medical Center
Institute of Environmental Medicine
550 First Avenue
New York, New York 10016

*Environmental Health Laboratory
Rancho Los Amigos Hospital
University of Southern California
Downey, California 90242

ABSTRACT

Total suspended particulate matter (TSP) samples from New York City have been extracted sequentially with cyclohexane, dichloromethane and acetone. The masses of extractable material have been compared to older data obtained by benzene/acetone extractions and have been examined for correlations to several trace elements and other indices of pollutant sources.

The results indicate that the extractable organic matter has not shown any obvious trends during the period 1968-77 when the concentrations of TSP and several elements have markedly declined.

The correlations indicate that source allocations may be successfully made with more complete data. Local sources (autos and oil burning) appear to be related to the moderately polar and more polar fractions, while oxidants (photochemical reactions) may influence the concentration of the moderately polar material in the summer.

INTRODUCTION

Organic compounds comprise a significant fraction of the urban aerosol both in terms of mass and possibly in terms of hazard to health. Our knowledge of the chemical identities of compounds present in the aerosol and of the relationships of these materials to other aerosol variables, however, is relatively limited.

Many of the compounds present may be products of photochemical reactions and measurements of these can aid in defining precursor compounds and mechanisms of production. Of more significance, perhaps, are the potential health effects. A fraction of all respiratory cancers, estimated at 5 to 10 per 100,000 population, is believed to be related to urban environments (1). Many of the compounds already shown to exist in urban aerosols are known to be carcinogens or co-carcinogens (2). All of the materials in these groups are of interest because of their potential involvement in the excess respiratory cancers in urban populations.

Our studies have been undertaken to identify and define the concentrations of several classes of potentially hazardous compounds in the atmosphere, to investigate seasonal and long term trends in aerosol concentrations, and to seek source relationships where measured concentrations appear to be of some significance.

EXPERIMENTAL

Total suspended particulates (TSP) samples are collected on pre-ignited glass fiber filters on the roof of the N.Y.U. Medical Center on the east side of mid-Manhattan. The samples are sequentially extracted with increasingly polar solvents, cyclohexane, dichloromethane and acetone, respectively, for 8 hours each in a Soxhlet apparatus. The cyclohexane extracts non-polar organics including polycyclic aromatic (PAH), and aliphatic (AHC) hydrocarbons while the dichloromethane extracts moderately polar oxidized hydrocarbons. Acetone extracts polar oxidized hydrocarbons as well as some inorganic materials such as Zn, Cu, Cd and NO_3^- (3). Organic solvent extractable compounds were determined for 1968, 1969 and 1975 by sequential extraction with benzene followed by acetone. Trace metals were determined by atomic absorption (4). Nitrate and sulfate were determined by chemical colorimetric techniques by the Brookhaven National Laboratory and the laboratory of the John B. Pierce Foundation of Yale University (5,6). Ozone, NO_x and CO data were obtained from the State of New York.

RESULTS

Total suspended particulate matter in the air of U.S. cities has declined in

the past 10 years. Regulatory efforts have been rewarded, as exemplified by the reduction in TSP in New York City from a level of 120-130 $\mu g/m^3$ in the late 1960's to less than 80 $\mu g/m^3$ in the last few years. This decline in New York City is due principally to the burning of cleaner, low sulfur oil in large boilers for the production of power and heating. The overall decline in TSP has been accompanied by an even more significant reduction in vanadium and SO_2 concentrations and, due to other regulatory steps, for other reasons, by reductions in lead and copper concentrations (7,8,9). Airborne concentrations of organic solvent extractable materials, however, have not changed significantly in these years, as shown by the data in Table 1. A comparison of total solvent extractables in 1968-1969 with values for 1975-1976 does not indicate a shift in the concentrations of these materials. The combination of cyclohexane and dichloromethane might be expected to extract 20% more material than benzene alone (9); however, comparisons of the values fail to show a downward trend even if this is taken into account. The winter data for 1977 does appear higher than in past years, however. As more data is accumulated, we will determine whether this difference continues to occur. Possible changes in automotive combustion, in heating fuels, and other major sources must be examined if this appears to represent a real change.

Daily concentrations of PAH compounds have been determined for two alternate weeks in August, 1976 by a combination thin-layer/gas-liquid chromatographic method. The aerosol concentrations were comparable to those reported for New York for 1974 (10) and for the summers of 1962 and 1973 (11). Typical values are given in Table 2. Data are being collected to define seasonal or longer term trends for these compounds.

Table 2. Average ambient aerosol concentrations of some polycyclic aromatic hydrocarbons, August, 1976.

	Carcinogenicity	$ng/m^3 \pm S.D.$
Chrysene/Triphenylene	±	1.1±1.0
Benz(a)anthracene	+	1.1±0.8
Benzo(a)pyrene	+++	1.4±1.1
Benzo(e)pyrene	-	2.7±1.4
Benzo(ghi)perylene	-	0.8±0.4

Table 1. Airborne concentrations of extractable organic matter in total suspended particulate matter, $\mu g/m^3$ - extractable.

	Summer			
Solvent	1968 July-Aug.	1969 July-Aug.	1975 July-Aug.	1976 Aug.
Benzene	5.7	6.4	5.2	-
Cyclohexane	-	-	-	3.1
Dichloromethane	-	-	-	3.1
Acetone	5.9	6.2	-	7.1
Total	11.6	12.6	-	13.3
TSP	119	126	55	86

	Winter			
Solvent	1968 February	1969 Jan.-Feb.	1975 February	1977 February
Benzene	3.8	7.9	5.4	-
Cyclohexane	-	-	-	7.6
Dichloromethane	-	-	-	2.3
Acetone	5.5	7.3	-	12.1
Total	9.3	15.2	-	22.0
TSP	125	134	54	(a) 96

(a) First floor level, all other data for 14th floor.

We have also begun to test solvent extracts of TSP for the presence of alkylating agents and oxidizing compounds such as peroxides. Although no data exist for these classes from earlier studies in New York, it is important to establish baseline data in view of the known carcinogenic and cocarcinogenic properties of these types of compounds (12). Alkylating agents have been found in both the dichloromethane and acetone extracts for composites of samples taken during Summer, 1976 (13). For composite samples from the following winter, alkylating activity was 7 times lower for the dichloromethane extract and 11 times lower for the acetone extract, suggesting a major source difference or a photochemical relation for the materials in the summer samples. (Data were not obtained for the cyclohexane soluble fraction because of sample size limitations.) Oxidizing materials have been found in all three extracts with some preliminary evidence of higher levels in the summer.

Correlations have been sought between organic solvent extractable materials and a number of other variables measured in two intensive cooperative programs. Figure 1 shows a typical set of data used in these calculations. Results for the August, 1976, and February, 1977, study are given in Table 3.

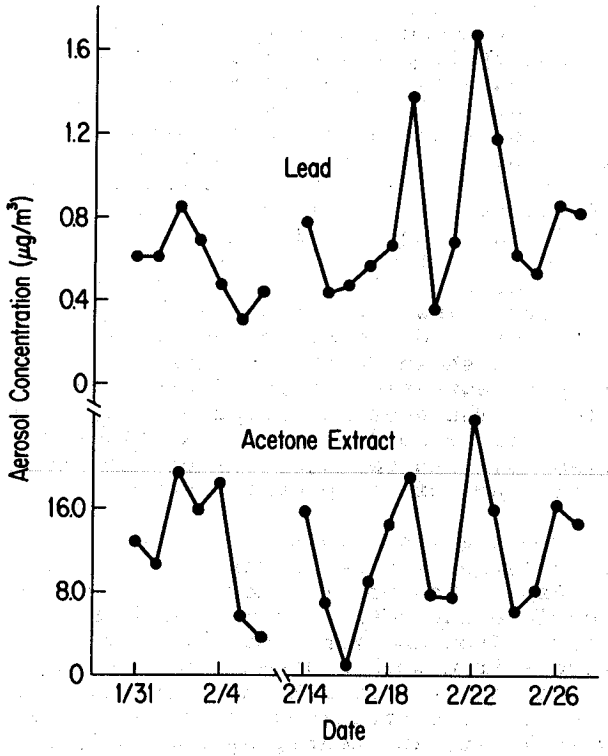

Figure 1. Concentrations of lead and acetone extractable materials in 24-hour samples from January and February, 1977.

Table 3. New York Aerosol Study. Kendall rank correlations between concentrations of organic solvent extracts of TSP and other variables.

	Summer, 1976		Winter, 1977	
Variables	r(a)	p(n)(b)	r(a)	p(n)(b)
Cyclohexane Extract with:				
Mn	0.49	0.006(15)	0.30	0.032(21)
Fe	0.45	0.011(15)	0.33	0.025(19)
Dichloromethane Extract with:				
O_3	0.59	0.001(17)	-0.156	0.18(19)
Pb	0.58	0.001(16)	0.125	0.22(21)
Traffic	0.59	0.001(16)	-	-
Zn	0.58	0.003(13)	0.26(c)	0.062(19)(c)
V	0.34	0.044(14)	0.44	0.008(16)
Acetone Extract with:				
Pb	0.74	0.001(16)	0.62	0.001(21)
Zn	0.74	0.001(13)	0.19(c)	0.124(19) (c)
NO_2	0.91	0.001(8)	0.60(d)	0.001(20) (d)
O_3	0.45	0.006(17)	-0.50	0.002(19)
Traffic	0.46	0.007(16)	-	-
CO	-	-	0.56	0.001(19)
NO_3^-	0.42	0.037(11)	0.58	0.002(15)
$SO_4^=$	0.48	0.021(11)	0.48	0.005(16)
V	0.13	0.255(14)	0.40	0.015(16)
Total Organics	-	-	0.63	0.001 (21)

(a) r=Kendall rank correlation coefficient
(b) p(n)= level of statistical significance (number of data pairs)
(c) Analysis for copper rather than zinc
(d) Winter data for NO_x

Kendall Rank correlations have been chosen for these comparisons. This affords non-parametric evaluation of interrelated trends and avoids the assumption that the data is normally distributed. The results show a correlation of the non-polar cyclohexane soluble material with aerosol concentrations of both iron and manganese in February, 1977, similar to a correlation found in August, 1976. The dichloromethane extract correlated to vanadium during February, 1977, but correlated to lead, ozone and more strongly to the cross product of lead and ozone the previous summer, as shown by the results of the multiple regression analysis given in Table 4. The acetone extractable compounds correlated to lead plus several other variables, with no major difference from the findings of the previous summer.

The results suggest that a more or less constant source is responsible for the mass of non-polar materials extracted by cyclohexane both in summer and in winter. Iron and manganese are found in aerosols from soil sources, but are also present in coal fly ash and possibly other sources. Concentrations of manganese in New York City are nearly as low as levels 30-70 miles to the northwest, suggesting that strong local sources of these materials are not important (7,8).

The correlations of the acetone extractable material suggest that the polar oxidized hydrocarbons are directly emitted by automobiles and thus correlate with lead concentrations in both summer and winter. The moderately polar organics extracted by dichloromethane seem to originate from fuel burning in the winter as shown by the correlation with vanadium. The correlation with O_3 X Pb, seen for this fraction during the summer, suggests that these materials may have contained large quantities of secondary aerosols during this period. A weak correlation with vanadium in the summer indicates a continuing relation to oil burning sources such as power production.

The correlations which we have found are useful in suggesting more important fractions to be subjected to detailed analysis as well as indicating directions for future work on source allocation modeling.

ACKNOWLEDGEMENTS

The authors wish to thank R. Hershman and B. Naumann for sample collection and preparation, and J. Miller for the sample analyses. We would also like to express our appreciation to Roger Tanner and Brian Leaderer and their co-workers for making available the data for a number of ionic species of sulfur and nitrogen.

This work is supported by Grant No. RP 1058-1 of the Electric Power Research Institute and by the American Petroleum Institute and is part of Center programs supported by Grant No. ES 00260 from the National Institute of Environmental Health Sciences and by Grant No. CA-13343 from the National Cancer Institute.

REFERENCES

1. Friberg, et al., "Air pollution and cancer: Risk assessment methodology and epidemiological evidence". Environ. Health Persp. (In press).

2. E. Sawicki, "Analysis of atmospheric carinogens and their cofactors". In: INSERM Symposia Series Vol. 52, IARC Scientific Publications No. 13, Environmental Pollution and Carcinogenic Risks, 297-354.

3. J. M. Daisey, Unpublished data, this laboratory.

4. T. J. Kneip, J. Eisenbud, C. D. Strehlow, P. C. Freudenthal, "Airborne particulates in New York City", J. Air Poll. Con. Asso. 20(3):144-149, 1970.

5. R. T. Tanner, Personal Communication.

Table 4. Results of multiple regression analysis

Solvent	Organic Compound Class	Significant Regression Variables ($p<0.01$)	F	% Variation Explained by Regression
Acetone	Polar	Pb	43.4	77
Dichloro-methane	Slightly Polar	Pb X O_3	18.8	59
Cyclohexane	Non-Polar	-	-	-

6. B. Leaderer, Personal Communication.

7. M. Eisenbud and T. J. Kneip, Trace metals in urban aerosols, Final report to Electric Power Research Institute, October, 1975. NTIS #Pb-248-324, 1976.

8. M. T. Kleinman, The Apportionment of sources of airborne particulate matter, Thesis submitted to the New York University Graduate School of Arts and Sciences, June, 1977.

9. D. Grosjean, "Solvent extraction and organic carbon determination in atmospheric particulate matter: The organic extraction--organic carbon analyzer (OEOCA) technique". Anal. Chem. 47(6):797-805, 1975.

10. M. Dong, D. C. Locke and E. Ferrand, "High pressure liquid chromatographic method for routine analysis of major parent polycyclic aromatic hydrocarbons in suspended particulate matter. Anal. Chem. 48:369-372, 1976.

11. J. M. Colucci and C. R. Begeman, "Carcinogenic air pollutants in automotive traffic in New York. Environ. Sci. Technol. 5:145-150, 1971.

12. B. L. Van Duuren, "Part II. Chemical carcinogenesiscarcinogenic epoxides, lactones, haloethers and their mode of action", Ann. N. Y. Acad. Sci. 163:633-651, 1969.

13. S. Agarwal, Unpublished data, this laboratory.

DIURNAL AND SPATIAL VARIATIONS OF ORGANIC AEROSOL CONSTITUENTS IN THE LOS ANGELES BASIN

Bruce R. Appel, Emanuel M. Hoffer, Evaldo L. Kothny,
Stephen M. Wall, Meyer Haik and Richard L. Knights
Air and Industrial Hygiene Laboratory, Laboratory Services Branch,
Calif. State Dept. of Health, 2151 Berkeley Way, Berkeley, CA 94704
Chemistry Department, University of Washington, Seattle, WA 98195

ABSTRACT

Two-hour and fourteen-hour hi-vol aerosol samples were collected simultaneously at Pasadena, Pomona and Riverside, California on four successive days in July 1975. Simultaneous ozone and visibility measurements were made for correlation with aerosol constituents. Samples were analyzed for primary (C_p), secondary (C_s), and elemental carbon (C_e) by selective solvent extraction-carbon analysis. In addition, high resolution mass spectrometry was used to provide detailed analysis of organic constituents and to evaluate the selective extraction procedure. The composition of the carbonaceous material at the three sites was found to be similar with $C_s/C_p \geq 2$. The C_e, as estimated by insoluble carbon, was the most abundant carbon form. Adipic and glutaric acids were among the more abundant aerosol constituents of probable secondary origin. Elevated morning levels of C_s, dicarboxylic acids and acid nitrates as well as low morning Br/Pb ratios gave evidence of the retention of secondary organic aerosol from preceding days. Cycloalkenes appear to be the principal secondary organic aerosol precursor. Primary organics show evidence of a motor vehicle origin plus additional unidentified sources. Comparison between 2-hour and 14-hour samples reveals evidence of both loss of organics by volatilization and increased collection efficiency for organics with increased particle loading.

I. INTRODUCTION

A previous paper [1] reviewed various techniques which have been applied to characterization of atmospheric carbonaceous particulate matter and described a new procedure for such characterization. The latter employed a combination of solvent extraction and carbon determinations. It was postulated that cyclohexane was a selective solvent for the extraction of "primary" particle phase organics (i.e. those injected into the atmosphere in the particle state), while total organics could be approximated as those solubilized by successive extraction with benzene and 1:2 v/v methanol-chloroform. Insoluble carbon was used to estimate the elemental carbon present. "Secondary" organics (i.e. those formed as a result of chemical reactions in the atmosphere) were determined by subtracting primary from total organics, all expressed as carbon. Insoluble carbon also includes carbonates, if present, as well as carbon in various polymeric forms (e.g. pollen, spores, rubber particles). Samples were analyzed for carbonates but not for carbon in rubber or viable particles. Thus the results cited for elemental carbon were upper-limit values.

The present paper reports on the validation of the selective extraction approach and its application to samples collected simultaneously at Pasadena, Pomona and Riverside, within California's South Coast Air Basin (SCAB) [figure 1]. Results of analyses employing high resolution mass spectrometric thermal analysis (MSTA) [2,3] on the same samples are also reported.

In addition to analyses for carbonaceous species, the samples were analyzed for lead and bromine. The ratio of these elements can be used to assess the age of an air mass when motor vehicle exhaust is the principal source of both elements [4]. Such information was employed in interpreting diurnal and spatial variations of carbonaceous materials. Ozone was monitored at each site to provide additional evaluation of the correlation between mean daytime ozone concentrations and secondary organics [1].

At each site two hi-vol filter samplers were used, one sampling for 14 hours and the second, for 7, 2-hour periods. This design permitted assessment of diurnal and spatial variations of primary and secondary organics and elemental carbon in the SCAB. A comparison of analyses made on short and long term samples provided measurement of sampling errors for carbonaceous materials. A more detailed account of this work is available elsewhere [5].

II. RESULTS AND DISCUSSION

A. Validation of the Selective Solvent Extraction Technique

The extraction efficiency for atmospheric particulate carbon of the solvents used are compared in table 1. Cyclohexane extracted significantly less carbon compared with the other solvent systems. To evaluate the hypothesis that cyclohexane is selective for the extraction of primary organics, results of the MSTA of cyclohexane extracts were compared with MSTA for direct analysis of the same filter samples without

extraction (table 2). MSTA provides information on individual compounds and in some cases, on classes of compounds. The sum of alkanes plus alkenes and alkylbenzenes was used as a model for primary organics while the dicarboxylic acids and difunctional nitrates plus nitrites were used as model secondary organics. Comparing the MSTA of cyclohexane extracts and filter samples, cyclohexane enhanced the recovery of alkanes plus alkenes relative to direct filter analysis. Alkylbenzenes recovered in cyclohexane were about equal to the level on the filters and their concentration was substantially lower relative to alkanes plus alkenes. On average cyclohexane extracted about 40% of the hexanedioic acid and a small fraction of the pentanedioic acid and difunctional nitrates and nitrites. The ratio, total model secondary organic indicators/total model primary organics for the filters was about 10 times higher than in the cyclohexane extracts. The enhanced recovery of alkanes plus alkenes in cyclohexane accounts for, on average, a value of 1.7 for the above ratio. The remainder reflects the relatively low solubility of secondary organics in cyclohexane.

Additional indications of the selectivity of cyclohexane is seen in figure 1 which plots the ratio of secondary to primary organics by solvent extraction against the ratio of total model secondary organics to total model primary organics by MSTA of 14-hour samples. A relatively high correlation coefficient ($\rho = 0.81$) is observed with a small intercept. A slope less than one is consistent with the omission of significant contributors to the total secondary organics from the set of compounds used as model secondary organics in MSTA. We conclude that while cyclohexane is not perfectly selective for primary organic aerosol constituents, it provides a useful upper limit to the primary organics.

B. Composition of 14-Hour Samples

Table 3 lists the results obtained by the solvent extraction-carbon analysis technique for 14-hour samples. Insoluble carbon, as a measure of elemental carbon, was the largest C constituent averaging somewhat more than 40% of the total C. Secondary organic carbon was 2-3 times more abundant than primary. In Riverside, which can receive pollutants formed during transport from locations to the west, there was somewhat more secondary organics in two of the four trials. In three of the four sampling days, the abundance of primary organic carbon was slightly less at Riverside although the differences are relatively small. In all cases the proportion of secondary organic carbon was somewhat lower at Pomona compared with the other sites.

Table 4 shows MSTA results for 14-hour filter samples for the two days of highest ozone levels previously given in Table 3, here shown relative to the concentration of total alkanes plus alkenes in the same sample. Dicarboxylic acids are seen to be about as abundant as the model primary organics. The relative concentration of secondary organics at Riverside was higher than at the other sites on both days. Similar to the solvent extraction-carbon analysis results, the proportion of secondary organics was significantly below that at the other sites on July 10th.

C. Diurnal Variations of Aerosol Constituents

The diurnal variations of carbonaceous materials on July 9 and 10, 1975, obtained by the solvent extraction-carbon analysis and MSTA techniques (on filter samples), are shown for Pomona in figures 2 and 3. July 9th was the first day of a relatively polluted episode with ozone maxima up to 0.38 ppm. On July 9 the peak in secondary organics by solvent extraction followed that for O_3 while primary organic carbon showed two weak maxima and elemental carbon peaked earlier in the day. MSTA showed a similar pattern, two weak maxima for total model primary and a single afternoon maximum for total model secondary organics. The lead concentration peaked in early morning, consistent with the early morning traffic peak, low windspeed and the expected low mixing height. The Br/Pb ratio was fairly constant throughout the day which contrasts greatly with results for the following day. On July 10th, both primary and secondary organic particulate levels were greatly elevated in the early morning. While the morning Pb level was high, the low morning Br/Pb ratio suggests that relatively aged aerosol was being sampled. The high Br/Pb ratio observed during the evening, 0.7, reflects either non-automotive sources of Br or analytical error in this sample. Results at Pomona are similar to those observed in Pasadena and Riverside on these two days.

D. Sampling Errors

Table 5 compares the 14-hour sample results with those calculated from the corresponding seven, successive, 2-hour samples for total carbon (C_t), elemental carbon (C_e), cyclohexane (CEC), benzene (BEC) and methanol-chloroform (MCC) soluble carbon. The calculated 14-hour average values for C_t consistently exceeds those observed at all sites. Of the fractions contributing to the total carbon, MCC and C_e showed similar ratios. Ratios > 1.0 for carbonaceous materials may reflect the loss of more volatile constituents not strongly adsorbed on other materials during the prolonged

(14-hour) sampling, consistent with Della Fiorentina's observations [8,9]. This hypothesis can serve to rationalize the high ratio for MCC (1.7). However, a ratio of 1.2 for C_e cannot be explained by volatilization and may be indicative of other sources of error. Thus, only ratios > 1.2, (e.g. 1.7 for MCC) are here considered to be indicative of losses of organics due to volatilization.

Ratios < 1.0 may reflect both sampling and analytical errors. If gas phase organics are adsorbed on previously collected, non-volatile materials (e.g. soot) the efficiency of such collection of gas phase organics should increase with increased particulate loading. This would result in greater levels of carbon from this source on 14-hour samples than calculated from the two hour samples. Since the atmospheric concentration of hydrocarbons in the gas phase appears to be substantially greater than that of polar organic materials, the collection of gas phase organics by adsorption on particulate matter would be expected to enhance the BEC and CEC fractions. Possible sources of analytical errors leading to ratios < 1.0 were considered as part of quality assurance studies reported elsewhere [5]. The results suggest these errors to be of minor importance.

III. CONCLUSIONS

We conclude that the solvent extraction-carbon analysis approach for estimating primary and secondary organics is a useful technique and correlates reasonably well with results by mass spectrometry. For four days in July 1975 in California's South Coast Air Basin the carbonaceous fractions in order of abundance were elemental C > secondary organic C > primary organic C. The extent to which polymeric forms of carbon (e.g. in spores, pollen, tire dust) contributed to the estimate for elemental carbon remains unclear. The period July 9-10, 1975, represented a stagnation episode during which aerosols were retained in the SCAB from one day to the next. The indicators of such aerosol retention are elevated concentrations of secondary organics preceding the diurnal ozone peak and low Br/Pb ratios for early morning aerosol samples. Because of the possible retention of aerosols from one day to the next, pollutant transport and/or dilution may be dominant factors in determining concentrations of secondary organics rather than degree of conversion of precursors. Accordingly, high correlations between concentrations of secondary organic materials and indicators of smog intensity (e.g. ozone) may not be observed. Finally, hi-vol sampling for particulate organics is subject to both positive and negative errors. Improved sampling procedures are needed to obtain measures of ambient carbonaceous particulate matter which are less subject to error.

ACKNOWLEDGEMENTS

The authors wish to express their appreciation to A. Alcocer, D. Grosjean, S. K. Friedlander, S. Heisler, S. Marsh and the staff of the Southern California Air Pollution Control District for assistance in various phases of this study. The work was carried out under the sponsorship of the California Air Resources Board Research Section.

REFERENCES

1. Appel, B.R., Colodny, P. and Wesolowski, J.J., Environ. Sci. Technol., 10 359 (1976).

2. Schuetzle, D., Cronn, D., Crittenden, A.L., and Charlson, R.J., Environ. Sci. Technol., 9 838 (1975).

Cronn, D.R., Charlson, J.J., Knights, R.L., Crittenden, A.L. and Appel, B.R., Atmos. Environ., 11 929 (1977).

4. Robbins, J.A. and Snitz, F.L., Environ. Sci. Technol., 6 164 (1972).

5. Appel, B.R., Hoffer, E.M., Haik, M., Wall, S.M., Kothny, E.L., Knights, R.L. and Wesolowski, J.J., Final Report to California Air Resources Board, Contract No. ARB 5-682 "Characterization of Organic Particulate Matter," 1977.

6. Della Fiorentina, H., DeWiest, F., and DeGraeve, J., Atmos. Environ. 9 517 (1975).

7. Rondia, D., DeWiest, F. and Della Fiorentina, H., "Organics in Atmospheric Aerosols in Belgium," Vol. 2, Paper No. 24-5, presented at the International Conference on Environmental Sensing and Assessment, Las Vegas, NV, Sept. 1975.

Table 1

Mean Extraction Efficiency of Solvents for Carbonaceous Material in Atmospheric Samples

Solvent	% of Total C in Extract
cyclohexane	17
benzene	25
benzene plus MeOH-$CHCl_3$	57

Table 2

Comparison of Cyclohexane Soluble Organics and Direct Analysis of Filter Samples by MSTA ($\mu g/m^3$)[a]

Episode	Site	Alkanes + alkenes		Alkylbenzenes		Hexanedioic acid		Pentanedioic acid		Organic nitrates + nitrites[b]	
		C_6H_{12}	filter	C_6H_{12}	filter	C_6H_{12}	filter	C_6H_{12}	filter	C_6H_{12}	filter
July 9	Pasadena	7.1	3.0	0.13	0.38	1.0	1.4	0.0	1.6	0.16	0.39
July 9	Pomona	5.8	3.0	0.16	0.41	0.11	1.6	0.05	1.4	0.047	0.22
July 9	Riverside	4.0	1.3	0.13	0.15	0.47	0.88	0.15	0.84	---	0.17
July 10	Pasadena	5.3	2.3	0.16	0.38	1.0	1.8	---	1.3	---	0.17
July 10	Pomona	6.2	2.6	0.09	0.32	0.29	1.1	---	1.4	0.022	0.090
July 10	Riverside	2.7	1.0	0.16	0.20	0.18	1.0	---	0.96	---	0.032

Mean Ratio $\frac{\text{Total secondary organics}^c}{\text{Total primary organics}^d}$ = 1.1 (filters); 0.11 (cyclohexane extract)

a. The compounds determined and their identifying mass fragments are: total alkanes plus alkenes ($C_5H_{11} + C_5H_9$), alkylbenzenes ($C_7H_7 + C_8H_{10} + C_9H_{11} + C_9H_{12}$), hexanedioic acid ($C_5H_8O_2$), pentanedioic acid ($C_4H_6O_2$) and organic nitrates plus nitrites ($C_xH_yNO_z$ where x = 5,6,7; y = 7,9,11; z = 4,5).

b. The sum of acid nitrates and nitrites and aldehyde nitrates and nitrites.

c. Hexanedioic acid + pentanedioic acid + organic nitrates and nitrites.

d. Alkanes + alkenes + alkylbenzenes.

Table 3

Composition of 14-hour Carbonaceous Samples by Solvent Extraction-Carbon Analysis

(% of Total Carbon)

Episode	Site	Soluble C	Primary C	Secondary C	Elemental C
July 9	Pasadena	58.2	17.5	40.7	41.8
	Pomona	54.1	18.5	35.6	45.9
	Riverside	58.5	15.3	43.2	41.5
July 10	Pasadena	57.8	13.7	44.1	42.2
	Pomona	48.5	16.8	31.7	51.5
	Riverside	58.5	15.3	43.2	41.5
July 11	Pasadena	67.7	19.9	47.8	32.4
	Pomona	58.6	20.8	37.8	41.4
	Riverside	57.6	15.4	42.2	42.4
July 12	Pasadena	55.8	20.4	35.4	44.2
	Pomona	50.1	16.5	33.5	50.0
	Riverside	42.8	14.1	38.6	47.2
	Mean:	56.5	17.0	39.5	43.5

Table 4

Analysis of 14-Hour Filter Samples by MSTA[a]

Episode	Site	Total Alkanes + Alkenes	Alkylbenzenes	Hexanedioic Acid	Pentanedioic Acid	Organic Nitrites + Nitrates	ΣSecondary[b]
July 9	Pasadena	1.0	0.12	0.45	0.52	0.13	1.1
July 9	Pomona	1.0	0.14	0.53	0.47	0.07	1.1
July 9	Riverside	1.0	0.12	0.68	0.65	0.13	1.5
July 10	Pasadena	1.0	0.19	0.78	0.57	0.07	1.4
July 10	Pomona	1.0	0.13	0.42	0.54	0.03	1.0
July 10	Riverside	1.0	0.24	1.0	1.0	0.03	2.0

a. Results relative to the concentration of total alkanes plus alkenes in the same sample.

b. The sum of hexanedioic, pentanedioic acids and organic nitrates plus nitrites.

Figure 1

CORRELATION BETWEEN MSTA AND SOLVENT EXTRACTION-CARBON ANALYSIS

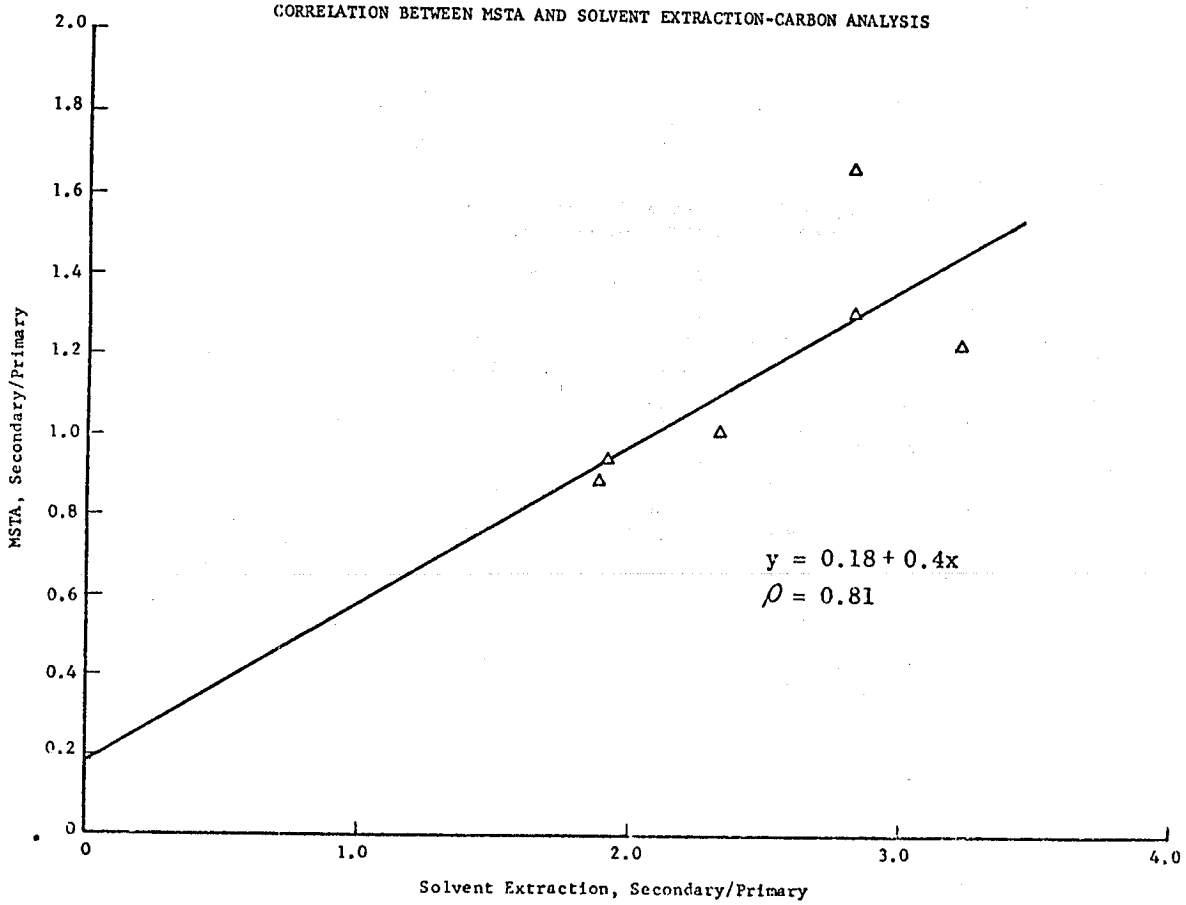

Figure 2 DIURNAL VARIATIONS IN AEROSOL CONSTITUENTS AT POMONA ($\mu g/m^3$)
JULY 9, 1975

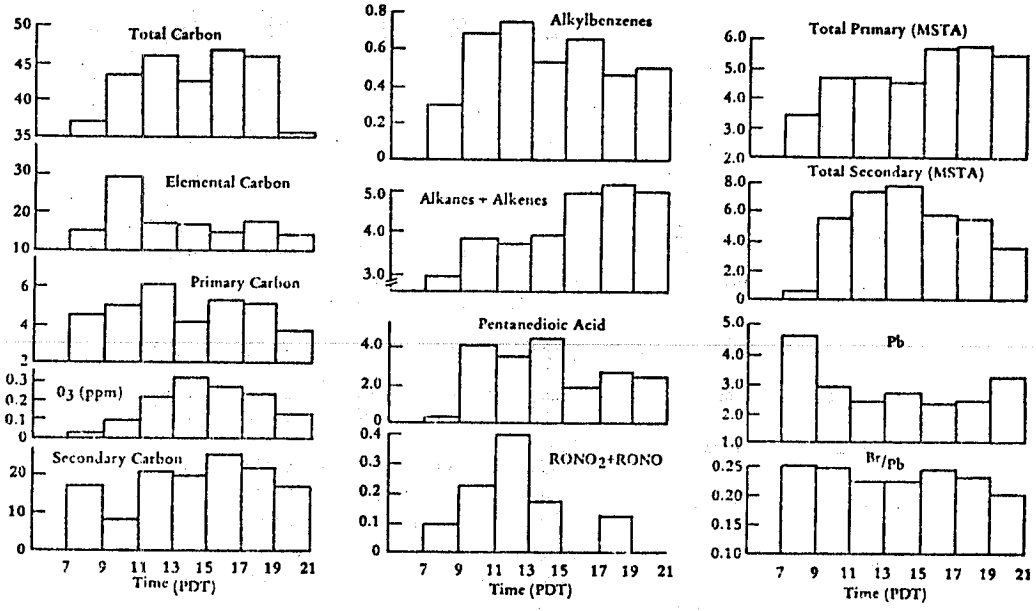

Figure 3 DIURNAL VARIATIONS IN AEROSOL CONSTITUENTS AT POMONA ($\mu g/m^3$)
JULY 10, 1975

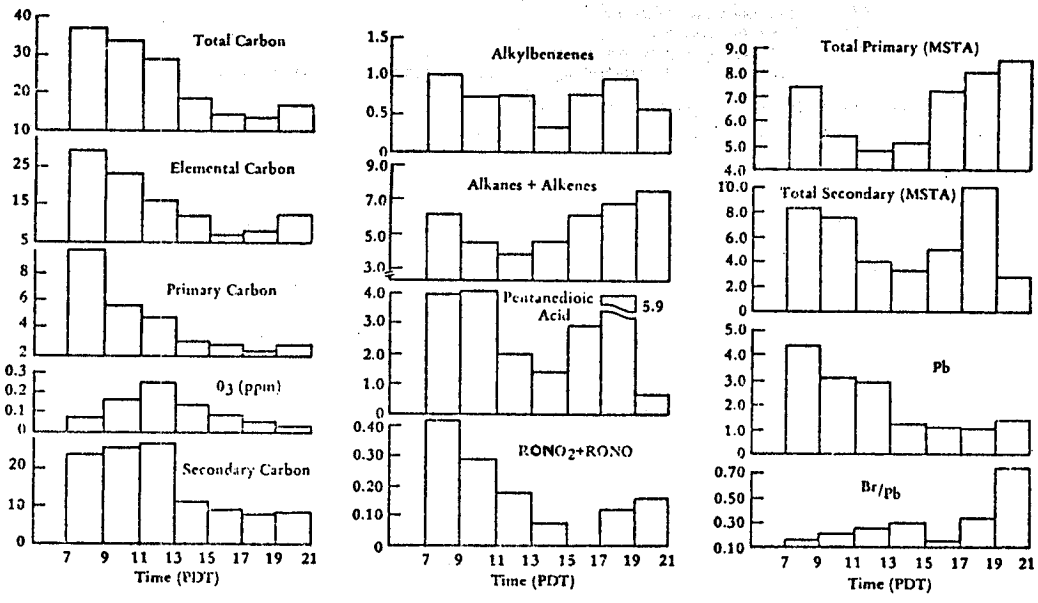

Table 5

COMPARISON OF OBSERVED AND CALCULATED 14-HOUR VALUES[a]

Episode	Site	Calculated/Observed 14-Hour Analyses[b,c] C_T	CEC	BEC	MCC[d]	C_e
July 9	Pasadena	1.11 (.04)	.73 (.13)	.52 (.07)	1.60 (.18)	1.11 (.15)
July 9	Pomona	1.21 (.04)	.75 (.13)	.60 (.08)	1.98 (.22)	1.15 (.13)
July 9	Riverside	1.18 (.04)	.63 (.11)	.53 (.07)	1.52 (.17)	1.29 (.16)
July 10	Pasadena	1.12 (.04)	1.02 (.18)	.59 (.08)	1.59 (.18)	1.08 (.15)
July 10	Pomona	1.10 (.04)	.79 (.15	.67 (.09)	1.85 (.21)	.92 (.11)
July 10	Riverside	1.26 (.05)	.66 (.13)	.68 (.09)	1.65 (.18)	1.21 (.15)
July 11	Pasadena	1.28 (.05)	.64 (.13)	.54 (.07)	1.45 (.16)	1.78 (.29)
July 11	Pomona	1.35 (.05)	.77 (.14)	.87 (.11)	1.72 (.19)	1.34 (.19)
July 11	Riverside	1.16 (.04)	.60 (.12)	.59 (.08)	1.58 (.18)	1.15 (.16)
July 12	Pasadena	1.34 (.06)	.54 (.12)	.65 (.09)	1.68 (.19)	1.46 (.19)
July 12	Pomona	1.09 (.04)	.67 (.13)	.59 (.08)	1.80 (.20)	.93 (.12)
July 12	Riverside	1.34 (.05)	1.12 (.15)	.58 (.08)	1.94 (.22)	1.36 (.15)
	Mean Ratio	1.21	.74	.62	1.70	1.23

a. Calculated from 7, successive 2-hour samples collected simultaneously with the 14-hour sample.

b. C_T = total carbon
CEC = cyclohexane soluble C
BEC = benzene soluble C
MCC = methanol-chloroform soluble C
C_e = elemental C estimated by insoluble carbon, C_T-(BEC + MCC)

c. One sigma value shown below each ratio.

d. Following extraction for BEC.

Discussion by Lara Gundel (Lawrence Berkeley Laboratory

At LBL we have applied the solvent extraction technique of Bruce Appel et al.[1] to ambient particulate samples collected in Berkeley in December 1977 and January 1978. Our intent has been to analyze and compare particulate samples collected under nonphotochemical conditions to the Los Angeles samples collected during the July 1975 episode which Dr. Appel discussed earlier today.[2]

Four quartz hi-vol filters which had been loaded with ambient particulates for 48-72 hours were extracted and analyzed using the established protocol. Three samples of fresh vehicle exhaust collected in the Caldecott Tunnel were also analyzed. Figure 1 shows these results as well as the average of the 14-hour Los Angeles hi-vols presented earlier. Soluble carbon is carbon extracted by successive extraction with benzene and a methanol chloroform (1:2 vv) mixture. Cyclohexane is used to extract a separate portion of each hi-vol, so that soluble carbon can be divided into cyclohexane soluble compounds, labeled nonpolar (PRI), and compounds labeled polar (SEC). The unextracted carbon is obtained by difference, since the total carbon of the original sample is known.

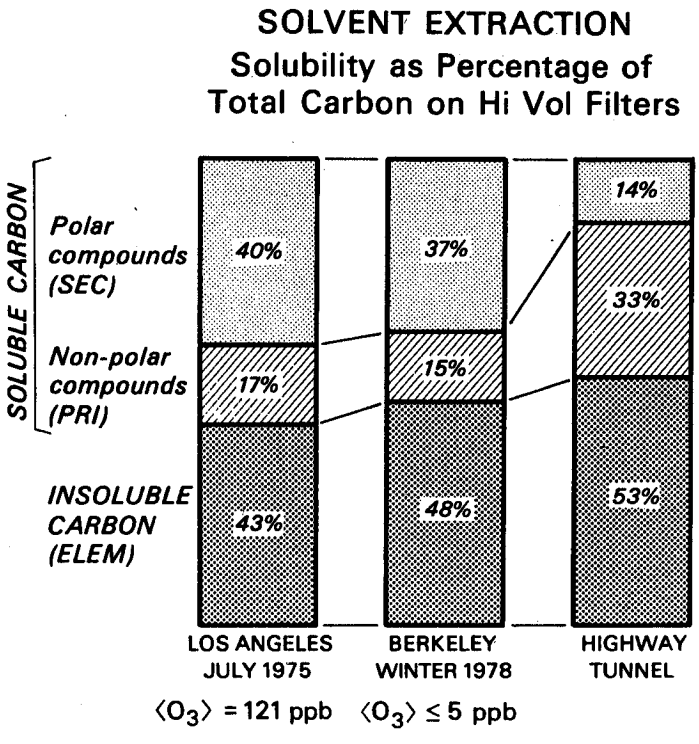

Figure 1.

A large fraction of Berkeley particulate carbon — 37% — can be attributed to polar (SEC) compounds, which is very similar to Los Angeles's polar fraction of 40%. In comparison only 14% of diluted vehicle exhaust from the tunnel is polar. Mean ozone levels during the sampling times are < 5 ppb for Berkeley and 120 ppb for Los Angeles.

These results indicate that polar compounds are associated with ambient particulate matter which has been collected under conditions of low ozone as well as high ozone concentration. The intensity of photochemical activity as monitored by ozone level does not significantly affect the fraction of polar material in the aerosol. Diluted vehicle exhaust appears to contain less polar material than ambient particulate; however, total soluble carbon is similar.

Possible explanations for these results include non-ozone related conversion of adsorbed nonpolar to polar material in the atmosphere, admixture of particulate material from other sources, and conversion of adsorbed nonpolar to polar material during the sampling period. Displacement of adsorbed nonpolar by less volatile polar compounds on the collected filter is also possible during the first 24 hours of sampling.[3] We favor the first of these lines of thought and plan to investigate suitable model systems.

References

1. B.R. Appel, E.M. Hoffer, M. Haik, S.M. Wall, E.L. Kothny, R.L. Knights, and J.J. Wesolowski, Final Report to California Air Resources Board, Contract No. ARB 5-682, "Characterization of Organic Particulate Matter" (1977).
2. B.R. Appel, E.M. Hoffer, E.L. Kothny, S.M. Wall, M. Haik, and R.L. Knights, "Diurnal and Spatial Variations of Organic Aerosol Constituents in the Los Angeles Basin," paper presented at the Conference on Carbonaceous Particles in the Atmosphere, Lawrence Berkeley Laboratory, March 20-22, 1978.
2. H. Della Diorentina, F. de Wiest, J. De Graene, "Determination per spectrometrie infrarouge de la matière organique nonvolatile associée aux particles en suspension dans l'air — II. Facteurs influencant l'indice aliphatique," Atmos. Environ. 9, 517 (1975).

Discussion by P. T. Cunningham (Argonne National Laboratory)

We have heard throughout this opening today of the Conference a number of reports describing the use of very powerful and sophisticated methods to identify specific carbonaceous compounds that may be present in the atmosphere. There is certainly a need for extensive use in this kind of instrumentation, but it must be kept in mind that the costs involved are high and the number of samples that must be analyzed to establish cause-and-effect relationships is extremely large. Thus, it seems appropriate to call for the development of rapid low-cost analytical procedures that can be used to determine specific compounds or classes of compounds in a very large number of samples. With such methods in hand, the detailed characterization provided by the more sophisticated methods could be used to identify materials that are characteristic of certain processes or pollution sources and the low-cost methods used to determine the behavior of these characteristic materials in large numbers of samples. It seems that only through such a two-level approach can we hope to accumulate sufficient data regarding temporal and spatial distributions to answer the numerous questions regarding mechanisms of formation, compound origin, atmospheric transport, and the fate of pollutants.

Discussion by P. T. Cunningham (Argonne National Laboratory)

I believe that there is a need for all of us to be a little more careful in the use of our terms in discussing carbonaceous materials. I am not sure that we always make it clear what we are talking about. Such terms as benzene soluble carbon compounds, graphitic carbon, noncarbonate carbon, total carbon, hydrocarbon, and so forth are not always sufficiently precise in their usage. For example, it appears that benzene soluble carbonaceous material may include hydrocarbons, polymeric carbonaceous material, and organic compounds containing a variety of hetero-atoms. It really is difficult to come up with terms that will have the same meaning for all of us since we use such a wide variety of analytical techniques and procedures; but, nevertheless, we should address ourselves to the problems of establishing accepted definitions or, at the least, be sure that the way in which we are using terms cannot be misunderstood within the audience we are addressing.

Transport, Formation, and Reactions

LONG DISTANCE TRANSPORT OF CARBONACEOUS MATTER

Cyrill Brosset
Swedish Water and Air Pollution Research Laboratory
Gothenburg, Sweden

ABSTRACT

In Sweden carbonaceous particles have been measured during many years. Sampling has been carried out in urban as well as in rural sites. Measurement results from rural sites have been compared with wind-trajectories. Noticeable flows of carbonaceous particles from Central Europe towards Scandinavia have been observed. The size of long-distance transported carbonaceous particles are in general less than 2 µm (aerodynamic diameter). They are probably generated mainly through coal combustion and contain, as a rule, more or less acid ammonium sulphate. They have catalytic ability to oxidise SO_2. In this respect they differ from in Sweden emitted particles which mainly derive from oil combustion. Thus in the air above a Swedish urban site the oxidation of SO_2 is faster in the presence of larger concentrations of long-distance transported carbonaceous particles than otherwise. The same type of catalytic effect has been found even in precipitation. At the present, it is not clear if the catalytic effect of the particles should be ascribed to their concentration of graphite or of certain metals.

Introduction

Black particles and SO_2 were long regarded as the major air pollutants in urban areas. They were consequently the subject of comprehensive measurements. Today a large bulk of data from different parts of the world on so called soot concentrations is available.

So far, these data have been regarded with a certain amount of scepticism. One reason is that the measurements have been carried out with somewhat dubious methods; another is that the substance (soot) measured is generally felt to be ill defined.

However, it is agreed that soot measurements could be used as an index of the general pollution.

Lately, however, it has been shown[1)] that the black component in soot is most likely graphite and thus a defined phase. This means that black, carbonaceous aerosols must have properties which are to some part determined by the concentration of graphite. The effect of the deposition of black carbonaceous particles observed in different recipients may therefore be associated with these properties mentioned.

A renewed interest seems to have resulted to study the black carbonaceous particles, primarily with a view to identifying the properties dependent on the graphite concentration of the particles. Of course, such investigations require entirely different methods than those used previously (and still being used) to determine the "soot concentration" of the air. However, also the methods used so far may provide certain information of interest. Among other things, they have led to the identification of episodes, a case of increased particle concentration caused by long-distance atmospheric transport. This, in turn, has initiated a closer examination of the chemical and physical properties of the long-distance transported black particles. A review of some investigations of this kind is given below.

Extent of the review

The purpose of the present paper is to provide a compilation of such previously obtained measurement results as will illuminate the significance of long-distance transport of carbonaceous particles.

The measurement series discussed were carried out at sampling stations located at the Swedish south and west coasts. Four of these stations were placed at the light-houses Nidingen, Kullen, Falsterbo and Sandhammaren. More detailed measurements were made at the monitoring station at Råö, a peninsula 10 km north-east of Nidingen and approx. 40 km south of Gothenburg. Data have also been included from a station located in the western part of the island Hisingen, 20 km north-west of central Gothenburg. Location of sampling stations is shown in the map outline in Fig. 1, including the letters that will be used forthwith to designate these stations. The above-mentioned measurement series date back to October, 1966. They comprise primarily measurements of "soot concentrations" with the OECD-method[2]. The results obtained are discussed in the light of meteorological observations.

Finally, in connection with a discussion of the effects to which carbonaceous particles may give rise, measurement results concerning their composition with respect to water-soluble substances and their catalytic properties will be presented.

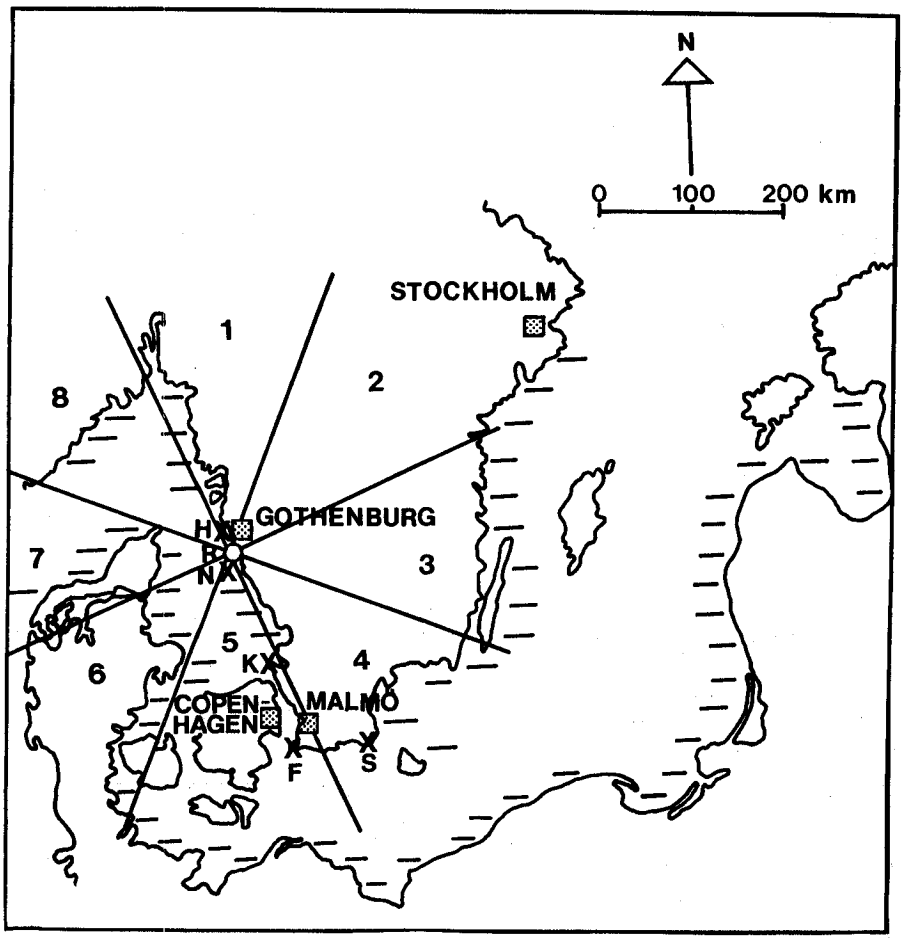

The figures (1-8) indicate trajectory sectors

Fig. 1.

- communities
- monitoring station
- sampling stations

H	Hisingen	Stockholm, pop. 0.7 million
R	Råö	Gothenburg, pop. 0.5 million
N	Nidingen (lighthouse)	Copenhagen, pop. 1.6 million
K	Kullen "	Malmö, pop. 0.3 million
F	Falsterbo "	
S	Sandhammaren "	

Carbonaceous particles (soot) and their long distance transport

Methods. As in most other countries "soot-measurements" in Sweden are carried out in several communities. The method used is the so-called OECD-method[2], based on drawing approx. 2 m^3 of air/24 h through a white filterpaper, and determining the reflectance of the resulting stain. Gravimetrically determined calibration curves are then used to convert reflectance to concentration of soot in $\mu g/m^3$ air.

Many objections can be raised against such a method. However, it is a simple and inexpensive method ghat gives remarkably good reproducibility and consistency of the results obtained. This is most probably due in part to the graphite concentration of the particles being about proportional to particle mass in the cases when the particles have been generated in the combustion of fossil fuels and in part to the frequent predominance of such particles in the fine fraction of the total particulate air pollution.

Concentrations of black carbonaceous aerosols at the Swedish south and west coasts

The reason why the "soot concentration" in Sweden has become the focus of quite extensive measurements is the suspicion arising in 1965 that a considerable part of these aerosols were from sources outside of Sweden. This gave rise to projects in the period 1966 - 1973 comprising, i.a. determination of daily means of black aerosol (soot) at the sampling stations in Fig. 1. It was found, as was expected, that the concentrations of black particles in the summer months were everywhere low. In winter, i.e. during the heating period, on the other hand, the concentrations were considerably higher and also dependent on the location of the sampling stations. Table 1 contains a summary of these half-year values. They actually represent the result of over 12,000 measurements.

Table 1. Winter and summer mean values of black aerosol (soot) in μg/m^3 during the period 1966-1973 at the stations F, K, N, H and S. (See Fig.1) w indicates the period October-March; s the period April-September.

Year		F	K	N	H	S
66-67	w	12.0	9.9	5.5	7.6	9.2
67	s	4.9	4.3	2.1	2.5	3.4
67-68	w	8.8	6.5	4.2	9.7	6.0
68	s	4.1	1.4	1.7	4.0	1.4
68-69	w	13.5	9.9	8.4	15.0	10.5
69	s	4.4	2.3	2.2	6.3	2.8
69-70	w	10.1	7.4	4.9	19.9	6.3
70	s	3.4	2.0	1.1	6.3	1.6
70-71	w	9.9	7.1	3.7	13.0	8.8
71	s	3.1	2.5	1.6	4.9	3.0
71-72	w	10.7	9.3	5.6	15.2	8.3
72	s	3.4	2.4	1.7	7.0	2.3
72-73	w	10.8	8.5	5.9	10.9	9.4
73	s	3.4	2.6	2.2	5.2	3.0
Grand	w	10.8	8.4	5.5	13.0	8.4
average	s	3.8	2.5	1.8	2.5	2.5

Grand averages from Table 1 will also be found in Fig. 2. As the stations are situated more or less on a straight line in almost north-southerly direction, the abscissa is the distance in km from the southernmost station F.

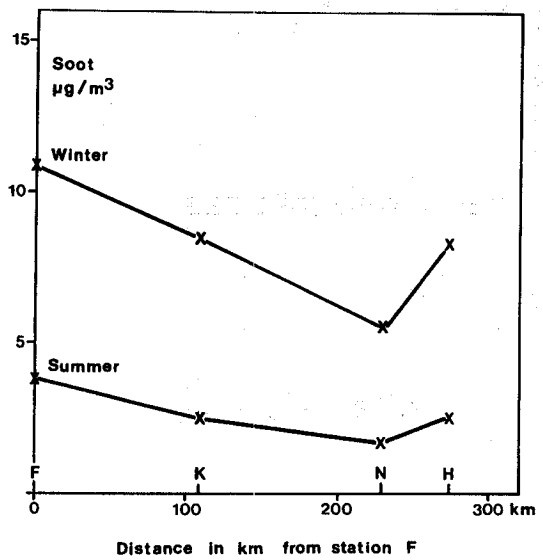

Fig. 2. Winter and summer mean values (grand averages) of black aerosol (soot) in μg/m^3 for the period 1966-1973 at stations F, K, N and S (see map in Fig. 1.)

Using the map in Fig. 1 the result in Table 1 and Fig. 2 can be summarised as follows.

Station S is relatively far from any large local sources. The values obtained here may thus be said to be representative of the background level of black aerosol in southern Sweden.

Station F is not far from Copenhagen and Malmö. It should therefore be affected by these large source areas. Higher values were actually recorded here compared to station S.

Stations K and N have no large sources in their vicinity. Here it is interesting to note the decrease in soot concentration which seems to occur when moving north from the south.

Station H, near Gothenburg, is affected during south-easterly winds by the emissions from the central parts of the city. In addition, it is exposed to local emissions from the near-by industrial area. The soot concentration here is also clearly higher than at station N. The latter may be said to represent the background level in a belt located about 300 km north of station S.

Transport of black carbonaceous aerosol

The measurements reported above indicate that transport of black particles occurs from sources in the south, in a northerly direction. As this atmospheric transport seems to cover vast distances, it is likely that it is caused by upper-level winds. The ground-level concentrations of the black particles are then built up primarily through turbulent diffusion since their aerodynamic diameter is usually below 2 μm.

These conclusions led to investigations of the variation in the concentration of black aerosols with the direction of upper-level winds. The first study of this kind was carried out by Rhode et al.[3] with data from stations S, F and N from September through December 1969. They found that the concentration at the three stations was highest at upperlevel winds from the southern sector.

When 72-h trajectories for air movements at the 850 mb level were made available through calculations carried out at the Norwegian Institute of Air Research (Nilu), more detailed studies of long distance transport of different airborne particle types became possible. Part of the data material thus collected is compiled in Fig. 3 a-f. The data comprise measurements of daily mean values of soot concentration at stations S, N and H during the period October 1972 - March 1973. For stations S and N it is also indicated in what sectors of the wind-rose diagram the 72-h trajectories predominated for the air parcel arriving at the sampling station at 18^{00} GMT on the day the respective sample was taken. The sector notations are given in Fig. 1. A dash means that the trajectory was short and/or very curved.

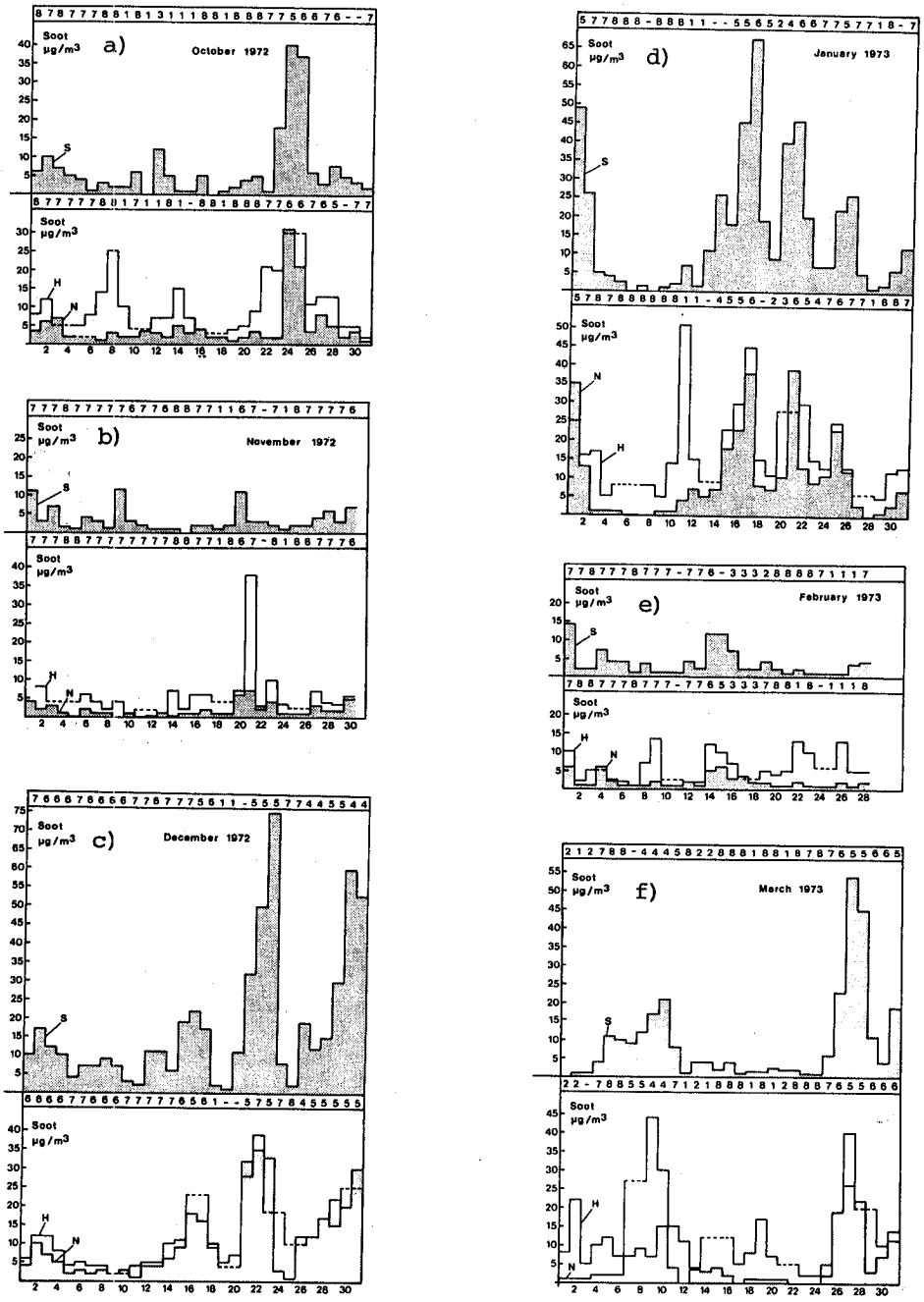

Fig. 3 a - f. Daily mean values of soot in $\mu g/m^3$ at stations S, N, and H as well as trajectory sectors for S and N (indicated by figures). Dash - indicates short trajectory or stagnation. Dashed line -- indicates mean value of several days.

Fig. 3 a-f illustrates rather well the build-up of the concentration level of black aerosol in southern Sweden. As will be seen, at stations S and N all peak concentrations are found in connection with sectors 5-7, i.e. at transport from the south. This also explains the fact that the concentration at station N is lower than at station S.

Fig. 3 a-f also show concentrations observed at station H. A comparison between these and corresponding values from station N gives an idea of the part of the total concentration made up of local contributions in the area in question.

As regards the distance to the sources responsible for the long-distance transported particles observed in Sweden there are as yet no conclusive investigations. Rhode et al.[3] made an assessment and arrived at distances of approx. 1000 km.

Some information can also be obtained from the OECD-study on long range transport of SO_2, if one assumes that the same sources are responsible for SO_2 and soot emissions.[4]

Certain chemical and physical properties of carbonaceous aerosols

The content in black carbonaceous particles of certain other components. Around 1969 the soot measurements at the above-mentioned stations were supplemented by determinations of sulphur concentration in the samples, using X-ray fluorescence[5]. It was thereby ascertained that maxima in soot concentration were practically always accompanied by maxima in sulphur concentration[6]. On the other hand, it was found that the opposite need not be the case. Later[7], it was shown that sulphur in carbonaceous particles is largely present as somewhat acid ammonium sulphate.

In Table 2 and Fig. 4 will be found monthly mean values of soot and sulphur concentrations recorded at station S in the winter season 1972-1973. The equation of the inserted regression line is:

$$y = 0.477\,x + 5.637 \qquad (r = 0.986)$$

where x is soot concentration and y is sulphur concentration expressed as $(NH_4)_2SO_4$ in $\mu g/m^3$.

Table 2. Monthly mean values of black aerosol (soot) and sulphur expressed as $(NH_4)_2SO_4$ in $\mu g/m^3$.

Station S, November 1972 - March 1973

		soot	$(NH_4)_2SO_4$
1974	Oct	9.1	9.9
	Nov	3.5	6.9
	Dec	17.5	13.4
1973	Jan	15.8	13.7
	Feb	3.7	7.3
	March	6.6	9.4

As will be seen, it seems possible for particulate sulphate to occur without the presence of soot.

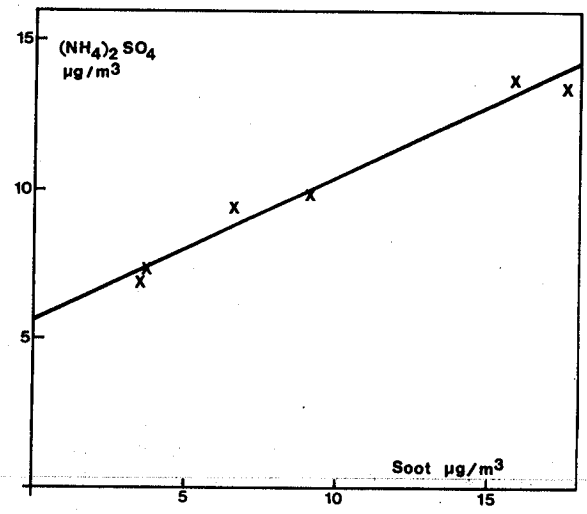

Station S, Oct. 1972 – March 1973

Fig. 4. Concentrations of black aerosol (soot) and sulphur expressed as $(NH_4)_2SO_4$ in $\mu g/m^3$.

A more detailed picture of the ion composition found as a rule in black carbonaceous particle is given in Table 3[8].

Table 3. Ion composition in black carbonaceous particles at Råö, autumn 1975.

Date 1975	$\mu g/m^3$ soot	n equiv./m^3 SO_4^{2-}	NO_3^-	$SO_4^{2-} + NO_3^-$	NH_4^+	H^+	$NH_4^+ + H^+$
Oct 25	13	393	58	451	405	5.6	411
31	11	193	21	214	232	2.7	236
Nov 1	32	151	22	173	164	4.1	168
2	39	627	40	667	604	19.9	624
16	14	177	11	187	213	2.8	216
17	14	195	6	201	210	3.8	214
25	24	325	40	365	452	5.4	457
26	36	402	64	466	458	9.4	467

Of interest in this context is the question of whether the observed sulphate concentrations are, like the graphite concentration (expressed as soot), to be regarded as primary emissions or whether the sulphate , to a greater or lesser part, has been formed through atmospheric reactions.

The catalytic properties of carbonaceous particles. In September 1969 observations were made in several places in Sweden of a distinct increase in soot concentration lasting for a number of days. It was a clear result of long distance transport from the south. At the same time, measurements in Swedish towns showed that soot concentration maxima were accompanied by a drastic drop in SO_2 concentration, often below the detection limit (then at approx. 5 $\mu g/m^3$) [6]. With this observation, suspicions arose that the aerosol brought into city air had the ability to catalyse oxidation of SO_2 to sulphate.

This hypothesis was later tested on a larger data material [9]. This comprised daily means of soot and sulphate in Gothenburg, at Råö and partly at a station 45 km north of Gothenburg; it also included daily means of SO_2 in Gothenburg. The data cover parts of the period 1972-1975.

The objective of the investigation was to determine the relationship, if any, between the concentration of black particles in and outside of Gothenburg, and sulphate formed in Gothenburg. For this purpose, the quantity q was defined as follows

$$q = \frac{\Delta\ SO_4^{2-}}{SO_2\ (G) + \Delta\ SO_4^{2-}}$$

$\Delta\ SO_4^{2-}$ is here the difference between the sulphate concentration (as daily mean) observed in central Gothenburg and the sulphate concentration observed in areas outside of Gothenburg not affected by local sources.

$\Delta\ SO_4^{2-}$ thus corresponds to the SO_2 concentration which, during the 24 h sampling period was oxidised to sulphate. SO_2 (G) are daily means of SO_2 recorded in central Gothenburg.

The denominator in the above expression is consequently the SO_2 concentration which would have been recorded if no oxidation had occurred. Thus q is the fraction of the originally existing SO_2 which during the 24 h period is oxidised to sulphate.

Calculated values of q were then compared with observed mean values of soot both in Gothenburg and at station N. The result of such a measurement series is given in Table 4.

Table 4. Mean values of q (in %), of soot concentration at Nidingen – P (N) – and in Gothenburg – P (G) – expressed in $\mu g/m^3$.
n is the number of daily means measured and T is the trajectory sector as per Fig. 1
Data from October - December 1972 and January, March and October 1973.

T	n	q	P (N)	P (G)	P (G)-P (N)
6-4	24	14.5	17.2	24.4	7.2
7-8	63	7.8	3.1	14.8	11.7
1-3	8	5.1	2.0	30.7	28.7

Data in Table 4 indicate that an increase in concentration of black particles in Gothenburg caused by long distance transport from the south brings about an increase in the rate of oxidation of SO_2.

Black particles produced within Gothenburg do not seem to have this effect. This interesting result has been confirmed also in another way. In connection with certain other investigations, a simple method was developed for the determination of the catalytic ability of solutions and suspensions to oxidise SO_2 [10]. The method is based on the exposure, under defined conditions, of a liquid surface to a flow of air with a known SO_2 concentration, and determination of the part remaining in the liquid in the form of sulphate after a certain period of exposure. The method has mainly been used for determining the catalytic activity of fly-ash from different fossil fuels. It has also been used to quantify the catalytic ability of precipitation samples. A series of such samples was taken during the summer of 1977 at a station about 50 km north-east of station K, and analysed in the manner mentioned. The results obtained expressed as annual means for the different trajectory sectors (Fig. 1) are shown in the form of a wind-rose diagram in Fig. 5.

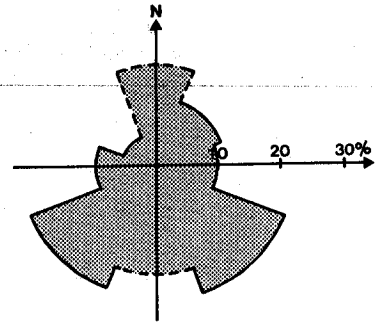

Fig. 5. Catalytic activity of precipitation in % for eight trajectory sectors. Sampling location 50 km NE station K. 1977.
Dashed line indicates unsatisfactory statistics.

It will be seen from this figure that precipitation that has washed out air masses coming from the south seems to acquire an increased ability to oxidise SO_2.

As long-distance transported black particles seemed to have catalytic ability in connection with SO_2 oxidation, it was of interest to establish whether these particles contain catalytic metals, primarily Mn and Fe. Analysis through neutron activation of samples taken at station R gave the results listed in Table 5.

Table 5.
Concentrations of soot, sulphate, manganese and iron in particle samples from Råö, February – March 1975

Date		µg/m^3	n mole/m^3	ng/m^3	
1975		soot	SO_4^{2-}	Mn	Fe
Feb	11	3.5	122	15	<10
	12	45.3	290	550	710
	13	16.2	107	153	<10
	14	∿0	77	20	<10
March	1	2.0	140	19	<10
	2	19.7	300	148	380
	3	6.0	77	14	250
	4	26.6	200	145	210
	5	23.4	176	87	300
	6	3.6	51	19	60
	7	14.2	136	142	70
	8	7.8	61	43	<10
	9	6.3	75	32	<10
	20	∿0	10	1	<10
	21	∿0	15	10	<10
	22	1.3	22	16	<10
	23	2.1	27	<1	<10

This table shows that the concentrations of soot, Mn and Fe, as regards magnitude, seem to be interrelated. The increase in oxidation rate observed at concentration peaks of long-distance transported black particles may thus be due to an increase in the concentration of particle-borne Mn and Fe.

On the other hand, tests in the U.S.A.[11], and also our own laboratory experiments, have shown that active carbon (graphite) in this context may function as a very active catalyst.

It is therefore not clear if the catalytic effect of long-distance transported black particles observed in Sweden should be ascribed to their concentration of graphite or of certain metals. Also, the possibility of a combined effect can not be dismissed.

Summary

It was established that the presence of black airborne particles in the rural parts of southern Sweden are largely a result of long distance transport from the south. This transport also contributes noticeably to the pollution load in built-up areas. The black carbonaceous particles contain, as a rule, weakly acid ammonium sulphate and nitrate.

In the winter half of the year there seems to be an approximately linear relationship in the long-distance transported aerosol between soot concentration (graphite concentration) and sulphate concentration. The black long-distance transported aerosol contains, i.a. the metals Mn and Fe in concentrations approximately proportional to the aerosol mass. The aerosol has catalytic ability to oxidise SO_2. It is at present unclear which phases that are responsible for this ability.

References

1 H. Rosen, A.D.A. Hansen, L. Gundel and T. Novakov; Identification of the graphitic carbon component of source and ambient particulates by Raman spectroscopy and an optical attenuation technique. Proceedings of the Conference on Carbonaceous Particles in the Atmosphere, March 20-22, 1978. National Science Foundation and Lawrence Berkeley Laboratory, California 94720, USA

2 Methods of Measuring Air Pollution of the Working Party on Methods of operation and Development, Paris, 1964. OECD publication No. 17913, January 1965

3 H. Rodhe, C. Persson, O. Åkesson; An investigation into regional transport of soot and sulfate aerosols. Atm. Env. 1972, Vol. 6, p. 675.

4 The OECD Programme on Long Range Transport of Air Pollutants, Measurements and Findings, OECD, Paris 1977

5 C. Brosset, Å. Åkerström: Atmospheric Environment 1972, Vol. 6, pp. 661-673

6 C. Brosset, A. Nyberg in Proceedings of the Second International Clean Air Congress, Washington, December 1-6, 1970. H.M. Englund, W.T. Beery Eds. (Academic Press, New York and Lindong, 1971) pp. 481-489

7 C. Brosset, Ambio 2, 1973, pp. 2-9

8 C. Brosset, Ambio Vol. 5, No. 4, 1976, pp. 157-163

9 C. Brosset in Proceedings of the International Conference on Environmental Sensing and Assessment (ICESA), Las Vegas, Nevada, September 14-19, 1975 (Institute of Electrical and Electronics Engineers, Inc. 345 East St. New York, 1976) IEE Catalogue No. 75-CH 1004-1 ICESA, Vol. I.

10 C. Brosset: Measurement of catalytic activity in SO_2-oxidation. Paper presented at International Symposium on Meteorological Aspects of Atmospheric Pollution, Leningrad, March 10-19, 1977

11 S.-G. Chang, R. Brodzinsky, R. Toossi, S.S. Markowitz and T. Novakov: Catalytic Oxidation of SO_2 on Carbon in Aqueous Suspensions. Proceedings of the Conference on Carbonaceous Particles in the Atmosphere, March 20-22, 1978, National Science Foundation and Lawrence Berkeley Laboratory, California 94720, USA

CARBON IN DENVER'S URBAN PLUME

J.L. Durham and R.K. Patterson
U.S. Environmental Protection Agency
Environmental Sciences Research Laboratory
Research Triangle Park, North Carolina 27711

and

R.G. Draftz
IIT Research Institute
Chicago, Illinois 60616

ABSTRACT

Field data collected in Denver during air pollution episodes in November 1971 and November 1973 are examined. Optical and scanning electron microscopy of size resolved aerosol samples collected downwind of Denver in the urban plume showed that the coarse aerosol principally consists of mineral dust, while the submicrometric fraction is dominated by auto exhaust aerosols. Chemical analyses of the fine aerosol fraction revealed that carbon (total), nitrate, sulfate, and lead accounted for 54-70% of the mass on episode days, and only 33% on a clean day in 1971. Chemical analysis of two combined samples for 16 and 17 NOV 73 accounted for 70% of the fine aerosol mass as: nonpolar organics, sulfates, lead, nitrates, and ammonium. The nonpolar organics consisted of 76% carbon, which permitted elemental (amorphous/graphitic) carbon concentrations to be estimated at 1.7-4.4 micrograms/m^3 for episode days. The results tend to indicate little or no photochemical activity in Denver's urban plume.

INTRODUCTION

What are the chemical and morphological forms of carbon in aerosols in the atmosphere? This question is being asked with greater frequency. Unfortunately, there have been few studies that have established a chemical balance for carbon and identified its principal morphological forms in fine (<1 μm) and coarse (>1 μm) aerosols in urban environments. We have not specifically directed field studies at identifying the role of carbon, but we have performed field studies in several urban areas to deduce the source types for atmospheric aerosols. Generally, we have used such techniques as (a) quantitative chemical analysis on size-resolved aerosol samples and total filter samples, and (b) light and scanning electron microscopy. Although our chemical data do not include values for elemental amorphous or graphitic carbon, C(O), we are able to imply an upper limit for the Denver aerosol. Figure 1 shows the location of our field sites in 1971 and 1973.

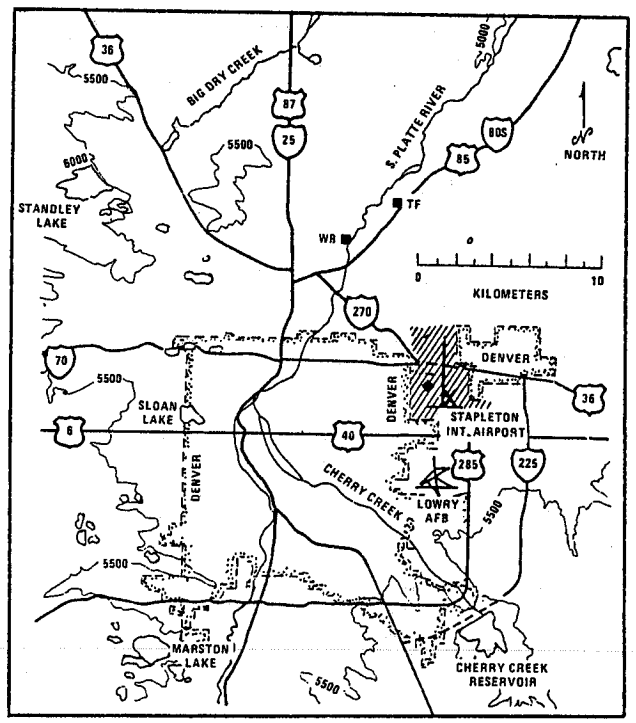

Figure 1. Map of the Denver area. The 1971 sampling site was at Welby (WB), which is approximately 10 kilometers northwest of Stapleton International Airport. The 1973 sampling site was at a trout farm (TF), about 10 kilometers north of Stapleton. The sampling sites are shown as squares (■). Major highways and elevation contours (in feet above mean sea level) are also shown.

FIELD MEASUREMENTS

Denver, 1971

In 1971, we performed a field study in Denver to investigate the origin of the aerosol in the urban plume. Local interest in this plume was intense because of its brownish color when viewed toward the northeast from Denver[1,2] during the fall and winter months. Prior to the 1971 experiment, it was generally speculated that this urban plume was of photochemical origin, and light absorption by nitrogen dioxide was suggested as the cause of the brownish appearance. Subsequent analysis of aerosol size distribution data[3] and microscopy indicated the bimodal character of the aerosol, and the dominance of

the suspended mass concentration by coarse mineral particles. The experimental measurements of aerosol size distributions by Willeke et al[3] demonstrated that the surface area distribution has a steep negative slope over the particle size range of 0.05-0.5 μm. This behavior is sufficient to produce the brown coloration due to selective scattering by aerosols of light on the blue end of the visible spectrum.[4]

High volume samplers were operated with and without Andersen heads, a 4-stage, 20 cfm impactor designed for use on the high volume sampler, and calibrated by Eaton, et al.[5] The filters from both hivol configurations were analyzed for benzene soluble organics, total carbon, total hydrogen, total nitrogen, nitrate, ammonium, lead, and sulfate. Table 1 reports the results of these analyses for the coarse and the fine aerosol. The data illustrate the history of the episode. The episode began on 10 Nov 71, and reached its peak on the 11th. Dispersion increased on the 12th, and the 13th was a clean day. Another episode began to form on the evening of the 14th. Of the species identified in the fine aerosol, carbon was present in the greatest amount. The non-polar organic carbon extracted by benzene appears to account for a substantial (but unknown) portion of the carbon. Of course, of great interest is the chemical composition of the fine aerosol. It can be seen from the data in Table 1 for 10,11,12,13,14 Nov 71, that 66%, 61%, 54%, 33%, 70%, respectively, of the fine aerosol mass as sulfate, nitrate, ammonium, carbon (total), and lead was accounted for. Not included in our analyses are organic H, N, and O. On 13 Nov 71, the date for which we account for only 33%, the wind was from the north and the samplers were not in Denver's urban plume.

Table 1. Chemical analysis of the filters for the total and the fine (<0.93 μm) aerosol fraction. 1971

NOV 1971:	10	11	12	13	14
	Mass, μg/m^3				
Carbon[a]					
Total Sample	11.8	20.6	14.5	5.3	12.5
Fine Fraction	10.6	11.0	7.7	5.0	7.0
BSO[b]					
Total Sample	10.7	14.6	11.5	4.7	7.7
Fine Fraction	9.2	11.1	6.8	3.6	6.1
Hydrogen					
Total Sample	1.1	2.9	1.7	0.41	1.5
Fine Fraction	1.0	0.85	0.64	0.44	0.65
Nitrogen					
Total Sample	1.0	2.1	1.1	0.25	0.94
Fine Fraction	1.0	0.89	0.52	0.14	0.64
Lead					
Total Sample	3.2	4.9	3.2	1.7	2.4
Fine Fraction	1.9	2.7	1.9	0.89	1.5
Sulfate					
Total Sample	3.8	3.9	3.3	2.4	2.2
Fine Fraction	2.3	2.3	2.1	2.0	2.0
Nitrate					
Total Sample	4.8	5.0	3.4	1.0	2.6
Fine Fraction	3.2	3.6	1.5	0.68	1.9
Ammonium					
Total Sample	0.38	0.78	0.41	0.24	0.22
Fine Fraction	0.38	0.50	0.21	0.14	0.20
Suspended Mass					
Total Sample	140	196	160	80	79
Fine Fraction	28	33	25	26	18

[a] Includes organics, amorphous graphitic carbon, and carbonates.
[b] Benzene soluble organics.

Optical and scanning electron microscopy were used to obtain the morphology of the aerosol.[6] The samples collected by an 8-stage Andersen impactor (operated at 1.0 cfm and with glass fiber collection surfaces) were morphologically characterized, and the results are in Table 2 for 10 Nov 71. The aerosol morphology as a function of size was the same for 10,11,12,13 and 14 Nov 71, even though 13 Nov was a clean day and that sample was not taken in the urban plume. Generally, minerals dominated the coarse aerosol population down to 1-2 micrometers; below that size, auto exhaust particles became the primary component of the aerosol. The fractionated samples were sufficiently resolved according to morphological types that semi-quantitative microscopy combined with gravimetric and chemical analyses were sufficient to establish the importance of source type to both aerosol fractions. The mass distributions for 10 Nov 71 are presented in Table 3. Table 2 shows that the primary components of the submicrometer fraction are particles derived from auto exhaust. Thus, the combination of chemical analysis of the fine aerosol and microscopy have demonstrated that auto exhaust is the primary contributor to the aerosols with diameters less than 1.0 μm, which probably dominate light scattering in Denver's urban plume.

Less important source types are: mineral dust, tire dust, coal combustion products, and fuel oil combustion products. The questions left unanswered are: (1) are photochemically produced aerosols important to the visibility problem, and (2) what is the role of elemental (amorphous/graphitic) carbon? The 1971 study cannot answer these questions because we did not investigate the nature of the benzene soluble organic and the extent of sulfate and nitrate artifact for these samples is unknown.

Denver, 1973

A second study was conducted in 1973 to provide more physical characterization of the urban plume, such as wind flow measurements, aerial plume mapping, and investigation of the light scattering properties of the aerosols. Most of these results have been reported in two volumes of a proceedings[1,2] and a third volume[8] which will be published in 1978. In regard to the role of carbon, we found that the polarizing light and scanning electron microscopy indicated the same source types for the coarse and for the fine aerosol as found in 1971; that is, auto exhaust particles dominate the aerosol mass below 1 μm. The filters collected with high volume samplers with and without an Andersen head

Table 2. Estimated weight percent of particle types on impactor stages. 10 NOV 71

Stage :	0	1	2	3	4	5	6	7	Filter
Diameter[a], μm:	>11	11-6.9	6.9-4.3	4.3-2.6	2.6-1.7	1.7-0.68	0.68-0.28	0.28-0.11	<0.11
Particle Types									
quartz	P	P	M	m	t				
limestone	t	m	M	P	P	P	t		
mica	t	t							
mica needles	t	m	M	M	m	t			
tire dust	m	t	t	t	m				m
auto exhaust						P	P	P	P
coal fragments	t	m	m	m					
flyash (spheres)	t	t	t	t	t		t		
oil soot					t				
iron oxides	t	t	t	t	t				
magnetic metal	t	t							
cornstarch	t	t	t						
paper fibers									
plant parts	t	t	t	t					

P = >25%, M = 5-25%, m = 0.5-5%, t = <0.5% (Estimated mass percentaged determined by the microscopist.)

Table 3. Mass distribution from impactor. 10 NOV 71

Stage :	0	1	2	3	4	5	6	7	Filter
Diameter[a], μm:	>11	11-6.9	6.9-4.3	4.3-2.6	2.6-1.7	1.7-0.68	0.68-0.28	0.28-0.11	<0.11
Mass, mg/m^3 :	39.7	21.5	20.4	19.1	21.8	7.8	6.1	7.3	18.1
Mass % :	24.6	13.3	12.6	11.8	13.4	4.8	3.8	4.5	11.2

[a]Size intervals were estimated from Hu's[7] values; See reference 8 for details. Microscopy showed that the fractionation efficiency of the impactor was not good for aerosols below 0.5 μm diameter. and this was attributed to the fact that glass fiber filters were used as impactor stage collection surfaces.

impactor were chemically analyzed. The data for seven air pollution episodes are shown in Table 4. For the fine fraction, we have data for four episode days. Carbon analyses were not performed on any of the samples collected during the 1973 study. For the samples collected on 14,16,17,21 Nov 73, we have accounted for 18-27% of the mass of the fine aerosol. However, the fine aerosol for 16 and 17 Nov 73 episode days were combined and subjected to functional class analysis by Miller et al[9]. These samples were extracted with methylene chloride to recover the nonpolar organics. The methylene chloride-extracted nonpolar organics were 45% of the fine aerosol mass. Insufficient material remained after the methylene chloride extraction to permit an extraction with dioxane for the polar organics. Miller et al.[9] stated that the expected dioxane extract would be insignificant compared to the dioxane blank. However, the infrared analyses performed on the methylene chloride extract by Miller et al.[9] show that the band corresponding to peroxides and organic carbonates (1770 cm^{-1}) was not present, and the bands corresponding to organic nitrate (1660 cm^{-1} to 1625 cm^{-1}) were low. These results indicate little or no photochemically derived aerosol in the sample. The analysis results of the nonpolar organics after pyrolysis were: 76% C, 10% H, 0.8% N, and 12% O (estimated by difference). Unfortunately, a total carbon analysis was not made for these two filter samples. However, for the combined samples of 16 and 17 Nov 73, we are able to account for 70% of the fine aerosol mass as: 45% nonpolar organics, 14% sulfate, 8% lead, 3% nitrate, and 0.4% ammonium.

An estimate of the elemental carbon, C(O), present in 1971 can be made by making two assumptions:

1. The aerosol character for 1971 and 1973 is the same.

2. Benzene (1971) and methylene chloride (1973) extracted the samples with the same efficiency, since the nonpolar organics of the 1973 sample were in a highly reduced form, similar to primary auto exhaust.

If the assumptions are valid, then the benzene soluble organic (BSO) extracted from the 1971 samples should have a carbon content accounting for 76% by weight. Using the values in Table 1, C(O) may be estimated by subtracting 76% of the BSO mass from the total carbon mass. These estimated concentrations of C(O) are presented in Table 5; the range of values is 2.3 to 3.6 μg/m^3. From these 1971 data, the ratio of estimated C(O) to lead was found to be 1.0-2.5, with an average of 1.7. Using this ratio the estimated C(O) concentration for fine aerosol for the 1973 episodes were 1.7 to 4.4 μg/m^3 (see Table 6).

CONCLUSIONS

Microscopy of aerosol samples collected with a cascade impactor and chemical analysis of the fine aerosol have demonstrated that auto

STRUCTURE-ACTIVITY RELATIONSHIPS IN POLYNUCLEAR AROMATIC HYDROCARBONS*

Stephen S. Hecht, Edmond J. LaVoie and Dietrich Hoffmann
American Health Foundation
Naylor Dana Institute for Disease Prevention
Valhalla, N.Y. 10595

ABSTRACT

Current concepts on the metabolic activation and carcinogenicity of polynuclear aromatic hydrocarbons are reviewed. A major process in metabolic activation of some common PAH carcinogens, such as benzo(a)-pyrene, benz(a)anthracene, and chrysene and their methylated derivatives is apparently formation of angular ring diol-epoxides in which one carbon terminus of the epoxide is in a bay region position. Among the four to six ring unsubstituted PAH, one structural requirement for carcinogenicity is a free peri position adjacent to an angular ring. Substitution of a methyl group in the angular ring may decrease carcinogenicity while substitution at other positions may increase carcinogenicity, especially when the molecule becomes non-planar. Three bioassay systems - complete carcinogenicity and tumor initiation on mouse skin, and mutagenesis in S. typhimurium TA 100 were compared for certain PAH derivatives. Complete carcinogenicity assays were the most sensitive to minor structural changes. Tumor initiation and mutagenicity assays had the advantages of lower material requirements and more rapid results.

INTRODUCTION

The metabolic activation and mechanism of action of polynuclear aromatic hydrocarbons (PAH) has been the subject of intense research beginning with the earliest studies on the structural requirements for the carcinogenicity of coal tar derivatives. A number of reviews have thoroughly discussed developments in this field, especially in the period up until 1975 [1-8]. In the last 2-3 years, remarkable progress has been made towards a thorough understanding of the mechanism of PAH carcinogenesis. This has been due, in part, to the development of new techniques such as high pressure liquid chromatography and mutagenicity assays with *S. typhimurium* which are particularly well suited to studies of PAH activation. In addition, organic chemical methods of synthesis for many of the important metabolites have been developed and refined. In this review, we will discuss the most recent work on BaP and other unsubstituted and methylated PAH. Structure-activity relationships among the four-six ring PAH will also be considered. Finally, we will discuss some results of comparisons between mutagenicity assays in *S. typhimurium* TA 100 and bioassays for carcinogenicity in mice.

RECENT STUDIES ON THE METABOLIC ACTIVATION OF PAH

The earliest evidence for the important role played by non-K-region diols of BaP (1, Fig. 1) in activation of this compound was obtained by Borgen, Yang and coworkers [9]. These workers found that the binding of BaP-7,8-diol (2, Fig. 1) to DNA in the presence of rat liver microsomes was favored, suggesting that this compound was a proximate form of BaP. Subsequently, Sims and Grover demonstrated that BaP-7,8-diol (in the presence of microsomes) and the corresponding diol epoxides (3 and/or 4, Fig. 1) gave binding products to DNA which were chromatographically identical with those formed from BaP and DNA in the presence of liver microsomes [10]. Further studies by the same group showed that hydrocarbon-DNA adducts formed in BaP treated human bronchial mucosa and mouse skin were chromatographically indistinguishable from those formed by reaction of 3 and/or 4 with DNA in solution [11].

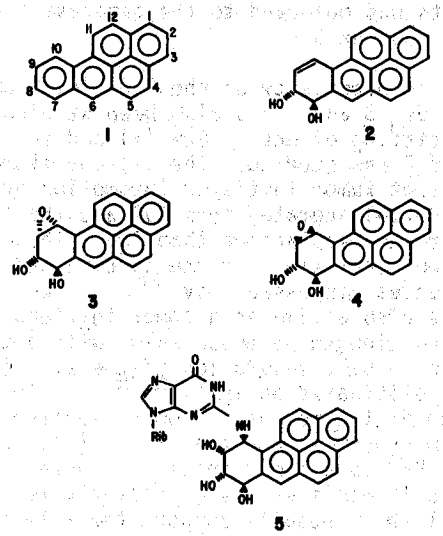

Fig. 1. Intermediates and products involved in metabolic activation of BaP.

Detailed studies on the metabolic formation of diol epoxides 3 and 4 and on the nature of the adducts formed by reaction of BaP diol epoxides with nucleic acids *in vitro* and *in vivo* have been carried out. The structure and absolute configuration of the major adduct formed by reaction of BaP with the RNA of cultured bovine bronchial mucosa was determined by Weinstein, Nakanishi, Harvey, and coworkers to be 5, which resulted from reaction of a single enantiomer of 3 with guanosine [12-14]. Similar results were obtained

after application of BaP to mouse skin; the major adducts resulting from nucleic acid binding were formed from a single enantiomer of 3, but adducts resulting from one enantiomer of 4 were also observed [15]. Diol epoxide 3 can be formed from BaP by stereospecific oxygenation of the 7,8 bond to give a single enantiomer of the 7,8-epoxide followed by stereospecific enzymatic hydration to optically pure (-)trans-7,8-diol and further stereoselective oxidation to a single enantiomer of 3 as demonstrated by Yang and Gelboin[16]. The formation of 3 as the major 7,8-diol-9,10-epoxide isomer from BaP was demonstrated in several studies, including an investigation of metabolism of BaP by cultured human bronchus[17-20].

Bioassays for mutagenicity, transformations *in vitro*, and carcinogenicity have, for the most part, supported the results of the studies of the molecular mode of action of BaP discussed above. The diol epoxide 3, (Fig. 1), a powerful mutagen, was more mutagenic than the isomer 4 or the 4,5 epoxide of BaP in Chinese hamster V79 cells[17, 21-23]. When the 7,8-diol was assayed in these cells in the presence of hepatic enzymes, it was also more mutagenic than BaP, but the other diols tested (4,5- and 9,10-) showed little activity[17]. In the Ames assay, both diol epoxides 3 and 4 were powerful mutagens with 4 being the more active[22]. Malignant transformation of M2 mouse fibroblasts was observed to the greatest extent with diol epoxide 3[23].

The carcinogenicity of the 7,8-diol 2 and the diol epoxides 3 and 4 has also been studied. The tumor initiating effect of the (+) and (-) enantiomers of 2 was studied. The (-) enantiomer was a more potent tumor initiator (promotion by tetradecanoylphorbol acetate) than BaP and the (+) enantiomer was less active than BaP. These results support the conclusions of the binding and metabolic studies discussed above[24]. The racemic diol 2 was also active as a tumor initiator and complete carcinogen on mouse skin, with activity comparable to BaP; saturation of the 9,10-double bond in 2 eliminated activity[25,26]. In another study, the diol 2 isolated from metabolism of BaP by liver microsomes, and presumably (-), was as active as BaP as a tumor initiator, whereas the 4,5- and 9,10-diols were significantly less active[27]. All these results support the role of 2 as a proximate carcinogen of BaP and of 3 or 4 as an ultimate carcinogen. However, assays of the isomers 3 and 4 as tumor initiators on mouse skin have shown little activity. In one study, the anti isomer 3 gave only 22% tumor bearing animals, compared to 94% for BaP, when the compounds were applied in acetone[26]. When the diol epoxide 3 was applied as a tumor initiator on mouse skin in THF solution, the tumor yield was increased, but was still less than that obtained with BaP[28]. Both 3 and 4 were also less active than BaP as initiators when applied to mouse skin in acetone/DMSO[29]. Neither 3 nor 4 was active as a complete carcinogen on mouse skin[25]. These negative results may be due to the high reactivity of epoxides 3 and 4 which may undergo solvolysis to inactive tetraols before reaching the critical targets. However, in another carcinogenicity study the anti-diol epoxide 3 was as active as BaP in inducing pulmonary adenomas in newborn mice when given at one fiftieth the dose. In addition, the racemic 7,8-diol was more active than BaP in this system[30].

The carcinogenicity of a number of other BaP derivatives has also been tested. All of the twelve possible monohydroxy-BaP derivatives have been tested as complete carcinogens on mouse skin and all were inactive except for 2-hydroxy-BaP which was as active as BaP[31,32]. However, 2-hydroxy-BaP has not been detected as a metabolite of BaP. The 4,5-, 7,8-, 9,10- and 11,12-epoxides of BaP were also tested for carcinogenic activity on mouse skin. Only the 7,8-epoxide showed activity and this activity was less than that of BaP[32,33]. Recently we completed a bioassay of 7,10-dimethyl-BaP as a tumor initiator. These studies were done in collaboration with Professor M. Newman, who synthesized the compound. This compound was inactive at the doses studied, in contrast to BaP. These results provide further evidence for involvement of the 7,8-diol-9,10-epoxide.

The involvement of a 7,8-diol-9,10-epoxide as an ultimate carcinogenic form of BaP gave rise to the "bay region" theory of hydrocarbon carcinogenesis, proposed by Jerina and coworkers[34,35]. According to this concept, ring opening of an epoxide with one carbon atom in the bay region (positions 10-11 in BaP) will give rise to a stabilized carbonium ion at the bay region (benzylic) position. Thus, ring opening of the 9,10-epoxide of BaP to give a carbonium ion at position 10 would be favored. This is supported by experimental data, as described above. The same reasoning can be applied to other PAH. Thus, these investigators predicted that the diol epoxides 6 and 7 (Fig. 2) derived from benz(a)anthracene and chrysene would be more active than the other possible diol epoxides which did not have a bay region epoxide.

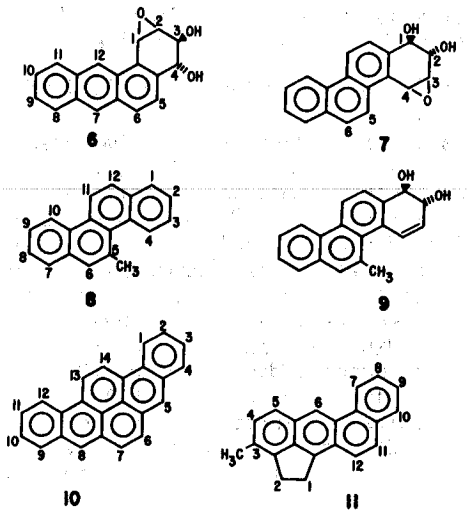

Fig. 2. Structures of derivatives of benz(a)-anthracene and chrysene and structures of dibenz(a,i)pyrene and 3-methylcholanthrene.

To test this hypothesis for benz(a)anthracene the corresponding diols were synthesized[36] and tested for mutagenic and carcinogenic activity. In the case of benz(a)anthracene, the 1,2-, 3,4-, 5,6-, 8,9- and 10,11-diols were assayed. The most mutagenic and carcinogenic diol was the 3,4-diol which is capable of transformation to diol epoxide 6 [37,38]. The diol epoxide isomers of 6 and the isomers of the 10,11-diol-8,9-epoxide and the 8,9-diol-10,11-epoxide of benz(a)anthracene, as well as the 1,2-epoxide and 3,4-epoxide of 1,2,3,4- tetrahydrobenz(a)anthracene were also synthesized and tested for mutagenicity in *S. typhimurium* and Chinese hamster V79 cells. In *S. typhimurium*, the isomers of 6 were both highly active, as was the 1,2-epoxide of tetrahydrobenz(a)anthracene. The least active derivative was the 10,11-diol-8,9-epoxide. Similar results were obtained with the hamster cells[39]. The metabolic formation of the diols of benz(a)anthracene and of the 8,9-diol-10,11-epoxide has been described, although not quantitatively[40-42].

Both 7-methylbenz(a)anthracene (7-MBA) and 7,12-dimethylbenz(a)anthracene (7,12-DMBA) are carcinogenic and evidence is mounting that these hydrocarbons may be activated through formation of bay region diol-epoxides. Studies with the diols of 7-MBA indicated that the 3,4-diol was the most mutagenic and most capable of inducing cell transformation, when activated with liver microsomes [43,44]. The 8,9-dihydrodiol of 7-MBA was more active than the parent hydrocarbon in inducing transformation of M-2 mouse fibroblasts[45]. However, the 3,4-diol of 7-MBA was the most active of the 7-MBA diols, when tested as a tumor initiator on mouse skin, and was more active than the parent hydrocarbon[46]. These results suggest that the 3,4-diol-1,2-epoxide of 7-MBA may be the ultimate carcinogen derived from this hydrocarbon. Bioassay of monofluoro-7-MBA derivatives indicated that 5-fluoro-7-MBA was the least active and that fluorine substitution in the 1-4 ring also decreased activity [35,47]. The low activity of these derivatives agrees with the bay region hypothesis.

In the case of 7,12-DMBA, a recent study by Baird, Dipple and Moschel indicated that binding of this carcinogen to DNA took place in the 1-4 ring; this was established by comparing the uv spectra of the bound carcinogen to those of model compounds[48]. A study of fluorinated-DMBA derivatives was also carried out by J. Miller, E. Miller and M. Newman. The results were similar to those found in the 7-MBA series[35,47]. A study of the binding of the 7,12-DMBA-5,6-epoxide to polyguanylic acid showed that the adducts were formed by reaction of the epoxide with the 2-amino group of guanine, as was found for the BaP epoxide-diols[49]. However, in the case of 7-MBA, the binding products of the 5,6-epoxide with RNA were not identical to those formed from the parent hydrocarbon[50].

Evidence for bay-region activation in the chrysene series is also developing (see 7, Fig.2 for nomenclature). The 1,2-, 3,4- and 5,6 diols of chrysene, as well as the 1,2,3,4,-tetrahydro-1,2-diol were synthesized and tested for mutagenic activity in *S. typhimurium* TA 100 with activation. The 1,2-diol was the only active compound indicating activation of chrysene *via* a bay region diol epoxide (7, Fig. 2)[51]. However, chrysene, like benz(a)anthracene is only weakly carcinogenic and it is expected that metabolic formation of 7 would be minimal. By contrast, 5-methylchrysene (5-MeC, 8, Fig. 2) is a strong carcinogen with activity comparable to BaP[52-54]. Interestingly, the other methylchrysene isomers are only weakly carcinogenic[52,55]. Of further interest is the environmental occurrence of the methylchrysenes which are found in tobacco smoke at levels comparable to those of BaP[52].

In our laboratories, a detailed study of the metabolic activation of 5-MeC was undertaken using the Miller-Newman fluorine probe approach. The following fluorinated 5-MeC derivatives were synthesized by unambiguous methods; 1-fluoro-5-methylchrysene (1-F-5-MeC), 3-F-5-MeC, 6-F-5-MeC, 7-F-5-MeC, 9-F-5-MeC, 11-F-5-MeC, and 12-F-5-MeC[56]. Each compound was tested for mutagenicity in *S. typhimurium* and for tumor initiating and complete carcinogenic activity on mouse skin. The results of the assays as tumor initiators indicated that the least active fluoro derivative was 3-F-5-MeC; 1-F-5-MeC and 12-F-5-MeC were also significantly less active than 5-MeC[57,58]. Complete carcinogenicity studies gave similar results. These results are summarized in Fig. 3 which indicates that 5-MeC has 2 bay regions, 2 K-regions, 2 non-K-regions, and 2-peri positions, but that only half the molecule (positions 12, 1-4) is involved in metabolic activation.

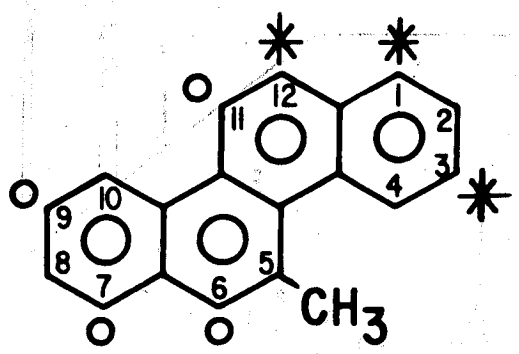

Fig. 3. Metabolic activation of 5-methylchrysene according to the fluorine-probe approach. The starred positions are involved in metabolic activation and the circled positions are not involved.

To investigate the nature of the proximate form(s) of 5-MeC, high pressure liquid chromatographic (HPLC) analysis of metabolites formed *in vitro* from 5-MeC was combined with mutagenicity assays of these metabolites in *S. typhimurium* TA 100 [59]. Figure 4 shows an HPLC trace of metabolites formed from 5-MeC upon incubation with Aroclor induced rat liver homogenates. Each peak was collected and assayed for mutagenicity with activation.

The peak corresponding to the greatest activity was E which was identified as the 1,2-dihydrodiol of 5-MeC (9, Fig. 2). Some activity was also detected for peak D, which was the 7,8-dihydrodiol. No significant activity was detected for the 9,10-dihydrodiol (peak A), 5-hydroxymethylchrysene (peak F), or the chrysenols (peaks G-I). These results demonstrate that 5-MeC-1,2-diol is a major proximate form of 5-MeC and are in agreement with the fluorine-probe studies described above. Quantitation of metabolite formation in this experiment using 5-MeC-5-^{14}C showed that formation of the 1,2-diol was favored over the 7,8-diol. Both diols could give rise to the corresponding bay region diol epoxides but, clearly, the extent to which these metabolites are actually formed is critical in determining the pathway of metabolic activation. Nevertheless, these experiments agree with the bay region hypothesis of Jerina and provide further evidence for its extenstion to methylated PAH.

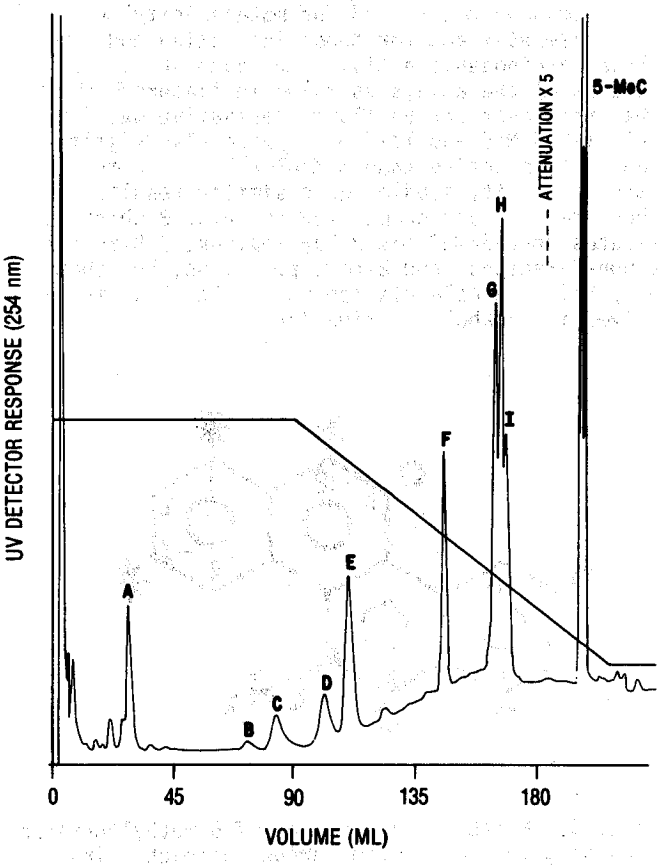

Fig. 4. High pressure liquid chromatogram of metabolites formed from 5-methylchrysene *in vitro*.

The fluorine probe approach has also been applied recently to dibenzo(a,i)pyrene (10, Fig. 2). In studies by Boger and coworkers[60], it was demonstrated that substitution of fluorine at the 2-, 3-, or 2,10-positions of 10 resulted in a decrease in activity, as tested by subcutaneous injection. Thus, the angular rings of this hydrocarbon may be involved in its activation.

A recent study has indicated possible bay region activation of the potent experimental carcinogen, 3-methylcholanthrene (3-MC, 11, Fig. 2). The major metabolites from 3-MC formed *in vitro* from rat liver microsomes were the 1-hydroxy and 2-hydroxy derivatives, with only minor amounts of diols being formed. This is somewhat surprising since 3-MC is a powerful carcinogen. However, diols were formed when 1-hydroxy-3-MC was incubated with rat liver microsomes. These diols were identified as the 2 diastereomeric 9,10-diols of 1-OH-3-MC. Both were more active than 3-MC towards *S. typhimurium* TA-100 with activation[61]

STRUCTURE-ACTIVITY RELATIONSHIPS

The carcinogenic activities of some unsubstituted 4-6 ring PAH are summarized in Fig. 5-8 [1,8,62]. While one still cannot generalize completely about structure activity relationships in this class, an understanding of the metabolic activation of certain PAH now permits more accurate prediction of activity. Among the tetracyclic compounds (Fig. 5), moderate activity is observed only when there is a free peri-position adjacent to an angular ring.

The presence of a free peri position and adjacent angular ring is also evident for the carcinogenic pentacyclic PAH shown in Fig. 6. Both dibenz(a,h)anthracene and dibenz(a,j)anthracene have this structural feature. However, the inactive isomer, dibenz(a,c)anthracene, has no free peri position adjacent to the angular rings. A similar explanation could account for the difference in activity between benzo(a)pyrene and benzo(e)pyrene. Some of the other compounds in Fig. 6 fulfill the structural requirement for carcinogenicity but nevertheless do not show activity.

Among the dibenzopyrenes shown in Fig. 7, only dibenzo(e,l)pyrene does not have a free peri position adjacent to an angular ring and this is the only inactive isomer. Similarly, the fluoranthenes (Fig. 8) show greatest activity when an angular ring and adjacent free peri position are present. Thus, the most active isomers are benzo(j)fluoranthene, benzo(b)fluoranthene, and dibenzo(a,e)-fluoranthene. Dibenzo(b,k)fluoranthene appears to be an exception. The activity of compounds having an available angular ring is consistent with the "bay region hypothesis", as discussed in the previous section. However, metabolic studies are necessary on many of these compounds to define the nature of the active forms and the role of the adjacent peri position.

Among methylated PAH, substitution of a methyl group in the angular ring which would be involved in activation of the parent hydrocarbon may decrease activity. Thus, 7,10-dimethylBaP was inactive when tested in both rats and mice [63,64]. Both 7-methylBaP and 10-methylBaP were also less active than BaP, but 2-,3-,4-,11-, and 12-methylBaP were all highly carcinogenic [64,65].

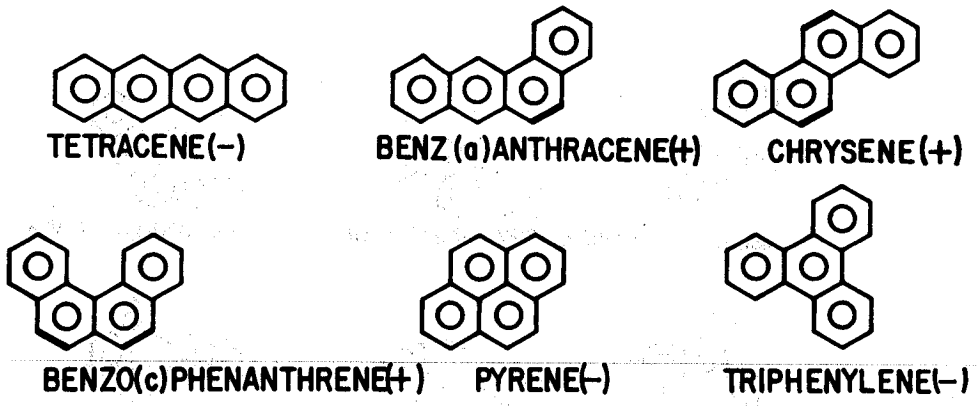

Fig. 5. Carcinogenic activity of tetracyclic PAH.

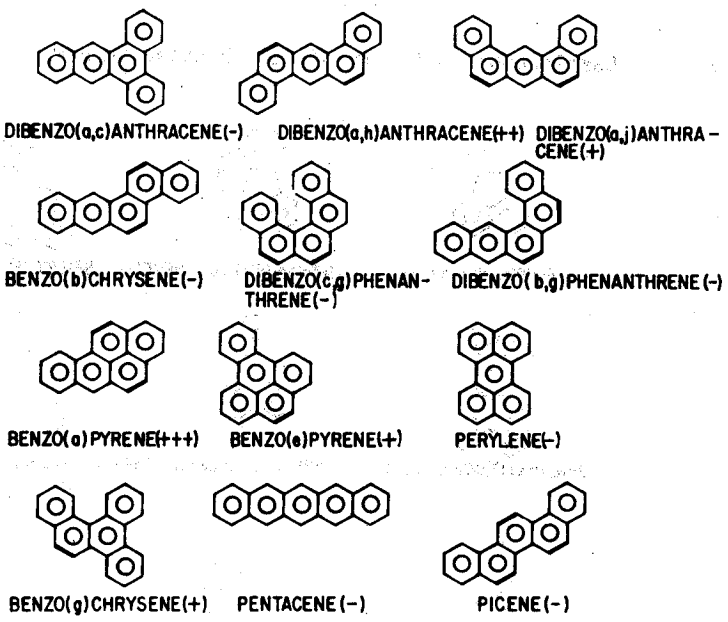

Fig. 6. Carcinogenic activity of some pentacyclic PAH.

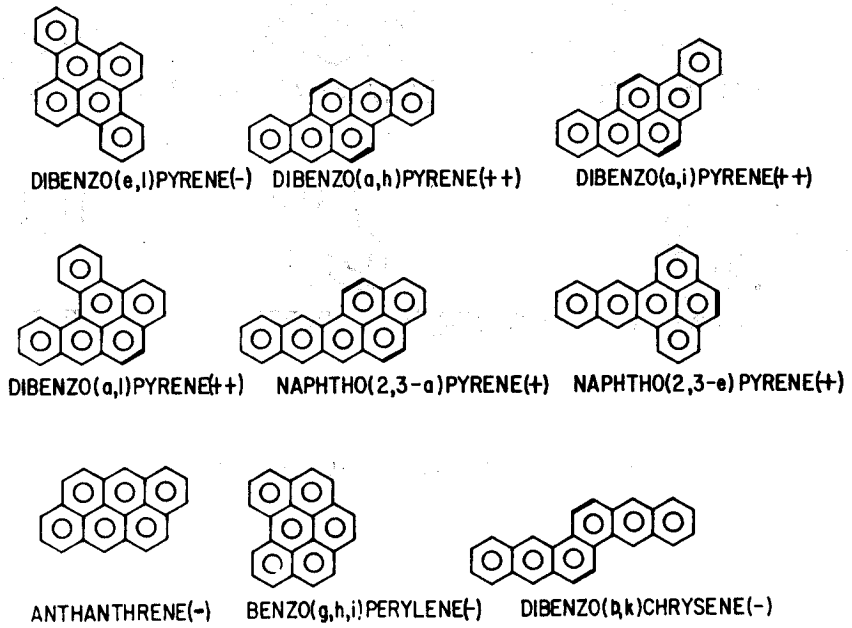

Fig. 7. Carcinogenic activity of some hexacyclic PAH.

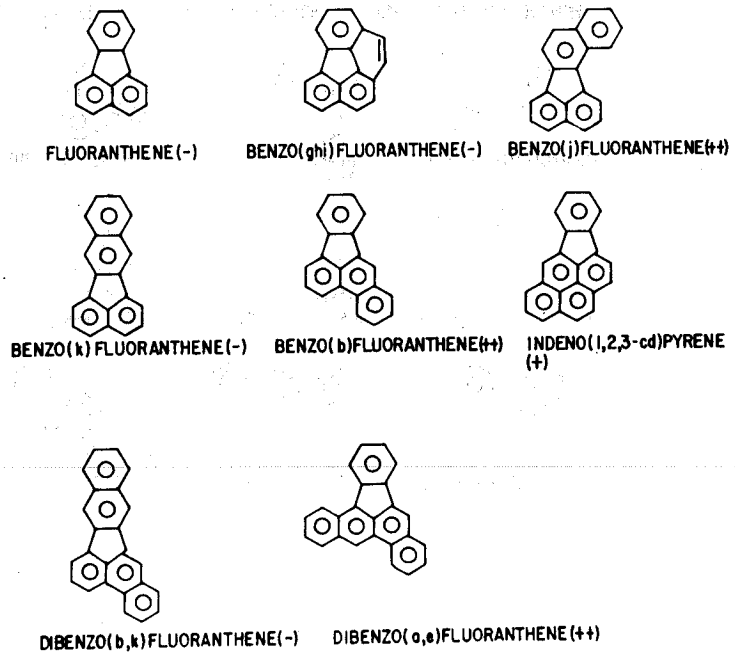

Fig. 8. Carcinogenic activity of fluoranthenes.

Substitution of a methyl group at positions other than the angular ring, for example in chrysene and benz(a)anthracene, can markedly increase carcinogenicity, especially when the substitution results in steric deformation of the molecule. The best examples of this are 5-MeC and 7,12-DMBA. In the methylchrysene series, the structural requirement favoring carcinogenicity is a bay region methyl group and a free peri position adjacent to an unsubstituted angular ring[52-58]. Only 5-MeC, the most carcinogenic isomer, fulfills this requirement. Similar generalizations apply to 7,12-DMBA derivatives and to cyclopentaphenanthrenes [47,66-68]. However, exceptions are also noted; for example, 4,7,12-trimethylbenz(a)anthracene, which has substitution in the angular ring, is nevertheless a potent carcinogen[64].

COMPARISON OF CARCINOGENICITY AND MUTAGENICITY ASSAYS FOR SOME PAH

Assays for mutagenicity in *S. typhimurium* TA 100 have been used widely in studies on PAH. In recent work on the methylchrysenes, this assay as well as assays for tumor initiating activity and complete carcinogenicity on mouse skin were used to evaluate the biological effects of a series of closely related compounds. A comparison of the results in the three systems is instructive in considering the most suitable bioassay for PAH.

These comparisons can be readily made since all assays for tumor initiating activity and complete carcinogenicity have been done in our laboratory under standard conditions. To determine tumor initiating activity, groups of 20 Ha(ICR) female outbred Swiss albino mice were treated with an initiating dose of the PAH during the early part of the second resting phase (50-55 days) of the hair cycle. Each compound was applied in solution to the shaved mouse back. Each initiating PAH was given in 10 subdoses; one dose every other day. Ten days after initiation, promotion began with application of 2.5 µg tetradecanoylphorbol acetate (TPA) three times weekly. Promotion continued for twenty weeks and tumors were counted weekly. For complete carcinogenicity assays on mouse skin, treatment also began during the second resting phase of the hair cycle. The PAH was applied three times weekly for 65-75 weeks. Typically, a dose of 5 µg PAH/100 µl acetone was applied each time. At the termination of these assays, all skin tumors were processed by standard histopathological techniques.

When the six isomeric methylchrysenes were compared as mutagens in *S. typhimurium* TA 100, with activation, 5-MeC was the most mutagenic [69,70]. This agrees well with assays for tumor initiating activity and complete carcinogenicity; in both cases, 5-MeC was more active than the other five isomers [52]. In the tumor initiation assays of the methylchrysenes, 3-methylchrysene and the other isomers also showed activity, although less than 5-MeC. The difference between 5-MeC and the other isomers was much more pronounced in the complete carcinogenicity assay. This is an example of a phenomenon which we have frequently observed; namely, that mouse skin is often more sensitive to the effect of a PAH as an initiator, with TPA as the promoter, than to the PAH as a complete carcinogen. Therefore, the complete carcinogenicity assay is often superior for distinguishing between closely related compounds. However, it requires more material and takes longer than the initiation assay.

A comparison of results among seven fluorinated 5-MeC derivatives showed that the mutagenicity assay in *S. typhimurium* TA 100 was less sensitive to minor differences in structure than the mouse skin assays. For example, the mutagenicity of 3-fluoro-5-MeC and 5-MeC is compared in Fig. 9. The two compounds were equally mutagenic towards *S. typhimurium* TA 100 with activation. However, inspection of Fig. 10 shows that 3-fluoro-5-MeC was significantly less active than 5-MeC as both a tumor initiator and complete carcinogen; in fact, no significant activity was detected for 3-fluoro-5-MeC in these assays. A similar comparison is shown for 12-fluoro-5-MeC and 5-MeC in Figs. 11 and 12. In both the mutagenicity and tumor initiation assays, the relative activity of the two compounds was dose dependent. At the lower doses in both cases, 12-fluoro-5-MeC was less active than 5-MeC, but this difference disappeared at higher doses. However, in the complete carcinogenicity assay, 12-fluoro-5-MeC was significantly less active than 5-MeC. These results indicate that the mutagenicity and tumor initiation assays are less able to distinguish between compounds with minor structural differences than the complete carcinogenicity assay. Nevertheless, we have found the Ames assay to be extremely useful in studies on PAH carcinogenesis, especially for detection of

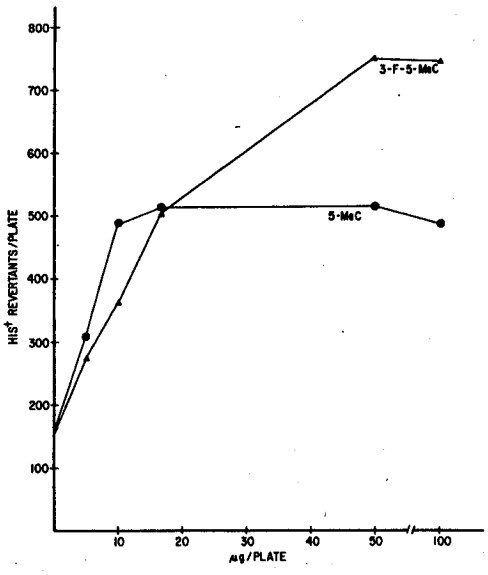

Fig. 9. Mutagenic activity of 3-fluoro-5-methylchrysene (3-F-5-MeC) and 5-methylchrysene (5-MeC) in *S. typhimurium* TA 100.

activated metabolites as discussed in the first section. The differences observed between these mutagenicity and carcinogenicity assays may be due, at least partially, to differences in the activating systems (rat liver homogenates *vs.* mouse skin) or to actual differences in mutagenic *vs.* carcinogenic activity of the metabolites formed.

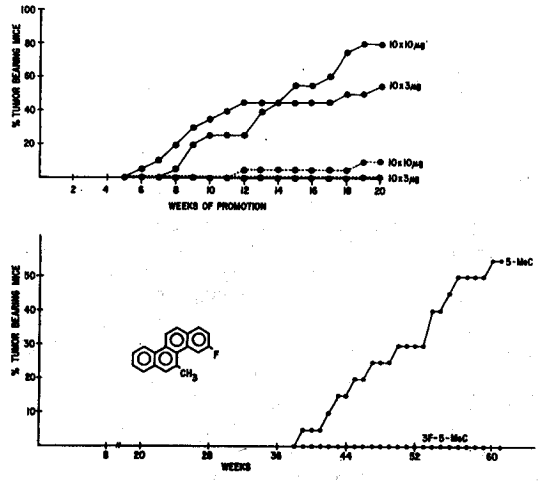

Fig. 10. Tumor initiating activity (upper) and complete carcinogenicity (lower) of 3-fluoro-5-methylchrysene (----) and 5-methylchrysene (——)

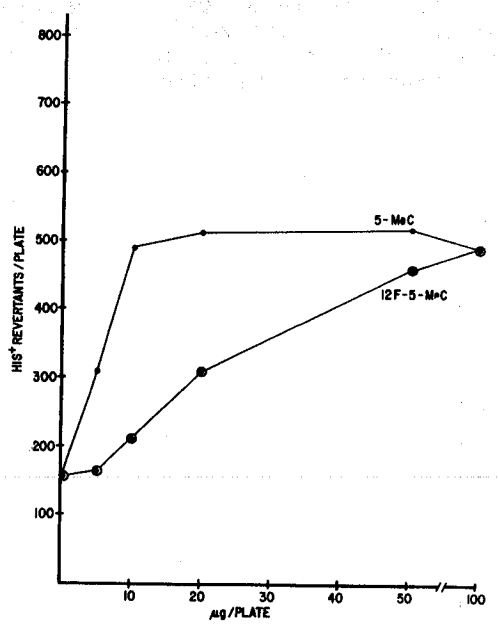

Fig. 11. Mutagenic activity of 12-fluoro-5-methylchrysene (12-F-5-MeC) and 5-methylchrysene (5-MeC) in *S. typhimurium* TA 100.

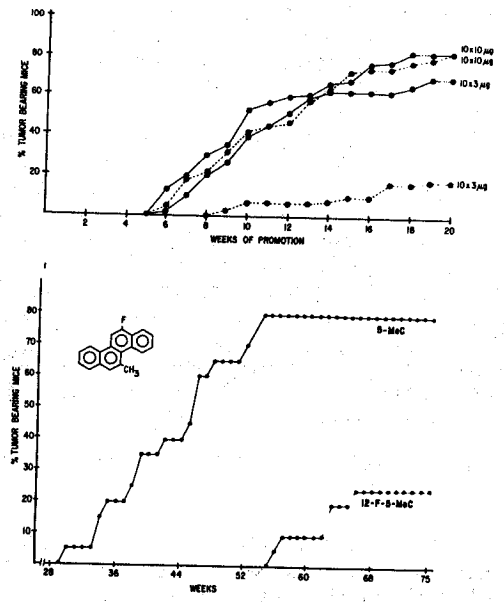

Fig. 12. Tumor initiating activity (upper) and complete carcinogenicity (lower) of 12-fluoro-5-methylchrysene (----) and 5-methylchrysene (——)

ACKNOWLEDGEMENTS

This study was supported by Grant CA-012376 from the National Cancer Institute. Stephen S. Hecht is recipient of National Cancer Institute Research Career Development Award NO. 5K04 CA-00124.

REFERENCES AND FOOTNOTES

* This is paper No. 13 of the series "A Study of Chemical Carcinogenesis."

1. A. Dipple, In "Chemical Carcinogens", C.E. Searle, ed., ACS Monograph 173, Washington, D.C., American Chemical Society, 1976, pp 245-314.
2. J.C. Arcos and M.F. Argus "Chemical Induction of Cancer" Vol. IIA, New York, Academic Press, 1974, pp 15-76
3. P. Sims and P.L. Grover Advan. Cancer Res. 20 165-274, (1974)
4. D.M. Jerina and J.W. Daly Science 185 537-582, (1974)
5. C. Heidelberger In "Topics in Chemical Carcinogenesis" W. Nakahara, S. Takayama, T.Sugimura, and S. Odashima, eds. Tokyo, Japan, Univ of Tokyo Press, pp 371-386
6. H. Gelboin and P.O. T'so Polycyclic Hydrocarbons in Cancer: Chemistry, Molecular Biology and Environment, New York, Academic Press, (1978) *In press*
7. R. Freudenthal and P.W. Jones, eds. "Carcinogenesis, A Comprehensive Survey, Vol. 1, Polynuclear Aromatic Hydrocarbons." New York, Raven Press, 1976, p 449

8. D. Hoffmann, S.S. Hecht, I. Schmeltz and E.L. Wynder In "Structural Correlates of Carcinogenesis and Mutagenesis; A Guide to Testing Priority", Washington D.C., U.S. Food and Drug Administration, (1978) *In press*

9. A. Borgen, H. Darvey, N. Castagnoli, T.T. Crocker, R.E. Rasmussen and I.Y. Yang J. Med. Chem. 16 502-504 (1973)

10. P. Sims, P.L. Grover, A. Swaisland, K. Pal, and A. Hewer Nature 252 326-328 (1974)

11. P. Grover, A. Hewer, K. Pal and P. Sims Int. J. Cancer 18 1-6 (1976)

12. I.B. Weinstein, A.M. Jeffrey, K.W. Jennette, S.H. Blobstein, R.G. Harvey, C. Harris, H. Autrup, H. Kasai, and K. Nakanishi Science 193 592-595 (1976)

13. A.M. Jeffrey, K.W. Jennette, S.H. Blobstein, I.B. Weinstein, F.A.Beland, R.G. Harvey, H. Kasai, I. Miura and K. Nakanishi J. Am. Chem. Soc. 98 5714-5715 (1976).

14. K. Nakanishi, H. Kasai, R.G. Harvey, H.Cho, A.M. Jeffrey, K.W. Jennette and I.B. Weinstein J. Am. Chem. Soc. 99 258-260 (1977)

15. M. Koreeda, P.D., Moore, P.G.Wislocki, W. Levin, A.H. Conney, H. Yagi and D.M. Jerina Science 199 778-781 (1978)

16. S.K. Yang, D.W. McCourt, J.C. Leutz and H. Gelboin Science 196 1199-1201 (1977)

17. E. Huberman, L. Sachs, S.K. Yang and H. Gelboin Proc. Natl Acad. Sci.USA 73 607-611 (1976)

18. D.R. Thakker, H. Yagi, A.H. Lu, W. Levin, A.H. Conney and D.M. Jerina Proc. Natl. Acad. Sci. USA 73 3381-3385 (1976)

19. S.K. Yang, D.W. McCourt, P.P. Roller and H. Gelboin Proc. Natl. Acad. Sci. USA 73 2594-2598 (1976)

20. S.K. Yang, H.Gelboin, B.F Trump, H. Autrup and C.C. Harris Cancer Res 37 1210-1215 (1977)

21. R.F. Newbold and P. Brookes Nature 261 52-54 (1976)

22. A.W. Wood, P.G. Wislocki, R.L. Chang, W. Levin. A.Y.H. Lu, H. Yagi, O. Hernandez, D.M. Jerina and A.H. Conney Cancer Res. 36 3358-3366 (1976)

23. H. Marquardt and S. Baker Cancer Letters 3 31-36 (1977)

24. W. Levin, A.W. Wood, R.L. Chang, T.J. Slaga H. Yagi, D.M. Jerina and A.H. Conney Cancer Res. 37 2721-2725 (1977)

25. W. Levin, A.W. Wood, P.G. Wislocki, J. Kapitulnik, H. Yagi, D.M. Jerina and A.H. Conney Cancer Res. 37 3356-3361 (1977)

26. T.J. Slaga, A. Viaje, D.L. Berry and W. Bracken Cancer Letters 2 115-122 (1976)

27. I. Chouroulinkov, A. Gentil, P.L. Grover and P. Sims Br. J. Cancer 34 523-532 (1976)

28. T.J. Slaga, A. Viaje, W.M. Bracken, D.L. Berry, S.M. Fischer, D.R. Miller and S.M. Leclerc Cancer Letters 3 23-30 (1977)

29. T.J. Slaga, W.M. Bracken, A. Viaje, W. Levin, H.Yagi, D.M. Jerina, A.H. Conney Cancer Res. 37 4130-4133 (1977)

30. J. Kapitulnik, P.G. Wislocki, W. Levin, H. Yagi, D. Jerina, and A.H. Conney Cancer Res. 38 354-358 (1978)

31.J. Kapitulnik, W. Levin, H. Yagi, D.M. Jerina and A.H. Conney Cancer Res. 36 3625-3628 (1976)

32. P.G. Wislocki, R.L. Chang, A.W. Wood, W. Levin, H. Yagi, O. Hernandez, H.D. Mah, P.M. Dansette, D.M. Jerina and A.H. Conney Cancer Res. 37 2608-2611 (1977)

33. W. Levin, A.W. Wood, H. Yagi, P.M. Dansette, D.M. Jerina and A.H. Conney Proc Natl Acad Sci USA 73 243-247 (1976)

34. R.E. Lehr and D.M. Jerina J. Toxicol. and Environ. Health 2 1259-1265 (1977)

35. D.M. Jerina and J.W. Daly In D.V. Parke and R.L. Smith, eds. "Drug Metabolism-from Microbe to Man" London, Taylor and Francis, Ltd., pp 13-32 (1976)

36. R.E. Lehr, M. Schaefer-Ridder and D.M. Jerina J. Org. Chem. 42 736-743 (1977)

37. A.W. Wood, W.Levin, A.Y.H. Lu, D. Ryan, S.B. West, R.E. Lehr, M. Schaefer-Ridder, D.M. Jerina and A.H. Conney Biochem. Biopys. Res. Commun. 72 680-686 (1976)

38. A.W. Wood, W. Levin, R.L. Chang, R.E.Lehr, M. Schaefer-Ridder, J.M. Karle, D.M. Jerina and A.H. Conney Proc. Natl Acad Sci. USA 74 3176-3179 (1977)

39. A.W. Wood, R.L. Chang, W. Levin, R.E.Lehr, M. Schaefer-Ridder, J.M. Karle, D.M. Jerina and A.H. Conney Proc. Natl Acad Sci. USA 74 2746-2760 (1977)

40. E. Boyland and P. Sims Biochem J. 91 493-506 (1964)

41. E. Boyland, M. Kimura and P. Sims Biochem J. 92 631-638 (1964)

42. J. Booth and P. Sims FEBS Lett. 47 30-33 (1974)

43. C. Malaveille, B. Tierney, P.L. Grover, P. Sims, H. Bartsch Biochem Biophys Res. Commun. 75 427-433 (1977)

44. H. Marquardt, S. Baker, B. Tierney, P.L. Grover and P. Sims Int J. Cancer 19 828-833(1977)

45. H. Marquardt, P.L. Grover and P. Sims Cancer Res. 36 2059-2064 (1976)

46. I. Chouroulinkov, A. Gentil, B. Tierney, P. Grover and P. Sims Cancer Letters 3 247-253 (1977)

47. M.S. Newman, In " Carcinogenesis, Vol. I, R.I. Freudenthal, P.W. Jones, eds, New York, Raven Press, 1976, pp 203-207

48. R.C. Moschel, W.M. Baird, and A. Dipple Biochem. Biophys. Res. Commun. 76 1092-1098 (1977)

49. A.M. Jeffrey, S.H. Blobstein, I.B. Weinstein F.A. Beland, R.G. Harvey, H. Kasai and K. Nakanishi Proc Natl Acad. Sci. USA 73 2311-2315 (1976)

50. W.M. Baird, P.L. Grover, P. Sims and P. Brookes Cancer Res. 36 2306-2311 (1976)

51. A.W. Wood, W. Levin, D. Ryan, P.E. Thomas, H. Yagi, H.D. Mah, D.R. Thakker, D.M. Jerina and A.H. Conney Biochem. Biophys. Res. Commun 78 847-854 (1977)

52. S.S. Hecht, W.E. Bondinell, and D. Hoffmann J. Natl Cancer Inst. 53 1121-1133 (1974)

53. S.S. Hecht, M. Loy and D. Hoffmann, in "Carcinogenesis" Vol. 1, R.I. Freudenthal, P.W. Jones, eds. New York, Raven Press, 1976, pp 325-340

54. S.S. Hecht, M. Loy, R.R. Maronpot and D. Hoffmann Cancer Letters 1 147-154 (1976)
55. D. Hoffmann, W.E. Bondinell and E.L. Wynder Science 183 215-216 (1974)
56. S.S. Hecht, M. Loy, R. Mazzarese and D. Hoffmann J. Med. Chem. 21 38-44 (1978)
57. S.S. Hecht, M. Loy, R. Mazzarese and D. Hoffmann in "Polycyclic Hydrocarbons in Cancer: Chemistry, Molecular Biology, and Environment", H. Gelboin and P.O. T'so, eds New York, Academic Press, 1978, *In press.*
58. S.S. Hecht, N. Hirota, M. Loy and D. Hoffmann Cancer Res. 38 1694-1698 (1978)
59. S.S. Hecht, E. LaVoie, R. Mazzarese, S.Amin, V. Bedenko and D. Hoffmann Cancer Res. (1978) *In press*
60. E. Boger, R.F. O'Malley and D.J. Sardella J. Fluorine Chem 8 513-525 (1976)
61. D.R. Thakker, W. Levin, A.W. Wood, A.H. Conney, T.A. Stoming and D.M. Jerina J. Am. Chem. Soc. 100 645-647 (1978)
62. National Institute of Health: "Survey of Compounds Which Have Been Tested for Carcinogenic Activity" Publ. Health Service Publ. No. 149,1951, pp. 583; Suppl. 1, 1957, pp. 388; Suppl. 2, 1969; pp. 655; DHEW Publ No. (NIH) 73-75, 1973, Vol. I and Vol. II, pp. 2343; DHEW Publ. No. (NIH) 74-75, 1977, pp. 1667; DHEW Publ. No. (NIH) 75, 1975, pp 1638
63. S.S. Hecht, N. Hirota and D. Hoffmann Cancer Letters, *Submitted*
64. R.G. Harvey and F.B. Dunne Nature (1978) *In press*
65. A. Lacassagne, F. Zajdela, N.P. Buu-Hoi, O. Chalvet and G.H. Daub Int. J. Cancer 3 238-243 (1968)
66. J. Pataki and C. Huggins Cancer Res. 29 506-509 (1969)
67. A. Butenandt and H. Dannenberg Arch. Geschwulstforsch 6 1-7 (1953)
68. M.M Coombs and C.J. Croft Prog. Exp. Tumor Res. 11 69-85 (1969)
69. M.M. Coombs, C. Dixon and A.M. Kissonerghis Cancer Res. 36 4525-4529 (1976)
70. E. LaVoie, V. Bedenko, N. Hirota, S.S. Hecht and D. Hoffmann Proc. Third International Symposium on Polynuclear Aromatic Hydrocarbons, Battelle Columbus Laboratories, 1978

MUTAGENIC ACTIVITY IN ORGANIC FRACTIONS OF AIRBORNE PARTICULATE MATTER

J. M. Daisey, I. Hawryluk,
T. J. Kneip and F. Mukai
New York University Medical Center
Institute of Environmental Medicine
550 First Avenue
New York, New York 10016

ABSTRACT

Airborne particulate matter collected recently in New York City was sequentially extracted with cyclohexane, dichloromethane and acetone respectively, to extract non-polar and polar organic compound fractions. The fractions were assayed for mutagenic activity with the Ames Salmonella typhimurium test system. Direct-acting mutagens (no microsomal activation) of a wide range of polarity have been found in both the winter and summer aerosol samples. The moderately polar, dichloromethane extractable compounds exhibited the greatest activity. These results indicate the presence of biologically active compounds other than polycyclic aromatic hydrocarbons. Ongoing separation work indicates the presence of more than one compound or class of compounds although structures have yet to be determined.

INTRODUCTION

Despite many studies, relationships between air pollution and the etiology of environmental diseases remain unclear. One reason for this may be our limited knowledge of the organic compound fraction of the urban aerosol. It has been estimated that "over 99% of the organic pollutants in the air have never been determined".[1] In view of the large numbers of organic compounds present[2] and the complex problems of sampling and analysis, identification and quantitation of all compounds present for the purpose of making judgments on possible human health hazards is clearly an extremely difficult task.

Short-term bacterial mutagenicity tests [2-4] provide an alternate and complementary means for screening organic compound fractions of the aerosol for biological activity as well as a criterion for deciding which fractions should be subjected to more intensive fractionation and chemical characterization. The significance of those compounds which are isolated and identified with the aid of such a screening program can then be evaluated on the basis of available toxicological information. For those compounds for which such information is unavailable, their identification in the aerosol should provide an impetus for toxicological testing.

We have begun such a screening program with the objectives of separating and identifying previously unidentified compounds which may be of significance to human health. Our results to date are reported here.

EXPERIMENTAL

Twenty-four hour total suspended particulate samples (TSP) which were collected in New York City during Summer, 1976, and Winter, 1977, were sequentially extracted with increasingly polar solvents, cyclohexane, dichloromethane and acetone, respectively, to separate non-polar, moderately polar and polar organic compounds. Extracts were filtered and then reduced to a 10 ml volume with a rotary evaporator (35-40°C). The individual cyclohexane and dichloromethane extracts of daily samples or composites of these extracts were evaporated just to dryness under argon at 35-40°C and redissolved in acetone for testing. The acetone extracts were reduced in volume, but not taken to dryness. Final sample concentrations, determined by weighing duplicate 100 µl aliquots which had been taken to dryness, were generally in the range of 0.5-5 mg/ml.

A composite of dichloromethane extracts of particulate samples collected in August, 1977, was taken to dryness, as described above and redissolved in methanol for a chromatographic fractionation on a Waters Associates Model 440 High Pressure Liquid Chromatograph with a Model 660 Solvent Programmer. Separation was effected on a µ-Bondapak C_{18} column using 90% methanol in water at a flow of 2.0 ml/min. Ultraviolet absorbance was monitored at 254 nm and 280 nm. The collected fractions were reduced to a 1.0 ml volume and weights of the fractions were determined by weighing duplicate 100 µl aliquots, which had been taken to dryness, on a microbalance.

Fractions were generally screened for the presence of direct-acting (no microsomal activation) bacterial mutagens using the Ames Salmonella typhimurium assay system.[3] Aroclor 1254-induced rat liver microsomal fraction S-9 and cofactors were used for tests employing

microsomal activation. Testing was carried out at levels ranging from about 50 to 540 μg per plate (0.1 ml).

Results, in units of revertants per plate (control subtracted) are expressed as averages of duplicate plates. The standard deviation of a particular value is calculated as [Total revertants per plate plus revertants per plate for the control]$^{1/2}$.

The uncertainty in values of revertants per μg or per m^3 of air is estimated from the standard deviation calculated above plus the uncertainty in the weighing procedure (approximately 10%).

RESULTS AND DISCUSSION

As an initial experiment, solvent extracts of individual 24-hour TSP samples were screened with 5 strains of Salmonella typhimurium. Mutagenic activity at levels 2 to 14 times higher than controls was found for all three solvent extracts. Solvent extracts of filter blanks were found to be inactive. S. typhimurium strains TA-1537, TA-1538 and TA-98, which respond to frame-shift mutagens, and TA-100, which responds to base-pair substitution mutagens, exhibited the greatest number of histidine revertants per plate. Strain TA-1535 (base-pair substitution) showed significant activity over the control only for the acetone-extractable compounds.

Dose-response relationships were determined for composites of Summer, 1976, and Winter, 1977, solvent extracts with S. typhimurium TA-98 and TA-100. Results are shown in Figures 1 and 2. A summary of the results in terms of revertants per microgram of extractable organic material is presented in Table 1. Mutagenicity, in the linear region of the dose response curves (Figures 1 and 2), was found to be greatest for the dichloromethane extractable compounds followed by the acetone and cyclohexane extractable compounds. The dichloromethane extract (Summer, 1976) exhibits some toxic effects on TA-100 at higher doses as can be seen in Figure 1.

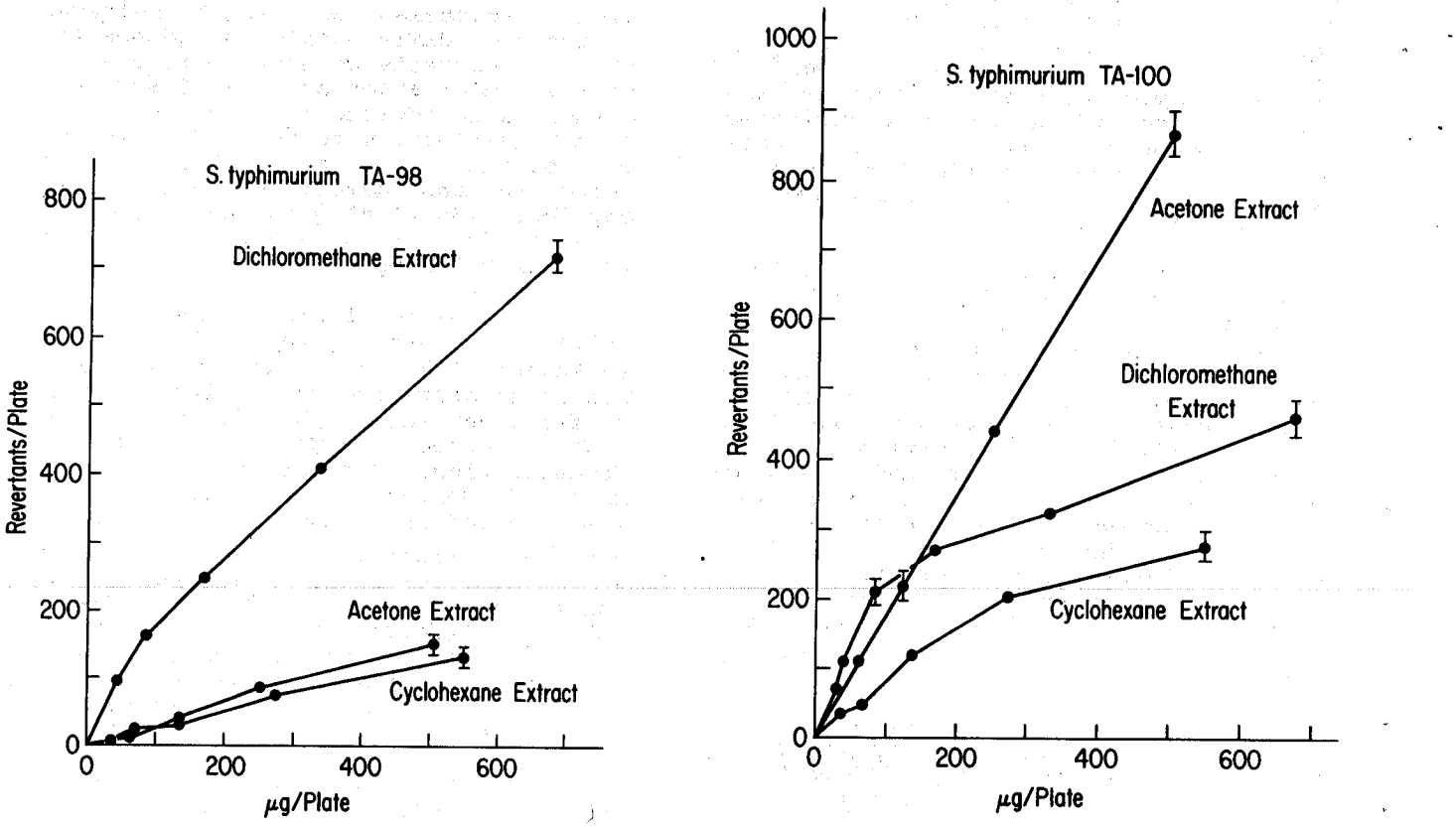

Figure 1. Mutagenic activity of several organic solvent extracts of airborne particulate matter collected in New York City during August, 1976. Extracts were tested with S. typhimurium strains TA-98 and TA-100.

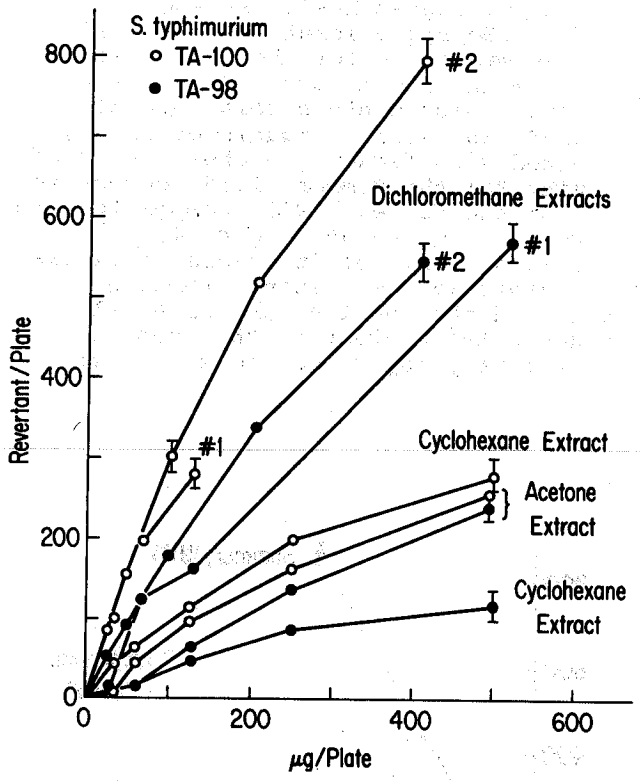

Figure 2. Mutagenic activity of several organic solvent extracts of airborne particulate matter collected in New York City during February, 1977. Extracts were tested with S. typhimurium strains TA-98 and TA-100.

Two dichloromethane composites, #1 and #2, covering the first and third weeks, respectively, of February, 1977, were tested to determine week-to-week variability. As can be seen in Figure 2, no significant difference was found for these two composites for either bacterial strain. The response of TA-100 to each of the extracts is somewhat higher than that of TA-98 for both the summer and winter composites.

Bacterial mutagenicity on a revertants per m^3 of air basis, has been calculated and is reported in Table 1. The order of activity here is acetone $\gtrsim$ dichloromethane > cyclohexane. The shift in order occurs because acetone extractable materials are a larger proportion of the organic fraction of the aerosol.

Table 1. Bacterial mutagenicity of organic solvent extracts of total suspended particulate matter from New York City.

Organic Solvent Extract	Revertants/μg-Extract TA-98	Revertants/μg-Extract TA-100	Revertants/m^3 - Air TA-98	Revertants/m^3 - Air TA-100
CYCLOHEXANE:				
Summer, 1976	0.28±0.06	0.9±0.2	2.0±0.4	6.0±1.2
Winter, 1977	0.34±0.06	1.1±0.3	1.9±0.3	6.1±1.7
DICHLOROMETHANE:				
Summer, 1976	1.6±0.05	2.50±0.04	5.1±1.6	8.0±0.1
Winter, 1977	1.3±0.3	2.8±0.5	4.2±0.8	8.6±1.6
ACETONE:				
Summer, 1976	0.31±0.06	1.9±0.2	1.8±0.3	10.9±1.4
Winter, 1977	0.46±0.10	0.5±0.3	6.5±1.4	7.2±4.1

Non-polar compounds extracted with cyclohexane, including polycyclic aromatic hydrocarbons (PAH) were tested both with and without microsomal activation. Slightly reduced activity was found with microsomal activation, as shown in Figure 3. Since most PAH compounds are not active without microsomal activation, this suggests the presence of other active mutagens. Similar results, i.e., somewhat reduced activity with microsomal activation, have been reported for extracts of particulate samples collected in Berkeley, California[5] and Los Angeles.[6]

Seasonal differences in the response of S. typhimurium strains TA-98 and TA-100 to the solvent extracts on a revertant per microgram basis are shown in Table 1. No significant seasonal differences were found for the cyclohexane or dichloromethane extracts. The acetone extracts, whioh contain polar organic compounds and some inorganic material, exhibited significantly higher levels of activity for the Summer, 1976, composite than for the Winter, 1977, composite with S. typhimurium TA-100 (Figure 4). Seasonal differences in levels of alkylating agents in the acetone extracts paralleled the results for bacterial mutagenicity[7] suggesting that some of this activity may be due to such compounds.

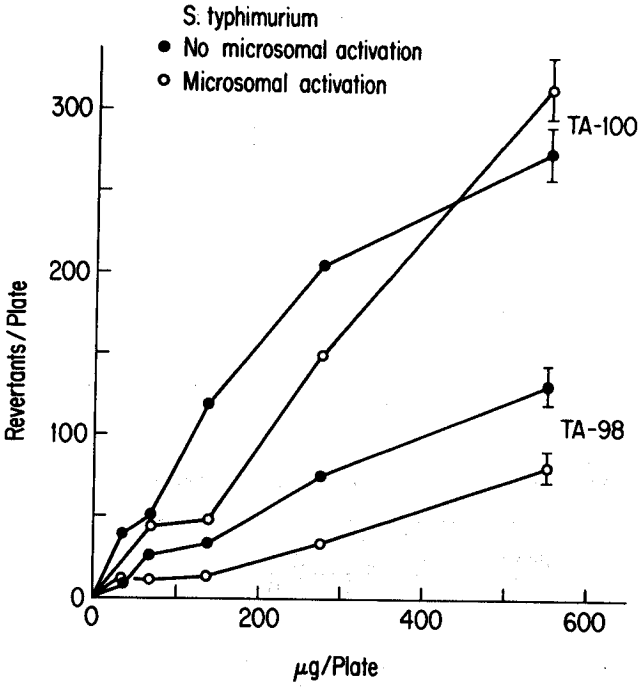

Figure 3. Effect of microsomal activation on the bacterial mutagenicity of the cyclohexane extractable fraction of aerosol samples collected in New York City. Aroclor 1254-induced rat liver microsomal fraction S-9 and co-factors were used. 2-Acetylaminofluorene was used as a positve control for confirmation of the S-9 mix.

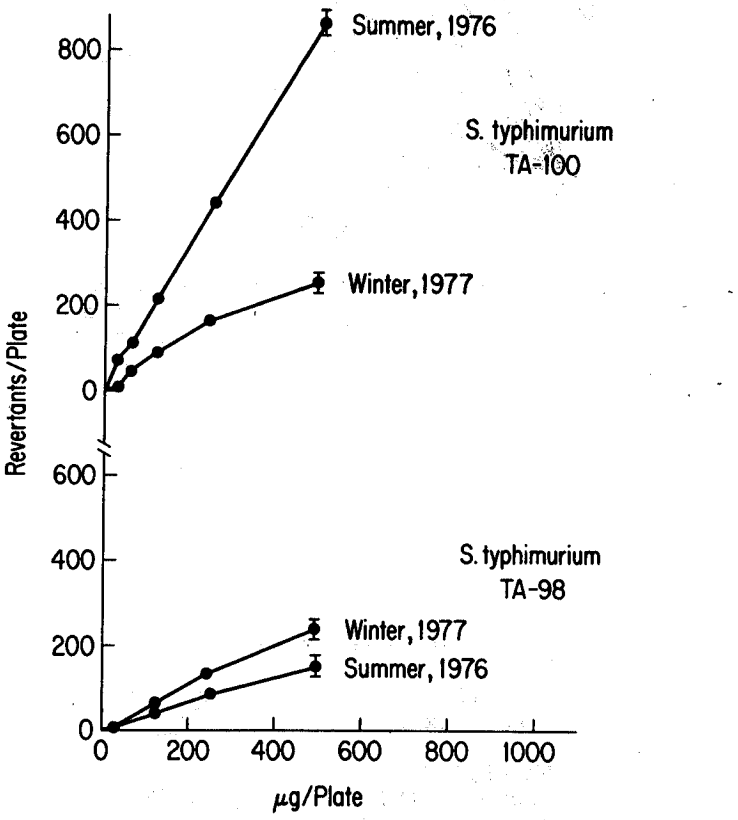

Figure 4. Seasonal comparison of the bacterial mutagenicity of composite samples of the acetone-extractable fraction of New York City aerosol samples.

Additional insight into seasonal relationships is provided by correlations found between aerosol concentrations of the organic solvent extracts and certain other aerosol variables. Aerosol concentrations of the dichloromethane extracts from Summer, 1976, were highly correlated with the cross-product of the concentrations of lead and ozone suggesting that these materials were strongly related to automotive emissions.[6] The dichloromethane extracts for Winter, 1977, in contrast, correlated significantly only with vanadium[9], a tracer for oil burning. Thus, while no seasonal difference in mutagenic activity was found for the dichloromethane extractable fraction, the nature and source of the materials within the fraction may differ from one season to the next.

As the dichloromethane extractable material exhibited the greatest bacterial mutagenicity (on a revertants/µg basis) a composite sample of dichloromethane extracts was fractionated by HPLC and the fractions were tested. Results are presented in Table 2 for the original composite and for the fractions. Fractions 4' and 5', of intermediate polarity,

Table 2. Bacterial mutagenicity of HPLC(1) fractions of composite dichloromethane extract of total suspended particulate matter (2)

Sample	µg per Plate	Revertants/µg ± S.D. TA-98	TA-100
ORIGINAL COMPOSITE:	414	1.19±0.06	0.56±0.05(3)
	207	1.36±0.09	1.31±0.11
	103	1.64±0.14	1.55±0.19
FRACTIONS:			
1'	10.4	1.7±2.1	1.2±1.7
2'	23.0	0.7±0.8	0.7±0.8
3'	40.0	1.5±0.6	0.5±0.5
4' *	40.8	3.8±0.9	3.1±0.7
5' *	22.6	5.1±0.9	5.1±1.3
6'	55.0	1.7±0.5	1.0±0.5
7' *	21.5	1.7±0.9	2.8±1.1
8'	25.5	0.8±0.7	0.9±0.6

(1) High pressure liquid chromatography.
(2) 12-hr. samples, New York City, August, 1977.
(3) Toxicity noted at this concentration.
* Fractions exhibiting activity significantly higher than original composite sample.

showed 2-3 times higher levels of activity than the original material with both strains of bacteria while fraction 7' showed about twice as much activity with TA-100 only. While no gross toxic effects were observed for the plates, the numbers in Table 2 must be interpreted with caution as they were determined from a single dose (duplicate samples) rather than a dose-response curve due to the limited amounts of material available. The doses for the fractions were, however, 2-10 times lower than the lowest dose tested for the composite sample and the sum of the activity of the fractions was equal to the activity of the original composite, within experimental uncertainty.

SUMMARY AND CONCLUSIONS

The presence of direct-acting bacterial mutagenic compounds of a wide range of polarity has been demonstrated at comparable levels for both the winter and summer aerosols of New York City. Although the chemical identities of the compounds responsible for this activity remain to be determined, the results to date indicate the presence of compounds other than PAH in the aerosol which may be of concern to human health. Additionally, the nature and source of some of these materials may differ from one season to the next. Work is now in progress in our laboratory to identify and test the compounds responsible for the observed bacterial mutagenicity.

ACKNOWLEDGEMENTS

The authors wish to thank M. A. Leyko, R. Hershman and B. D. Naumann for sample collection and preparation and Dr. S. Kline for help with the HPLC work.

This work is supported by Grant No. RP 1058l of the Electric Power Research Institute and by the American Petroleum Institute and is part of Center programs supported by Grant No. ES 00260 from the National Institute of Environmental Health Sciences and by Grant Nc. CA-13343 from the National Cancer Institute.

REFERENCES

1. E. Sawicki, "The genotoxic environmental pollutants," Paper presented at the Symposium in Management of Residuals from Synthetic Fuels Production, Denver, Colorado, May 25, 1976.

2. F. Mukai and W. Troll, "The mutagenicity and initiating activity of some aromatic amine metabolites," Ann. N.Y. Acad. Sci. 163, 828 (1969).

3. B. N. Ames, J. McCann and E. Yamasaki, "Methods for detecting carcinogens and mutagens with the Salmonella/mammalian-microsome mutagenicity test," Mut. Res., 31, 347 (1975).

4. J. McCann, E. Choi, E. Yamasaki, and B. N. Ames, "Detection of carcinogens as mutagens in the Salmonella/microsome test: Assay of 300 chemicals," Proc. Nat. Acad. Sci., U.S.A., 72, 5135 (1975).

5. R. Talcott and E. Wei, "Brief communication: Airborne mutagens bioassayed in Salmonella typhimurium," J. Nat'l. Cancer Inst., 58, 449 (1977).

6. J. N. Pitts, Jr., D. Grosjean, T. M. Mischke, V. F. Simmon and D. Polle, "Mutagenic activity of airborne particulate organic pollutants," Toxicology Letters, 1, 65 (1977).

7. S. Agarwal, New York University Medical Center, Unpublished data.

8. J. M. Daisey, M. A. Leyko, M. T. Kleinman and E. Hoffman, "The nature of the organic fraction of the New York City Summer Aerosol," Presented at the 1977 American Industrial Hygiene Conference, New Orleans, La., May 22-27, 1977.

9. T. J. Kneip, M. A. Leyko, M. T. Kleinman, M. Lippmann and J. M. Daisey, "Organic matter in New York City TSP: Comparisons of seasonal variations and relationships to source tracers," Conference on Carbonaceous Particles in the Atmosphere, Berkeley, Calif. March 20-22, 1978.

MUTAGENIC ACTIVITY OF FOSSIL FUEL COMBUSTION PRODUCTS

Debra A. Kaden
William G. Thilly
Toxicology Group
Department of Nutrition and Food Science
Massachusetts Institute of Techology
Cambridge, Massachusetts

ABSTRACT

The methylene chloride extracts of several soots, containing the polycyclic aromatic hydrocarbon fraction, were examined for their mutagenic activity in Salmonella typhimurium. Resistance to the purine analog 8-azaguanine was used as a genetic marker. To allow metabolism of pro-mutagens to their biologically active forms, a postmitochondrial supernatant drug-metabolizing system derived from livers of phenobarbitol and/or aroclor pretreated rats was incorporated into all assays. The observed mutagenicity of the soot extracts was ten to twenty times higher than could be accounted for by the amount of benzo(a)-pyrene present. Synergistic activity between benzo(a)pyrene and other components of the soot extracts was discounted by the simple additive mutagenicity of soot extract and added benzo(a)pyrene. The predominant polycyclic aromatic hydrocarbon components of a representative soot extract were quantitatively assayed for their mutagenic potential. Nine of these components were found to be mutagenic to S.typhimurium. Two components, perylene and acepyrylene, exhibit more mutagenic activity than benzo(a)pyrene on a equimolar level. Utilizing the measured mutagenic activities of the polycyclic aromatic hydrocarbon components of a fresh kerosene soot sample, we were able to account for the mutagenicity of the methylene chloride extract by an additive contribution of its various components.

INTRODUCTION

Byproducts of fossil fuel combustion processes are found distributed throughout the environment. Polycyclic aromatic hydrocarbons (PCAH) are formed as a result of the incomplete combustion of any organic material, and are generally found bound to particulate matter such as soot or fly ash. Two to fifteen percent of the fine particle mass in the atmosphere of a typical city is soot. The size range of these particles, 0.01-10.0 μm in diameter, makes the bulk of this material very likely to be retained in the lower respiratory tract (1).

It has now been two centuries since the biohazards of soot were first suspected. Percival Pott, a British physician, noted a high correlation between the occurrence of cancer of the scrotum and the occupation of chimney sweep (2). Since that time, numerous experiments have demonstrated soot as an animal carcinogen (3-10). Extracts of atmospheric particulate matter have been shown to induce transformation in rat and hamster embryo cells in culture (11) and mutation in the bacteria Salmonella typhimurium (12-16).

Although the mutagen/carcinogen benzo(a)pyrene (BaP) has been identified as one component of soot, fly ash, and particulate atmospheric matter, it is not present in high enough concentration to account for the high activity of these substances.

We present here the results of our investigations, demonstrating the full accounting of mutagenicity of soot extracts, utilizing a new quantitative bacterial mutation assay which is particularly well suited for the analysis of complex mixtures (17).

RESULTS AND DISCUSSION

Mutation was measured as the fraction of the treated bacterial culture resistant to the purine analog 8-azaguanine. A complete description of the procedure has been previously reported (17). BaP-induced mutation was carried out in each assay to act as an internal control.

Using this assay, the methylene chloride extracts of soots produced through the combustion of high nitrogen-, high sulfur-, and kerosene-containing fuels were all found to be mutagenic at concentrations of 20 to 50 μg/ml in a two-hour exposure (Figure 1). Initial slopes of the concentration dependence of induced mutation divided by background mutant fraction show the kerosene soot to have 20 percent of the activity of pure BaP, the S-containing soot 13 percent, and the N-containing soot 11 percent.

As BaP constitutes less than one percent of these soot extracts, its presence could not account for the high activity of the soot extracts. Two possible explanations for this activity were examined: mutagenic components could act synergistically with each other and non-mutagenic components with respect to their mutagenic activity; or there may be other components of the soots with undiscovered mutagenic activity which could cumulatively account for all of the activity of the soot extracts.

The mutagenic activity of a soot extract and added BaP appears to be completely additive over a wide range of BaP concentrations (Figure 2). This would indicate that synergism of the order necessary to explain soots' high activity is not occurring.

To test the alternative hypothesis of other components having undiscovered high mutagenicity, the major components of a kerosene soot extract were

assayed for their mutagenic potential. Nine of the fourteen major components of a kerosene soot extract exhibited significant mutation in S. typhimurium (Figures 3-10 and Table).

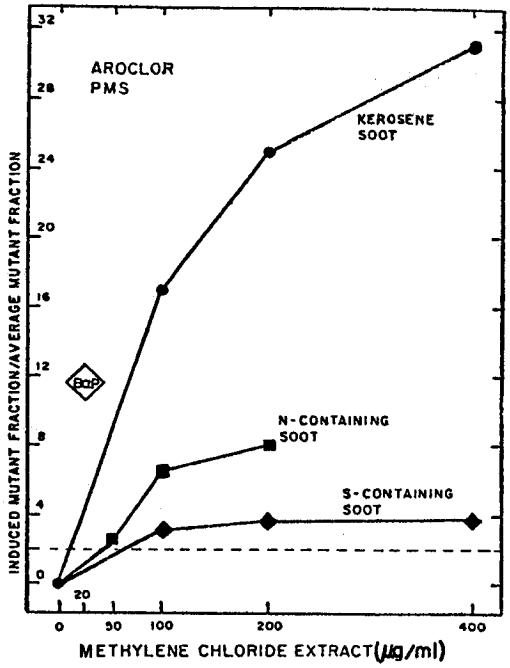

Fig. 1. Dose-dependent mutagenicity of methylene chloride extracts from kerosene, nitrogen-, and sulfur-containing soots to S. typhimurium TM677 in the presence of aroclor-induced post-mitochondrial supernatant (PMS). Each point represents the average of two independent determinations.

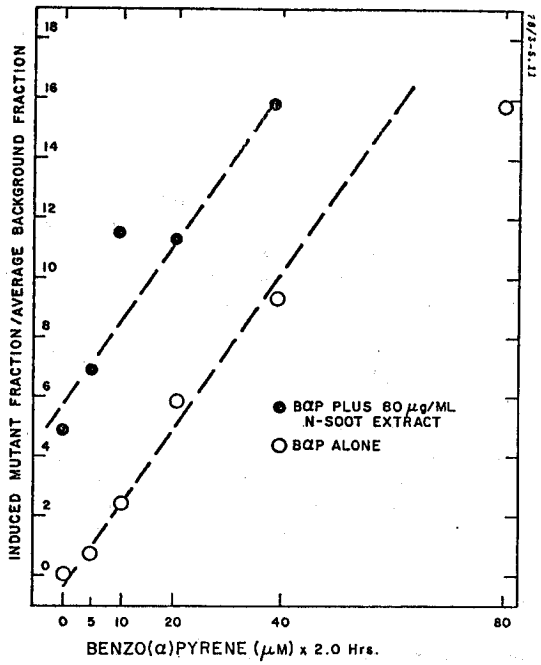

Fig. 2. Dose-dependent mutagenicity of benzo(a)-pyrene to S. typhimurium TM677 in the presence and absence of 80 μg/ml of a methylene chloride extract of a nitrogen-containing soot. An aroclor-induced PMS drug-metabolizing system was incorporated into the assay. Each point represents the average of two independent determinations.

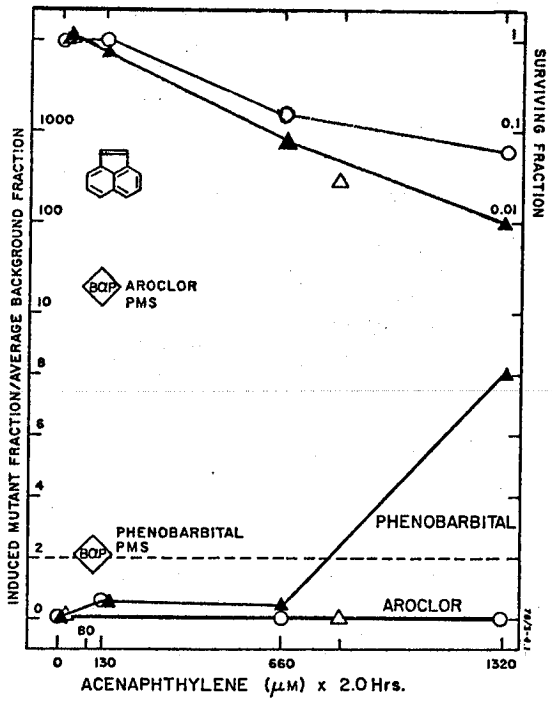

Fig. 3. Dose-dependent mutagenicity and toxicity of acenaphthylene to S. typhimurium TM677 in the presence of aroclor-induced PMS and phenobarbital-induced PMS. Each point represents the average of two independent determinations.

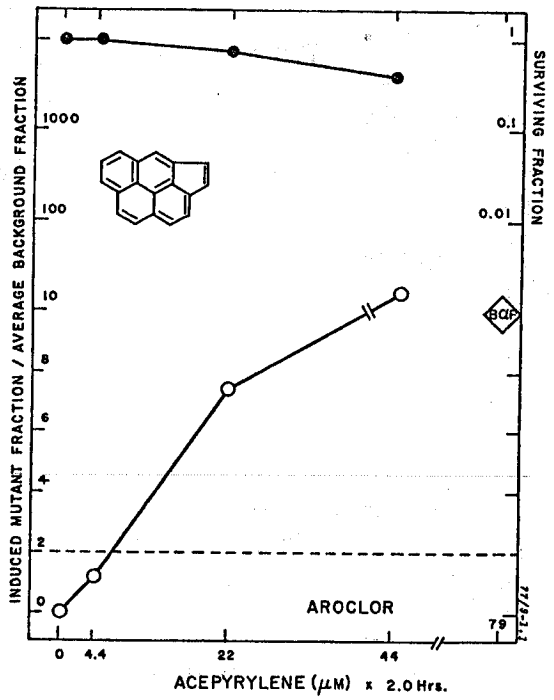

Fig. 4. Dose-dependent mutagenicity and toxicity of acepyrylene to S. typhimurium TM677 in the presence of aroclor-induced PMS. Each point represetns the average of two independent determinations.

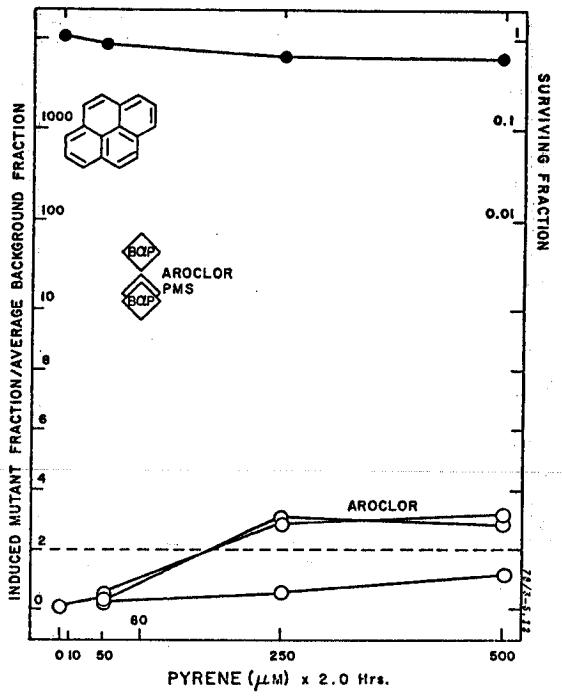

Fig. 5. Dose-dependent mutagenicity and toxicity to pyrene to S. typhimurium TM677 in the presence of aroclor-induced PMS. Each point represents the average of two independent determinations.

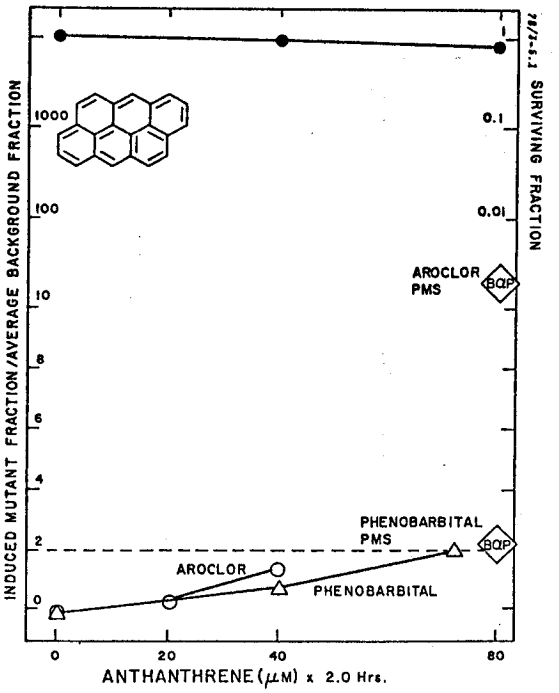

Fig. 6. Dose-dependent mutagenicity and toxicity of anthanthrene to S. typhimurium TM677 in the presence of aroclor-induced PMS and phenobarbital-induced PMS. Each point represents the average of two independent determinations.

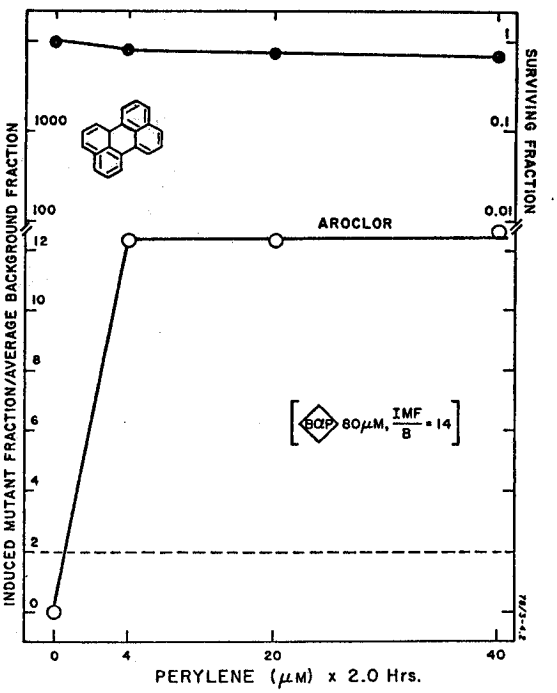

Fig. 7. Dose-dependent mutagenicity and toxicity of perylene to S. typhimurium TM677 in the presence of aroclor-induced PMS. Each point represents the average of two independent determinations.

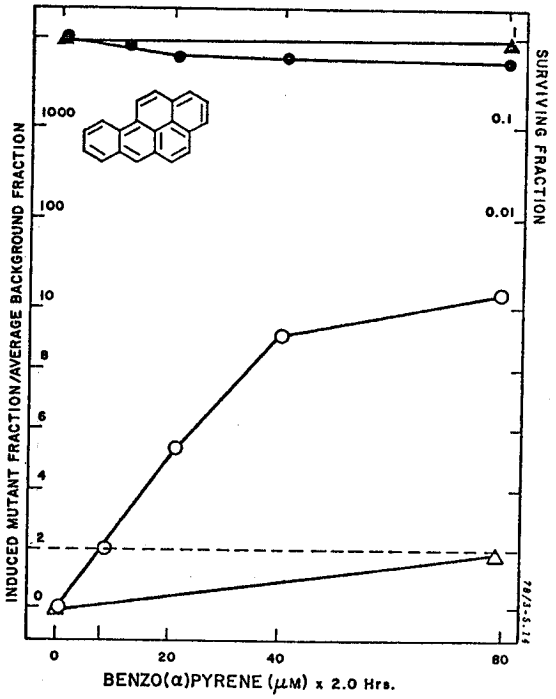

Fig. 8. Dose-dependent mutagenicity and toxicity of benzo(a)pyrene to S. typhimurium TM677 in the presence of aroclor-induced PMS and phenobarbital-induced PMS. Each point represents the average of two independent determinations.

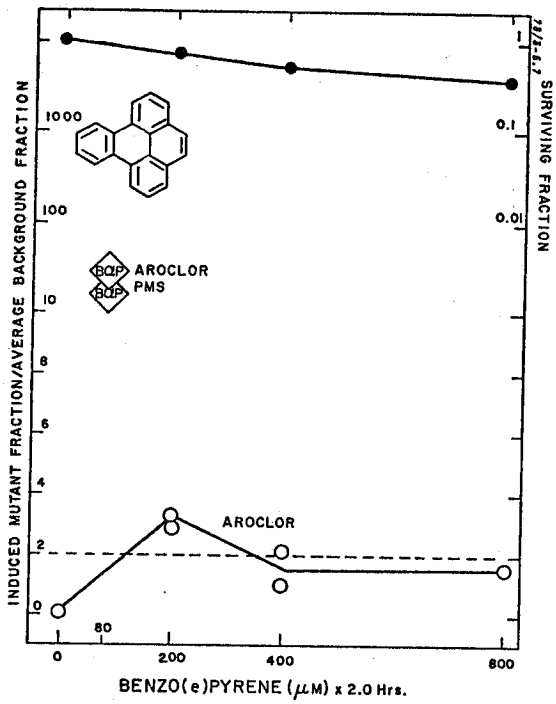

Fig. 9. Dose-dependent mutagenicity and toxicity of benzo(e)pyrene to S. typhimurium TM677 in the presence of aroclor-induced PMS. Each point represents the average of two independent determinations.

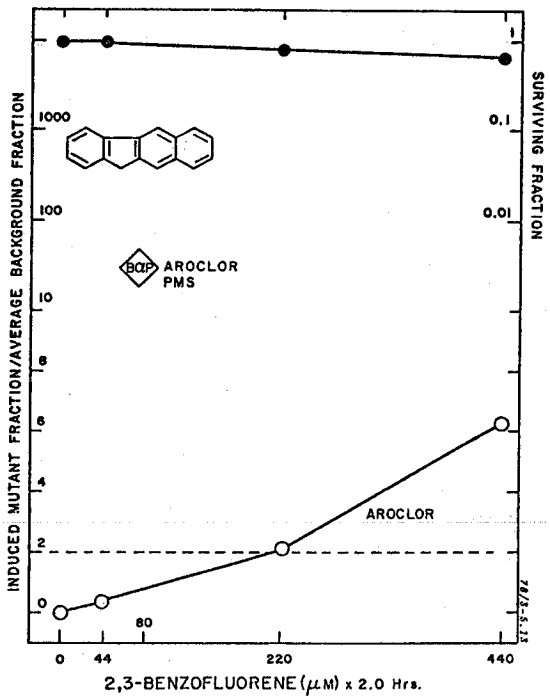

Fig. 10. Dose-dependent mutagenicity and toxicity of 2,3-benzofluorene to S. typhimurium TM677 in the presence of aroclor-induced PMS. Each point represents the average of two independent determinations.

Of particular interest is the high mutagenicity of perylene which induced six times the amount of mutation as BaP on an equimolar level (Fig. 7). Perylene is widely distributed throughout the environment and although it was found to be non-carcinogenic when painted upon the skin of mice (18), it appears to be responsible for the finding that 40 percent of a certain population of salamanders developed skin tumors (19).

Acepyrylene [cyclopenta(c,d)pyrene] also exhibits high mutagenicity in S. typhimurium (Fig. 4). It constitutes 15 percent of the weight of the kerosene soot extract, and appears to be one to two times as active as BaP on an equimolar level. Thus, acepyrylene alone can account for almost all of the mutagenicity of the soot extract.

As can be seen in the Table, the mutagenicity of the kerosene soot extract can now be totally accounted for through the additive contribution of its PCAH components. That the complex mixture now appears to be somewhat less active than would be expected on the basis of its components may be due to either the impression of our estimates to to a partial competition for the metabolizing reactions.

Compound	Relative Mutagenic Activity	Weight	Expected Relative Weighted Activity
Acenaphthylene	0.07	23	0.02
Acepyrylene	1.5	15	0.23
Pyrene	0.07	8	0.01
Benzo(ghi)perylene + Anthanthrene	<0.01 0.09	8	0.00
Coronene	--	5	--
Fluoranthene	--	4	--
Naphthalene	<0.01	3	0.00
Benzo(ghi)fluoranthene	--	3	--
Phenanthrene + Anthracene	<0.01 <0.01	2	0.00
Benzacenaphthalene	--	2	--
Benzofluoranthene	--	2	--
Perylene	6.0	2	0.12
Acenaphthalene	0.01	1	0.00
Indeno(1,2,3-cd)pyrene	--	1	--
Benzo(a)pyrene + Benzo(e)pyrene	1.00 0.11	1	0.01
4H-Cyclopenta(def)-phenanthrene	--	1	--
Benzofluorene	0.08	0.4	0.00
Fluorene	<0.01	0.3	0.00
Uncharacterized Material	--	18.3	--
Σ COMPONENTS			0.39
$MeCl_2$ Extract	0.20	100.0	0.20

Table 1. Mutagenic Activity Accounting of Kerosene Soot $MeCl_2$ Extract.

REFERENCES

1. Macias, E. S. (1978). Presentation at Conference on Carbonaceous Particles in the Atmosphere. Berkeley, CA; National Science Foundation and Lawrence Berkeley Laboratory.

2. International Agency for Research on Cancer (1973). Vol. 3. Lyon, France: IARC.

3. Passey, R.D. (1922). Brit. Med. J. 2:1112-1113.

4. Passey, R.D. and Carter-Braine, J. (1925). J. Path. and Bact. 28:133-144.

5. Seelig, M.G. and Benignus, A.B. (1936). Am. J. Cancer 28:96.

6. Campbell, J.A. (1939). Brit. J. Exp. Path. 20:122-132.

7. McDonald, J.C., Drinker, P. and Gordon, J. (1951). Am. J. Med. Sci. 221:325-342.

8. Shimkin, M.B. and Leiter, J. (1960). J. Natl. Cancer Inst. 1:241-254.

9. Leiter, J., Shimkin, M.B. and Shear, M.J. (1942). J. Natl. Cancer Inst. 3:155-165.

10. Epstein, S.S., Joshi, S., Andrea, J., Mantel, N. Sawicki, E., Stanley, T. and Tabor, E.C. (1966). Nature 212:1305-1307.

11.Freeman, A.E., Price, P.J., Bryan, R.J., Gordon, R.J., Gilden, R.V., Kelloff, G.J., and Huebner, R. J. (1971). PNAS 68:445-449.

12. Tokiwa, H., Morita, K., Takeyoski, H., Takahashu, K., Ohnishi, Y. (1977). Mutation Res. 48:237-248.

13. Pitts, Jr., J.N., Grosjean, D., Mischke, T.M. (1977). Toxicology Letters 1:65-70.

14. Daisey, J.M., Hawryluk, I., Kneip, T.J. and Mukai, F.H. (1978). Presentation at Conference on Carbonaceous Particles in the Atmosphere. Berkeley, CA: National Science Foundation and Lawrence Berkeley Laboratory.

15. Teranishi, K., Hamada, K. and Watanabe, H. (1978). Mutation Res. 56:373-380.

16. Chrisp, C.E., Fisher, G.L. and Lammert, J.E. (1978). Science 199:73-75.

17. Skopek, T.R., Liber, H.L., Krolewski, J.J. and Thilly, W.G. (1978). Proc. Natl. Acad. Sci., USA. 75:410-414.

18. Horton, A.W. and Christian, G.M. (1974). J. Natl. Cancer Inst. 53:1017-1020.

19. Rose, F.L. and Harshburger, J.C. (1977). Sci. 196:315-317.

Sources and Physical Properties

SIZE DISTRIBUTION AND PHYSICAL PROPERTIES OF COMBUSTION AEROSOLS

Kenneth T. Whitby
Department of Mechanical Engineering
University of Minnesota, Minneapolis, MN 55455

ABSTRACT

The results from combustion aerosol research on diffusion flames, premixed propane flames, diesel aerosols, and aerosols from automobiles on Los Angeles freeways and from catalyst-equipped cars are described. Aerosol size distributions have been modeled by fitting three log-normal distributions to the observed modes. The nuclei mode usually has a geometric mean diameter by volume, DGV_n, in the 0.005 to 0.04 μm range, and a σ_g in the 1.3 to 1.7 range, and may account for most of the aerosol mass for clean-burning fuels such as propane or methanol. The accumulation mode usually has a size in the 0.15 to 0.5 μm range with a σ_g of from 1.6 to 2. The higher the concentration of aerosol, the greater the mass fraction found in the accumulation mode. If the log of the mass concentration of combustion aerosols is plotted vs. the log of DGV overall, then most rapidly diluted combustion aerosols are found to the left of a line given by mass concentration, $\mu g\ cm^{-3}$, = $1.14 \times 10^8 (DGV)^{6.35}$. It has been found that the exhaust aerosol from moving vehicles is diluted very rapidly by 10^3 to 10^4, effectively stopping coagulation and condensation after the aerosol leaves the exhaust pipe.

Introduction

Since 1965, there have been significant advances in our ability to measure atmospheric aerosols, which in turn have led to a good understanding of the physical and chemical size distributions. However, these techniques have only been recently applied to combustion aerosols because high concentrations, high temperatures, and the great variety of different sampling situations encountered make good size distribution measurements of combustion aerosols much more difficult than for atmospheric aerosols.

Much of the work on combustion aerosol size distributions has concentrated on either the aerosols produced by quite dirty combustion resulting from problems with the combustor itself or on the details of the aerosol formation process itself in the flame. However, the combustion aerosol characteristics of interest in air pollution also include aerosols produced by combustion that is in compliance from an air pollution point of view as well as the many processes which affect the growth and chemical characteristics of the aerosols from the flame to the mixing of the plume into the ambient atmosphere.

This paper will review the combustion aerosol research performed by the University of Minnesota group over the past eight years. Since our interests have been primarily in the contribution of primary aerosols from clean combustion to the ambient atmosphere, and because our early capabilities were limited mostly to size distribution measurements, this paper will be limited to the discussion of combustion aerosol size distributions.

Following are the main combustion aerosol-related experiments in which our group has been involved.

* Electrical aerosol analyzer size distribution measurements of simple diffusion flames (1970).
* Size distributions, concentration and humidity dependence of aerosols from premixed propane flames (1972 to 1977).
* Size distributions and chemistry of aerosols measured alongside of the Harbor Freeway in Los Angeles as part of the ACHEX program (1972).
* Size distributions and chemistry of aerosols on and alongside of the General Motors test track during the GM sulfate experiment (1975).
* Size distributions and chemistry of aerosols on Los Angeles freeways (1976).
* Size distribution, sampling problems and dilution of diesel aerosols in the laboratory and on the roadway (1974 to present).
* Size distribution modeling studies of combustion aerosols (1974 to present).

Early Size Distribution Measurements of Aerosols from Clean Diffusion Flames

In 1970, Husar and Whitby[1] used the newly developed electrical aerosol analyzer (EAA) to measure the size distributions produced by diffusion flame, burning such fuels as alcohol, wax, kerosine, and benzene. In these experiments, a small wick burning the fuel was placed in a glove box supplied with clean air for dilution, and the aerosols measured at the outlet after the combustion products had been diluted with from 100 to 400 l/min of clean air. Typical surface area size distributions showing a nuclei mode and an accumulation mode are shown in Fig. 1. Modal parameters are shown in Table 1.

Two submicron modes, one at about 0.01 μm called the nuclei mode, and one in the 0.1 to 0.5 μm range called the accumulation mode, were observed. The cleaner the flame, the greater the fraction in the nuclei mode. Dirty flames from benzene-kerosine produced mostly accumulation mode particles. From Table 1, it will be noted that

Table 1. Modal and overall distribution parameters of selected combustion aerosol size distributions.

No.	Aerosol and Source	Nuclei Mode DGV, μm	σ_g	V_n, $\mu m^3 cm^{-3}$	Accumulation Mode DGV, μm	σ_g	V_a, $\mu m^3 cm^{-3}$	Overall Distribution DGV, μm	VT, $\mu m^3 cm^{-3}$
1	Diesel[9] - 1.8 Kw	0.016	1.21	392	0.12	1.9	1.8×10^4	0.12	1.8×10^4
2	Diesel[11]	---	---	---	0.2	1.7	5×10^4	0.2	5×10^4
3	Premixed acetylene - oxygen[16]	0.03	1.5	1.7×10^4	---	---	---	0.03	1.7×10^4
5	Premixed propane[3]	0.007 - 0.05	1.3 - 1.6	2-5000 x 10^{-4}	---	---	---	0.007 - 0.05	2-5000 x 10^{-4}
6	Premixed kerosene[17]	0.05	1.5	3.5×10^3	---	---	---	0.05	3.5×10^3
7	Jet engine[18]	---	---	---	0.15	1.8	7×10^3	0.15	7×10^3
8	Auto engine - leaded fuel, 30 & 50 mph[4]	0.03 - 0.06	1.7	7-44 x 10^3	---	---	---	0.03 - 0.06	7-44 x 10^3
9*	30 m from Harbor Freeway[4]	0.04	1.7	17	---	---	---	0.04	17
16*	Freeway average in Los Angeles[8]	0.029	1.7	8.7	0.17	1.9	15.2	0.09	23.9
17*	G. M. Sulfate Study, parallel wind[5]	0.033	1.6	21.0	0.31	1.8	12.6	0.08	33.6
18*	G. M. Sulfate Study, typical[5]	0.025	1.5	3.32	---	---	---	0.025	3.32
19	Candle flame	0.020	1.56	.25	0.29	1.58	5.6	0.26	5.85
20	Tobacco smoke off of end	---	---	---	0.64	1.9	414	0.64	414
22	Acetone diffusion flame	0.017	1.42	0.26	0.33	1.56	31.4	0.32	31.7
23	Acetone diffusion flame - rapid dilution	0.028	1.44	0.64	0.31	1.69	129	0.31	129.6
24	Methanol diffusion flame	0.016	1.49	0.52	---	---	---	0.016	0.52

* Difference distribution = roadway - background.

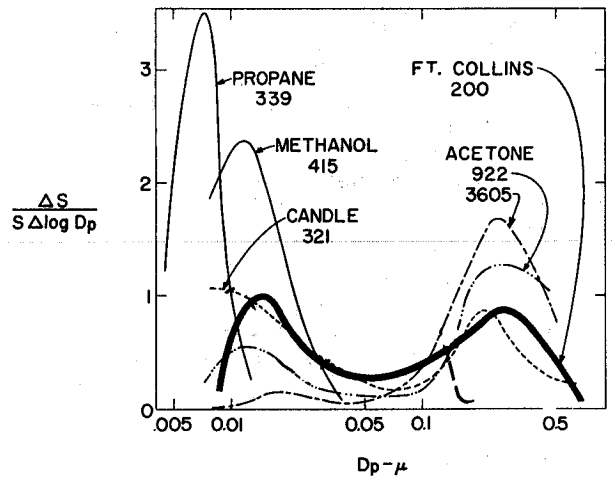

Fig. 1. Surface size distributions of the aerosol produced by several diffusion flames with moderate dilution. Numbers under each label are the total surface area in $\mu m^2 cm^{-3}$.

the volume in the nuclei mode, V_n, is relatively constant for these aerosols even though the volume in the accumulation mode, V_a, varies from 6 to 414 $\mu m^3 cm^{-3}$. Since the time between formation in the flame and sampling was relatively constant at a few seconds, this suggests that if a higher mass concentration is formed by the flame, the extra mass coagulates over to the accumulation mode, leaving a relatively constant amount in the nuclei mode.

Size Distributions, Concentration and Humidity Dependence of Aerosols Produced by Premixed Flames

In 1972, Fissan[2] found that the aerosols produced by a clean propane premixed flame were very hygroscopic, and that the number concentration seemed to depend strongly on the relative humidity of the air surrounding the flame. He found that the size of these aerosols was very small, on the order of 0.01 μm.

This was followed up by Barsic,[3] who made a thorough study of the variables affecting aerosol

size and concentration from a propane diffusion flame. Using a small premixed flame with as rapid a dilution as could be accomplished without adversely affecting the flame, he studied air fuel ratios from 0.5 to 1.4, relative humidities around the flame from 31 to 92%, commercial and research purity propane, and some of the effects of varying the sulfur content of the fuel. Number concentrations were measured with a G.E. Aitken nuclei counter, and size distributions were measured with an EAA, a diffusion battery, and a parallel plate ion counter.

A typical size distribution is shown in Fig. 2. For a fuel-rich flame diluted with unfiltered air, three modes could be observed in the submicron size distribution. There were two nuclei modes, one a little smaller than 0.01 μm and one around 0.03 μm. An accumulation mode was only observed when the flame was diluted with unfiltered air. Apparently this mode came from transformed or untransformed aerosols already in the dilution air.

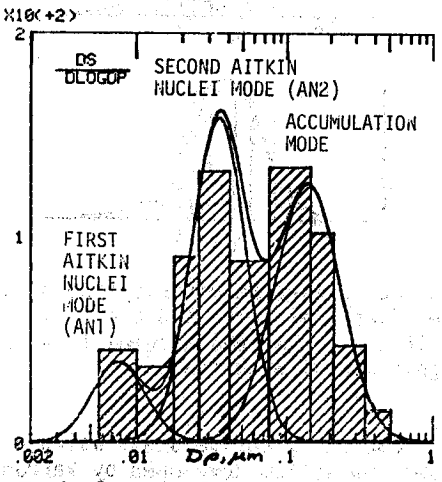

Fig. 2. Typical aerosol from a rich propane flame diluted with unfiltered air. Nuclei mode 1 is produced by sulfur in the fuel; nuclei mode 2 is carbon, dependent on the A/F ratio. The accumulation mode is only observed when unfiltered air is used for dilution.

Figure 3 shows that when the A/F ratio was stoichiometric, the volume of aerosol in the AN1 mode was much larger than the volume in the AN2 mode, and the volume was very dependent on the RH. From the fact that the volume concentration of AN1 was dependent on the sulfur content of the fuel, Barsic concluded that AN1 probably consisted of a hygroscopic sulfur compound, probably H_2SO_4. Electron microscope examination combined with the relatively hydrophobic nature of the AN2 mode suggest that it is carbon.

Barsic's work shows that at least three modes having different chemical composition and different origins may be observed from propane combustion.

Size Distributions and Chemistry of Aerosols Measured alongside of the Harbor Freeway in Los Angeles during the ACHEX Program in 1972

In 1972, as part of the Aerosol Characterization Experiment (ACHEX) sponsored by the Air Re-

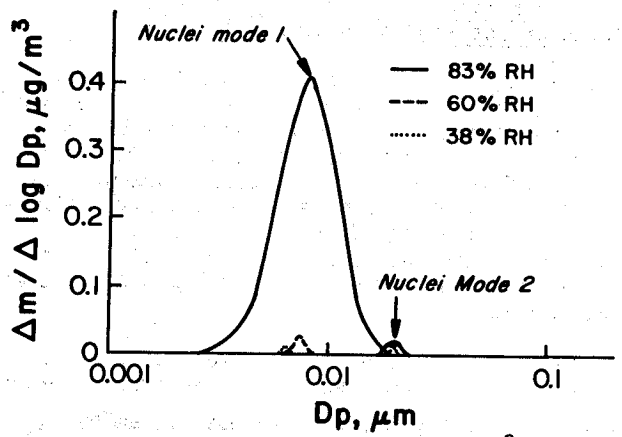

Fig. 3. Nuclei modes measured by Barsic[3] in the products of combustion of a sulfur-containing propane flame at a stoichiometric A/F ratio. Mode 1 is quite hygroscopic while Mode 2 is not. It is believed that Mode 1 is formed by the sulfur in the fuel. Mode 2 is carbon.

sources Board of the State of California, aerosols and gases were measured at a distance of about 50 m in the plume from the Harbor Freeway in Los Angeles.[4] During the morning rush hour, the parameters of the difference distribution (observed distribution - the background distribution) were found to be DGV = 0.04 μm, σ_g = 1.73, and volume concentration, V_n = 17 $\mu m^3 cm^{-3}$. The resolution of the techniques used in that study was not sufficient to determine whether there was a significant addition to the accumulation mode. However, it was clear that most of the aerosol was in the nuclei mode and smaller in size than that usually reported from laboratory studies in dilution tunnels at that time. It thus appeared that the dilution behind moving automobiles was more rapid than in most dilution tunnels. This rapid dilution stopped coagulation and condensational aerosol growth at a smaller size than was the case in many dilution tunnels.

Size Distributions Measured on and alongside of the Test Roadway during the General Motors Sulfate Experiment

In 1975, measurement of the size distribution and concentration of aerosols on and about 50 m from the GM Milford test track were made using a specially instrumented Ford sedan on the track and the EPA large moveable laboratory alongside.[5] The design and major results of the overall experiment have been described by Cadle et al.[6] and Wilson et al.[7] Because the cars were all new, well-tuned and -operated automobiles equipped with catalysts, it was expected that the emitted aerosols would be primarily H_2SO_4. Except for one run where the wind was almost exactly parallel to the roadway, the aerosols showed only a single mode having DGV_n = 0.025 μm, σ_g = 1.5 and V_n = 3.5 $\mu m^3 cm^{-3}$. For the parallel wind case, sufficient aerosol had coagulated to form an accumulation mode. Parameters of the two modes are in Table 1.

Size Distributions and Chemistry of Aerosols Measured on Los Angeles Roadways in 1976

In 1976, as part of an EPA-sponsored roadway study, the University of Minnesota used its mobile laboratory to make measurements of aerosols and gases on several Los Angeles freeways under a variety of traffic conditions.[8] Because upwind distributions were easy to measure accurately, difference distributions could be obtained under all conditions. Under all conditions of traffic, it was found that aerosol was added to both the nuclei and accumulation modes.

Figure 4 shows the grand average size distribution from the seven best runs. The grand average amount added to the nuclei mode was 9.2 $\mu m^3 cm^{-3}$, and to the accumulation mode, 16.3 $\mu m^3 cm^{-3}$. Comparison of these ΔV's with the ΔV's in Fig. 4 shows that because of the Santa Anna conditions prevailing during these experiments, most of the aerosol measured on the freeways came from the vehicles on the freeway.

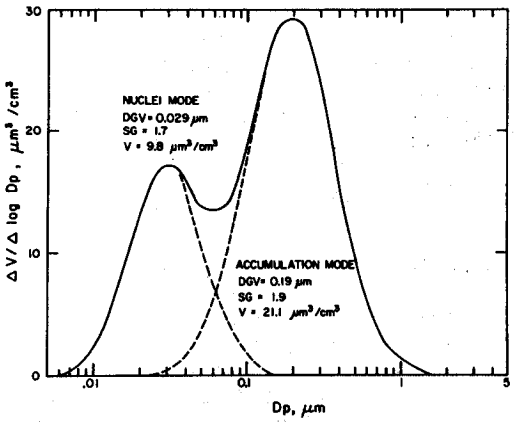

Fig. 4. Grand average volume size distribution of aerosol measured on several Los Angeles freeways showing the predominant two modes. This distribution was calculated by averaging the modal parameters and then calculatinag the distribution from them.

During this study, the concentration as a function of distance, with the wind in cross-flow, was measured up to 1 Km from the freeway. Examination of the size distribution data and comparisons with plume models showed that the decay in nuclei mode concentration was entirely by dilution. This means that chemically different aerosols emitted by different vehicles will not coagulate together until long after the roadway plume has been diluted by the ambient aerosol if the wind is across the roadway at anything near normal velocities. Coagulation in the roadway plume will only be significant if the wind is parallel to the roadway or is very low in velocity.

Diesel Exhaust Aerosol Size Distributions

Beginning in 1975, Kittelson and his students began to apply the EAA to the measurement of diesel aerosols. Since he has presented a separate paper at this conference describing this work, only a few important findings and some work on the modeling and comparisons of diesel exhaust size distributions will be discussed here.

One of the early size distributions is presented in Fig. 5. This figure shows that a nuclei and an accumulation mode are observed and that they are strong functions of the load.

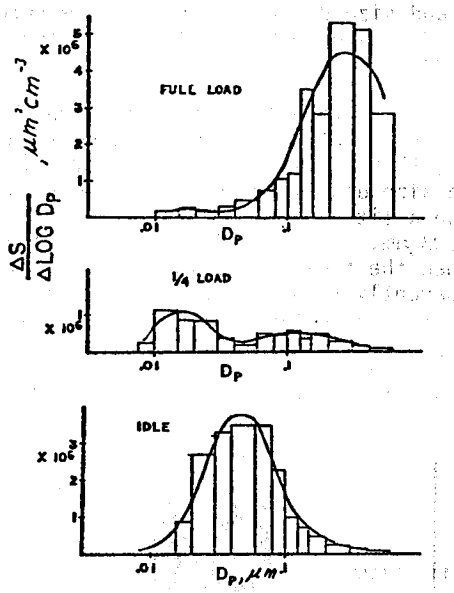

Fig. 5. Surface area-size distribution of a 6 cyl. open chamber diesel at idle, 1/4 and full load. The amount in the nuclei and accumulation modes changes significantly with load.

Dolan[9] made an extensive study using a much improved sampling system developed by Verrant.[10]

Most size distribution studies have been made using a cascade impactor or an optical particle counter. Figures 6 and 7 compare one of Dolan's average size distributions obtained at a medium load with an impactor distribution measured by Vuk et al.[11] and an optical counter distribution measured by Laresgoiti et al.[12] These figures show that if the various kinds of data are modeled and compared correctly, they are in substantial agreement. These figures also show that the diesel aerosol also may have a small coarse particle mode with a geometric mean size in the 3-4 μm range.

The procedures by which the amounts in the three modes can be obtained by the fitting of three log-normal size distributions to the individual modes have been described recently by Whitby.[13]

Thus, diesel aerosols may have a nuclei, an accumulation, and a coarse particle mode. It is known that the nuclei and accumulation modes are primarily carbon that has stayed suspended through the exhaust system. The coarse mode may be aerosol which has been deposited on the exhaust system, agglomerated, and resuspended.

Figure 7 also shows that by themselves, the cascade impactor (CI), the electrical aerosol analyzer (EAA), and the optical particle counter (OPC)

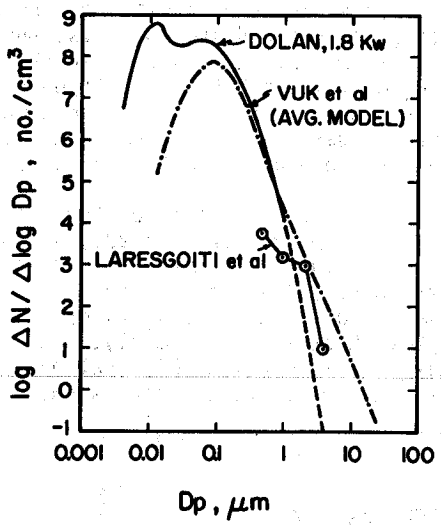

Fig. 6. Comparison of three diesel engine aerosol number size distributions. Further data on these aerosols is given in Table 1.

are incapable of characterizing the entire diesel size distribution. The CI has inadequate resolution below 0.5 μm, the EAA cannot measure above 1 μm, and the OPC cannot obtain reliable data below a few μm without extensive dilution. Of the three, the EAA probably provides the best data because most of the mass to be measured is normally below 1 μm, and the measurement can be made in situ with less dilution than is required by the OPC.

Kittelson's work, as discussed by him at this conference, has shown that unless diesel aerosol is diluted to ratios in excess of 500 to 1, condensation of volatile vapors in the dilution system may have a significant effect on the size distribution and mass concentration of the sampled aerosol. Furthermore, the 1976 Los Angeles roadway studies,[8] plus some more recent unpublished studies presently underway in our laboratory, suggest that real roadway dilution is very rapid due to the turbulence behind moving vehicles under most conditions. These recent experiments suggest that beyond 5 m behind a moving diesel automobile, the dilution is already between 10^3 and 10^4.

Size Distribution Modeling of Combustion Aerosols

It will already have been noted that the geometric standard deviation and geometric mean of multiple log-normal modes have been used to characterize combustion aerosols. This scheme, which was

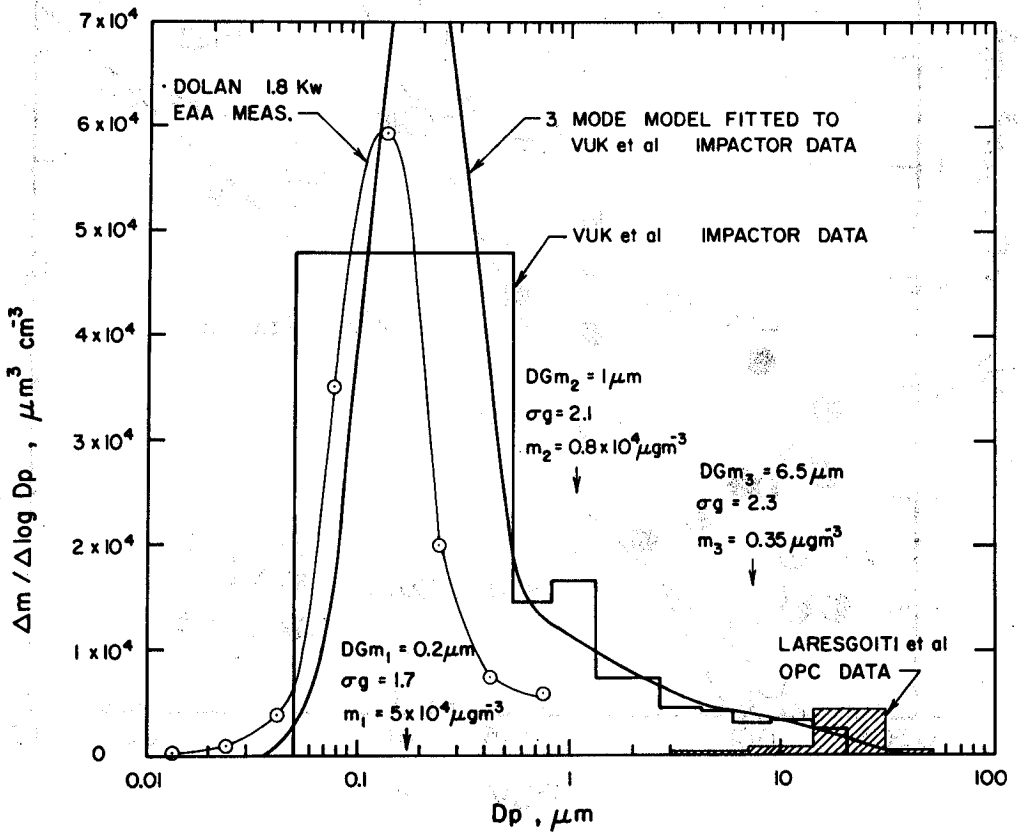

Fig. 7. Volume distributions of three diesel engine aerosols corresponding to the data in Fig. 6. Modal parameters of the best fit additive log-normal distributions are shown. Note that neither the OPC nor the impactor alone can provide a true characterization of the whole distribution.

originally developed for the description of atmospheric aerosols,[13,14] has also been found to be useful for the description of combustion aerosols.[3,15] Apart from the fact that it is convenient, examination of combustion aerosol size distributions shows that they can have up to three modes. Typically they have a nuclei mode with a DGV_n in the range from 0.007 to 0.04 μm, an accumulation mode with a DGV_a in the 0.1 to 0.6 μm range, and sometimes a coarse particle mode at several μm. In the case of vehicle emissions, the coarse particle mode seems to result from precipitation of fine particles on the walls of the exhaust system and subsequent reentrainment.

The accumulation mode seems to result primarily from coagulation and condensational growth of the nuclei mode-sized primary particles. The modal parameters of many of the aerosol size distributions that have been discussed previously are tabulated in Table 1 along with a few from the literature. The geometric mean diameter of the overall distributions is plotted in Fig. 8 vs. the total volume concentration. The numbers in the figure correspond to those in Table 1. Although comparing these DGV's and VT's is a little like comparing apples and oranges, there are some general conclusions that may be drawn from this figure.

Note that except for some of the diffusion flame aerosols (19, 20, 22, and 23), all of the aerosols are to the left of the dashed line. All of the aerosols to the left of the dashed line, whether measured in the laboratory or in the environment, have been diluted rapidly. It is observed that their size is considerably smaller for a given concentration. However, the more slowly diluted

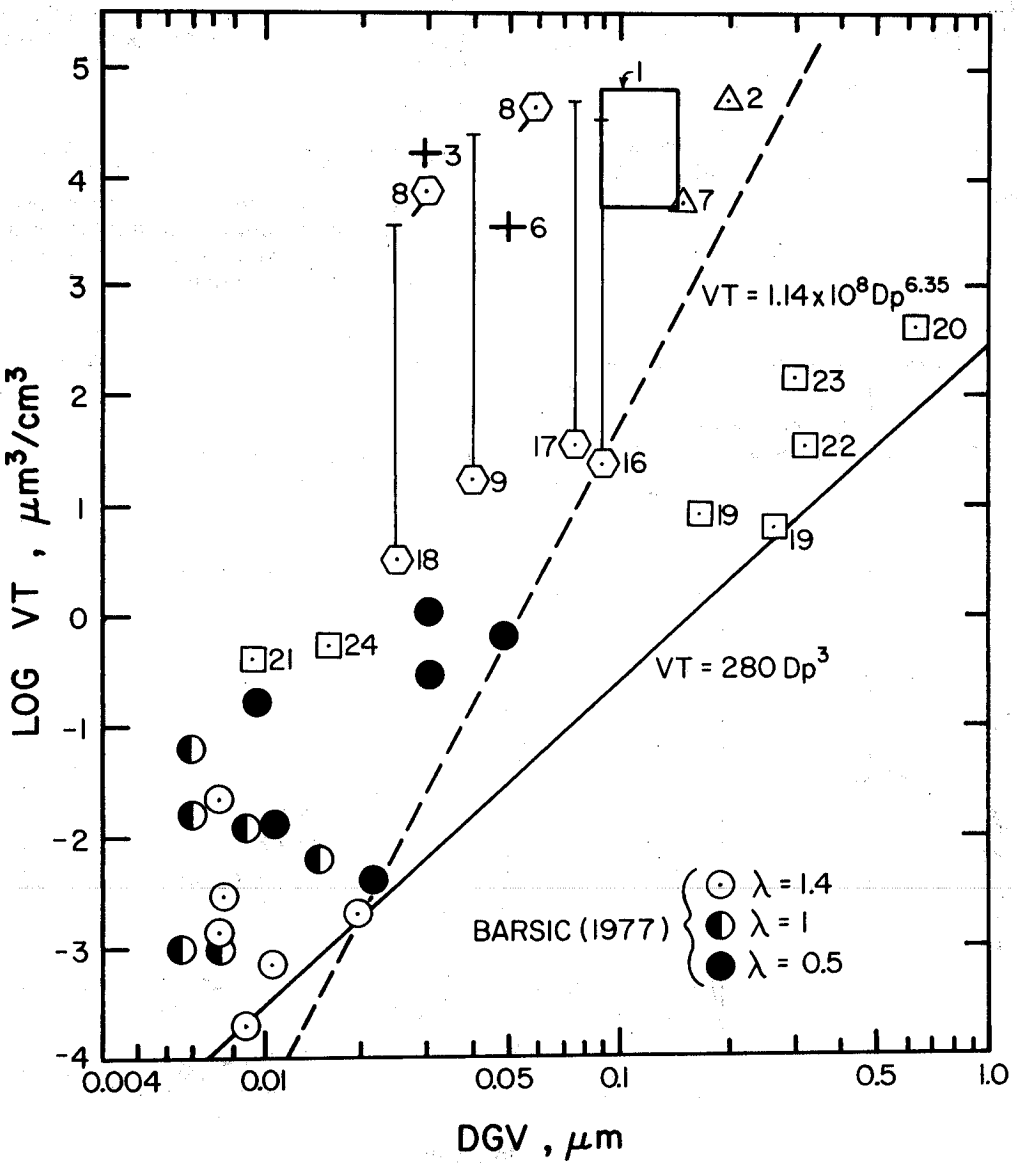

Fig. 8. Plot of the geometric mean diameters of the total distribution vs. either the mass or volume concentration corresponding to the data in Table 1. Note that except for the miscellaneous diffusion flames (19, 20, 22, and 23), all distributions fall to the left of the dashed line. For the roadway measured aerosols (7, 9, 16, and 18), a bar has been extended three orders of magnitude to higher concentration as a lower estimate of the tailpipe concentration.

diffusion flame aerosols have a significantly larger size for a given concentration.

For the roadway aerosols (9, 16, 17, and 18), the concentration bar has been extended three orders of magnitude to higher concentrations in order to provide an estimate of what the probable tailpipe concentration was. The position of these aerosols to the left of the dashed line, even after 10^3 dilution, shows just how effective is the rapid dilution at the tailpipe of a moving automobile.

Nomenclature

DGV	volume geometric mean diameter, μm
D_p	particle diameter, μm
m	mass concentration, $\mu g\ m^{-3}$
N	number concentration, no. cm^{-3}
S	surface area concentration, $\mu m^2 cm^{-3}$
V_n	nuclei mode volume concentration, $\mu m^3 cm^{-3}$
V_a	accumulation mode volume concentration, $\mu m^3 cm^{-3}$
VT	overall distribution volume concentration, $\mu m^3 cm^{-3}$
λ	oxidation ratio
	Subscripts
n	nuclei mode
a	accumulation mode

References and Footnotes

1. Husar, R. B. and K. T. Whitby (1970), Unpublished data.

2. Fissan, H. J., D. B. Kittelson and K. T. Whitby (1972), "Measurements of Aerosols Produced by a Propane-Air Flame in a Controlled Environment", Particle Technology Laboratory Publication No. 190, Mechanical Engineering Department, University of Minnesota, Minneapolis, MN.

3. Barsic, N. A. (1977), "Size Distributions and Concentrations of Fine Particles Produced by Propane-Air Combustion in a Controlled Humidity Environment", Ph.D. Thesis, Particle Technology Laboratory, Mechanical Engineering Department, University of Minnesota, Minneapolis, MN.

4. Whitby, K. T., W. E. Clark, V. A. Marple, G. M. Sverdrup, G. J. Sem, K. Willeke, B. Y. H. Liu and D. Y. H. Pui (1975), "Characterization of California Aerosols--Part I. Size Distributions of Freeway Aerosols", Atmos. Environ. 9:463-482.

5. Whitby, K. T., D. B. Kittelson, B. K. Cantrell, N. J. Barsic and D. F. Dolan (1977), "Aerosol Size Distributions and Concentrations Measured During the General Motors Proving Grounds Sulfate Study", to be published in Proceedings of the Symposium on Chemical Properties of Automotive Emissions from Catalyst-Equipped Cars and Biological Effects of Auto Emissions-Related Pollutants, R. K. Stevens (ed.), Ann Arbor Sciences Publ., Inc.

6. Cadle, S. H., D. P. Chock, P. R. Munson and J. M. Heuss (1977), "General Motors Sulfate Dispersion Experiment: Experimental Procedures and Results", J. Air Pollut. Control Assoc. 27:33-38.

7. Wilson, W. E., L. L. Spiller, T. G. Ellestad, P. J. Lamothe, T. G. Dzubay, R. K. Stevens, E. S. Macias, R. A. Fletcher, J. D. Husar, R. B. Husar, K. T. Whitby, D. B. Kittelson and B. K. Cantrell (1977), "General Motors Sulfate Dispersion Experiment: Summary of EPA Measurements", J. Air Pollut. Control. Assoc. 27:46-51.

8. Whitby, K. T., B. K. Cantrell, N. J. Barsic, R. L. McKenzie and D. B. Kittelson (1978), "Aerosol Size Distributions and Concentrations on Los Angeles Freeways", submitted to Atmos. Environ.

9. Dolan, D. F. (1977), "Experimental and Theoretical Investigation of Diesel Exhaust Particulate Matter", Ph.D. Thesis, Mechanical Engineering Department, University of Minnesota, Minneapolis, MN.

10. Verrant, J. A. (1976), "Development of a Dilution System for Measuring Diesel Exhaust Particulate Matter", M.S. Thesis, Mechanical Engineering Department, University of Minnesota, Minneapolis, MN.

11. Vuk, C. T., M. A. Jones and J. H. Johnson (1976), "The Measurement and Analysis of the Physical Character of Diesel Particulate Emissions", SAE Paper No. 760131.

12. Laresgoiti, A., A. C. Loos and G. S. Springer (1977), "Particulate and Smoke Emission from a Light Duty Diesel Engine", Environ. Sci. Technol. 11:973-978.

13. Whitby, K. T. (1978), "The Physical Characteristics of Sulfur Aerosols", Atmos. Environ. 12:135-159.

14. Whitby, K. T. (1974), "Modeling of Multimodal Aerosol Distributions", Proceedings of the Annual Meeting of the Association for Aerosol Research (GAF), Bad Soden, Germany.

15. Dolan, D. F., D. B. Kittelson and K. T. Whitby (1975), "Measurement of Diesel Exhaust Particle Size Distributions", ASME Paper #75-WA/APC-5.

16. Wersbork, B. L., J. B. Howard and G. C. Williams (1972), "Physical Mechanisms in Carbon Formation in Flames", presented at the 14th Symposium on Combustion, Pennsylvania State University, University Park, PA.

17. Prado, G. P., M. L. Lee, R. A. Hites, D. P. Hoult and J. B. Howard (1976), "Soot and Hydrocarbon Formation in a Turbulent Diffusion Flame", presented at the 16th Symposium on Combustion, Massachusetts Institute of Technology, Cambridge, MA.

18. Sem, G. J. (1975), Unpublished data on jet engine aerosol size distributions.

A ROLE FOR CARBON AND CARBON COMPOUNDS IN THE PARTICULATE EMISSIONS OF SMALL WOOD STOVES

Samuel S. Butcher
Chemistry Department, Bowdoin College
Brunswick, Maine 04011

ABSTRACT

Emission factors for particulate matter have been measured for small wood stoves operated under a variety of conditions. The emission factors, which range from 1 to 25 g(particulate matter)/kg(fuel), may be represented as a simple function of stove operating parameters. The particulate matter samples lose up to 55% of their weight on heating to 175°C, indicating that a substantial portion of the material collected on the filters consists of volatile or decomposable organic matter.

INTRODUCTION

The northern New England states have heating loads which range from 6,000 to 10,000 heating degree days per heating season and rely heavily on #2 oil for residential space heating. The increasing cost of oil has already brought about a shift toward the use of indigenous fuelwood[1], which is mainly used in small stoves[2].

A few measurements of the emissions from fireplaces and industrial scale forced-draft wood burners have been reported in the literature. On the other hand, very few measurements have come to light on small stoves (natural draft system, less than 100,000 BTU/hr fuel input) which appear to be coming into common use for cooking and residential space heating.

A significant feature of many of these stoves is that the superfluous air leaks are minimized so that the combustion rate may be controlled by the air supplied through the inlet draft system. Convenience (longer refuel times) and comfort (smaller room temperature fluctuations) considerations cause these stoves to frequently be operated in an air-poor mode which results in incomplete combustion of the fuel.

This paper reports an extension of our preliminary study[3] to conditions which are felt to more closely represent actual operating conditions. Measurements have also been made on an additional type of stove and some preliminary measurements have been made on a chip burner which employs a forced draft system and higher temperatures than the small stoves. A simple model has been developed which represents the emission factor as a function of stove operating conditions.

EXPERIMENTAL

The emission factors have been measured by a method described earlier[3]. A weighed charge of wood is placed on a bed of coals in a preheated stove and allowed to burn at a constant draft setting until it is reduced to an amount of coals similar to that present initially. The particulate matter from the entire flue gas stream is collected on a series of glass fiber high volume filters. The emission rate during the combustion of a charge of wood is shown in figure 1. The emission rate is integrated over the time of the burn to determine the total amount of particulate matter emitted for a known charge of wood.

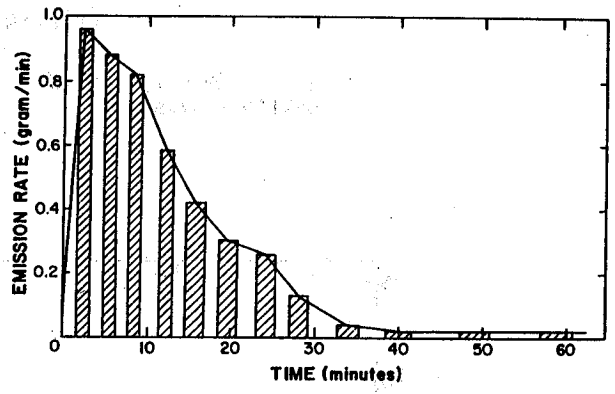

Fig. 1. Emission rate during the combustion of 2.77 kg of oak.

The report describes the measurements made on three small stoves (Jotul #602, Franklin #2, and Riteway #2000) and on a chip burner described by Riley[4]. The stoves are felt to be representative of those in common use; the chip burner has a greater capacity (ca. 200,000 BTU/hr) and has been developed for commercial and light industrial applications. Red Oak (Quercus rubra) and eastern white pine (Pinus strobus) have been used as fuel.

The emission factors for the three small stoves range from 1 to 25 g(particulate matter)/kg(fuel) and are sensitive functions of the manner in which the stoves are operated. It has been found, however, that the emission factor (E) is fairly well represented by a function of the fuel load (m) and the fuel combustion rate (q). (The combustion rate is taken to be the heat of combustion of the fuel (corrected for moisture content) divided by the length of the burn.) A number of functions relating E to m and q have been examined; the relationship $E = A + Bm/q$ accounts for as much of the variance in the data as any of the other functions. The regression line for E as a function of m/q is shown in figure 2 for oak and in figure 3 for pine. These figures include the data collected earlier[3] and 27 burns conducted more

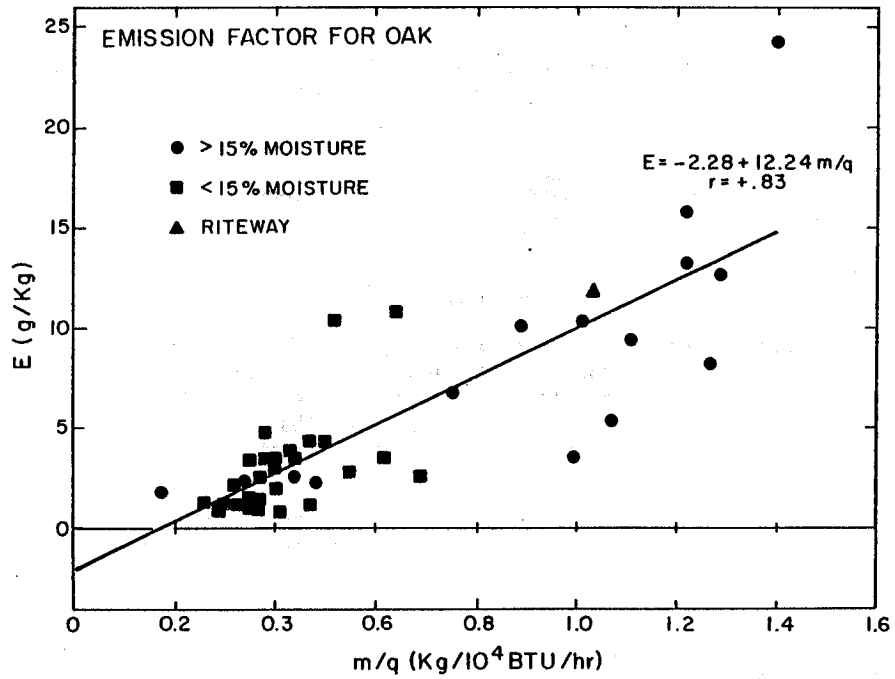

Fig. 2. Emission factor for oak. Jotul, Riteway, and Franklin stoves.

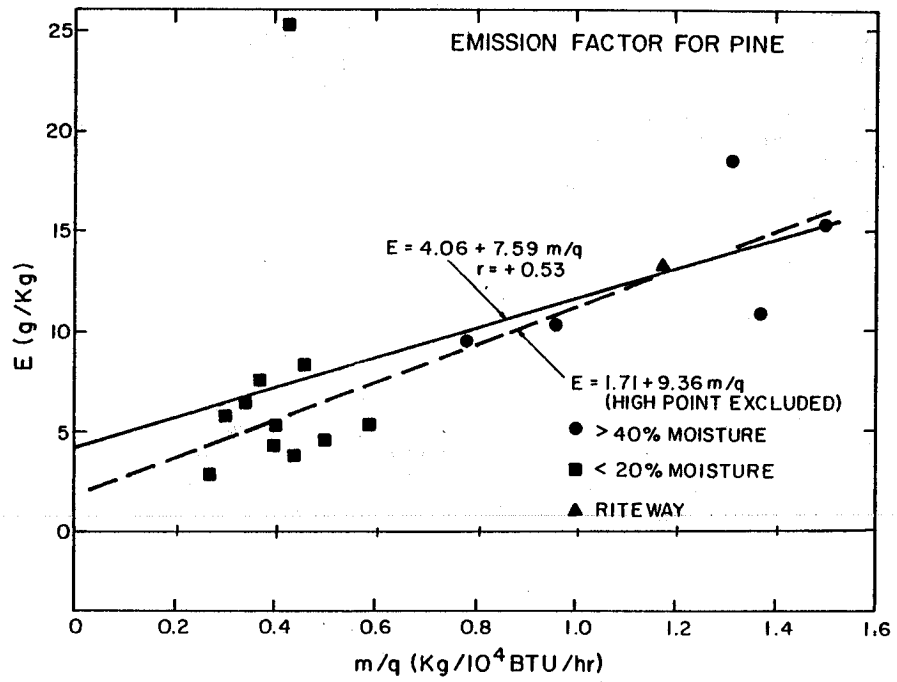

Fig. 3. Emission factor for pine. Jotul and Riteway stoves.

recently. Care should be exercised not to extend the emission factor model beyond the range of values of m and q represented by the experiments. Fuel loads ranged from 0.49 to 5.23 kg and burn times ranged from 0.26 to 1.95 hr in these studies.

All data have been included in the analysis except where noted. The observation of occasional high emission factors for dry wood is consistent with the report by Shelton[5] that significantly lower combustion efficiencies are observed with very dry wood. Apparently this results from a greatly increased combustion/pyrolysis rate (since there isn't as much water to evaporate) which, for constant draft setting, results in a reduced air/fuel ratio.

The measurement of the emission factor for the chip burner was hampered by the lack of accurate flow rate data. A best estimate for the chip burner emission factor is 0.8 g/kg, with an upper limit of 1.4 g/kg.

Previously dried particulate matter samples from the small stoves are typically black, lose up to 21% of their weight on heating to 65°C, and about 55% of their weight on heating to 175°C. The particulate matter from the chip burner is very light in color and loses about 6% of its weight on heating to 175°C.

DISCUSSION

The particulate matter yields per unit of fuel energy from this work are collected in the following table along with the value for #2 oil and the range of values expected for the inorganic ash content of wood.

Particulate matter yields per energy unit for residential heating systems

System	grams/10^9joules
#2 oil	30
Small stoves	80-1600
Chip burner	60
Ash content of fuelwood	100-500

The amount of particulate matter obtained from small stoves as well as its appearance and the fact that much of the inorganic ash remains behind in these stoves all suggest an important role for carbon and carbon-containing compounds in the particulate matter emitted to the atmosphere. On the other hand, the properties of the particulate matter obtained from the chip burner and the knowledge that the temperature is higher and the turbulence is greater than in the small stoves suggest a relatively more important role for inorganic species in the emissions from these units.

The results from the small stoves point out that those operating conditions which are most convenient for the stove user (large m/q and thus, longer refuel times) tend to produce the most particulate matter. At present, there seems to be no data available which indicates just how people operate their stoves.

Two surveys[1,2] in Maine and New Hampshire suggested that fuelwood was providing 4-8% of the space heating requirement in 1976. The emission data, when combined with heating requirements, meteorological data, and an assumption of a one hour refuel time indicates that ambient 24 hr average particulate matter concentrations could reach 100 $\mu g/m^3$ under poor atmospheric dispersion conditions in northern New England communities if the entire space heating load were carried by wood.

ACKNOWLEDGEMENTS

This research was supported in part by a contract administered by the Maine Department of Environmental Protection. The support and assistance of John G. Riley in conducting the measurements on the chip burner is also gratefully acknowledged.

REFERENCES

(1) Use of wood and other fuels for home heating in Bangor, Old Town, and Milford. Dept. of Agricultural and Resource Economics, University of Maine, Orono, Maine, 1977.

(2) M.M. Dalton, J.H. Herrington, O.B. Durgin, and R.A. Andrews, "Household fuel wood use and procurement in New Hampshire," Research Report #59, Agricultural Experiment Station, University of New Hampshire, Durham, N.H., 1977.

(3) S.S. Butcher and D.I. Buckley, J. Air Poll. Control Assoc. 27, 346 (1977).

(4) J.G. Riley, Proceedings, Wood Heating Seminar I, Wood Energy Institute, Waitsfield, Vermont, 1977.

(5) J. Shelton, Proceedings, Wood Heating Seminar II, Wood Energy Institute, Waitsfield, Vermont, 1977.

DYNAMICS OF SAMPLING AND MEASUREMENT OF DIESEL ENGINE EXHAUST AEROSOLS

David B. Kittelson
Daniel F. Dolan
Department of Mechanical Engineering
University of Minnesota
Minneapolis, Minnesota 55455

ABSTRACT

This paper examines the dynamics of sampling and measurement of diesel exhaust aerosols and presents the results of measurements made on the exhaust of a single cylinder prechamber diesel engine. Diesel engine exhaust aerosols appear to consist primarily of approximately 0.02 μm diameter carbonaceous nuclei which have grown by coagulation into chain aggregates of approximately 0.1 to 0.2 μm diameter. These aggregates may also contain condensed hydrocarbons, sulfates, and other materials. The form in which these particles appear in the atmosphere depends not only upon processes occurring inside the engine and exhaust systems, but also upon the dynamics of the process of dilution in the exhaust plume, and finally upon coagulation and condensation processes which occur after emission into the atmosphere. Because of the complex nature of these interactions, great care must be taken in attempting to relate laboratory measurements of diesel exhaust aerosols with their potential atmospheric impact. In this study an electrical aerosol analyzer, transmission electron microscope, and filter sampler were used in conjunction with a rapid dilution sampling system for measurements of particle size distribution, particle morphology, and total particle mass concentration. Particle size distributions were found to be bimodal with modes at approximately 0.02 and 0.10 μm diameter. Total aerosol mass concentrations in the exhaust were found to vary from about 10 to 110 mg m^{-3} and depended on engine load and fuel.

INTRODUCTION

Diesel engine exhaust particles consist primarily of carbonaceous nuclei which have grown by coagulation into chain aggregates of approximately 0.1 to 0.2 μm mass mean diameter. A typical particle is shown in Fig. 1. These particles may also contain condensed hydrocarbons, sulfur compounds, and other materials. They may contribute to environmental problems including: health hazards associated with their inhalation and visibility reductions associated with light scattering and absorption. Such problems may be further compounded by interactions between these particles and other atmospheric pollutants. Both health effects and optical properties of the particles depend on their particle size distributions and chemical compositions, which in turn depend not only upon processes taking place within the engine but also within the exhaust plume where dilution with ambient air occurs.

EXHAUST AEROSOL DYNAMICS

It is important to examine the relationship between the roadway dilution process and the laboratory dilution process. Figure 2 compares the roadway dilution process with a typical dilution tunnel measurement system. Measurements made by Verrant and Kittelson[1] in the exhaust plume of a diesel car on a roadway suggest that at a speed of 20 m s^{-1}, a dilution ratio of more than 100 to 1 is reached in less than 0.5 s. Tunnels, on the other hand, typically achieve maximum dilution ratios between 5 and 20 and have transit times of 1-5 seconds. Processes which may lead to differences between dilution tunnel aerosols and roadway aerosols are coagulation, condensation, evaporation, and chemical reactions on the particles.

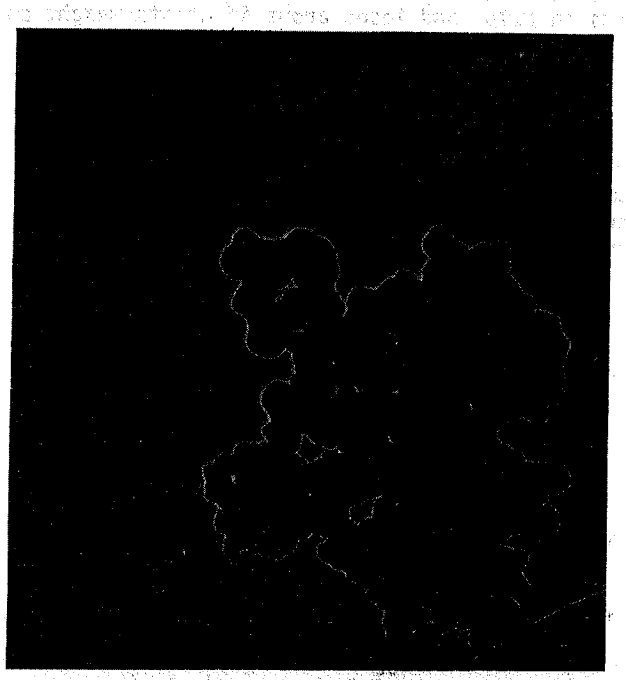

Fig. 1. Transmission Electron Microscope Photo of Large Diesel Exhaust Particle

Coagulation results from interparticle collisions which lead to clusters of small primary particles like those shown in Fig. 1. The rate of coagulation is given by:

$$\frac{dN}{dt} = -kN^2 \qquad (1)$$

where N, t, and k are the number concentration, time, and coagulation coefficient, respectively. For thermal coagulation k is a function of size

distribution, pressure, and temperature[2]. Within the exhaust system k and N are approximately 2×10^{-9} cm^3 s^{-1} and 5×10^8 particles cm^{-3}, respectively. The pseudo first order time constant associated with Eq. (1) is $\tau = 1/kN$, which is 1 s for the stated conditions. Under roadway conditions similar to those described above, dilution is so rapid that negligible coagulation should occur. However, in a typical tunnel with a 10:1 dilution ratio and a 5 s residence time, significant coagulation may occur.

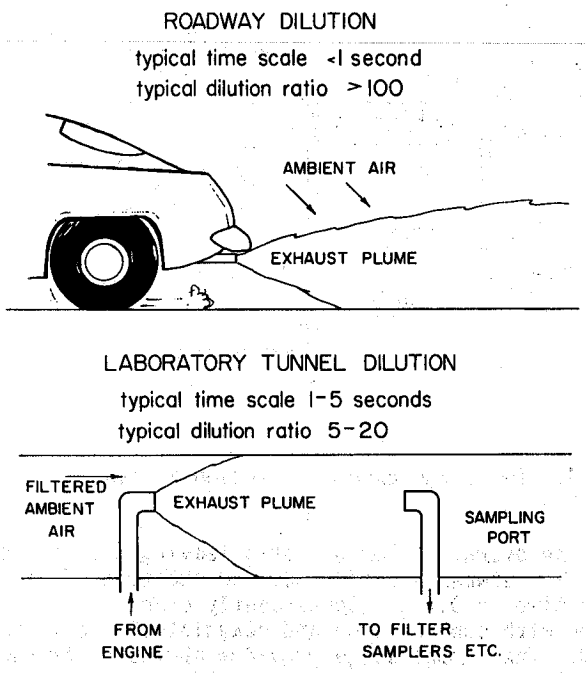

Fig. 2. Comparison of Typical Roadway and Laboratory Dilution Processes

Condensation and evaporation processes are considerably more difficult to quantify because neither the condensing species nor its concentration is known. However, Hare et al.[3], Laresgoiti et al.[4], and numerous other investigators have reported significant organic extractable fractions in diesel exhaust particles collected on filters. This material apparently condenses on the surfaces of primary combustion particles sometime during the exhaust, dilution, or sample collection process. A simple analysis was performed in order to examine condensation and evaporation of a single component during exhaust dilution. The following assumptions were made:

a. The exhaust is adiabatically diluted with clean, dry air

b. The specific heats of the dilution air and exhaust are constant and equal.

c. The condensible material obeys Trouton's rule, i.e., $\Delta H_{vap}/RT_B = 10.5$ where ΔH_{vap} is the molar heat of vaporization, R is the gas constant, and T_B is the boiling temperature.

d. The variation of vapor pressure with temperature is given by the Clasius-Clapeyron Equation with ΔH_{vap} assumed constant.

e. The initial mole fraction of condensible in the undiluted exhaust is 20 ppm.

f. The dilution air temperature is 300 K.

These assumptions have been used to calculate the variation of the degree of saturation of the condensible species with dilution ratio for various exhaust temperatures and condensible boiling points. Figure 3 shows the results for exhaust temperatures of 480 K and 600 K and condensible boiling points of 720 K and 810 K. All curves exhibit a maximum in the intermediate dilution ratio range between about 5 and 50 to 1. It is in this range that the maximum driving force for condensation or adsorption onto the exhaust particles exists.

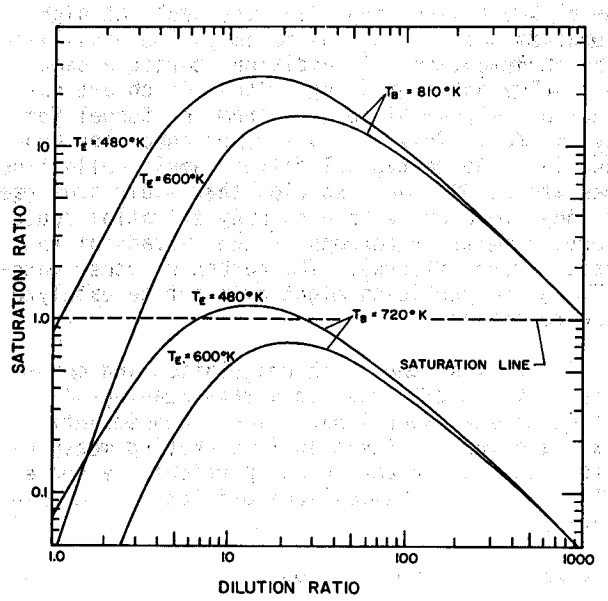

Fig. 3. Calculated Saturation Ratios for Condensible Hydrocarbons in an Exhaust Stream Undergoing Adiabatic Dilution with Clean Ambient Air. The saturation ratio is the ratio of the partial pressure of the condensible to its vapor pressure. T_E is the exhaust temperature and T_B is the boiling point temperature of the condensible species. The exhaust mole fraction of condensible is assumed to be 20 ppm. Dilution air is assumed to be at 300 K.

The rate of mass transfer by condensation to submicron particles may be calculated using expressions given by Fuchs.[2] These expressions may be rearranged to give:

$$1/\tau = (1/m)dm/dt = D(\rho_{oo} - \rho_s)f(d_p,Kn)/\rho_p \quad (2)$$

where τ is the condensation time constant, m is the particle mass, t is time, D is the diffusion coefficient, ρ_{oo} and ρ_s are the bulk and surface densities of the condensible, ρ_p is the particle density, d_p is the particle diameter, and Kn is its Knudsen number. Using the results shown in Fig. 3 for exhaust and condensible boiling temperatures of 480 and 720 K, respectively, a dilution ratio of 13, which gives the maximum saturation ratio of 1.23, a condensible molecular weight of 400, a diffusion coefficient of 3×10^{-2} cm^2 s^{-1}, and a particle diameter of 0.1 μm, gives a characteristic time for condensation of 81 ms. Under roadway conditions dilution ratios greater than 100 are achieved in less than 0.5 s; thus the time available at dilution ratios between about 5 and 50 (where the highest saturation ratios are obtained) may be long enough to lead to some condensation. This may be followed by reevaporation at higher dilution ratios and consequently lower saturation ratios. Dilution tunnels operating in the dilution ratio range of 5 to 20 with residence time of 1-5 s make long times available at high saturation ratios and thus maximize the possibility of condensation. In addition, particle samples are usually obtained using filters which are exposed to a stream of aerosol from the tunnel for many minutes. This should further encourage condensation. Since typical filter sample collection times are 10-30 min, species that would condense and then reevaporate in a roadway situation could undergo chemical reactions on the surface of the particles (or filters). The carbon or other materials in the particles might even act to catalyze these reactions.

It is clear that both coagulation and condensation make it difficult to obtain meaningful samples of diesel exhaust particles. Consequently, great care must be taken in interpreting measurements made on such particles, particularly those dealing with the chemical composition of condensed materials.

MEASUREMENT OF EXHAUST AEROSOLS

A program is currently under way in the University of Minnesota Power and Propulsion and Particle Technology Laboratories to develop methods for the sampling and measurement of diesel exhaust aerosols. Emphasis has been placed on physical measurements; i.e., size distribution measurements in the .01 to 1.0 μm diameter range using an electrical aerosol analyzer (EAA), particle morphology studies using a transmission electron microscope (TEM), and total mass measurements using a filter sampler. A single-cylinder precombustion chamber Onan MDJA engine running at 1800 RPM has been used as an aerosol source in all tests. The two-stage dilution sampling system shown in Fig. 4 has been developed to attempt to minimize the problems associated with coagulation and condensation discussed previously. Dilution ratios are measured for each operating condition using NO_x as a tracer. The first stage provides aerosols for filter sampling. Dilution ratios between 5 and 50 and a residence time of 8 ms are typical. Condensation could influence filter samples obtained in this manner. The extent of this problem is currently being explored by investigating the variation of total mass collected with dilution ratio.

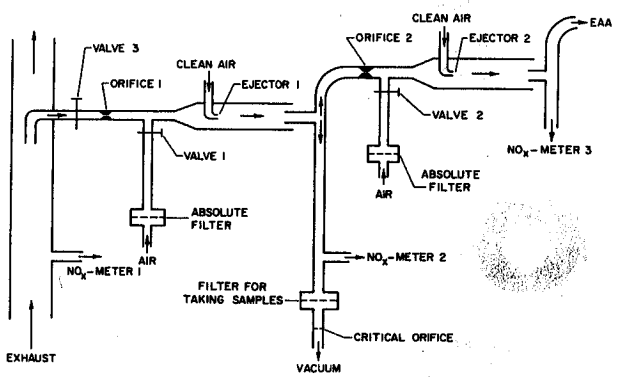

Fig. 4. Two Stage Exhaust Dilution System

The overall dilution ratio leaving the second stage is between 400 and 2000 and the total residence time is 0.1 s. Consequently problems associated with condensation and coagulation are minimized. The second stage provides aerosols for the EAA. Figure 5 shows the results of the EAA measurements made using several different test fuels. In all cases the engine was operated at 1/3 load at 1800 rpm. The volume distribution function, $\Delta V/\Delta \log D_p$, has been plotted against particle diameter. The total volume (or mass assuming constant density) of aerosols is proportional to the area under the curve. Note that the results are bimodal with modes at approximately 0.02 and 0.1 μm diameter. Little volume appears in particles larger than 0.5 μm diameter. The mode at 0.02 μm is probably associated with primary particles formed by the combustion process whereas the mode at 0.1 μm probably results from coagulation of these particles during the expansion stroke. Such size distribution measurements are useful for several reasons: health effects of small particles appear to be size dependent, the optical properties of aerosols are strongly size dependent, and because size distributions provide important additional information about the mechanism of formation and growth of these particles within the engine.

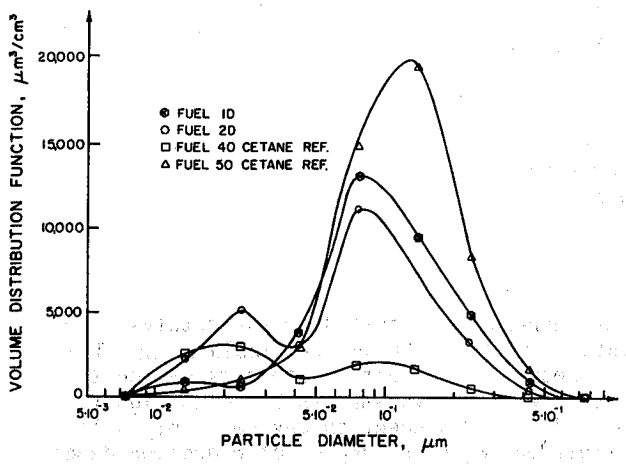

Fig. 5. Diesel Exhaust Aerosol Volume Distribution Function, $\Delta V/\Delta \log D_p$, plotted against particle diameter. The exhaust is from an Onan MDSA prechamber diesel engine operating at 1800 rpm and 1/3 load.

Figure 6 shows the variation of total aerosol mass determined with filters and total aerosol volume determined with the EAA with load for the four fuels. The results for no. 1 and no. 2 diesel fuels (both with a cetane number of about 50) and 50 cetane reference fuel fall on essentially the same lines. The 40 cetane number reference fuel produces both significantly smaller aerosol concentrations than do the other fuels and mean particle diameters. This fuel should have a longer spontaneous ingition delay period than the other three; apparently more complete mixing of the fuel and air occurs before combustion begins, and a smaller, more uniform concentration of particles is formed within the combustion chamber. A more detailed examination of this behavior will be described by Kittelson et al.[5] in a forthcoming paper.

In all cases the filter mass and EAA volumes shown in Fig. 6 track one another very well. For perfect agreement and a particle density of 1 gm cm^{-3}, the curves would be coincident. The rather good agreement between these two very different measurement techniques is encouraging and adds confidence to the size distribution results obtained with the EAA.

ACKNOWLEDGEMENTS

This work is being supported by a grant from General Motors Corp. Additional equipment support has been provided by U.S.E.P.A. Grant No. R803851 and by the Onan Corp.

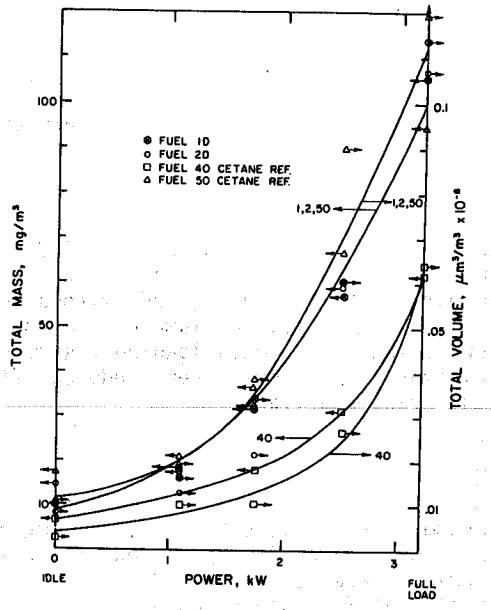

Fig. 6. Plots of Total Aerosol Mass and Volume Against Engine Load. For a particle density of 1 gm cm^{-3}, 1000 μm^3 cm^{-3} corresponds to a mass of 1 mg m^{-3}.

REFERENCES

1. J. A. Verrant and D. B. Kittelson. "Sampling and Physical Characterization of Diesel Exhaust Aerosols," Society of Automotive Engineers, Paper No. 770720.

2. N. A. Fuchs. "The Mechanics of Aerosols," U.S. Dept. of Commerce, Office of Technical Services, Washington, D.C. CWL Special Publications, 4-12, 1955.

3. C. T. Hare, K. J. Springer and R. L. Bradow. "Fuel and Additive Effects on Diesel Particulate Development and Demonstration of Methodology," Society of Automotive Engineers, Paper No. 760130.

4. A. Laresgoiti, A. C. Loos, and G. S. Springer. "Particulate and Smoke Emission from a Light-Duty Diesel Engine," Environmental Science and Technology, Vol. 11, No. 10 (October 1977), pp. 973-978.

5. D. B. Kittelson, D. F. Dolan, R. B. Diver, and E. Anfterheide, "Diesel Exhaust Particle Size Distribution--Fuel and Additive Effects," Society of Automotive Engineers, Paper No. 780787, to be presented in Milwaukee, Wisconsin, September 1978.

ANALYSIS OF CARBONACEOUS DIESEL EMISSIONS

D. E. Seizinger
Department of Energy
Bartlesville Energy Research Center
Bartlesville, Oklahoma

ABSTRACT

Carbonaceous diesel emissions were sampled before and after exhaust treatment devices--catalyst, particulate trap and water scrubber--for determination of particulate size distribution, particulate mass loading, polynuclear aromatics levels, and hydrocarbon character. Results show particulate size was on the order of 0.1 micron mass median diameter. Although the exhaust treatment systems exhibited no significant effect on particulate size, mass loading was reduced from 20 to 70 pct dependent on device. Polynuclear aromatics and hydrocarbon levels were reduced after exhaust treatment with the degree of reduction dependent on engine speed and load.

INTRODUCTION

The Department of Energy's Bartlesville (Okla.) Energy Research Center (BERC) has an ongoing project of measuring diesel emissions produced by engines typically used in underground mines. Since engine emissions are exhausted into the mine atmosphere, pollution levels in the mines are dependent on mine ventilation; therefore, reduction of diesel emission levels using add-on exhaust treatment devices could result in reducing mine ventilation requirements and may be necessary or desirable for environmental purposes.

In view of these concerns, an investigative program is being conducted to evaluate the effect of exhaust emission control add-on devices on the carbonaceous diesel emissions including particulate size distribution, particulate mass loading, polynuclear aromatics (PNA) characterization, and hydrocarbon characterization.

EXPERIMENTAL EQUIPMENT AND METHODS

Two diesel engines #1 and #2 were used as exhaust generators with maximum horsepower ratings of 100 and 80, respectively. Both engines were four-stroke cycle, indirect-injected, light-to-medium duty engine types. These engines are used in light-duty trucks and mining equipment. The engines were operated at four steady-state speed and load modes (idle, idle-light load, mid-speed and load, full speed and load). The engines were fueled with #2D diesel fuel commercially available locally.

Exhaust treatment devices including oxidation catalysts, particulate traps and water scrubber were installed in the exhaust system individually or in series combination as shown in Fig. 1. The noble metal catalysts were experimental units of both monolithic and pelletized types. The particulate traps were 7½ inches O.D., either 11- or 22-inches long, and packed with alumina coated steel wire. An experimental water scrubber with improved exhaust-water contact for cooling the exhaust to <200° F was used.

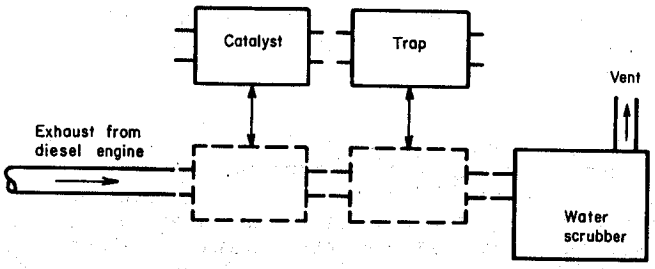

Fig. 1. Diesel emission reduction devices installed singly or in serial combination.

Emission measurements of carbon monoxide (CO), carbon dioxide (CO_2), total hydrocarbons (HC_T), oxides of nitrogen (NO_X), (NO + nitrogen dioxide), and smoke (exhaust opacity) were monitored continuously before and after exhaust treatment devices. Batch samples for hydrocarbon characterization by carbon number and class, oxygenates (formaldehyde, acrolein, and total aldehydes plus ketones), particulate-size distribution, mass loading[1] and PNA, benzo(a)anthracene (BaA) and benzo(a)pyrene (BaP), and sulfur oxides (sulfur dioxide and sulfates) were collected and measured for all operating modes before and after exhaust treatment devices. This discussion is limited to exhaust hydrocarbons in the vapor phase and exhaust particulate.

RESULTS

Particulate Size Distribution

Size distribution measurements of diesel exhaust particulate produced by engine 1 were measured before and after 11- and 22-inch particulate traps; and particulates produced by engine 2 were measured before and after catalyst plus water scrubber. These data (Fig. 2) show the particulate aggregate mass diameter ranges from 0.05 to 0.25 micron with a mass median diameter of approximately 0.13 micron.

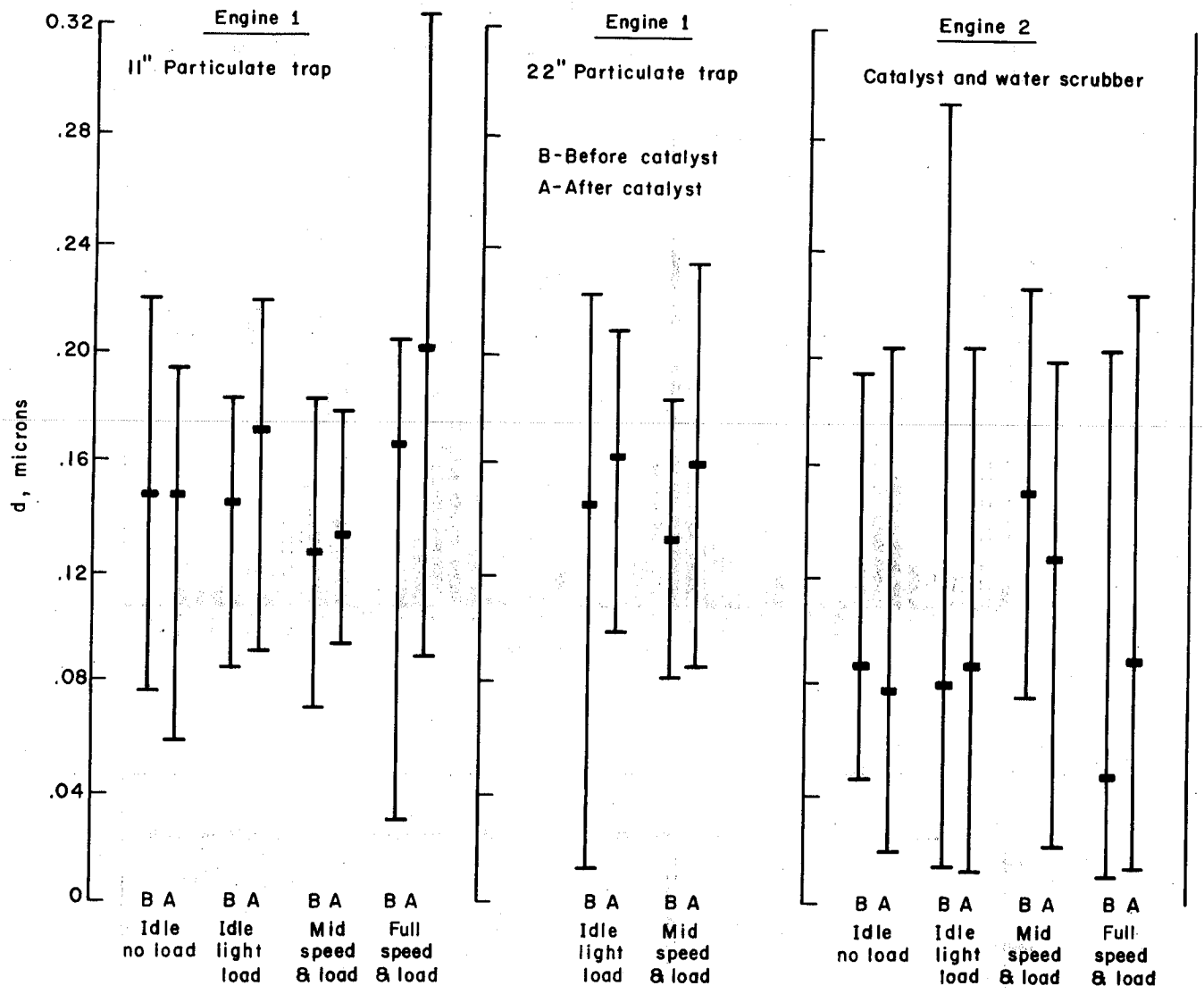

Fig. 2. Particulate size distribution measurements before(B) and after(A) 11- and 22-inch particulate traps and catalyst plus water scrubber. (The solid bar on each size range is the mass median diameter.)

Diesel exhaust size distribution measurements made at BERC using electron microscopic and electrical aerosol analyzer techniques show the particulate size data were independent of the engines tested, engine operating modes, fuels tested, and the emission control devices tested. Kittleson, et. al.,[2] has reported similar diesel exhaust particulate size distribution data using a four-stroke cycle diesel engine fueled with #1 and #2 diesel fuels.

Hydrocarbon Characterization

Diesel exhaust hydrocarbons from engine 2 were characterized by carbon number (C_1 through C_{23} range) and class (saturates and unsaturates) using GLC techniques.[3,4] Samples were collected before and after catalyst plus water scrubber. The resulting hydrocarbon characterization data (Fig. 3) represent only the vapor state hydrocarbons since the exhaust was filtered through a glass wool plug during hydrocarbon sample collection.

The amount of unsaturated hydrocarbons in the exhaust ranged from 50 to 80 pct of the total hydrocarbons. C_2 unsaturated hydrocarbons ranged from 9 to 36 pct of the total hydrocarbon dependent on engine mode and exhaust treatment. Usually C_2 through C_7 unsaturates were the principal light-end hydrocarbons, especially at higher power engine operating modes. Hydrocarbon exhaust samples collected after exhaust water scrubber (exhaust temperature <180° F) show that appreciable levels of C_{10} + hydrocarbons were not condensed by the scrubber and not oxidized by the catalyst.

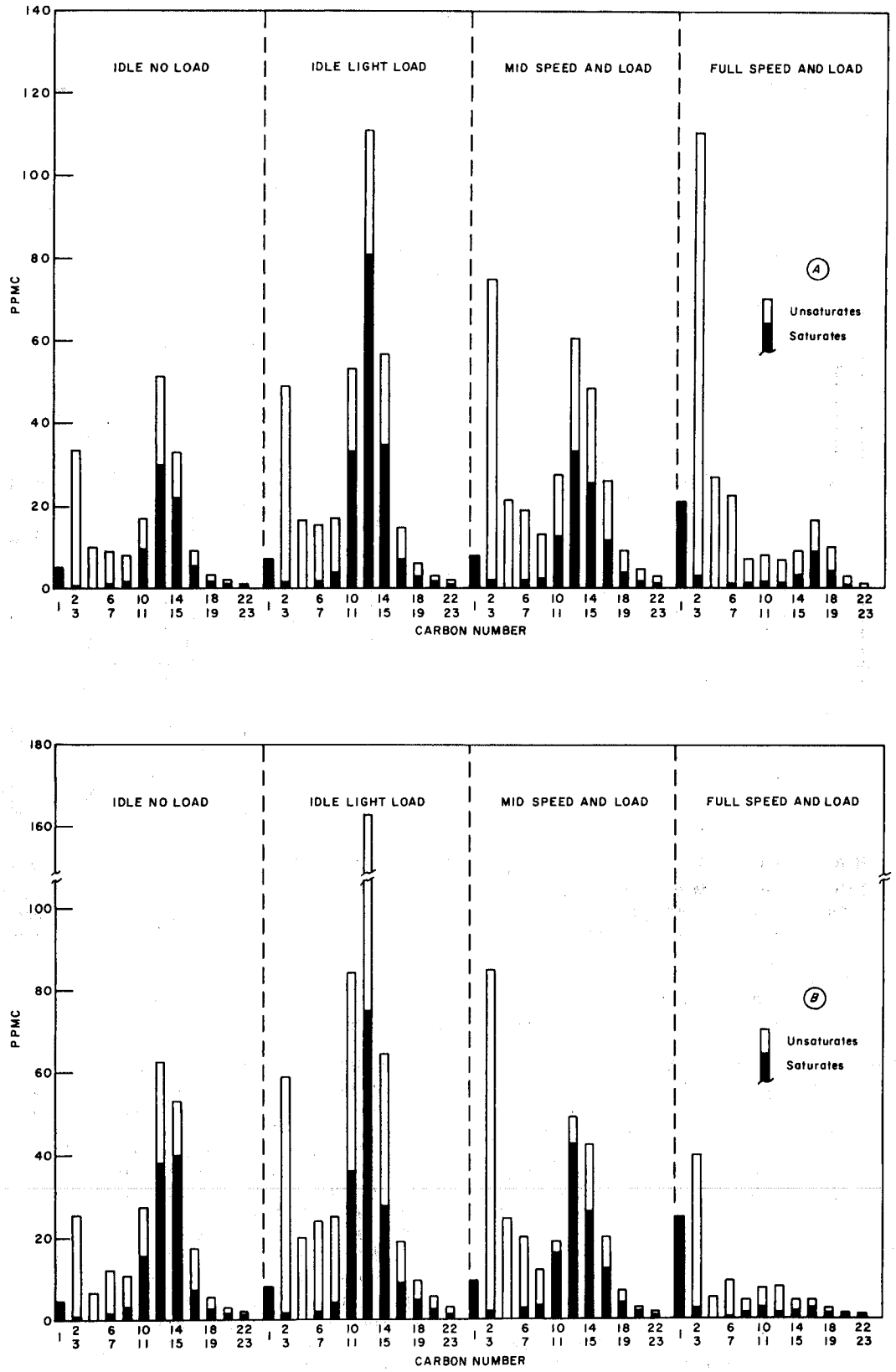

Fig. 3. Exhaust hydrocarbon characterization by carbon number and class--saturates vs unsaturates measured at four different engine speed and load operating modes.

A -- Samples collected before catalyst plus water scrubber.
B -- Samples collected after catalyst plus water scrubber.

Table 1. Diesel emission measurements before(B) and after(A) exhaust treatment.

Engine mode	Particulate mass loading, mg/m³ B	A	BaP, µg/m³ B	A	Exhaust temperature, °F
CATALYST					
Idle, 0 load	66	56	1.7	0.9	178
Idle, light load	63	58	1.6	0.4	191
Mid-speed and load	100	71	3.5	0.4	573
Full-speed and load	119	93	9.6	0.1	1,150
TRAP (11 in. long)					
Idle, 0 load	79	26	0.5	0.3	160
Idle, light load	89	45	0.9	0.5	166
Mid-speed and load	109	70	2.3	-	522
Full-speed and load	112	52	5.4	0	1,137
CATALYST + TRAP					
Idle, 0 load	122	34	1.4	1.0	174
Idle, light load	57	32	1.5	1.1	148
Mid-speed and load	90	32	1.7	0.7	600
Full-speed and load	129	58	9.7	0.6	1,170

Particulate Mass Loading

Mass loading levels ranged from 25 to 130 mg/m³ dependent on engine operation and exhaust treatment (Table 1). The catalyst reduced mass loading levels by 20 to 30 pct compared to non-catalyst operation. The 11- and 22-inch particulate traps reduced mass loading levels about 50 and 70 pct of the untreated exhaust respectively; however, a penalty of increased backpressure (from 15 to 60 inches of water) was experienced during prolonged operation (6 to 8 hours at steady-state mode) with exhaust temperature <850° F. The trap was self cleaning at exhaust temperatures >850° F (full speed and load) or the trap could be regenerated by backwashing with detergent, water, and oven drying while removed from the exhaust system.

PNA Measurements

PNA measurements were made on the benzene extract of the particulate deposited on the filter. Liquid chromatograms of PNA extracts from particulate filters collected before and after a catalyst with the engine operated at full speed and load are shown in Fig. 4. The principal peaks of interest are BaA and BaP which have been indentified as carcinogens.[5] These chromatograms show the catalytic reactor was 80 to 100 pct effective in reduction of all PNA compounds. BaP levels (µg/m³) measured before and after different exhaust treatment devices are included in Table 1.

Table 2 shows the pct reduction of BaP, and pct reduction of particulate, after catalyst, after particulate trap, and after catalyst plus particulate trap with the engine operated at four different engine modes. These data show BaP reduction was directly associated with increasing exhaust temperature through the exhaust treatment devices. These data also show that catalytic exhaust treatment reduced particulate levels only about 20 to 30 pct; whereas, BaP levels were reduced from 45 to 99 pct with increased engine power. The particulate trap was more effective in reducing particulate levels (about 50 to 70 pct) and less effective in BaP reduction--approaching 100 pct reduction of BaP only at full speed and load. Emission levels for the case of the catalyst coupled with the particulate trap were similar to the particulate trap data. In this series combination, the catalyst appeared to have only limited effect on emissions.

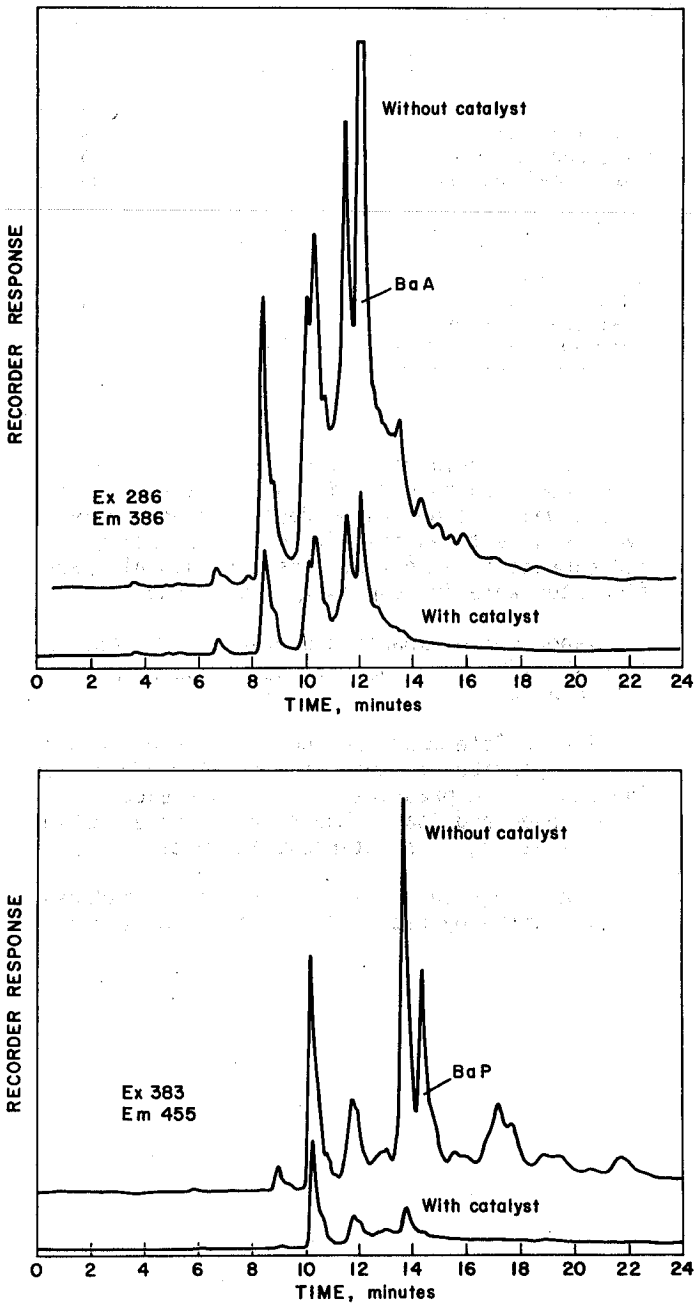

Fig. 4. Liquid chromatograms of exhaust samples collected before and after catalyst and analyzed at different excitation(Ex) and emission(Em) wavelengths of BaA and BaP.

Table 2. Pct reduction of BaP and particulates vs engine operating mode using different exhaust treatment devices.

Engine mode	BaP, pct reduction	Particulates, pct reduction
CATALYST		
Idle, 0 load	45	15
Idle, light load	73	8
Mid-speed and load	88	29
Rated speed and load	99	22
TRAP (11 in. long)		
Idle, 0 load	29	67
Idle, light load	41	49
Mid-speed and load	-	36
Rated speed and load	100	56
CATALYST + TRAP		
Idle, 0 load	25	72
Idle, light load	35	44
Mid-speed and load	57	64
Rated speed and load	94	55

SUMMARY

The particulates in diesel exhaust range in size from 0.05 to 0.25 micron in diameter; the size appears to be independent of four-stroke cycle engine types tested, engine operating mode, and exhaust treatment devices tested. All particulates were in respirable size range.

Vapor phase exhaust hydrocarbon characterization shows 50 to 80 pct of the hydrocarbons to be unsaturated.

Particulate mass loading was reduced 50 pct using a particulate trap at a penalty of increasing engine backpressure at all modes except at rated speed and load. The trap was regenerable by backwashing with detergent and water.

PNA levels in diesel exhaust can be reduced significantly by catalytic treatment of the exhaust.

REFERENCES AND FOOTNOTES

1. Gravimetric measurement of particulate deposited on filters.

2. Kittelson, D. B., and D. F. Dolan. "Dynamics of Sampling and Measurement of Diesel Engine Exhaust Aerosols." Presented at Conference on Carbonaceous Particles in the Atmosphere, Berkeley, CA, March 20-22, 1978, Paper #33.

3. Raible, C. J., and D. E. Seizinger. "Development of High Temperature Subtractive Column and Chromatographic Analysis of Hydrocarbons Present in Diesel Exhaust." BERC Report of Investigation. In publication process.

4. Dimitriades, B., C. F. Ellis, and D. E. Seizinger. "Gas Chromatographic Analysis of Vehicular Exhaust Emissions." Ch. in Advances in Chromatography (J. C. Giddings and R. A. Keller), Marcel Dekker, New York, vol. 8, 1969, pp. 327-362.

5. National Academy of Sciences. Particulate Polycyclic Organic Matter. Washington, D. C., 1972, pp. 4-12.

PARTICULATE ORGANIC MATTER AND TOTAL CARBON FROM VEHICLES ON THE ROAD

William R. Pierson
Scientific Laboratory, Ford Motor Company
P.O. Box 2053, Dearborn, Michigan 48121

ABSTRACT

Experiments in urban and highway vehicle tunnels have indicated the emission rates and characteristics of carbonaceous aerosol directly emitted by vehicles on the road. Advantage is taken of the fluctuations in traffic composition to differentiate the emissions according to vehicle type. The heavy-duty Diesel trucks play the dominant role, emitting some 700 mg/km of aerosol carbon, elemental and combined. Carbonaceous material comprises some 2/3, by mass, of the vehicle aerosol. The elemental and combined carbon are present in comparable amounts, the latter primarily as long-chain alkanes. The particles have large surface areas, reaching 90 m^2/g when the hydrocarbon material is extracted, suggesting structures that are very porous and very much plugged with hydrocarbon material. Perhaps it is for this reason that the oxidation of SO_2 to sulfate on the vehicle aerosol particles is only ~ 2% even after several minutes residence time in the tunnel. Light scattering by the vehicle aerosol is inefficient and appears minor compared to light absorption, mostly by the carbon from Diesels. A simple projection of urban aerosol loadings indicates that extensive conversion from gasoline to Diesel automobiles could add a considerable amount of carbonaceous aerosol.

Beginning in 1970, we have studied vehicle particulate emissions at the Detroit & Canada Tunnel and two tunnels on the Pennsylvania Turnpike.[1-9] In the Turnpike tunnels (Allegheny Mountain, Tuscarora Mountain), the average traffic composition is ~ 90% gasoline-powered vehicles (predominantly cars) and 10% Diesel trucks. Enormous variations in traffic composition (Fig. 1) permit one to separate the contributions of cars and Diesel trucks to the various particulate species. The vehicle aerosol is isolated from the ambient aerosol by concurrent measurement and subtraction of the latter. With known fluxes of ventilation air and traffic, the mg/km emission rates for the various species are computed.

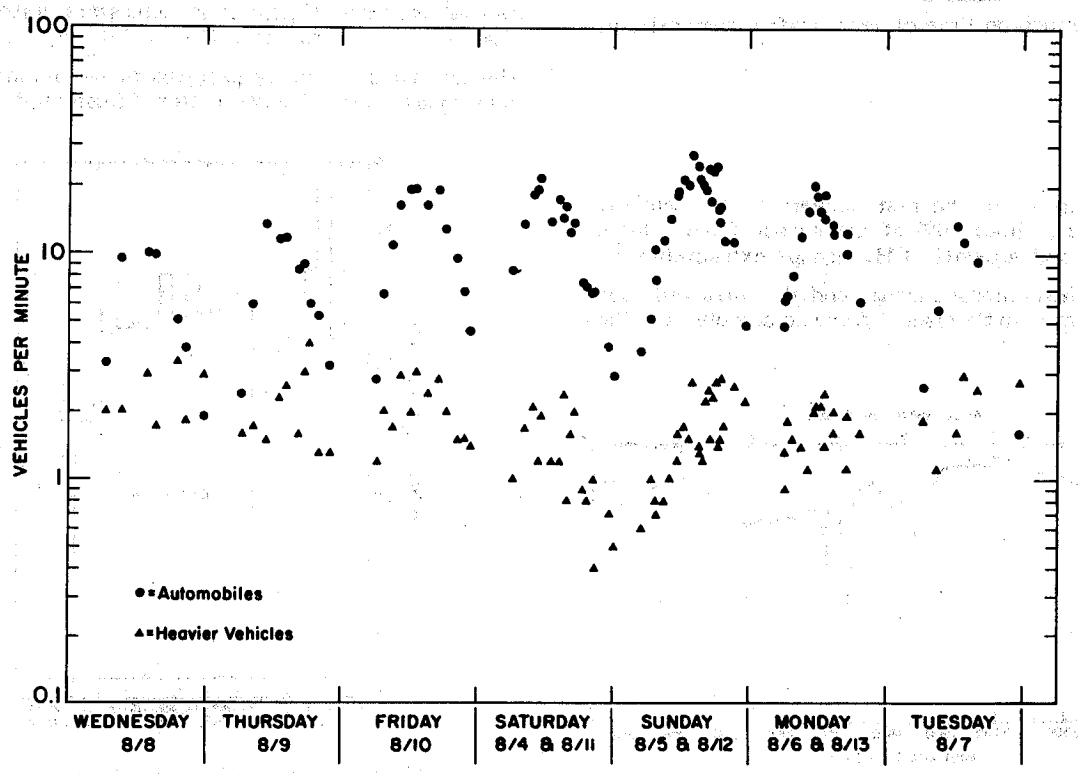

Fig. 1. Visual counts of eastbound traffic, by categories, in the Allegheny Tunnel 4 to 13 August 1973. Patterns in later years are similar. Note that the ordinate is logarithmic.

The purpose of our discussion is to describe some chemical and physical characteristics of the carbonaceous component of the particulate matter from vehicles in roadway driving - as observed near the source, before photochemical processes have had a chance to act.

Two thirds of the airborne particulate mass emitted by vehicles in the Turnpike tunnels is carbon - free and combined (Table 1). Of this carbon, about 40% consists of

Table 1. Average composition of vehicle aerosol, from the Turnpike tunnels, % by mass.

Extractable [a]	28 ± 11
H [b]	5.5 ± 0.5
C (total) [b]	68 ± 11
N	1.4 ± 0.4
Sulfate	3.7 ± 2.0
Pb	5.6 ± 2.0 [c]

Other elements measured (total ~ 8%):
Li, B, Na, Mg, Al, Si, P, Cl, K, Ca, Sc, Ti, V, Cr, Mn, Fe, Zn, Br, Sr, Zr, I, Cs, Ba (Tuscarora Tunnel, 1977).

[a] Mostly alkanes.

[b] Figures for H and C include the extractable material.

[c] Depends very much on time of year, traffic composition, etc.

long-chain alkanes and the rest appears to be elemental carbon. That is, about 40% of the carbon from vehicles exists as CH_3 and aliphatic CH_2 groups extractable into benzene or orthodichlorobenzene, and the infra-red spectrum (Fig. 2) shows little else. Aromatic and olefinic lines

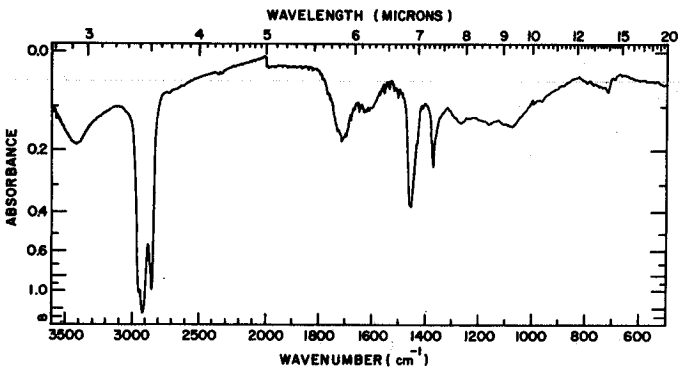

Fig. 2. Infra-red spectrum of benzene extract of airborne particulate matter collected in the Allegheny Tunnel eastbound tube 0754-1959 EDT Sunday 5 August 1973.

are essentially absent, aside from a small amount (more apparent in the o-$Cl_2\emptyset$ extracts) attributable to tire rubber.[1-5] There are no lines of nitro or other substitutional groups, and no significant carbonyl beyond what was already present in the tunnel intake air (Fig. 3).

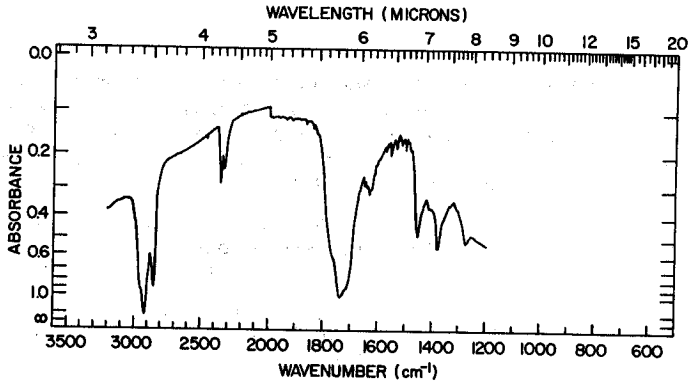

Fig. 3. Infra-red spectrum of benzene extract of airborne particulate matter in the intake air (east fan room) of the Allegheny Tunnel 1 to 12 August 1973.

The atom ratio H/C ~ 0.9 of the (unextracted) vehicle aerosol material (Table 1) is consistent with the ratio (0.4) between extractable CH_3 + CH_2 and total carbon.

The diurnal and weekly patterns of particulate extractable hydrocarbon concentration (illustrated in Fig. 4),

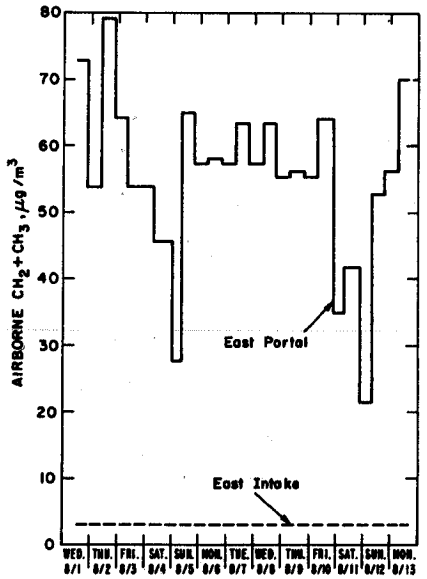

Fig. 4. Concentrations of airborne particulate alkanes (extractable CH_3 + CH_2) in the Allegheny Tunnel eastbound (solid line) and in the ambient air (dashed line), 1 to 13 August 1973.

total carbon, and total mass are all strongly correlated to truck traffic (e.g., r ~ 0.97) and to one another.

At the relatively slow and erratic speeds characteristic of the Detroit & Canada Tunnel, about half of the airborne particulate carbon emitted by vehicles was extractable (Table 2).

Table 2. Composition of vehicle aerosol from Detroit & Canada Tunnel (1973), % by mass.

Extractable [a]	24
C (total) [b]	43 ± 5
Pb	11 ± 6

[a]Not analyzed.

[b]Figure for C includes the extractable material.

The ambient aerosol, in contrast to the vehicle aerosol, contains by mass only ~ 20% carbon (Table 3) - of which the % extractable covers an enormous range. Especially notable is the extensive oxygenation of the extractable organic material (the bands at ~ 1710 to 1770 cm^{-1} in Fig. 3; compare with Fig. 2).

The vehicle-generated $\Delta C/\Delta Pb$ mass ratio in the tunnel can be divided by the C/Pb ratio in the local air to give an upper limit on the fraction of the carbonaceous particulate matter in the outside air that could be of motor-vehicle origin (given that the atmospheric Pb is predominantly from gasoline-powered vehicles and that some of the carbonaceous material, unlike the Pb, is labile). Table 4 suggests that the upper limit is 1/4 (driving in Detroit) to 1/2 (highway driving).

The measurements in the Detroit & Canada Tunnel in Table 3 also fix an upper limit of ≤ 4 for the C/Pb aerosol mass ratio from automobiles in an urban driving regime (fluctuating speeds, speed limit 30 mi/hr).

From measurements at the Summer Tunnel in 1961 and 1963, the motor vehicle was estimated to be the source of some 47 to 74% of the airborne extractable carbonaceous particulate matter in Boston.[10-12] Our data at Allegheny, showing particulate-mass HC/Pb ~ 4.5 from vehicles and ~ 9 in the outside air (Table 4), suggest that at least half of the hydrocarbon particulate matter at this rural site was from non-automotive sources even though the roadway and tunnel were nearby.

There are several detailed studies[13-17] of the organic particulate matter from spark-ignition and Diesel engine exhaust; hundreds of compounds have been identified,[14,15] the commonest by mass being alkanes of chain lengths in the C_{24} to C_{33} region, generally presumed to represent or originate from the engine lubricant and the heavier fuel hydrocarbons. It should be noted that the presence of these compounds in the particulate phase is in spite of gas-phase partial pressures far below saturation.

Table 3. Composition (examples) of ambient aerosols, % by mass.

	Allegheny and Tuscarora Mountains [a]	Detroit (16 m above street)	Dearborn (12 m from road) [b]
Extractable $CH_3 + CH_2$	4.3 [d]	22	25
H [c]	4 ± 4 [d]	f	f
C [c]	21 ± 9 [d]	19	19
N	6.5 ± 0.6 [d]	f	f
Sulfate	24 ± 10 [d]	f	f
Pb	0.4 [e]	1.3	2.7

[a]Also measured (total ~ 7%): Li, B, Na, Mg, Al, Si, P, Cl, K, Ca, Sc, Ti, V, Cr, Mn, Fe, Zn, Se, Br, Rb, Sr, Zr, Ag, Sb, I, Cs, Ba, La, Ce, Eu, Lu, Hf, Ta (Tuscarora, 1977).

[b]Rotunda Drive, a 4-lane suburban artery.

[c]Figures for H and C include the extractable material.

[d]Tunnel intake air.

[e]On radio tower on top of Allegheny Mountain.

[f]Not measured.

Table 4. Summary of vehicle and ambient C/Pb and HC/Pb mass ratios.

	C/Pb		$(CH_3 + CH_2)$/Pb	
	Vehicle[a]	Ambient	Vehicle[b]	Ambient
Detroit & Canada	4 ± 1	15.5 ± 3	—	—
Allegheny, Tuscarora	13 ± 5	25 ± 10	4.5	9.4

[a] Tunnel concentrations corrected for intake-air concentrations, i.e., $\Delta C/\Delta Pb$.
[b] $\Delta(CH_3+CH_2)/\Delta Pb$.

Rubber tire debris comprises 1 to 15% (depending on driving conditions, road surface, etc.) of the airborne carbonaceous mass from vehicles.[1-5] Part of it is rubber hydrocarbon, some of which is degraded (devulcanized, etc.); and part of it is carbon black.

Certainly one of the salient features of the vehicle aerosol is its large BET specific surface area - up to 30 m^2/g, or as high as 90 m^2/g after removal of extractable organic material (Table 5). The fact that the extraction of the organic material representing only ~ 1/4 of the mass produces a many-fold increase in specific surface area, and the fact that the size distribution of the extractable hydrocarbon (extrapolated mass median equivalent diameter ~ 0.5 μm, Fig. 5) resembles that of the gross particulate mass (m.m.e.d. ~ 1 μm), evokes a picture of the vehicle aerosol particles as porous or open networks very much plugged with condensed hydrocarbon material.

The foregoing picture may explain why the $SO_2 \rightarrow SO_4^{-2}$ conversion in the Turnpike tunnels was only ~ 2%, despite carbon loadings and SO_2 concentrations $\approx 10^2$ $\mu g/m^3$, several minutes residence time, and many hours exposure of the aerosol deposit to SO_2 during collection;[5-7] namely, a layer of hydrocarbon on the carbon surface may quench the process. (In the laboratory, very rapid and extensive $SO_2 \rightarrow SO_4^{-2}$ conversion on combustion-soot-particle surfaces had been reported.)[18]

The SO_2 and airborne carbon generated in the tunnel originate mostly from Diesel trucks.[5-7] The 2% conversion is the same as is found in dynamometer/dilution-tube studies of Diesel exhaust. There is some evidence[19] that the % $SO_2 \rightarrow SO_4^{-2}$ conversion and gross particulate loading in Diesel exhaust tend to track each other. Together, these observations suggest that Diesel-exhaust SO_2 oxidation on carbon occurs, but only within the exhaust system (or at least faster than ~ 2 seconds, the residence time of exhaust in a dilution tube) before being quenched by hydrocarbon condensation, and that little further oxidation occurs in the tunnel air. A corollary of this scenario is that SO_2 oxidation on carbon explains the SO_4^{-2} emissions from Diesel vehicles - 30 to 35 mg/km in the case of the heavy-duty rigs.[5-7]

Table 5. Summary of BET specific surface areas (Kr at 77°K), m^2/g.

	Initial	After extraction by benzene	After extraction by o-$Cl_2\phi$
Detroit & Canada Tunnel			
aerosol	4.7	—	42
wall deposit	0.45	—	9.1
Allegheny Tunnel			
aerosol	31	57	91
dustfall in tunnel	0.3	1.3	7.7
Ambient			
Detroit	3.1	—	11.2
Dearborn[a]	1 to 3	6	12 to 25

[a] 12 meters from a 4-lane suburban roadway (Rotunda Drive)

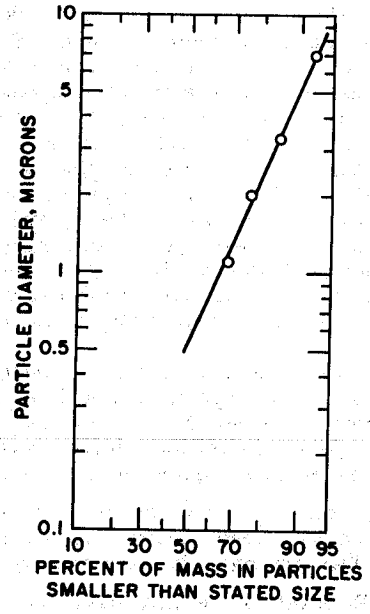

Fig. 5. Size distribution of extractable alkanes in the airborne particulate matter in the Allegheny Tunnel eastbound tube 10 to 13 August (Fri.-Mon.) 1973.

Light scattering in the Tuscarora Tunnel is dominated by the Diesel trucks, but even so is inefficient; the mass attenuation coefficient for scattering is only 1.8 ± 0.4 m^2/g (or, for Diesels alone, 3.1 m^2/g).[8] But the total light extinction coefficient of Diesel aerosol - scattering plus absorption (from opacity and mass measurements)[20] - appears to be ~ 8 m^2/g. And from data from the Caldecott Tunnel[21] one can extract a mass absorption coefficient of ~ 5 m^2/g carbon for the carbon in a vehicle aerosol. Thus it seems probable that light extinction along a roadway, to the extent that it is significant at all, consists mostly of absorption by aerosol carbon - which comes mostly from Diesel vehicles.

Diesel trucks are responsible for most of the airborne particulate mass, total carbon, and hydrocarbon generated by vehicles in the Turnpike tunnels; the respective average percentages are 89%, 91%, and 80%. The mg/km emission rates from cars and Diesels are listed in Table 6. These rates were determined by regression of emission rate (mg per vehicle-km) vs. traffic composition (% Diesel trucks) as detailed in reference 7 and as illustrated in Fig. 6.

Undoubtedly, the exhaust is the origin of the carbonaceous aerosol associated with Diesels. The relatively low carbon content of the dustfall, wall dirt, and gutter debris in the tunnels ($\leq$ 20%, Table 7; compare with Tables 1 and 2) shows that re-entrainment is unimportant. A tendency of filters in the tunnel to clog is strongly associated with Diesel traffic, reminiscent of the behavior[22] of Diesel exhaust particles in dynamometer experiments. The composition (Table 1) - that is, the H, C, N content - and the apportionment of carbon between elemental and combined are consistent with reported properties of Diesel exhaust (refs. 16, 17, 19, 20, 22-26; also see Table 13 of ref. 5). The infra-red spectrum of the extracted material (Fig. 2) is indistinguishable from the spectrum[16] of extractable Diesel-exhaust particulate matter. Diesel exhaust particles have 28 to 50 m^2/g specific areas,[27,28] similar to that encountered at Allegheny (Table 5). Specific surfaces of that magnitude would correspond to carbon spheres in the nuclei-mode size range, typical of combustion/condensation aerosols and typical also of the individual spherical carbon particles in the Diesel-exhaust-aerosol agglomerates.[20] Finally, our inferred hydrocarbon coating appears amply demonstrated in recent studies of Diesel exhaust aerosol.[20,28]

Table 6. Airborne particulate emission rates, mg/km - averages from the Turnpike tunnels.[a]

	Cars	Diesel trucks	r[b]
Total mass	20 $\pm$ 14	988 $\pm$ 103	0.98
Carbon[c]	9 $\pm$ 11	695 $\pm$ 290	0.97
Hydrocarbon	11 $\pm$ 5	272 $\pm$ 50	0.85

[a] The results are the least-squares regressions of the form

$$\frac{mg}{km} = a + b \cdot (\% \text{ Diesel-powered})$$

where mg/km from cars = a

and mg/km from Diesels = a + 100b.

[b] Average correlation coefficients from the various experiments.

[c] Total, free and combined. Includes hydrocarbon listed in next row.

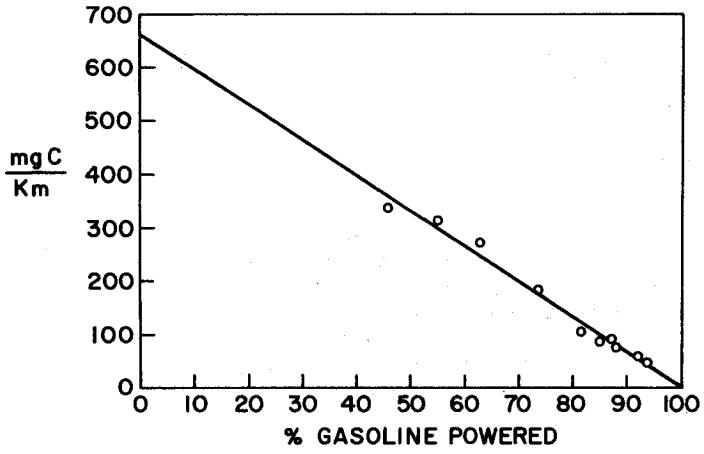

Fig. 6. Plot of particulate carbon emission rate (mg per vehicle-km) vs. traffic composition (gasoline-powered vehicles, % of total), Tuscarora Tunnel eastbound 18 to 24 August 1976. Each point represents one of 10 consecutive 12-hour runs. Least-squares regression in this example gives 3 ± 7 mg/km from gasoline-powered vehicles (predominantly cars), 661 ± 24 mg/km from Diesel trucks, $|r| = 0.991$.

Table 7. Carbon and Pb content of tunnel dustfall, wall deposit, and gutter debris, % by mass.

	C	Pb
Dustfall[a]	20%	0.53%
Wall deposit[b]	19	0.35
Walkway gutters[a]	17	0.28
Roadway gutters[a]	8.8	0.19
Topsoil[c]	—	0.0013

[a]Allegheny Tunnel

[b]Detroit & Canada Tunnel

[c]70 meters from Turnpike near Allegheny

The amount of settleable particulate matter generated by vehicles in the Allegheny Tunnel (~ 9 g/km over-all) outweighs the amount of airborne material (0.16 g/km over-all average) by nearly two orders of magnitude.[5] The chemical differences between the airborne and settled material (compare Table VII with Table I) indicate that most of the latter does not come from engine exhausts. Despite the low carbon content of the settled material, the g/km amount far exceeds that of the airborne carbon. Tire debris accounts for a few percent of the carbon in the gutters but about half of the carbon in the wall deposits and dustfall in the tunnels.

To summarize: Our experiments demonstrate the dominant role of Diesel exhaust in the area of primary automotive particulate emissions, and the dominant role of carbonaceous matter in these emissions. Elemental and combined carbon are seen in comparable amounts, the latter mostly as alkanes. The material is found to have a huge surface area per unit mass, which signifies that environmental assessment of vehicle emissions should give serious attention to this feature. Further work on optical effects should consider light absorption, the light scattering being relatively feeble. Other questions that call for further study are: What is the adsorption process by which so much hydrocarbon is held in the condensed phase? Since so much of the carbonaceous material is alkanes, what happens to them in the atmosphere?

Finally, one should consider carbonaceous Diesel particulate from the standpoint of what it would do to Los Angeles if present-design Diesel cars supplanted some fraction x of the spark-ignition cars ($0 < x < 1$). It would increase the particulate loading in Los Angeles by some 30x $\mu g/m^3$, i.e., by 30x%, mostly carbonaceous material. If x becomes large enough, this could be a serious problem. [The estimate is obtained by noting that atmospheric Pb levels in the L.A. basin are a few $\mu g/m^3$ (e.g., 3 $\mu g/m^3$ in 1972[29]), that airborne Pb emission rates on the road[5,10-12] or in dynamometer simulations of urban driving[30-38] at the 1972 prevailing Los Angeles gasoline Pb levels are ~ 25 mg/km, and that the average particulate emission rate from a light-duty Diesel is ~ 300 mg/km.[17,19,22-24,26,39,40]]

ACKNOWLEDGMENTS

Collaborators at Ford in this work were Wanda W. Brachaczek, James W. Butler, Robert H. Hammerle, Joseph T. Kummer, Douglas E. McKee, and John L. Parsons. We wish to thank Ronald J. Delaney for permission and assistance in carrying out the Detroit & Canada Tunnel experiments. Among our many colleagues now or formerly on the Pennsylvania Turnpike staff, we wish especially to acknowledge the consistent and gracious assistance by Charles E. Barron, Joseph R. Ciabocchi, Calvin L. Ewig, Jr., John R. Foor, John A. Hook, Warren E. Kipp, Guy Oakman, Robert K. Peffer, William J. Raves, Franklin V. Summers, the late William H. Sherlock, the crew at Tuscarora headed by Donald Peterson, and the crew at Allegheny headed by Robert J. Hauger.

REFERENCES

1. W. W. Brachaczek and W. R. Pierson, "Analytical method for measuring SBR tire debris in the environment," Rubber Chem. Technol. 47, 150 (1974).

2. W. R. Pierson and W. W. Brachaczek, "Airborne particulate matter from rubber tires," Paper #23, Ecology Symposium, ACS Rubber Division, Toronto, May 8, 1974; Rubber Chem. Technol. 47, 1275 (1974).

3. W. R. Pierson and W. W. Brachaczek, "Airborne particulate debris from rubber tires," EPA Toxicology Conference, University of Akron, Akron, Ohio, March 12-14, 1975; Environmental Aspects of Chemical Use in Rubber Processing Operations, EPA-560/1-75-002,

Franklin A. Ayer, compiler (Office of Toxic Substances, U. S. Environmental Protection Agency, July 1975).

4. W. R. Pierson and W. W. Brachaczek, "In-traffic measurement of airborne tire-wear particulate debris," J. Air Pollution Control Assoc. 25, 404 (1975).

5. W. R. Pierson and W. W. Brachaczek, "Particulate matter associated with vehicles on the road," SAE Paper 760039 (1976); SAE Transactions 85, 209 (1976).

6. W. R. Pierson, R. H. Hammerle, and W. W. Brachaczek, "Sulfate formed by interaction of sulfur dioxide with filters and aerosol deposits," Analytical Chem. 48, 1808 (1976).

7. W. R. Pierson, W. W. Brachaczek, R. H. Hammerle, D. E. McKee, and J. W. Butler, "Sulfate emissions from vehicles on the road," J. Air Pollution Control Assoc. 28, 123 (1978).

8. W. R. Pierson and D. E. McKee, "Light scattering by particulate emissions from vehicles on the road," J. Air Pollution Control Assoc. 28 (June 1978).

9. W. R. Pierson, D. E. McKee, W. W. Brachaczek, and J. W. Butler, "Methylcyclopentadienyl Manganese Tricarbonyl: Effect on manganese emissions from vehicles on the road," J. Air Pollution Control Assoc. 28 (July 1978).

10. R. I. Larsen and V. J. Konopinski, "Sumner Tunnel air quality," Arch. Environ. Health 5, 597 (1962).

11. R. I. Larsen, "Air pollution from motor vehicles," Ann. N. Y. Acad. Sci. 136, Art. 12, p. 275 (1966).

12. C. J. Conlee, P. A. Kenline, R. L. Cummins, and V. J. Konopinski, "Motor vehicle exhaust at three selected sites," Arch. Environ. Health 14, 429 (1967).

13. T. R. Hauser and J. N. Pattison, "Analysis of aliphatic fraction of air particulate matter," Environ. Sci. Technol. 6, 549 (1972).

14. F. W. Karasek, R. J. Smythe, and R. J. Laub, "A gas chromatographic-mass spectrometric study of organic compounds adsorbed on particulate matter from Diesel exhaust," J. Chromatography 101, 125 (1974).

15. K. W. Boyer and H. A. Laitinen, "Automobile exhaust particulates," Environ. Sci. Technol. 9, 457 (1975).

16. C. T. Hare, Methodology for Determining Fuel Effects on Diesel Particulate Emissions, EPA-650/2-75-056, March 1975; C. T. Hare, K. J. Springer, and R. L. Bradow, "Fuel and additive effects on Diesel particulate - development and demonstration of methodology," SAE Paper 760130 (1976), SAE Transactions 85, 527 (1976).

17. K. J. Springer and T. M. Baines, "Emissions from Diesel versions of production passenger cars," SAE Paper 770818 (1977).

18. T. Novakov, S.-G. Chang, and A. B. Harker, "Sulfates as pollution particulates: Catalytic formation on carbon (soot) particles," Science 186, 259 (1974); B. Barbaray, J. P. Contour, and G. Mouvier, "Sulfur dioxide oxidation over atmospheric aerosol - x-ray photoelectron spectra of sulfur dioxide adsorbed on V_2O_5 and carbon," Atmos. Environ. 11 351 (1977).

19. J. N. Braddock and P. A. Gabele, "Emission patterns of Diesel-powered passenger cars - Part II," SAE Paper 770168 (1977).

20. C. T. Vuk, M. A. Jones, and J. H. Johnson, "The measurement and analysis of the physical character of Diesel particulate emissions," SAE Paper 760131 (1976); SAE Transactions 85, 556 (1976).

21. H. Rosen, A. D. A. Hansen, R. L. Dod, and T. Novakov, "Characterization of the carbonaceous component of ambient particulate samples by an optical absorption technique," Lawrence Berkeley Laboratory Report LBL-6819 (1977), pp. 8-17.

22. J. N. Braddock and R. L. Bradow, "Emissions patterns of Diesel-powered passenger cars," SAE Paper 750682 (1975); SAE Transactions 84, 1603 (1975).

23. A. Laresgoiti, A. C. Loos, and G. S. Springer, "Particulate and smoke emission from a light-duty Diesel engine," Environ. Sci. Technol. 11, 973 (1977).

24. K. J. Springer and R. C. Stahman, "Diesel car emissions - emphasis on particulate and sulfate," SAE Paper 770254 (1977).

25. K. J. Springer and R. C. Stahman, "Unregulated emissions from Diesels used in trucks and buses," SAE Paper 770258 (1977).

26. 1977 annual report of General Motors on advanced emission control system development progress, submitted to U. S. Environmental Protection Agency, Jan. 16, 1978.

27. J. W. Frey and M. Corn, "Physical and chemical characteristics of particulates in a Diesel exhaust," Amer. Ind. Hyg. Assoc. J. 28, 468 (1967); "Diesel exhaust particulates," Nature 216, 615 (1967).

28. J. A. Verrant and D. A. Kittelson, "Sampling and physical characterization of Diesel exhaust aerosols," SAE Paper 770720 (1977).

29. R. H. Hammerle and W. R. Pierson, "Sources and elemental composition of aerosol in Pasadena, Calif., by energy-dispersive x-ray fluorescence," Environ. Sci. Technol. 9, 1058 (1975).

30. D. A. Hirschler, L. F. Gilbert, F. W. Lamb, and L. M. Niebylski, "Particulate lead compounds in automobile exhaust gas," Ind. Eng. Chem. 49, 1131 (1957); D. A. Hirschler and L. F. Gilbert, "Nature of lead in automobile exhaust gas," Arch. Environ. Health 8, 109 (1964).

31. J. B. Moran and O. J. Manary, PB196783 (1970); J. B. Moran, O. J. Manary, R. H. Fay, and M. J. Baldwin, APTD0949, PB207312 (1971); J. B. Moran, M. J. Baldwin, O. J. Manary, and J. C. Valenta, EPA-R2-72-066 (1972); J. E. Gentel, O. J. Manary, and J. C. Valenta, APTD1567 (1973).

32. K. Habibi, "Characterization of particulate lead in vehicle exhaust - experimental techniques," Environ. Sci. Technol. 4, 239 (1970); P. K. Mueller, "Discussion," ibid. 4, 248 (1970).

33. K. Habibi, E. S. Jacobs, W. G. Kunz, Jr., and D. L. Pastell, "Characterization and control of gaseous and particulate exhaust emissions from vehicles," APCA West Coast Section Fifth Technical Meeting, San Francisco, Oct. 8-9, 1970; K. Habibi, "Automotive particulate emissions and their control," SAE Paper 710638 (1971); K. Habibi," Characterization of particulate matter in vehicle exhaust," Environ. Sci. Technol. 7, 223 (1973).

34. J. S. Ninomiya, W. Bergman, and B. H. Simpson, "Automotive particulate emissions," Second International Clean Air Congress of the International Union of Air Pollution Prevention Association, Washington, D. C., Dec. 6-11, 1970; W. Bergman, "Characterizing and measuring automotive particulate emissions with two improved sampling techniques," Central States Section of the Combustion Institute, Ann Arbor, Michigan, March 23-24, 1971.

35. G. L. Ter Haar, D. L. Lenane, J. N. Hu, and M. Brandt, "Composition, size and control of automotive exhaust particulates," APCA 64th Annual Meeting, Atlantic City, N. J., June 27 - July 2, 1971; J. Air Pollution Control Assoc. 22, 39 (1972).

36. Associated Octel Ltd., "The elimination of vehicle particulate emissions," Report OP 72/5, 1972.

37. K. Campbell and P. L. Dartnell, "Vehicle particulate emissions, "Paper C123 in Air Pollution Control in Transport Engines (Institution of Mechanical Engineers, 1972), pp. 14-20. Proceedings of a Symposium of the Automobile Division and the Combustion Engines Group, Institution of Mechanical Engineers, Nov. 9-11, 1971.

38. C. W. Melton, R. I. Mitchell, D. A. Trayser, and J. F. Foster, "Chemical and physical characterization of automotive exhaust particulate matter in the atmosphere," Battelle-Columbus Summary Report to Coordinating Research Council and EPA, Project APRAC CAPE-19-70, June 14, 1973; J. F. Foster, D. A. Trayser, C. W. Melton, and R. I. Mitchell, Fourth Annual Summary Report, July 25, 1974; J. F. Foster, D. A. Trayser, E. R. Blosser, F. A. Creswick, D. F. Miller, A. Levy, R. I. Mitchell, and J. H. Oxley, Fifth Annual Summary Report, March 22, 1976.

39. C. R. Begeman, M. W. Jackson, and G. J. Nebel, "Sulfate emissions from catalyst-equipped automobiles," SAE Paper 741060 (1974).

40. K. J. Springer and R. C. Stahman, EPA-460/3-77-077 (1977).

CARBONACEOUS PARTICLES IN COAL FLY ASH

G. L. Fisher, C. E. Chrisp
Radiobiology Laboratory
University of California, Davis, CA 95616
and
T. L. Hayes
Donner Laboratory
University of California, Berkeley, CA 94720

ABSTRACT

The relative mass contribution and numerical abundance of carbonaceous particles in coal fly ash is described. The materials studied were stack-collected fly ash samples obtained by in situ size-classification into four fractions. The carbon content based on residue analysis of the four fractions was less than 0.3% of the total mass. Light microscopic analysis indicated that the abundance of carbonaceous particles was small relative to other particle types. Single particle X-ray analysis supported the light microscopic identification of the carbonaceous particles. The relative abundance of carbonaceous particles increased with the size of the particulate fractions. In contrast, mutagenicity studies indicated increased biological activity with decreasing particle size.

INTRODUCTION

In our assessment of the bioenvironmental significance of combustion by-products associated with fossil fuel utilization in electric power production, we are evaluating in detail the physical and chemical properties and biological activity of coal fly ash. We[1] have estimated that, in 1974, coal-fired power plants generated 60 million metric tons of fly ash of which 2.4 million metric tons were emitted to the atmosphere. The fly ash resulting from conventional coal combustion technologies consists predominantly of aluminosilicate spheres, although a variety of morphological particle types are present.[1] Volatile trace elements[2] as well as relatively refractory elements[3] have been demonstrated to be enriched in fine fly ash fractions. A surface enhancement of many trace elements has been observed.[4] Organic compounds including polynuclear aromatic hydrocarbons have also been reported to be associated with fly ash surfaces.[5,6] Furthermore, it has been postulated that surface crystal growth may result from SO_2 oxidation to H_2SO_4 with subsequent formation of alkaline-earth sulfates.[7] Also, matrix heterogeneity of morphologically similar fly ash particles has been demonstrated.[8] Thus, the existing data on the physical and chemical properties of fly ash indicate the complexity of this material in terms of physical and chemical heterogeneity and size-dependent properties.

This report will evaluate the relative abundance of carbonaceous particles in coal fly ash and will compare the abundance to the demonstrated biological (mutagenic) activity of fly ash extracts.

MATERIALS AND METHODS

As previously described, kilogram quantities of fly ash were aerodynamically fractionated in situ from the stack breeching after the electrostatic precipitator of a coal-fired electric power plant, burning low-sulfur, high ash, high moisture coal.[10] The specifically designed fractionator consisted of a series of two cyclone separators and a 25-jet centripeter. The resulting four fractions were collected directly in aluminum hoppers (cyclone fractions) or on fiberglass fabric filters which were pulsed at 2-minute intervals with high velocity jets of air and thence to aluminum containers (centripeter fractions). The four size-classified fractions had volume median diameters (VMD's) of 20.0, 6.3, 3.2, and 2.2 μm with associated geometric standard deviations of approximately 1.8.

Chemical analysis of matrix and trace elements have been performed by atomic absorption spectroscopy (AAS) at the Radiobiology Laboratory, by ion chromatography at Brigham Young University, and by instrumental neutron activation analysis (INAA) at the Lawrence Livermore Laboratory.[11] Sample preparation for AAS analysis involved room temperature digestion in $HF\text{-}H_3BO_3$.[12]

Light microscopic investigations of the fly ash fractions indicated that the fly ash was composed of a variety of morphological particle types.[1] We have defined eleven major classes of coal fly ash particles: (A) amorphous, non-opaque; (B) amorphous, opaque; (C) amorphous, mixed opaque and non-opaque; (D) rounded, vesicular, non-opaque; (E) rounded, vesicular, mixed opaque and non-opaque; (F) angular, lacy, opaque; (G) non-opaque, cenosphere (hollow sphere); (H) non-opaque, plerosphere (sphere packed with other spheres); (I) non-opaque, solid sphere; (J) opaque, sphere and (K) non-opaque sphere with either surface or internal crystals. On the basis of these morphological classes

Table 1. Major Element Composition (%) of Fly Ash Fractions[a]

Element	Fraction 1 (VMD = 20 μm)	Fraction 2 (VMD = 6.3 μm)	Fraction 3 (VMD = 3.2 μm)	Fraction 4 (VMD = 2.2 μm)
Si	29.6	28.0	27.5	26.8
Al	13.8	14.4	14.2	14.1
Fe	2.55	3.09	3.14	3.44
Ca	2.12	2.23	2.30	2.38
Mg	0.47	0.56	0.60	0.63
Na	1.19	1.75	1.83	1.85
K	0.74	0.80	0.82	0.81
Ti	0.62	0.76	0.77	0.78
SO_4[b]	0.15	0.67	0.99	1.62
C[c]	0.18	0.23	0.15	0.27
Undissolved residue	0.22	0.20	0.21	0.27
Total as oxides[d]	100.7	101.0	100.3	99.9

[a] Analysis by AAS

[b] Aquaeous extract analyzed by ion chromatography

[c] Carbon analysis by high temperature CO_2 evolution

[d] Oxide totals assuming simple oxides of the major elements excluding carbon and undissolved residue contribution

and their probable matrix compositions we have developed a particle genesis scheme. Opacity, shape and type of inclusions were used as characteristics for classification.

Mutagenicity studies were performed with the five Ames tester strains with and without addition of rat liver homogenates (S-9) which were derived from rats previously treated with polychlorinated biphenyl.[13] Tests were performed using the spot test methodology, as well as soft top agar pour plates. Extraction of the fly ash was performed at 37°C over a 7-day period with pooled horse serum.

RESULTS AND DISCUSSION

Major elemental composition determined by AAS of the four size-classified fly ash fractions is presented in Table 1. On the assumption that the major elements existed as simple oxides, mass recovery ranged from 99.9 to 101.0%. Carbon analyses by gravimetric CO_2 evolution from the undissolved residues, which accounted for 0.15 to 0.27% of the total mass, indicated that the residues are predominantly composed of elemental carbon. Previous analysis of electrostatic precipitator-collected coal fly ash samples indicated that the carbon content of the undissolved residue was similar to that of the parent coal.

Based on light microscopic studies of the four fly ash fractions, the relative abundances of the 11 morphological particle types has been quantitated as a function of particle size.[1] Two morphologies appear carbonaceous upon examination under the light microscope, i.e., class B, the opaque, amorphous particles which appear similar to unburned coal and class F, the opaque, lacy particles which are sootlike.

Elemental analyses of individual particles representing the eleven morphological classes have also been performed.[14] Scanning electron microscopy in combination with energy dispersive X-ray analysis was utilized to study the light-microscopically determined particle types.[8] The amorphous, opaque particles (class B) and angular, lacy opaque particles (class F) were composed of low atomic number matrices as determined from measurements of total count rates and characteristic X-ray production. The total count rates of classes B and F are significantly ($p < 0.001$) less than class I, a major morphological class. Class I is composed of non-opaque, solid spheres which appear to have aluminosilicate matrix composition.

The relative abundances determined by light microscopy of classes B, F and I in the four size fractions are presented in Table 2. These data indicate that the carbonaceous particles are most abundant in the coarser fly ash fractions and are generally small contributors to the total particulate composition.

We have performed mutagenicity assays on serum extracts from the four fly ash fractions utilizing the Ames Salmonella assay system (Fig. 1). Analyses of the finest fraction indicated that the bulk of the mutagenic activity is probably associated with compounds deposited on fly ash surfaces. Furthermore, preliminary analyses indicate that the mutagenic activities of the coarser fractions, with VMD's of 20 and 6.3 μm, are approximately one-tenth and one-third that of the fine fractions, respectively.

Table 2. Frequency Distribution (%) of Particle Classes in Size-Classified Coal Fly Ash[a]

Particle Class	Fraction 1 (20 μm)	Fraction 2 (6.3 μm)	Fraction 3 (3.2 μm)	Fraction 4 (2.2 μm)
Class B opaque, amorphous	0.4	0.2	-	-
Class F opaque, lacy	1.3	0.6	0.3	0.3
Class I non-opaque, solid sphere	25.6	56.0	79.2	87.0

[a]3000 particles were classified in each fraction

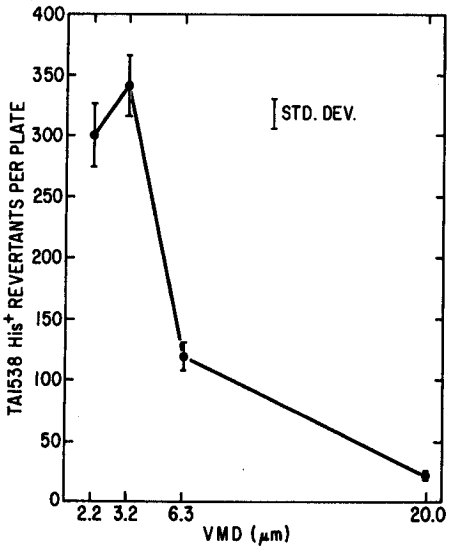

Fig. 1. Effect of particle size on the mutagenic activity of serum extracts of size-classified fly ash fractions. Tests were performed with TA 1538 utilizing 80 mg of fly ash per ml of serum.

SUMMARY

In summary, our studies indicate that the vast majority of particles in samples of western fly ash collected from the stack of a power plant over a thirty-day period are aluminosilicates. Carbonaceous particles provide small contributions to either the total mass or the total light-microscopically determined number distribution of coal fly ash particles. Mutagenicity testing indicates that although light-microscopically classified carbonaceous particles are most abundant in the coarser fly ash fractions, the finer fly ash fractions are most mutagenic.

ACKNOWLEDGEMENTS

This work was supported by the U. S. Department of Energy. The authors also gratefully acknowledge the technical assistance of B. A. Prentice, D. Silberman, J. Lammert and C. Lai.

REFERENCES

1. Fisher, G. L., B. A. Prentice, D. Silberman, J. M. Ondov, A. H. Biermann, R. C. Ragaini, and A. R. McFarland. 1978. *Environ. Sci. Tech.* 12, 447-451.

2. Davison, R. L., D. F. S. Natusch, J. R. Wallace, and C. A. Evans, Jr. 1974. *Environ. Sci. Tech.* 8, 1107-1113.

3. Fisher, G. L. and C. E. Chrisp. 1978. *Symposium on Application of Short-term Bioassays in the Fractionation Analysis of Complex Environmental Mixtures*, Williamsburg, VA, in press.

4. Linton, R. W., A. Loh, D. F. S. Natusch, C. A. Evans, Jr., and P. Williams. 1976. *Science* 191, 852-854.

5. Natusch, D. F. S. 1978. *Environ. Health Perspectives*, in press.

6. Sucre, L., W. G. Jennings, G. L. Fisher, O. G. Raabe, and J. Olechno. 1978. *National Bureau of Standards Ninth Materials Research Symposium; Trace Organic Analysis*, Gaithersburg, MD, in press.

7. Fisher, G. L., D. P. Y. Chang, and M. Brummer. 1976. *Science* 192, 553-555.

8. Pawley, J. B. and G. L. Fisher. 1977. *J. Micros.* 110, 87-101.

9. Chrisp, C. E., G. L. Fisher, and J. E. Lammert. 1978. *Science* 199, 73-75.

10. McFarland, A. R., R. W. Bertch, G. L. Fisher, and B. A. Prentice. 1977. *Environ. Sci. Tech.* 11, 781-784.

11. Ondov, J. M., R. C. Ragaini, R. E. Heft, G. L. Fisher, D. Silberman, and B. A. Prentice. 1977. *Proc. NBS 8th Materials Research Symposium*, Gaithersburg, pp. 565-572.

12. Silberman, D. and G. L. Fisher. 1977. *Pacific Conference on Chemistry and Spectroscopy*, October 1977, Anaheim, CA

13. Ames, B. N., J. McCann, and E. Yamasaki. 1975. *Mutat. Res.* 31, 347-363.

14. Fisher, G. L. and T. L. Hayes. Unpublished data.

BIOGENIC LIPIDS IN EOLIAN PARTICULATES COLLECTED OVER THE OCEAN *

Bernd R.T. Simoneit
Institute of Geophysics and Planetary Physics
University of California
Los Angeles, California 90024

ABSTRACT

The elemental and mineralogical composition and the microfossil and detritus content of particulate fallout from the lower marine troposphere has been extensively documented in earlier work, and it was possible to associate terrigenous source areas with such fallout. The lipids of eolian dusts trapped from the lower tropospheric air mass over the Atlantic, Pacific and Indian Oceans, and Sea of Japan have been investigated in this work.

The solvent soluble organic matter consists mainly of normal alkanes (C_{25}-C_{33}, strong odd-to-even carbon number predominance), fatty acids (C_{12}-C_{26}, strong even-to-odd carbon number predominance), and fatty alcohols (C_{12}-C_{30}, even-to-odd carbon number predominance), with relative amounts and molecular weight distributions varying according to the terrigenous source area. These lipids have distributions predominantly characteristic of vascular plant waxes. The non-soluble organic matter consists mainly of plant detritus, carbon particulates and probably humates.

Compound distribution patterns attributable to terrigenous sources, superimposed on the autochthonous marine lipids have been described for Deep Sea Drilling Project sediment samples from the North Atlantic Ocean, where no potamic influx was evident. The major terrigenous compound series encountered are normal alkanes maximizing at C_{29} or C_{31} with strong odd-to-even carbon number predominances and normal fatty acids maximizing at C_{24} or C_{26} with strong even-to-odd carbon number predominances.

Based on these data it was concluded that the organic compound distributions and the mineralogy of eolian dusts could be correlated with the same species in certain deep sea sediments. Hence, eolian transport can contribute significant amounts of organic matter to certain marine sedimentary environments over geologic time periods.

INTRODUCTION

Natural particulates from non-anthropogenic sources in tropospheric air masses contain biogenic lipids (Simoneit et al., 1977). These lipids are derived from terrestrial vascular plants and in part from dessicated lacustrine muds. The particles consist of plant detritus, soil and mineral fragments. In urban areas, the particulates and the associated organic compounds are derived predominantly from anthropogenic activity (e.g., Hauser and Pattison, 1972; Simoneit et al., 1975; Karasek et al., 1978). However, the natural background of biogenic lipids is not always supressed by the anthropogenic components. It is this background of biolipids and particulate matter which will be described here in further detail. These examples are derived from the large tropospheric wind masses over the ocean.

Darwin (1846) and Ehrenberg (1847) described the earliest examinations of eolian dust fallout in the Atlantic Ocean. They concluded that Africa was the most likely source of the dust based on the fresh-water fossil content. The identification of eolian material in marine sediments was initially made by Radczewski (1937a,b). He used iron oxide-coated quartz particles (Wüstenquarz) as a diagnostic marker for eolian dust derived from Central Africa. The presence of Melosira granulata in the eolian dust collected at Barbados (Delany et al., 1967) and the report that this same freshwater diatom species was present in deep-sea sediments of the tropical belt of the Atlantic Ocean (Kolbe, 1957) indicated the wind transport of these diatoms across the ocean from Africa. They originate in Central African lakes, rivers, and swamps, where after the dry season desiccation the fine dust from the bottom muds (often with plant ash and detritus) is taken up by the trade winds and blown out to sea (Delany et al., 1967; Kolbe, 1957).

Various dust storms blowing out to sea from the North African continent have been observed by satellite imagery and some were correlated with dust samples collected over the ocean at the same time (e.g., Prospero, et al., 1970; Parkin et al. 1972). An example of such a satellite photograph is shown in Fig. 1. It depicts a portion of the dust storm at 1102 GMT on May 5, 1973 (Lepple, 1975) at Cape Timiris, Mauritania. The diffuse dust is seen over the dark background of the coastal waters (cf. insert Fig. 1) and some cloudiness is present at the base and left edge of the photograph.

Rex and Goldberg (1962) have surveyed wind-transport mechanisms and summarize three genetic classes for such materials:

1. extra-terrestrial materials
2. solids of biological origins from the Continents

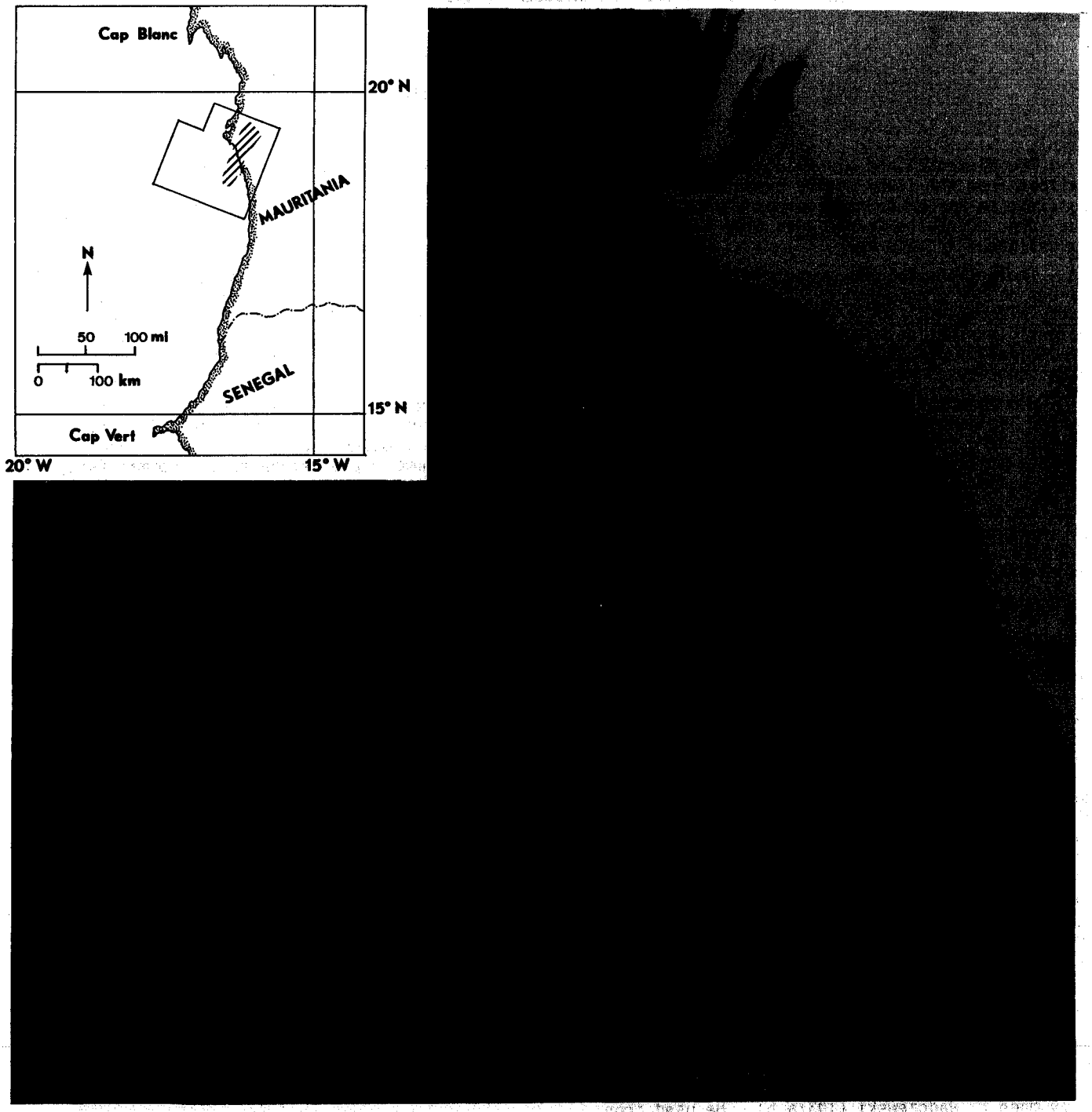

Figure 1. Photograph of Cape Timiris, Mauritania obtained by NASA ERTS satellite (ID No. E-1286-11020, MSS 7) from an altitude of 910 km at 1102 GMT on May 5, 1973. The approximate magnitude of the dust cloud is indicated on the insert.

3. solids of inorganic origins from the lithosphere, including debris from volcanic activity

The genetic class (2) above is the major contributor of organic matter to eolian dust and it includes man's activities.

The major provinces in the World Ocean where eolian input to the sediments is presently significant are mainly the Atlantic Ocean (15°N-50°N, jet stream; 15°S-15°N, trade winds and rivers; 15°S-50°S, jet stream); Indian Ocean (15°S-20°N, trades; 20°S-50°S, jet stream); and some areas of the Pacific Ocean (15°N-50°N, jet stream; 15°N-15°S, trades; 15°S-50°S, jet stream)(Griffin, et al., 1968). The eolian dust veil over the Atlantic has been investigated more extensively than any other area (Chester, 1972). This area is used here as a type setting for an attempted correlation of organic matter in deep-sea sediments with the organic matter of eolian dust. To illustrate the distribution of terrigenous organic matter in deep-sea sediments removed from river input, the lipids of some core samples from the Deep Sea Drilling Project (DSDP) are described here. The organic matter of some dusts from other areas is also detailed.

Experimental

The dust samples were collected by both the net technique (Chester et al., 1972) and by high volume filtering (Lepple, 1975). The experimental details of the sample handling, preparation and analyses have been discussed (Simoneit and Eglinton, 1977; Simoneit, 1977a). Briefly, the parameters for a typical net sampling (e.g., sample 5 in Table 1) are: 28 hours, clear weather, wind SSW-SW force 3-4, anemometer 697 km (corresponds to about $7 \times 10^5 m^3$ of air sampled). The high volume air samplers were operated from 5 to 60 hours per filter, depending on conditions (Lepple, 1975). The net collection efficiency is about 50% of the <2 μm size fraction and about 70% of the <4 μm size fraction (Goldberg, 1971). The high volume air sampler traps essentially 100% of all particles 0.3 μm or greater in diameter (Pate and Tabor, 1962). The dusts were removed from both nets and filters by agitation and settling in distilled water (recovery about 90%).

The dusts were extracted with two aliquots of toluene and methanol (3:1) only. After capillary gas chromatographic (GC) and gas chromatography-mass spectrometric (GC/MS) analyses all total extracts were treated with diazomethane in ether in order to esterify free fatty acids and reanalyzed by GC and GC/MS. Some extracts were further derivatized with BSA reagent to silylate the fatty alcohols and subjected to GC and GC/MS analysis. The extracts from large samples were separated by thin layer chromatography (TLC) on silica gel with hexane:ether (9:1) as eluent into fractions corresponding to the retention times of hydrocarbons, esters and alcohols. These fractions were also subjected to instrumental analysis.

The total extract fractions from the DSDP samples were treated with diazomethane in ether and subjected to silica gel TLC. The hydrocarbon and ester bands were scraped off, eluted with ethyl acetate, concentrated and analyzed by GC and GC/MS. Preliminary analyses of the total extracts of these samples have appeared (Simoneit et al., 1973; Simoneit, 1977b); Simoneit and Mazurek, 1978). The details of the instrumental analyses are found elsewhere (Simoneit 1977a; Simoneit and Eglinton, 1977).

Results

The sample locations are given in Table 1 and shown in Figure 2. The dust loadings and lipids yields are also cited in Table 1. The Saharan dusts (samples 2 and 3) are beige in color and yielded relatively low amounts of solvent-soluble organic matter. The dust loading is high, resulting in the high concentration of lipids (5-10 ng/m^3). The dusts from the more tropical and more vegetated environments (samples 1, 4-10, 12-14) are gray to brown in color and yielded large amounts of solvent-soluble organic matter. The dust loading in most of these cases is low, resulting in lower overall concentrations of lipids.

The contents of organic carbon and clay minerals of these dusts have been presented (Simoneit and Eglinton, 1977; Simoneit, 1977a). Some examples of distribution diagrams for the n-alkanes and n-fatty acids are shown in Figure 3. The n-alkanes exhibit maxima at mainly n-C_{27}, n-C_{29} and n-C_{31}, with strong odd-to-even carbon number predominances (cf. CPI in Table 1). The n-fatty acids maximize at n-C_{16} and either n-C_{24} or n-C_{26}, with strong even-to-odd carbon number predominances (cf. CPI in Table 1). Both n-alkanes and n-fatty acids of all samples were distinguished from iso-, anteiso- and isoprenoidal compounds by coinjection of suitable standards on capillary GC, mass fragmentography and interpretation of individual low resolution mass spectra from GC/MS analyses. Monounsaturated fatty acids (mainly $C_{18:1}$ and $C_{16:1}$) are present in most samples as significant components (cf. Figure 2). Some examples of n-fatty alcohol distributions for dusts are given in Figure 4. The n-alcohols exhibit a maximum at n-C_{28}, with a strong even-to-odd carbon number predominance. Trace amounts of triterpenoidal compounds have been detected in samples 4-10, but not in samples 1-3. Diterpenoidal compounds, which have been proposed as terrigenous markers of resinous higher plants (Simoneit, 1977c) and sesquiterpenoidal compounds have not been detected in these dusts. Polynuclear aromatic hydrocarbons have also not been detected. TLC analyses of some of the dust extracts showed no fluorescence and in the GC/MS analyses no polynuclear aromatic hydrocarbons could be detected to a limit of about 0.1 ppm. All dust samples contained significant amounts of phthalate esters (various C_2, C_4 and C_8 diesters), probably derived from mainly the nets, polyethylene bags and sample vials.

Dust sample 1 was taken off the coast of Morocco and represents mainly trade wind flux of North African material (cf. Figure 2). Samples 2 and 3 were taken essentially in the same area along the coast of Mauritania, but in different seasonal times. They represent trade wind flux of Saharan material. Samples 4 and 5 were

Table 1. Dust sample descriptions and analytical results

Sample (cf. Fig. 2)	Ship's Tracks[1]	Dust loading (µg/m³)	Total lipids[2] (ng/m³)	n-alkanes: Approx. yield[2] (µg/g)	n-alkanes: CPI[3]	n-alkanes: Max. at C no.[4]	n-fatty acids: Approx. yield[2] (µg/g)	n-fatty acids: CPI[3]	n-fatty acids: Max. at C No.[4]
1	34°44'N, 13°38'W 28°30'N, 15°54'W	0.18	0.13	10	10.2	27	740	n.d.	16
2	21°41'N, 17°41'W 14°04'N, 18°07'W	36	4.7	40	1.4	25,29	20	6.1	16,24
3	17°47'N, 17°42'W 19°24'N, 17°40'W	20	10.0	400	7.5	27≃29	35	22	16,24
4	03°44'N, 12°00'W 08°50'N, 15°44'W	9.6	8.0	340	5.0	29	160	11.6	16,20
5	01°14'S, 08°01'W 03°44'N, 12°00'W	0.4	1.0	860	3.2	29	900	7.5	16,24
6	07°12'S, 04°02'W 02°37'S, 07°42'W	0.18	1.8	2200	5.6	29	3400	14	16,24
7	11°52'S, 00°29'W 07°12'S, 04°02'W	0.08	0.03	45	6.0	29	n.d.	--	--
8	09°40'S, 01°31'W 14°42'S, 02°06'E	1.4	3.8	1150	5.2	29≃31	400	4.1	26
9	22°26'S, 07°58'E 17°01'S, 03°30'E	0.29	0.08	120	6.5	29≃31	40	26	16,26
10	14°42'S, 02°06'E 19°26'S, 05°47'E	2.0	0.2	40	5.2	31	12	7.5	16,26
11	29°03'S, 13°22'E 25°06'S, 09°59'E	5.6	n.d.	n.d.	--	hump	n.d.	--	--
12	30°03'S, 31°03'E 24°24'S, 24°07'E	4.0	12.0	1050	7.5	27	260	8.4	16,26
13	04°38'S,106°44'E 08°02'S,102°02'E	0.1	0.12	1180	4.6	27≃29	300	10.0	16,24
14	33°55'N,132°40'E 34°37'N,135°07'E	n.d.	n.d.	80	7.1	29	25	10.3	16,26
15	20°56'N, 17°02'W	13,420	1.5	74	1.6	19,29	3	8.2	16,24
16	20°56'N, 17°02'W	2,520	0.11	30	1.6	17,23,29	1	9.9	16,22
17	13°08'N, 59°28'W	n.d.	n.d.	40	2.0	27≃29	n.d.	--	--

[1] Indicates the ship position at the start and finish of each sampling run (except for stationary land sampling, numbers 15 to 17).

[2] Determined by weighing an aliquot of extract on a microbalance (±20%) or by GC quantitation

[3] CPI - carbon preference index, summed from C_{10} to C_{35}.

[4] The predominant homolog is underscored.

n.d. - not determined

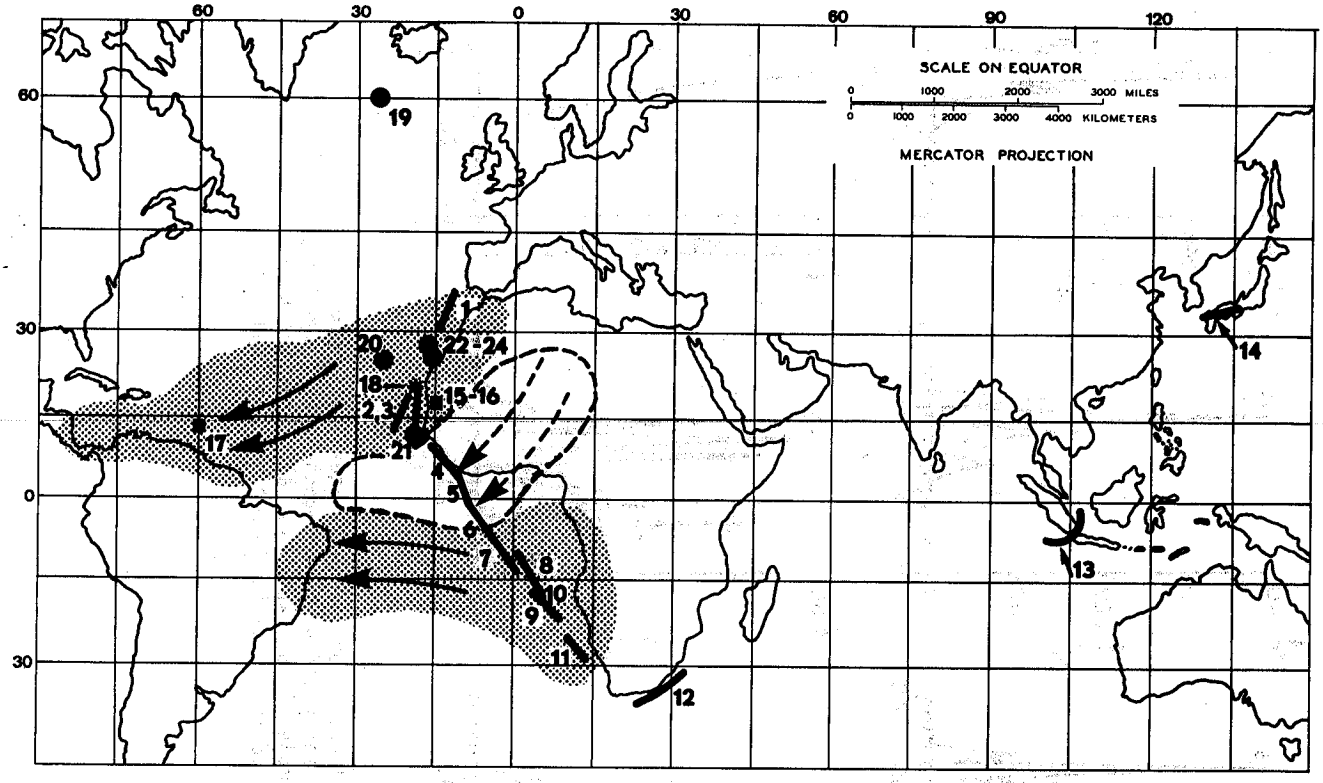

Figure 2. Map showing the sample locations (—— dust collection; *,● - DSDP sediments; ■- land-based dust collections).

collected off West Africa and probably represent both Saharan and West African material carried by the Harmattan winds. Samples 6-10 represent fall-out from the south-east trades, deriving material mainly from the soils of southern Africa, the Namib and Kalahari deserts and probably from the lower Guinea area of Africa. Samples 9 and 10 were taken in the same geographic area but at different seasonal times. A seasonal variation of lipid content was observed on a qualitative level. Sample 12 represents material derived from the soils of south-eastern Africa. Sample 13 was collected through the Sunda Strait and represents material blown off tropical Indonesia. Sample 14 was collected on the Inland Sea off Japan and consists of predominantly urban material. Samples 15 and 16 were sampled on land at Nouadihbou, Mauritania and were analyzed here in order to assess the contribution of lacustrine lipids to the dusts. Some preliminary analyses of samples 15 and 16 have been carried out (Lepple and Brine, 1976). Sample 17 was taken on land at Barbados.

Three examples of marine sediments, where a significant eolian input of organic matter has occurred, are illustrated by the n-alkane and n-fatty acid distributions in Figure 5. Sample 18 (cf., Table 2) is a near-surface sediment from the continental shelf off Cape Blanc in the fall-out zone of the northeast trades. It has a low clay content (high marine carbonates) and exhibits a strongly terrigenous distribution pattern in the n-alkanes and n-fatty acids (Gaskell et al., 1975). This distribution is similar to those of dust samples 8 and 9 (cf., Table 1). The DSDP samples 21 and 22 (cf., Table 2 and Figs. 5b and e) are from the continental slope off Spanish Sahara and the eastern edge of the Cape Verde Basin, respectively. They are both of Pliocene age and consist of nannoplankton marl. The n-alkanes and n-fatty acids exhibit mainly allochthonous terrigenous distributions with a minor autochthonous marine ($< C_{20}$) component. Sample 20 (cf., Table 2 and Figs. 5c and f) is from the abyssal plain at the foot of the continental rise about 850 km northeast of Cape Blanc. This site was at the base of the continental rise off West Africa during the Oligocene. The sample exhibits n-alkane and n-fatty acid distribution patterns resembling those of dust samples 3, 6 and 14. The clay content of this sample is high and coated quartz grains (Wüstenquarz) have been identified in some of the DSDP Leg 14 samples (Simoneit and Eglinton, 1977). Samples 23 and 24 (cf., Table 2) also exhibit

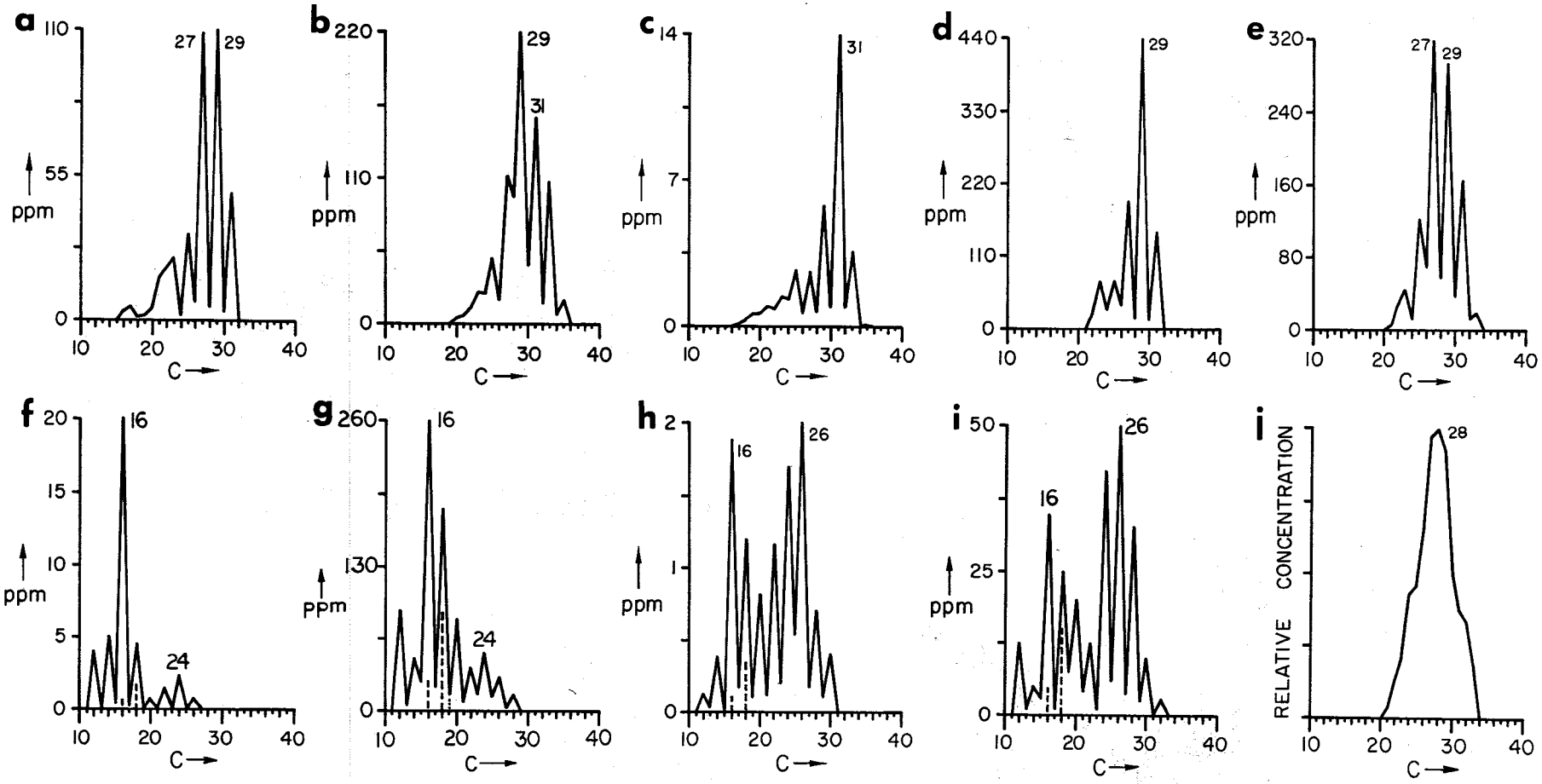

Figure 3. Distribution diagrams for homologous compounds in typical eolian dusts: n-alkanes (a) sample 3, (b) sample 5, (c) sample 10, (d) sample 12, (e) sample 13, n-fatty acids (----- mono-unsaturated fatty acids) (f) sample 3, (g) sample 5, (h) sample 10, (i) sample 12, n-alkanes (j) aliphatic fraction of Los Angeles urban air particulates (January, 1970), plotted from data by Hauser and Pattison, 1972).

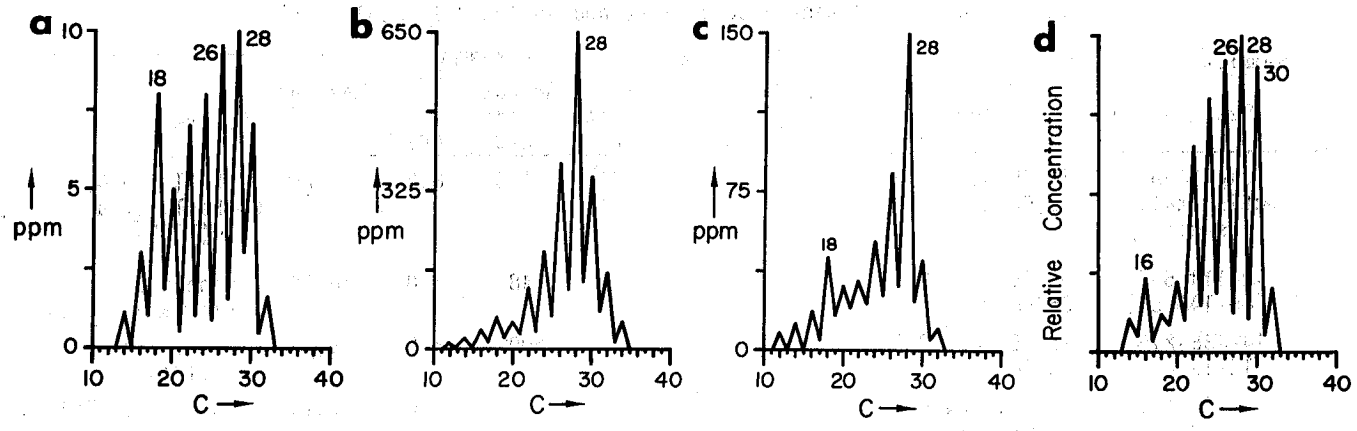

Figure 4. Distribution diagrams for n-alcohols in typical eolian dusts and sediments: (a) sample 2, (b) sample 6, (c) sample 8, (d) sediment sample 19.

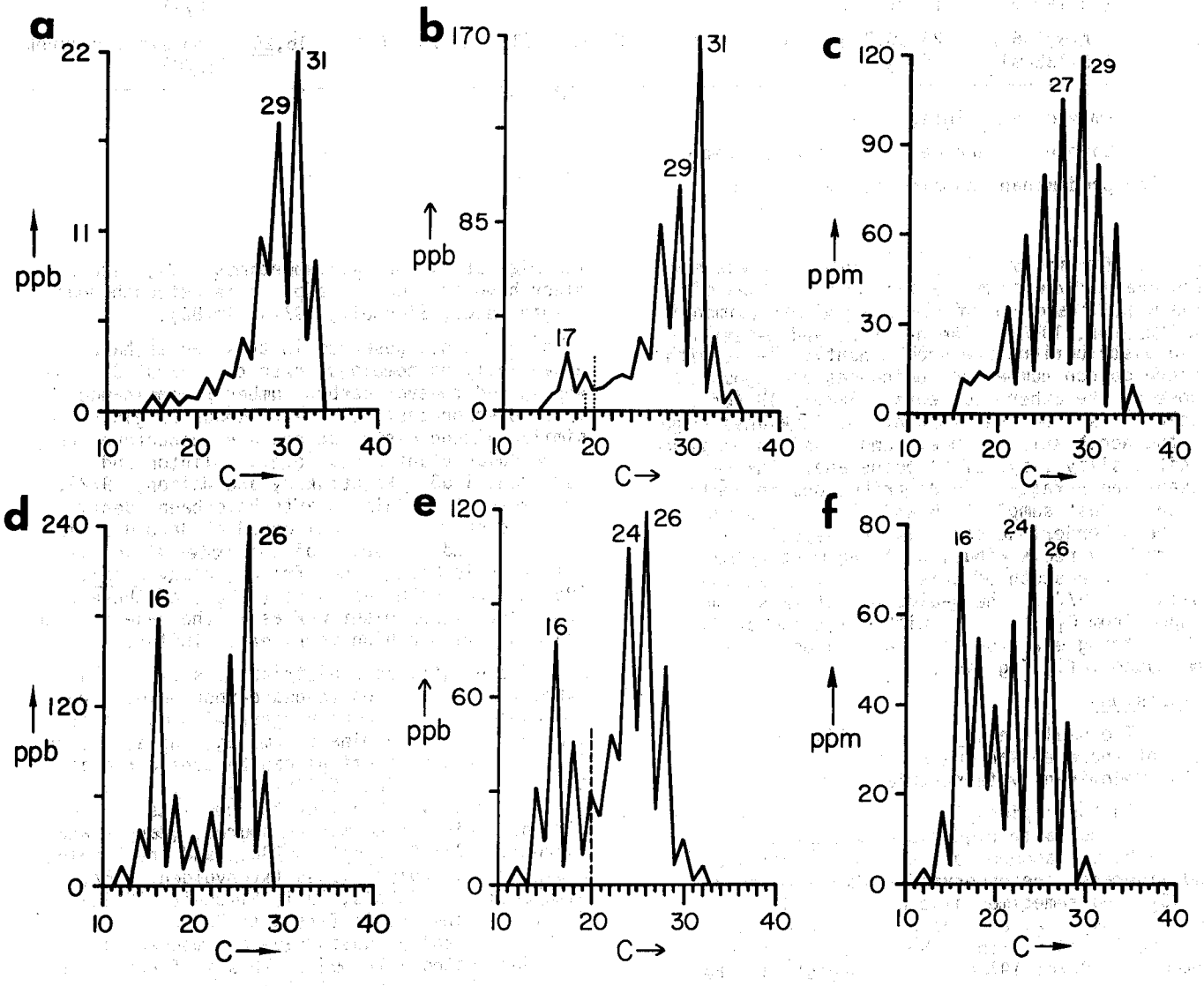

Figure 5. Distribution diagrams for n-alkanes and n-fatty acids in marine sediment samples: n-alkanes (····· isoprenoids) (a) sample 18, (b) sample 22, (c) sample 20, n-fatty acids (----- dehydroabietic acid) (d) sample 18, (e) sample 22, (f) sample 20.

Table 2. Marine Sediment Descriptions and Analytical Results

Sample Number (cf. Fig.2)	Designation	Location	Org. C (%)	n-alkanes Approx. yield[1] (µg/g)	n-alkanes CPI[2]	n-alkanes Max.at C no.[3]	n-fatty acids Approx. yield[1] (µg/g)	n-fatty acids CPI[2]	n-fatty acids Max. at C no.[3]	References
18	Cap Blanc (Continental shelf)	20°45'N, 18°02'W	1.3	0.1	2.6	29≈31	1.0	8.2	16,<u>26</u>	Gaskell (1974); Gaskell, et al. (1975)
19	12-114-5-5 (80-140 cm)	59°56'N, 26°48'W	0.2	290	5.8	29	48	7.8	16,<u>24</u>	Simoneit and Burlingame (1973)
20	14-138-2-6 (12-13 cm)	25°55'N, 25°34'W	2.3	710	5.2	29	500	5.2	16,<u>24</u>	Simoneit et al., (1973)
21	41-367-4-3 (0-10 cm)	12°29.2'N, 20°02.8'W	0.2	2.7	4.0	31	0.1	3.6	16,<u>24</u>	Simoneit (1977b)
22	41-369-2-6 (135-140 cm)	26°35.6'N, 14°59.9'W	0.1	0.7	3.6	31	0.8	3.2	16,<u>26</u>	Simoneit (1977b)
23	47A-397-2-5 (120-150cm)	26°50.7'N, 15° 10.8'W	0.47	2.1	1.7	23,<u>31</u>	5.7	5.5	16,<u>26</u>	Simoneit & Mazurek (1978)
24	47A-397-6-3 (120-135cm)	26°50.7'N, 15°10.8'W	0.81	0.8	1.8	17,23,<u>31</u>	3.3	6.1	16,<u>26</u>	Simoneit & Mazurek (1978)

[1] Determined by GC integration.

[2] CPI-Carbon preference index, summed from C_{10} to C_{35}

[3] The predominant homolog is underscored

evidence for influx of eolian lipids. These samples are derived from the continental slope off Cape Bojador and are of Pleistocene age (Simoneit and Mazurek, 1978). The n-alkane and n-fatty acid distributions are predominantly >n-C_{23} with strong carbon number predominances analogous to those of the other sediments. Sample 19 (cf., Table 2) is from the flank of the Reykjanes Ridge in the North Atlantic Ocean and consists of glauconitic silty clays of Pliocene age. The n-alkane and n-fatty acid distributions resemble those of dust sample 4, 5 and 12. This sediment may be a borderline case, as the deposition occurred by redistribution of sedimentary material from the south of this site (Simoneit and Eglinton, 1977). The n-alcohols of this sample ranged from C_{14} to C_{32}, with a maximum at C_{28} and a strong even-to-odd carbon number predominance (cf., Fig. 4d).

Discussion

The n-alkanes, n-fatty acids and n-alcohols of these eolian dusts can be correlated with predominantly terrestrial sources.

In the lipids of a typically marine sediment, without a terrigenous component as inferred by the absence of terrestrial detritus and minerals, the observed n-alkanes maximize at <C_{20} and sometimes also at C_{22} or C_{23}, with no homologs >C_{26}; and the n-fatty acids maximize at C_{16} only with no homologs >C_{21} (e.g., Simoneit, 1977c; 1978a). By contrast, in the lipids of marine sediments with a major terrigenous component, as inferred by the high contents of clays and quartz, the n-alkanes maximize at either C_{27}, C_{29} or C_{31} with essentially no homologs < C_{25}; and the n-fatty acids maximize at C_{24} or C_{26} (sometimes C_{28}), with only minor homologs <C_{20} of a probable autochthonous origin (e.g., Simoneit, 1977d; 1978a).

The n-alkanes observed in these dusts have essentially no homologs lower than about C_{22} and a strong odd-to-even carbon number predominance. This corroborates their terrigenous origin since similar alkane distributions are encountered only in vascular plant waxes (e.g., Eglinton and Hamilton, 1963; Kolattukudy and Walton, 1972). Fragments of vascular plants have been identified the eolian dusts collected at Barbados, indicating wind transport of that material across the Atlantic Ocean from Africa (Delany et al., 1967). Thus, the n-alkanes (> C_{25}) of these dusts represent higher plant wax as is the case for the sediments with a high terrigenous influx.

The n-fatty acid distributions of the dusts exhibit a strong even-to-odd carbon number predominance and a bimodal pattern with maxima at C_{16}, usually the dominant homolog, and at C_{24} or C_{26}. These distributions can be considered as typically lacustrine (Eglinton et al., 1974; Cooper and Bray, 1963), or the homologs <C_{20} can also be derived from marine sources (Barger and Garrett, 1976; Simoneit, 1978a), and the homologs > C_{20} from vascular plants (Kvenvolden, 1967; Hitchcock and Nichols, 1971; Simoneit, 1978a). The lacustrine origin fits with Kolbe's proposal (1957) that eolian dusts have a component derived from desiccated lake muds. This is further corroborated by the analytical results on samples 15 and 16, which were sampled on land and do not contain a marine component. The n-fatty acids < C_{20} of these two samples are therefore derived from lacustrine sources. The relative

concentrations of the lipids in these samples are low, probably due to the content of coarse mineral detritus.

The n-alcohol distributions of the dusts, with the maxima at C_{28} and the strong even-to-odd carbon number predominances, are directly correlatable with the fatty alcohol contents of higher plant waxes (Eglinton and Hamilton, 1963; Simoneit, 1978b). They also correlate well with the sedimentary n-alcohols (e.g., sample 19, Fig. 4d).

The absence of diterpenoids, which have been used as molecular markers of resinous plants (Simoneit, 1977c), may reflect the over-abundance of plant wax rather than resin residues in the dust, especially in those dusts from the more vegetated areas of the African steppes. The triterpenoidal compounds were detected in samples with a high wax content.

Waxy material has also been identified by microscopy in eolian dusts collected at Barbados (Delany et al., 1967). A series of scanning electron micrographs for some typical morphologies of surface waxes from vascular plants is shown in Fig. 6 (I am grateful for Dr. P.J. Holloway, Long Ashton Research Station, University of Bristol, Bristol,England and Academic Press, Ltd. for kindly providing these photographs). The extreme fragility of the white wax protrusions is evident from the photomicrographs. Wax particles are easily sloughed off from plant surfaces and can become airborne.

The distributions of the n-alkanes from the dusts do not resemble the distributions of these compounds in urban dusts. An example of the n-alkane distribution from particulates sampled in Los Angeles is shown in Fig. 3j (Hauser and Pattison, 1972). The n-alkanes of urban air particulates are present as minor components as part of a general "hump" typical of petroleum products. They range from $\sim C_{20}$ to C_{33}, with a maximum at $\sim C_{28}$ and no carbon number predominance (e.g., Hauser and Pattison, 1972; Grimmer and Böhnke, 1972; Cukor et al., 1972).

The n-alkanes, n-fatty acids and n-alcohols with such terrigenous distributions have been identified in various marine sediments ranging in age from Recent to Cretaceous (Simoneit, 1978a; Simoneit and Burlingame, 1972; 1974). Some of these sediments were deposited in paleoenvironments where no obvious potamic influx had occurred and thus the allochthonous terrigenous lipids may have been brought in by eolian transport.

The minerals composing eolian dusts that are considered terrigenous markers are clays, quartz (usually coated with iron oxide) and feldspars (Chester, 1972; Chester and Elderfield, 1970). The clays consist of montmorillonite, illite, chlorite and kaolinite and are all of a land-derived origin (Aston et al., 1973). The clay content of these dusts is greater than 80% of the total minerals (Aston et al., 1973). The mineralogy of eolian dusts correlates well with that of sea-bed sediments under the fallout blanket. The clay mineral distributions in the World Ocean have been mapped (Griffin et al., 1968). Quartz has also been documented in the oceanic sediments (e.g., Beltagy et al., 1972; Rex and Goldberg, 1958). The major transport mechanisms of these minerals to the marine environment are potamic, eolian, and/or ice rafting (e.g., Griffin et al., 1968; Chester, 1972).

The problem of organic contamination with phthalate ester plasticizers could not be avoided entirely with these dusts. The presence of phthalates on the eolian dusts can therefore not be demonstrated. Shipboard stack contamination was not a problem. Moyers et al. (1972) found that to be minimal when collections were made in the bow. A sample (#11, Table 1) contaminated by the ship's stack has also been examined. This black dust contained about 80% organic carbon mostly derived from the burning of marine fuel oil in the vessel's steam turbine. The yield of solvent-soluble organic matter was low. It appears that the bulk of this organic carbon is amorphous ("lampblack"). The GC analysis of the total extract exhibits a hump in the C_{20} retention region with no obvious high molecular weight n-alkanes.

Conclusions

Tropospheric dusts from non-urban areas contain plant wax and natural biogenic detritus. The relatively high concentrations of this wax can make it a significant component of suburban particulates.

Eolian transport is a significant mechanism for the input of organic material to some marine environments and ultimately to sediments. The n-alkanes, n-fatty acids and n-alcohols of eolian dusts were found to have homologous distributions similar to those of marine sediments recovered from areas where eolian dust falls out and no obvious river and ice-rafting inputsoccur. The presence of terrigenous organic markers in sediments remote from potamic inputs indicates eolian fallout in that particular paleoenvironment. Thus, the identification of eolian input, both organic and inorganic, in old sediments may be a useful tool in the assessment of paleoenvironments.

Eolian transport is a rapid dispersal mechanism for organic matter over vast global areas.

Acknowledgements

I thank Drs. R. Chester, S. Aston and F.K. Lepple for dust samples and the National Science Foundation for making the core samples available via the Deep Sea Drilling Project. I acknowledge the Atmospheric Research Section, National Science Foundation (Grant ATM77-19980) for financial support.

References and Footnotes

* Contribution No. 1824 from the Institute of Geophysics and Planetary Physics, University of California, Los Angeles, California 90024

Aston, S.R., R. Chester, L.R. Johnson and R.C. Padgham (1973). Eolian dust from the lower atmosphere of the Eastern Atlantic and Indian Oceans, China Sea and Sea of Japan, Mar. Geol. 14, 15-28.

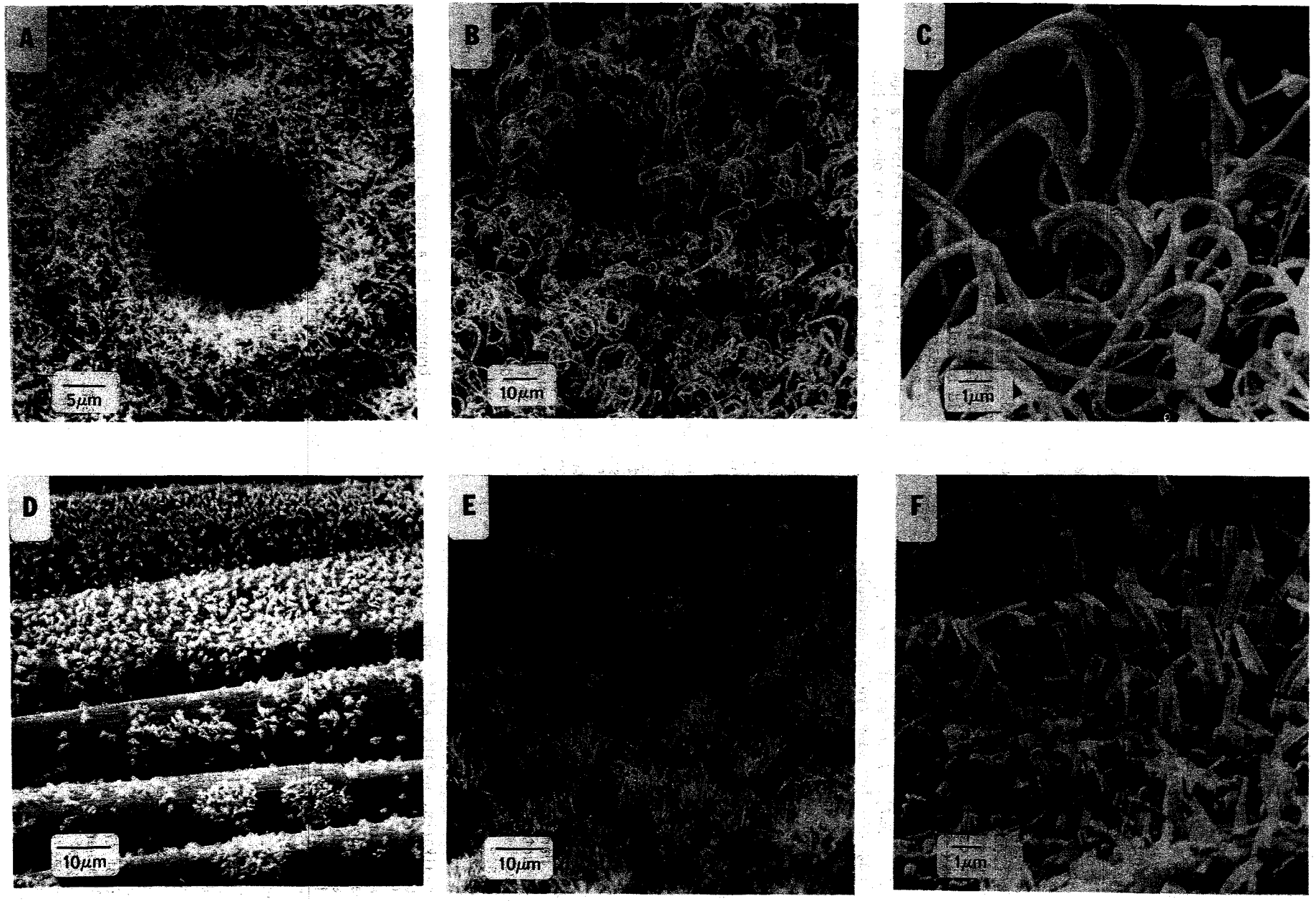

Figure 6. Examples of leaf wax morphologies (SEM photomicrographs, courtesy of Dr. P.J. Holloway, Long Ashton Research Station, University of Bristol). (A) Pinus sylvestris (needle), (B) Musa paradisaica (Banana, leaf), (C) Musa paradisaica, (D) Dactylis glomerata (cocksfoot grass, lower surface of leaf), (E) Eucalyptus (F) Brassica oleracea (brussel sprout, upper leaf surface). (D reprinted from Holloway, 1971, with permission of Academic Press, London).

Barger, W.R. and W.D. Garrett (1976). Surface active organic material in air over the Mediterranean and over the eastern equatorial Pacific, J. Geophys. Res. 81, 3151-3157.

Beltagy, A.O., R. Chester, and R.C. Padgham (1972). The particle-size distribution of quartz in some North Atlantic deep-sea sediments, Mar. Geol. 13, 297-310.

Chester, R. and H. Elderfield (1970). Dust over the oceans, New Scientist 47, 432-434.

Chester, R. (1972). Geological, geochemical and environmental implications of the marine dust veil, Proc. 20th Nobel Symp., The Changing Chemistry of the Oceans, D. Dyrssen and D. Jagner, eds., Wiley-Interscience, New York, 291-305.

Chester, R., H. Elderfield, J.J. Griffin, L.R. Johnson and R.C. Padgham (1972). Eolian dust along the eastern margins of the Atlantic Ocean, Mar. Geol. 13, 91-105.

Cooper, J.E. and E.E. Bray (1963). A postulated role of fatty acids in petroleum formation, Geochim. Cosmochim. Acta 27, 1113-1127.

Cukor, P., L.L. Ciaccio, E.W. Lanning and R.L. Rubino (1972). Some chemical and physical characteristics of organic fractions in airborne particulate matter, Env. Sci. and Tech. 6, 633-637.

Darwin, C. (1846). An account of the fine dust which often falls on vessels in the Atlantic Ocean, Quart. Journ. Geol. Soc. (Lond.) 2, 26-30.

Delany, A.C., Audrey C. Delany, D.W. Parkin, J.J. Griffin, E.D. Goldberg and B.E.F. Reimann (1967). Airborne dust collected at Barbados, Geochim. Cosmochim. Acta 31, 885-909.

Eglinton, G. and R.J. Hamilton (1963). The distribution of alkanes, in: Swain, T., Ed., Chemical Plant Taxonomy, Academic Press, New York, 187-217.

Eglinton, G., J.R. Maxwell and R.P. Philp (1974). Organic geochemistry of sediments from contemporary aquatic environments, in: Advances in Organic Chemistry 1973, B. Tissot and F. Bienner, Eds., Editions Technip , Paris, 941-961.

Ehrenberg, C. (1847). Passatstaub und Blutregen, Abhandl. Königl. Akad. Wiss. Berlin, 269-460.

Gaskell, S.J. (1974). The environmental geochemistry of sterols, Ph.D. Thesis, University of Bristol, 90-103.

Gaskell, S.J., R.J. Morris, G. Eglinton and S.E. Calvert (1975). The geochemistry of a recent marine sediment off northwest Africa: An assessment of source of input and early diagenesis. Deep-Sea Res. 22, 777-789.

Goldberg, E.D. (1971). Atmospheric dust, the sedimentary cycle and man, Comments in Geophys., Earth Sci. I, 117-132.

Griffin, J.J., H. Windom and E.D. Goldberg (1968). The distribution of clay minerals in the world ocean. Deep-Sea Res. 15, 433-459.

Grimmer, G. and H. Böhnke (1972). Bestimmung des Gesamtgehaltes aller polyzyclischen aromatischen Kohlenwasserstoffe in Luftstaub und Kraftfahrzeugabgas mit der Kapillar-Gas-Chromatographie, Z. Anal. Chem. 261, 310-314.

Hauser, T.R. and J.N. Pattison (1972). Analysis of aliphatic fraction of air particulate matter, Env. Sci. Tech. 6, 549-555.

Hitchcock, C. and B.W. Nichols (1971). Plant Lipid Biochemistry, Academic Press, London, 387 pp.

Holloway, P.J. (1971). The chemical and physical characteristics of leaf surfaces, in: Ecology of Leaf Surface Microorganisms, T.F. Preece and C.H. Dickinson, Eds., Academic Press, London, p. 49.

Karasek, F.W., D.W. Denney, K.W. Chen and R.E. Clement (1978). Analysis of complex organic mixtures on airborne particulate matter. Anal. Chem. 50, 82-87.

Kolbe, R.W. (1957). Fresh-water diatoms from Atlantic deep sea sediments, Science 126, 1053-1056.

Kolattukudy, P.E. and T.J. Walton (1972). The biochemistry of plant cuticular lipids, in: Progress in the Chemistry of Fats and Lipids, R.T. Holman, Ed., Vol. 13, Pt. 3, Pergamon Press, Oxford, pp. 121-175.

Kvenvolden, K.A. (1967). Normal fatty acids in sediments, J. Amer. Oil Chem. Soc. 44, 628-636.

Lepple, F.K. (1975). Eolian dust over the North Atlantic Ocean, Ph.D. Thesis, University of Delaware; 270 pp.

Lepple, F.K. and C.J. Brine (1976). Organic constituents in eolian dust and surface sediments from Northwest Africa. J. Geophys. Res. 81, 1141-1147.

Moyers, J.L., R.A. Duce and G.L. Hoffman (1972). A note on the contamination of atmospheric particulate samples collected from ships, Atmos. Env. 6, 551-556.

Parkin, D.W., D.R. Phillips, R.A.L. Sullivan and L.R. Johnson (1972). Airborne dust collections down the Atlantic. Q. J. Roy. Meterol. Soc. 98, 798-808.

Pate, J.B. and E.C. Tabor (1962). Analytical aspects of the use of glass fiber filters for the collection of and analysis of atmospheric particulate matter. Amer. Ind. Hyg. Assn. J. 23, 144-150.

Prospero, J.M., E. Bonatti, C. Schubert and T.N. Carlson (1970). Dust in the Caribbean atmosphere traced to an African dust storm. Earth Planet. Sci. Lett. 9, 287-293.

Radczewski, O.E. (1937a). Eolian deposits in marine sediments, in: Recent Marine Sediments, P. Trask, Ed., Amer. Assoc. Pet. Geol., Tulsa, 496-502.

Radczewski, O.E. (1937b). Die Mineralfazies der Sedimente des Kapverden Beckens, Wiss. Ergebn. Deut. Atlant. Expd. "Meteor"., 1925-1929, B.3, T1-3, 262-277.

Rex, R.W. and E.D. Goldberg (1958). Quartz contents of pelagic sediments of the Pacific Ocean, Tellus 10, 153-159.

Rex, R.W. and E.D. Goldberg (1962). Insolubles, in: The Sea, M.N. Hill, Ed., Interscience, New York, Vol. I, 295-312.

Simoneit, B.R.T. (1977a). Organic matter in eolian dusts over the Atlantic Ocean, Mar. Chem. 5, 443-464.

Simoneit, B.R.T. (1977b). Leg 41 sediment lipids--search for eolian organic matter in Recent samples and examination of a black shale, in: Initial Reports of the Deep Sea Drilling Project, Vol. 41, Y. Lancelot, E. Seibold, et al., Eds., U.S. Government Printing Office, Washington, D.C., 855-858.

Simoneit, B.R.T. (1977c). Diterpenoidal compounds and other lipids in deep sea sediments and their geochemical significance, Geochim. Cosmochim. Acta 41, 463-476.

Simoneit, B.R.T. (1977d). The Black Sea, a sink for terrigenous lipids, Deep-Sea Res. 24, 813-830.

Simoneit, B.R.T. (1978a). Terrigenous and marine organic markers in lipids of marine sediments, in: Organic Geochemistry of Deep Sea Drilling Project Sediments, E.W. Baker, Ed., Science Press, Princeton, (in press).

Simoneit, B.R.T. (1967b). The organic chemistry of marine sediments, in: Chemical Oceanography, R. Chester and J.P. Riley, Eds., Vol. 7, Academic Press, London, 2nd Ed., (in press).

Simoneit, B.R.T. and A.L. Burlingame (1972). Preliminary organic analyses of the DSDP (JOIDES) cores, Legs V-IX, in: Advances in Organic Geochemistry 1971, H.R. von Gaertner and H. Wehner, Eds., Pergamon Press, Oxford-Braunschweig, pp. 189-228.

Simoneit, B.R.T. and A.L. Burlingame (1973). Preliminary organic analyses of DSDP cores, Legs 12 and 13, in: Initial Reports of the Deep Sea Drilling Project, Vol. 17, E.L. Winterer, J.L. Ewing, et al., Eds., U.S. Government Printing Office, Washington, D.C., 561-590.

Simoneit, B.R.T. and A.L. Burlingame (1974). Study of the organic matter in the DSDP (JOIDES) cores, Legs 10-15, in: Advances in Organic Geochemistry 1973, B. Tissot and F. Bienner, Eds., Editions Technip , Paris, 629-648.

Simoneit, B.R.T. and G. Eglinton (1977). Organic matter of eolian dust and its input to marine sediments, in: Advances in Organic Geochemistry 1975, R. Campos and J. Goni, Eds., ENADIMSA, Madrid, 415-430.

Simoneit, B.R.T. and M.A. Mazurek (1978). Search for eolian lipids in the Pleistocene off Cape Bojador and lipid geochemistry of a Cretaceous mudstone DSDP/IPOD Leg 47A, in: Initial Reports of the Deep Sea Drilling Project, Vol. 47A, W.B.F. Ryan, U. von Rad, et al., Eds., U.S. Government Printing Office, Washington, D.C. (in press).

Simoneit, B.R.T., R. Chester and G. Eglinton (1977). Biogenic lipids in particulates from the lower atmosphere over the Eastern Atlantic, Nature 267, 682-685.

Simoneit, B.R.T., E.S. Scott and A.L. Burlingame (1973). Preliminary organic analyses of DSDP cores, Leg 14, Atlantic Ocean, in: Initial Reports of the Deep Sea Drilling Project, Vol. 16, T.H. van Andel, G.R. Heath, et al., Eds., U.S. Government Printing Office, Washington, D.C., 575-600.

Simoneit, B.R.T., D.H. Smith and G. Eglinton (1975). Application of real-time mass spectrometric techniques to environmental organic chemistry: I. Computerized high resolution mass spectrometry and gas chromatography low resolution mass spectrometry. Arch. Env. Contamin. Toxicol. 3 (4), 385-490.

THE EFFECT OF CARBON PARTICLES ON ATMOSPHERIC RADIATION

by

Robert W. Bergstrom
Systems Applications, Incorporated
San Rafael, California

and

NASA Ames Research Center
Moffett Field, California

SUMMARY

The solar radiation absorption properties of graphitic carbon and soots are well documented. What is not as well known is that small carbon particles less than 0.1 μm in radius are extremely effective absorbers per unit mass; this suggests that a small amount of submicron particles of graphitic carbon has a large effect on atmospheric radiation. Figure 1 shows the absorption and light scattering per unit mass for a variety of indices of refraction. For nonabsorptive particles, those from 0.1 to 1 μm in radius are the most effective light scatterers per unit mass, thus explaining the importance of secondary aerosols to visibility and atmospheric radiative properties. As the absorption index increases, small particles become more effective scatterers per unit mass.

Further enhancing the role of carbon particles, a coating of nonabsorbing material (water/sulfate compound) increases their abosprtion. This result has been shown by Kattawar and Hood (1976), who computed the absorption cross section as a function of the ratio of the core radius (carbon) to the total particle radius (carbon plus water/sufate). For values between 0.85 and 1.0, the absorption efficiency for the entire particle is actually larger than that for a particle with no coating. The coating of water/sulfate acts as a lens in focusing the radiation onto the particle.

Previous calculations have shown that large heating rates (about 1 degree per hour) could occur for polluted atmospheres containing a small amount of carbon particles. Such rapid heating is important to local dynamics and global climate energetics. However, these calculations assume that all of the energy absorbed by the particles contributes to the bulk properties of the air. It has not yet been established whether the carbon particles have the same temperature as the surrounding air. After studying the energetics of weakly absorbing particles, Fiocco, Grams, and Mugnai (1976) concluded that the temperature of the particles may differ from that of the ambient gas. Also, if the particle is coated with water, a significant fraction of the energy can be released through evaporation. Baker (1976) studied the energetics of a weakly absorbing particle with properties similar to water and determined that a 0.5 μm particle evaporates in several minutes as a

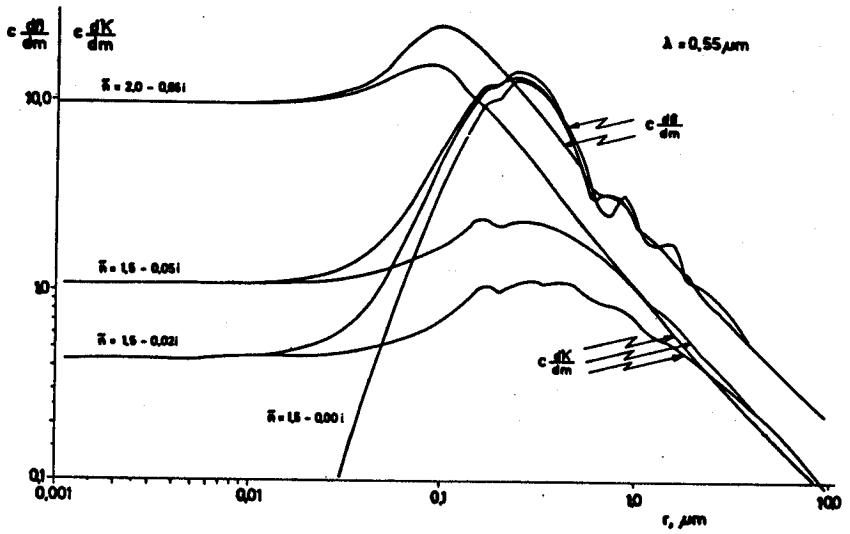

Fig. 1. Extinction and Absorption Coefficients per Unit Mass as a Function of Particle Radius for Four Different Refractive Indices at a Solar Wavelength of 0.55 μm

result of absorption of solar radiation. She found that roughly half of the energy was accounted for by evaporation.

The presentation discussed (1) the effect of a small amoung of submicron carbon particles on atmospheric radiative properties and (2) the various processes that govern the energetics of highly absorbing particles.

REFERENCES

Baker, M. B. (1976), "Energy Absorption by Volatile Atmospheric Aerosol Particles," Atmos. Environ., Vol. 10, p. 241.

Fiocco, G., G. Grams, and A. Mugnai (1976), "Energy Exchange and Temperature of Aerosols in the Earth's Atmosphere (0-60 km)," J. Atmos. Sci., Vol. 33, p. 2415.

Kattawai, G. W., and D. A. Hood (1976), "Electromagnetic Scattering from a Spherical Polydispersion of Coated Spheres," Appl. Opt., Vol. 15, p. 1996.

OPTICAL PROPERTIES OF URBAN AEROSOLS CONTAINING CARBONACEOUS MATERIAL

E. M. Patterson
National Center for Atmospheric Research
P.O. Box 3000
Boulder, Colorado 80307

ABSTRACT

We have measured the imaginary index of refraction for Denver, Colorado urban aerosols. The absorptive properties of these aerosols are strongly influenced by the absorptive properties of both elemental carbon and the benzene soluble organics. The consequences of the change in absorption due to the carbonaceous compounds on the optical effects of the aerosol will be discussed.

INTRODUCTION

Carbon and carbonaceous compounds are known to be important components of the Denver, Colorado urban aerosol; and it is reasonable that the presence of these carbon compounds will affect the absorptive properties and, possibly, the optical effects of the aerosol. We have made a number of measurements of the optical properties of the Denver urban aerosol that have been related to the size distribution and composition of these aerosols. We have found that the absorptive properties of the aerosol are strongly influenced by the absorptive properties of two general types of carbonaceous material: elemental, possibly graphitic, carbon and benzene soluble organics (BSO), two types of material with very different absorptive properties. We will discuss some probable sources for the carbonaceous material in the Denver aerosol and will relate the properties of the source material to the measurements of the optical properties. We will also discuss some of the consequences of the presence of the carbonaceous material on the aerosol optical effects.

METHOD OF ANALYSIS

The optical effects of an aerosol will be determined by the size-distribution for the aerosol, the shapes of the aerosol particles and the optical properties of the aerosol material. The optical properties of an aerosol material may be described by a complex index of refraction

$$m = n_{RE} - i\, n_{IM} \qquad (1)$$

where the n_{RE} is the usual real index of refraction and n_{IM}, the imaginary index of refraction, is an absorption parameter that is related to the usual Bouguer-Lambert absorption parameter, k, by the equation n_{RE} for the aerosols may be determined by optical microscopic techniques[1]; n_{IM} may be determined as a function of wavelength in the visible by means of transmission measurements on suitable samples, a method that was used for the determination of the absorption of the benzene soluble component or by means of measurements of sample reflectance, such as our measurements of the total diffuse reflectance of a sample with analysis using the Kubelka-Munk Theory.

Kubelka-Munk Theory

The Kubelka-Munk (K-M) theory is a phenomenalogical theory that relates the total diffuse reflection from a material to the effective scattering and absorbing properties of the material. As discussed by Kortum[2], the K-M theory is a two-flux theory in which the radiation is assumed to be composed of two oppositely directed radiation fluxes through a continuous medium. This material is assumed to have an absorption coefficient per unit distance k and a scattering coefficient per unit distance s, with the term scattering referring only to radiation redirected into the backward hemisphere. The K-M theory assumes diffuse radiation onto the surface of the material, as well as diffuse radiation within the material, which results in an increased effective path length within the material. The scattering and absorption coefficients are generally redefined as S = 2s and K = 2k, to take into account this increased path length. Gate[3] has shown that the K-M constants S and K are related to the usual scattering and absorption cross sections, σ_S and σ_A, and are defined for radiation transfer calculations by the equations

$$K \doteq 2\sigma_A \qquad (2)$$

and

$$S = (3/4)\sigma_S \qquad (3)$$

which are valid for isotropically scattering, weakly absorbing materials (K/S < 0.01). These relations have been verified experimentally [Gate[3], Brinkworth[4]] and have been found to be valid within approximately 5%.

Since the definitions K = 2k and S = 2s have been made, these results imply that the quantity k is the same as the usual Bouguer-Lambert absorption coefficient, although $s = (3/8)\sigma_S$. The difference in the scattering coefficients arises because s is defined as scattering into the backward hemisphere. Since k is the usual Bouguer-Lambert absorption coefficient appropriate to a bulk material, the values for n_{IM} may be determined from k using Eq. (2).

According to K-M theory, the total diffuse reflectance from a semi-infinite thickness of material, R_∞, will depend only on the ratio k/s by means of the equation

$$\frac{k}{s} = F(R_\infty) = \frac{(1-R_\infty)^2}{2R_\infty} \quad (4)$$

F(R) for any reflectance is called the Kubelka-Munk function for R. Kortum has shown that the K-M scattering coefficient S may be determined from measurements of the reflectance of a thin layer of material against a dark background if the layer thickness, d, and R_∞ for the material are known. The absorption coefficient k may then be determined from a measurement of R_∞ if the scattering coefficient has been measured. Kortum has shown that there are deviations from K-M theory under conditions of high absorption, but that the K-M theory is applicable when the highly absorbing material whose absorption is to be measured is diluted with an excess of a white standard. These are the same conditions under which the relationships discussed by Gate are valid. Under these conditions, also, directed incident radiation may be used in place of the diffuse incident radiation and the applicability of the K-M theory is maintained. Because the K-M theory is based on multiple scattering calculations, the K-M theory is completely independent of the usual Mie theory analysis and is not dependent on the shape of the particles.

Measurements Procedures

Aerosols were collected at surface stations and aboard an aircraft during a series of studies of Denver area pollution aerosols using high-volume samplers operated at flow rates of approximately 1-2 m/ min. Collection was made onto both fibreglas and Delbag® polystyrene filters; a series of size separated aerosol collections was made with a high-volume cascade impactor. Benzene extractions of the material on the fibreglas filters were made and the absorptive properties of the benzene soluble fraction were determined as a function of wavelength using standard transmission techniques on the sample dissolved in benzene.

The aerosol material on the polystyrene filters was analyzed using the reflectance method, following the general procedures described in Patterson et al[5]. Briefly, the aerosol material was separated from the polystyrene filters by dissolving the polystyrene material in toluene and sedimenting out the aerosol material. The collected aerosol was washed several times with toluene to remove the remaining plastic material, with the toluene remaining after the last wash removed by evaporation. The reflection measurements were made with a C-14 spectrophotometer equipped with a 15 cm integrating sphere coated with a barium sulfate paint. The total diffuse reflectance was measured for pure barium sulfate and for a mixture of the barium sulfate and the aerosol sample.

The dilution ratios of aerosol and barium sulfate are chosen so that the scattering is determined by the barium sulfate whose scattering properties have been previously measured [6]. With the knowledge of the optical properties of the barium sulfate, the K-M theory may be used to determine k and n_{IM} for the aerosol.

The method described is similar to that used by Lindberg and Laude[7] to measure n_{IM} for atmospheric dust in the southwestern United States and has been used by us in a number of measurement programs. In one particular study, we have measured n_{IM} for Saharan soil aerosols as a function of wavelength in the visible as shown in Fig. 1.from Patterson et al[5]. These measurements were in agreement with measurements of n_{IM} for the same aerosols made using a direct-diffuse radiation method by Carlson and Caverly [8], also shown in Fig. 1.

MEASUREMENT RESULTS

The results of measurements of n_{IM} for two different aerosol samples obtained under conditions of relatively light pollution are shown in Fig. 2. The mass distributions for these aerosol samples were dominated by the mineral aerosol component with radii greater than approximately 0.5 μm, and so the measured absorption is dominated by aerosols in this size range. The lower curve shows the values of n_{IM} measured for an aerosol sample obtained when the wind direction was from a predominately rural area; values of n_{IM} measured for this aerosol are similar to our measured values for Saharan aerosols and appear to be typical of soil aerosol n_{IM} measurements. The upper curve in Fig. 2 is more typical of our measurements when the wind direction was from the city center. The values of n_{IM} for this aerosol are generally uniform across the visible spectrum and considerably higher than those for the lower curve, although the mass distribution was again dominated by minerological aerosols. The high and relatively constant values of n_{IM} across the visible lead us to identify the source of increased absorption as elemental, probably graphitic, carbon. (See for example Rosen et al.[9]) Microscopic analysis of the aerosol particles showed that the sample contained an appreciable amount of black particles, some of which appeared to be tire rubber fragments. Tire rubber contains an appreciable amount of carbon black which has the required absorption properties.

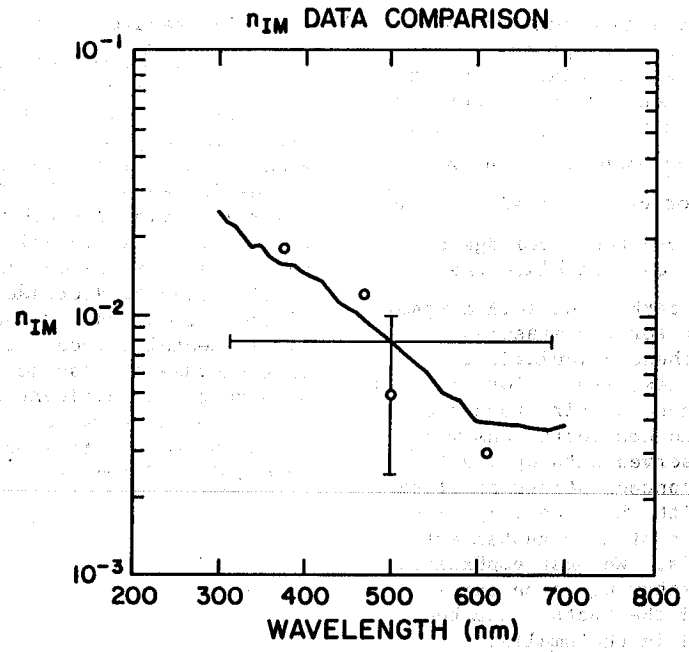

Figure 1. Measurements of the imaginary index of refraction for Saharan and other soil-derived aerosols. The solid curve represents our best estimate of the imaginary index of refraction as a function of wavelength for the Saharan aerosols. The circles at 375, 468, and 610 nm are from measurements of Carlson and Caverly for Saharan aerosols; the circle with error bars at 500 nm represents an average of some measurements of soil derived aerosols by Grams et al., and the solid line (——) at n_{IM} = 0.008 represents an average value measured by DeLuisi et al. for similar aerosols in the Southwestern U.S.

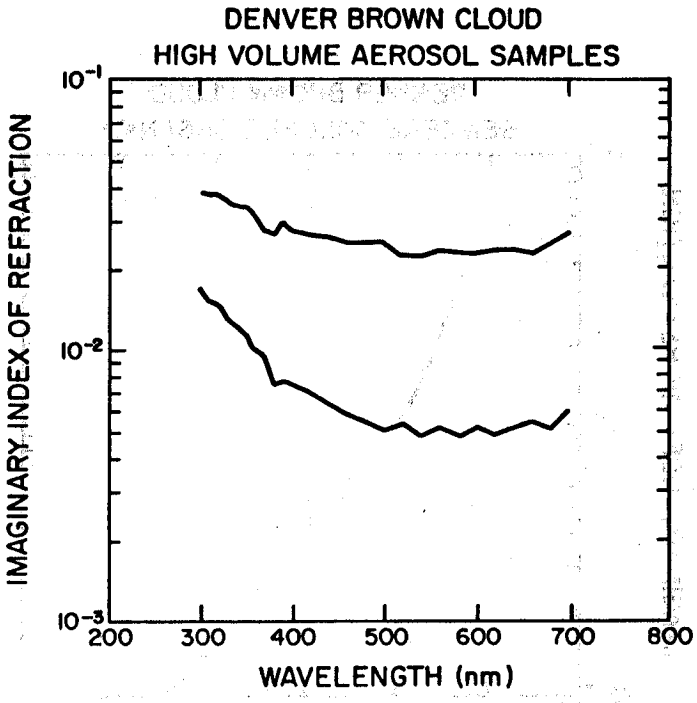

Figure 2. Imaginary index of refraction for two samples of Denver aerosol. The upper curve is the imaginary index for a sample containing a relatively large amount of a dark uniformly absorbing material; the lower curve is for a sample not containing this material.

The identification of a component may be checked by a consideration of the optical properties of the components since the relative concentrations for two components needed to account for a given value of n_{IM} for a mixture may be calculated if the values of n_{IM} for each component are known. The value of n_{IM} for carbon is known to be approximately 0.6 so that with the knowledge of n_{IM} for the soil aerosol we can calculate the relative concentrations of carbon and soil-aerosol particles needed to account for the measured absorption. We have made these calculations assuming both carbon particles, (soots for example) and carbon that is a component of tire rubber and have compared the calculated concentrations with relative concentrations observed with optical microscopy. The observed concentrations of black particles are consistent with the identification of the carbon as a component of tire rubber but not as pure carbon particles. We must emphasize, however, that these were measurements on samples of the larger particles and the soots would be expected to be concentrated in the smaller size fraction. We can estimate that the relative concentration of elemental carbon in our absorbing sample in Fig. 2 is approximately 3% by volume, although the relative concentration of tire particles is of course higher.

The results of the measurements of n_{IM} for the benzene soluble component of the aerosols are shown in Fig. 3. The imaginary index of refraction is quite different from that of elemental carbon, being relatively low throughout much of the visible and showing a sharp rise with decreasing wavelength. The low value of the imaginary index throughout the visible implies that if the benzene soluble organic component of the aerosol is present in large quantities then it will tend to decrease the average absorption of the aerosol rather than increase it, as does the elemental carbon. This is potentially important because our cascade impactor measurements show that a significant portion of the benzene soluble organic was concentrated in the small fraction and can thus serve to reduce the average absorption of this size fraction.

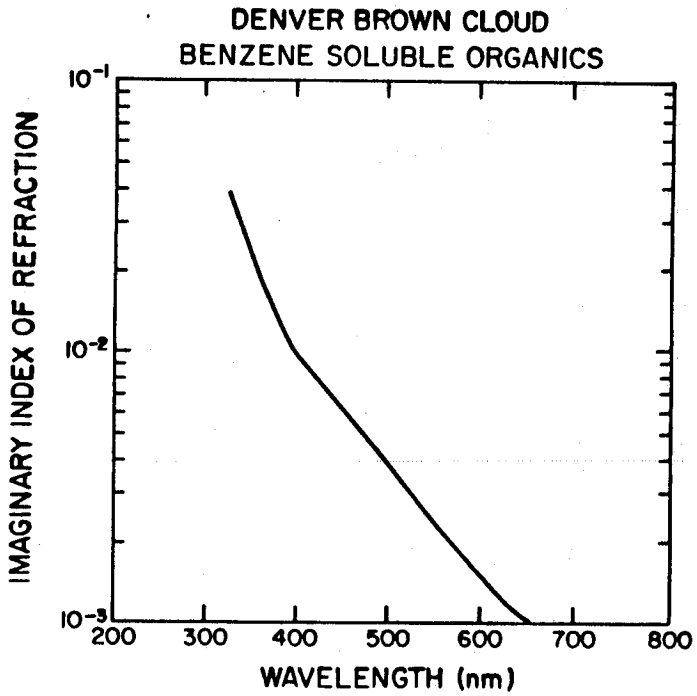

Figure 3. Imaginary index of refraction for the benzene soluble organic component of the Denver aerosol.

CONCLUSIONS

Our measurements indicate that the Denver urban aerosol is relatively highly absorbing, in agreement with results reported by Waggoner and Charlson[10] with a relatively constant value of n_{IM} across the visible. The source for this absorption is likely elemental carbon, with tire rubber possibly accounting for a significant portion of the absorption in the larger size ranges. The benzene soluble fraction, unlike the elemental carbon fraction has a low value of n_{IM} throughout much of the visible and will thus serve to reduce the absorption when this aerosol component is present in large quantities.

This relatively high aerosol absorption will affect the haze coefficient measurements and will affect the atmospheric heating rates for the aerosol, possibly affecting the dynamical behavior of the regional pollution cloud.

We have however calculated the wavelength dependence of the phase function for these absorbing aerosols and have found that the wavelength dependence does not appear to be significantly different from that determined for the non-absorbing case. These calculations indicate that the observed optical effects of the aerosols will not be highly sensitive to the absorption properties of the aerosol.

ACKNOWLEDGMENT

The National Center for Atmospheric Research is sponsored by the National Science Foundation.

REFERENCES

1. F. E. Wright, "The index ellipsoid (optical indicatrix) in petrographic microscope work", Am. J. Sci., 185, 133-138 (1913).

2. G. Kortum, Reflectance Spectrocospy, Interscience, New York, 366 pp. (1969).

3. L. F. Gate, "Comparison of the photon diffusion model and Kubelka-Munk equation with the exact solution of the radiative transport equation", Appl. Opt., 13, 236-238 (1974).

4. B. J. Brinkworth, "On the theory of reflection by scattering and absorbing media", J. Phys. D:Appl. Phys., 4, 1105-1106 (1971).

5. E. M. Patterson, D. A. Gillette, B. H. Stockton, "Complex index of refraction between 300 and 700 nm for Saharan aerosols", J. Geophys. Res., 82, 3143-3160 (1977).

6. E. M. Patterson, C. E. Shelden and B. H. Stockton, "Kubelka-Munk optical properties of a barium sulfate white reflectance standard", Appl. Opt., 16, 729-732 (1977).

7. J. D. Lindberg and L. S. Laude, "Measurement of the absorption coefficient of atmospheric dust", Appl. Opt., 13, 1923-1927 (1974).

8. T. N. Carlson and R. S. Caverly, "Radiation characteristics of Saharan dust at solar wavelengths", J. Geophys. Res., 82 (1976).

9. H. Rosen, A.D.A. Hansen, L. Gundel, and T. Novakov, "Identification of the Graphitic Carbon Component of Source and Ambient Particulates by Raman Spectroscopy and Optical Attenuation Techniques", paper presented at the Conference on Carbonaceous Aerosols, Berkeley, CA (March 1977).

10. A. P. Waggoner and R. J. Charlson, "Measurements of Aerosol Optical Properties", in Denver Air Pollution Study-1973, Proceedings of a Symposium, Vol II, Edited by P. A. Russell available from NTIS as EPA-600/9-77-001 (1977).

LIGHT ABSORPTION MEASUREMENTS IN EUROPE

Jost Heintzenberg
International Meteorological Institute in Stockholm
Arrhenius Laboratory
S-106 91 STOCKHOLM, Sweden

ABSTRACT

European studies on the absorption of electromagnetic radiation by atmospheric aerosol particles in the wavelength range 0.2 to 17μm are reviewed, starting with the first radiation models which incorporated light absorption. Mass absorption indices derived with an integrating sphere and a spectrometer from impactor aerosol samples under various continental and maritime conditions are shown. The paper includes results for size-segregated aerosol samples together with those for precipitation recidues and fog-activated aerosol samples. In a preliminary analysis of the latest field experiment in southern Sweden a combination of optical and chemical characteristics of the haze layer over Europe is presented.

Atmospheric aerosol particles play an important role in the processes of scattering and absorption of electromagnetic radiation in the atmosphere. Here we concentrate on the absorption of light (and other electromagnetic radiation) by the atmospheric aerosol and review European research in this area. The paper is based on studies covering the wavelength range which contains the major part of the solar input into the troposphere (2 to 2.4μm) as well as on investigations of the long-vawe range between 2.4μm and 17μm where the heat radiative transfer in the lower atmosphere is most intense.

Long before the first reliable experimental results on the absorption properties were derived, a grey aerosol absorption had been suspected and used successfully in radiative transfer calculations to explain measurements of direct and diffuse sun radiation 1.2.

Even though various experimental attempts had been made to establish quantitative results on the aerosol absorption, the numbers were rather uncertain because of the weak bulk absorption effect of atmospheric particles: When comparing air to ground transmission with light scattering measurements Waldram found cases with high aerosol absorption [3]. Volz [4] found high UV absorption by soot-free precipitation residues from European locations with a very fast decrease with increasing wavelenghts i.e. about a factor of 10 from 0.22μm to 0.6μm wavelength In the sixties the amount of energy absorbed by aerosol particles was deduced from several European studies of radiation in the atmosphere, [5-8]. In urban aerosol an average amount of 30% of the extinction of sun radiation was attributed to light absorption.

For a reliable determination of bulk absorption properties of the aerosol material such as the imaginary part k of the complex refractive index, particle collection tehniques had to be applied to enhance the observed optical effects. Furthermore an integrating sphere was used to discriminate between the pure absorption of an aerosol sample and the combined light scattering and absorption effects which are seen by a regular photometer [9].

With jet impactors collecting particles above 0.15μm aerodynamic radius Fischer sampled probes under various continental and maritime conditions. The samples are deposited either on glass slides for wavelengths below 2.4μm or on silver chloride plates for the analysis of the infrared absorption spectrum. The collection times vary from hours in polluted air to more than a week in clean air masses.

Only up to wavelenghts of 2μm is scattering a significant part of the total extinction by an aerosol collection. Therefore a simple spectrograph without integrating sphere could be used for the infrared analysis [11].

A summary of his results is present in figure 1. Since the absorption measurements require an independent measurement of the bulk density ϱ of the collected material (which most of the time was not available) the results are given in terms of the so called mass absorption index k/ϱ. One should use values between 1.8 and 3 for the density to convert the results to the imaginary part of the refraction index [10]. The full bars give the range he found for urban aerosols in the visible while the dashed bar shows results derived with a different technique by Chin i Lin et al. in New York city. As spectra typical continental (Namibia), high tropospheric (Jungfraujoch) and maritime (Mace Head) aerosol absorptions are depicted.

Infrared absorption spectra taken from [11] are plotted on the right part of fig. 1. With the exception of the maritime samples all of Fischers aerosol probes have absorption bands in the region of atmospheric transparencey between 7.5 and 12μm wavelength. The dominating bands can be attributed to the oscillations of certain atom-groups like the $SO_4^=$-ion (9.2, 16.3μm), the NH_4^+-ion (3.2, 7.1μm) and silicates 8-10μm). However, quantitative chemical analysis is difficult without additional separation techniques because of the coincidence of bands of inorganic and organic substances and the shift of absorption bands with the size of the particles (surface-phonon-modes in particles with a size $\ll$ than the wavelength compared to bulk-phonon-modes of compact cristalline substances). Furthermore internal mixing of different salts within aerosol particles smooths the band structure.

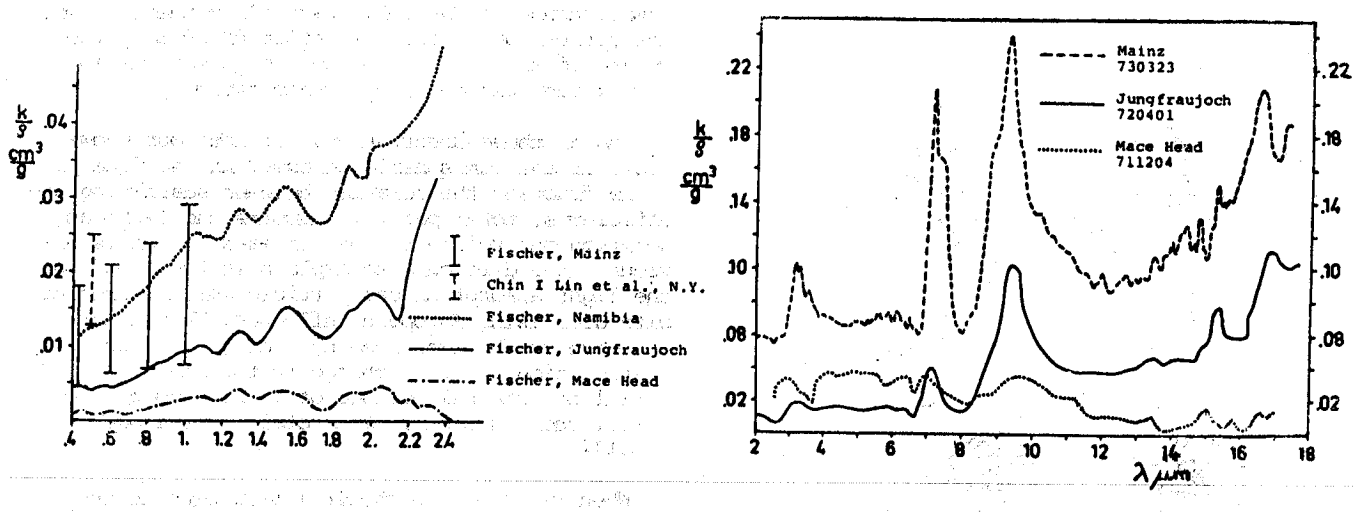

Fig. 1. Spectra of mass absorption indices under various continental and maritime conditions 8, 9, 11.

The spectral mass absorption indices, however, have been used in radiative transfer models to calculate heating or cooling effects of the atmospheric aerosol. Eschelbach [12] showed that in the visible and near infrared part of the spectrum absorbing particles lead to a heating of the particle-loaden layers of the atmosphere. Grassl [13] included the terrestrial part of the spectrum in the model calculations and calculated net effects of heating due to short wave absorption and cooling due to long wave emission. The absorption index strongly depends on relative humidity in both parts of the spectrum. Therefore he always finds a distinct relative humidity where cooling balances heating.

In recent studies size-segregated aerosol samples have been analyzed together with precipitation residues and fog-activated aerosol samples which had been collected with several stages of impactors [14]. In figs. 2 and 3 the results are summarized. The curves show a distinct decrease of the absorption index with particle size in the dry aerosol as well as in aerosols where condensations processes have activated larger particles.

In the latest field experiment in Velen, Sweden 1977, optical in situ measurements were combined with physical and chemical analysis of aerosol samples in study of charecteristic parameters of the European smoke cloud, i.e. an aerosol layer being centered over Western Europe having an extent of about 1000 km.

The changes in optical and chemical parameters of the aerosol with the transition from air masses with direct European influence to those without is demonstrated with the results of four consecutive sampling periods. In fig. 4. 72 hours trajectories to Velen are collected for each of the sampling intervals. They indicate that sample one is under strong influence of England and Northern Ireland. Sample 2 covers a longer period of time with higher wind speeds and trajectories scattering from Southern Norway over the British Isles down to the Biscaya. Sample 3 is characterized by low wind

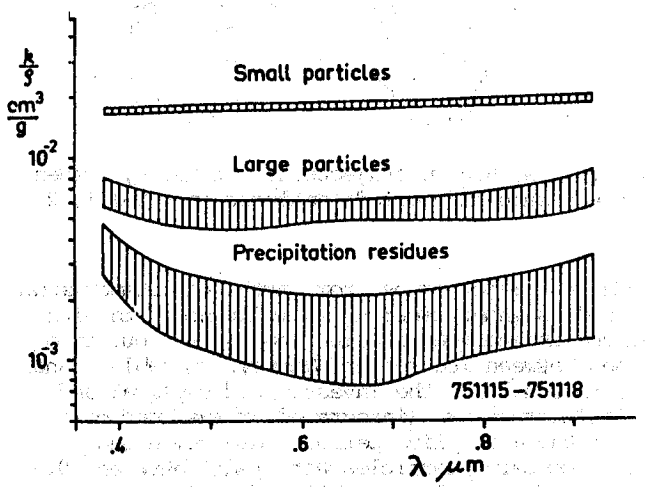

Fig. 2. Spectra of mass absorption indices for size-segregated aerosol samples and precipitation residues[14]. Dashed areas indicate uncertainties due to systematic measuring errors.

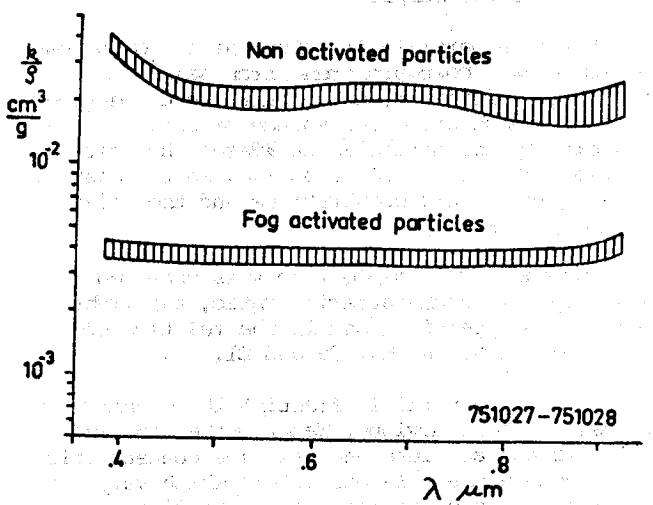

Fig. 3. Spectra of mass absorption indices of non activated and fog activated aerosol particles[14]. Dasted areas indicate uncertainties due to systematic measuring errors.

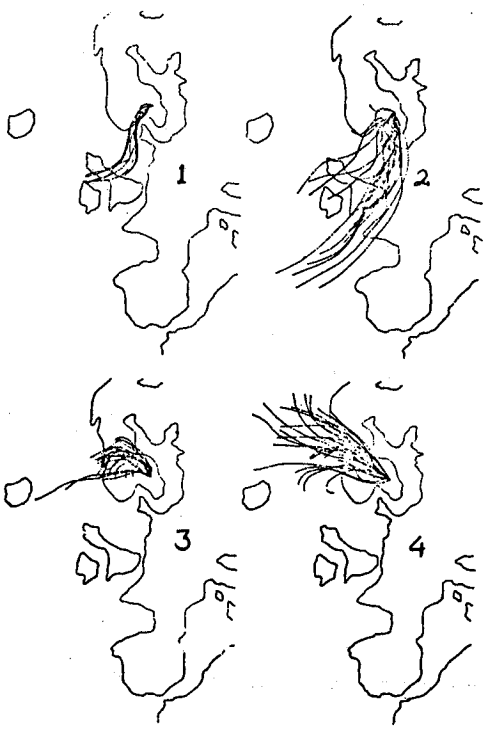

Fig. 4. 72 h, 850 mb trajectories to Velen, Sweden for the 4 sampling periods analysed in tabel 1, 2.

speeds and trajectories from North West Scandinavia. Sample 4 is under clear polar influence with high wind speeds and trajectories leading far out into the sea between Iceland and Norway. In table 1 and 2 the results from the investigated physical and chemical parameters (integrated or averaged over each of the 4 sampling periods) are collected. Table 1 concerns particles with radii between 0.2-0.3 μm and about 1.5 μm while table 2 gives results for larger particles up to radii of 8 μm. Let us see now how the origin of the air masses is reflected in the physical and chemical parameters of the respective samples.

In the fine particle fraction the following parameters show a downward trend from sample 1 to 4: scattering coefficient, total particle concentration, light absorption per volume of air, the water uptake by the particles at 90%rel. humidity, the hysteresis in the water uptake, in the absolute NH_4^+, $SO_4^=$, and iron-concentrations and the relative NH_4^+ concentrations.

An increase from sample 1 to 4 is observed in the hemispheric backscattering ratio, the light absorption per particle and in the relative concentrations of Na, K, Mg, Ca and Cl.

In the coarse particle fraction the trends with air mass are less obvious. Water uptake and its hysteresis and absolute and relative concentrations of clorine are the only parameters which vary for the large particles as they do in the fine particle range. However, several other parameters form a group with similar variation with air mass (or just sample number): The total particle concentration, the optical depth for absorption divided by the volume of air or by the number of particles in that volume and the iron-concentration.

How do these observations fit into our knowledge of the atmospheric aerosol? In the fine particle fraction the relation between scattering coefficients, total particle numbers and light absorption per volume to the air mass origin is obvious. More difficult to explain is the trend in the light absorption per particle which increases with decreasing European influence. This apparent increase can be explained by a change in the size distribution and by a change in the state of internal or external mixture of light absorbing material such as soot in the total aerosol population[12].

When relating the chemical variables to the aerosol orgin we include the concentrations relative to those for $SO_4^=$ in the analysis. This is done with the following reasoning. Rodhe[15] has shown that 80-100% of the sulfur in the European aerosol cloud is of anthropogenic orgin. With increasing distance from the source its concentration should go down according to our knowledge of long-range transport and wet/dry deposition mechanisms. For elements with other sources such as Na, Ca and Cl the relative concentrations should go up with distance from the sulfur source. Allowing a maritime source for Na, Ca and Cl the trends in the elementary concentrations with sample number are consistent with the trajectory analysis. The hygroscopic behaviour and the hemispheric backscatter ratio should be analysed together because they are closely related. It has been shown that the backscatter ratio of continental aerosol is directly proportional to the real part of the refractive index. On the other hand aquous solutions like droplets formed by strongly hygroscopic aerosols have a low refractive index compared to that of an undissolved salt crystal. For instance the transitition from an aerosol consisting of an acid like H_2SO_4 to the neutralized salt is characterized by an increase in the backscatter ratio due to the increase in refractive index[16].

On the other hand the humidity uptake of an H_2SO_4 aerosol is far above that of the neutralized salt and these acid droplets have no hysteresis in their water uptake while neutralized salts usually found in the atmosphere have distinct deliquescence points between 70 and 80% rel. humidity with hysteris occuring above 50% rel. humidity[17]. So except for the hysteresis behaviour of sample 1 (where no wet chemical analysis was available) the changes in backscatter ratio and hygroscopic behaviour with air mass can be explained by a change in the acidity of the aerosol.

With the exceptions of the hygroscopic behaviour and the clorine concentrations the large particle fraction seems to be rather decoupled from the accumulation mode indicating a more local origin of the aerosols. Here the light absorption per particle follows a different trend than in the accumulation mode which is also seen in the total particle number and in the iron-concentration.

Table 1

VELEN 1977

Accumulation mode

Sample Nr.	b_s .55 μm km^{-1}	$\frac{b_{bs}}{b_s}$	N >.3μm cm^{-3}	τ_{aV}	τ_{aN}	m_w f=.9	$\frac{\mu'}{\mu''}$ f=.5	Na $\frac{\mu g}{m^3}$	K $\frac{\mu g}{m^3}$	Mg $\frac{\mu g}{m^3}$	Ca $\frac{\mu g}{m^3}$	NH_4 $\frac{\mu g}{m^3}$	Cl $\frac{\mu g}{m^3}$	NO_3 $\frac{\mu g}{m^3}$	SO_4 $\frac{\mu g}{m^3}$	Fe $\frac{ng}{m^3}$
1	.079	.11	24.	7.9	3.2	3.5	2.8	./.	./.	./.	./.	./.	./.	./.	./.	21.9
2	.033	.13	9.4	4.2	5.0	./.	./.	.12 (.11)	.02 (.018)	.04 (.036)	<.01	.86 (.77)	.14 (.12)	.06 (.054)	1.12 (1.0)	10.3
3	.021	.15	3.0	1.55	6.3	./.	./.	.03 (.091)	.01 (.03)	.01 (.03)	.01 (.03)	.20 (.61)	.12 (.36)	.01 (.03)	.33 (1.0)	15.2
4	.012	.17	2.3	./.	./.	2.6	1.1	.06 (.35)	.03 (.18)	.02 (.11)	.02 (.12)	.04 (.24)	.16 (.94)	.03 (.18)	.17 (1.0)	8.5

Table 2

VELEN 1977

Coarse particle mode

Sample Nr.		N >1.3μm cm^{-3}	τ_{aV}	τ_{aN}	m_w f=.9	$\frac{\mu'}{\mu''}$ f=.5	Na $\frac{\mu g}{m^3}$	K $\frac{\mu g}{m^3}$	Mg $\frac{\mu g}{m^3}$	Ca $\frac{\mu g}{m^3}$	NH_4 $\frac{\mu g}{m^3}$	Cl $\frac{\mu g}{m^3}$	NO_3 $\frac{\mu g}{m^3}$	SO_4 $\frac{\mu g}{m^3}$	Fe $\frac{ng}{m^3}$
1		.28	.79	2.3	2.3	3.6	./.	./.	./.	./.	./.	./.	./.	./.	26.5
2		.071	.26	.40	./.	./.	.11 (1.2)	.01 (.11)	.03 (.33)	.01 (.11)	<.01	.05 (.55)	.06 (.66)	.09 (1.0)	10.0
3		.026	.37	1.3	./.	./.	.01 (1.0)	.01 (1.0)	<.01	.02 (2.0)	<.01	.06 (6.0)	.01 (1.0)	.01 (1.0)	19.5
4		.028	.40	1.4	2.1	1.5	.04 (2.0)	.01 (.50)	.01 (.50)	.02 (1.0)	.01 (.50)	.17 (8.5)	.02 (1.0)	.02 (1.0)	25.7

Table 1, 2. Optical and chemical characteristics of atmospheric aerosols with varying influence from western Europe.

List of symbols

b_s = scattering coefficient at .55 μm wavelength

b_{bs}/b_s = ratio of hemispheric backscattering coefficient to scattering coefficient

N = particle concentration

τ_{aV} = optical depth for absorption divided by the sampling volume of air

τ_{aN} = optical depth for absorption divided by the number of particles in the sampling volume

m_w = the mass of water taken up by the sample at 90% rel. humidity divided by the dry mass

μ'/μ'' = the mass of water in the sample when decreasing the rel. humidity to 50% divided by the mass of water taken up when increasing the rel. humidity to 50%

Na - SO_4 = elementary concentrations from wet chemistry analysis of filter samples. The numbers in parenthesis give the concentrations relative to those for SO_4

Fe = elementary concentrations from PIXE-analysis of filter samples

./. = no data

Iron compounds like hematite are strongly light absorbing. Under clean air conditions we can expect the major anthropogenic particulate light absorber, i.e. soot, to have a greatly reduced effect and other light absorbing materials like hematite might have to be accounted for.

REFERENCES

1. Gordov, A., 1936: Gerl. Beitr. Geophys., 48, 131.
2. Hinzpeter, H., 1957: Z. f. Met., 11, 1.
3. Waldram, I.M., 1945: Quart. J. R. Met. Soc., 71, 319.
4. Volz, F., 1956: Meteorol. Rundsch., 9, 169.
5. Bolle, H.J., 1967: Bundesministerium f. wissenschaftl. Forschung, W 67-17.
6. Leupolt, A.B., 1965: Ph.D. Thesis, University of München.
7. Quenzel, H., 1967: "Meteor"-Forsch.-Ergebnisse B1, 36.
8. Eiden, R., 1971: Appl. Opt., 10, 749.
9. Fischer, K., 1970: Contr. Atm. Phys., 43, 244.
10. Thudium, J., 1976: Aerosol Sci., 7, 167-173.
11. Fischer, K., 1975: Appl. Opt., 14, 2851.
12. Eschelbach, G., 1971: J. Quant. Spectrosc. Radiat. Transfer, 11, 757.
13. Fischer, K., H. Grassl, 1975: Tellus, XXVII, 522.
14. Schnatz, G., K. Andre, 1977: Proc. Symposium on Radiation in the Atmosphere, Garmisch-Partenkirchen 1976, 54.
15. Rodhe, H., 1976, in SCOPE Report 7. Ecol. Bull. (Stockholm) 22, 89-134.
16. Heintzenberg, J., 1978: Staub., 38, 2, 62-63.
17. Winkler, P., 1973: Aerosol Sci., 4, 373-382.
18. Heintzenberg, J., 1978: Light scattering parameters of internal and external mixtures of soot and non-absorbing material in atmospheric aerosols, paper submitted to the conference on carbonaceous particles in the atmosphere, Berkeley, Cal.

STUDIES OF THE OPTICAL, PHYSICAL & CHEMICAL PROPERTIES OF LIGHT ABSORBING AEROSOLS

R.E. WEISS, A.P. WAGGONER, R.J. CHARLSON
University of Washington, Seattle, WA
D.L. THORSELL
Seattle University, Seattle, WA
J.S. HALL, L.A. RILEY
Lowell Observatory, Flagstaff, AZ

ABSTRACT

The optical, physical and chemical characteristics of light absorbing aerosol particles are investigated and the results for several urban and rural locations are compared. In addition, a simple technique for measuring the absorption coefficient of an aerosol is discussed and calibration results are shown. The results indicate that: (1) The average values of the single particle scattering albedos range from 0.5 to 0.7 for urban areas and 0.8 to 0.95 for rural areas, (2) with the exception of samples from Barbados, B.W.I. absorption was wavelength independent for all sampling locations, (3) particles of diameter less than 2.5 μm dominated absorption at all sites where the aerosol was size fractinated and (4) solvent washes of nuclepore filters containing aerosol removed most of the aerosol mass but essentially none of the gray absorbing material indicating it is probably a graphite like material(e.g. soot).

INTRODUCTION

Of the aerosol optical properties useful in modeling effects on climate and weather, least is known about light absorption. Distributed in the ambient air, absorbing particles heat the atmosphere, cool the surface and reduce optical transparency.

An aerosol absorbing quality is described by an absorption coefficient, b_{ap}, or an imaginary part of a complex refractive index, κ. b_{ap} is a property of the system of particles in air that describes absorption of optical radiation passing through the system. κ is a property of the bulk material composition of the particles. Optical effects are due to b_{ap}. However, κ can be used to calculate b_{ap} if the size distribution is known and the particles are assumed to be spherical.

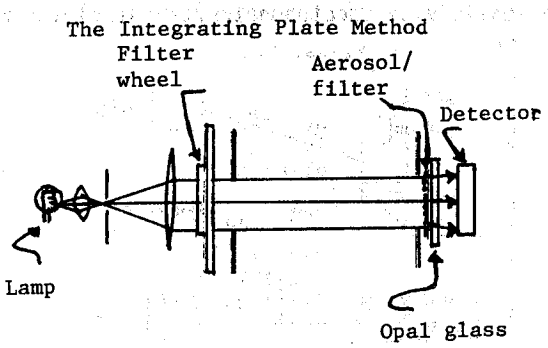

Fig. 1. The optical system of the Integrating Plate Method.

We have developed a simple technique to directly measure the absorption coefficient of an aerosol that is independent of assumptions about the physical properties of the aerosol particles (e.g. size, shape, refractive index). Named the Integrating Plate Method (I.P.M.), the technique is based on comparing the transparency of a nuclepore filter containing a small amount of aerosol with that of a clean filter. The original paper describing the method reported its accuracy to be within a factor of two[1]; testing included in this report suggest that accuracies are much better.

Utilizing the I.P.M., three areas of research regarding the optical and physical properties of ambient absorbing aerosols are described in this report: (1) laboratory and field experiments checking the accuracy of the I.P.M. for measuring light absorption extinction coefficients, (2) absorption data from several urban and rural locations comparing $1-\omega$; $b_{ap}(\lambda)$; b_{ap}/ρ; κ and b_{ap} vs. size (above and below 2.5 μm) and (3) results of chemical stripping technique indicating that for all but one sampling location the ambient light absorbing material collected is resistant to solution when washed with several solvents and acids; a characteristic of graphitic or amorphous carbon.

Tests of the Integrating Plate Method

A. Laboratory Test

The method was originally tested by comparing calculated and measured absorption coefficients of a dyed lacquer aerosol. The absorption properties of the dyed lacquer were determined from transmission measurements of carefully prepared thin films of the material. There are several disadvantages to this approach: (1) thin, uniform

layers of known thickness are difficult to prepare, (2) the aerosol must be accurately sized from scanning electron micrographs and (3) the shape of the lacquer particles are highly irregular but must be approximated as spheres for Mie calculations. Uncertainties in the calibration method limited confidence in the accuracy of the I.P.M. to within a factor of two.

These disadvantages can be largely eliminated if colored, monodispersed particles, large enough to be opaque are used for comparison of calculated and measured b_{ap} values. The absorption cross

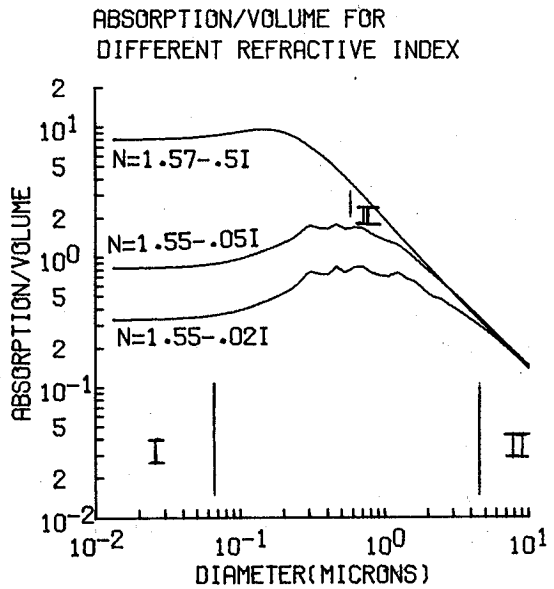

Fig. 2. Mie calculations of absorption cross sections per unit volume. Particles in region I absorb proportionally to their volume whereas those in region II absorb proportionally to their cross sectional area.

section is independent of refractive index for these particles (non-metallic) and depends only on the geometric cross section (figure 2). One micron or larger particles of moderate to high absorbing materials (e.g. $\kappa \gtrsim .1$) are essentially opaque so only the size and concentration (or mass) are needed to calculate the absorption cross section.

Monodispersed aerosols of Methylene Blue were prepared with a Berglund-Liu vibrating orifice aerosol generator and collected on nuclepore filters. A scanning electron microscope was used to determine the size of the particles; filters were weighed with a model 4700 Cahn electrobalance. For the range of particle sizes (D_p = .8 to 2μm), measured absorption is within 10 percent of the calculated value (figure 3). The experimental error is estimated to be on the order of 10 percent.

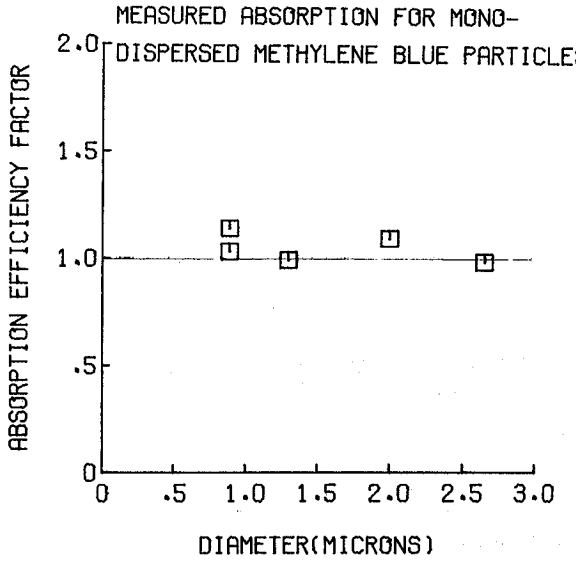

Fig. 3. Measured absorption efficiency factors for monodispersed Methylene Blue particles using the Integrating Plate Method. The absorption efficiency factor should be approximately equal to 1 for opaque non-metallic particles.

B. Field Test

In November, 1974 and November, 1977, the University of Washington and Lowell Observatory (Hall & Riley) cooperated in field experiments to compare horizontal extinction as measured by high sensitivity, long path transphotometry with that measured from combined absorption and scattering measurements. The earlier experiment was done on a plateau outside of Flagstaff, Arizona where aerosol absorption was thought to be less than 10 percent of extinction; the latter at Phoenix, Arizona where absorption is generally greater than 30 percent of extinction.

The total extinction coefficient, b_{ext}, was measured by the Lowell Observatory using long path, high sensitivity spectrophotometry at eleven wave-

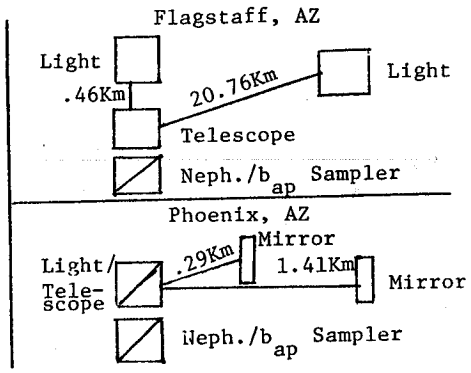

Fig. 4. Experimental set-up for extinction comparison measurements at sites (1) near Flagstaff, AZ (6Nov74) and (2) Phoenix, AZ (23 Nov77).

length bands from .3225μm to .665μm[2]. The scattering coefficient was determined with a 3-wavelength integrating nephelometer[3] at Flagstaff (λ=.45μm, .55μm, .65μm) and two single wavelength nephelometers at Phoenix (λ=.45μm, .5μm). Absorption was measured using the I.P.M. At Phoenix, mirrors were used to fold the optical path of the transphotometer (see figure 4).

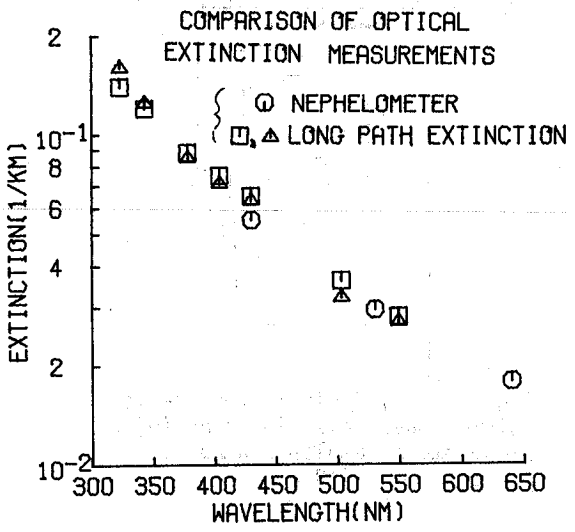

Fig. 5(a). Measurements of $b_{ext}(\lambda)$ by long path extinction and by nephelometer. Data taken near Flagstaff, AZ on 6 Nov 74.

The results for two nights are shown in figure 5. The aerosol extinction at Flagstaff was dominated by scattering and good agreement exists between the transphotometer and the nephelometer. The absorption to extinction ratio was on the order of 5 percent. However at Phoenix, absorption was generally 35 to 45 percent of aerosol extinction. The results for the evening of November 23 are shown as time plots of the three extinction coefficients. The sum of absorption and scattering coefficients agree with total extinction for measurement periods when the air was spatially homogeneous. During the period from 0215 to 0245 the wind was changing direction and the air was not spatially uniform; cleaner air was moving through the transmissometer path before reaching the nephelometer - a disadvantage of comparing point and line measurements. The good agreement suggest the I.P.M. as a useful and accurate technique for measuring absorption extinction coefficients.

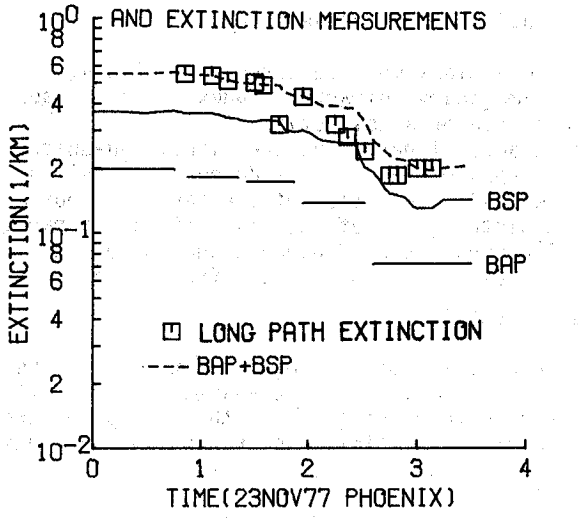

Fig. 5(b). Comparison of b_{ext} measured by long path extinction and $b_{ext} = b_{sp} + b_{ap}$ as measured with a nephelometer (b_{sp}) and the I.P.M. (b_{ap}). Data was taken at Phoenix, AZ., 23 Nov., 1977, λ=.55μm.

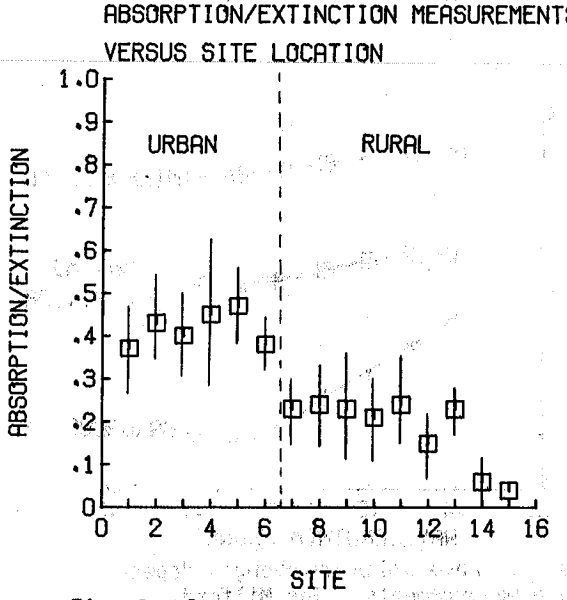

Fig. 6. $1-\omega_o$ averages for several locations (below). The bars represent the range of values.

1. Industrial Seattle, WA.
2. Downtown Portland, OR.
3. Industrial St. Louis, MO.
4. Denver, CO. (fairgrounds)
5. Denver, CO. (trout farm).
6. Central Phoenix, AZ.
7. Residential Seattle, WA.
8. Residential St. Louis, MO
9. Tyson, MO. (1973)
10. Tyson, MO. (1975)
11. Milford, MI.
12. Hall Mt., AR.
13. Puget Island, WA.
14. Flagstaff, AZ.
15. Mauna Loa Observatory, HI

Absorption Data

The sources of absorbing materials in the ambient air have not been specifically identified but are suspected to be primarily urban effluents. If true, then urban and rural aerosols are likely to have dissimilar optical characteristics. Absorption and related properties for several urban and rural locations are compared below.

A. $1-\omega_o$

The sites are arranged on the abscissa of figure 6 so that interurban sites or sites strongly affected by industrial plumes are on the left and residential, rural and remote areas are on the right. Average values for the urban/industrial areas range from 0.36 to 0.47 compared with 0.07 to 0.26 for the residential/rural areas.

B. b_{ap} vs. λ

The absorption wavelength responses (λ=.3μm to .7μm) for all the sites listed in figure 6 are essentially gray. Characterisitic examples from four sites are shown in figure 7. Also shown in figure 7 is a characterisitic wavelength response of filter samples from Barbados, B.W.I. indicating strong blue absorption. The Barbados aerosol is suspected of being Saharan dust from long distance transport. The wavelength dependence is similar to that measured from flux divergence and satellite measurements[4].

CHARACTERISTIC ABSORPTION WAVELENGTH DEPENDENCE MEASUREMENTS

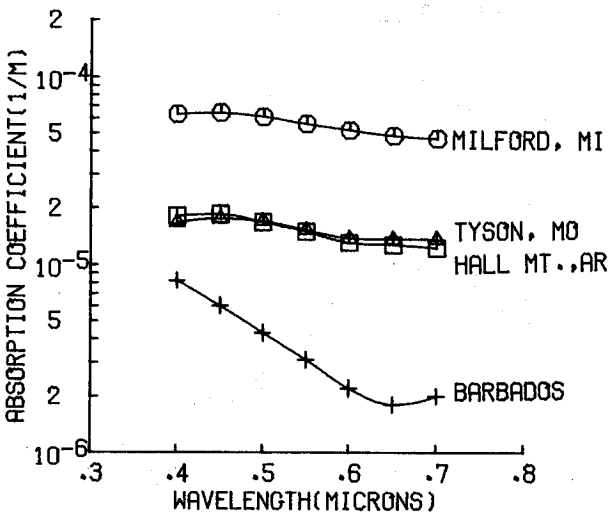

Fig. 7. Absorption wavelength dependence measurements. The Milford, Tyson and Hall Mt. curves are typical of the sites listed in fig. 6. The strong wavelength dependence curve is characteristic of all the Barbados samples.

C. b_{ap} vs. Size and ρ

Suspensions of particles in the atmosphere comprise a broad range of sizes from molecular clusters on the order of .001μm to dust particles of 100μm or larger. Due to production mechanisms, coagulative and settling processes, particle mass tends to accumulate in two modes: above and below diameters of about 2μm[5] (figure 8). Because the sources and production mechanisms of the two modes are different, the chemistry and optical constants are likely different.

The two modes were separated with a dichotomous sampler[6] and collected separately on filters. The absorption coefficients of the two modes were then measured. The absorption coefficient for the large particles was corrected for fine particles on the filter.

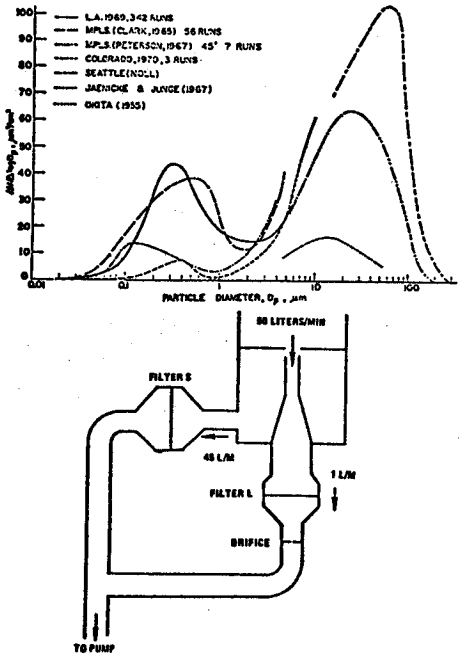

Fig. 8. (a) Typical atmospheric volume (mass) distributions (b) a dichotomous sampler schematic. source: Higy (1972).

At all the sites, urban and rural, absorption is dominated by the fine particles (<2.5μm); values of the ratio of fine to coarse particle absorption varied from four to fifty. The fine particles are generall ten times more effective as absorbers on a per unit mass basis. However, the data is not sufficient to say that the absorbing material is primarily in the fine fraction since small particles are more efficient absorbers on a per mass basis.

D. Imaginary Refractive Index

Precautions must be taken in assigning a single imaginary refractive index, κ, to an aerosol particle or a collection of particles: (1) ambient aerosol particles are highly non-uniform and the apparent value of κ depends not only on the chemical composition of the particles but also on the distribution of material within the particle (2)κ may be size dependent due to source differences associated with the different particle size classes.[6]

An estimate of the lower limit of κ can be made using the I.P.M. if we assume (1) the particles are uniform and (2) that the absorption cross section of the particles is proportional to their volume (or mass). Then,

$$\sigma_{ap}(r) \propto \kappa M_p(r) \quad (1)$$

$$b_{ap} = \int \sigma_{ap}(r) M(r)/M_p(r) dr \quad (2)$$

$$b_{ap} \propto \kappa \int M(r) dr = \kappa M_{tot} \quad (3)$$

The second criterion suggest that the particles must be small. Consequently these calculations were done only on the less than 2.5 μm size fraction.

Imaginary refractive indices for the fine particle fractions are shown in figure 9. Values range from .05 to .09 for the urban areas and .002 and .05 for the others. If graphite were the absorbing material, this would imply mass fractions up to about 20 percent.

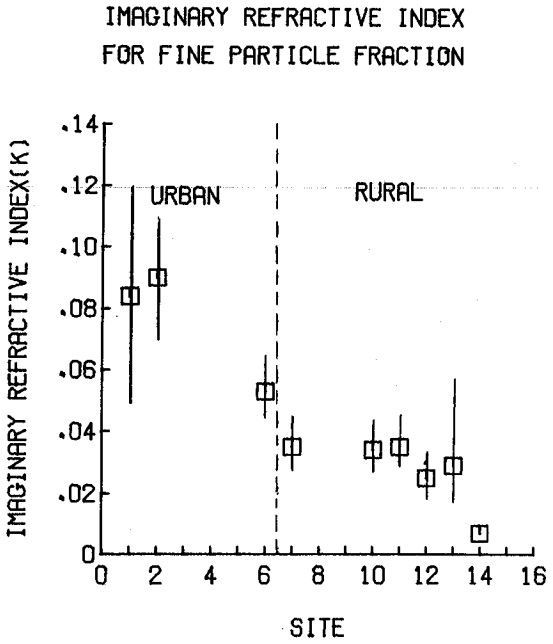

Fig. 9. Calculated, average imaginary refractive indices (λ=.55μm) for fine particles (<2.5 μm) at the sites listed in fig. 6. At sites 3,4,5,8, 9 and 15 there was no dichotomous sampler for size fractionating the particles.

Chemical Composition of the Absorbing Material

We have developed a technique to determine the resistance of the absorbing species collected on nuclepore filters to various solvents and acids. Solutions of H_2O, dilute and concentrated HCL, HF and Aqua Regia (3 parts HCL and 1 part HNO_3) were aspirated sequentially through the sample filters; differential mass and absorption measurements were taken after each elution step. The pretreated filters were analyzed for elemental concentration by x-ray florescence; effluents after each treatment were saved for future ion analysis. Scanning electron microscope photographs taken before and after treatments indicated that the particles on the filters were not severely altered by the stripping procedure.

The results of differential mass and absorption measurements are shown in figure 10. For all the samples that were gray absorbers little change in absorption occurred though from 49 to 96 percent of the mass was removed from the filters. The absorbing material was removed from the Barbados sample (not a gray absorber) which appeared to be a soil derivative material.

Graphitic or amorphous carbon is the most likely material to be gray, resistant to these solvents and a ubiquitous aerosol component.

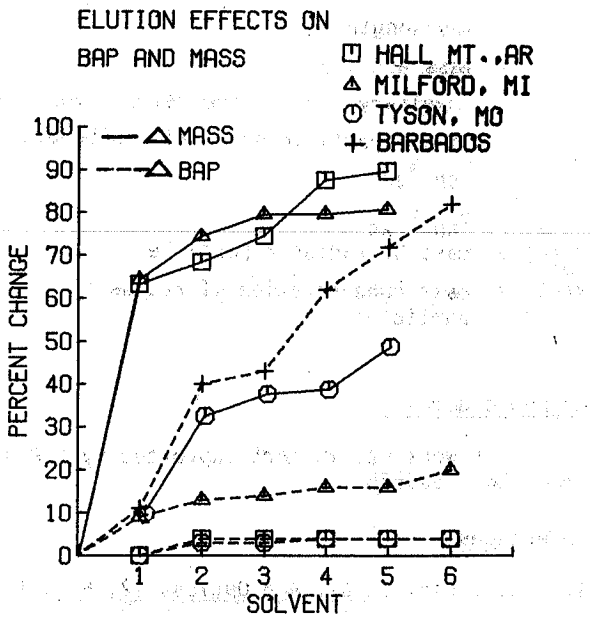

Fig. 10. Shows the effectiveness of the solvent washes (abscissa) on removing both the mass and the absorbing material from typical urban and rural samples. The absorbing material on the Barbados sample (the only non-gray absorber) was effectively removed by the washes.

Conclusions

A. The I.P.M. is accurate to much better than a factor of two. It provides a technically simple, inexpensive method for determining the aerosol absorption coefficient.

B. Absorption is usually a significant fraction of optical extinction by aerosols; particularly in urban-industrial areas where it generally exceeds 30 percent.

C. Particles less than 2.5 μm in diameter dominate absorption except during periods when the large particle mass fraction is many times that of the fine fraction (e.g. dust storms).

D. Graphitic or amorphous carbon is probably the gray absorbing material that controls absorption at U.S. urban and rural locations.

Definitions

b_{ext} ≡ aerosol extinction coefficient

b_{sp} ≡ aerosol scattering coefficient

b_{ap} ≡ aerosol absorption coefficient

σ_{ap} ≡ absorption cross section

λ ≡ wavelength

ρ ≡ mass density

κ ≡ imaginary part of the refractive index

ω_o ≡ single particle scattering albedo, b_{sp}/b_{ext}

$1-\omega_o$ ≡ b_{ap}/b_{ext}

$M_p(r)$ ≡ mass of radius r particle

$M(r)$ ≡ mass concentration of radius r particles

Acknowledgements

This work was in part supported by E.P.A. Grant No. R800665.

References

1. C.I. Lin, et al. App Optics, 12, 6 (1973).

2. J.S. Hall, and L.A. Riley, Progress in Astronautics and Aeronautics, 49 (1976)

3. A.P. Waggoner, N.C. Ahlquist, R.J. Charlson, Proc. of: Atmospheric Aerosols: Their Optical Properties and Effects, NASA CP-2004 (1976).

4. T.N. Carlson, and R.S. Caverly, Journal of Geophysical Research, 82, 21, (1977).

5. Hidy, Aerosol and Atmospheric Chemistry, Academic Press (1972).

6. F.S. Goulding, J.M. Jaklevic and B.W. Loo EPA Environmental Protection Technology Series, EPA-650/2-75-048 (1975).

EFFECT OF CARBONACEOUS PARTICLES ON VISIBILITY

Thomas A. Cahill
Department of Physics and Crocker Nuclear Lab
University of California, Davis, CA. 95616

ABSTRACT

Investigations made of factors statistically associated with visibility reduction in four California cities included a short study of the role of fine (<0.6 micron) carbonaceous particles during one summer month in the Los Angeles air basin. Visibility degradation at this site, Los Alamitos, was dominated by intermediate size (0.6 to 3.6 micron) sulfur containing particles, and gaseous NO_2, while negligible improvement in fit resulted through addition of fine carbonaceous particles. However, negligible improvement in fit was also exhibited by fine sulfur containing particles. Intermediate size carbonaceous particles were not studied.

INTRODUCTION

In an effort to establish the sources of visibility impairment in California, long term studies have been initiated in the statistical associations between visibility reduction and atmospheric conditions. The morphological and chemical complexity of the atmosphere especially under the highly photochemical conditions common during summer months demands an approach that does not prejudge the factors that may be influential at any given time and place. The method of multiple regressions can provide a method that is able to encompass the large data sets that are generated in such studies. The data set consists of weather data (usually from NOAA and originating at airports) and pollutant data (originating from air monitoring stations run by either local districts of the California Air Resources Board). The effort is based upon the changes in visibility that occur under synoptic weather changes, which have a typical time period of 5 to 7 days, and thus must last many such periods in order to have statistical weight. Long study durations are also demanded by the magnitude of the data sets, as the initial set normally included 8 weather variables, 8 gas pollutants, and about 50 elemental values on particulates in three size ranges (20 to 3.6, 3.6 to 0.6 , 0.6 to 0 microns). Thus, at least 67 24 hour periods are required in the dependent variable, visibility, which was also derived from airport values and averaged over each day. For these reasons, 90 day periods were chosen, coinciding with the summer (July, August, and September) and winter (January, February, and March) quarters.1)

STATISTICAL METHODOLOGY

The data sets were first examined via bivariate correlations in order to strip out strongly correlated variables. An example would be soil-derived particles, which at most locations, included Al, Si, K, Ca, Ti, Mn, and Fe containing particles in large size ranges.2) Another involves all the oxides of nitrogen. Initial tests also showed that any influence that the largest particles had on visibility was also mirrored in the intermediate sized particles, 0.6 to 3.6 microns, and thus large particle data could be omitted from the search. In these cases, one parameter was retained, such as Si for soils and NO_2 for the oxides of nitrogen.

The remaining parameters were used in the multiple regression fit via the physically reasonable equation,

$$b_{scatt} = A\,(P_1)^{b_1}\,(P_2)^{b_2}\ldots\,(P_n)^{b_n} + E\ ,$$

in which P_1, P_2, ... P_n are values of the parameters (weather and pollutant), and A, b_1, b_2,... b_n, and E are constants that are fixed by the fit to the 90 days of visibility data, 3).

RESULTS

In the initial study, four sites were included for summer, 1973: Los Angeles, Los Alamitos, Bakersfield, and Oakland, representing three major atmospheric regimes in California. The fit to the visibility data varied from site to site, but generally it was good, with multiple R^2 values running from 0.63 (Oakland) to 0.85 (Los Alamitos) (Figure 1). The significant beta coefficients were limited to only 15 of the parameters, and at each site only a few parameters dominated the fit to the visibility data. At this point, one has to reiterate the caution that association does not prove causality, although lack of association can deny a direct causal relationship. Results are shown in Table 1.

Table 1
All Significant Beta Coefficients

Parameter	Sources	Los Alamitos	Los Angeles
Sodium (2)	Sea Salt	-0.189	-0.172
Silicon(2)	Soils	none	+0.201
Sulfur (2)	Fuels	+0.386	+0.283
Lead (2)	Autos	none	none
Sulfur (3)	Fuels	none	none
Lead (3)	Autos	none	-0.369
Humidity		+0.644	+0.624
Temperature		+0.198	none
Oxidant		+0.240	none

Table 1
(con't)

NO_2	+0.296	+0.282
SO_2	+0.233	not measured
Multiple R^2 fit	+0.848	+0.730

(2) particles 0.6 to 3.6 microns diam.
(3) particles less than 0.6 microns
\+ parameter assoc. with visibility loss

Some of the effects seen are a result of wind direction (i.e. sea salt on brisk ocean breezes, fine lead at Los Angeles), but the correlation with intermediate size sulfur particles occurred at all sites and no correlation was ever seen with fine sulfur particles. The elements H, C, and O were also studied at the Los Alamitos site, and negligible improvement in the fit and poor qualitative fit with visibility showed that it was not important. Unlike the sulfate fraction, the fine carbonaceous fraction appears to be relatively non-hygroscopic and possessed median diameters much smaller than the wavelength of light, hence limiting its influence on visibility. Carbon was not studied in the intermediate size range that had the most correlation with visibility, and so some correlation with carbon is possible.

Figure 1

Fit to Visibility at Los Alamitos

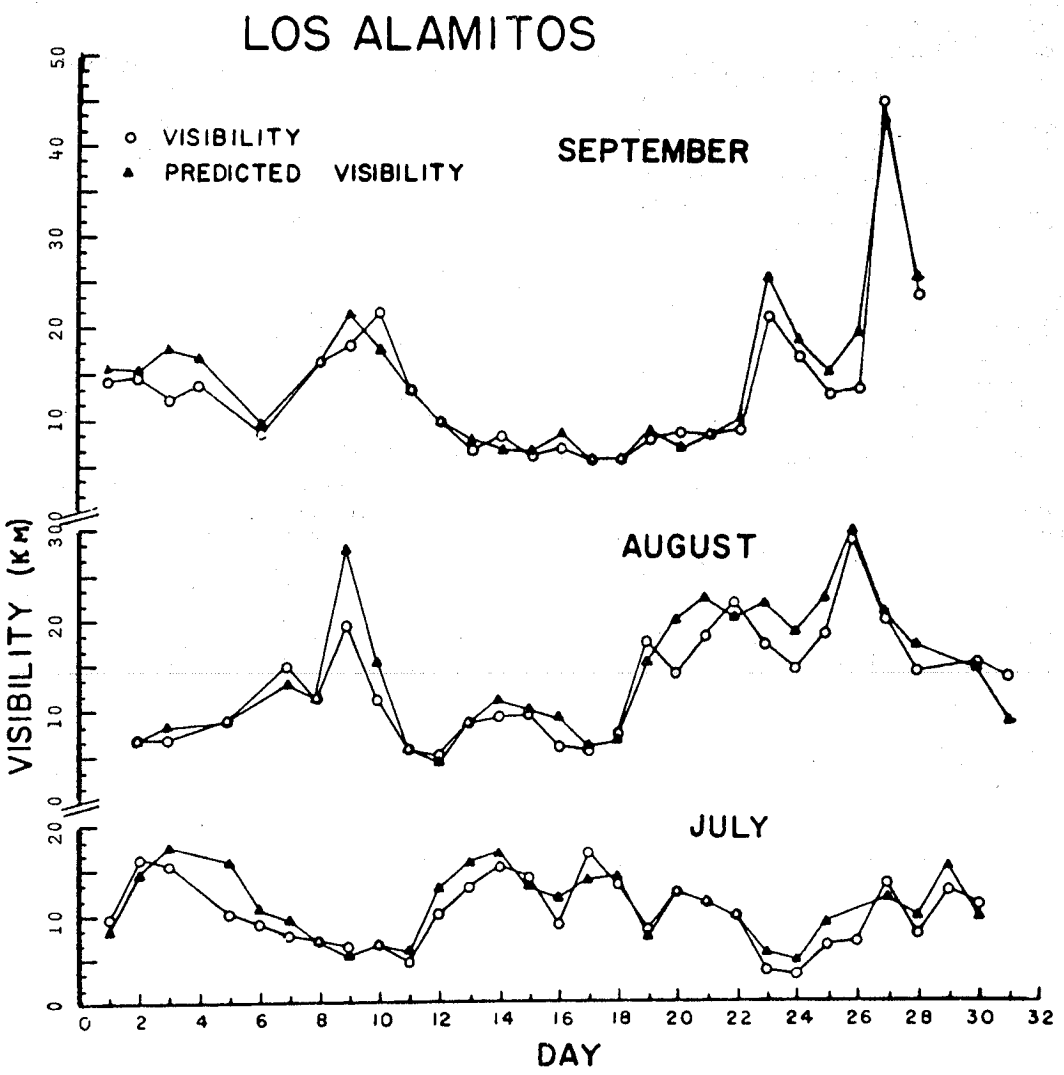

REFERENCES

1. Flocchini et al., "Monitoring California's Aerosols by Size and Elemental Composition", Envir. Sci. and Techn. 10, 76 (1976)

2. Cahill et al., "Statistical Techniques for Handling PIXE Data", Nucl. Instr. and Methods 142, 259 (1977)

3. Barone et al., "A Multivariate Statistical Analysis of Visibility at Four California Cities", Atm. Environment (in press)

Measurement of Light Absorbing Aerosols from Combustion Sources

James L. Nolan
Rhode Island Department of Health
Providence, Rhode Island

ABSTRACT

The absorption coefficients of the exhaust gas streams from a forest slash burn, a coal fired boiler, an oil fired home heating furnace and a natural gas fired home heating furnace were measured by diluting the samples dynamically and analyzing the filters via the Integrating Plate Method. Using a simple inversion technique, the average imaginary index of refraction was then calculated for each source. The results indicated that the forest fire and the coal boiler were not appreciable sources of highly absorbing aerosol. Since the calculated imaginary index of refraction of both the fuel oil and natural gas furnaces were comparable to the value reported for carbon, the particulate emissions from these sources were concluded to be comprised primarily of carbonaceous soot. Finally, an attempt was made to estimate emission rates of soot from these sources.

INTRODUCTION

It has been known for many years that black particles known as soot are commonly found in filtered samples of polluted air. In fact, a number of measurement techniques are based on the principle that such particles absorb visible light[1]. These techniques consist of measuring either the change of reflectance or transmittance of a filter after a known amount of air has been sampled.

This study was designed to identify some of the sources of these soot particles by measuring the absorption coefficient in the exhuast gas stream of various combustion sources.

The sources chosen to be tested included a coal fired boiler, a laboratory burn of forest slash material, an oil fired home heating furnace and a natural gas fired home heating furnace.

Since carbonaceous soot is believed to result from pyrolitic reactions of unburned fuel vapors in the exhaust streams of combustion sources, the samples were diluted with filtered ambient air to assure that all particles were condensed prior to collection on a nuclepore filter. To accomplish this, a stack sampling probe was designed which dynamically mixed the sample gas with filtered air at a known dilution ratio to simulate conditions that would exist just as the gas was released into the air. A portion of the diluted sample was then drawn through a nuclepore filter and the absorption coefficient was measured using the Integrating Plate Method developed by Lin[2]. The average imaginary index of refraction was then calculated using an inversion technique suggested by Lin.

Sampling Probe

The dilution probe designed by Mehra[3] is depicted in Figure 1. It was constructed from aluminum irrigation conduit, reinforced wire mesh screen covered with cotton cloth, aluminum end plates and a high volume air sampler. According to the original design, the incoming air would be filtered by a glass fiber filter on the high vol head and the cotton cloth on the inner screen would maintain a pressure drop across the screen to assure that particles would remain in the inner tube. During the initial tests of this probe it was found that there was significant particle deposition on the cotton cloth, indicating that the desired pressure drop was not being maintained. To alleviate this problem, the high vol head was removed from the probe and the wire mesh inner screen was covered with glass fiber filter paper rather than cotton cloth. Further tests showed that the pressure drop with the new design was adequate to eliminate particle deposition on the screen and still maintain the flexibility to throttle the dilution air through the port left by the removal of the high vol head.

While the total flow through the system was constant, the flow across the orifice was a function of the chosen dilution ratio. Sampling probes were chosen for each source so the flow across the orifice would be within 10 percent of isokinetic, therefore the size of the probe was a function of the exhaust gas flow rate and the dilution ratio. A single size sampling thimble was used to take the grab sample from the chamber prior to the high vol blower since the flow through this region was independent of the source sampled.

Integrating Plate Method

This technique developed by Lin[2] required that the particles be concentrated on a filter, thus increasing the measured extinction and removing the effect of all the scattered light, so that the measured extinction is due solely to absorption. As shown in Figure 2, the clean nuclepore filters are zeroed and then read again after particles have collected on them. The amount of light absorbed by the particles on the filter is measured and the absorption coefficient can be calculated using the Beer-Lambert relationship:

$$I/I_o = \exp(-bap\ x) \qquad (1)$$

where x = the length of the air column drawn through the filter (m)

I_o = the intensity of light transmitted through the clean filter

I = the intensity of light transmitted through the filter with particles on it.

bap = the absorption coefficient (m^{-1})

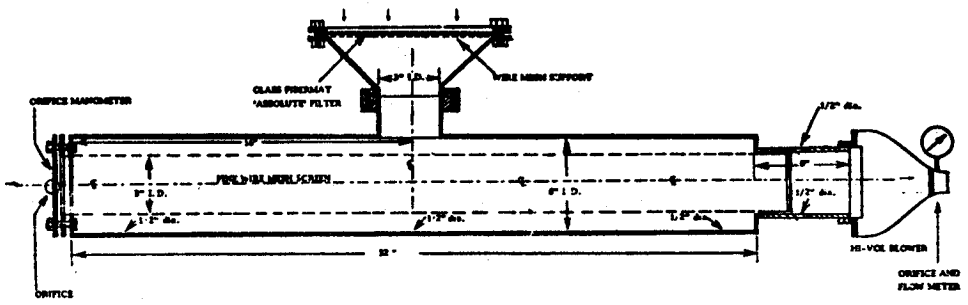

Figure 1. Diluting probe. Material of construction is aluminum.

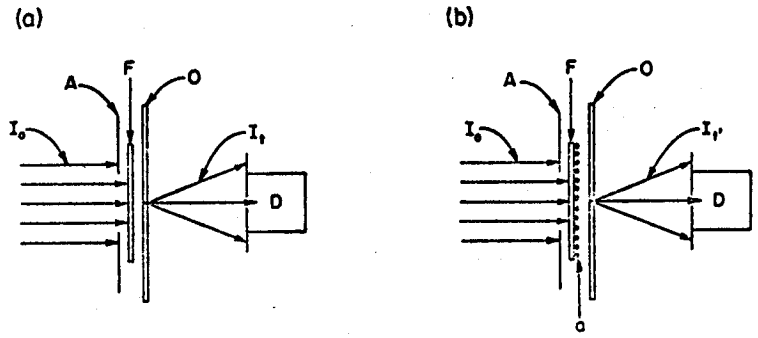

Figure 2. (app.) The experimental arrangement used in the opal glass method: (a) filter without aerosol, (b) filter with aerosol.

The absorption coefficient is a function of the shape of the particles, the size of the particles, the mass concentration of particles, the imaginary part of the complex index of refraction and the wavelength of light. For spherical submicron, homogeneous particles Lin[2] suggested the following inversion was good to within a factor of 2:

$$n_2 = \frac{bap \lambda V \bar{P}}{4 \pi m} \quad (2)$$

where: n_2 = imaginary part of the complex index of refraction ($n_1 - \ell n_2$)

V = volume of air sampled (m^3)

bap = absorption coefficient (m^{-1})

λ = wavelength of light (m)

$\bar{P}$ = density of particles (g/m^3)

m = mass of particles collected (g)

Source Characteristics

Coal Fired Boiler This boiler was a Riley Stoker Company unit rated at 45,000 kg steam/hr at maximum continuous load. It burned pulverized coal through horizontal flare-type forced draft burners and was equipped with both a multiclone collector and an electrostatic precipitator. Throughout the test period this unit burned low sulfur (0.6%) Utah coal with a gross heating value of 12,847 Btu/lb, an ash content of approximately 10% and equal amounts of volatile and fixed carbon. During the sampling the boiler was operated in a steady state mode at approximately 50% capacity.

Slash Burn Apparatus

The laboratory burning facility of the Forestry Department of the University of Washington was used to simulate a burn of Ponderosa Pine slash. This fuel was collected from a selectively logged area near Cle Elum, Washington. The procedure was to cut an area of the forest floor material and place it in a wire basket under a large hood in the laboratory. The bed was lit from one end and flamed vigorously until the entire bed was ignited; the flaming then stopped and the bed continued to smolder. One sample was taken during the flaming and the rest were taken during the smoldering.

Oil and Natural Gas Furnaces

The residential oil furnace was a forced hot air type, approximately 15 years old. The burner was an atmospheric pressure, conventional head type of one gallon per hour capacity, which had been serviced just prior to the test. The natural gas furnace was a forced hot air unit approximately ten years old. It had a capacity of 200 cubic feet per hour of gas and was equipped with a conventional head, atmospheric pressure burner and a primary air control orifice. This burner had also just been serviced prior to the test. The procedure for sampling both furnaces was the same; the first filter was taken during coldstart and the subsequent filters reflected steady state operation.

Discussion

A summary of the results from the four sources is contained in Table I. As noted previously, the coal boiler was tested while operating in steady state and the low error bars reflect this fact. The slash burn, distillate oil and natural gas were sampled from start-up through steady state. The start-up filters contained much more soot as could be expected, and caused large errors in the mean bap and n_2. When the steady state results alone are considered the error is decreased dramatically.

The n_2 of 0.02 for the coal fly ash shows good agreement with the value of 0.01 reported by Twitty and Weinmann[4] and indicates that coal fly ash does not contain an appreciable amount of soot. This result is also in good agreement with the findings of Fisher, et al[5], that the vast majority of such particles are aluminosilicates and that carbonoceus particles represent a very small percentage.

The mean of all the slash burn samples was roughly the same as the coal, but the filters were not as consistant. The start-up filter contained an appreciable amount of soot but the subsequent smoldering filters contained little if any soot. The mean n_2 of 0.009 for all the samples, however is probably representative of a forest fire since it contains both flaming and smoldering particulate.

Both the distillate oil and natural gas samples were composed of highly absorbing aerosol since the mean n_2 for each was on the order of 0.45. This is in good agreement with the value of 0.66 reported for the graphite[6]. The steady state values are reported in the table to show the smaller error bars for those samples. Again the start-up filter for each contained much more mass than the steady state filters, but it is assumed that the mass on all the filters is predominantly carbonaceous soot. It is interesting to note that the absorption coefficients for both sources are so similar.

The gas furnace was 45 percent larger than the oil so this might account for some of it; but even if the bap was normalized for heat release the oil furnace put out only 3.5 times the soot emitted from the gas furnace. This initially was a surprise but a check of the EPA emission factors for such sources[7] showed that oil furnaces put out approximately 4.5 times the soot emitted from natural gas, therefore, these numbers are quite consistent.

Conclusions

As a result of this study it is possible to conclude that sources such as forest fires, wood and leaf burning and coal fired boilers are not significant producers of carbonaceous soot. However, the aerosols from such sources can absorb an appreciable amount of light when found in high concentrations. Conversely, fuel oil and gas fired furnaces are sources of graphitic soot and have the same order of magnitude emission rate. Assuming that the particulate emissions from such sources is almost all soot, the EPA emission factors in Table II might be a good approximation of the soot emission rates from these sources.

TABLE 1.

Absorption Coefficients at 530 nm Wavelength

Source	b_{ap} (m^{-1})	$\bar{P}$ ($\frac{g}{cm^3}$)	% Attenuation ($g/10^6$Btu)	n_2
coal boiler	$4X10^{-2}\pm3.6X10^{-2}$	1.5	0.26	0.02 ± 0.01
slash burn	$4X10^{-2}\pm1.6X10^{-1}$	1.3	0.27	0.009 ± 0.04
(w/o start-up)	$4X10^{-3}\pm4X.10^{-3}$	1.3	0.08	0.0004 ± 0.0002
distillate oil	$7X10^{-3}\pm6X10^{-3}$	2.5	3.33	0.45 ± 0.27
(w/o start-up)	$5X10^{-3}\pm4X10^{-4}$	2.5	3.5	0.39 ± 0.11
natural gas	$3X10^{-3}\pm5.2X10^{-3}$	2.5	3.44	0.45 ± 0.68
(w/o start-up)	$2X10^{-3}\pm8X10^{-4}$	2.5	2.8	0.30 ± 0.11

all values reported to the 2σ level

TABLE 2.

ENVIRONMENTAL PROTECTION AGENCY PARTICULATE EMISSION FACTORS

Source	Emission Rate ($g/10^6$Btu)
distillate oil	33
natural gas and propane	7
residual oil	76

Acknowledgements

This work was sponsored by a fellowship grant from the United States Environmental Protection Agency. I wish to thank Bob Charlson for his enthusiasm and his advice on this project. I would also like to thank Ray Weiss for helping with the Integrating Plate Method and the very helpful discussions on the physics of absorption.

References

1. Waller, R.E., "Experiments on the Calibration of Smoke Filters", Journal of the Air Pollution Control Association, 14(8):323 (August 1964).

2. Lin, C., Baka, M., Charlson, R.J., "Absorption Coefficient of Atmospheric Aerosol: a Method for Measurement", Applied Optics, 12:1356 (June 1973).

3. Mahra, V.S. "Design, Construction and testing of a probe for Source Sampling", MSE Thesis, University of Washington, 1968

4. Twitty, J. T., and Weinman, J. A., "Radiative Properties of Carbonaceous Aerosols", J. Appl., Met., 10:725-731 (1971)

5. Fisher, GL, Chrisp, C.E., Hayes, T.L., "Carbonaceous Particles in Coal Fly Ash", Proceedings of Conference on Carbonaceous Particles in the Atmosphere, Berkeley, California, (March 20-22, 1978)

6. Handbook of Chemistry and Physics, Chemical Rubber Co., 45th Edition, 1964

7. Compilation of Air Pollutant Emissions Factors (AP-42), United States Environmental Protection Agency, Office of the Air Quality Planning and Standards, Research Triangle Park, North Carolina (1976)

SPECTROPHOTOMETRIC MEASUREMENTS OF EXTINCTION

J. S. Hall and L. A. Riley
Lowell Observatory
Flagstaff, Arizona

ABSTRACT

Nighttime extinction measures made with a transmissometer and interference filters over the spectral range of 0.32 to 0.66 μm at ten carefully selected sites are discussed in this report. The main purpose of the program was to obtain absolute and objective baseline data which can be used at some future time for comparison. Data obtained at nine of the ten sites believed to be generally outside the normal air flow patterns from industrial and smog-producing areas have air of very high quality, with aerosol extinction in the visual region of the spectrum of less than a factor of two or three times Rayleigh extinction alone. Several different procedures tried in an effort to make accurate extinction measures in full sunlight are described.

BACKGROUND

We have been using astronomical photometric techniques since 1971 to determine atmospheric extinction (the total loss of transparency caused by absorption and scattering by both aerosols and gases) over horizontal paths of from one to twenty kilometers and in at least nine wavelength bands within the spectral domain bounded by ozone and water vapor absorption (0.32 to 0.66 μm).

We have had three objectives in mind: 1) to determine very accurate extinction coefficients at Flagstaff, Arizona, and in other areas of different elevation in the United States where clear air is most likely to be found, in order to establish baseline data so that a future possible influx of man-made pollutants can be monitored quantitatively; 2) to find a simple means of making accurate measurements of both background intensity and extinction in full daylight for the purpose of determining reliable and objective values of visibility; and 3) to determine, if possible, the nature of the aerosols responsible for the extinction observed in each environmental situation. We believe that a good way to do this is to start from very clear air and learn what happens whenever a known aerosol is introduced by man or nature.

The only comparable spectrophotometric data which we have found are those obtained in Pasadena by Baum and Dunkelman[1] and near Chesapeake Bay by Knestrick *et al.*[2] These data were used extensively by Elterman[3] in compiling his tables of "representative" aerosol extinction for different wavelengths at low elevations. For higher elevations, the tabular values are derived by combining these data with observations made in the upper air by a variety of techniques. The data presented here include some of that previously published by the authors.[4,5]

APPARATUS AND METHODS

The data presented here have all been obtained at night using a very carefully regulated quartz-halogen 45-W lamp powered by two 12-volt storage batteries. Immediately in front of the lamp is a thin 20-mm quartz disk, which has been ground on both sides to produce what is essentially an isotropic beam in the forward direction. The receiving equipment consists of a six-inch reflecting telescope, a set of narrow-band interference filters, an EMI 6526Q photomultiplier, high-voltage supply, and pulse-counting components. The data from the pulse counter can be stored and reduced on-line by a 9815-A Hewlett-Packard programmable calculator. Figure 1 is a schematic diagram of the observing equipment.

Early in the program we measured the same light source placed alternately at two different distances from the telescope. This procedure provides good absolute extinction data but requires a significant amount of time to move the source and an easily traversable terrain. More recently, in an effort to provide data of greater accuracy and to avoid physical limitations imposed by certain sites, we have attached the light source to the telescope and measured the energy reflected from two mirrors placed at widely separated distances. These mirrors must be optically flat, firmly mounted on a stable base, and aimed so that the reflected beam is precisely centered on the telescope. The aperture of the telescope accepts an isotropic beam reflected from an area on the flat mirror of half the diameter of the primary mirror of the telescope. The reflectivity of the two mirrors at the same distance was compared at regular intervals to an accuracy of one quarter of one percent using the same filters and light source as those used in the observing program. The ratio of their reflectivities is close to unity and varies very little when measured at monthly intervals.

The use of two mirrors rather than alternate locations of the light source proved to be advantageous at Mount Hopkins and near the center of Phoenix, where there were severe restraints on the choice of sites. At Bryce Canyon the light beam passed within a few feet of the ground and on one calm night jumped around to such a large extent due to rapid changes in refraction that the returning beam was not always centered on the telescope. Thereafter the configuration used at Bryce Canyon and elsewhere was selected on the basis of weather conditions and the nature of the terrain. At Lake Powell, Organ Pipe Cactus National Monument, and White Sands National Monument, the direct beam method gave excellent results because of the long path lengths (more than 4 km) and stable atmospheric conditions.

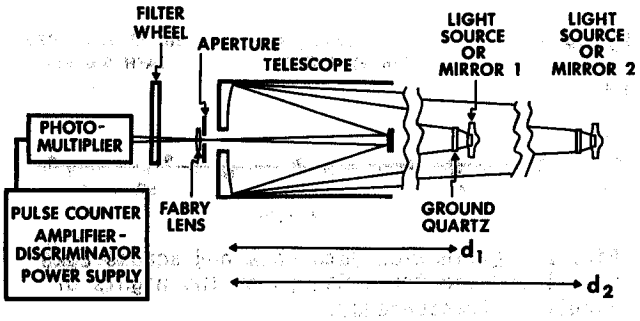

Fig. 1. Schematic diagram of our equipment, illustrating the two modes of observation. The same light source can be measured at two different positions, d_1 and d_2, or optical flats at d_1 and d_2 reflect the light source (attached to the telescope) at essentially normal incidence back to the photometer.

Since, in the absence of any extinction, the amount of light entering the telescope aperture varies as the square of its distance from the source, the pertinent distances must be accurately determined. A Wild theodolite and a good tape measure were used in measuring distances. These were measured to better than one part in 2000.

In order to present the data in an homogeneous and objective form, we have used a power relation of the form $y = ax^b$ to compute a curve representing a least-squares solution for each set. Except at the two ends of the spectral range, the output from the light source alone has shown a standard deviation of one-half percent at all wavelengths; at each end it has been about twice this value. In the field there are additional errors due to scintillation and short-term transparency changes during a run. Under good atmospheric conditions, the observed error in $\beta_p(km^{-1})$ is usually between 0.005 and 0.010. When least-square solution power curves are used to provide the value of $\beta_p(km^{-1})$ in the visual range, the error whould be about one-third these values, which is probably comparable to atmospheric fluctuations.

It is easy to convert the values of β_p in the graphs to the range of visibility. One will make only a very small error if the Rayleigh coefficient at 0.550 μm is assumed to be 0.012 km^{-1} at all elevations. The range of visibility for a two-percent threshold is simply 3.9 divided by $(\beta_p + 0.012)$. A value of $\beta_p(km^{-1})$ of 0.020 therefore corresponds to a visual range of visibility of 122 km; 0.050 would be 63 km.

We normally used a Gardner Small Particle Detector to measure the number of condensation nuclei per cubic centimeter. The size range of these particles is 0.001 to 0.1 μm, which is just below the size range causing visual extinction.

Experimental Daylight Observations

For three months in 1975 we collaborated with Drs. Kenneth O'Dell and William Malm of the Physics Department at Northern Arizona University to take advantage of their experience in laser technology.

With a helium-neon laser at a distance of 3 km and a narrow-band interference filter at 0.6328 μm, it was not difficult to produce intensities which greatly exceeded ambient daylight. Presumably because of the unstable image patterns which we always observed, we were not able to obtain consistent results.

We then decided that a mercury arc might be an ideal light source for daylight observations, as a low-pressure mercury arc provides several very narrow emission lines extending from the yellow to the ultraviolet. Many of these individual lines produced by a 100-watt arc have about a thousand times more power than the single wavelength produced by a standard laser having a power output of one or two milliwatts. Furthermore, the mercury green line at 0.5461 μm is very near the wavelength of maximum sensitivity of the eye.

Several attempts to modulate the beam and to use synchronous detection failed, probably because of the highly random energy fluctuations introduced into the beam by the atmosphere under the influence of sunlight. The simple pulse-counting techniques used in our nighttime work have proven to be adequate. In full sunlight, over a round-trip range of 2 km, with no lenses or mirrors to concentrate the beam and with interference filters 5 Ångstroms wide, the observed background intensity was less than 10 percent of that from the mercury green line.

The remaining problem is to minimize the effects of the relatively large seeing fluctuations which occur in full or intermittant sunshine. It seems probable that errors caused by these fluctuations can be reduced to reasonable limits by the use of a larger telescope (with correspondingly larger mirrors) and by selecting sites well above the terrain. Our limited experience with an over-water site (Lake Powell) provided very consistent results during early evening hours.

Laboratory Measures of Extinction by Selected Aerosols

A plastic cylindrical container with quartz windows at each end has been constructed in such a way that aerosols can be easily introduced. The light source and receiving equipment already described can be used to obtain the wavelength dependence of the extinction of selected aerosols. We hope to make a few measures of this type before the termination of this project.

DISCUSSION OF OBSERVATIONS

The air quality to be found at a given site should, of course, be judged by measures made over a long period of time, in different seasons of the year and different times of day. However, one can observe for a short period at a given site and, by taking several factors into account, use his

observations to predict the probable long-term air quality at that site. For instance, the very clear air found on a run of only two nights at Lake Powell could not be expected to be present when the winds come from the general direction of the Navajo Power Plant or when stagnant air conditions exist.

All of our observations were made along light paths which were inclined less than three degrees from the horizontal. After the light intensity is corrected by the inverse-square law, the observed intensity I is related to the initial intensity I_0 by the relationship $I = I_0 e^{-\beta(h,\lambda)d}$, where β is the total extinction coefficient at an elevation h above sea level and d is the path difference ($d_2 - d_1$ in Fig. 1). When intensities from two mirrors at different distances are compared, small corrections must also be made for the ratio of their reflectivities at different wavelengths.

The Rayleigh extinction due to air molecules is subtracted, and the extinction coefficients due to aerosols only, (β_p), expressed in units of reciprocal kilometers, are plotted against wavelength. The Rayleigh values were interpolated from Elterman's Tables for the elevation of a given site. No corrections were applied to account for the atmospheric pressure at the time of observation. (These would be very small corrections.) A discussion of the accuracy of the Rayleigh scattering coefficients is not within the scope of this paper.

Data have been obtained at night at ten different sites with elevations ranging from zero to 2.3 km. Conditions have been encountered at both low and high elevations under which the visibility was not significantly affected by the presence of aerosols.

At Flagstaff, Arizona (elevation 2.2 km), in October of 1973, measures obtained over a 3.3-km differential path well above a sparsely settled area showed virtually no aerosol extinction on two nights when the air movement was gentle and downslope from the nearby San Francisco mountains. The absence of aerosols was indicated on these two nights alone from a total of 25 nights.

Observations made across Lake Powell and the Grand Canyon (elevation 1.2 km) over a 6.6-km path on two nights showed no significant departure from Rayleigh scattering throughout the entire spectral range (Fig. 2). Under favorable wind conditions this area, which has only desert vegetation, can be remarkably clear. (The Navajo power station was about 3 miles east and downwind from the line of sight.) The Gardner counted 1000 particles per cubic centimeter, which is about one-quarter the number usually measured in the vicinity of the Lowell Observatory.

Conditions of Rayleigh scattering only were also found in March 1977 on several occasions immediately after rainy periods on Puget Island, Washington, a few meters above the Columbia River and about 50 km from its mouth.

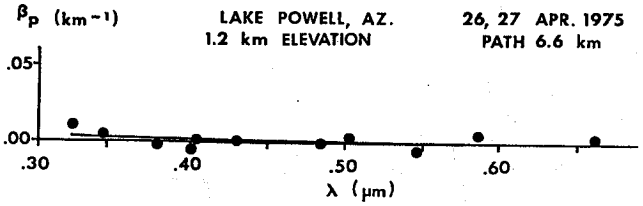

Fig. 2. Extinction data obtained across Lake Powell and the Grand Canyon on two nights of excellent transparency.

We have encountered a wide variety of aerosol sizes which produce effects ranging from dominant absorption to dominant scattering, that is, from aerosols large to small when compared to visual wavelengths. All of our aerosol extinction data for Flagstaff are represented by the four power curves in Fig. 3. The mean values for all nights (curve C) are 25 percent smaller than Elterman's tabulated data for the visual wavelengths and about equal to them in the ultraviolet. (The abrupt change in the shape of curve B is at the junction of the data published by Baum and Dunkelman[1] and that of Knestrick *et al.*[2]) The Flagstaff data include nights in which the aerosol extinction is nearly constant with wavelength (curve D), suggesting absorption by large particles, and other nights in which the ultraviolet data show pronounced selective scattering by small particles (curve E); as mentioned above, on two nights the aerosol extinction was close to zero.

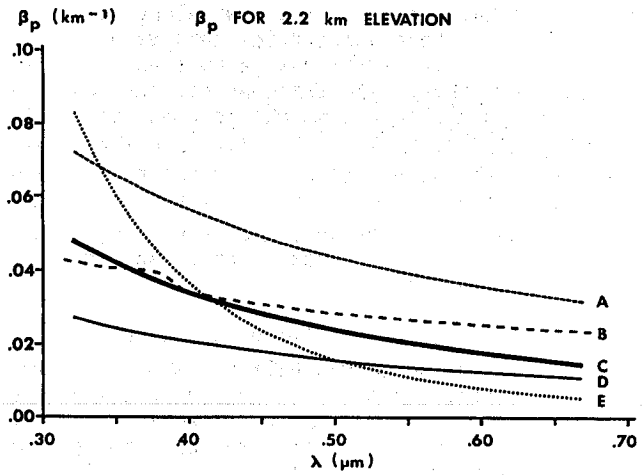

Fig. 3. Summary of aerosol extinction data for Flagstaff, Arizona. The mean best-fit power curves only are plotted. Curve C represents a mean of 25 nights of observations; compare this to curve B, which represents data interpolated from Elterman's Tables for 2.2 km. Curve A is the mean of seven poor nights; curve E represents five nights affected by forest fire particles or similar small particles. Curve D is a mean of the 13 clearest nights, including nights in which the extinction is nearly constant with wavelength.

Observations were made on eight nights at Mount Hopkins, Arizona (elevation 2.3 km), 55 km south-southeast of Tucson, over a light path well above the local terrain. The data for those periods which were free of aerosols brought in by high winds show mean extinction coefficients in the visual which are comparable to those obtained on the 13 best nights in Flagstaff (Fig. 3, curve D). In the far ultraviolet, however, the extinction is less than at Flagstaff, presumably due to the absence of nearby auto fumes and wood fires. Typical clean air data obtained at Mount Hopkins are plotted in the lower half of Fig. 4.

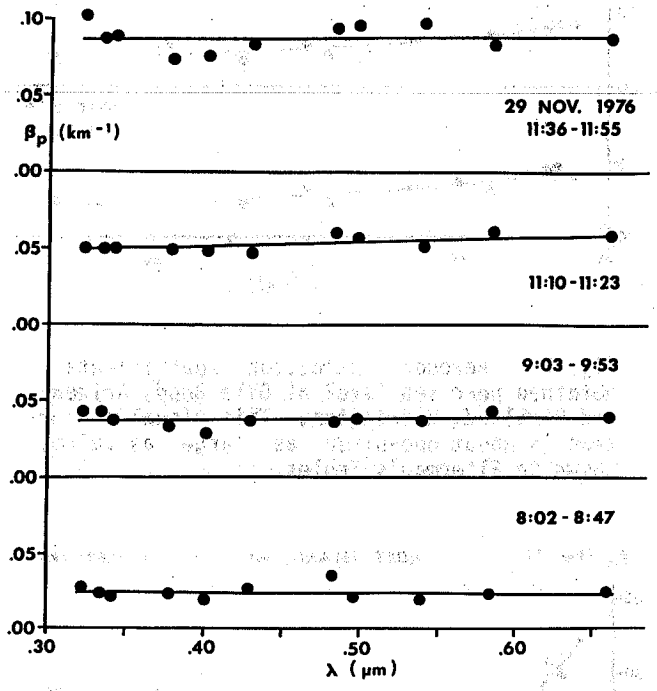

Fig. 4. Aerosol extinction coefficients obtained at Mount Hopkins, Arizona (2.3-km elevation). Typical clean air data are plotted in the two lower curves, while the two upper curves show the effect of continuously increasing extinction by large particles.

On two nights at Mount Hopkins, the aerosol extinction increased markedly during the course of the evening. This was particularly so on November 29, 1976, when the winds were very strong and dust either from local roads or from the fields several thousand feet below was observed on horizontal surfaces. On such nights, the extinction curves were essentially horizontal straight lines with increasing ordinate as the number of particles, large compared to wavelength, increased. Examples are shown in the upper half of Fig. 4.

Observations were also made at an elevation of 2.3 km at the airport just west of the entrance to Bryce Canyon, in southeastern Utah. Data obtained on nine nights indicated that this region had clearer air than any we have found.

Ray Weiss (University of Washington) worked with us at Bryce Canyon with a variety of instruments designed to measure air quality. Among these were instruments for measuring scattering coefficients and size distributions of large and small particles. The purpose of this collaboration (and several other joint efforts) was to calibrate the Integrating Plate Method of determining absorption coefficients which he has developed. The absorption encountered at Bryce Canyon, however, proved to be so small that no reliable calibration could be obtained. (The comparison was later made in Phoenix.)

On three of the nine nights on which we observed, the aerosol density was below our limit of detection; there were about as many negative coefficients (due to errors of measurement) as there were positive ones. Graphs showing data obtained on nights of good and poor transparency are included in Fig. 5. Weiss returned later in November and made further measurements which confirmed his opinion that Bryce Canyon has exceptionally clean air.

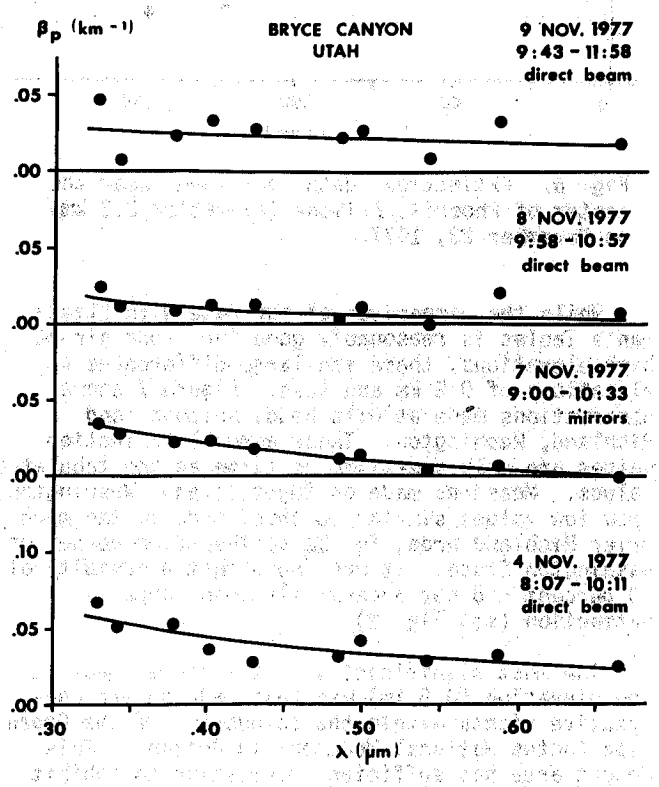

Fig. 5. Aerosol extinction data obtained near Bryce Canyon (elevation 2.3 km).

Observations made on a number of nights near the center of Phoenix showed large variations in air quality, depending on the time of night and on wind direction. On an exceptional night, however, about twelve hours after a rain shower, the aerosol extinction in the visual was only three or four times the Rayleigh extinction, or comparable to the air quality found in isolated areas. Data obtained in Phoenix on November 23, 1977, showing widely different degrees of extinction, are shown in Fig. 6.

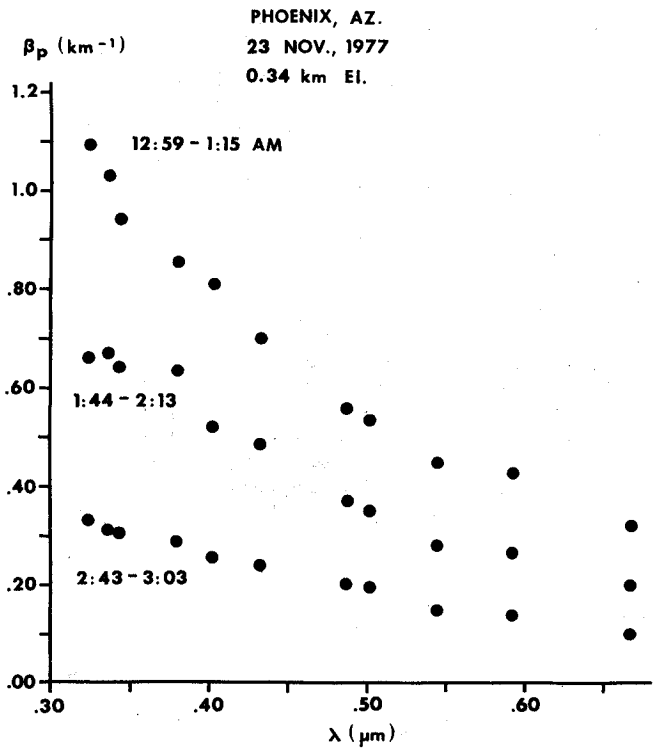

Fig. 6. Extinction data obtained near the center of Phoenix, Arizona (elevation 0.3 km) on November 23, 1977.

While the comparison of our data with Elterman's Tables is reasonably good for clear air at high elevations, there are large differences at elevations of 0.2 km and less. Figure 7 shows observations made at Gila Bend, Arizona, and Richland, Washington. These aerosol extinction values are only one-sixth as large as the tabulated values. Measures made on Puget Island, Washington, show low values similar to those made in the much drier Richland area, in the southeastern corner of Washington State. It was found that a humidity of 90 percent did not necessarily mean large extinction (see Fig. 8).

The most significant set of measures made at low elevation (0.5 km) was that made on ten consecutive nights within the boundaries of the Organ Pipe Cactus National Monument in Arizona. This desert area has sufficient vegetation to inhibit the development of numerous dust devils. It is roughly 500 km east-southeast of San Diego, bordered on the west by a government proving ground and on the south by Sonora, Mexico, with the Gulf of California and Baja California to the southwest. The lands south of the Mexican border are used for grazing. We found no evidence of contamination from a copper smelter at Ajo, 72 km north of our site.

With the exception of the second run on April 15, 1978, and both runs on the following night when strong winds associated with a frontal passage were present, the air quality was high. As shown in Fig. 9, on about half the nights the computed extinction curves were virtually straight lines and close to horizontal. On other nights they slope upward slightly in the ultraviolet.

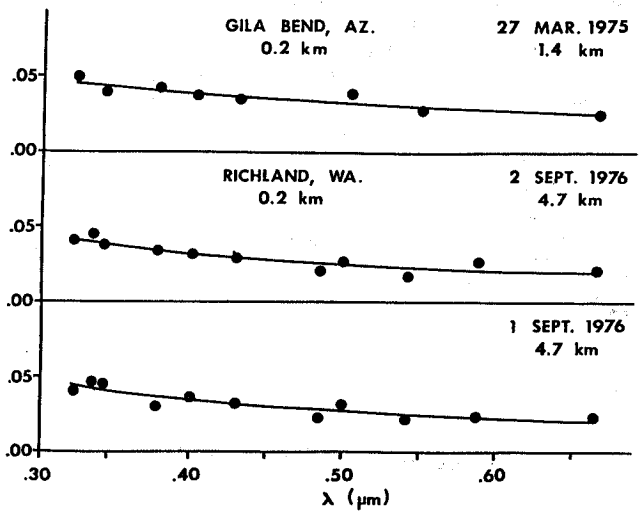

Fig. 7. Aerosol extinction coefficients obtained near sea level at Gila Bend, Arizona, and Richland, Washington, This visual extinction is about one-sixth as large as values shown in Elterman's Tables.

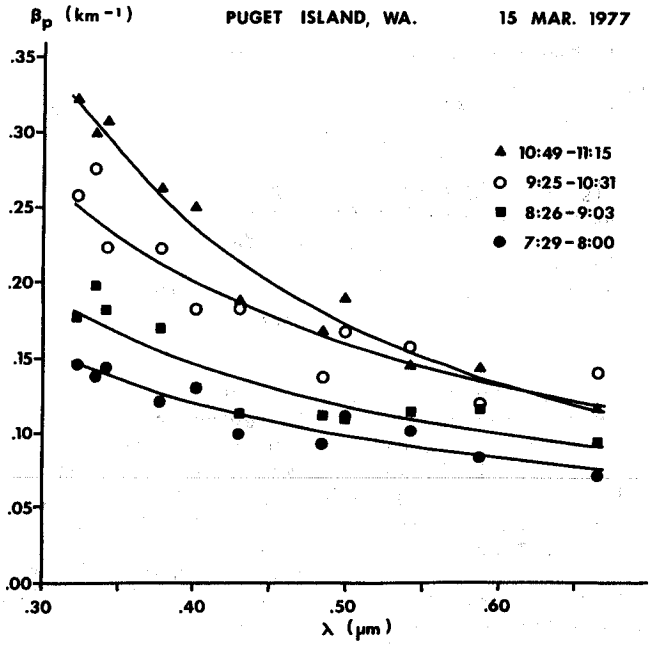

Fig. 8. Aerosol extinction coefficients obtained at Puget Island, Washington. The extinction increased rapidly, particularly in the ultraviolet, as the number of condensation nuclei increased. A heavy fog developed a few hours later.

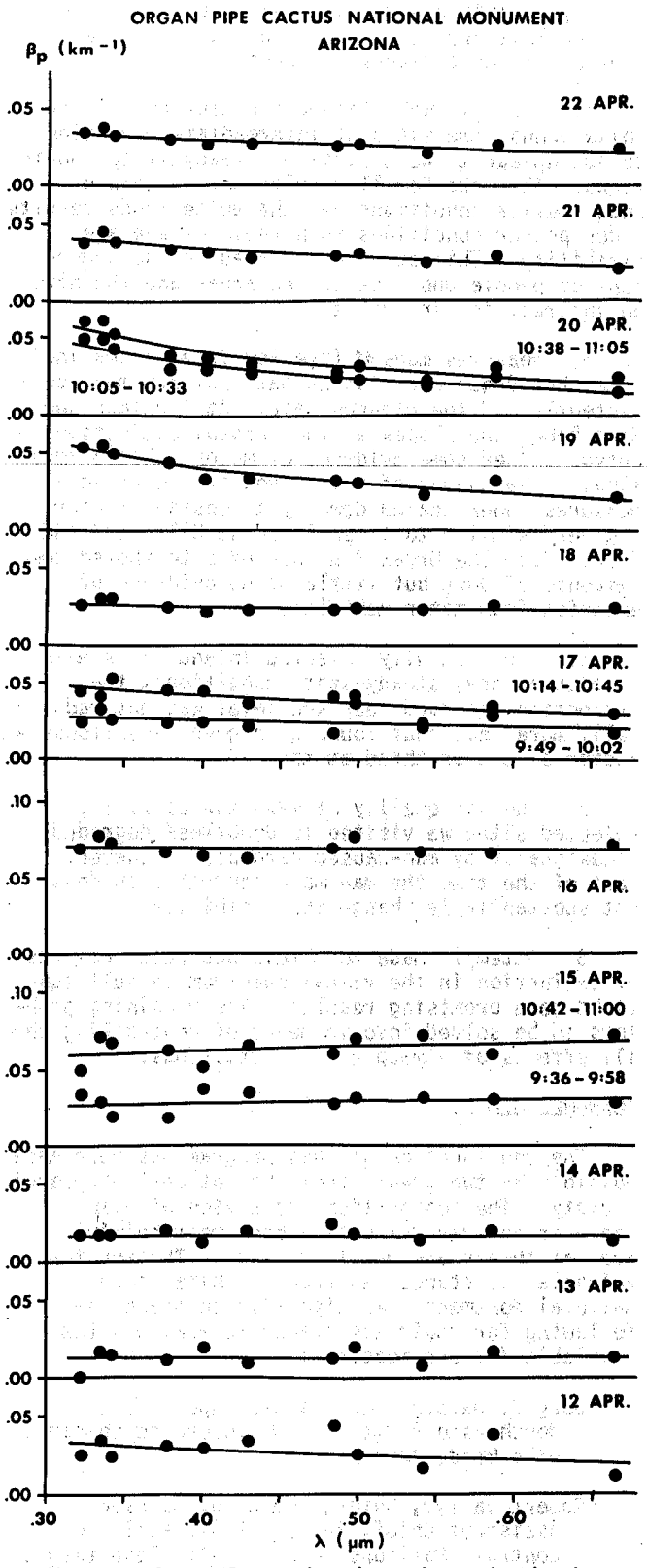

Fig. 9. Aerosol extinction data obtained during April 1978. The influx of strong frontal winds almost doubled the extinction on 15 April and kept it at a high level through 16 April.

The generally flat curves with small or no slopes suggest large aerosols, perhaps stirred up by local winds (dust devils). Vehicles travelling over unpaved roads within the Monument also create small amounts of dust.

Very recently we have measured air quality on seven consecutive nights at the White Sands National Monument. This Monument, at an elevation of 1.23 km, is surrounded on the north, west, and south by desert. Alamogordo, a city of 22,000 people, is 25 km to the east, Las Cruces (43,000) is 80 km to the southeast, and El Paso (370,000) is 110 km to the south. The prevailing winds from the west and southwest have blown the gypsum sand from a nearby lake bed to form the dunes.

On the nights of May 23 to 26, 1978, the winds were light and variable; on May 27 the wind was about 15 km/hr from the southwest. On May 29 it was 20-25 km/hr from the south-southeast. On May 28 there was little or no wind and a very large temperature gradient, a condition which caused very large and variable refraction of the light beam.

Air quality data secured on the nights of May 23-27 inclusive were so similar that they were combined and plotted at the bottom of Fig. 10. The variable refraction of May 28 caused such a serious loss of accuracy that the data are not presented. The data of May 29, plotted at the top of Fig. 10, show a definite increase in aerosol extinction toward the ultraviolet. It is quite possible that the air quality on this night was degraded by aerosols from the El Paso area.

The data for May 23-27 show low extinction with only a small increase toward the ultraviolet. There was no noticeable change based on wind direction.

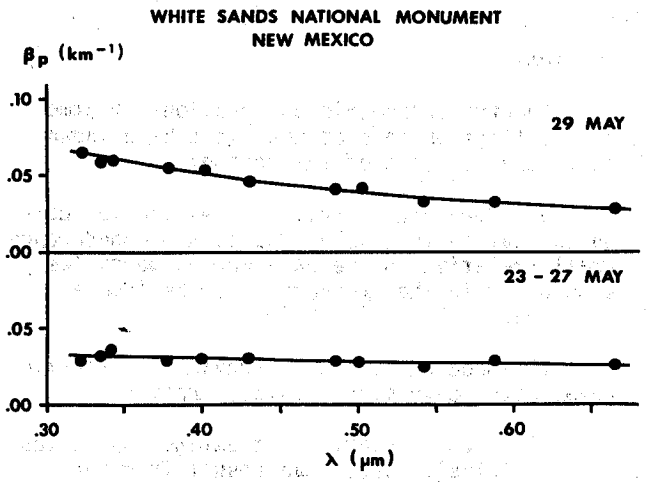

Fig. 10. Aerosol extinction data obtained during May 1978. The data for five nights shown at the bottom indicate a range of visibility of 100 km, a value very similar to that for the average of the last five nights of observation at Organ Pipe Cactus National Monument (see Fig. 9).

Puget Island was the only site where observations were made under very humid conditions. As shown in Fig. 8, on March 15, 1977, the aerosol extinction coefficients increased rapidly as the night progressed, particularly in the ultraviolet, and a nearby nephelometer showed a rapid increase in the number of particles. These evidently were the result of emission from a pulp mill about 2 km to the south, which always had plumes of water droplets associated with it. At sunrise on the next day, a heavy fog covered the island from the surface to a height of perhaps 50 meters.

Accurate measures were made during a severe dust storm at Gila Bend, Arizona, on March 26, 1975. The particles were large compared to a wavelength of visible light, and the visual extinction was about twelve times larger than that observed on the following clear night. The Gardner indicated a very low particle count (1000 per cc) during the dust storm. It appears that the large particles swept out the very small condensation nuclei.

During measures made while a forest fire was burning near Flagstaff, unusually large extinction in the ultraviolet and blue was observed (curve E, Fig. 3). A similar result was obtained on two nights in late July of 1976, also at Flagstaff, under very dry conditions.

Measures were made from the Observatory's dark-sky site 16 km southeast of Flagstaff over a 20.3-km path to the Flagstaff Station of the Naval Observatory, 8 km west of the city. The light path extended 100 to 300 meters above wooded terrain and over several roads, including I-17 from Flagstaff to Phoenix. These data also show an abnormal amount of extinction in the ultraviolet, which could be due in part to automobile emission and/or smoke from a few local dwellings (curve E, Fig. 3).

CONCLUSIONS

1. Spectrophotometric observations of atmospheric extinction made at ten sites have shown three general classes of extinction:

a) Very high ultraviolet extinction compared to that in the visual due to a preponderance of small (relative to the wavelength) particles. This occurred in the presence of smoke from a forest fire.

b) Moderately high ultraviolet extinction in areas with heavy motor vehicle traffic.

c) Flat or nearly flat extinction curves (large particles). These can result from the presence of windblown dust.

2. Very clear air was encountered at all elevations. At inland sites this was the case for air which had descended from high elevations or had been cleaned by rain showers. Measures on Puget Island showed that air coming in from the Pacific Ocean appeared to be very clear.

3. Three sites at high elevation were examined. Although Flagstaff and Mount Hopkins usually exhibited very clear air, we are led to believe that Bryce Canyon would prove to have clearer air on a year-round basis.

4. The data we obtained for Lake Powell and White Sands, two sites at intermediate elevation, do not appear to be typical of steady-state conditions. The Lake Powell results were obtained under better conditions and the White Sands results under poorer conditions than those of average visibility. This opinion is based on the judgement of people who live in the areas and who have an interest in air quality.

5. Measures made at five low-level sites indicate that Organ Pipe Cactus National Monument consistently had the clearest air. At Richland and Gila Bend, the slopes of the aerosol extinction curves showed some evidence of motor vehicle emission. (The shapes of the curves of the Phoenix measures, when scaled down by a constant factor, are very similar to those found at Gila Bend and Richland.) The Organ Pipe Cactus site showed some evidence of dust but little or no evidence of emission from motor vehicles.

6. For carefully selected inland sites examined under dry, steady-state conditions, the extinction observed near sea level was not radically more than that found at higher elevations--a factor of two or three at most.

7. The air quality at even the carefully selected sites we visited is doubtless degraded occasionally by man-caused aerosols. However, most of the time the man-made contribution does not substantially change the visibility.

8. Attempts made to obtain accurate measures of extinction in the visual spectrum in full sunlight gave promising results. The remaining problems to be solved involve means of controlling the ill effects of atmospheric fluctuations.

ACKNOWLEDGEMENTS

The continuation of this program has been made possible by two grants from the National Geographic Society. The cooperation and advice of Alan Waggoner and Ray Weiss have been most helpful. Special thanks are due to Robert J. Thomson for valuable assistance rendered at White Sands National Monument. We also wish to thank the following for their assistance in making sites available for our measures:

Doug C. Nelson, Real Estate Supervisor, Northwestern Mutual Life Insurance Company, Gila Bend, Arizona.

Robert Taylor, Chief, and G. W. Johnson, Assistant Chief, Bureau of Air Pollution Control, Maricopa County Health Department, Phoenix, Arizona.

Clark A. Lowry, President, American Estate Life Insurance Company, Phoenix, Arizona.

J. Bartlett, Manager, Bryce Canyon Airport, Utah.

R. G. Martinez, Jr., Superintendent, Organ Pipe Cactus National Monument, Arizona.

Willis Ramsey, Port Director, Lukeville, Arizona.

J. M. Thomson, Superintendent, White Sands National Monument, New Mexico.

REFERENCES

[1]W. A. Baum and L. Dunkelman (1955). "Horizontal Attenuation of Ultraviolet Light by the Lower Atmosphere. *Journal of the Optical Society of America,* Vol. 45, pp. 166-175.

[2]G. L. Knestrick, T. H. Cosden, and J. A. Curcio. (1962). "Atmospheric Scattering Coefficients in the Visible and Infrared Regions." *Journal of the Optical Society of America,* Vol. 52, pp. 1010-1016.

[3]L. Elterman (1968). "UV, Visible, and IR Attenuation for Altitudes to 50 km, 1968." AFCRL-68-0153, *Environmental Research Papers* No. 285, Air Force Cambridge Research Laboratories, L. G. Hanscom Field, Bedford, Massachusetts.

[4]J. S. Hall, M. Jerzykiewicz, and L. Riley (1975). "Extinction Measurements for Sensitive Assessment of Air Quality." *Journal of the Air Pollution Control Association,* Vol. 25, pp. 1045-1048.

[5]J. S. Hall and L. A. Riley (1976). "Basic Spectrophotometric Measures of Air Quality Over Long Paths." *Progress in Astronautics and Aeronautics,* Vol. 49, pp. 205-212.

LIGHT SCATTERING PARAMETERS OF INTERNAL AND EXTERNAL MIXTURES OF SOOT AND NON-ABSORBING MATERIAL IN ATMOSPHERIC AEROSOLS

Jost Heintzenberg

International Meteorological Institute in Stockholm,
Arrhenius Laboratory, S-106 91 Stockholm, Sweden

ABSTRACT

Extinction, scattering and absorption coefficients of single particles are calculated allowing three different ways of mixing a fixed volume fraction of soot with non-absorbing ammonium sulfate:
1. one homogeneous sphere with the soot being 'dissolved' in the ammonium sulfate,
2. an external mixture of two independently scattering soot and ammonium sulfate spheres,
3. two concentric spheres with the soot being the kernel.

The results are integrated over Whitby's Los Angeles Grand Average aerosol size distribution to demonstrate the influence of the state of internal or external mixture on the light scattering parameters of an urban aerosol. Four different possibilities of distributing a fixed total soot volume over the three modes of the size distribution have been investigated. The calculated light extinction coefficients for the 4 models differ only by 5% while the corresponding scattering coefficients vary by 10% depending on the state of mixture. The absorption coefficients however vary by a factor of 3 with changing location of the fixed absorber volume within the particles and/or within the size distribution.

INTRODUCTION

In this study the location of the absorbing material is varied within a trimodal urban aerosol model (Whitby's L. A. grand average[1]) and the effect on integral light scattering and absorption properties has been investigated. Soot with a complex refractive index of $1.57 - .48i$[2] is assumed to be the light absorber while ammonium sulfate with a real refractive index of 1.525 represents the non-absorbing fraction of the atmospheric aerosol. For each individual particle size three different ways of distributing a given absorber volume were considered:

1. volume mix: The absorber is 'dissolved' in the non-absorbing material forming homogeneous particles of a complex refractive index of $1.53 - .01i$, a frequently published value for the refractive index of atmospheric aerosol. The volume mix though chemically unsound repsents about the state of the art in the optics of the atmosphere,
2. external mix: Absorbing and non-absorbing material exists as two separate particles acting as independent scatterers,
3. internal mix: The absorber is the kernel of two concentric spheres with ammonium sulfate as the shell.

Four different possibilities for locating a given absorber volume within the over all size distribution have been used.

1. symmetrically, leading to the same volume fraction of absorber/non-absorbing material in all theree modes, (M1-M3),
2. the total absorber volume in the fine particle mode, (M4),
3. the total absorber volume in the accumulation mode, (M5),
4. internal mixing in the accumulation mode while the rest of the absorber volume is externally mixed into the fine particle mode, (M6).

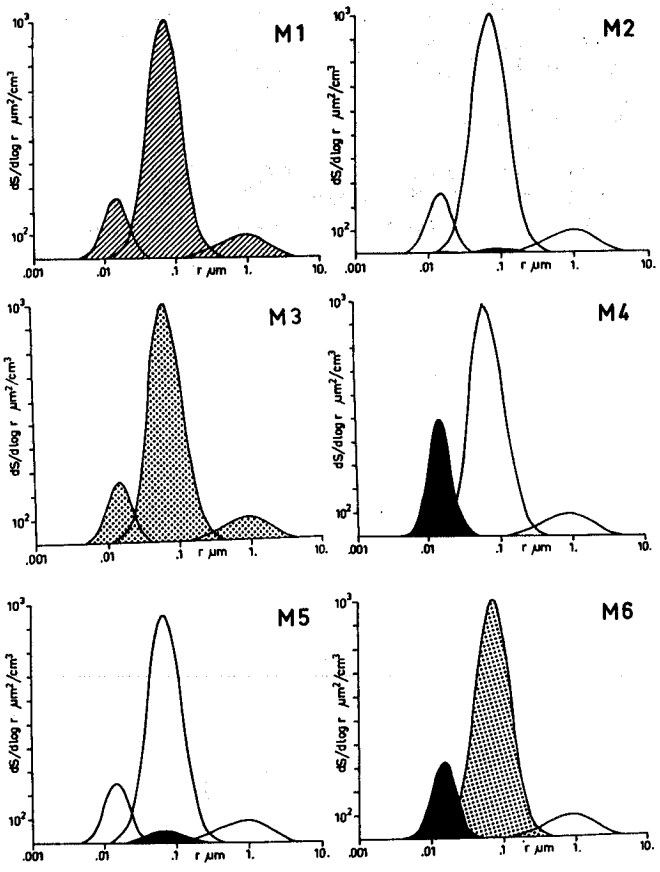

Fig. 1 Aerosol models used in the light scattering calculations. Dashed areas stand for a volume mix. Dotted areas stand for an internal mixture. Black areas represent pure soot.

RESULTS

Results of the scattering calculations are first given for individual particles to demonstrate the effects of the different internal or external mixtures of absorbing and non-absorbing material on single particle light scattering and absorption. Here the fraction of soot to total volume is kept the same for all particle sizes. Setting it to about 2% yields a bulk value of 1.53 - .01i for the refractive index at each radius. Figures 2-4 show extinction, scattering and absorption per volume as a function of particle size.

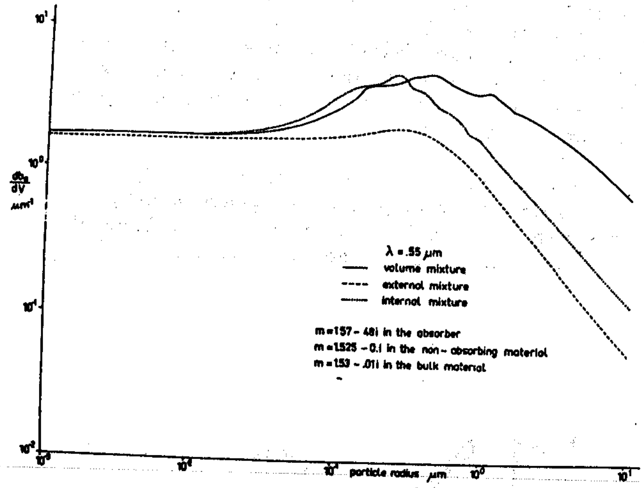

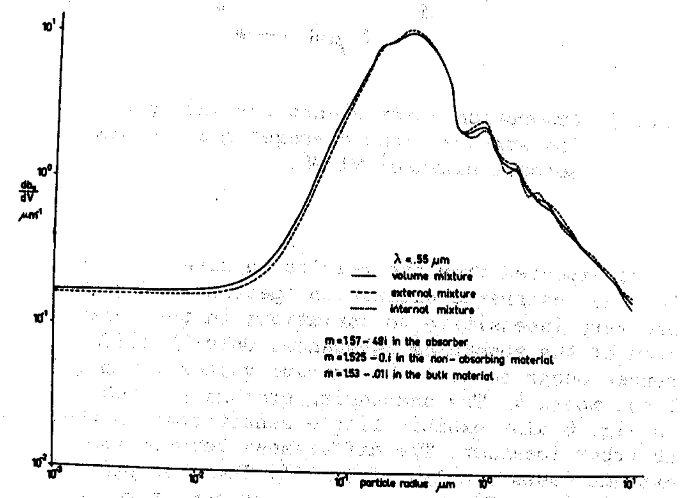

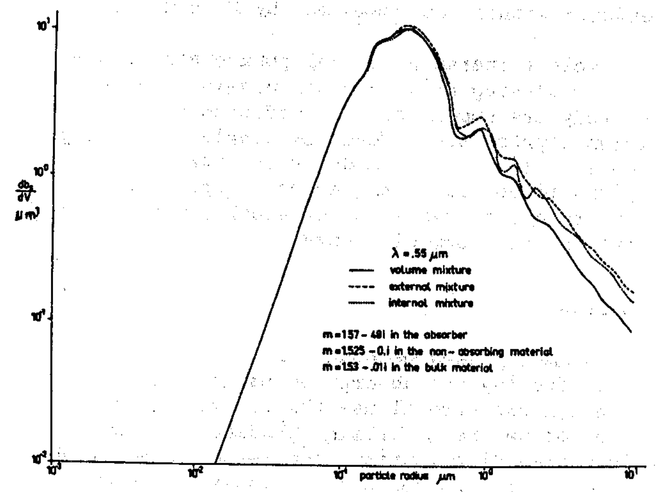

Fig. 2-4 Extinction, scattering and absorption coefficients per volume as a function of particle size.

As for the extinction coefficient, no striking differences appear between the 3 ways of distributing a given volume fraction of soot within each particle. The external mixture sets the lower limit for the first 2 decades of particle size but above that the 3 mixtures follow the same curve with only slight deviations.

For the scattering coefficients the differences between 3 kinds of mixture are even smaller for particle radii up to about .2 μm. For larger sizes however the curves diverge markedly. The volume mixture sets the lower limit and the external mixture sets the upper limit for the scattering coefficients per volume.

However, the most striking effects of varying the distribution of a fixed volume fraction of absorbing material can be seen in the absorption coefficients. For particles with radii above .01 μm the curves spread increasingly with more than one order of magnitude between external and volume mixture at the upper end of the investigated size range. The external mixture yields the lowest absorption coefficients for all particles sizes. Particles with a soot kernel show strongest absorption up to the maximal radius at about .2 μm. For larger sizes, the volume mixture causes increasingly stronger light absorption than the other two mixtures.

For the extinction, being the sum of absorption and scattering it does not matter how the absorber is distributed within the aerosol particle. Spreading it over the total particle volume maximizes its damping effect on the electromagnetic field, causing highest absorption and lowest scattering. However, below the main resonance maximum a significant part of the light entering the particle traverses the center of the sphere. Through this focussing effect a soot kernel causes higher absorption than the volume mixture.

For larger particle sizes a concentric absorber still yields higher light absorption than an external soot particle absorbing independently but distributing the same absorber volume over the entire particle volume causes the strongest damping of the internal field.

Extinction, scattering and absorption spectra are presented for Whitby's L. A. grand average size distribution (note that the total volume of soot is the same in all 6 aerosol models).

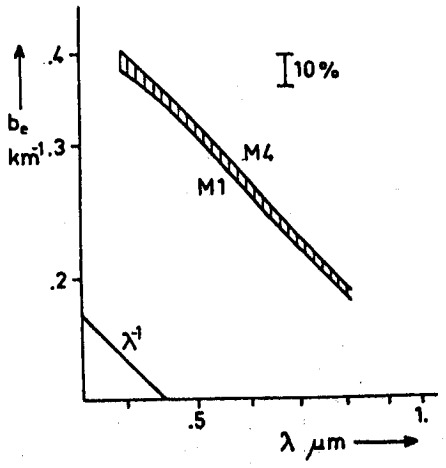

Fig. 5 Extinction coefficients for Whitby's Los Angeles Grand Average[1] and the six aerosol mixtures M1-M6.

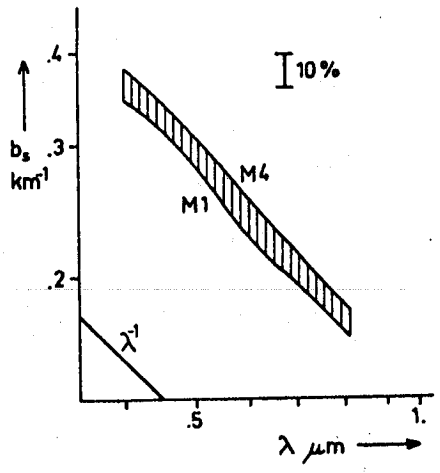

Fig. 6 Scattering coefficients for Whitby's Los Angeles Grand Average[1] and the six aerosol mixtures M1-M6.

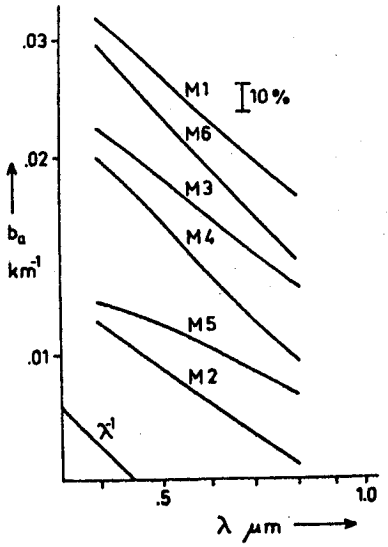

Fig. 7 Absorption coefficients for Whitby's Los Angeles Grand Average[1] and the six aerosol mixtures M1-M6.

As expected from the results on single particles the integrated extinction spectra in Fig. 5 are very insensitive to variations in the location of the absorbing substance. Only 5% differences occur between the extreme values for model 1 and model 4. The scattering spectra plotted in Fig. 6 also exhibit little sensitivity to the absorber location. The differences between the extreme cases are less than 10%. The absorption spectra (Fig. 7) however, are very sensitive to the location of the absorber material. The symmetrical external mixture (M2) sets the lower limit while the symmetrical volume-mixture causes the highest light absorption with three-forld values, (see Fig. 4 as explanation). The results for the other four models scatter with varying wavelength dependence within the range set by M2 and M1.

In table 1 characteristical parameters of the carbon containing urban aerosol models used in this study are summarized. In addition to the coefficients presented before the single scattering albedo ω is listed. $1 - \omega$ describes how much of the light illuminating the aerosol population is converted into radiation of another wavelength or into another form of energy.

CONCLUSIONS

The commonly used methods for calculating light scattering and absorption parameters of the atmospheric aerosol use the volume-mixture (M1) to locate the absorbing substance in the particle size distribution. The results presented here show that this approach yields the lowest extinction and scattering and the highest absorption coefficients of all investigated models concerning the distribution of a given absorber volume in the aerosol.

model	aerosol material			λ = .55 µm			
	mode 1	mode 2	mode 3	extinction coefficient km^{-1}	scattering coefficient km^{-1}	absorption coefficient km^{-1}	single-scattering albedo
M1	volume-mix	volume-mix	volume-mix	.281	.257	.0246	.91
M2	external mix	external mix	external mix	.284	.275	.00898	.97
M3	internal mix	internal mix	internal mix	.280	.263	.0173	.94
M4	soot	$(NH_4)_2SO_4$	$(NH_4)_2SO_4$	.293	.279	.0144	.95
M5	$(NH_4)_2SO_4$	soot,$(NH_4)_2SO_4$	$(NH_4)_2SO_4$	.285	.274	.0107	.96
M6	soot	internal mix	$(NH_4)_2SO_4$	.288	.267	.0209	.93

Table 1 Characteristic parameters of a carbon containing trimodal urban aerosol size distribution[1].

The aerosol can cause either cooling or heating of the atmosphere depending on the relation between its absorption and its scattering properties (including the angular distribution of the scattered radiation[3]). In aerosol particles with radii comparable to the wavelength, the absorption influences most strongly the radiation scattered into the backward hemisphere. Therefore in a separate study the effect of the absorber location on the angular distribution of scattered light will be investigated. In conclusion it is recommended that the commonly used models for locating the absorber material in the aerosol be revised and more knowledge about the state of internal and external mixture of soot and non-absorbing substances gathered before assessing the netto effect of aerosol on the atmospheric heat balance.

REFERENCES

1. Whitby K T, 1974, Proceedings of the GAF-Conference, Bad Soden, W Germany.

2. Dalzell W H and Sarofim A F, 1969, J. Heat Transfer, Feb. 1969, 100-104.

3. Charlson R J and Pilat M J, 1969, J. Appl. Met. 8, 6,1001-1002.